Draft v 9.02
June 07, 2013

SEARCHING for a QCD MIXED PHASE at the NUCLOTRON-BASED ION COLLIDER FACILITY (NICA White Paper)

From: "T.D. Lee" <tdl@phys.columbia.edu>
To: "Sisakian A.N." <sisakian@jinr.ru>
Sent: Wednesday, January 14, 2009 7:01 PM
Subject: Comment on the goals of the NICA heavy ion collider

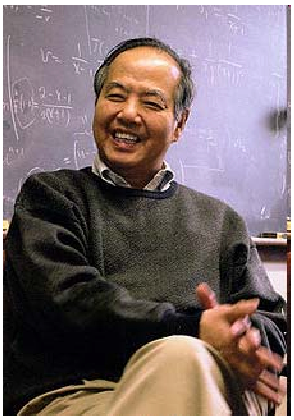

Dear Prof. Sissakian:

The NICA heavy ion collider will be a very major step towards the formation of a new phase of quark-gluon matter.

The goal of relativistic heavy ion physics is to modify the properties of the physical vacuum. Of particular interest is a possibility to create a phase of quark-gluon matter where some of the fundamental symmetries may be altered. Recent RHIC results indicate that there may be an evidence of parity violation (on an event-by-event basis) in heavy ion collisions at high energies. It would be of great importance to search for this phenomenon in the energy range covered by the NICA collider where a high baryon density is reached.

I am very much looking forward to the completion and future success of the NICA heavy ion collider. Warm regards and very best wishes,

T. D. Lee
--
T. D. Lee
University Professor
Dept. of Physics - MC 5208
Columbia University
New York, NY 10027

Foreword to the ninth Edition

We present the ninth Edition of the NICA White Paper with 6 new and one revised contributions (marked in red color) which demonstrates that the interest in the development of the Nuclotron-NICA facilities is as big as before and has even grown over the past months. So has the NICA White Paper which now comprises 104 contributions on 300 pages of text written by 188 authors from all over the world. This makes it necessary reconsider the structure of the White Paper and to invoke a prioritization of contributions according to their relevance for the planned experiments.

In the present Edition, we have made a first step towards a prioritization of NICA White Paper contributions. To that end a working group has prepared short summaries to contributions in five topical directions:

1. Equation of state and phases of QCD (D. Blaschke)
2. Mixed phase and chiral magnetic effect (V. D. Toneev)
3. Collective dynamics, medium effects, dileptons, strangeness and elementary reactions (E. Bratkovskaya)
4. Spin and polarization phenomena with polarized beams (O. Teryaev)
5. Lambda-nucleon interaction, hypernucleus production and rare objects (J. Aichelin)

The result is given in the Subsection "1.3 Priority directions for NICA experiments", which is newly added to the present White Paper Edition. Note for example that as a result of this first "evaluation" process, a critical assessment of pursuing the Chiral Magnetic Effect (Section 8) in NICA experiments has been suggested!

We want to underline that this is still a very preliminary result since even the group members themselves had not enough time to discuss the contents of this Subsection 1.3, not even to speak about a backreaction from the community.

Nevertheless, this first step shall demonstrate the direction of a priorization process which herewith has been started and which shall contribute to the preparation of a discussion in a broader context, for instance at a "NICA Round Table" to be held in Dubna later this year.

With these introductory remarks we recommend the present Edition of the NICA White Paper to the attention of the growing community of compressed baryon matter research and hope it will prove useful for the further development of scientific collaborations for the NICA/MPD and BM@N experiments.

Yours sincerely,

D. Blaschke,
E. Bratkovskaya,
D. Kharzeev,
V. Matveev,
A. Sorin,
H. Stöcker
O. Teryaev,
I. Tserruya,
N. Xu

Dubna, June 2013

Foreword to the eighth Edition

We present the eighth Edition of the NICA White Paper with 14 new contributions (marked in red in the Table of Contents) which make this document a milestone on the way towards the development of the Scientific Programme of the Nuclotron-NICA facilities. These new articles represent a rather broad spectrum and contribute to 8 of the 11 scientific sections of the White Paper. A common feature to all of them is their emphasis of the special role and merits of the fixed target programme (BM@N) at NICA.

Let us mention a few of the interesting arguments in favor of BM@N. Nonequilibrium modeling of the phase transition shows that the energy range $E_{\rm Lab} = 2 - 4$ A GeV may be optimal for detecting the growth of spinodal fluctuations (clumping) as characteristic for a first order phase transition (4.19) and for disentangling them (4.20) from a second order/crossover scenario . It has been pointed out (9.3) that BM@N is a place to test the idea that multi-nucleon quark clusters may be formed between the hadron-dominated and quark-dominated regions with the consequence of binding energy anomalies in hypernuclei. Three new contributions are directly related to the measurements of hypernuclei production with the BM@N detector (12.7, 12.8, 12.9). The fixed target experiment may be the ideal place to test mechanisms of hadron production (2.9, 6.8) and dilepton production (7.8, 7.9) in the corresponding energy range. If accessible at all in heavy-ion collisions, here may be the unique place to see effects of color superconductivity (3.14).

During the past year, special attention has been dedicated to the development of the Physics Program and Conceptual Design Report of the BM@N experiment

`http://nica.jinr.ru/files/BM@N/bmn_documents.htm`

Despite the existence of the special Section "Fixed Target Experiments", we would like to stress here that there is no actual separation of contributions to experiments at the collider NICA (i.e. MPD, SPD) and to the fixed target experiment at the Nuclotron (BM@N). Indeed, the physical ideas at the "crossing"-energies between NICA and Nuclotron (i.e. for $\sqrt{s} < 4.5$ GeV) are applicable for collider as well as for the fixed target modes and provide a unique possibility to obtain a combined experimental information on the same physical phenomena: the multi-strange hadron and hypernuclei production, the study of hadron properties in a dense medium, hadron production in elementary reactions etc.

We point out that besides the contributions in Sect. 12 also the following ones are relevant for the BM@N experiment:

2.4, 2.5, 2.6, 2.9;
3.3, 3.6, 3.7;
4.2, 4.3, 4.6, 4.12, 4.13, 4.16, 4.17, 4.19, 4.20;
5.5, 5.6, 5.7, 5.8;
6.4, 6.6, 6.7 6.5, 6.8;
7.1, 7.2, 7.7, 7.3, 7.8, 7.9;
8.1, 8.2, 8.3, 8.4, 8.5, 8.6, 8.8;
9.1, 9.2, 9.3;
10.1, 10.2, 10.3, 10.4;
11.4, 11.5

We hope that the present Edition of the NICA White Paper will prove useful for the further development of scientific collaborations for the NICA/MPD and BM@N experiments.

Yours sincerely,

D. Blaschke,
E. Bratkovskaya,
D. Kharzeev,
V. Matveev,
A. Sorin,
H. Stöcker
O. Teryaev,
I. Tserruya,
N. Xu

Dubna, January 2013

Foreword to the seventh Edition

We present the seventh Edition of the NICA White Paper with eight new contributions (marked in red color) which make this document a milestone on the way towards the development of the Scientific Programme of the NICA facility.

The present Edition has an intermediate character. Since the document has grown substantially, a major Editorial work becomes necessary to account for the fact that the fixed target experiment (BM@N) is taking shape and requires special attention. Besides that, it is desireabe to restructure the presentation so that it resembles more adequately the aspects of the scientific programme at NICA, i.e. accounting for the basic physical phenomena and corresponding observables, as summarized in the Table of the Editorial section 1.1.

Six of the eight new contributions in the present Edition iterate on topics that were already discussed before

- QCD phase diagram (3.12, 3.13)
- Hadronic signals of the chiral and deconfinement transition (4.17, 4.18)
- Fluctuation signals (5.9)
- Local P/ CP violation and CME (8.8)

These new contributions make the picture more complete and serve for a more balanced presentation of the physics issues at NICA.

The contribution 4.16 raises a new issue, namely the role of nuclear clusters in the determination of flow and signals of the QCD phase transition. This contribution is a direct response to recent discussions at the PAC meeting where the question of MPD design was discussed with particular emphasis on the possible role of light nuclear clusters (d, t, h, α).

We would like to recommend to the readers of the NICA White Paper the new contribution by Stanley Brodsky (2.7) which presents a portfolio of ideas for the experimental programme in itself. It is in particular devoted to the perspectives of heavy flavor physics at NICA energies. If at least part of these ideas becomes feasible this would substantially enrich the physics programme at NICA.

Yours sincerely,

D. Blaschke,
D. Kharzeev,
V. Matveev,
A. Sorin,
H. Stöcker
O. Teryaev,
I. Tserruya,
N. Xu

Foreword to the sixth Edition

We present the sixth Edition of the NICA White Paper with seven new contributions which make this document a stepping stone on the way towards the development of the Scientific Programme of the NICA facility.

A qualitatively new aspect of the present Edition is that most of the new contributions make use of the expected parameters of the NICA facility for both, the collider (MPD) and the fixed target (BM@N) experiments. This is a nice justification of the decision taken by the Editorial board in the previous edition to add the new "Editorial" section where the basic parameters of the facility have been summarized for the convenience of the contributors to the White Paper. In subsection 1.2 we added a table, taken from the Conceptual Design Report (CDR) of the Multi-Purpose Detector (MPD), summarizing the expected particle multiplicities in central Au+Au collisions at energies covered by the NICA facility.

The present Edition becomes particularly valuable as its new elements may be considered as facets of the evolving Scientific Programme for NICA, with specific predictions for the possible outcome of experiments with the foreseen concrete parameters.

We want to emphasize here the new contribution by Peter Senger in Subsection 12.5 which presents a detailed programme to study strangeness and hypernuclei production in heavy-ion collisions using the fixed target experiment BM@N at the refurbished Nuclotron facility.

We wish to express our hope that the present Edition of the NICA White Paper will prove useful for the further development of the collaborations for the NICA/MPD and BM@N experiments and for shaping up their scientific programme.

Yours sincerely,

D. Blaschke,
D. Kharzeev,
V. Matveev,
A. Sorin,
H. Stöcker
O. Teryaev,
I. Tserruya,
N. Xu

Foreword to the fifth Edition

The present fifth Edition of the NICA White Paper represents a milestone towards the realization of the NICA project. Besides new contributions and revision of previous ones, in this Edition we have added a new "Editorial" Section which provides a summary of the basic parameters of the planned NICA accelerator facility, such as its beam characteristics and design parameters. This new Section also gives an overview on the physical phenomena which shall be investigated and the experimental observables which are suggested to reach this goal. Table 1.1 in Subsection 1.1 summarizes the most promising suggestions contained in the White Paper with reference to the chapters where more details are given. It shall be regarded as an important step towards a more detailed scientific programme for the NICA facility and shall help to identify the discovery potential of NICA in the context of the existing and planned heavy-ion collision experiments at RHIC, CERN and FAIR.

We hope that the present Edition of the NICA White Paper will prove useful for the further development of scientific collaborations for the NICA/MPD and BM@N experiments.

Yours sincerely,

D. Blaschke,
D. Kharzeev,
V. Matveev,
A. Sorin,
H. Stöcker
O. Teryaev,
I. Tserruya,
N. Xu

Foreword to the fourth Edition

The present fourth Edition of the NICA White Paper became necessary not only because newly submitted contributions had to be included to this open forum for the discussion of the "search for the quark-hadron mixed phase and QCD critical point". After the third Edition had been released in June 2010, an additional programme is being developed at the NICA facility for fixed target experiments with heavy ion beams extracted from the Nuclotron-N at energies up to $E_{\rm lab} = 5.5$ AGeV (start date: 2014). This programme was discussed, e.g., at the V$^{\rm th}$ Round Table Workshop "Physics at NICA" held on August 28, 2010, during the 6$^{\rm th}$ International Workshop on "Critical Point and Onset of Deconfinement" (Dubna) and at a dedicated Meeting on "Fixed target @ Nuclotron-N and SIS100 @ FAIR" (GSI Darmstadt, November 3, 2010). Links to these events are to be found on the NICA White Paper Wikipage

http://theor.jinr.ru/twiki-cgi/view/NICA/WebHome

Accordingly, we have introduced a new section for "Fixed target experiments" in the present Edition which contains already three new contributions.

Moreover, we have split from the big section 2 on "Phases of QCD matter at high baryon density" (which grew too big) a new section dedicated to "Hydrodynamics and hadronic observables" and reordered the contributions correspondingly.

Among the new contributions (marked in red) to this Edition the reader will find for the first time contributions on astrophysical constraints on dense matter and on lattice QCD, which put the NICA programme into a broader context. A separate contribution is devoted to the challenging new idea of a so-called "quarkyonic phase" and a triple point in the QCD phase diagram which directly concern the energy range of experiments planned at NICA.

With the present fourth Edition the NICA White Paper has grown to some maturity but it is still considered an open process and an invitation to the international heavy-ion physics community for collaborating with NICA and for discussing the physics of dense matter.

We are looking forward to your contribution!

Yours sincerely,

D. Blaschke,
D. Kharzeev,
A. Sorin,
O. Teryaev,
V. Toneev,
I. Tserruya

Foreword to the first Edition

Theoretical and experimental investigations of the QCD phase diagram belong to the most topical research directions in modern physics. The search for the quark-gluon plasma (QGP) at RHIC Brookhaven and CERN SPS has revealed first indications for rich physics going beyond the naive picture of a gas of quarks and gluons: a strongly coupled QGP (sQGP). Results from the energy scan program of the NA49 experiment, however, suggest that the physics of the onset of the hadron-to-quark matter transition should be expected at lower c.m. energies of the colliding heavy-ion systems. Therefore, new experimental programs are being developed which aim at investigations of the QCD phase diagram at lower temperatures and high baryon densities: low-energy RHIC, NA61 (SHINE), CBM @ FAIR Darmstadt and NICA-MPD in Dubna.

The Nuclotron-based Ion Collider fAcility (NICA) with its multi-purpose detector (MPD) has been defined as the new flagship of the Joint Institute for Nuclear Research (JINR) Dubna within the roadmap for the JINR development. Being the "CERN of the East", the JINR Dubna plans to provide with this instrument a dedicated collider experiment for exploring the high density region of the QCD phase diagram, thus filling a niche in the global plans.

In order to support the realization of heavy-ion collider facilities like NICA, it is important to continue the process of theory-experiment discussions which has been initiated with the now completed CBM White Book. As it has become clear during the preparations for the CBM experiment, it is of utmost importance to use the chance which a new experiment provides in order to stimulate this dialogue and to trigger the generation of new and the sharpening of known ideas on the phase structure of dense QCD and the possibilities for its experimental verification.

In this spirit, a series of Round Table discussions on the development of the NICA project has been organized, the next one on "Physics at NICA" to be held at JINR Dubna in the week of September 7 - 11, 2009.

In preparation of this event, a call for contributions to the physics programme at NICA has been issued in April 2009 and a Wiki-page has been created to provide a public forum making the submitted suggestions accessible to the community at:

http://theor.jinr.ru/twiki-cgi/view/NICA/WebHome

At the present stage, we have decided to assemble the submitted material into a unified document as a basis for the clarification of the key topics for the preparation of NICA and above mentioned experiments:

- Phases of dense QCD matter and conditions for their possible realization
- Characteristic processes as indicators of phase transformations
- Estimates for events and event rates
- Comparison to other experiments
- Interdisciplinary aspects, e.g. astrophysical constraints for dense matter phases

shall be continuously all interested at the Bogoliubov Laboratory for Theoretical Physics in Dubna (please, find attached the file with brief information on the NICA project) and invite you to participate in a discussion of the Physics potential of such a facility! As a forum for the discussions we will organize a Round Table on "Physics at NICA", to be held at JINR Dubna, tentatively in the week September 7 - 11, 2009. In preparation of this event, and

The recent developments in dense matter physics have shown that we must be prepared for the unexpected! Three examples:

- Only ten years ago, Frank Wilczek and Edward Shuryak with their groups have initiated the exploration of color superconducting quark matter which triggered an avalanche of papers with suggestions how the dense QCD phase diagram should look like and what consequences one could expect for the explanation of astrophysical phenomena. Unfortunately, up to now we don't know what dilepton spectrum we should expect from diquark annihilation in superconducting quark matter!

- Just two years ago, Rob Pisarski and Larry McLerran found out that in dense QCD chiral symmetry restoration may not be accompanied with deconfinement and suggested that in the yet unexplored high-density corner of the QCD phase diagram we shall find "quarkyonic matter", a quantum liquid of confined, but massless quarks! What observables shall identify such a phase once it gets "accidentally" created in a heavy-ion collision? We don't know yet.

- Last not least, Dmitry Kharzeev and collaborators suggested an observable effect from P-parity violation in heavy ion collisions - is this effect relevant for the exploration of dense matter phases?

We need to identify the challenges and the discovery potential of such machines like NICA, creating the densest forms of matter in terrestrial laboratories. It requires concerted efforts to understand the stuff which constitutes the interiors of neutron stars and governs fantastic astrophysical phenomena like supernova explosions and neutron star mergers, the possible origins for the mysterious gamma-ray bursts and cosmic rays. In order to support the process of construction or modification of heavy-ion collider facilities which would be suitable to study QCD phase transformations at high baryon densities in laboratory experiments (see Appendix for a sketch of the QCD phase diagram), we invite you to contribute with your expertise to a "White Paper" under the working title:

"Searching for the mixed phase of QCD matter at the Nuclotron-based Ion Collider fAcility".

In order to initiate the process and estimate the spectrum of items, we suggest that you draft your brainstorming ideas on just one or two pages and send them to the editors (nica@theor.jinr.ru). In the week April 12-18, we will assemble the ideas into topics on a Wiki Forum, which shall be maintained by the NICA group at JINR. We expect that the creation and feeding of such a forum accessible to all researchers involved in theoretical and experimental investigations of superdense QCD matter will prove successful whenever the actual status and potential of dense matter research shall be discussed or reported.

After another iteration of the available inputs during May, a first version of the "White Paper" shall be prepared by the NICA group, to be ready for presentation at the Program Advisory Committee on Particle Physics meeting beginning June in Dubna.

We are looking forward to your contribution!

Yours sincerely,

D. Blaschke,
D. Kharzeev,
A. Sissakian,
A. Sorin,
O. Teryaev,
V. Toneev,
I. Tserruya

Contents

1 Editorial

1.1 Physical phenomena and relevant observables

The realization of the NICA project has been started at the Joint Institute for Nuclear Research (JINR) in Dubna as a flagship project in High Energy Physics. In addition to beams extracted from the Nuclotron (the existing accelerator of heavy ions) the project foresees the construction of a Nuclotron based Ion Collider fAcility (NICA), a Multi-Purpose Detector (MPD), and a Baryonic Matter at Nuclotron (BM@N) experiment.

With the energy range of $\sqrt{s_{\rm NN}} = 4 - 11$ GeV, the collider experiment will provide a unique possibility to explore the properties of strongly interacting matter in a region of temperatures and baryon densities where the critical point (and possibly a triple point) is suspected in the QCD phase diagram (see the left panel of Fig. 1.1). As indicated in a series of theoretical works [1–3] (see, e.g., Cleymans and Randrup in the following Section), for heavy ion collisions within this energy range the highest possible baryon densities at freeze-out are reached (see the right panel of Fig. 1.1).

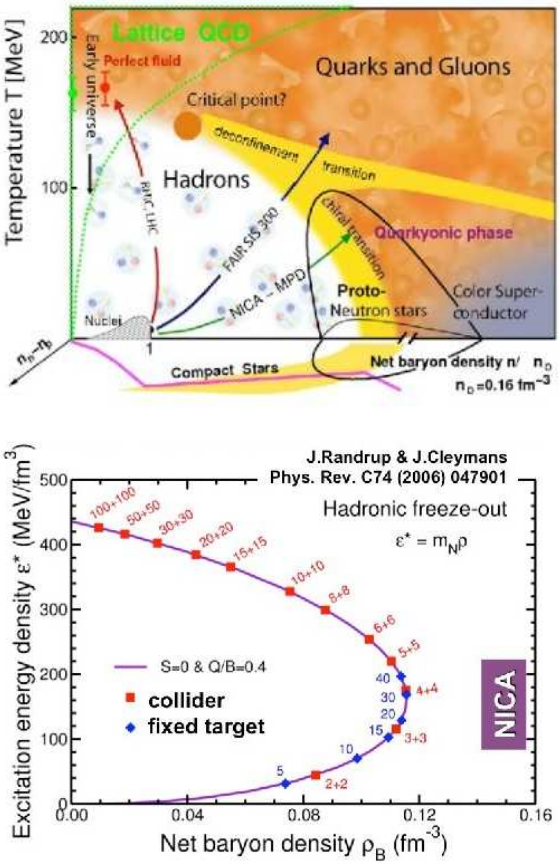

Figure 1.1: Upper panel: QCD phase diagram. Lower panel: Barion density in A + A collisions.

The experimental program aims at investigating physical properties and phenomena in hot and dense baryonic matter such as:

- in-medium modification of hadron properties (MMH)
- the nuclear matter equation of state (EoS);
- the onset of deconfinement (OD);
- chiral symmetry restoration (CSR);

- signals of a phase transition (PT);
- the mixed phase and the critical end-point (CEP);
- possible local parity violation in strong interactions (LPV).

This shall be achieved by measuring a large variety of observables systematically changing the collision conditions (energy, centrality, system size). An attempt to summarize the correlations between observables and physical phenomena is given in the Table 1.1.

Observables	Physical Phenomena							Detectors	Reference in the White Paper
	MMH	EoS	OD	CSR	PT	CEP	LPV		
yields of hadrons, normal and exotic light nuclei	x	x	x					tracking, TOF	3.6, 3.9, 3.11, 3.12, 4.3, 4.12, 4.18, 4.19, 6.7, 6.8, 9.3, 12.7, 12.8, 12.9
yields and spectra of multistrange hyperons	x	x	x					precision tracking (seconday vertices)	2.6, 5.3, 6.4, 12.3, 12.5, 12.6, 12.7
electromagnetic probes			x	x				tracking, electron identifiers (e.g. RICH)	7.1, 7.2, 7.3, 7.7, 7.8, 7.9
azimuthal charged particle correlations					x		x	tracking	2.9, 8.1 - 8.7, 8.8, 10.4
event-by-event (EBE) fluctuations						x		tracking, TOF	2.1, 2.6, 3.10, 5.4, 5.9
Radial, elliptic and triangular flow of hadrons		x	x		x			tracking, TOF	4.4, 4.8, 4.14, 5.8, 11.5
higher moments of hadron distributions			x		x	x		tracking, TOF	3.10, 4.1, 4.5, 4.6, 4.10, 4.12-4.15, 4.17, 4.19, 4.20
interferometric parameters		x			x			tracking	3.5, 5.1, 5.2, 5.5

Table 1.1: The correlations between observables and physical phenomena.

This table shall provide a basis for the development of the scientific program to be pursued at the NICA accelerator facility, with the BM@N experiment (in fixed target mode) and the MPD experiment (collider mode). For details on the technical parameters of these experiments, see the following Section.

1.2 Parameters of the NICA accelerator facility

The Nuclotron is an existing accelerator facility of JINR in HEP put in operation in 1993. It is based on the unique technology of superconducting fast cycling magnets developed at JINR. The Nuclotron provides proton, polarized deuteron and multi-charged ion beams. The layout of the planned NICA facility and its various components are shown in Fig. 1.2

The maximum magnetic field of the dipole magnets $B = 2.0$ T corresponds to the following ion beam energies:

- 5.81 GeV/u for d (A = 2, Z = 1);
- 3.64 GeV/u for Xe (A = 124, Z = 42); and

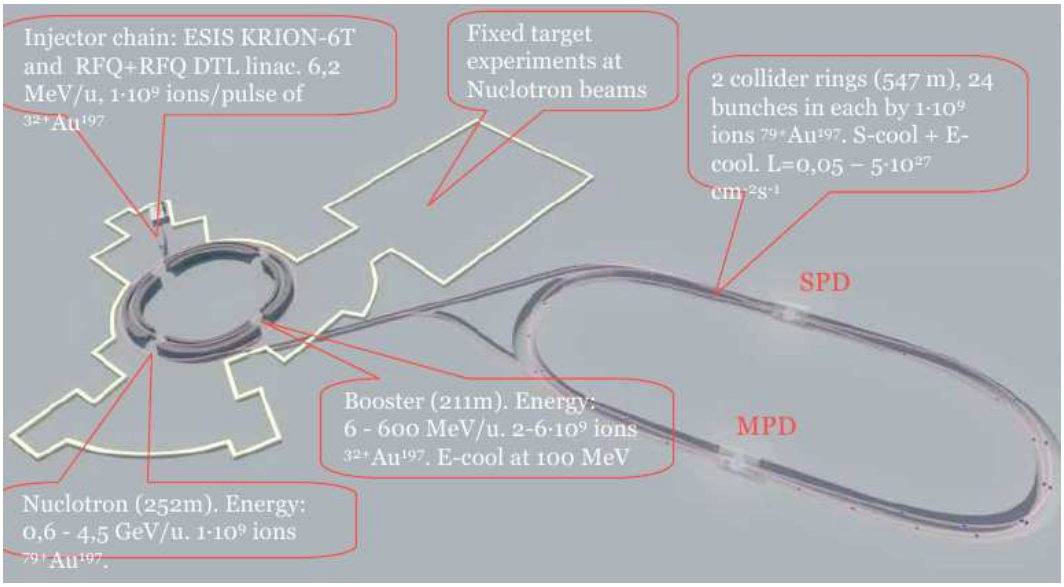

Figure 1.2: NICA facility and its components.

- 4.56 GeV/u for Au (A = 197, Z = 79).

The new accelerator facility NICA [4] includes:

- an injector complex including ion sources and a linac providing a wide spectrum of ions up to the heaviest $^{197}Au^{32+}$ at the energy of 6.2 MeV/u with an intensity of $2 \cdot 10^9$ ion/s;
- a booster accelerating ions up to 600 MeV/u;
- the Nuclotron accelerator up to the maximum energy of 4.5 GeV/u and
- two storage rings with two interaction points (IP).

The ions are additionally stripped before injection into the Nuclotron. The main parameters of the NICA collider are as follows:

- $B\rho_{\max} = 45$ Tm;
- vacuum in the beam chamber 10^{-11} Torr;
- maximum dipole field 2 T;
- kinetic energy from 1 GeV/u to 4.5 GeV/u for Au^{79+} ;
- zero beam crossing angle at IP;
- 9 m space for detector allocations at IP's;
- average luminosity for heavy ions $1 \cdot 10^{27}$ cm^{-2}s^{-1} (at 3.5 GeV/u).

The required Nuclotron upgrade has started in 2008 and will be fully completed by 2014 - 2015. The booster and the new linac will be put in operation. The overall construction schedule foresees that the storage ring and basic infrastructure facility should be available for the first ion collisions already in 2016 [5]. The beams provided by the Nuclotron at the different stages of the project realization are listed in Table 1.2.

The energy of the extracted beams provided by the upgraded Nuclotron-NICA will finally reach 5.81 GeV/u for typical values of A/Z = 2. The typical range of planned maximum beam energies is presented in the Table 1.3.

Beam	Nuclonron Beam Intensity (particles per cycle)		
	June 2011	Ion source type	New ion Source + booster
p	$3 \cdot 10^{10}$	Duoplasmotron	$5 \cdot 10^{12}$
d	$3 \cdot 10^{10}$	—··—	$5 \cdot 10^{12}$
^{4}He	$8 \cdot 10^{8}$	—··—	$1 \cdot 10^{12}$
$d\uparrow$	$2 \cdot 10^{8}$	SPI	$1 \cdot 10^{10}$
^{7}Li^{6+}	$8 \cdot 10^{8}$	Laser	$5 \cdot 10^{11}$
^{1,10}B	$1 \cdot 10^{9,8}$	—··—	
^{12}C	$1 \cdot 10^{9}$	—··—	$2 \cdot 10^{11}$
^{24}Mg	$2 \cdot 10^{7}$	—··—	
^{1}4N	$1 \cdot 10^{7}$	ESIS ("Krion-6T")	$5 \cdot 10^{10}$
^{40}Ar	$1 \cdot 10^{9}$	—··—	$2 \cdot 10^{11}$
^{56}Fe	$2 \cdot 10^{6}$	—··—	$5 \cdot 10^{10}$
^{84}Kr	$1 \cdot 10^{4}$	—··—	$1 \cdot 10^{9}$
^{124}Xe	$1 \cdot 10^{4}$	—··—	$1 \cdot 10^{9}$
^{197}Au	-	—··—	$1 \cdot 10^{9}$

Table 1.2: Beams provided by the Nuclotron.

beam	Z/A	max $\sqrt{s_{\rm NN}}$ (GeV/n)	max $T_{\rm kin}$ (GeV/n)
p	1	≈5.2	≈ 12
d	1/2	≈3.8	≈ 5.7 (including polarized deuterons)
Au	0.4	≈ 3.5	≈4.5 (at 2T in dipoles)

Table 1.3: Planned beam energies at the Nuclotron.

The BM@N Experiment

To realize the first stage of experiments using extracted beams from the Nuclotron with fixed target a new set-up – BM@N (Baryonic Matter at Nuclotron) will be constructed using an existing dipole magnet, tracking devices and other necessary parts for particle ID etc. The new silicon vertex detector will be constructed in cooperation with partners from GSI (Darmstadt). Further details, such as the layout of the BM@N detector and its components are presently under development. The NICA White Paper contributions shall assist in this process.

The MPD Experiment

The MPD experiment should be competitive and at the same time supplementary to the ones operating at RHIC [6], and those constructed in the framework of the FAIR project [7]. The MPD will be installed at the first IP of NICA. The major sub-detectors of the MPD are (see Fig.1.3):

- a solenoidal superconducting magnet with a magnetic field of 0.5 T (5 m in diameter and 8 m in length);
- a time projection chamber (TPC);
- an inner tracker (IT);
- a time-of-flight (TOF) system;
- an electromagnetic calorimeter (ECAL);
- an end cap tracker (ECT) and
- two forward spectrometers based on toroidal magnets (optional).

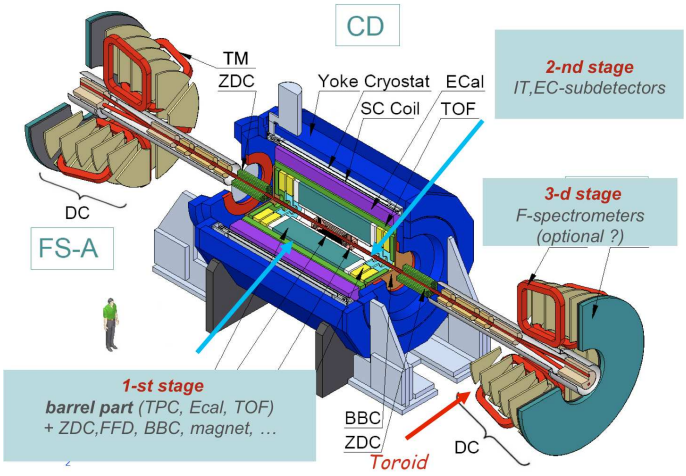

Figure 1.3: The MPD.

Three stages are foreseen for putting MPD into operation. The first stage of operation involves magnet, TPC, TOF, ECAL (partially) and IT (partially), and should be ready for the first collision of beams in 2016.

The processes studied with MPD were simulated using the dedicated software framework (MpdRoot). This software is based on the object-oriented framework FairRoot [8] and provides a powerful tool for detector performance studies, development of algorithms for reconstruction and physics analysis of the data. The evaluated rate in Au + Au collisions at $\sqrt{s_{\rm NN}} = 7.1$ GeV (10 % central interactions) taking into account the luminosity of $L = 10^{27}$ cm^{-2}s^{-1} is 7 kHz. More than ten working groups from 12 institutions are intensively working on sub-detector R&D, and on prototyping of all detector elements. Further detailed information could be found in the corresponding conceptual design report [9]. It has been shown that the MPD is well optimized for the study of in-medium effects caused by high baryon densities, such as: changing particle properties in the hot and dense medium (broadening of spectral functions etc.), event-by-event dynamical fluctuations of strange to non-strange particle ratios, and others. These studies could be done with better precision than the one achieved at presently performed experiments. The simulations of the MPD experiment show that a high statistics of studied events could be accumulated (10^9 minimum bias events and 10^8 central events per week) which provide the best precision for femtoscopy studies with respect to RP correlation of multistrange particles. In ten weeks of running more than 10^7 of Ω-decays will be recorded.

Charged particles are reliably identified using both techniques: by measuring the dE/dx of tracks in the TPC, and by the TOF system. A sufficiently high resolution of vertex reconstruction has been obtained, as illustrated in the left panel of the Fig. 1.4.

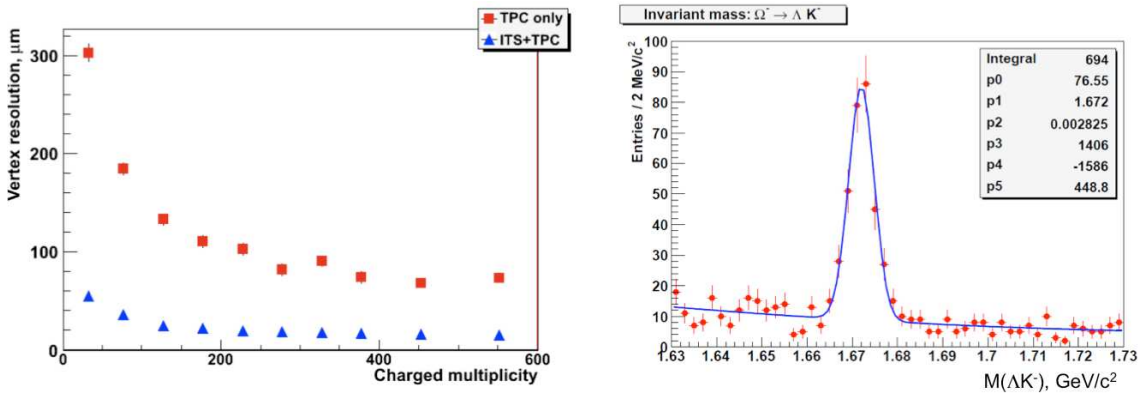

Figure 1.4: Left panel: The resolution of vertex reconstruction. Right panel: $\Omega \to \Lambda K^-$ decay reconstruction.

The right panel of this figure also shows the example of an $\Omega \to \Lambda K^-$ decay reconstruction implementing the full chain of simulations: central Au + Au collision generation at $\sqrt{s_{\rm NN}} = 7.1$ GeV; hyperon productions and decays; decay product detection and their reconstruction using necessary MPD subdetectors.

In Table 1.4 we summarize the mean particle multiplicities in central Au+Au collisions at an impact parameter $b < 3$ fm for selected energies $\sqrt{s} = 4$ GeV, 7 GeV and 11 GeV. The simulations have been performed with UrQMD [10].

Part.	4 GeV		7 GeV		11 GeV	
	4π	$\|\eta\| < 1$ $p > 100$ MeV/c	4π	$\|\eta\| < 1$ $p > 100$ MeV/c	4π	$\|\eta\| < 1$ $p > 100$ MeV/c
charged	430	250	870	430	1300	550
p	170	91	160	63	160	49
n	200	110	180	68	170	53
π^+	110	65	310	160	470	230
π^-	120	78	340	170	520	240
π^0	120	72	340	180	520	240
K^+	12	7.6	38	19	57	24
K^-	1.3	0.82	12	6.2	26	12
K^0	12	7.7	38	19	57	26
Λ	10	6.2	26	12	31	12
Σ^+	3.4	2.1	8.0	3.7	9.2	3.6
Σ^-	4.0	2.4	8.8	4.0	10	3.8
Σ^0	3.2	1.9	7.9	3.6	9.4	3.8
Ξ^-	0.16	0.11	0.87	0.42	1.7	0.66
Ξ^0	0.13	0.077	0.86	0.42	1.3	0.62
Ω^-	0.003	0.002	0.022	0.011	0.038	0.015

Table 1.4: The mean particle multiplicity in central Au+Au events (impact parameter $b < 3$ fm) calculated by UrQMD.

1.3 Priority directions for NICA experiments

In this Subsection, we collect summary statements to main perspective directions of research at the NICA experiments in the attempt to make first steps towards a priorization of the suggestions collected in the NICA White Paper. The statements concern comments and critical assignments by a working group which was appointed at rather short notice. Therefore, we apologize beforehand for the rather preliminary character of this Subsection. Nevertheless, the first step into the priorization era is made and the floor is open for discussion and comments from the community which we are happy to receive by email to nica@theor.jinr.ru

Equation of state and phases of QCD

D. Blaschke

Bogolyubov Laboratory for Theoretical Physics, JINR, Dubna, Russia
Institute for Theoretical Physics, University of Wrocław, Wrocław, Poland

Summary on NICA WP contributions: 3.1 - 3.16, 4.19

The very goal of the NICA facilities (see the title of this White Paper) is the search for the mixed phase of quark matter and baryon rich hadronic matter as a consequence of a first order phase transition, bearing strong analogies with a liquid-gas phase instability. The latter is quite established for nuclear matter and its theoretical description has recently been advanced a lot by deepening the understanding of its interrelation with nuclear bound state (cluster) formation in the framework of a combined quantum statistical and relativistic mean field approach [S. Typel et al., Phys. Rev. C 81, 015803 (2010)]. The van-der-Waals like behaviour of an EoS like

this, but now in the domain of the nuclear-to-quark-matter transition has been used as a basis for the suggestion to study the phenomenon of "spinodal enhancement" **(4.19)**, see also the summary in Subsection 1.3.3.

However, a microscopic approach to a van-der-Waals like EoS for the suspected first order QCD phase transition at sufficiently low temperatures, below the critical endpoint, is still absent. Lattice QCD as the only ab-initio approach to QCD at finite temperature and density, suffers the fermion sign problem and cannot (yet) be extended to the relevant high baryon densities. Therefore, one is bound to effective models where a lot of progress has been made recently, in conjunction with Lattice QCD studies for the inputs entering these models. However, this concerns effective meanfield approaches for the QCD phase diagram and quark matter EoS. The step beyond the meanfield, by consistently including the formation of hadronic bound states and their dissolution at high densities and temperatures (Mott effect) is notoriously difficult and only first steps in this direction have recently been achieved [L. Turko et al., Acta Phys. Pol. B (Suppl.) 5, 485 (2012), D. Blaschke et al., arxiv:1305.3907]. Probably the most promising approach would be an extension of the hadron resonance gas model including the Mott effect by a generic spectral function for all relevant hadronic states, to be calibrated with lattice QCD data where available.

As this is a programme for the near future, in the White Paper the status concerning the QCD phase diagram comprises chiral quark model studies on the meanfield level which in the best case consider a most complete set of possible order parameters, like in the recent study by Zhang and Kunihiro **(3.16)**. Key question is the existence and position of a critical end point (CEP) of a first-order phase transition **(3.13)** or even many of them. An extremely interesting problem in this context is the role of the $U_A(1)$ anomaly since its origin can be manyfold. Within the Kobayashi-Maskawa-'t Hooft determinant interaction model, there is a strong effect already on the meanfield, which would be particularly prominent at low temperatures where the Fierz transformed channel of that interaction leads to a coexistence phase with color superconductivity, making the very low temperature region of the QCD phase diagram a crossover. So there are many possibilities on this level of description, shortly summarized in **(3.13)** as

- no CEP at all, since the transition is crossover in the whole phase diagram.
- no CEP, but a Lifshitz point,
- one CEP, but with largely differing predictions of its position
- second CEP
- CEP and triple point, possibly coincident, due to another phase (i.e. color superconducting or quarkyonic matter) at low temperatures and high densities

It is unclear how the multi-faceted picture drawn on the quark meanfield level **(3.1), (3.8), (3.13), (3.14), (3.16)** will change when the phase transition to hadronic matter is included! Here one is bound basically to the Maxwell construction of phase equilibrium with hadronic EoS which are taken as realistic as possible, see for instance **(3.6), (3.7), (3.9), (3.11), (3.12), (3.15)**.

This situation underlines the necessity to perform the experiments at NICA because of the huge discovery potential in the low-temperature, high-density domain of the QCD phase diagram. One of the most thrilling possibility would be the discovery of exotic signals of a high-temperature (T_c 180 MeV) color superconducting phase which, according to estimates in **(3.7)** would be accessible at NICA for $3 < E_{lab}[\text{A GeV}] < 7$.

More detailed theoretical studies and simulations of possible signals from the population of such a (metastable) color superconducting phase in a heavy-ion collision have to be performed.

Mixed quark-hadron phase and chiral magnetic effect at NICA ?

V. D. Toneev

Joint Institute for Nuclear Research, Dubna, Russia

Summary on NICA WP contributions: 2.2, 2.4, 2.9, 3.11, 4.4, 4.19, 4.20, 5.8, 8.1, 8.4 - 8.8

The NICA facilities will provide a unique possibility to study nuclear matter under extreme conditions - at large baryon density and high temperature - where according to lattice QCD the hadronic matter transforms to the strongly interacting quark-gluon plasma. The different phases of the excited nuclear matter are not so

well settled and a mixed phase of partons and hadrons may be be formed. Depending on the order of the phase transition the structure of the mixed phase (MP) may be different. If the first order phase transition occurs, the MP is nonhomogeneous, structured having domains consisting from one or another pure phase. At the crossover the system is homogeneous mixture of its components characterized by their relative concentration C, $0 \leq C \leq 1$. A general physics problem is to define properties (signals) of the MP and the order of phase transition, to locate the MP of the deconfinement phase transition on the QCD phase diagram.

The MP is mentioned few times in the White Paper (WP). Really, these contributions ascertain a particular experiment and confront it with expectation:

- The constituent quark scaling observed at the RHIC energies apparently is broken at the top NICA energy where the formation of the MP is possible; the v_2 is expected to soften at the transition temperature but such effect is not visible (contribution **(2.2)**;
- In **(2.4)** the possible MP formation is only noted;
- The structure in the excitation function of the directed v_1 flow (observed earlier) is emphasized as a signal of the transient phase (MP ?) **(4.4)**;
- In **(5.8)** a general hope what a comprehensive study of Fourier-coefficients of the azimuthal particle distributions for non-central collisions at the NICA energies could help in clarifying the question, whether the mixed quark-hadron phase is formed;
- The hadron-quark phase transition is investigated **(3.11)** in the Two-EoS approach describing the hadron matter with nonlinear Walecka model and separately the quark matter with the MIT-Bag and the NJL(PNJL) models. Boundaries of the mixed phase are defined and consequences of the Isospin Distillation as a kind of neutron trapping in the quark phase are discussed. Observable sensitive to this isospin distillation are noted but without their dynamical estimates.

There are only a few definite proposals which propose a dedicated search for mixed phase formation and suggest corresponding signals as due to spinodal decomposition **(4.19)** and **(4.20)**. In particular **(4.19)** comes to the conclusion that right at Nuclotron energies ($E_{lab} \sim 3$ A GeV) there is a maximum for the "spinodal amplification".

A very important statement has been made by D. Kharzeev that in relativistic heavy ion collisions in the created hot deconfined QCD matter and strong magnetic field the topologically induced local P and CP violation may occur (so called Chiral Magnetic Effect (CME)). A corresponding experimental signal, charge asymmetry with respect to the reaction plane, has been proposed. This statement has attached much attention of both theorists and experimentalists and is reflected in many contributions into the WP:

- In **(8.1)** it is emphasized that NICA would provide a necessary and complementary information on the CME but the asymmetry should significantly decrease in magnitude;
- In the NICA energy region the deconfined state defined as ϵ >1 GeV/fm^3 is inside the range of the maximal magnetic field strength and therefore the necessary conditions for the CME are fulfilled but not yet sufficient ones **(8.5)**;
- Experimental studies with the NICA facilities of the QCD tricritical point may well detect a more complicated phase structure due to the interplay with the parity violation phase as noted in **(8.4)**;
- The attention was called to the point that for the same charge pairs STAR measurements in-plane back-to-back correlations is in contradistinction to the prediction from the Chiral Magnetic Effect, which predicts out-of plane same side correlations **(8.7)**.

High activity in this field results in new interesting results. The most important one for the physics NICA program is that the expected CME signal, the charge separation effect between the same $(++, --)$ and opposite $(+-)$ charge pairs, is NOT observed at the energy $\sqrt{s_{NN}} = 7$ GeV and, therefore, the Chiral Magnetic Effect is NOT be realized in the NICA energy range. This has been shown in the RHIC energy beam-scan experiments (D. Gangadharan (for the STAR Collaboration), J. Phys. G: Nucl. Part. Phys. **38**, 124166 (2011); I. Selyuzhenkov (for the ALICE Collaboration), PoS WPCF 2011 , 044 (2011)) and in theoretical papers (V. Toneev and V.

Voronyuk, Phys. Part. Nucl. Lett. **8** , 938 (2011); Acta Phys. Pol. Suppl. **B 5**, 887(2012); V. Toneev et al., Phys. Rev. **C 85**, 034910 (2012)). Unfortunately, these findings are reflected in neither WP nor MPD Physics Program.

Another new possibility to test experimentally signatures of P-odd effects is related with the Chiral Vortaic Effect (CVE) of the medium as proposed in **(8.6)**. The CVE is preferable for the NICA energy because there is its intimate connection to the baryon chemical potential. The two-particle correlation for neutrons might be used as one of the probes of CVE. In **(8.6)** is assumed that the magnitude of the CVE is of the same order as CME (but see the above conclusion on the CME !?). In analogy with CME to look for the baryon charge separation, the $n-n$ and $n-\bar{n}$ correlations should be studied, however, the identification of anti-neutrons at the NICA energy poses a challenge to the experiment. Real simulations of the CVE are needed to conclude about feasibility of this effect for the NICA energy as well as a search for new observables is indispensable.

The generation of strong magnetic fields occurs in peripheral heavy-ion collisions due to mainly charged spectators moving at almost the speed of light. These strong magnetic fields can create the conditions for observable QCD effects **(8.8)** by influence in general on confinement/deconfinement and chiral transitions, the location of the critical point, inhomogeneous condensates. In **(8.8)** a large reference list is given exemplifying various possible effects of nuclear matter in an external magnetic field without any comments and estimates.

The study of the spectator-induced electromagnetic phenomena is proposed as a new, independent source of information on the space-time evolution of the reaction and of the non-perturbative process of particle production (**2.9**). The corresponding measurements would, in particular, include particle spectra, charged particle ratios ($\pi^+/\pi^-, K^+/K^-$, etc.) and directed flow. The investigation of electromagnetic distortion of charge particles has started more than 30 years ago but it is still not without interest now. This effect is expected and do really seen in a low-energy part of spectra what is also demonstrated in (**2.9**). The expected NICA cut $p_{tr} > (100-150)$ MeV/c will essentially suppress this effect and simulation with the proper account for experimental acceptance is needed.

In **(10.2)** spin correlations for the $\Lambda\bar{\Lambda}$ pairs, generated in relativistic heavy ion collisions, as well as related angular correlations at the joint registration of hadronic two hyperons decays with nonconservation of space parity are analyzed. It is mentioned that such a situation may arise when the system passes through the mixed phase.

Collective dynamics, medium effects, dileptons, strangeness and elementary reactions.

E. L. Bratkovskaya

Institute for Theoretical Physics and FIAS, Frankfurt University, Frankfurt-am-Main, Germany

Summary on NICA WP contributions: 2.4, 2.6, 2.9, 3.12, 4.2, 4.3, 4.4, 4.6, 4.8, 4.10, 4.12, 4.17, (5), 6.2, 6.4, 6.5., 6.6, 6.7, (7), 12.1-12.6

The NICA facility in Dubna together with the CBM experiment at FAIR (GSI) will provide a unique possibility to study nuclear matter under extreme conditions - at high baryon density and temperature - where according to lattice QCD the hadronic matter transforms to the strongly interacting quark-gluon plasma (sQGP) - cf. [2.4,2.6]. In spite of active experimental investigations on this issue going on at present accelerators at CERN and RHIC the different phases of the sQGP are not so well understood and there might be a mixed phase of partons and hadrons at higher baryon density, too. There are several indications for a critical endpoint in the QCD phase diagram - separating the cross over at low quark chemical potential μ_q from a first order phase transition at high μ_q, but a rigorous proof is not yet available. The experimental investigations at NICA and CBM are required to provide a reliable experimental information on the nature of transition and of the deconfinement and the properties of the QGP as well as the dense and hot hadronic matter.

For the experimental observation of the appearing phenomena the following observables are important for the NICA/Nuclotron energies [2.4,2.6,12.3,12.5]:

1. 'bulk' observables:
   particle multiplicities and their ratios, transverse mass spectra, rapidity distributions, collective flow and high angular harmonics, different type of fluctuations and correlations

2. rare probes as dileptons and photons,

3. strangeness,

4. charm.

The measurements have to be done in heavy-ion collisions and in elementary reactions as well. The latest is important as a 'reference frame' for the interpretation of heavy-ion data. As stressed in [2.6] a successful future heavy-ion research program has to perform a comprehensive scan of observables, beam energies and collision systems. NICA is designed for high luminosities at the collision energies where high net-baryon densities are created and the MPD can run over long periods. This offers the possibility to perform systematic measurements of multi-differential observables, including particles with low production cross sections. In contrast to the fixed-target CBM, the collider experiment MPD has a uniform acceptance which is almost independent of the collision energy. Therefore, MPD at NICA and CBM at FAIR will be able to perform complementary measurements, covering different regions of phase space.

'Bulk' observables

1) Particle multiplicities and their ratios, transverse mass spectra and rapidity distributions.
They provide information about the collective dynamics of the system [2.6]. The observation of a non-monotonic behaviour of the excitation functions of particle ratios or increase/flattening of the excitation function for the inverse slope are considered as a signal of the deconfiment and the phase transition from hadronic to partonic matter whereas a global m_T-scaling of all mesons as a signal for chiral symmetry restoration [2.4]. It is important to measure the excitation functions of different hadrons including the rare particles since they freeze-out at different times.

2) Collective flow v_1, v_2 and higher-order harmonics $v_3, v_4, ..$ in the azimuthal angular distribution:
At low energies the measurement of angular harmonics will provide information about the EoS and the influence of hadronic potentials. As high energies the observation of strong collective flow v_2 and a 'wiggle' in v_1 signals the non-hadronic nature of the initial pressure in the system. The scaling of v_2 with the quark content is considered as a signal that the QGP is approximately an ideal liquid with low viscosity-to-entropy ratio [2.4]. The deviation from the scaling behavior will correspond to the transition from partonic dominated matter to hadronic degrees of freedom [4.8]. To obtain the information about the order of the phase transition it is suggested [4.6] to measure the midrapidity reduced curvature of the (net)proton rapidity spectrum as a function of the center-of-mass energy of colliding nuclei C_y which expected to have 'zig-zag' irregularity in the first-order-transition scenario, while the hadronic scenario produces purely monotonous behaviour. The analysis of higher-order harmonics $v_3, v_4, ..$ in the azimuthal angular distribution [2.4,2.6] shows the growing deviations between partonic and purely hadronic models with increasing collision energy. This demonstrates that the excitation functions of azimuthal anisotropies reflect the increasing role of quark-gluon degrees of freedom in the early phase of relativistic heavy-ion collisions.

3) Fluctuations and correlations, femtoscopy:
The fluctuations and correlations are the signals of the critical behaviour of the system, the femtoscopy provides the space-time history of the collisions (cf. Section 5). Fluctuations of baryon number, electric charge as well as strangeness have been shown to be sensitive indicators for such a critical behavior [4.10]. E.g. the higher moments of baryon number fluctuations will diverge on the chiral phase transition line $T_c(\mu_B, m_q = 0)$. Experiments at NICA will probe a regime of high baryon number density in which the QCD transition may well be of first order. In this high density regime direct lattice QCD calculations will be difficult. Thus, one has to make a careful energy/system size scan in order to observe a phase transition.

Electromagnetice probes - dileptons and photons

Dileptons (e^+e- or $\mu^+\mu^-$ pairs) and photons are a powerful tool to diagnose the hot and dense matter produced in relativistic heavy-ion collisions [7.1, 7.2, 2.4, 7.7, 7.8]. This signal is not distorted by the final strong interaction, contrary to the hadronic observables, and provide direct information about their creation origin. The energy range covered by the planned NICA facility, $\sqrt{s_{NN}} = 4 - 11$ GeV, is unique in several respects [7.1]. It fills a very important gap in energy where no dilepton measurements exist, providing a crucial complement to the measurements at lower (DLS and HADES) and higher (SPS and RHIC) energies. This is a very promising energy range with considerable discovery potential.

Observations of an enhancement of the dilepton rates - at low invariant masses - due to in-medium changes of the vector meson spectral functions may serve as a signal of chiral symmetry restoration in the hot and dense matter; thermal dileptons from the QGP show up at intermediate invariant masses (1.2 GeV $< M <$ 2.5 GeV) [2.4, 7.2, 7.8] which can be identified as an enhancement of invariant mass spectra over the expected hadronic cocktail as well as a modification of p_T spectra. The top NICA energy $\sqrt{s_{NN}}$ =11 GeV allows also to investigate the hidden charm meson production (J/Ψ) via the dilepton decay mode [7.4, 7.5, 7.6].

As proposed in [4.12] the dileptons can be used as a probe to search for the production of color-neutral bound states which might survive slightly above T_C in the region of high density. These bound states will be resonant states either above (quasi-particle clusters) or below (chirally symmetric color-neutral states) the known resonance spectrum.

As emphasize in [7.9] it is important to measure the dilepton spectra from elementary pp reactions, particular at lower Nuclotron energies since at this energy regime must be a transition between resonance mechanism for the hadron production - dominated at low energies - to the multi-particle production via the excitation and fragmentation of strings. The NICA fixed target experiment $BM\&N$ is an ideal possibility to provide these important experimental data. Moreover, it is interesting to measure ϕ meson at this low energies via dilepton mode (as well as via K^+K^- channel) since the formation of ϕ in heavy-ion collisions is strongly modified due to the in-medium modification of (anti-)kaons, thus is is sensitive to the reaction dynamics and EoS.

Strangeness

An enhancement of strangeness production in heavy ion collisions has been considered as a signal for quark-gluon plasma formation [6.4,2.6]. The discovery of the sharp peak of $K^+/\pi+$ multiplicity ratio for collisions at beam energy of 30 AGeV and the flattening of the inverse slope parameter T of kaon spectra might be interpreted as a signal for QGP formation, since purely hadronic models without a deconfinement phase transition were not able so far to reproduce such a peak. However this issue is not fully settled and in this respect NICA can provide an important contribution to the field.

The systematic measurement of strange hadrons in elementary pp, pA and AA reactions from low Nuclotron to the top NICA energies will provide a comprehensive information to the existing data from the SIS, AGS, SPS and low energy scan RHIC program as well as from the future CBM experiment at FAIR. This will allow to make solid conclusions on different fundamental problems as mechanisms for the strangeness production in elementary reactions (especially important for the transition regime from 'resonance dominated' at SIS energies to the 'string picture' at high energies), in-medium modifications of strange hadron properties due to the (partial) chiral symmetry restoration, the consequences on strangeness production at the vicinity of phase transition from hadronic to partonic matter, the dynamical equilibration of strangeness at chemical free-out [6.5]. Also the measurement of strangeness gives additional information about the EoS.

Since the in-medium effects on strangeness are more visible at low energies near the threshold of strange particle productions it will be an important aspect for the BMN experimental program [12.3,12.5]. A complementary information on the production mechanisms can be extracted from the centrality dependence of the particle yields since it provides the excess to the different density regimes and production mechanisms at the same bombarding energy of heavy-ions. As stressed in [6.4, 7.8] it is mandatory to measure hyperons and ϕ mesons additionally to the strange mesons.

The search for strange matter - hypernuclei, multi-strange meta-stable objects - will explore the 3D - "strange" axis of the QCD phase diagram (cf. [6.6, 12.3, 12.5]). The production of multi-strange hyperons close to the threshold in elementary reactions, can be enhanced though strangeness-exchange processes like $\Lambda K \to \Xi\pi$ or $\Lambda\Xi \to \Omega n$ with previously produced strange particles in the entrance channel. Their yield is thus sensitive to both the strangeness production mechanism and the baryon density.

Elementary reactions

The NICA and Nuclotron allow to study the elementary reaction in the wide energy range which is mandatory for the correct interpretation and understanding of the heavy-ion data [12.1, 7.8] since the elementary reactions are considered as a 'reference' for the heavy-ion measurements. The knowledge on the multi-particle production in elementary reactions is a very important input for the dynamical transport model which are aimed to describe the complicated collisional dynamics of nuclei [12.1]. Moreover, we need to know it not only from the pp, but from pn, too, due to the strong isospin dependence of the particle production at lower energies. Thus, the measurement of the $p+d$ or $p+A$ collisions with light nuclei are highly requested. Moreover, the understanding

of the origin of the particle production in elementary collisions is an interesting subject for the investigation itself. The transition from the 'resonance' production (i.e. by the excitation and decay of mesonic and baryonic resonances) to the direct production of light hadrons within the 'string' picture is presently an open field since there is very little experimental information available.

Spin and exotic phenomena.

O. V. Teryaev

Joint institute for Nuclear Research, Dubna, Russia

Summary on NICA WP contributions: 8.6, 10.1 - 10.4

This section contains the discussion of two important related issues:
i) polarization effects in heavy ion collisions and
ii) the spin program with polarized beams.

The studies of polarization effects in heavy ion collisions have just began and their general program is outlined in the contribution of A.V. Efremov, O.V. Teryaev and V.D. Toneev (10.1). Possible (at least partial) conversion of the huge initial angular momentum available in a heavy ion collision into the angular momentum carried by dense matter, and possibly to the angular asymmetries and spin polarization of produced particles is an extremely interesting problem. Understanding it will undoubtedly allow to penetrate deeper into the collision dynamics. A number of observables are proposed in this section - most of them have never been studied before in heavy ion experiments. The physics issues include the dynamics of the collision, the chiral properties of the produced medium, and of the possible local violation of P and CP invariances discussed above. The recent development includes the updated contribution (M. Baznat, K. Gudima, O. Rogachevsky, A. Sorin and O. Teryaev - 8.6) where such P-odd hydrodynamical charcteristics as vorticity and helicity entering the earlier expressions for neutron asymmetries are calculated using the kinetic QGSM model.

The spin program is an important and integral part of the NICA project. Indeed, ever since the "spin crisis" of 1987, the composition of the nucleon's spin in terms of the fundamental constituents - quarks and gluons - remains in the focus of attention of many physicists. Currently one of the main problems is the extraction of transverse momentum and spin dependent parton distributions. The cornerstone of this activity is the developing Drell-Yan program at at NICA with transverse polarized beams described in the contribution of A. Efremov, A. Nagaytsev, I. Savin, O. Shevchenko and O. Teryaev (10.2). It is competitive and complementary to other polarized Drell-Yan programs, in particular the one at COMPASS sharing with NICA common expertise.

The common ingredient to heavy ions and hadronic spin programs is the polarization of hyperons, discussed in the contribution of V. Ladygin, A. Jerusalimov and N. Ladygina (10.3), which includes the simulation and etimates of background effect.

The contribution of V.L. Lyuboshitz and V.V. Lyuboshitz (10.4) is dedicated to the spin correlations of hyperon pairs whose observation is requiring very high statistics.

Multifragmentation, hypernuclei and elementary reactions.

J. Aichelin

Subatech, Universit? de Nantes, ?cole des Mines de Nantes, Nantes, France

Summary on NICA WP contributions: 3.3, 4.11, 4.12, 9.3, 12.7-12.9

Hypernuclei are very interesting objects because they allow for determining the lambda (sigma) nucleon interaction which is otherwise only accessible by theoretical calculations. The mass of the ground state and that of excited states as well as the life time are here of interest. These quantities can then be compared with theoretical calculations. That hypernuclei can be observed in heavy ion reactions has been demonstrated at SIS energies by the FOPI collaborations and at RHIC energies by the Star collaboration. There are presumably two different ways to produce hypernuclei in heavy ion reactions:

1. By coalescence in the midrapidity region. During the reaction in the midrapidity region the system comes probably close to a thermal equilibrium and the fragments form in this region are low mass fragments.

Therefore either a coalescence models based Boltzmann type equations (12.8) or a statistical models (12.7) are theoretical tools to describe this production. One expects at midrapidity that the yield decreases exponentially with the mass number of the nuclei, so midrapidity is well suited for nuclei like hyper triton. It fits well that this system can also be treated relatively easy in theoretical calculations.

2. By conserving initial final state correlations in target and projectile region (12.9). Spectator matter is usual of little interest in heavy ion reactions at energies about 1 GeV. It maintains to a large extend the initial correlations and disintegrates into fragments which can be observed in projectile resp. target rapidity. It happens, however, once a while that a hyperon, produced in collisions between projectile and target, enters the spectator matter and forms then with a correlated cluster of spectator nucleons hyper-nuclei. These hypernuclei can be larger in mass which may have excited states. The study of the transition adds to the studies which are possible for light mass hypernuclei listed in a). If hypernuclei can be produced in mass the study at NICA opens a quite new field, little explored so far, the study of hyperons in interaction with nonstrange matter. The difference between excited states and the ground state will shed light on the structure of the hypernuclei especially by comparing the excitation of closed shell nuclei with neighboring ones like $17O_\Lambda$ and $16O_\Lambda$ (9.3). Are they more to consider as a 48 (51) quark cluster or a as 16 (17) nucleons.

The hyperon - nucleon interaction is not only interesting in itself it has also far reaching consequences for astrophysics, especially for neutron stars. The maximal mass of a neutron star depends among other things from the nuclear equation of state (4.11). The stiffer the equation of state the larger the star masses can be. Hyperons have the tendency to soften the equation of state but precise information on the hyperon nucleon interaction is necessary for quantitative predictions. In the Star experiment, with a chemical potential close to zero, nuclei and antinuclei with masses up to A=4 have been observed at midrapidity. For the high chemical potential expected for the NICA energies, it is not excluded that other color neutral multi quark states exist which may be formed inside the quark matter and survive the phase transition (4.12). If they exist their multiplicity and their mass would give information about quantumchromodynamics in the nonperturbative regime and will allow for a better understanding of the transition between the quarks and hadron, one of the still very little understood phenomena in ultrarelativistic heavy ion collisions (3.11). For large chemical potentials the transition between quarks and hadrons is presumably a first order phase transition. How a first order phase transition in finite size systems takes place is rather unknown, even more how such a transition takes place in a rapidly expanding system? It has been argued that the formation of hadrons can be understood as a spinodal instability (3.3). It would be very interesting if this could be observed. All the above ideas require detectors which are able to identify clusters at midrapidity and have the capacity to measure the mass of the observed objects or the invariant mass of the objects are short living. The detection of large hyper nuclei requires cluster detectors in the target or projectile rapidity domain as well as the possibility to measure the decay products.

Bibliography

[1] A. N. Sissakian, A. S. Sorin, M. K. Suleimanov, V. D. Toneev, and G. M. Zinovjev, Part. Nucl. Lett. **5**, 1 (2008).

[2] M. Gazdzicki, M. Gorenstein, and S. Mrowczynski, Phys. Lett. **B 585,** 115 (2004).

[3] J. Cleymans, and J. Randrup, Phys. Rev. **C 74,** 04791 (2006).

[4] I. Meshkov, *Status of the NICA project, Proceedings of CPOD 2010*, Yad. Fiz. (2011), in press.

[5] A. Sissakian *et al.*, *Design and Construction of Nuclotron-based Ion Collider fAcility (NICA). Conceptual Design Report* (JINR, Dubna, 2008); http://www.nica.ru.

[6] G. S. F. Stephans, J. Phys. G. **32,** 447 (2006) [arXiv: nucl-ex/0607030].

[7] P. Senger, J. Phys. G. **30,** 1087 (2004).

[8] D. Bertini *et al.*, J. Phys. Conf. Ser. **119**, 032011 (2008); http://cbmroot.gsi.de.

[9] A. Sissakian *et al*, *Multi Purpose Detector Conceptual Design Report, v.1.2* (JINR, Dubna, 2010); http:// www.nica.ru.

[10] A. Sissakian *et al., The MultiPurpose Detector (MPD) to study Heavy Ion Collisions at NICA*. (Letter of Intent (JINR, Dubna, 2008)).

2 General aspects

The contributions in this section address the important question of the niche that will be occupied by the NICA project within the current and planned international effort on heavy ion research. The physics in the energy range of the NICA collider has been studied in the experiments at CERN SPS; this program will soon be extended at RHIC during the low energy scan, and then eventually at the FAIR facility. RHIC will work in the collider mode similarly to what is planned at NICA, whereas CERN and FAIR use the fixed target. The forthcoming experimental results from RHIC will help to identify even more precisely the most promising directions for research that would benefit from a higher beam luminosity at NICA and a dedicated detector design. Regarding the comparison to FAIR, the approaches taken by FAIR and NICA are complementary to each other – the fixed target at FAIR makes easier access to rare probes, whereas the collider set-up at NICA provides a symmetrical, uniform and energy-independent acceptance that is beneficial for the studies of various fluctuations and correlations.

2.1 MPD at the JINR NICA in the landscape of heavy ion projects

M. Gazdzicki

Institut für Kernphysik, University of Frankfurt, Frankfurt, Germany
J. Kochanowski University, Kielce, Poland

A. MPD [1] at NICA together with **CBM** [2] at SIS-100/300 belong to the third generation of experiments planned to study nucleus-nucleus collisions at energies of the CERN SPS. Heavy ion physics in this energy range is very attractive for experimentalists and theorists mainly due to two reasons.

- First, following predictions of Ref. [3] the NA49 discovered a rapid change of the energy dependence of hadron production properties in central Pb+Pb collisions which starts at about $E_{\rm lab}$ =30 AGeV ($\sqrt{s_{\rm NN}} \approx$ 7.6 GeV) [4]. This result gives an evidence for the onset of deconfinement at the low CERN SPS energies. Clearly, the pilot NA49 study should be followed by systematic and precision measurements.

- Second, the critical point of strongly interacting matter may be located in the phase diagram region accessible in heavy ion collisions at energies larger than the energy of the onset of deconfinement ($\sqrt{s_{\rm NN}} \approx$ 7.6 GeV) [5]. Thus, measurements in this domain may lead to a discovery of the critical point.

B. The three generations of the experiments at energies of the CERN SPS are:

- NA49 at the CERN SPS. The pilot study of the energy dependence of hadron production properties in central Pb+Pb collisions, which resulted in the discovery of the onset of deconfinement [3]. The detector was designed for the study of hadron production at the top SPS energy and not optimized for the performed energy scan. Data were registered in the period 1999-2002.

- NA61 [6] at the CERN SPS and STAR/PHENIX [7] at the BNL RHIC. The second generation study will be performed with the beams and detectors originally designed for the top SPS and RHIC energies and subsequently upgraded/optimized for the new measurements, in particular for the study of event-by-event fluctuations. The basic goals are: systematic studies of the onset of deconfinement and search for the critical point. The two dimensional scans in the plane (system-size/centrality)-(energy) will be performed. Data will be registered in the period 2009-2014.

- MPD at the JINR NICA and CBM at the FAIR SIS-100/300. The third generation studies which are planned to be performed using dedicated accelerators and detectors. Due to the financial/technical constraints the maximum energy will be about $\sqrt{s_{\rm NN}} \approx 11$ GeV for MPD and $\sqrt{s_{\rm NN}} \approx 8$ GeV for CBM. In the latter case the event rate will be orders of magnitude higher than the NA61 and STAR/PHENIX one. The basic goals are precision studies of the properties of the dense confined matter and of the transition to the deconfined phase. The first data are expected in 2015.

C. The above information provokes **general comments** concerning the third generation projects.

- Planning and construction of the third generation projects starts well before the results of the second generation experiments are known. In particular, it may happen (as suggested by the first NA49 results [8]) that the critical point will be discovered close to the top SPS energy, $\sqrt{s_{\rm NN}} \approx 17$ GeV, i.e. above the maximum energies of NICA and SIS-300. It would be important to consider a possibility of future upgrades to higher energies.

- The performance of the second generation experiments is limited by the use of the facilities which were originally designed for other studies. This, in particular, negatively impacts event-by-event fluctuation and correlation measurements and excludes studies of low cross section processes. The third generation projects should be designed in order to overcome these limitations.

D. The third generation projects, MPD at the JINR NICA and CBM at the FAIR SIS-100/300 are to a large extend complementary. The fixed target collision geometry and a very high event rate make the CBM experiment ideal for the study of rare probes of dense confined matter. The collider collision geometry of the MPD project allows to have a complete and uniform acceptance. The designed maximum energy is significantly above the energy of the onset of deconfinement. These two features make the MPD project perfect for the study of fluctuation and correlation probes of the transition between confined and deconfined matter.

Clearly, there will be a significant overlap between the MPD and CBM measurements which will allow for important cross-checks of the final results.

E. A significant progress in comparison to the second generation experiments and complementarity with the CBM project will be achieved by the MPD at the JINR NICA providing the following.

The MPD detector will allow for:

- charged particle measurements in the full acceptance,

- measurements of proton and neutron spectators of both colliding nuclei,

- an almost unique particle identification in a a large acceptance. The scans in two dimensional planes, (system-size)-(energy) and (centrality)-(energy), will be performed.

2.2 Comments on the Mixed Phase Physics (MPP)

Nu Xu

Nuclear Science Division, Lawrence Berkeley National Laboratory, Berkeley, CA, USA

Number-of-quark scaling in event anisotropy (n_q-scaling of v_2)

In high-energy nuclear collisions at RHIC, the scaling of the event anisotropy v_2 for all hadrons has been observed providing a clear evidence for the formation of a partonic system in such collisions [9]. In order to reach the observed scaling, the system must have been in the state of deconfinement, and hadrons are then formed via coalescence [10, 11]. In case of hadron gas or mix-phase, on the other hand, the scaling will be violated. Results of simulations, for Au + Au collisions at $\sqrt{s_{\rm NN}} = 9$ GeV, from both partonic and hadronic system are shown in Fig. 2.1. Therefore the measurement of v_2 for (π, K, ρ, p, ϕ, Λ, Ξ, Ω) will provide info on the nature of the system created in the collision. It is important to point out that when the system at the mixed phase the expansion is stalled one expects a reduction of the strength of the collective flow. This has been predicted in Ref. [12]. For this study, the measurement of the v_1 (the direct flow) and v_2 for (π, K, p) and a function of the bombarding energy should be sufficient.

The measurement requires the capability for determine event plane, preferably at high rapidity range in order to avoid auto correlations and particle identification.

High order correlation of net-proton

Recent Lattice Gauge Theory (LGT) calculations [13–15] predicted a spike in quark susceptibility ratios χ_4/χ_2 at the finite values of temperature and chemical potential, see Fig. 2.2.

On the other hand, for a system with hadronic degrees of freedom, the ratio is expected to be one. *The secret of the degrees of freedom of the system is reflected by the ratio of susceptibilities.* In an experiment,

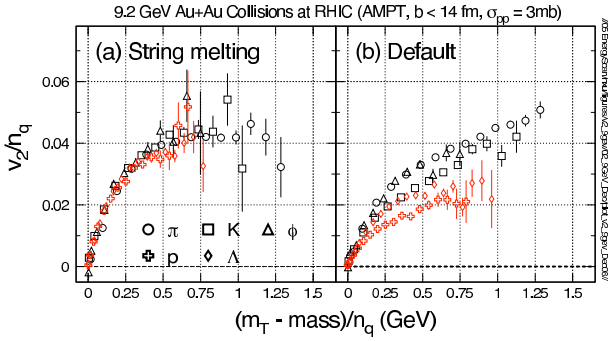

Figure 2.1: Number of quark scaled v_2 plotted as a function of the transverse mass (m_T-mass)/n_q, also scaled by n_q. Plot (a) and (b) represent partonic and hadronic system, respectively. It is clear that in the hadronic case no scaling in v_2 is observed in this simulation. The AMPT model [12] is used in the simulations.

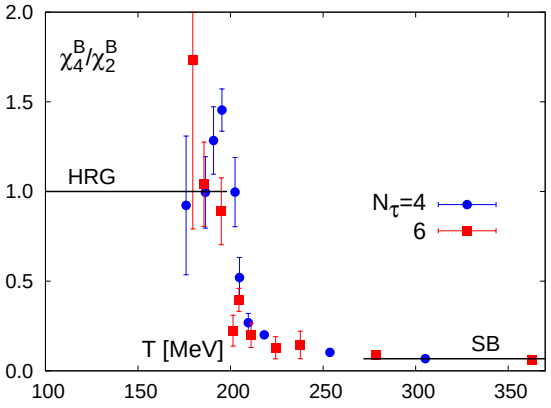

Figure 2.2: The ratio of the 4^{th} and 2^{nd} order cumulants of baryon number as a function of temperature. The value from hadronic gas model (HRG) is for the temperature range 100-200 MeV.

the ratio of the susceptibility can be readily constructed by the high order correlation function for conserved quantities in high-energy nuclear collisions. Baryon numbers are conserved in strong interactions. Simulations have shown that net-proton correlation function is a fair good representation of the net-baryons [16]. Note, at the critical point, the smallness (or disappearance) of the correlation length will lead to a large value of the quark susceptibility ratio. The systematic measurements of the net-charge and net-proton Kurtosis will provide info on the nature of the system.

Advantages for NICA

There is no comparison in terms of the control of systematic errors in a high-density tracking environment with the collider mode comparing with the fixed target experiment. In this sense, NICA provide a clear advantage compare to the proposed experiment CBM at FAIR. The possible shorting coming is the limitation of the luminosity with the collider. Therefore a careful selection of observable becomes more important. The above mentioned observables are, in my view, doable with the proposed collider.

2.3 Experimental advantages of collider over fixed target

B. Mohanty

Physics group, Variable Energy Cyclotron Center, Kolkata, India

Uniform acceptance for different particle species and for different beam energies in the same experimental setup

This is illustrated in Fig. 2.3 from the STAR experiment at the Relativistic Heavy-Ion Collidier in Brookhaven National Laboratory. The plot shows the uncorrected distribution of hadron transverse momentum versus rapidity within STAR Time Projection Chamber for three different beam energies and three types of hadron-pion, kaon and proton.

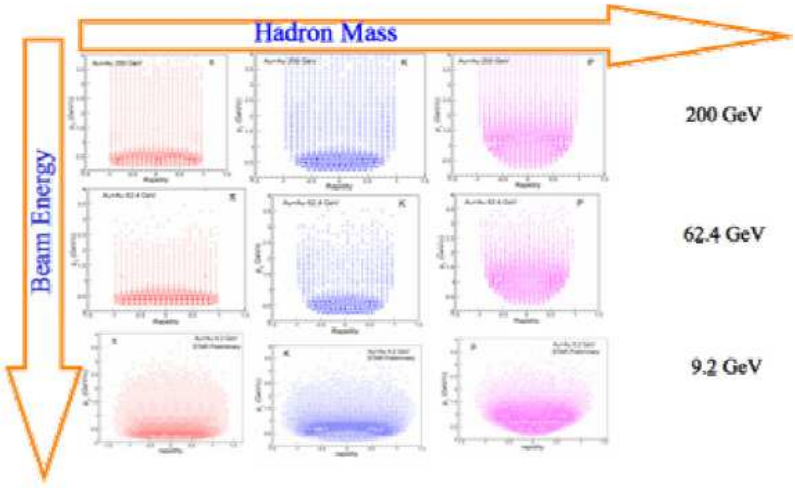

Figure 2.3: Acceptance for the collider mode [17]

Contrast this to similar plot from a typical fixed target experiment - NA49 at SPS, CERN Fig. 2.4. We can observe variation in acceptance for different hadrons at different beam energies.

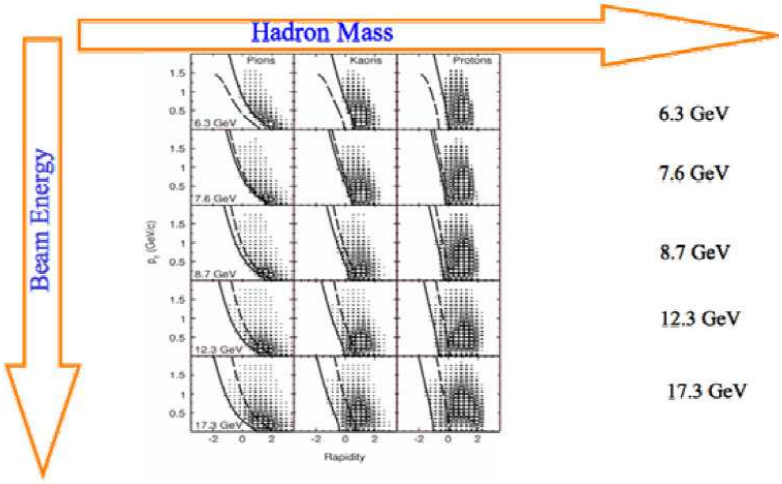

Figure 2.4: Acceptance in the fixed target mode [18]

For studies such as fluctuations (signatures for a phase transition and diverges at the QCD critical point) where having a correct knowledge of the acceptance is crucial for correct interpretation of results, it is desirable to have uniform acceptance at all beam energies for different hadrons.

Variation of particle density with beam energy

In a collider experiment: the variation of particle density with beam energy slower compared to fixed target experiments at similar colliding beam energies. This can be seen in Fig. 2.5, which shows the number of particles

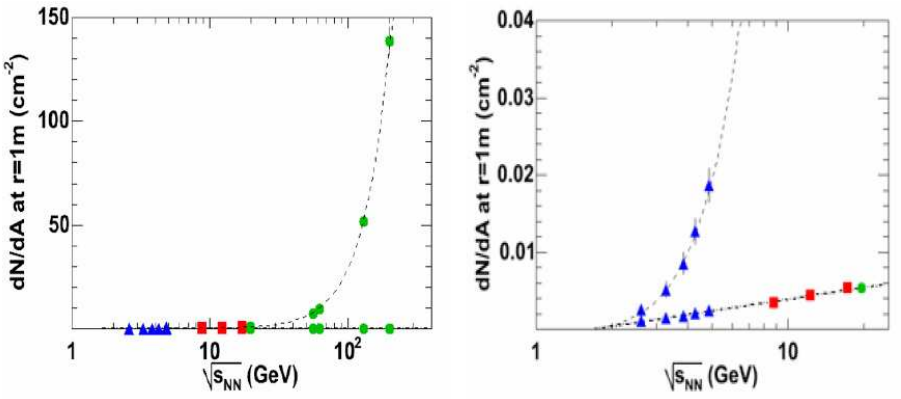

Figure 2.5: A number of particles per unit area at a distance of 1 meter from the collision point [19]. The low energy part of the left figure is zoomed in the right panel.

per unit area at a distance of 1 meter from the collision point [19]. A enlarged version of the figure is presented in the right panel, which clearly shows the difference in variation of particle density between collider and fixed target experiment.

A higher particle density affects the detector occupancy, which in turn could affect physics performance if not properly handled. A higher occupancy can lead to difficulties in reconstruction of tracks in the detector, also particle identification using techniques such as specific ionization energy loss, increase in double hit probability and space charge effects in tracking detectors.

One advantage which the fixed target experiments have over collider experiments is ability to reach higher luminosity for the same colliding beam energies.

2.4 Observables and open problems for NICA

E. Bratkovskaya[a] and W. Cassing[b]

[a] *Institut für Theoretische Physik, Universität Frankfurt*
[b] *Institut für Theoretische Physik, Universität Giessen*

Recent efforts of the world-wide heavy-ion community have been made to develop the physical program of the future CBM experiment at FAIR. The results obtained directly apply for the NICA experimental program, too - cf. the CBM Physics Book [20].

The NICA and CBM facilities will provide a unique possibility to study nuclear matter under extreme conditions - at high baryon density and temperature - where according to lattice QCD the hadronic matter transforms to the strongly interacting quark-gluon plasma (sQGP). The different phases of the sQGP are not so well settled and there might be a mixed phase of partons and hadrons at higher baryon density, too. There are several indications for a critical endpoint in the QCD phase diagram - separating the cross over at low quark chemical potential μ_q from a first order phase transition at high μ_q, but a rigorous proof is not yet available. Ultimately, the experimental investigations at CBM and NICA should solve this issue.

However, the main difficulty of the problem is that the information about the initial sQGP stage of matter can only be obtained indirectly from the measurement of final (color neutral) hadronic observables. One should expect that a sQGP signal can be strongly distorted by the hadronization process itself as well as by (resonant) final state interactions of the hadrons. In order to subtract the "trivial" hadronic contribution from the sQGP signal, one needs nonequilibrium transport approaches for the phase transition from hadronic to partonic matter (Quark-Gluon-Plasma) on a microscopic level which include the partonic dynamics explicitly as well as the dynamics of hadronization and hadronic final state interactions.

The microscopic Parton-Hadron-String-Dynamics approach (PHSD) [21, 22] developed recently is based on a dynamical quasiparticle model (DQPM) matched to reproduce lattice QCD results in thermodynamic equilibrium [23, 24]. It includes a nontrivial partonic equation of state - in line with lattice QCD - as well as

covariant transition rates from partonic to hadronic degrees of freedom. Additionally PHSD incorporates the hadron and string dynamics which have been tested in the HSD approach for more than 15 years [25] in the energy range from about 100 AMeV to 21 ATeV.

A systematic analysis from the theoretical and experimental side for a large variety of observables - as a function of beam energy and centrality of the collision - will allow to study extensively the properties of hadronic/partonic matter and their phase transition.

The promising observables for NICA energies are considered to be:

- **Excitation function of particle yields and ratios:**
  Observation of a non-monotonic energy dependence of the particle yields and ratios as well as an enhancement of multi-strange particle production which can not be reproduced in hadron-based models [25, 26].

- **Transverse mass spectra and rapidity distributions:**
  Observation of a non-monotomnic increase/flattening of the excitation function for the inverse slope; global m_T-scaling of all mesons as a signal for chiral symmetry restoration. [26].

- **Collective flow:**
  Observation of strong collective flow v_2 and a "wiggle" in v_1 signals of non-hadronic nature of the initial pressure in the system; scaling of v_2 with quark content as a signal of the QGP as an approximately ideal liquid with low viscosity-to-entropy ratio [27].

- **Open and hidden charm:**
  Observation of an enhancement of D meson production due to a dropping mass in the hot and dense environment or a strong in-medium modification of the initial $c\bar{c}$ pair in the plasma phase; anomalous J/ψ suppression beyond the trivial "comover" or "QGP threshold melting" scenarios; ratio ψ'/ψ as a probe of charm equilibration; large v_2 as a signal of strong initial pressure of partonic nature [28].

- **Dileptons:**
  Observation of an enhancement of the dilepton rates - at low invariant masses - due to in-medium changes of the vector meson spectral functions as a signal of chiral symmetry restoration in the hot and dense matter; thermal dileptons from the QGP at intermediate invariant masses (1.2 GeV $<$ M $<$ 2.5 GeV) [29, 30].

- **Fluctuations and correlations:**
  Observation of strong fluctuations in the number of charged particles, baryon number, electric charge, transverse momenta p_T, K/π, K/p, p/π ratios etc. as well as correlations beyond the hadron based model predictions [31, 32].

2.5 Exploring high-density baryonic matter: Maximum freeze-out density

J. Randrup[a] and J. Cleymans[b]

[a] *Nuclear Science Division, LBNL, Berkeley, California, USA*
[b] *Department of Physics, University of Cape Town, South Africa*

Over the past decade a striking regularity has been established in heavy-ion collisions: From the lowest beam energies to the highest, the yields of various hadronic species are consistent with the assumption of chemical equilibrium [16, 17, 19, 33, 37]. Analyses of the experimentally obtained hadronic yield ratios at a variety of collision energies have shown that the data can be well reproduced within the conceptually simple statistical model that describes an ideal hadron resonance gas in statistical equilibrium. Furthermore, the extracted freeze-out values of the temperature T and the baryon chemical potential $\mu_{\rm B}$ exhibit a smooth and monotonic dependence on the collision energy and can be simply parametrized.

The beam energy thus plays a determining role for the thermodynamic properties of the final state in relativistic heavy-ion collisions. However, there is no simple relationship between the collision energy and the freeze-out value of the (net) baryon density: At low collision energies the freeze-out density increases with the energy, whereas it decreases when the collision energy is high due to the onset of nuclear transparency. Thus there must exist a certain range of collision energies within which the freeze-out values of the net baryon density displays a maximum.

The optimal collision energy leading to this highest freeze-out density was discussed in [38] on the basis of the up-to-date results on the properties of the final state. It was pointed out there that since neither $\mu_{\rm B}$ nor T is subject to a conservation law they may be less suitable in a dynamical context. Furthermore, when a first-order phase transition is present, they become multivalued functions of the basic mechanical variables $\rho_{\rm B}$ (net baryon density) and ε (energy density) inside the mixed-phase region. It is therefore of interest to reexpress the thermodynamic variables in terms of those mechanical densities. Accordingly, we considered in [38] how the freezeout line appears when represented in terms of the basic baryon and energy densities, rather than chemical potential and temperature.

In [38], we presented the freeze-out line in terms of the net baryon density $\rho_{\rm B}$ and the energy density ε. We show below (in Fig. 2.6) the corresponding (ρ_B, ε^*) representation, where the "excitation energy density" $\varepsilon^* \equiv \varepsilon - n_{\rm N}\rho_{\rm B}$ is the energy density above the minimum value $m_{\rm N}\rho_{\rm B}$ dictated by the specified net baryon density. Thus ε^* has both compressional and thermal contributions.

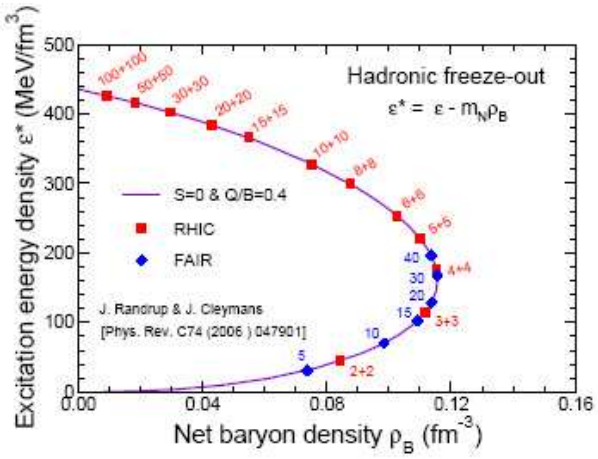

Figure 2.6: The hadronic freeze-out line in the $\rho_{\rm B} - \varepsilon^*$ phase plane as obtained from the values of $\mu_{\rm B}$ and T that have been extracted from the experimental data [16]. The calculation employs values of $\mu_{\rm Q}$ and $\mu_{\rm S}$ that ensure $< S >= 0$ and $< Q >= 0.4 < B >$ for each value of $\mu_{\rm B}$. Also indicated are the beam energies $E_{\rm lab}$ (in AGeV) for which the particular freeze-out conditions are expected at either a collider (red) or a fixed-target facility (blue).

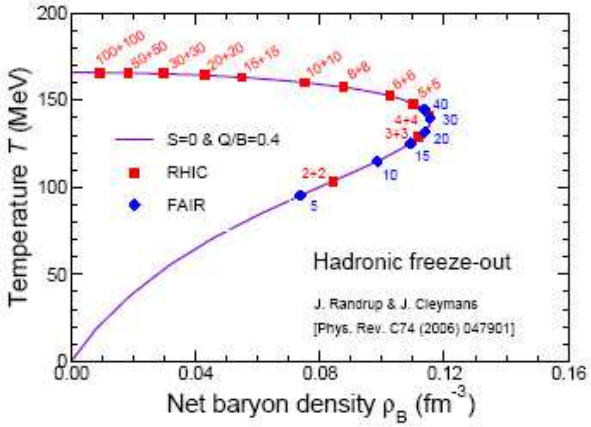

Figure 2.7: The hadronic freeze-out line in the $\rho_{\rm B} - T$ phase plane as obtained from the values of $\mu_{\rm B}$ and T that have been extracted from the experimental data [16]. The calculation employs values of $\mu_{\rm Q}$ and $\mu_{\rm S}$ that ensure $< S >= 0$ and $< Q >= 0.4 < B >$ for each value of $\mu_{\rm B}$. Also indicated are the beam energies (in AGeV) for which the particular freeze-out conditions are expected at either a collider (red) or a fixed-target facility (blue).

The corresponding ($\rho_{B,T}$) diagram, where T is the freeze-out temperature is perhaps more easily grasped and we show it in Fig. 2.7 below:

These novel representations of the freeze-out line bring out very clearly that there is a maximum value of the net baryon density: At the highest collision energies, freeze-out occurs for a negligible value of ρ_B and at an energy density of nearly one half GeV/fm^{-3}; then, in the range of μ_B = 400 - 500 MeV (and a temperature of T = 140 - 130 MeV), the freeze-out line exhibits a backbend and approaches the origin. Thus, the net baryon density at freeze-out has a maximum value which amounts to about three quarters of the familiar nuclear saturation density of $\rho_0 \approx 0.16\ fm^{-3}$.

The fact that the freeze-out value of the net baryon density exhibits a maximum as the collision energy is being scanned suggests that the corresponding collision energy (range) is optimal for the exploration of compressed baryonic matter. This suggested optimal beam kinetic energy is 15 - 30 GeV per nucleon for a fixed-target configuration (such as FAIR at GSI), corresponding to $\sqrt{s_{NN}}$ = 5.6 - 7.8 GeV for a collider (such as RHIC at BNL).

The results presented here should provide valuable guidance for establishing the desired capabilities of the contemplated NICA at JINR. In particular, our results suggest that freezeout densities all the way up to the maximum value could be explored at a collider facility delivering beam kinetic energies of up to $\approx$ 2.4 AGeV.

2.6 Nuclear matter physics at NICA

P. Senger

GSI Helmholtzzentrum für Schwerionenforschung, D-64291 Darmstadt, Germany

The exploration of the QCD phase diagram is one of the most exciting and challenging projects of modern nuclear physics. In particular, the investigation of nuclear matter at high baryon densities offers the opportunity to find characteristic structures such as a first-order phase transition with a region of phase coexistence and a critical endpoint. The experimental discovery of these prominent landmarks of the QCD phase diagram would be a major breakthrough in our understanding of the properties of nuclear matter. Equally important is quantitative experimental information on the properties of hadrons in dense matter which may shed light on chiral symmetry restoration and the origin of hadron masses. Worldwide, substantial efforts at heavy-ion accelerators like RHIC/BNL and SPS/CERN are devoted to the clarification of these fundamental questions, and new dedicated experiments are planned at future facilities like CBM at FAIR in Darmstadt and MPD at NICA/JINR in Dubna. In this article the perspectives for MPD at NICA are discussed.

Exploring the phases of nuclear matter

Ordinary substances exist in different phases such as gas, liquid, and solid, depending on the temperature and pressure. A variation of these conditions may cause a transition from one phase to the other, and the boundaries between the different lines can be drawn in a diagram as function of temperature and pressure. These lines could meet at the triple point where several phases coexist. In general there is also a critical point where the distinct phase boundary between liquid and gas ends, and beyond which there is a continuous "crossover" between the two phases. The phase boundaries, the triple point and the critical point represent fundamental landmarks in the phase diagram of each substance.

Fig. 2.8 illustrates the possible phases of nuclear matter and their boundaries in a diagram of temperature versus net-baryon density. At moderate temperatures and densities, nucleons are excited to short-lived states (baryonic resonances) which decay by the emission of mesons. At higher temperatures, also baryon-antibaryon pairs are created. This mixture of baryons, antibaryons and mesons, all strongly interacting particles, is generally called hadronic matter, or baryonic matter if baryons prevail. At very high temperatures and/or baryon densities the hadrons melt, and the constituents, the quarks and gluons, form a new phase, the Quark-Gluon-Plasma (QGP). In the first microsecond after the big bang the early universe underwent a phase transition from the primordial matter consisting of quarks, antiquarks and gluons into hadronic matter. This confinement process happened at zero net-baryon densities i.e. at equal numbers of particles and anti-particles, where modern theory predicts a smooth crossover transition from partonic to hadronic matter. For larger net-baryon densities theory predicts the existence a critical endpoint, followed by a first-order deconfinement phase transition with a phase coexistence region. High-density but rather cold nuclear matter is expected to exist in the core of neutron stars, and at very high densities correlated quark-quark pairs are predicted to form a color superconductor. A very fundamental but still open question is whether the deconfinement phase-transition coincides with the chiral

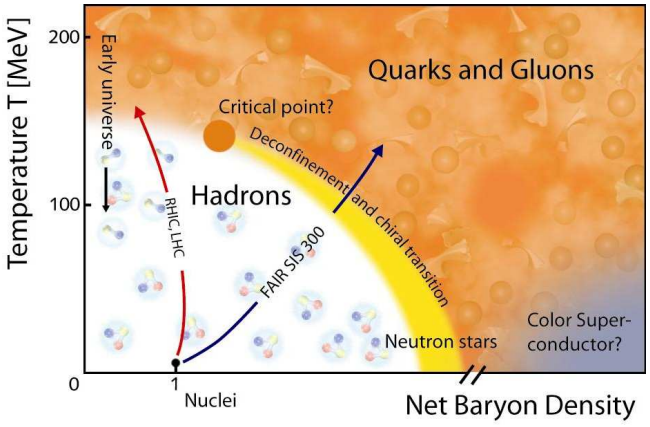

Figure 2.8: Sketch of the phase diagram of nuclear matter

phase-transition which is responsible for the generation of constituent quark masses, i.e. for the origin of the mass of the visible matter in our universe.

In the laboratory, hot and dense nuclear matter can be produced and studied in collisions between atomic nuclei at high bombarding energies. However, quantitative experimental information on the QCD phase diagram is still restricted to the freeze-out points of heavy-ion collisions as derived from statistical (thermal) model fits to measured particle yields and ratios [39]. The freeze-out points are shown in Fig. 2.9 as function of temperature T and baryon-chemical potential μ_B (full and open circles). A freeze-out temperature of T $\approx$ 160 MeV has been derived at very low values of μ_B from nucleus-nucleus collisions at the Relativistic Heavy Ion Collider (RHIC) at BNL . This number coincides with the critical temperature T_c found by lattice QCD calculations which varies between 150 and 180 MeV [40, 41]. The RHIC experiments made intriguing observations which support the picture that partonic degrees of freedom prevail in the early phase of the fireball evolution [42]. These studies will be continued at even higher energies at the Large Hadron Collider (LHC) at CERN.

It is worthwhile to note that the thermal model fits to the experimental data extract freeze-out temperatures which rise sharply up to beam energies of about 30 AGeV and then level off. The observation of a limiting freeze-out temperature is nontrivial, and may indicate a change of the degrees-of-freedom in the fireball which happens at FAIR (low SPS) beam energies. Around the same beam energy various structures in excitation functions have been observed by the NA49 experiment at the CERN-SPS [43]: the ratio of strange to non-strange hadrons exhibits a sharp peak, and the inverse slope parameters of the kaon transverse mass spectra (which are dominated by transverse flow) reach a plateau. Moreover, the dynamical fluctuations of the kaon-to pion ratio measured event-by-event increase with decreasing beam energy. Critical fluctuations are expected in the vicinity of the critical endpoint, like in macroscopic systems where the density fluctuations cause the phenomenon of "critical opalescence".

In Fig. 2.10 the freeze-out points are plotted as function of temperature and net-baryon density [38]. The numbers refer to either the total collision energy (from 2+2 to 100+100 AGeV)), or to laboratory kinetic energies for fixed target experiments (from 5 – 40 AGeV). The freeze-out density clearly exhibits a maximum at low CERN-SPS, NICA or FAIR energies indicating that beam energies between 30 and 40 AGeV (on fixed target), or total energies between $\sqrt{s_{\rm NN}} = 6$ and 10 AGeV are best suited to create the highest net-baryon densities in the laboratory.

In conclusion, the systematic and comprehensive exploration of the QCD phase diagram in the region of high net-baryon densities using novel observables will have a large discovery potential. In particular, future high-energy heavy-ion collision experiments such as CBM at FAIR or MPD at NICA will have to address the following fundamental questions:

- What is the equation-of-state of nuclear matter at neutron star densities (up to 6 ρ_0), and what are the relevant degrees-of-freedom at these densities?
- Are there structures in the QCD phase diagram such as a phase boundary between hadronic and partonic matter, a region of phase coexistence, a triple point or a critical endpoint ?

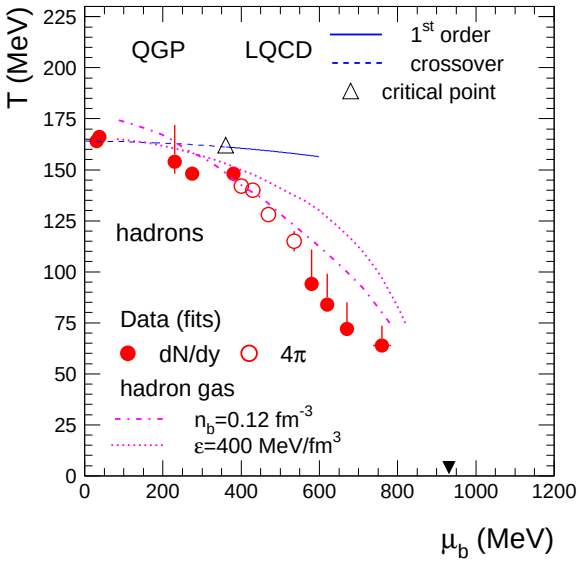

Figure 2.9: The QCD phase diagram as function of temperature and baryon chemical potential plane with chemical freeze-out points. The red dashed-dotted line corresponds to a constant total baryon density of n_b=0.12 fm^{-3}. The red dotted line represents a freeze-out curve for a hadron gas at constant energy density of ε = 500 MeV/fm^3. The black dashed line illustrates the location of a crossover transition as predicted by LQCD calculation, and the triangle represents the critical end point of a first order phase transition. Figure taken from [39].

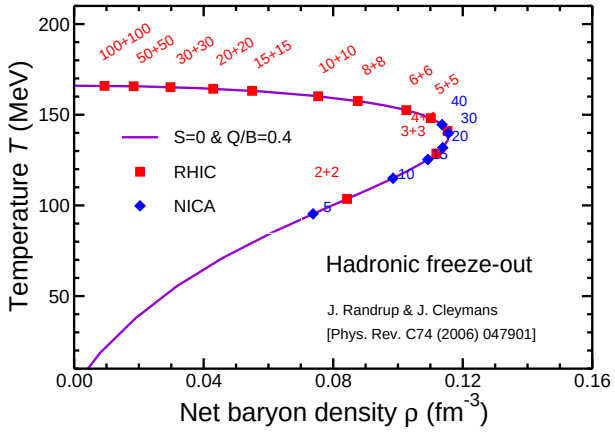

Figure 2.10: Chemical freeze-out curve as function of temperature and net-baryon density [38].

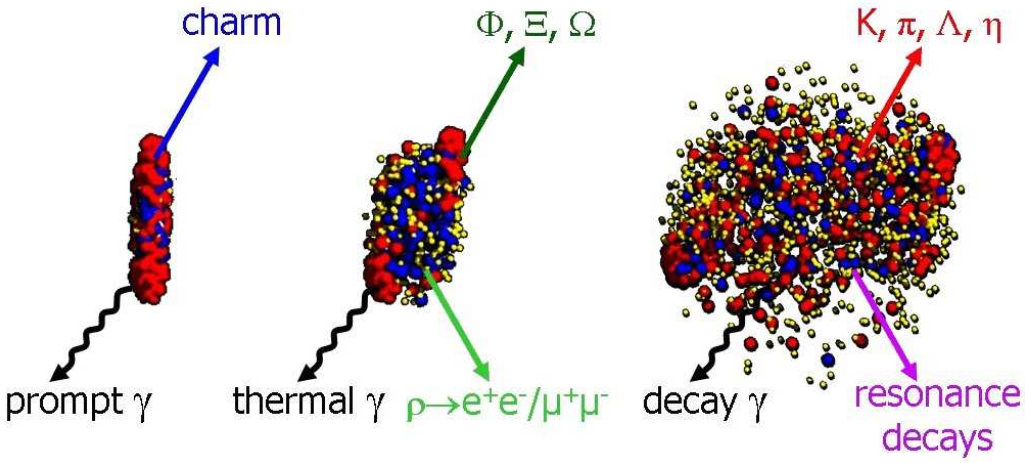

Figure 2.11: Sketch of the expansion phase of a U + U collision at a laboratory beam energy of 23 AGeV ($\sqrt{s_{\rm NN}}$ = 7 GeV) at different time steps: initial stage where the two Lorentz-contracted nuclei overlap (left), high density phase (middle), and final stage ("freeze-out") when all hadrons have been formed (right). Different particles are created in different stages of the collisions or escape from the interaction region at different times (see text). Almost 1000 charged particles are created in such a collision, most of them are pions.

- Does strange matter exist in the form of heavy multi-strange short-lived objects?
- To what extent are the properties of hadrons modified in dense baryonic matter, and are there signatures for chiral symmetry restoration?

The theoretical understanding of nuclear matter properties at large net-baryon densities is still in its infancy. Therefore, the scientific progress in this field is mainly driven by new experimental results. This requires high-precision measurements of new experimental observables as discussed in the next section.

Observables in heavy-ion collisions

In order to explore the properties of dense baryonic matter one has to find observables which serve as diagnostic probes of the early stage of the fireball. One of these observables is the elliptic flow of hadrons which reflects the initial almond shaped collision volume in momentum space. This is particularly true for particles which do not suffer from rescattering like Ω hyperons or ϕ mesons because of their low hadronic cross sections. Moreover, heavy quarks are produced in hard processes which occur predominantly in the initial phase of the collision.

The emission time of various particle species is illustrated in Fig. 2.11 which depicts three snapshots of the evolution of a heavy-ion collision at NICA/FAIR energies. Particles containing charm quarks are expected to be created in the very first stage of the reaction, and, therefore, offer the possibility to probe partonic degrees-of- freedom. Vector mesons like ρ, ω and ϕ mesons are produced continuously via $\pi - \pi$ annihilation during the course of the reaction, and decay either again into mesons, or into a pair of leptons. The latter decay channel is suppressed by about 4 orders of magnitude (corresponding to the square of the electromagnetic coupling constant $(1/137)^2$). However, as leptons are not affected by final-state interactions, this decay offers the possibility to look into the fireball. In particular the short-lived ρ meson is a promising diagnostic probe of hot and dense nuclear matter. Due to their small hadronic cross sections, also multi-strange hyperons and ϕ mesons carry information on the dense phase of the collision, in particular via their collective flow. Finally, the bulk of the particles is emitted at densities below saturation density. Up to date, essentially these freeze-out probes have been measured in heavy-ion collisions at beam energies between 2 and 40 AGeV (on stationary target). In contrast, the messengers from the early and/or the high-density phase of the collision are produced very rarely, either because of the low cross section (charm) or because of the small branching ratios into lepton pairs (low-mass vector mesons). Therefore, a successful experimental program can only be realized with a combination of fast detector systems and high beam luminosity.

A successful future heavy-ion research program has to perform a comprehensive scan of observables, beam energies and collision systems. The observables should include low mass dilepton pairs, charmonia and open

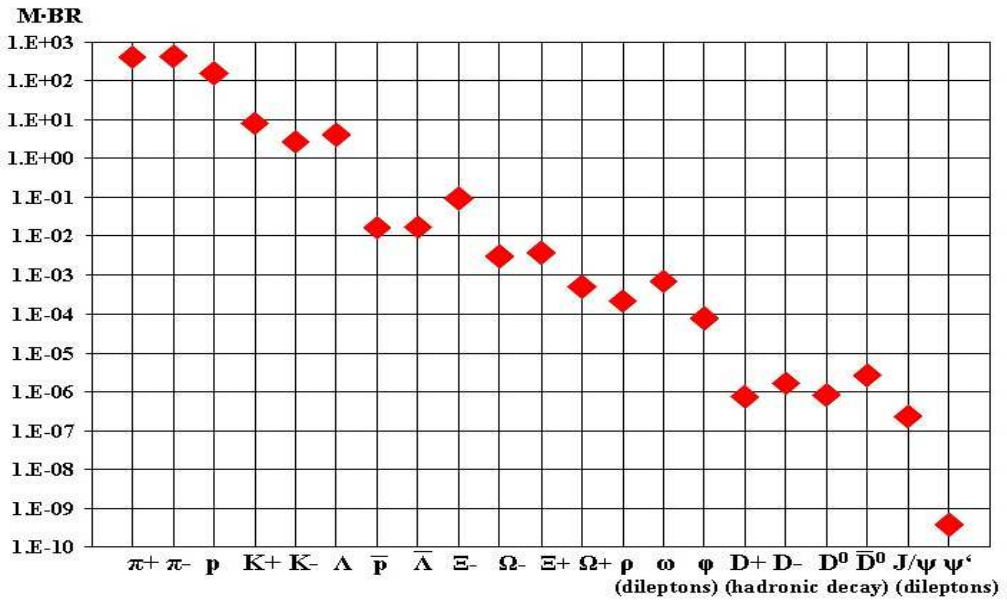

Figure 2.12: Particle multiplicities times branching ratio for central Au+Au collisions at 25 AGeV ($\sqrt{s_{\rm NN}}$ = 7.1 GeV) as calculated with the HSD transport code [44] and the statistical model [45]. For the vector mesons (ρ, ω, ϕ, J/ψ, ψ') the decay into lepton pairs was assumed, for D mesons the hadronic decay into kaons and pions.

charm, but also collective flow of rare and bulk particles, correlations and fluctuations. The experimental goal is to measure these rare probes with high precision in spite of the very low multiplicities. Fig. 2.12 quantifies the notation "rare probes" in terms of the product of particle multiplicity times branching ratio. The points are calculated for central Au + Au collisions at 25 AGeV (or at $\sqrt{s_{\rm NN}}$ = 7.1 GeV collider energy) using either the HSD transport code [44], or a thermal model assuming values for temperature and baryon chemical potential corresponding to a beam energy of 25 AGeV [45]. Mesons containing charm quarks are suppressed by about 9 orders of magnitude with respect to the pions (the ψ' meson is even more suppressed). The yield of lepton pairs from vector meson decays is about 6 orders of magnitude below the pion yield, similar to the yield of multi-strange hyperons.

Future experiments will have to be many orders of magnitude more sensitive than the ones which have been performed so far at AGS and low SPS energies. These experiments concentrated on the measurement of the most abundant hadrons which freeze out in the late and dilute stage of the collision. New insight will come from the measurement of multi-differential observables such as the elliptic flow of various particles as function of transverse momentum, and from the detailed analysis of rare diagnostic probes such as lepton pairs, multi-strange baryons and charmed hadrons.

Perspectives for NICA

The NICA energy range is ideally suited for the investigation of the equation-of-state of nuclear matter at neutron star core densities, and for the search for landmarks in the QCD phase diagram such as phase boundaries and critical/triple points. In order to characterize the properties of the fireball matter one has to measure the abundantly produced particles including their phase-space distributions and correlations, together with rare diagnostic probes like multi-strange particles, lepton pairs and charmed hadrons. The experimental challenge will be to identify these rare particles with high purity, and to collect samples with large statistics which is required for a multi-differential analysis.

Table 2.1 lists the multiplicities of the most important probes in minimum bias Au+Au collisions for two energies as calculated with the HSD transport model and the statistical model, and their yields which are estimated based on realistic detector and analysis efficiencies, and on the design NICA luminosity of of L=10^{27}cm^{-2}s^{-1}.

Particle (mass)	Multiplicity $\sqrt{s_{NN}}$ = 7.1 GeV	Multiplicity $\sqrt{s_{NN}}$ = 11 GeV	decay mode	BR	ε (%)	yield (s^{-1}) $\sqrt{s_{NN}}$ = 7.1 GeV	yield (s^{-1}) $\sqrt{s_{NN}}$ = 11 GeV	yield in 10 weeks $\sqrt{s_{NN}}$ = 7.1 GeV	yield in 10 weeks $\sqrt{s_{NN}}$ = 11 GeV
K^+ (494)	8	12	-	-	20	$9.6{\cdot}10^3$	$1.4{\cdot}10^4$	$5.8{\cdot}10^{10}$	$8.4{\cdot}10^{10}$
K^- (494)	2.6	5.6	-	-	20	$3.1{\cdot}10^3$	$6.7{\cdot}10^3$	$1.9{\cdot}10^{10}$	$4.0{\cdot}10^{10}$
ρ(770)	4.6	8	e^+e^-	$4.7{\cdot}10^{-5}$	2	$2.6{\cdot}10^{-2}$	$4.5{\cdot}10^{-2}$	$1.6{\cdot}10^5$	$2.7{\cdot}10^5$
ω(782)	7.6	13	e^+e^-	$7.1{\cdot}10^{-5}$	2	$6.5{\cdot}10^{-2}$	0.11	$3.9{\cdot}10^5$	$6.6{\cdot}10^5$
ϕ(1020)	0.24	0.4	e^+e^-	$3{\cdot}10^{-4}$	2	$8.6{\cdot}10^{-3}$	$1.4{\cdot}10^{-2}$	$5.2{\cdot}10^4$	$8.4{\cdot}10^4$
Ξ^-(1321)	0.16	0.2	$\Lambda\pi^-$	1	2	19	24	$1.1{\cdot}10^8$	$1.4{\cdot}10^8$
Ω^-(1672)	0.024	0.032	ΛK^-	0.68	2	1.9	2.9	$1.1{\cdot}10^7$	$1.7{\cdot}10^7$
D^0 (1864)	$7.5{\cdot}10^{-6}$	$7.5{\cdot}10^{-4}$	$K^+\pi^-$	0.038	2	$3.4{\cdot}10^{-5}$	$3.4{\cdot}10^{-3}$	200	$2{\cdot}10^4$
J/ψ (3097)	$2.4{\cdot}10^{-6}$	$5{\cdot}10^{-5}$	e^+e^-	0.06	10	$8.6{\cdot}10^{-5}$	$1.8{\cdot}10^{-3}$	520	$1.1{\cdot}10^4$

Table 2.1: Particle multiplicities and yields for minimum bias Au+Au collisions at energies of $\sqrt{s_{NN}}$ = 7.1 and 11 GeV (25 and 60 AGeV fixed target energy) as calculated with the HSD transport model and with the statistical model. The values have been calculated for central collisions, and then scaled down by 5 for minimum bias collisions. The yield estimates are based on the maximum NICA luminosity of L=10^{27}cm^{-2}s^{-1} corresponding to a reaction rate of 6 kHz for minimum bias Au + Au collisions.

The detector system should comprise the following components. The measurement of kaons, in particularly their separation from pions and protons, requires a magnetic field, a tracking detector like a Time-Projection-Chamber (TPC), and preferably a time-of-flight detector (TOF). Λ, Ξ, and Ω hyperons can be identified via the topology of their weak decays ($\Lambda \to p\pi$, $\Xi \to \Lambda\pi$, $\Omega \to \Lambda K$). Such a measurement requires tracking detectors inside a magnetic field. However, due to the short decay lengths of $c\tau$ = 7.89 cm (Λ), $c\tau$ = 4.91 cm (Ξ^-), and $c\tau$ = 2.46 cm (Ω^-) the track measurement should start close to the primary vertex where the track density is high. For this purpose, a high precision tracking detector based on Silicon micro-strip sensors would be the best choice. With a detector system in collider geometry it is very difficult to identify muons at midrapidity. Therefore, it would be preferable to add electron detectors such as a Ring Imaging Cherenkov (RICH) detector or an Electromagnetic Calorimeter (ECAL). Typically, in the NICA energy range on has to suppress the π yield by a factor of about 10^4 to see the electrons. If this cannot be achieved with RICH and ECAL one could add a Transition Radiation Detector (TRD) to identify electrons above 1 GeV. The rejection of physical background due to close electron pairs may require the use of a Hadron Blind Detector (HBD).

The identification of particles containing charm quarks poses a particular experimental challenge due the very low signal-to-background ratio at beam energies close to production threshold. Moreover, their yield would be very low even after 10 weeks of beam at highest luminosity, at least for beam energies where one expects the highest net-baryon densities to be produced (see Table 2.1). Therefore, the measurement of J/ψ and D mesons may be restricted to the highest NICA beam energies. Moreover, the identification of D mesons via their hadronic decay into pions and kaons (decay length of $c\tau$ = 123 μm for D^0, and $c\tau$ = 312 μm for $D^\pm$) would require the installation of an additional high-resolution low-mass micro-vertex detector.

Table 2.2 summarizes the major NICA physics cases, the corresponding observables and the required detector components. It turns out that the most interesting scientific questions can be tackled with a basic version of the MPD comprising a magnet, a TPC, a Silicon tracker, and a TOF detector. These measurements do not necessarily require the highest reaction rates as the production cross sections for strange particles are reasonably high. The electron detectors could possibly be part of an MPD upgrade program which could take place once NICA has reached the design luminosity.

The MPD/NICA project is part of a worldwide experimental research program which is devoted to the exploration of the QCD phase diagram at high net-baryon densities. This program was started about 30 years ago with pioneering experiments at the Bevalac at the LBL in Berkeley, and was continued at higher energies at AGS at BNL in Brookhaven and at the SPS at CERN. At the SPS, the fixed-target experiment NA61/SHINE is still taking data, mainly bulk particles like pions, kaons, and hyperons. At GSI/SIS18 the second generations experiments FOPI and HADES study nuclear matter properties at 2–3 time saturation density by measuring

Physics case	Observables	Detectors
nuclear EOS at high densities	proton flow, Λ, Ξ, Ω	Silicon tracker, TPC, TOF
deconfinement phase transition, phase coexistence	excit. funct. of yield and flow of K, Λ, Ξ, Ω. e-by-e fluctuations	Silicon tracker, TPC, TOF
strange matter	multi-strange short-lived objects (decay into Λ, Ξ, Ω)	Silicon tracker, TPC, TOF
chiral phase transition, hadrons in dense matter	dileptons (e+e-)	HBD, RICH, TPC, TOF, ECAL, (TRD ?)

Table 2.2: The possible NICA physics cases, related observables, and detector requirements

pions, strange particles and dileptons.

At RHIC, the energy scan program has been started mainly using the STAR detector with the goal to search for the critical endpoint. The scaling of the elliptic flow parameter v_2 with the number of constituent quarks as observed at RHIC is regarded as one of the most convincing signatures for partonic degrees-of-freedom prevailing in the early stage of the collision. Therefore, this signal should disappear at a certain beam energy when scanning down the energy. At the same energy, higher-order event-by-event fluctuations should appear indicating the location of the critical point. The statistical significance of these and other signals will be limited by the very low luminosity at RHIC injection energies. Moreover, the beam time available at RHIC for this kind of studies is very limited. In contrast, NICA is designed for high luminosities at the collision energies where high net-baryon densities are created and the MPD can run over long periods. This offers the possibility to perform systematic measurements of multi-differential observables, including particles with lower production cross sections. Extremely high beam intensities will be available at FAIR for the CBM experiment which is designed to measure bulk and rare probes with almost unlimited statistics [46]. In contrast to the fixed-target CBM, the collider experiment MPD has a uniform acceptance which is almost independent of the collision energy. Therefore, MPD at NICA and CBM at FAIR will be able to perform complementary measurements, covering different regions of phase space. Last but not least, the parallel development of two detector systems based on cutting-edge technology offers the opportunity of joint R&D activities which will be of large mutual benefit.

2.7 Hadron Physics at the Charm and Bottom Thresholds and Other Novel QCD Physics Topics at the NICA Accelerator Facility

S. J. Brodsky

SLAC National Accelerator Laboratory Stanford University, Stanford, California, USA

The NICA collider project at the Joint Institute for Nuclear Research in Dubna will have the capability of colliding protons, polarized deuterons, and nuclei at an effective nucleon-nucleon center-of mass energy in the range $\sqrt{s_{NN}} = 4$ to 11 GeV. I briefly survey a number of novel hadron physics processes which can be investigated at the NICA collider. The topics include the formation of exotic heavy quark resonances near the charm and bottom thresholds, intrinsic strangeness, charm, and bottom phenomena, hidden-color degrees of freedom in nuclei, color transparency, single-spin asymmetries, the RHIC baryon anomaly, and non-universal antishadowing.

Introduction

The NICA collider project at the Joint Institute for Nuclear Research in Dubna [47, 91] will have the capability of colliding nucleons, polarized deuterons, and nuclei at an effective nucleon-nucleon center-of mass energy in the range $\sqrt{s_{NN}} = 4$ to 11 GeV.

In tis brief report, I will discuss a number of novel hadron physics topics which can be investigated at the NICA collider. The topics include the formation of exotic heavy quark resonances near the charm and bottom thresholds, intrinsic strangeness, charm, and bottom phenomena, hidden-color degrees of freedom in nuclei, color transparency, single-spin asymmetries, the RHIC baryon anomaly, and non-universal antishadowing.

The Ultra-Low Energy Domain Using Variable-Angle Collisions

If the interaction region at NICA is designed so that A and B can collide at a variable finite center of mass angle $0 < \theta < \pi$, then the effective CM energy squared $s = (p_A + p_B)^2 = M_A^2 + M_B^2 + 2E_A E_B(1 - \beta_A \beta_B \cos\theta)$ will span from very low energies to beyond the bottom flavor threshold. (Here $\beta_i = |\vec{p}_i|/E_i$ are the colliding beam velocities.) For example, if the beams are arranged to collide while moving in the same direction ($\theta \to 0$), one could study collisions close to zero relative velocity at the NICA, a novel nonrelativistic regime for studying nuclear and Coulombic interactions. Bjorken has called this comoving configuration the "Fool's Intersecting Storage Ring" (FISR) [49]. The direction of the beam polarization could also be also modified from longitudinal to transverse if the colliding beams are perpendicular.

Charm and Bottom Physics at Threshold

The threshold for hidden-charm production in pp channels such as $pp \to pp J/\psi$ is $\sqrt{s} = 5$ GeV. The corresponding threshold for hidden-bottom production in $pp \to pp\Upsilon$ is $\sqrt{s} = 7$ GeV. Thus an array of interesting hidden and open heavy quark reactions is accessible at the NICA collider. One can also access open-charm reactions such as $pp \to \Lambda_c(cud)D(\bar{c}u)p$, the production of double-charm baryons $\Lambda(ccu)$, $\Lambda(ccd)$ single and double charmonium, charm-strangeness channels and, in principle, even open-bottom channels such as $pp \to \Lambda_b(bud)B(\bar{b}u)p$. One can also study strange or charm dijets and measure the asymmetries analogous to the $t\bar{t}$ asymmetries observed at the Tevatron [50, 51]. Such processes are sensitive to the correct choice of QCD renormalization scale [52], as well as the lensing effects due to the final-state interactions of the heavy quarks with the beam and target spectator quarks [53] .

The rates for heavy quark production processes near threshold in proton collisions is enhanced by the existence of intrinsic charm and intrinsic bottom Fock states within the proton wavefunction; i.e., five quark $|uudQ\bar{Q}>$ configurations in the proton's light-front wavefunction where the heavy quarks are multi-connected to the proton's valence quarks via two or more gluons . As discussed in more detail in the next section, the intrinsic contributions [55] correspond to $gg \to Q\bar{Q} \to gg$ gluon-gluon scattering insertions in the proton self energy. They scale as $1/M_Q^2$ due to the non-Abelian couplings of QCD [55, 56] and are maximal at equal rapidity; i.e. $x_i \propto \sqrt{m_i^2 + k_{\perp i}^2}$. Thus the heavy quarks carry most of the light-front momentum x_i of the proton. This allows the energy of the beam hadrons to be efficiently transferred to the production of heavy quark charm and bottom states [57, 58]. In addition, the gluonic interactions between heavy quarks of opposite color provide a strong attractive potential analogous to the Sommerfeld-Schwinger-Sakharov (SSS) Coulomb threshold enhancement in QED [59] For example, the cross section for $e^+e^- \to \mu^+\mu^-$ is enhanced by a power of $\frac{1}{\beta}$ canceling the phase space factor at small relative velocity β because of the SSS Coulombic interactions. In fact the rate just above the muon pair threshold matches the production of the infinite series of nS-state Bohr bound states of "true muonium" just below threshold [60, 61].

Hadrons interact very strongly when their relative velocity β is small, and the time for their interactions is maximal. This phenomenon has been observed at the thresholds for baryon-pair production in $e^+e^- \to p\bar{p}$, and $e^+e^- \to \Lambda\bar{\Lambda}$ reactions [62]. The baryon pair cross sections remain finite at $\beta \to 0$, even though the phase space vanishes. One also observes enhancements at $\beta_{p\bar{p}} = 0$ in the decay $J/\psi \to p\bar{p}\gamma$ [63].

The enhancement of hadronic interactions at threshold implies that new types of charm-based resonances can be formed and studied at NICA. This includes the production of possible $J/\psi-$ nucleon resonances at threshold in reactions such as $pp \to p[J/\psi p]$, $pd \to pp[J/\psi n]$, and "nuclear bound quarkonium" $pA \to pp[J/\psi A - 1]$ [64]. These heavy-quark bound states are expected in QCD from QCD gluonic interactions at small relative velocity. For example, nuclear-bound quarkonium $[J/\psi A]$ can be formed due to the attractive two-gluon exchange QCD van der Waals potential. [64–67] Furthermore, if hadrons share the same valence (or even intrinsic sea quarks), resonances can be formed due to attractive QCD covalent interactions in analogy to covalent molecular forces. In each case, the strength of the hadronic interactions can overcome the phase-space suppression at zero relative velocity.

Another example of enhanced dynamics near the heavy-quark thresholds is the remarkably large $4:1$ transverse-transverse spin correlation A_{NN} observed in large-angle elastic proton-proton scattering [68] at $\sqrt{s} \simeq 3$ GeV and $\sqrt{s} \simeq 5$ GeV. These center-of-mass energies correspond to the strange and charm thresholds relevant to the two-baryon system. In fact, the observed strong spin correlations are consistent with the formation in the s-channel of $J = L = S = 1$ $uuds\bar{s}uud$ and $uudc\bar{c}uud$ "octoquark" resonances near the heavy-quark pair production thresholds. [69]. It thus would be very interesting to study th collisions of polarized proton

beams at the NICA. Guy de Teramond and I used unitarity to estimate that the charm production cross section $\sigma(pp \to c\bar{c}X) \sim 1\ mb$ at the charm threshold.

Intrinsic strange and charm distributions at large x

As shown by Chang and Peng [70], the HERMES electroproduction data [71] for the strange quark distribution $s(x, Q^2)$ in the proton exhibits two components, a contribution at small $x_{Bj} < 0.1$ – consistent with $g \to s\bar{s}$ gluon splitting, as incorporated into DGLAP evolution – and an approximately flat component at $0.1 < x < 0.4$ which is consistent with a five-quark Fock state $|uud\bar{s}s>$ intrinsic to the proton eigenstate. The intrinsic strange quarks arise from diagrams which are multi-connected to the valence quarks; they are thus *intrinsic* to the structure of the proton itself.

In fact, the broad intrinsic strangeness contribution at large x is also consistent with the EMC [72] measurement of the charm structure function $c(x, Q^2)$ at large x as well as the BPHS model [55] for intrinsic charm. The charm structure function measured by EMC at $x = 0.42$ and $Q^2 = 75\ GeV^2$ is 30 times larger that the extrinsic contribution from gluon splitting. The probabilities for Intrinsic strangeness and charm scale as M_s^2/M_c^2, the scaling, as predicted by the operator product expansion [55, 56] for non-Abelian theory. The probability of intrinsic bottom is thus smaller than the intrinsic charm probability in the proton by a factor $m_c^2/m_b^2 \sim 1/10$.

The anomalously large $pp \to c\gamma X$ rate observed by D0 [73] at the Tevatron could be due to intrinsic charm in the subprocess $gc \to \gamma c$ at $x_c > 0.1$ [74]. This anomaly can be checked at NICA.

The intrinsic Fock states in the proton's eigensolution are a rigorous prediction of QCD. For example, the existence of QED intrinsic muons in the positronium Fock state wavefunction $|e^+e^-\mu^+\mu^->$ reflects the light-by-light muon-loop insertion into the positronium self-energy. There is no "tunneling" suppression. A bound-state wavefunction is an off-shell amplitude describing arbitrarily off-shell configurations. In the case of the Front Form [75], the frame-independent light-front wavefunction (LFWF) $\psi_n(x_i, \vec{k}_{\perp i})$ describes a hadron at fixed light-front time $\tau = t+z/c$ as as a function of its n constituents' invariant mass squared $\mathcal{M}^2 = \sum_i^n \frac{k_{\perp i}^2+m_i^2}{x_i}$.

As discussed in ref. [58], the cross section for charm production $\gamma p \to J/\psi p$ at the charm threshold measured in photoproduction at CESR [76] is considerably larger than extrapolations based on phase space suppression. This is expected from the intrinsic heavy quark configurations of the proton.The production of heavy quark states at threshold requires that the valence quarks of the proton efficiently transfer their four-momentum to the heavy quark production process. This is possible since the five-quark intrinsic charm Fock state $|uudc\bar{c}>$ in the proton has maximum probability at minimum off-shellness; i.e., when all of the quarks have the same rapidity.

Intrinsic charm can also be investigated at NICA by measuring the x_F distribution of processes such as $\frac{d\sigma}{dx_F}(pp \to \Lambda_c X)$. The Λ_c is created from the coalescence and combined momenta of the comoving quarks in the proton's five-quark Fock state $|uudc\bar{c}>$. Indeed the Λ_c [77, 78] and the $\Lambda_b >$ [79] was first discovered in pp collisions at large x_F using the split field magnet at the ISR. Diffractive open charm production such as $pp \to \Lambda_c pX$ has also been observed [80–83]

One can also study single- and double-quarkonium production [84] $pp \to J/\psi X$ and $pp \to J/\psi J/\psi X$ at high x_F at NICA. The double charmonium channels were first observed in pA and πA collisions at $x_F^{total} > 0.5$ in the NA3 fixed target experiment at CERN, evidently reflecting the existence of Fock states such as $|uudc\bar{c}c\bar{c}>$ The SELEX experiment at Fermilab [85] has observed doubly-charmed baryons $|ccu>$ and $|ccd>$; the anomalously large isospin spitting of the doubly-charmed baryons reported by the SELEX has not been explained. [86]

Gardner and I [88] have also shown that the existence of intrinsic charm in the higher Fock states B meson can affect the rare decays of the B meson, particularly the decay channels where "penguin" diagrams are important.

The intrinsic heavy quark distributions can be quark/antiquark asymmetric [87]; e.g. $s(x) \neq \bar{s}(x)$ as well as have novel spin properties since the five-quark Fock state $|uuds\bar{s}>$ is dual to off-shell hadronic excitations such as $|K^+(u\bar{s})\Lambda(sud)>$. For a recent review of intrinsic heavy quark phenomenology, see ref. [89]

Other Novel Physics Topics at NICA

1. **The anomalous nuclear dependence of high-x_F quarkonium production**

   One of the outstanding QCD puzzles is the nuclear dependence of $\frac{d\sigma}{dx_F}(pA \to J/\psi X)$. The observed A-dependence breaks QCD factorization since it is not a function of the gluon momentum, and it behaves as $A^{\alpha(X_F)} \simeq 2/3$ at high x_F. This phenomenon could reflect the special color-octet/color-octet composition

of the $|uud_{8C}c\bar{c}>$ intrinsic charm Fock state; because of its large color dipole moment the intrinsic charm fluctuation of incoming proton at high x_F will then interact to produce the J/ψ at the front surface, yielding the $A^{2/3}$ dependence [90, 91]. It will be very interesting to investigate such nuclear effects at NICA. The quarkonium polarization and other physics issues are reviewed in ref. [92]

2. **The Sivers effect: breakdown of pQCD leading-twist factorization**

   The Sivers pseudo-T-odd correlation of the target hadron's spin with the virtual photon to jet plane arises in deep inelastic lepton scattering from rescattering of the struck quark; i.e., a final-state lensing effect [93]. The Sivers effect satisfies Bjorken scaling and is leading twist, but it does not have the normal factorization properties of pQCD. In fact one predicts an opposite single-spin asymmetry in Drell Yan reactions from initial state interactions [94, 95]. One can study such lensing effects at NICA in polarized deuteron or polarized proton beam Drell Yan reactions such as $d^{\Uparrow}A \to \mu^+\mu^- X$.

   The source of the large single-spin asymmetries at large x_F in $p^{\Uparrow}A \to \pi X$ is not understood [96, 97]. This provides another an important NICA physics opportunity which can be studied in polarized deuteron reactions such as $d^{\Uparrow}A \to \pi X$, etc.

3. **The Double Boer-Mulders Effect: the breakdown of pQCD leading-twist factorization**

   As shown by Boer, Hwang, and myself [98], the Initial-state interactions of both the quark and antiquark in unpolarized Drell-Yan reactions $pp \to \mu^+\mu^- X$ generates an anomalous $\cos 2\phi \sin^2\theta$ distribution of the lepton pair and the breakdown of the Lam-Tung relation of pQCD at leading twist. This was first observed in $\pi^- A \to \mu^+\mu^- X$ by NA10 [99]. This type of lensing phenomena can be investigated in detail at NICA.

4. **Higher-Twist Effects in the Drell-Yan Reaction**

   At high x_F the Drell-Yan reaction can utilize multiparton correlations of the beam hadron. For example, the Chicago-Princeton fixed target experiment [100] observed a dramatic change of the muon angular distribution $1 + \lambda \cos^2\theta$ from $\lambda = +1$ to $\lambda = -1$ at high x_F in $\pi^- p \to \mu^+\mu^-$. This effect can be ascribed to the higher twist subprocess $(d\bar{u}) + u \to d\gamma^* \to d\mu^+\mu^-$ where both valence quarks of the pion contribute their momentum to the hard reaction at large x_F [101]. This interesting phenomenon can be investigated at NICA.

5. **Scaling of hard inclusive reactions**

   An important test of pQCD is the scaling behavior of inclusive cross sections [102, 103]

$$\frac{d\sigma}{d^3p_C/E_C}(AB \to CX) = \frac{F(\theta_{CM}, x_T)}{p_T^n}$$

   at fixed $x_T = \frac{2p_T}{\sqrt{s}}$ and fixed θ_{CM}. The conformal parton model predicts $n = 4$ simply from dimensional analysis. This become $n \sim 5$ for direct photon reactions $pp \to \gamma X$ due to evolution and running coupling, This is verified by experiment. However, the predicted pQCD power law $n \simeq 5.5$ fails to describe any experiment. For example, the Chicago Princeton experiment [104] as well as ISR measurements found that $\frac{d\sigma}{d^3p_C/E_C}(pp \to pX)$ scales with $n > 11$ far from the leading twist pQCD prediction $n \sim 5.5$. This breakdown of pQCD could be explained by the fact that one can also create hadrons directly from a hard subprocess such has $uu \to p\bar{d}$ in addition to the standard jet fragmentation $q \to qp$ [105]

   The breakdown of leading twist scaling is particular interesting to study at NICA in nuclear collisions such as $AA \to pX$, since the directly-produced proton is formed as a small color singlet and is thus color transparent [106]. This phenomenon can explain the "baryon anomaly" observed in high centrality heavy ion colisions at RHIC. [107]

   One can also study reactions such as $pA \to \mathrm{JetJetJet}X$ to check color transparency and measure aspects of the proton's three-quark light-front wavefunction [108–110].

6. **Exclusive Reactions**

   pQCD Counting rules predict the leading fall-off of hard exclusive reactions $\frac{d\sigma}{dt}(AB \to CD) = \frac{F(s/t)}{t^{n-2}}$ where n counts the minimum number of initial and final-state partons, according to the twist of the hadrons [111, 112]. This scaling is also predicted by AdS/QCD [113, 114]. These reactions are also quark

helicity-conserving [115] and "color transparent." Color transparency predicts no absorption of the hard scattering hadrons in the nucleus; i.e. the cross section scales as the number of nucleons [106] Experiments at BNL have in fact found evidence [116] for increasing color transparency in quasielastic pp scattering with p_T below the charm threshold.

The angular distribution of virtually all hard hadron-hadron exclusive reactions at fixed t/s appears to be consistent with quark interchange (e.g. u quark exchange in $K^+p \to K^+p$) rather than gluon exchange [117]. These experimental facts and phenomena could be evidence for the "sublimation" of gluons into an effective color-confining potential below gluon virtuality $Q^2 \sim 1\ GeV^2$, as suggested by the successful phenomenology of AdS/QCD [118].

As shown by Landshoff [119], an anomalous odderon contribution due to triple-gluon exchange with three equal momentum transfers $t/9$ can give a contribution $\frac{d\sigma}{dt}(pp \to pp) \propto s^0/t^8$, but this contribution has never been observed, perhaps again because of gluon sublimation.

Many such tests of QCD in hard exclusive reactions, including $pn \to pn$, $pp \to \Lambda Kp$, $pd \to pd$, and $pd \to npp$ with each hadron detected at fixed CM angle, can be performed at NICA. It will also be interesting to check the polarization dependence of exclusive reactions, such as single-spin asymmetries.

7. **Hidden-color of nuclear wavefunctions.**

   The deuteron six-quark $|uudddu>$ Fock state has five different color-singlet configurations. The *hidden color* [120] Fock states, which cannot be identified with the np configuration are activated when the six quarks have small transverse separation. Hard exclusive reactions involving the deuteron such $pd \to pd$ are thus particularly interesting since they probe the hidden-color Fock states of the deuteron six-quark Fock state. In addition to the usual pn configuration, there are four other color-singlet combinations of six color-triplet quarks in the deuteron's QCD eigensolution. Hidden-color QCD phenomena can thus be investigated at NICA in many different high Q^2 elastic and transition deuteron reactions.

8. **Non-universal antishadowing.**

   There is evidence that the nuclear dependence of structure functions measured in charged-current deep inelastic neutrino-nucleus scattering is different than in deep inelastic lepton-nucleus scattering [121]. This could occur, for example, if antishadowing is flavor-specific, since antishadowing is driven by diffractive contributions which involve Reggeon exchange [122] Experiments at NICA can investigate flavor-tagged Drell-Yan reactions to see whether shadowing and antishadowing are quark specific [123].

9. **Odderon phenomenology.**

   The existence of Odderon exchange, the $C = -$ three-gluon exchange analog of the Pomeron, is predicted to exist in QCD, but it has never been observed [124–128]. The interference of two-gluon and three-gluon exchange will lead to charm meson $D^{\pm}$ asymmetries in $pp \to D^+D^-pp$ reactions [129], a phenomenon which may be testable at the NICA.

Acknowledgements Contribution to the White Paper for the Nuclotron-Based Ion Collider Facility (NICA) at Dubna. I thank David Blaschke for helpful suggestions and comments. This research was supported by the Department of Energy, contract DE–AC02–76SF00515. SLAC-PUB-15050.

2.8 Excluded volume effects on baryon density and transition from baryon to meson dominated matter

V. V. Begun[a,b], M. Gaździcki[b,c], M. I. Gorenstein[a,d]

[a] *Bogolyubov Institute for Theoretical Physics, Kiev, Ukraine*
[b] *Institut für Kernphysik, Geothe-University, Frankfurt am Main*
[c] *Jan Kochanowski University, Kielce, Poland*
[d] *Frankfurt Institute for Advanced Studies, Frankfurt, Germany*

One of the main goals of the NICA [91] experimental program at JINR is to investigate physical properties and phenomena in dense baryonic matter. The position of the maximum in baryon density at freeze-out is estimated in [38] using statistical model of an ideal gas of hadrons and resonances (I–HRG). This model is

conceptually simple and has only few free parameters. In spite of this it is successful in describing the bulk properties of mean hadron multiplicities in a broad range of reactions, from $e^+ + e^-$, p+p, and p+$\bar{p}$ [66] at low energies to central Pb+Pb collisions at the highest LHC energy [132–134].

The I–HRG model takes into account attractive interactions between hadrons by including the full spectrum of known hadrons and resonances but ignores repulsive interactions. The latter are needed to catch basic qualitative features of strong interactions, e.g, the phase transition between hadron–resonance gas and the quark–gluon plasma [135–137]. Moreover, they strongly modify properties of the hadron–resonance gas. The most common way to include repulsive interactions in the hadron–resonance gas model is to follow the van der Waals excluded volume procedure and introduce hard–core radii of hadrons.

If radii of all hadrons are assumed to be the same, the chemical freeze–out parameters, temperature T and baryon chemical potential $\mu_{\rm B}$, fitted to data on mean hadron multiplicities using excluded volume hadron-resonance gas (EV–HRG) are identical to those obtained within the I–HRG model [138]. However, all densities calculated within the EV–HRG model are lower than the corresponding densities obtained within I–HRG and have maximum at lower energies, see Fig. 2.13 left [139]. In particular, the energy at which net–baryon density

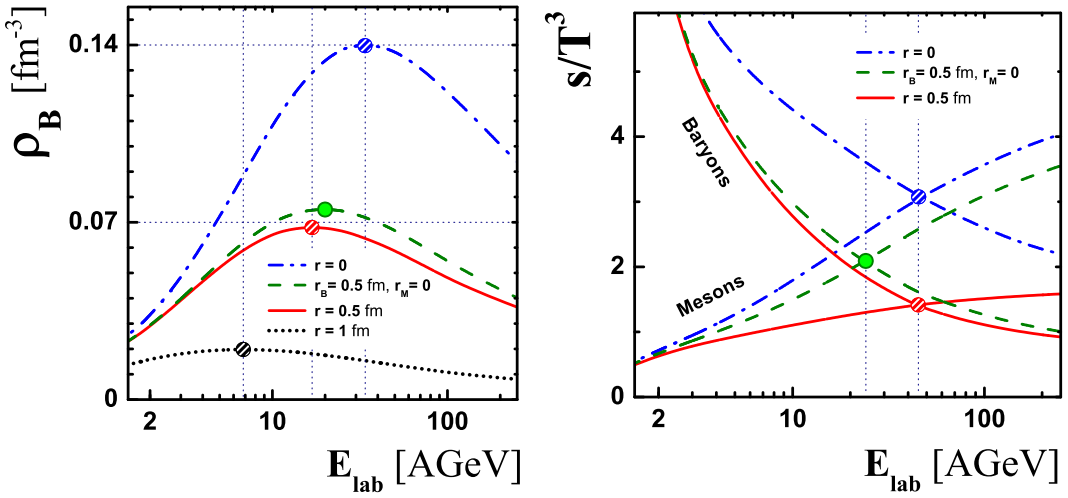

Figure 2.13: Left panel: The baryon density along the chemical freeze–out line [139]. Dashed–dotted line corresponds to the I–HRG model with point-like particles with zero hard core radius $r = 0$, dashed line to EV–HRG with baryon radiuses $r_{\rm B} = 0.5$ fm and meson radiuses $r_{\rm M} = 0$, solid line to EV–HRG with $r_{\rm B} = r_{\rm M} = r = 0.5$ fm, and dotted line to EV–HRG with $r_{\rm B} = r_{\rm M} = r = 1$ fm. Right panel: The ratios $s_{\rm B}/T^3$ and $s_{\rm M}/T^3$ along the chemical freeze–out line [139].

has a maximum decreases from about $E_{\rm lab} \cong 34A$ GeV ($\sqrt{s_{\rm NN}} \simeq 8.1$ GeV) for the I–HRG to about $E_{\rm lab} \cong 7A$ GeV ($\sqrt{s_{\rm NN}} \simeq 3.9$ GeV) for the EV–HRG with hard core radius of hadrons $r = 1$ fm [139].

The meson $s_{\rm M}$ and baryon $s_{\rm B}$ entropy densities as a function of collision energy following the freeze–out line [138] are shown in Fig. 2.13, right [139]. With increasing collision energy the baryon–dominated ($s_B > s_M$) matter changes to meson–dominated ($s_{\rm M} > s_{\rm B}$) matter. For the I–HRG model as well as for the EV–HRG with equal hard core radiuses for all hadrons this transition is located at $E_{\rm lab} \cong 46A$ GeV.

If the radii of hadrons are assumed to be different, densities of different hadrons are modified differently. In particular, the collision energy at which the transition between baryon and meson dominated matter takes place decreases from $E_{\rm lab} \cong 46A$ GeV ($\sqrt{s_{\rm NN}} \simeq 9.4$ GeV) for the I–HRG model to $E_{\rm lab} \cong 23A$ GeV ($\sqrt{s_{\rm NN}} \simeq 6.7$ GeV) for the EV–HRG model with the hard–core radii of baryons and mesons equal to 0.5 fm and 0, respectively [139]. Clearly, the excluded volume effects are even larger for the hadron matter at stages preceding the chemical freeze–out in nucleus–nucleus collisions, i.e. at larger values of the energy density.

Typical values of hard–core radii considered in the literature are $r = (0.3 \div 0.8)$ fm [140–144]. By varying the radii in the range r = (0-1.0) fm the collision energy at which the baryon density is maximal changes between $7A$ and $34A$ GeV. This range is fully covered by the NICA collider. Thus experiments at NICA will allow to study in detail freeze-out conditions in heavy ion collisions in the domain of their rapid changes. They will aslo shed light on the relation between the onset of deconfinement observed in central Pb+Pb collisions at about $30A$ GeV [145] and the freeze-out conditions.

2.9 Studying the Interplay of Strong and Electromagnetic Forces in Heavy Ion Collisions with NICA

A. Rybicki[a], *A. Szczurek*[a,b], *M. Kłusek-Gawenda*[a], *I. Sputowska*[a]

H. Niewodniczański Institute of Nuclear Physics, Polish Academy of Sciences, Kraków, Poland
University of Rzeszów, Rzeszów, Poland

In the following we stress the advantages of the NICA research programme in the context of studying the spectator-induced electromagnetic phenomena present in proton-nucleus and heavy ion collisions. We point at the specific interest of using these phenomena as a new, independent source of information on the space-time evolution of the reaction and of the non-perturbative process of particle production. We propose an extended series of measurements of well-defined observables to be performed in different types of nuclear reactions and in the whole range of collision energies available to NICA. We expect these measurements to bring very valuable new insight into the mechanism of non-perturbative strong interactions, complementary to the studies made at the SPS at CERN, RHIC at BNL, and the LHC.

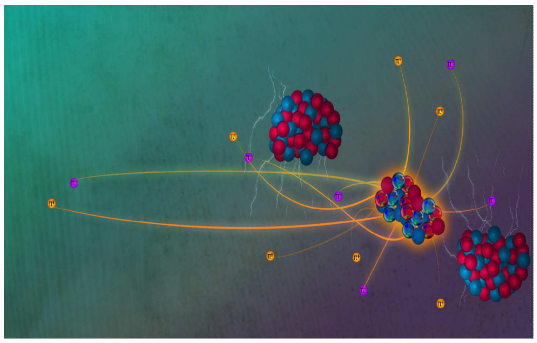

Figure 2.14: The general idea of the spectator-induced electromagnetic effect discussed in this chapter. The figure is redrawn from [146].

Introduction

The specific features of the NICA (Nuclotron based Ion Collider fAcility) research programme [147], and in particular (a) the broad range of reactions planned to be studied, (b) the relatively modest collision energy $\sqrt{s_{\rm NN}}$, placing the whole programme close to that of the CERN SPS, (c) the possibility to measure reactions at different energies, and (d) the elasticity of taking measurements both in fixed target and collider modes, make it well suitable for studying the interplay of strong and electromagnetic interactions in nuclear collisions. What we specifically address in the present proposal is the *electromagnetic interaction between charged particles produced in the collision and the nuclear remnant that does not participate directly in the reaction* (the "spectator system"). This latter phenomenon is of particular interest because, as discussed in our earlier works [148], *it provides independent information on the space time-evolution of the reaction*: the space-time evolution of the particle production process, the fragmentation (break-up) of the spectator system, and the interplay between the two. It is to be noted that with the well-known exception of HBT measurements [149,150], the experimental programmes at the SPS, RHIC and LHC provide direct information essentially only on the final (or near-to-final) state particles in *momentum space* (p_x, p_y, p_z). Much less is possible as far as providing information on the evolution of the reaction in *position space* (x,y,z), which on the other hand is extremely important in view of our understanding of the heavy ion reaction. Here NICA could strongly contribute to the overall knowledge in the whole heavy ion field, with very little competition from existing experiments. The corresponding measurements would in particular include *particle spectra, charged particle ratios* (π^+/π^-, K^+/K^-, etc.) and *directed flow*.

This discussion is organized as follows. Firstly, we discuss the principal features of the spectator-induced electromagnetic effect, with particular emphasis on its importance as a new source of information on the mechanism of the nuclear reaction. Then we define the possible future contribution of NICA. After that we shortly address the subject of competition from other experiments.

What do we know about the spectator-induced electromagnetic effect?

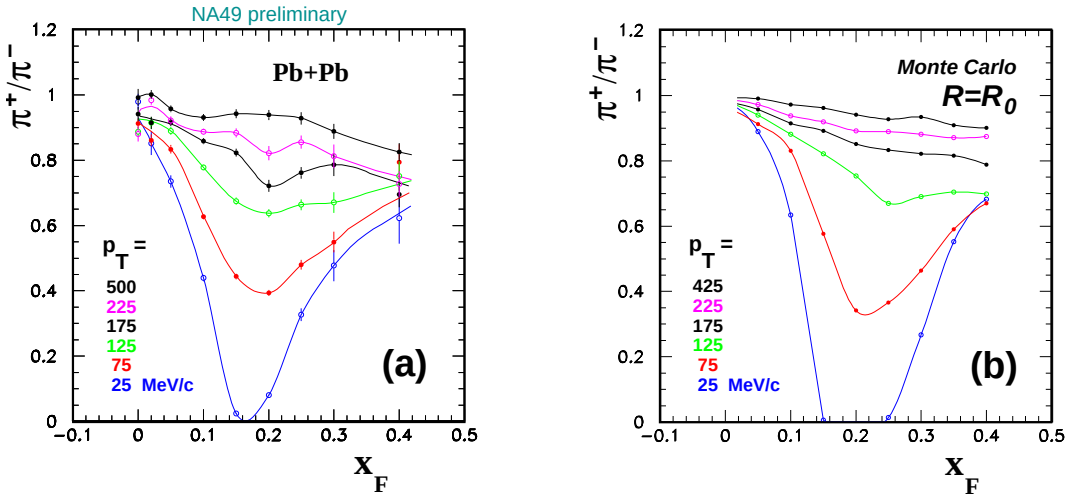

Figure 2.15: Electromagnetic distortion of charged pion ratios in the projectile hemisphere of the peripheral Pb+Pb reaction. (a) The π^+/π^- ratios measured by the NA49 experiment at the CERN SPS, drawn as a function of x_F at fixed values of p_T (listed from top to bottom curve); (b) Result of the Monte Carlo simulation described in the text. The figure comes from [157].

It is not surprising that various kinds of electromagnetic interactions in nucleus-nucleus collisions were studied in the past (a partial overview can be found in [151,152]). The problem of Coulomb corrections to HBT measurements belongs in fact to the "standard" in the analysis of heavy ion experimental data. Numerous works exist also on the influence of the electromagnetic field on the spectra of particles produced at *mid-rapidity* (that is, in the vicinity of $x_F = 0$) in central heavy ion reactions[1] [153–156]. However, these concentrate on the electromagnetic field induced by the presence of initial charge in the "participant zone", that is, the charge of the *participating nucleons*[2]. On the other hand, it seems that the theoretical and experimental analyses of the electromagnetic interactions between *nuclear remnants* and produced particles were performed mostly at lower energies. Very sizeable electromagnetically-induced distortions were observed there [158]. An important, much more recent result, was reported in nuclear collisions at several GeV/nucleon, where the non-relativistic approach to the Coulomb field brought information on the space-time evolution of the process of nuclear fragmentation [159]. In the energy regime of the CERN SPS and above, up to now our main range of interest, we were aware of only one earlier experimental measurement [160]. The latter was unfortunately restricted to a very narrow acceptance range (forward angles i.e. $p_T \approx 0$), and to an extremely small number of data points (between two and four, depending on collision centrality) which limited its scientific usefulness.

For this reason, we performed a series of experimental and theoretical studies of the influence which the spectator charge exerts on charged pion and charged kaon spectra[3] [146, 148, 157, 161–163]. Out of these, a consistent picture emerges which can be summarized as follows:

- The presence of the spectator-induced electromagnetic field brings a very sizeable distortion to π^+/π^- ratios observed in the final state of "peripheral" (large impact parameter) Pb+Pb reactions measured at a beam energy of 158 GeV/nucleon ($\sqrt{s_{\rm NN}} = 17.3$ GeV). This is shown in Fig. 2.15(a), where the x_F-dependence of π^+/π^- ratios is drawn in the projectile hemisphere of the reaction, for fixed values of pion transverse momentum p_T. This effect is so strong that the π^+/π^- ratio goes close to zero in the vicinity of $x_F = 0.15$, violating isospin symmetry and thus unequivocally confirming the electromagnetic origin of the whole phenomenon. Note that the latter value of $x_F = 0.15 = m_\pi/m_N$ corresponds, at

[1] We always define the Feynman $x_F = \frac{p_L}{p_L(max)}$ and rapidity $y = \frac{1}{2}\ln\left(\frac{E+p_L}{E-p_L}\right)$ in the nucleon-nucleon c.m.s.

[2] Note: the two electromagnetic effects discussed above, namely that induced by the participant and by the spectator charge, should be clearly differentiated as they have a different distribution over phase-space and a different centrality dependence. The participant charge will mostly influence the region closer to $x_F = 0$ in central nucleus-nucleus collisions, see above, while the spectator charge will produce the largest effect at higher values of x_F and in peripheral collisions.

[3] All the experimental results were obtained within the framework of the NA49 experiment at the CERN SPS (see [164] for a detailed description of the NA49 detector).

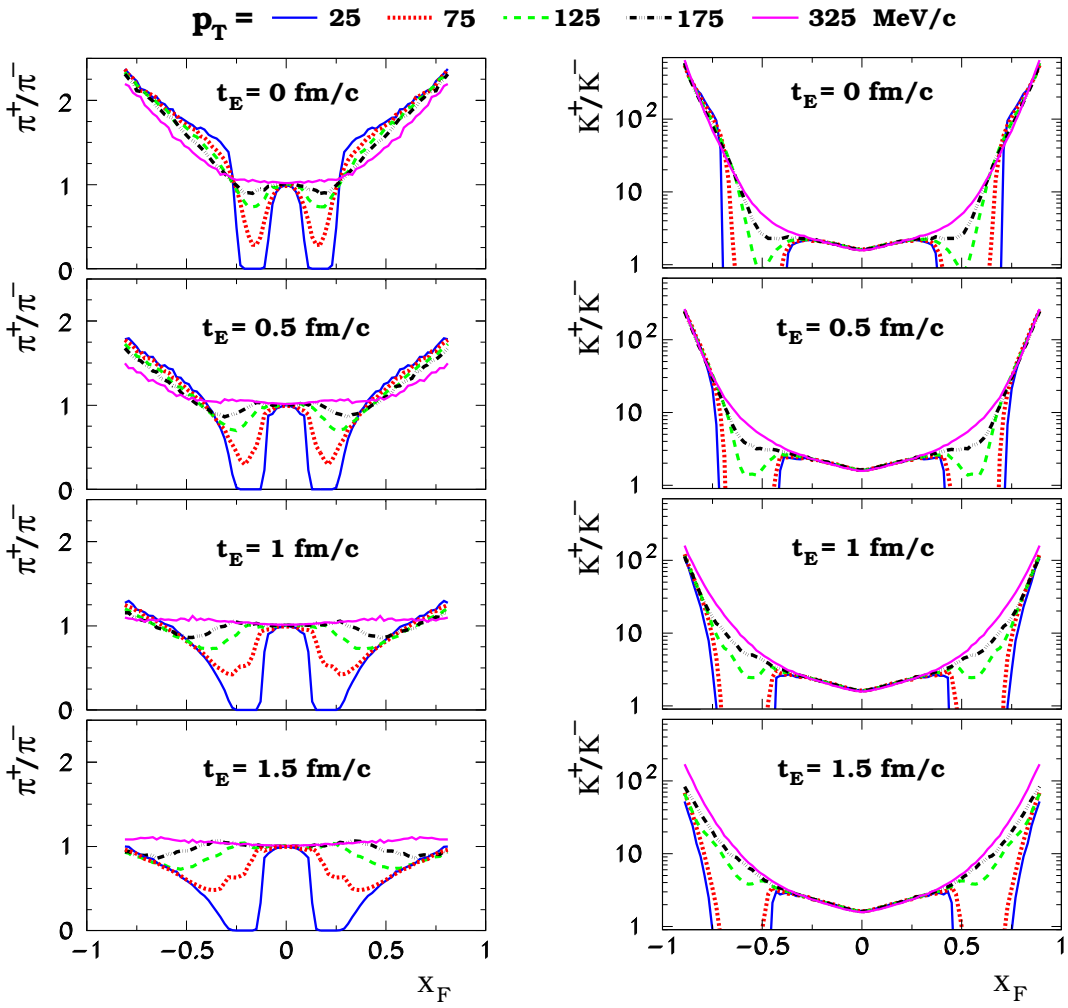

Figure 2.16: Dependence of the electromagnetic distortion of π^+/π^- (left) and K^+/K^- (right) ratios, for particles produced in peripheral Pb+Pb collisions. The different panels correspond to different pion and kaon emission times $t_{\rm E}$. The figure comes from [157].

low transverse momenta, to pions moving at the same velocity as the spectator system, thus confirming that electromagnetic repulsion (attraction) of positive (negative) pions from positively charged spectator protons is indeed at the cause of this behaviour.

- Our simple Monte Carlo model of the electromagnetic interaction [148, 161] brings a very reasonable description of the main features of this effect as shown in Fig. 2.15(b). The unique region where a more significant disagreement between data and model can be seen ($x_{\rm F} \approx 0.2$, low $p_{\rm T}$) has been identified as due to the process of *nuclear fragmentation (break-up) of the spectator system*; a discussion of this subject can be found in [163].

- A very similar electromagnetic effect is also present in high energy collisions of lead ions with lighter nuclei which we recently investigated [146].

- The electromagnetic distortion observed in Fig. 2.15(a) *depends on the specific space-time scenario imposed on pion emission.* This is illustrated in Fig. 2.16 (left) where the results of our model calculations are drawn in the full range of $x_{\rm F}$, $1 < x_{\rm F} < 1$, for different values assumed for the time of pion emission[4] $t_{\rm E}$. The characteristic distortion pattern imposed by the two spectator systems at positive and negative $x_{\rm F}$

[4]Note: we define the time of pion emission with respect to the moment of closest approach of the two colliding nuclei [148].

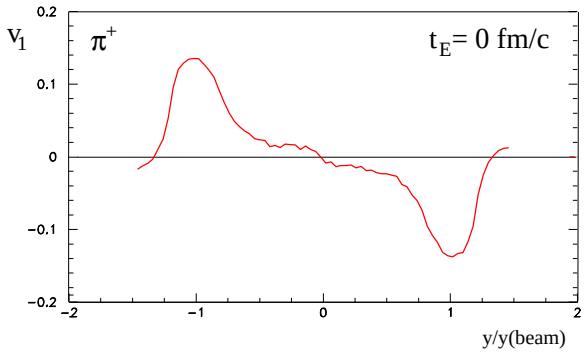

Figure 2.17: Dependence of the electromagnetically-induced directed flow of positively charged pions on the scaled pion rapidity y/y(beam). The simulation assumes the pion emission time t_E equal to zero. Directed flow is integrated over p_T from 0 to 1 GeV/c.

appears clearly sensitive to t_E (with typically lower π^+/π^- ratios obtained for larger t_E at higher values of x_F). *This implies that the electromagnetic effect provides independent information on the evolution of the non-perturbative process of pion production in space and time* [148, 161].

- The electromagnetic distortion of charged kaon (K^+/K^-) ratios, Fig. 2.16 (right), exhibits basic qualitative similarities to the effect seen for pions, however, with pronounced differences on the quantitative level. The position of the deep "valley" in the ratio is displaced towards higher values of x_F, and the region of highest sensitivity to the kaon emission time is moved towards very high x_F ($x_F > 0.75$).

- Finally, as apparent in Fig. 2.17, the spectator-induced electromagnetic force exerts also *a noticeable influence on pion directed flow, v_1*. Our very recent Monte Carlo calculation (not yet published) predicts a well-defined pattern in the rapidity dependence of the *electromagnetically-induced* directed flow of positive pions, with a large peak in the vicinity of projectile and target rapidities. As such, directed flow of charged pions (π^+, π^-) appears as another observable where, also through electromagnetic effects, new information on the space-time evolution of the reaction can become available.

The above description is, of course, highly simplified (the interested reader is invited to visit the enclosed bibliography for a more detailed account), but nevertheless constitutes a good starting point for the present proposal. As it comes from the considerations above, and as has also been suggested to us in numerous discussions with experts, the spectator-induced electromagnetic effects discussed here have very specific characteristics which make them attractive for numerous future studies:

- they can be large in specific regions of phase space;

- they can bring large distortions to various collision characteristics observed in the final state (like charged particle ratios or directed flow) and at the same time, they can provide information about the intrinsic space-time scenario of particle emission (formation times, parton fragmentation, resonance decays, hydrodynamics, etc).

As such, in principle they should be studied in any possible reaction at any possible energy, whenever this is possible. This is particularly important in the present situation where the available experimental information remains very limited. In the high energy regime (SPS energies and above), no experimental data set other than what was discussed above is known to us. No possibility of obtaining such information at RHIC or LHC is apparent to us due to strict experimental limitations. For this reason, we see here a good scientific prospect for NICA.

Possible measurements at NICA

The principal detector requirements needed in order to perform measurements of the spectator-induced electromagnetic effect are particle momentum vector reconstruction and particle identification capabilities (including in particular charge differentiation), as well as a relatively wide acceptance coverage defined in terms

of longitudinal and transverse momenta. Once these conditions are fulfilled, measurements of particle spectra (preferably double differential spectra of the type $\frac{d^2n}{dydp_T}$) become accessible. Measurements of directed flow (as well as possibly higher harmonics) are characterized by additional requirements well known to the community.

In the range of collision energies specified in [147], the NICA/MPD apparatus looks promising in view of the requirements specified above. With the extremely broad spectrum of reactions planned to be analysed, including in particular proton-nucleus and nucleus-nucleus collisions with an impressive versatility of projectiles and targets, we propose a *detailed, systematic experimental study of charged particle spectra and directed flow with a special emphasis on charge asymmetries induced by electromagnetic interactions*. Such a very broad study, taking full benefit of the possibility of cross-comparisons between different reactions (in particular also proton-nucleus collisions), of switching between fixed target and collider modes with different ranges of effective acceptance in both cases, and of comparisons of different collision energies, would in our view provide new information on the *space-time evolution of very different aspects of nuclear reactions*. In particular, these would be:

- the centrality and system-size dependence of particle production phenomena;
- the interplay between particle production and spectator fragmentation;
- azimuthal anisotropies and flow;
- the energy dependence of particle production.

All of the above are clearly basic, essential issues in heavy ion collision physics. With the advent of the NICA research programme, these could be analysed also with full use of the specific electromagnetic interaction as discussed in the present proposal.

Competition from existing experiments

As already specified above, we consider the competition from existing experiments as relatively weak with respect to the possibilities offered by NICA and its experimental community. We see at present no RHIC nor LHC experiment to be able to provide reliable measurements of the phenomena discussed here. What remains is clearly the SPS energy range where, as evident from the results presented in Fig. 2.15 above, new experimental analyses can be performed on the basis of data from the NA49 experiment [164] or from its extension, NA61/SHINE [165]. This could possibly make these experiments complementary to NICA/MPD, but with specific limitations which would require a more in-depth study.

Conclusions

The interplay of strong and electromagnetic interactions in nuclear collisions, including in particular the spectator-induced electromagnetic distortion of charged particle spectra and azimuthal anisotropies, constitutes a new, and in our opinion, very promising source of information on the space-time evolution of various processes present in the heavy ion reaction. The range of collision energies considered for NICA, together with its experimental elasticity in terms of data taking mode and of the versatile choice of interacting projectiles and targets, makes it in our opinion well suitable to bring a very valuable contribution to studies of this phenomenon.

Acknowledgments

This work was supported by the Polish National Science Centre (on the basis of decision no. DEC-2011/03/B/ST2/02634).

Bibliography

[1] A.N. Sissakian, A.S. Sorin and V.D. Toneev, *Proc. of the 33rd International Conference on High Energy Physics (ICHEP 06)*, (26 July - 2 August, Moscow 2006), p.421 [arXiv:nucl-th/0608032].

[2] P. Senger, T. Galatyuk, D. Kresan, A. Kiseleva and E. Kryshen, **PoS CPOD06,** 18 (2006).

[3] M. Gazdzicki and M. I. Gorenstein, Acta. Phys. Polon. **B 30,** 2705, (1999).

[4] C. Alt *et al.* (NA49 Collaboration), Phys. Rev. **C 77,** 024903, (2008) [arXiv:0710.0118].

[5] Z. Fodor and S. D. Katz, **JHEP 0404**, 050 (2004) [arXiv:hep-lat/0402006].

[6] N. Antoniou *et al.* (NA61/SHINE Collaboration), CERN-SPSC-2006-034.

[7] G.S.F. Stephans, *critRHIC: The RHIC low energy program*; nucl-ex/0607030.

[8] K. Grebieszkow *et al.* (NA49E Collaboration), *contributed talk at the Quark Matter 2009.*

[9] J. Adams, *et al.* (STAR collaboration), Nucl. Phys. **A 757,** 102, (2005).

[10] B.I. Abelev, *et al.* (STAR collaboration), Phys. Rev. Lett. **99,** 12301 (2007).

[11] R. J. Fries *et al.*, Phys. Rev. Lett. **90,** 202303 (2003) and references therein.

[12] C. Alt *et al.* (NA49 collaboration), Phys. Rev. **C 68,** 034903 (2003); [nucl-ex/0303001].

[13] M. Cheng et al., arXiv:0811.1006; M.A. Stephanov, arXiv:0809.3450.

[14] R.V. Gavai and S. Gupta, Phys. Rev. **D 71,** 114014, (2005).

[15] Y. Hatta and M. Stephanov, Phys. Rev. Lett. **91,** 102003 (2003).

[16] B. Mohanty, *private communication, 2009.*

[17] B. Mohanty, *talk at the Quark Matter 2009.*

[18] (NA49 Collaboration), arXiv:0808.1237.

[19] G. Roland, *talk at RHIC low energy running workshop, BNL*, March 2006.

[20] *CBM Physics Book, to be published.*

[21] W. Cassing and E.L. Bratkovskaya, Phys. Rev. **C 78,** 034919 (2008).

[22] W. Cassing, Eur. Phys. J. **ST 168,** 3, (2009).

[23] A. Peshier and W. Cassing, Phys. Rev. Lett. **94,** 172301, (2005).

[24] W. Cassing, Nucl. Phys. **A 791,** 365, (2007); **795**, 70, (2007).

[25] W. Cassing, E.L. Bratkovskaya, Phys. Rep. **308,** 65, (1999).

[26] E. L. Bratkovskaya et al., Phys. Rev. **C 69,** 054907, (2004).

[27] H. Stöcker et al., J. Phys. G. **31,** 929, (2005).

[28] O. Linnyk, E.L. Bratkovskaya and W. Cassing, Int. J. Mod. Phys. **E 17,** 1367, (2008).

[29] E. L. Bratkovskaya and W. Cassing, Nucl. Phys. **A 807,** 214 (2008);

[30] E.L. Bratkovskaya, W. Cassing and O. Linnyk, Phys. Lett. **B 67,** 428, (2009).

[31] V. P. Konchakovski *et al.*, Phys. Rev. **C 73,** 034902 (2006); **78**, 024906 (2008); **79**, 024907 (2009).

[32] V. P. Konchakovski *et al.*, Phys. Lett. **B 651,** 114 (2007).

[33] F. Becattini, J. Cleymans, A. Keränen, E. Suhonen, and K. Redlich, Phys. Rev. **C 64,** 024901, (2001).

[34] J. Cleymans, H. Oeschler, K. Redlich, and S. Wheaton, Phys. Rev. **C 73,** 034905, (2006).

[35] F. Becattini, J. Manninen, and M. Gazdzicki, Phys. Rev. **C 73,** 044905, (2006).

[36] J. Manninen and F. Becattini, Phys. Rev. **C 78,** 054901, (2008).

[37] A. Andronic, P. Braun-Munzinger, and J. Stachel, Phys. Lett. **B 673,** 142 (2009).

[38] J. Randrup and J. Cleymans, Phys. Rev. **C 74,** 047901, (2006).

[39] A. Andronic *et al.*, Nucl. Phys. **A 834,** 237, (2010)

[40] Y. Aoki *et al.*, **JHEP** 0906, 088, (2009); [arXiv:0903.4155].

[41] M. Cheng *et al.*, [arXiv:0911.3450 [hep-lat]]

[42] A. Adare et al. (PHENIX Collaboration), Phys. Rev. Lett. **98,** 162301, (2007)

[43] K. Grebieszkow (NA49 and NA61 Collaborations), Acta. Phys. Polon. **B 41,** 427, (2010); [arXiv:0911.1902 [nucl-ex]].

[44] E.L. Bratkovskaya, *private communication*

[45] A. Andronic, *private communication*

[46] http://www.gsi.de/fair/experiments/CBM/index_e.html

[47] G. Musulmanbekov (NICA Collaboration), Nucl. Phys. **A 862**, 244 (2011).

[48] http://theor.jinr.ru/twiki-cgi/view/NICA/WebHome

[49] J. D. Bjorken, Lect. Notes Phys. **56**, 93 (1976).

[50] T. Aaltonen *et al.* (CDF Collaboration), Phys. Rev. **D 83**, 112003 (2011) [arXiv:1101.0034 [hep-ex]].

[51] V. M. Abazov *et al.,* (D0 Collaboration), Phys. Rev. **D 84**, 112005 (2011) [arXiv:1107.4995 [hep-ex]].

[52] S. J. Brodsky and X. -G. Wu, [arXiv:1205.1232 [hep-ph]].

[53] S. J. Brodsky, B. von Harling, Y. Zhao (in preparation)

[54] S. J. Brodsky, P. Hoyer, C. Peterson and N. Sakai, Phys. Lett. **B 93**, 451 (1980).

[55] M. Franz, M. V. Polyakov and K. Goeke, Phys. Rev. **D 62**, 074024 (2000) [arXiv:hep-ph/0002240].

[56] S. J. Brodsky *et al.,* Proc. of the Snowmass Summer Study 1984:0227 DOE/ER/40048-21 P4.

[57] R. Vogt and S. J. Brodsky, Nucl. Phys. **B 438**, 261 (1995) [hep-ph/9405236].

[58] S. J. Brodsky, E. Chudakov, P. Hoyer and J. M. Laget, Phys. Lett. **B 498**, 23 (2001) [arXiv:hep-ph/0010343].

[59] A. Sommerfeld, Atombau und Spektralliniem (Vieweg, Braunschweig, 1944), Vol. 2, p.130. J. Schwinger, Particles, Sources, and Fields, Vol. III, p. 80. A. D. Sakharov, Zh. Eksp. Teor. Fiz. 18, 631 (1948) [Sov. Phys. Usp. 34, 375 (1991)].

[60] S. J. Brodsky and R. F. Lebed, Phys. Rev. Lett. **102**, 213401 (2009) [arXiv:0904.2225 [hep-ph]].

[61] http://nuclear.unh.edu/HPS/

[62] R. Baldini, S. Pacetti, A. Zallo and A. Zichichi, Eur. Phys. J. **A 39**, 315 (2009) [arXiv:0711.1725 [hep-ph]].

[63] R. Baldini Ferroli, S. Pacetti and A. Zallo, Nucl. Phys. Proc. Suppl. **219-220**, 32 (2011).

[64] S. J. Brodsky, I. A. Schmidt and G. F. de Teramond, Phys. Rev. Lett. **64**, 1011 (1990).

[65] S. J. Brodsky and G. A. Miller, Phys. Lett. **B 412**, 125 (1997) [arXiv:hep-ph/9707382].

[66] K. Tsushima, D. H. Lu, G. Krein and A. W. Thomas, Phys. Rev. **C 83**, 065208 (2011) [arXiv:1103.5516 [nucl-th]].

[67] S. J. Brodsky, A. H. Hoang, J. H. Kuhn and T. Teubner, Phys. Lett. **B 359**, 355 (1995) [arXiv:hep-ph/9508274].

[68] G. R. Court *et al.*, Phys. Rev. Lett. **57**, 507 (1986).

[69] S. J. Brodsky and G. F. de Teramond, Phys. Rev. Lett. **60**, 1924 (1988).

[70] W. C. Chang and J. C. Peng, Phys. Lett. B **704**, 197 (2011) [arXiv:1105.2381 [hep-ph]].

[71] A. Airapetian *et al.* (HERMES Collaboration), Phys. Lett. **B 666**, 446 (2008) [arXiv:0803.2993 [hep-ex]].

[72] J. J. Aubert *et al.* (European Muon Collaboration), Phys. Lett. **B 110**, 73 (1982).

[73] V. M. Abazov *et al.* (D0 Collaboration), Phys. Rev. Lett. **102**, 192002 (2009) [arXiv:0901.0739 [hep-ex]].

[74] S. J. Brodsky, AIP Conf. Proc. **1348**, 11 (2011) [arXiv:1012.0553 [hep-ph]].

[75] S. J. Brodsky, H. -C. Pauli and S. S. Pinsky, Phys. Rept. **301**, 299 (1998) [hep-ph/9705477].

[76] B. Gittelman, K. M. Hanson, D. Larson, E. Loh, A. Silverman and G. Theodosiou, Phys. Rev. Lett. **35**, 1616 (1975).

[77] W. S. Lockman *et al.,* Phys. Lett. **B 85**, 443 (1979).

[78] P. Chauvat *et al.* (R608 Collaboration), Phys. Lett. B **199**, 304 (1987).

[79] G. Bari *et al.*, Nuovo Cim. **A 104**, 1787 (1991).

[80] K. L. Giboni, D. DiBitonto, M. Barone, M. M. Block, A. Bohm, R. Campanini, F. Ceradini and J. Eickmeyer *et al.*, Phys. Lett. **B 85**, 437 (1979).

[81] A. Kernan and G. J. VanDalen, Phys. Rept. **106**, 297 (1984).

[82] S. P. K. Tavernier, Rept. Prog. Phys. **50**, 1439 (1987).

[83] M. H. L. S. Wang *et al.*, Phys. Rev. Lett. **87**, 082002 (2001).

[84] R. Vogt and S. J. Brodsky, Phys. Lett. **B 349**, 569 (1995) [hep-ph/9503206].

[85] J. Engelfried (SELEX Collaboration), Nucl. Phys. **A 752**, 121 (2005).

[86] S. J. Brodsky, F. -K. Guo, C. Hanhart and U. -G. Meissner, Phys. Lett. **B 698**, 251 (2011) [arXiv:1101.1983 [hep-ph]].

[87] S. J. Brodsky and B. -Q. Ma, Phys. Lett. **B 381**, 317 (1996) [hep-ph/9604393].

[88] S. J. Brodsky and S. Gardner, Phys. Rev. **D 65**, 054016 (2002), [hep-ph/0108121].

[89] S. J. Brodsky, [arXiv:1202.5338 [hep-ph]].

[90] S. J. Brodsky, A. S. Goldhaber, B. Z. Kopeliovich and I. Schmidt, Nucl. Phys. **B 807**, 334 (2009) [arXiv:0707.4658 [hep-ph]].

[91] S. J. Brodsky, B. Kopeliovich, I. Schmidt and J. Soffer, Phys. Rev. **D 73**, 113005 (2006) [hep-ph/0603238].

[92] J. P. Lansberg, S. J. Brodsky, F. Fleuret and C. Hadjidakis, [arXiv:1204.5793 [hep-ph]].

[93] S. J. Brodsky, D. S. Hwang and I. Schmidt, Phys. Lett. **B 530**, 99 (2002) [hep-ph/0201296].

[94] S. J. Brodsky, D. S. Hwang and I. Schmidt, Nucl. Phys. **B 642**, 344 (2002) [hep-ph/0206259].

[95] J. C. Collins, Phys. Lett. **B 536**, 43 (2002) [hep-ph/0204004].

[96] G. L. Kane, J. Pumplin and W. Repko, Phys. Rev. Lett. **41**, 1689 (1978).

[97] V. Barone, A. Drago and P. G. Ratcliffe, Phys. Rept. **359**, 1 (2002) [hep-ph/0104283].

[98] D. Boer, S. J. Brodsky and D. S. Hwang, Phys. Rev. **D 67**, 054003 (2003) [arXiv:hep-ph/0211110].

[99] S. Falciano *et al.* (NA10 Collaboration), Z. Phys. **C 31**, 513 (1986).

[100] K. J. Anderson *et al.*, Phys. Rev. Lett. **43**, 1219 (1979).

[101] E. L. Berger and S. J. Brodsky, Phys. Rev. Lett. **42**, 940 (1979).

[102] S. M. Berman, J. D. Bjorken and J. B. Kogut, Phys. Rev.**D 4**, 3388 (1971).

[103] D. W. Sivers, S. J. Brodsky and R. Blankenbecler, Phys. Rept. **23**, 1 (1976).

[104] J. W. Cronin *at al.,* Phys. Rev. **D 11**, 3105 (1975).

[105] F. Arleo, S. J. Brodsky, D. S. Hwang and A. M. Sickles, Phys. Rev. Lett. **105**, 062002 (2010) [arXiv:0911.4604 [hep-ph]].

[106] S. J. Brodsky and A. H. Mueller, Phys. Lett. **B 206**, 685 (1988).

[107] S. J. Brodsky and A. Sickles, Phys. Lett. **B 668**, 111 (2008) [arXiv:0804.4608 [hep-ph]].

[108] G. Bertsch, S. J. Brodsky, A. S. Goldhaber and J. F. Gunion, Phys. Rev. Lett. **47**, 297 (1981).

[109] L. Frankfurt, G. A. Miller and M. Strikman, Phys. Lett. **B 304**, 1 (1993) [hep-ph/9305228].

[110] L. Frankfurt, G. A. Miller and M. Strikman, Phys. Rev. **D 65**, 094015 (2002) [hep-ph/0010297].

[111] S. J. Brodsky and G. R. Farrar, Phys. Rev. Lett. **31**, 1153 (1973).

[112] V. A. Matveev, R. M. Muradian and A. N. Tavkhelidze, Lett. Nuovo Cim. **7**, 719 (1973).

[113] J. Polchinski and M. J. Strassler, Phys. Rev. Lett. **88**, 031601 (2002) [hep-th/0109174].

[114] G. F. de Teramond and S. J. Brodsky, [arXiv:1203.4025 [hep-ph]].

[115] S. J. Brodsky and G. P. Lepage, Phys. Rev. **D 24**, 2848 (1981).

[116] J. Aclander *et al.*, Phys. Rev. **C 70**, 015208 (2004) [nucl-ex/0405025].

[117] C. White *et al.*, Phys. Rev. **D 49**, 58 (1994).

[118] S. J. Brodsky and G. F. de Teramond, PoS QCD **-TNT-II**, 008 (2011) [arXiv:1112.4212 [hep-th]].

[119] P. V. Landshoff, Phys. Rev. **D 10**, 1024 (1974).

[120] S. J. Brodsky, C. R. Ji and G. P. Lepage, Phys. Rev. Lett. **51**, 83 (1983).

[121] K. Kovarik *et al.*, [arXiv:1111.1145 [hep-ph]].

[122] S. J. Brodsky and H. J. Lu, Phys. Rev. Lett. **64** (1990) 1342.

[123] S. J. Brodsky, I. Schmidt and J. J. Yang, Phys. Rev. **D 70**, 116003 (2004) [arXiv:hep-ph/0409279].

[124] L. Lukaszuk and B. Nicolescu, Lett. Nuovo Cim. **8**, 405 (1973).

[125] J. Bartels, Nucl. Phys. **B 175**, 365 (1980).

[126] B. Nicolescu, [arXiv:0707.2923 [hep-ph]].

[127] C. Ewerz, DESY-PROC-2009-02.

[128] E. A. Kuraev, L. N. Lipatov and V. S. Fadin, Sov. Phys. JETP **44**, 443 (1976) [Zh. Eksp. Teor. Fiz. **71**, 840 (1976)].

[129] C. Merino, S. J. Brodsky and J. Rathsman, Nucl. Phys. Proc. Suppl. **86**, 183 (2000).

[130] A. N. Sissakian *et al.* (NICA Collaboration), J. Phys. G **36**, 064069 (2009)

[131] F. Becattini and U. W. Heinz, Z. Phys. **C 76**, 269 (1997) [Erratum-ibid. **C 76**, 578 (1997)], F. Becattini, Z. Phys. **C 69**, 485 (1996).

[132] M. Floris, J. Phys. G **38**, 124025 (2011);

[133] A Kalweit (ALICE Collaboration), Acta Phys. Polon. B, Proc. Suppl. **5**, 225 (2012);

[134] B. Abelev *et al.* (ALICE Collaboration), Phys. Rev. Lett. **109**, 072301 (2012).

[135] M. I. Gorenstein, V. K. Petrov, and G. M. Zinovjev, Phys. Lett. **B 106**, 327 (1981); D. H. Rischke, M. I. Gorenstein, H. Stöcker, and W. Greiner, Z. Phys. **C 51**, 485 (1991);

[136] J. Cleymans, M. I. Gorenstein, J. Stalnacke, and E. Suhonen, Phys. Scripta **48**, 277 (1993).

[137] M. I. Gorenstein, H. Stoecker, G. D. Yen, S. N. Yang, and W. Greiner, J. Phys. G **24**, 1777 (1998).

[138] J. Cleymans, H. Oeschler, K. Redlich, and S. Wheaton, Phys. Rev. **C 73**, 034905 (2006).

[139] V. V. Begun, M. Gazdzicki and M. I. Gorenstein, arXiv:1208.4107 [nucl-th], submitted to Phys. Rev. C.

[140] G. D. Yen, M. I. Gorenstein, W. Greiner, and S. N. Yang, Phys. Rev. **C 56**, 2210 (1997); G. D. Yen and M. I. Gorenstein, Phys. Rev. **C 59**, 2788 (1999).

[141] P. Braun-Munzinger, K. Redlich and J. Stachel, *In *Hwa, R.C. (ed.) et al.: Quark gluon plasma* 491-599* [nucl-th/0304013];

[142] P. Braun-Munzinger, I. Heppe and J. Stachel, Phys. Lett. **B 465**, 15 (1999)

[143] A. Andronic, P. Braun-Munzinger, J. Stachel and M. Winn, Phys. Lett. **B 718**, 80 (2012)

[144] D. R. Oliinychenko, K. A. Bugaev and A. S. Sorin, [arXiv:1204.0103 [hep-ph]].

[145] M. Gazdzicki, M. Gorenstein and P. Seyboth, Acta Phys. Polon. **B 42**, 307 (2011).

[146] I. Sputowska, A. Rybicki, to appear in Eur. Phys. J. Web of Conf.

[147] G. Trubnikov, *NICA Project in Dubna, 1st JINR-CERN School on GRID and Management Information Systems*, (Dubna, October 2010).

[148] A. Rybicki, A. Szczurek, Phys. Rev. **C 75**, 054903 (2007).

[149] G. Baym, Acta Phys. Polon. **B29** (1998) 1839.

[150] K. Aamodt *et al.*, (ALICE Collaboration), Phys. Lett. **B 696**, 328 (2011) and references therein.

[151] J. Bartke, *Introduction to Relativistic Heavy Ion Physics*, (Hackensack, USA: World Scientific (2009)), and references therein.

[152] A. Rybicki, *Report no. 2040/PH, H. Niewodniczański Institute of Nuclear Physics, Polish Academy of Sciences, Kraków, Poland.*

[153] L. Ahle *et al.*, (E802 Collaboration), Phys. Rev. **C 57**, 466 (1998).

[154] (NA44 Collaboration), Nucl. Phys. **A 610**, 175 (1996).

[155] H. W. Bartz, J. P. Bondorf, J. J. Gaardhoje and H. Heiselberg, Phys. Rev. **C 57**, 2536 (1998).

[156] T. Osada, S. Sano, M. Biyajima and G. Wilk, Phys. Rev. **C 54**, 2167 (1996).

[157] A. Rybicki, A. Szczurek, E. Kozik, Acta Phys. Polon. Supp. **5**, 369 (2012).

[158] W. Beneson *et al.*, Phys. Rev. Lett. **43**, 683 (1979). J. P. Sullivan *et al.*, Phys. Rev. **C 25**, 1499 (1982).

[159] V. A. Karnaukhov *et al.*, Phys. Atom. Nucl. **69** (2006) 1142, and references therein.

[160] NA52 Collab., G. Ambrosini *et al.*, New J. Phys. **1**, 23 (1999).

[161] A. Rybicki, PoS(EPS-HEP 2009) 031.

[162] A. Szczurek, A. Rybicki, A. Z. Górski, J. Phys. **G 34**, 827 (2007).

[163] A. Rybicki, Acta Phys. Polon. **B 42**, 867 (2011).

[164] S. Afanasiev *et al.*,(NA49 Collaboration) Nucl. Instrum. Meth. **A 430**, 210 (1999).

[165] N. Abgrall *et al.*, (NA61/SHINE Collaboration), Phys. Rev. **C 84**, 034604 (2011).

3 Phases of QCD matter at high baryon density

There has been an impressive progress in the understanding of the QCD phase diagram in recent years. This concerns in particular the phases at high baryon density: at low temperature, one expects the emergence of the color superconductivity phase. The classification in terms of large N_c (number of colors) behavior suggests the confined baryonic phase where the thermodynamic quantities scale proportionally to N_c (resembling for example the Skyrme crystal) – the "quarkyonic" phase. At high baryon density, the confined and deconfined phases are separated by a first order phase transition line that is expected to terminate at a chiral critical point. This critical point is likely located at a baryon density that is within the reach of the NICA collider. A number of related phenomena amenable to experimental observation are considered in this section. An interesting set of problems discussed here is related to the non-equilibrium and finite-size behavior in deconfined matter.

3.1 Comments on a phase diagram and fluctuations

M. Stephanov

University of Illinois, Chicago, USA

QCD phase diagram (contemporary view, Fig. 3.1**)**

- Models (and lattice) suggest crossover turns into first- order at some $\mu_{\rm B}$.
- Large $\mu_{\rm B}$ - Color Flavor Locked phase ("QCD ice").
- Crossover - "supercritica" fluid. Almost perfect. Strongly coupled. New methods needed.

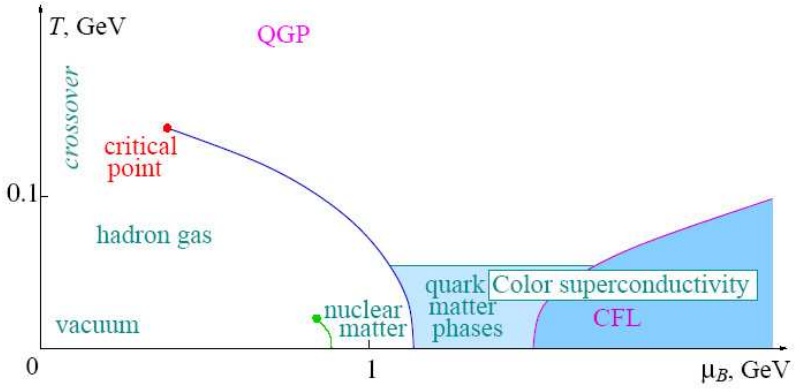

Figure 3.1: Phase diagram.

Location of the critical point vs freeze-out, Fig. 3.2
Needed:

- Energy-scan experiments:
  RHIC,
  NA61(SHINE)@SPS,
  CBM@FAIR/GSI,
  NICA
- Improve lattice predictions – understand systematic errors
- Understand critical phenomena in the dynamical environment of a heavy ion collision
  – understand background
  – develop optimal signatures.

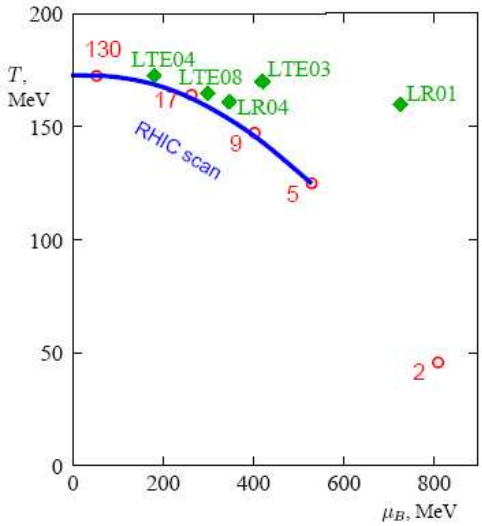

Figure 3.2: Estimates of a critical end point.

Fluctuation signatures, Fig. 3.3

- Experiments measure for each event: multiplicities $N\pi, N_p, ...$, momenta p, etc. These quantities fluctuate event-by-event.
  – Typical measure is standard deviation, e.g., $< (\delta N)^2 >$.
- What is the magnitude of these fluctuations near the critical point [41] ?
- *Universality* tells how it grows at the critical point: $< (\delta N)^2 > \sim \xi^2$.
  – Correlation length is a universal measure of the "distance" from the critical point. It diverges as $\xi \sim (\Delta\mu \text{ or } \Delta T)^{-2/5}$ as the critical point is approached.

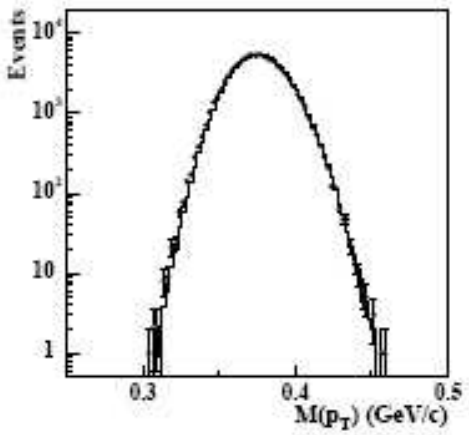

Figure 3.3: Transverse momentum fluctuation.

- Magnitude of ξ is limited by finite time/size effects: $\mathcal{O}(3 \text{ fm})$ – [2].
- "Shape" of the fluctuations can be also measured: non-Gaussian moments. As $\xi \to \infty$ fluctuations become more non-Gaussian.

- Higher cumulants show even stronger dependence on ξ [3]:

$$< (\delta N)^3 > \sim \xi^{4.5}, \quad < (\delta N)^4 > -3 < (\delta N)^2 >^2 \sim \xi^7$$

which makes them more sensitive signatures of the critical point.

Observables – theory comments

- Fluctuations:
  – Multiplicities –
  pro: larger signal – especially protons (coupled to critical mode);
  con: larger background (impact parameter fluctuations)
  – Ratios, mean $p_{\rm T}$ –
  pro: no impact parameter fluctuations;
  con: smaller signal.
  – Non-gaussian fluctuations (higher moments: skewness, kurtosis) –
  pro: strong dependence on ξ – large signal;
  con: difficult to estimate either signal or background.
  – Fluctuations from first- order transition (nonequilibrium)?
  pro: presumably more dramatic;
  con: difficult to predict – requires more detailed dynamic assumptions.
- Non-fluctuation observables: $\bar{p}/p$ – Asakawa-Bass-Möller-Nonaka; based on focusing – trajectories are "pulled" to larger $\mu_{\rm B}$ at earlier times + earlier freezeout of higher $p_{\rm T}$
- True critical point signal should show consistently in several observables.

3.2 Search for manifestation of medium effects in dense, excited hadron-quark matter

D. Voskresensky

Moscow Engineering Physics Institute, Russia

EoS and particle abundance. There are different possibilities for the behavior of the hadron masses, couplings, widths at finite temperature and density:

Following (partial) chiral symmetry restoration and the Brown-Rho scaling ideas, masses of hadrons and their coupling constants may decrease with increase of the density and the temperature. This behavior essentially affects particle occupations and the Equation of State (EoS). A rather appropriate EoS at $T = 0$ (fitted to the description of global properties of atomic nuclei and neutron stars) can be constructed at approximately the same suppression of masses and couplings (universal, or approximately universal suppression) [4]. Here one should stress necessity of *a simultaneous analysis of the relevant phenomena in different domains of nuclear physics (hadron scattering, atomic nuclei, neutron stars, heavy-ion collisions)* to construct an appropriate EoS, cf. [5]. Analysis of [6] shows that with mentioned approximately universal suppression the calculated pressure at large temperatures T proves to be much higher than that follows from the modern lattice calculations. Thus, if one believes the lattice data (for large temperatures, $T \gtrsim 170$ MeV), one should assume an additional suppression of the hadron couplings with the temperature at $T \sim T_c$, otherwise the phase transition to sQGP would not be energetically favorable. With suppressed couplings and masses the quasiparticle approximation proves to be operative in a broad temperature-density region at least for part of hadron species.

Opposite, in case when hadron couplings are assumed to be not decreased with the density and the temperature (strong coupling limit) the gap between upper and lower baryon continua may become blurred [7] with increase of the temperature. For $T \gtrsim T_{\rm bl}$ ($T_{\rm bl} \sim m_\pi$ at small baryon chemical potential) the abundance of baryon- antibaryon blurs (described by completely regular Green functions) is exponentially increased. Boson masses are diminished due to fermion blur - boson quasiparticle interactions. Some boson species may even undergo a hot boson condensation. The pressure increases substantially above that calculated on the lattice. If were so, one could expect a broad region of a hadron porridge of mesons and baryon blurs. Some of these hadron species can be melt into quark constituents leading to the state of strongly interacting hadron-quark porridge (a mixed phase).

Dynamics of the phase transition.

In assumption of the first-order hadron-sQGP phase transition in the vicinity of the endpoint all processes develop very slowly [8]. Thus in heavy ion collisions the expanding fireball may linger in the sQGP state, until $T(t)$ decreases well below the corresponding equilibrium value of the endpoint temperature. Far from the endpoint fluctuations may grow much faster provided the system reaches spinodal decomposition region. Appearing an aerosol mixture (a mixed phase) may manifest in observables. Ref. [8] also points on essential role of viscosity and finite size effects (surface tension) in the mixed phase preparing in the dynamics of the first-order phase transition. Fluctuations at the hadron-sQGP phase transition (at a finite baryon density) grow and dissolve, as if the fluid were effectively very viscous.

Critical fluctuations.

Analysis of [9] demonstrates that the fluctuation region (a mixed phase) at the color superconducting second-order phase transition at thermal equilibrium might be very broad ($0.5 \div 1.5\ T_c$) and thus, at least, some effects might be visible in heavy-ion collisions provided the critical temperature of the transition is sufficiently high. Although a critical slowing down effects smear effects of thermodynamical fluctuations, one may hope to observe some deviations in fluctuation effects compared to those from trivial statistical fluctuations.

Experiments with heavy-ions in a broad region of the beam energies (at a monotonous increase of the collision energy with a certain energy step) are welcome in order to distinguish above mentioned effects. One may hope to observe a non-monotonous behavior of different observables at a step-by-step increase of the collision energy in some energy interval.

3.3 Searching for evidence of spinodal decomposition

J. Randrup

Nuclear Science Division, Lawrence Berkeley National Laboratory, Berkeley, California, USA

The phase structure of strongly interacting matter forms a focal point for current theoretical and experimental investigations around the world. The Relativistic Heavy Ion Collider (RHIC) at BNL is preparing for a beam energy scan that aims to identify signals of the expected critical point and the CBM experiment at the future Facility for Antiproton and Ion Research (FAIR) at GSI will explore the properties of compressed baryonic matter in the deconfined phase as well as search for evidence of the expected confinement phase transition. The

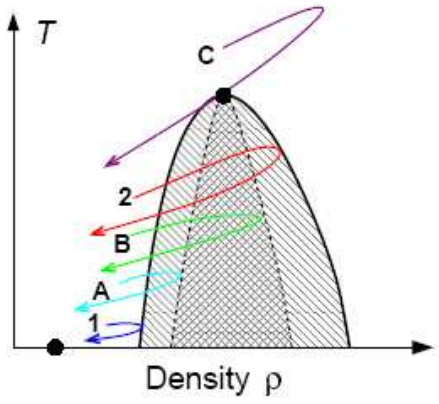

Figure 3.4: Dynamical phase trajectories for the most compressed matter produced at various threshold collision energies E_1, E_A, E_B, E_2, E_c. The solid curve shows the phase co-existence boundary: at a given temperature $T < T_c$, bulk systems at the densities $\rho_1(T)$ and $\rho_2(T)$ are in thermodynamic equilibrium; the lower and higher coexistence boundaries meet at the critical point (ρ_c, T_c); uniform matter is thermodynamically unfavored inside the coexistence region. The dashed curve shows the boundary within which uniform matter is mechanically unstable and entropy can be gained by infinitesimal irregularities.

contemplated Nuclotron-based Ion Collider Facility at JINR would complement those programs by focussing on collision energies where the bulk of the collision system receives maximum exposure to the mixed phase (these

relatively low collision energies can most likely not be provided by RHIC). Generally speaking, one may expect that the prospects for learning about the mixed phase would improve with the time spent by the bulk of the system inside the coexistence region of the phase diagram. Fig. 3.4 illustrates how this quantity develops with the collision energy.

A first-order phase transition is inherently accompanied by the phenomenon known as spinodal decompositon, a clumping with a characteristic spatial scale [10, 11]. Intuitively, one would expect that collision energies slightly below $E_{\rm B}$ would be optimal for maximizing the time spent by the phase trajectory inside the spinodal region. Such collisions, in turn, would presumably be most favorable for the spinodal instabilities to develop. Recent transport calculations of phase trajectories [12] suggest that this optimal beam energy is $E_{\rm lab} = 5 - 15$ AGeV for a stationary target setup, corresponding to a total beam energy of $1.8 - 2.8$ AGeV in a collider. [The precise values depend not only on the specific location of the spinodal phase boundaries, i.e. on the specific equation of state (which is still unknown), but also on the complications arising from the non-uniformity of the density and its time evolution.] Rough estimates indicate that collisions within a suitably tuned energy range may produce bulk matter that stays inside the mechanically unstable phase region sufficiently long for some degree of spinodal decomposition to develop [13]. However, reliable predictions cannot yet be made which underscores the need for identifying observable consequences of such a clumping.

3.4 Supercooled quark-gluon phase?

Yu. Ivanov

Kurchatov Institute, Moscow, Russia

A prime goal of planned experiments at NICA is search for onset of a phase transition to the quark-gluon phase. Presently theoretical models indicate that this should be a first-order phase transition. A phase transition, first of all, implies certain softening of the equation of state (EoS) as compared to a hadronic EoS without any transition. Therefore, experimental evidences of such softening can be viewed as a signal of the deconfinement transition. In fact, there are such evidences: directed flow data favor a steady softening of the EoS with increasing beam energy [14], proton rapidity distributions also require a softer EoS at lower SPS energies [15]. The above analysis was performed within a 3-fluid dynamical model [14]. At the same time, there is no model which, based on the same unique EoS (or mean-field interaction in kinetic models), reproduces all the body of available experimental data, from AGS to SPS energies, on such a "trivial" mechanical characteristics of nuclear collisions as proton rapidity distributions, transverse momentum spectra, directed and elliptic flows. It means that we do not quite well understand the global dynamics of nuclear collisions in this energy range. Hydrodynamical simulations with a EoS involving the first-order phase transition within the Maxwell construction do not help to improve this reproduction. A probable reason for these theoretical problems is that a phase transition occurs but the Maxwell construction is not applicable for its description in nuclear collisions at high incident energies. Indeed, the Maxwell construction implies adiabatically slow evolution of the matter, when seeds of the new phase have enough time to grow to their equilibrium value and thus form a mixed phase. As it was demonstrated in recent papers [8, 13], the rate of the fluctuation growth in the phase-transition region is very slow as compared with the collective evolution of the matter. Precisely this makes the Maxwell construction inapplicable. The slow growth of seeds of hadronic phase in the rapidly expanding quark-gluon matter may result in that the system pass by the mixed phase and directly gets into a phase of the supercooled quark-gluon matter. In particular, this supercooled matter will hadronize at lower temperatures and/or baryon densities than those predicted by thermodynamics based on the mixed-phase concept. Since growth of fluctuations in the supercooled state is already very fast, the hadronization of this supercooled quark-gluon matter has already an explosive character. This is an alternative scenario to the mixed-phase one which should be considered. The above scenario has its practical consequences. From the theoretical point of view:

- It is necessary to construct EoS's based on the concept of the supercooled quark-gluon matter rather than the corresponding mixed phase.
- It is necessary to adapt hydrodynamic models for work with such kind of EoS's.
- It is necessary to study fluctuations at the explosive hadronization of the supercooled matter and consider chances for these fluctuations to survive in the evolution of already hadronic phase to its freeze-out.

Note that while first steps in realization of the first two points have been already done [8, 13], the work on the last point has not been even started. From the experimental point of view:

- Excitation functions of such a conventional "mechanical" observables as rapidity distributions, transverse momentum spectra, directed and elliptic flows are required. A large body of such data is already available from experiments at AGS and SPS. However, in the range of lower SPS energies, which is most suspicious on the possible onset of deconfinement, these data are still fragmentary. NICA is going to well cover this energy range. These observables reflect softness of the EoS and hence are directly relevant to the search for a phase transition.

- Measurements of event-by-event fluctuations are required.

3.5 Rigorous investigation of surface tension and finite width of the QGP bags at NICA energies

K. Bugaev

Bogolyubov Institute for Theoretical Physics, Kiev, Ukraine

Extensive experimental and theoretical searches for the (tri)critical endpoint of the strongly interacting matter became one of the focal point of the modern nuclear physics. These searches are one of the primary goals of the planned low energy experimental programs at RHIC (BNL), SPS(CERN), NICA (Dubna) and FAIR (GSI). However, at present neither the Equation of State (EoS) of strongly interacting matter, nor the exact location of the deconfnement Phase Transition (PT) and/or cross-over are known. Moreover, on the one hand the lattice QCD simulations of different groups disagree with each other on the location of the (tri)critical QCD endpoint, and on the other hand the results of mean-field models are not informative. The commonly used Pisarski-Wilczek argument based on the universality properties is, strictly speaking, valid for the chiral restoration PT whereas for the deconfinement PT it might be irrelevant. Furthermore, such line of arguments does not explain the reason why, depending on the number of flavors, the finite masses of light quarks demolish the 1-st or 2-nd order PT at low baryonic densities and do not destroy it at high densities. Therefore, the searches for the physical cause that is responsible for a degeneration of the 1-st order deconfinement PT at high baryonic densities to a weaker PT at the (tri)critical endpoint and to a cross-over at low baryonic densities are of great importance for heavy ion phenomenology. Moreover, there exists a huge list of unanswered (and often ignored!) questions related to the following two main problems of modeling PT in finite systems which are probed in the nuclear laboratories:

- how the EoS with PT is modified in finite systems; and

- how the endpoint properties would look like in a finite system.

These problems are routed in the fact that, despite many progress reports, there are only a few general guesses how to define PT and the corresponding analogs of phases in finite systems while the rigorous treatment of this problem is at the initial stage of research [17].

It turns, however, out that investigation of the strongly interacting matter EoS based on the exactly solvable models [17–21] is vitally necessary for a success of NICA program. First of all the modern statistical model of the liquid-vapor PT teach us that the vanishing surface tension coefficient plays a crucial role in the (tri)critical endpoint existence [17]. This fact was put into the grounds of the Quark Gluon Bags with Surface Tension Model (QGBSTM) [18] which enable us to work out a unified statistical description of the 1-st and 2-nd order deconfinement PT with the cross-over. This model naturally explains that the reason for degenerating the 1-st order deconfinement PT into a weaker PT at the endpoint and into a cross-over at low baryonic densities is due to negative surface tension coefficient of the QGP bags at high energy densities [18]. It is shown that the QGBSTM has a tricritical point since the deconfined QGP phase must be separated from the cross-over QGP by another PT which is induced by the change of sign of the surface tension coefficient of large bags [18]. Very recently this model was developed further in order to generate the critical endpoint [19].

Despite the considerable success of the statistical models [17–19] discussed above and their remarkable features, all of them (and all other ones!) face two conceptual problems [20] that can be formulated as following:

- Why the QGP bags and/or strangelets are never directly observed in experiments?

- Why we do not observe more hadronic resonances with masses above 2.5 GeV?

These conceptual problems have been resolved recently [20] by the inclusion of the Gaussian width of the QGP bags which depends on the bag's volume. Such a model, the Finite Width Model (FWM), not only naturally generates the linear temperature dependence of the QGP pressure at low temperatures which is well known from the lattice QCD, but also it explicitly demonstrates that the large and/or heavy QGP bags can be regarded as the objects belonging to the Regge trajectories. Thus, at hight temperatures the average mass and width of the QGP bags behave in accordance with the upper bound of the Regge trajectory asymptotics (the linear asymptotics), whereas at low temperatures they obey the lower bound of the Regge trajectory asymptotics (the square root one) [20].

Counting all this I conclude that there are three main directions of research which will resolve two main problems of modeling a PT in finite systems and will help us to establish the leadership of NICA project both in theoretical and experimental studies compared to other low-energy programs (see the thorough discussions in [21]):

- **to drastically improve the exactly solvable models and rigorously extend them to finite systems**: to normalize the QGBSTM [18, 19] onto the existing lattice QCD data and reproduce the deviation of the QGP EoS from the Stefan-Boltzmann limit at zero baryonic densities; include the nonzero baryonic and strange chemical potentials into the QGBSTM inspired models [18,19] and test them on the measured particle yield ratios; study the critical exponents of the QGBSTM [18, 19] and their possible modifications in finite systems on the basis of the Laplace-Fourier method [17]; investigate the influence of the Fisher index τ on the values of critical indices of the QGBSTM inspired models and the possible determination of τ value from the cluster scaling picture [21] emerging from the heavy ion collisions data; include the Lorentz contraction of the excluded volumes of light hadrons into the QGBSTM [18, 19], improve the existing Van der Waals extrapolations according to relativistic prescription, calculate the kinetic coefficients for hadronic matter and QGP bags below and above cross-over and determine the free parameters from the comparison with the AdS/CF results.

- **to study all aspects of the surface tension of the QGP bags**: generalize the Hills and Dales model [17] to the clusters with the continuous base of deformations and use it to estimate the surface entropy of the QGP bags; examine the bimodal [17] and monomodal [21] properties of finite QGP matter with positive and negative surface tension coefficient, respectively, to formulate possible signals of the deconfinement PT, the cross-over transition and surface-induced PT [18] in finite systems; study the volume-surface fluctuations of QGP bags in the grand canonical, canonical and microcanonical ensembles in order to reconstruct an actual surface tension coefficient of the QGP bags; investigate the HBT radii of highly nonspherical QGP bags above the cross-over and the HBT emission volume event-by-event fluctuations for soft photons and pions as the possible signals of negative surface tension coefficient; elucidate the surface tension coefficient of QGP bags from the LQCD data and establish the relation between the surface tension coefficient and the string tension one; study the in influence of shape deformations with positive heights (hills) on the fusion and decay rates of QGP bags to describe the kinetics and hydro-kinetics of the 1-st order PT in finite systems.

- **to investigate the role of the QGP bags finite width**: estimate the mean width of heavy hadronic resonances from the review of the Particle Data Group; consider the large N_c limit of the FWM and establish the connection between the FWM and the corresponding limit of the QCD and QCD inspired models; elucidate the width of QGP bags directly from the LQCD data of the metastable branch of the QGP EoS; work out a microscopic model of sequential decay of heavy QGP bags and find out the constraints on the width of these bags from the particle yields data measured in the collisions of elementary particles at high energies and from the nuclear collisions data on the early hadronizing particles; investigate the processes of melting and propagation of QGP bags in the dense and hot media in order to study the low energy jet evolution; combine all the features of the EoS found while completing the projects related to the surface tension of the QGP bags. A completion of this proposal will essentially advance the theoretical backup of NICA project and will allow us to formulate the firm signals of the mixed phase formation in finite systems.

3.6 Isospin effects on phase transitions of hadronic to quark matter

M. Di Toro[a,b], V. Greco[a,b], B. Liu[c,d], and S. Plumari[2]

[a] *Laboratori Nazionali del Sud, Catania, Italy*
[b] *University of Catania, Catania, Italy*
[c] *Center of Theoretical Nuclear Physics, National Laboratory of Heavy Ion Accelerator, Lanzhou, China*
[d] *Institute of High Energy Physics, Chinese Academy of Sciences, Beijing, China*

The phase transition of hadronic to quark matter at high baryon and isospin density is analyzed. Nonlinear relativistic mean field models are used to describe hadronic matter, and the MIT bag model is adopted for quark matter. The boundaries of the mixed phase and the related critical points for symmetric and asymmetric matter are obtained. Isospin effects appear to be rather significant. The binodal transition line of the (T, ρ_B) diagram is lowered in a region accessible to heavy ion collisions in the energy range of the NICA project. Some observable effects are suggested, in particular a "neutron distillation" mechanism. Theoretically a very important problem appears to be the suitable treatment of the isovector part of the interaction in effective QCD lagrangian approaches.

On the transition to a mixed hadron-quark phase at high baryon and isospin density

Several suggestions are already present about the possibility of interesting isospin effects on the transition to a mixed hadron-quark phase at high baryon density [22–25]. This seems to be a very appealing physics program for the NICA project if heavy ion beams will be available with good intensities in the energy region $E_{\rm lab}$ =1 – 10 AGeV. The weak point of those predictions is the lack of a reliable equation of state that can describe with the same confidence the two phases, hadronic and deconfined. On the other hand this also represents a strong theory motivation to work on more refined effective theories for a strong interacting matter. The argument in favor of noticeable isospin effects on the hadron-quark transition at high density is very simple and can be easily derived from the Fig. 3.5, where we compare typical Equations of State for Hadron and Quark Matter (at zero temperature) for symmetric $\alpha \equiv \rho_n - \rho_p/\rho_B \equiv -\rho_3/\rho_B = 0$ and neutron matter ($\alpha = 1$). For the Hadron part we use a Relativistic Mean Field [26] result with non-linear terms and effective ρ-meson coupling for the isovector part, largely used to study isospin effects on meson production and collective flows [24, 27]. The energy density and the pressure for the quark phase are, respectively, given by the MIT Bag model [28] (two-flavor case):

$$\varepsilon = 3 \times 2 \sum_{q=u,d} \int \frac{d^3k}{(2\pi)^3} \sqrt{k^2 + m_q^2}\, (f_q + \bar{f}_q) + B \,, \tag{3.1}$$

$$P = \frac{3 \times 2}{3} \sum_{q=u,d} \int \frac{d^3k}{(2\pi)^3} \frac{k^2}{\sqrt{k^2 + m_q^2}}\, (f_q + \bar{f}_q) - B \,, \tag{3.2}$$

where B denotes the bag constant (the bag pressure), taken as a rather standard value from the hadron spectra (no density dependence), $m_{\rm q}$ is the quark mass, and $f_{\rm q}$, $\bar{f}_{\rm q}$ represent the Fermi distribution functions for quarks and anti-quarks. The transition to the more repulsive quark matter should appear around the crossing points of the two EoS. We see that such crossing for symmetric matter ($\alpha_{\rm H} = \alpha_{\rm Q} = 0$) is located at rather high density, $\rho_{\rm B} = \rho_{\rm Q} = 1$, while for pure neutron matter ($\alpha_{\rm H} = \alpha_{\rm Q} = 1.0$) the crossing is moving down to about three times ρ_0. Since we have a coexistence transition region we would expect to see some mixed phase effects already at relatively low density for asymmetric systems, easily reached in relativistic heavy ion collisions.

We note that the above argument is rather independent of the used Hadron EoS at high density, quite stiff in agreement with collective flow and kaon production data [6]. For the quark part the lack of explicit isovector interactions could represent a problem. In fact we can study in detail the isospin dependence of the transition densities [22–24]. The structure of the mixed phase is obtained by imposing the Gibbs conditions [30]

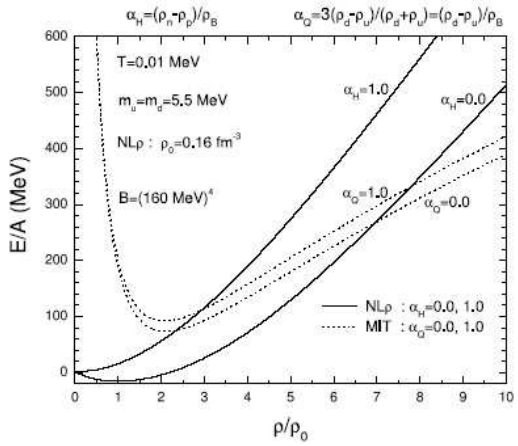

Figure 3.5: EoS of Symmetric/Neutron Matter: Hadron (NLρ), solid lines, vs. Quark (MIT-Bag), dashed lines. $\alpha_{\rm H,Q}$ represent the isospin asymmetry parameters respectively of the hadron,quark matter: $\alpha_{\rm H,Q}=0$, Symmetric Matter; $\alpha_{\rm H,Q}=1$ Neutron Matter.

for chemical potentials and pressure and by requiring the conservation of the total baryon and isospin densities

$$\begin{aligned}
\mu_{\rm B}^H(\rho_{\rm B}^H,\rho_3^H,T) &= \mu_{\rm B}^Q(\rho_{\rm B}^Q,\rho_3^Q,T)\ ,\\
\mu_3^H(\rho_3^H,\rho_3^3,T) &= \mu_3^Q(\rho_3^Q,\rho_3^3,T)\ ,\\
P^H(\rho_{\rm B}^H,\rho_3^H,T) &= P^H(\rho_{\rm B}^Q,\rho_3^Q,T)\ ,\\
\rho_{\rm B} &= (1-\chi)\rho_{\rm B}^H+\chi\rho_{\rm B}^Q\ ,\\
\rho_3 &= -\alpha\rho_{\rm B}=(1-\chi)\rho_3^H+\chi\rho_3^Q\ ,
\end{aligned}\tag{3.3}$$

where χ is the fraction of quark matter in the mixed phase. In this way we get the binodal surface which gives the phase coexistence region in the (T,$\rho_{\rm B}$, ρ_3) space. For a fixed value of the total asymmetry $\alpha_T=\rho_3/\rho_{\rm B}$ we will study the boundaries of the mixed phase region in the (T, $\rho_{\rm B}$) plane. In the hadronic phase the charge chemical potential is given by $\mu_3=2E_{\rm sym}(\rho_{\rm B})\rho_3/\rho_{\rm B}$. Thus, we expect that critical densities rather sensitive to the isovector channel in the hadronic EoS. In general for each effective interactive lagrangian we can simulate the solution of the highly nonlinear system of Eqs.(3.3), via a minimization procedure, in order to determine the binodal boundaries and the final critical point (T_c, $\rho_{\rm Bc}$) of the mixed phase. Typical results for isospin effects

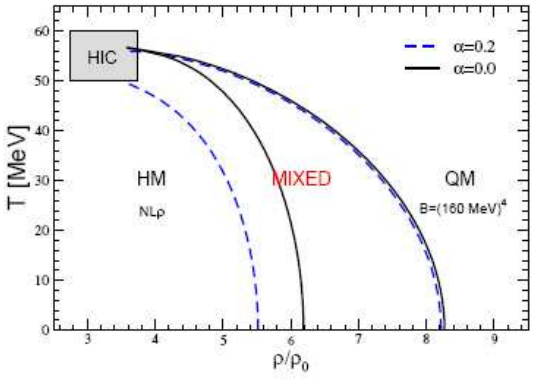

Figure 3.6: Binodal surface for symmetric (α =0.0) and asymmetric (α =0.2) matter. Hadron EoS from NLρ interaction. Quark EoS: MIT bag model with $B^{1/4}$=160 MeV. The grey region corresponds to the conditions reached in heavy ion collision simulations at few AGeV beam energies, see also Fig. 3.7.

on the binodal "surface" are presented in Fig. 3.6 for symmetric and asymmetric matter. For the hadron part we have started from a NLρ effective Lagrangian very close to other widely used relativistic effective models, e.g. see the GM3 of Ref. [30]. As expected, the lower boundary of the mixed phase is mostly affected by isospin effects. In spite of the relatively small total asymmetry, α =0.2, we clearly see a shift to the left of the first transition boundary, in particular at low temperature, and a relatively "early" critical point, around ($T = 53 \div 58$ MeV, $\rho_B = 2.5 \div 2.8\rho_0$), well within the reach of heavy ion collisions in the few AGeV range.

Collision simulations and NICA perspectives

In order to check the possibility of observing some precursor signals of a new physics even in collisions of stable nuclei at intermediate energies we have performed some event simulations for the collision of very heavy, neutron-rich, elements, using a consistent relativistic mean field approach with the same interactions [24, 27]. We have chosen the reaction $^{238}U + ^{238}U$ (average proton fraction Z/A = 0.39) at 1 AGeV and semicentral impact parameter $b = 7$ fm just to increase the neutron excess in the interacting region, see [24]. In Fig. 3.7 we report the evolution of momentum distribution and baryon density in a space cell located in the c.m. of the system. We see that after about 10 fm/c a local equilibration is achieved. We have a unique Fermi distribution and from a simple fit we can evaluate the local temperature (black numbers in MeV). We note that a rather exotic nuclear matter is formed in a transient time of the order of 10 fm/c with baryon density around $(3-4)\rho_0$, temperature 50 – 60 MeV, energy density 500 MeV fm^{-3} and proton fraction between 0.35 and 0.40, likely inside the estimated mixed phase region, close to the critical point. Which are the observable effects to look at if we enter and/or cross the mixed phase? A first expectation would be a general softening of the matter, due to the contribution of more degrees of freedom, with consequences on collective flows and particle/cluster production. For the latter point we can expect also a neutron distillation effect, a kind of *neutron trapping* in the quark phase, supported by statistical fluctuations as well as by a symmetry energy difference in the two phases, see Fig. 14 of Ref. [23]. In fact while in the hadron phase at high density we have a large neutron potential repulsion (in particular in the NLρ case), in the quark phase the neutron see only the much smaller kinetic contribution from the Fermi gas. If in a pure hadronic phase neutrons are quickly emitted or "transformed" in protons by inelastic collisions, when the mixed phase starts forming, neutrons are kept in the interacting system up to the subsequent hadronization in the expansion stage [24]. Observables related to such neutron "trapping" could be an inversion in the trend of the formation of neutron rich fragments and/or of the $\pi^-/\pi^+, K^0/K^+$ yield ratios for reaction products coming from high density regions, i.e. with large transverse momenta.

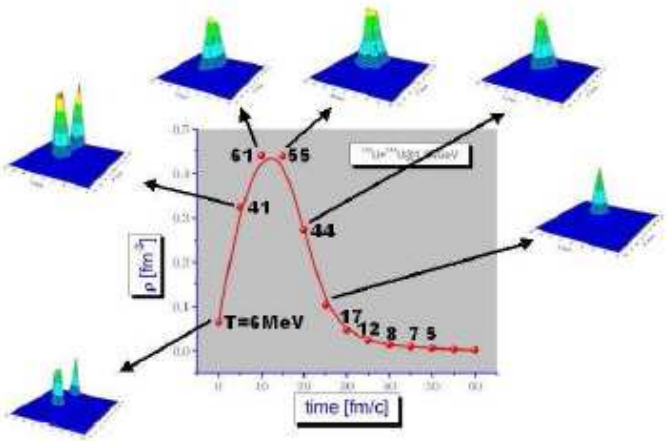

Figure 3.7: $^{238}U + ^{238}U$, 1 AGeV , semicentral collisions. Correlation between density, temperature (black values), momentum thermalization (3D plots), inside a cubic cell, 2.5 fm wide, in the center of mass of the system.

We note that all the above arguments, on the binodal boundaries of the mixed phase, on the critical point and on the neutron distillation are rather independent of the used Hadron EoS at high density, that should be relatively stiff in agreement with collective flow and kaon production data [6]. At variance for the quark sector there is the lack of explicit isovector interaction that could strongly affect the isospin effects on the location of the phase transition.

Isospin in effective partonic models

From the above discussion it appears extremely important to include the isospin degree of freedom in any effective QCD dynamics. A first approach can be supplied by a two-flavor NJL model [31] where the isospin asymmetry can be included in a flavor-mixing picture [32] via a Gap Equation like $M_i = m - i - 4G_1\Phi_i - 4G_2\Phi_j, i \neq j, (u,d)$, where the $\Phi_{u,d} =< \bar{u}u >, < \bar{d}d >$ are the two (negative) condensates and mu;d = m the (equal) current masses. Introducing explicitly a flavor mixing, i.e. the dependence of the constituent mass of a given flavor to both condensate, via $G_1 = (1-\alpha)G_0,\ G_2 = \alpha G_0$ we have the coupled equations

$$M_u = m - 4G_0\Phi_u - 4G_0(\Phi_u - \Phi_d) \tag{3.4}$$

$$M_d = m - 4G_0\Phi_u + 4(1-\alpha)G_0(\Phi_u - \Phi_d)\ . \tag{3.5}$$

For $\alpha = 1/2$ we go back to the usual NJL ($M_u = M_d$), while small/large mixing is for $\alpha \to 0/\alpha \to 1$, respectively. In neutron rich matter $|\Phi_d|$ decreases more rapidly due to the larger ρ_d and so $(\Phi_u - \Phi_d) < 0$. In the "realistic" small mixing case, see also [32,33], we will get a definite $M_u > M_d$ splitting at high baryon density (before the chiral restoration). This expectation is nicely confirmed by a full calculation [34] of the coupled gap equations with standard parameters (same as in Ref. [32]).

All that can indicate a more fundamental confirmation of the $m_p^* > m_n^*$ splitting in the hadron phase, as suggested by the effective QHD model with the isovector scalar δ coupling, see [27,35].

However such isospin mixing effect results in a very small variation of the symmetry energy in the quark phase. In fact this represents just a very first step towards a more complete treatment of isovector interactions in effective partonic models, and is of large interest for the discussion of the phase transition at high densities. We remind that confinement is still missing in these mean-field models. Stimulating new perspectives are open.

3.7 Accessibility of dense QCD phases in heavy-ion collisions

D. Blaschke[a,b], F. Sandin[c,d], V. Skokov[b,e,f] and S. Typel[e,g]

[a] *Institute for Theoretical Physics, University of Wrocław, Poland*
[b] *Joint Institute for Nuclear Research, Dubna, Russia*
[c] *Fundamental Interactions in Physics and Astrophysics, University of Liège, Belgium*
[d] *EISLAB, Luleå University of Technology, 971 87 Luleå, Sweden*
[e] *Gesellschaft für Schwerionenforschung mbH, Darmstadt, Germany*
[f] *Frankfurt Institute for Advanced Studies, Universität Frankfurt, Germany*
[g] *Excellence Cluster Universe, Technical University Munich, Garching, Germany.*

Theoretical studies of the QCD phase diagram have predicted a rich structure of nonperturbative phases under conditions of temperatures T below the deconfinement temperature $T_c \sim 180$ MeV found in lattice QCD studies [36] and baryochemical potentials $\mu_{\rm B}$ above $\sim m_{\rm N}$, where $m_{\rm N} = 939$ MeV is the nucleon mass. Of particular interest are the questions:

- How does the order and the location of the chiral phase transition depend on temperature, density, size and isospin asymmetry of the system?
- What is the nature of confinement and how does deconfinement occur?
- Can deconfinement and chiral symmetry restoration occur independent from each other at high densities? As a consequence, shall we expect massive deconfined quark matter or chirally symmetric but confined quark matter (quarkyonic matter)?
- Is dense quark matter (color) superconducting? Does confinement preclude color superconductivity? Is there a BEC or rather BCS phase of color superconductivity? What is the critical temperature? Can these phases be created in the laboratory?

The JINR Nuclotron and the Nuclotron-based Ion Collider fAcility (NICA) gives a unique opportunity to explore the above mentioned region of the phase diagram, and may thus complement alternative programs for systematic studies of heavy-ion collisons in the relevant range of collision energies $2 \leq E_{\rm lab} \leq 40$ AGeV. The energy scan program of the NA49 experiment has given indications for a phase change at $E_{\rm lab} \sim 30$ AGeV,

in particular from the peak ("horn") in the K^+/π^+ ratio. Experiments of the next generation (NA61-SHINE, low-energy RHIC, CBM and NICA) should, however, take into their focus the possibility that qualitatively new features could be found at still lower energies. This concerns in particular color superconducting quark matter phases like the 2SC phase and the recently conjectured quarkyonic phase [50]. As has been demonstrated in [37,38] the coupling to the Polyakov loop increases the critical temperature for the 2SC phase to the order of the deconfinement temperature $T_{2SC} \sim 150$ MeV, see the left panel of Fig. 3.8. In that figure, we show a modern QCD model phase diagram based on a quark matter EoS from a three-flavor NJL model with selfconsistent quark masses and diquark gaps [39–42], generalized here by the coupling to the Polyakov-loop potential to suppress unpysical quark degrees of freedom. The hadronic phase is modeled according to a density-dependent relativistic meanfield approach [43] which also describes the nuclear liquid-gas phase transition with a critical point, see the blue hatched region in Fig. 3.8 (left panel). The hadron-to-quark matter transition is obtained from the Maxwell construction with a mixed phase coexistence region shown by the turquoise hatched region. The unusual nose-like shape of this region is due to the Polyakov-loop potential which suppresses the quark pressure at finite temperatures below the deconfinement temperature, but not at $T = 0$. At low temperatures, the appearance of the diquark condensate shifts the chiral restoration transition to rather low densities, of the order of $(2-3)\ n_0$, $n_0 = 0.16$ fm^{-3}.

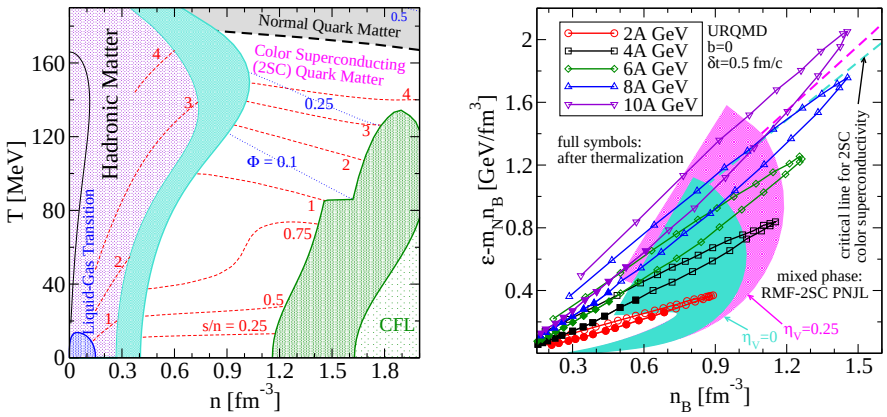

Figure 3.8: Left panel: QCD model phase diagram with mixed phase regions corresponding to the first order phase transitions: nuclear liquid-gas (blue), hadron - quark matter (turquoise), 2SC - CFL quark matter (green). The transition from color superconducting (2SC) quark matter to normal quark matter is of second order (dashed line). Right panel: trajectories of heavy-ion collisions at different energies in the excitation energy-density plane overlayed to the hadronic matter - 2SC quark matter mixed phase region of the model-QCD phase diagram. Hatched regions indicate the mixed phase for two parametrizations of the quark matter model, with ($\eta_V = 0.25$, magenta) and without ($\eta_V = 0$, turquoise) vector mean field. The dashed lines with corresponding colors denote the critical lines for 2SC color superconductivity of these parametrizations.

In order to answer the question of the accessibility of these new phases of dense QCD matter, we have examined the trajectories of the Lorentz contracted central region of central Au + Au collisions of given energies in the range $2 < E_{\rm lab} < 10$ AGeV from UrQMD simulations, see the right panel of Fig. 3.8. The hatched regions correspond to the mixed phase of hadronic and 2SC quarkyonic matter for two parametrizations of the PNJL model, with ($\eta_V = 0.25$, magenta) and without ($\eta_V = 0$, turquoise) vector mean field. The dashed lines with corresponding colors denote the critical lines for 2SC color superconductivity of these parametrizations. We conclude from this figure that for energies $4 < E_{\rm lab} < 8$ AGeV, which are in reach of the present Nuclotron facility already now, one may expect to enter the 2SC color superconducting quark matter phase with restored chiral symmetry and strong color correlations due to a low Polyakov-loop meanfield $\Phi < 0.25$, indicating a quarkyonic phase [95]. The exploration of the transition from color superconducting to normal quark matter and finally the ceasing of the mixed phase at the QCD critical point would require energies beyond 10 AGeV, aimed to be reached at NICA.

Finally, let us discuss two ideas for the experimental identification of the chiral restoration and the color superconductivity transition which should be considered when planning experiments and in particular when designing the MPD detector system.

- An enhancement of the two-photon invariant mass spectrum in the mass range $M_{2\gamma} \sim 300$ MeV, from the decay of the sigma meson which should become a long-lived "sharp" resonance when chiral symmetry gets restored and the dominant tw-pion decay channel gets closed [45, 46]. This signal shall also prevail in the hypothetic quarkyonic phase and more traditional estimates of the two-photon spectrum within the ordinary NJL model would have to be revised within the PNJL model.

- An enhancement of the lepton-pair invariant mass spectrum when approaching the critical temperature for color superconductivity from above (precursor effect [47]) which should eventually turn into a resonance-like structure when entering the 2SC phase, due to additional contributions to the diquark-antidiquark annihilation diagrams (generalized Aslamasov-Larkin and Maki-Thompson diagrams) containing anomalous propagator contributions.

In conclusion we would like to stress that our modern QCD model phase diagram suggests that new dense quark matter phases (color superconductor and quarkyonic matter) are accessible already at the present nuclotron energies and that both the study of the transition to normal quark matter and the vanishing of the mixed phase at the QCD critical endpoint will require higher energies than presently available at the Nuclotron but attainable at the NICA facility.

3.8 Transitional change to baryon-rich QCD matter at NICA energy

K. Fukushima

Yukawa Institute for Theoretical Physics, Kyoto University, Kyoto, Japan

The temperature T and the baryon chemical potential $\mu_{\rm B}$ at the chemical freeze-out are nicely determined by the Statistical Model. It is a tempting idea to associate the freeze-out curve unravelled in such a way with any of QCD phase transition. In fact both chiral and deconfinement transitions in QCD could crucially affect thermodynamic properties of the system and trigger the sudden freeze-out then.

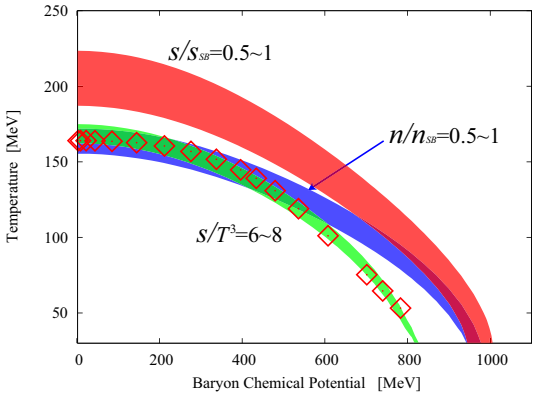

Figure 3.9: Thermodynamics from the Statistical Model by THERMUS [48]. The red and blue bands represent the regions where the entropy density s and the baryon number density n, respectively, normalized by the Stefan-Boltzmann value range from 0.5 to 1. The green band is the region in which s/T^3 takes a value from 6 to 8 so as to fit in with the freeze-out points represented by the red square dots.

One of the thermodynamic constraints that reproduce the freeze-out curve is the condition; $s/T^3 \approx 7$. The agreement is actually excellent as seen from Fig. 3.9. At the same time, as seen from Fig. 3.9, one may well consider that other conditions to detect the points where either the entropy density s or the baryon number density n rapidly increase lead to curves similar to the freeze-out one. Intuitively it should be rather natural to consider that not s/T^3 but s itself is a sensitive quantity to deconfinement. Let us try to fit the freeze-out curve by a condition to require that the entropy density itself is fixed.

Fig. 3.10 clearly shows that the constant-s cannot reproduce the freeze-out curve. It is interesting that the freeze-out curve suddenly drops down with a steeper slope than the constant-s curve. A possible interpretation for this is that a transitional change of the state of QCD matter occurs around $T \approx 150$ MeV and $\mu_{\rm B} \approx 400$ MeV

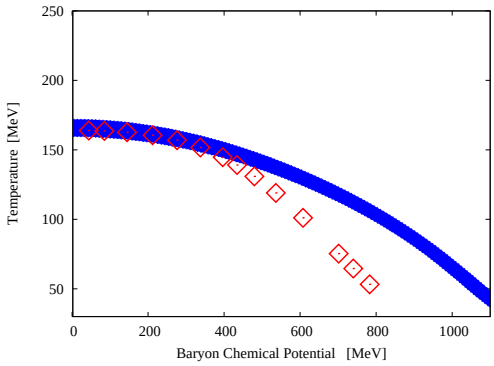

Figure 3.10: Blue band represents the thermodynamic constraint; $s = 4$ fm^{-3} and the freeze-out points are represented by the red square dots.

from where the deviation between the constant-s and freeze-out curves starts growing. It is quite interesting that this departing point corresponds to a collision with the energy $\sqrt{s_{\rm NN}} \approx 8$ GeV, which is just the NICA energy. Hence, it would be extremely intriguing to explore the character of QCD matter in this temperature and density region at NICA. It must be a special point.

A possible interpretation of this special point is the relevance of the triple-point-like region as depicted in Fig. 3.11 that presents a typical output from the PNJL model [95]. Here we see that the deconfinement transition is fairly flat and is to be interpreted as similar to the blue curve in Fig. 3.10. Therefore, in view of Figs. 3.10 and 3.11, the freeze-out points beyond $\mu_{\rm B} \sim 400$ MeV belong to some different physics, namely, a sudden jump in the baryon number in the system. If it is true, the collision energy $\sqrt{s_{\rm NN}} \approx 8$ GeV is a threshold above which abundant baryons can emerge. Such baryon dominant matter yet below deconfinement could be identified with so-called Quarkyonic Matter [49]. NICA would be an ideal facility to probe such an onset to enter the baryon-rich regime of QCD matter.

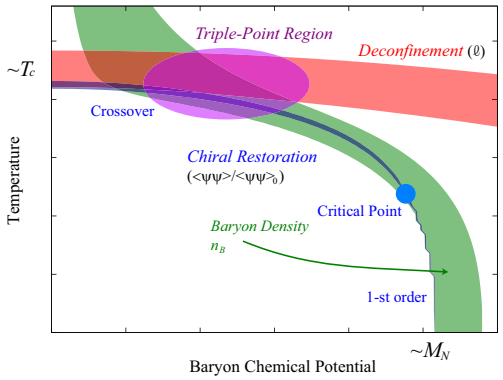

Figure 3.11: A typical example of the phase diagram from the PNJL model.

3.9 Triple point and quarkyonic matter in the QCD phase diagram

L. McLerran[a], K. Redlich[b,c], D. Blaschke[b,d]

[a] *BNL and Riken Brookhaven Center, Upton, NY, USA*
[b] *Institute for Theoretical Physics, University of Wrocław, Wrocław, Poland*
[c] *Theory Division, CERN, Geneva, Switzerland*
[d] *Joint Institute for Nuclear Research, Dubna, Russia*

Features of hadron production in relativistic nuclear collisions, mainly at CERN-SPS energies, may be explained by the existence of three forms of matter: Hadronic Matter, the Quark-Gluon Plasma, and a third

form introduced recently as Quarkyonic Matter [50]. It has been suggested [49] that these meet at a triple point in the QCD phase diagram. A schematic view of such a phase diagram is shown in the left panel of Fig. 3.12. If the transition(s) between the three phases are merely crossover(s), the triple point is only approximate. Some of the features explained by such a picture, both qualitatively and quantitatively, include the curve for the decoupling of chemical equilibrium (see the right panel of Fig. 3.12), along with the non-monotonic behavior of strange particle multiplicity ratios at center of mass energies $\sqrt{s}\lesssim$10 GeV (left panel of Fig. 3.13).

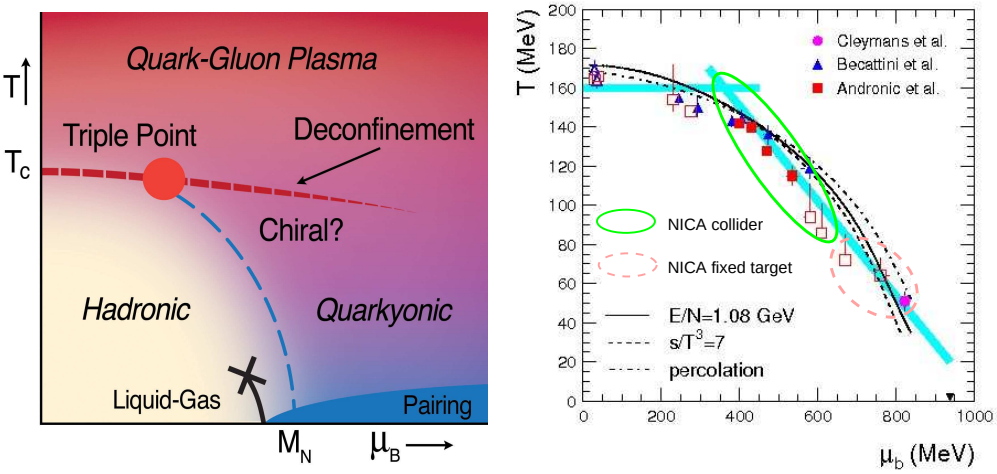

Figure 3.12: Left panel: The conjectured phase diagram of strongly interacting matter according to Ref. [49]. Right panel: Hadronic freeze-out temperatures and chemical potentials extracted by statistical model fits to experimental data on hadron production in heavy-ion collisions.

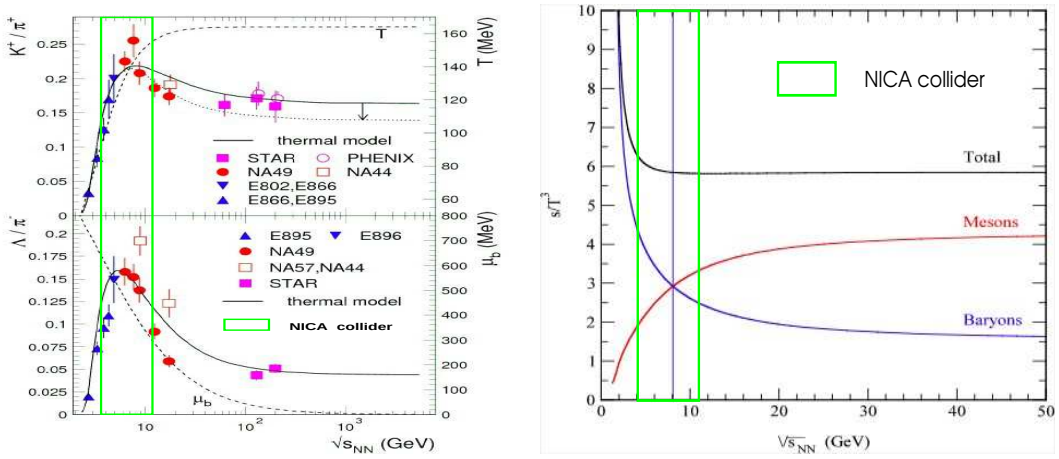

Figure 3.13: Left panel: Energy dependence of hadron yields relative to pions. Right panel: Baryonic and mesonic contributions to the entropy density as a function of the center of mass energy of heavy-ion collisions. When increasing the energy above that where the horn in the K^+/π^+ and Λ/π^+ ratios is observed, $\sqrt{s}\sim 10$ GeV, the system changes its character from baryon- to meson-dominated.

The energy range of the NICA facility at JINR Dubna will be ideally suited to provide more phenomenological evidence for the existence of the triple point and the characteristics of its underlying phase structure. This concerns heavy-ion collisions at both, the collider with the MPD experiment covering 4 GeV $\lesssim\sqrt{s}\lesssim$11 GeV (mirroring the fixed target CBM experiment at FAIR) and the fixed target experiments with the extracted Nuclotron beam of 2 AGeV $\lesssim E_{\rm lab}\lesssim$5.5 AGeV, filling the gap between GSI-SIS20 and AGS energies.

Let us explain the discovery potential of this facility related to the quarkyonic phase a bit more in detail.

According to the original motivation [50], and based on the large N_c limit of QCD, a new view of the QCD phase diagram emerges in the "quarkyonic" region where quarks are still confined like in the hadronic phase, but chiral symmetry is almost restored. A microscopic QCD-motivated approach for the simultaneous description of dynamical chiral symmetry breaking/restoration and confinement/deconfinement at finite temperatures and densities is still absent. Therefore, it is a challenge for theorists to develop approximative methods for characterizing the quarkyonic phase and its observable signatures.

Models of the Nambu-Jona-Lasinio (NJL) type may give valuable insights, in particular to the aspects of chiral dynamics in hot and dense matter. The absence of a confining interaction in this model can partly be remedied by the coupling to a Polyakov loop potential which effectively suppresses the unphysical appearance of quark degrees of freedom in the confinement domain [51,223]. Polyakov-loop NJL (PNJL) models have been used to discuss the phase diagram [95], where for low temperatures and high densities one finds a chirally restored but confined phase [53], typically accompanied by a diquark condensate signalling color superconductivity [37, 133].

Most studies are restricted to homogeneous phases although the thermodynamically favored ground state at low temperatures generally is a chiral crystalline one characterized by an inhomogeneous order parameter (see Ref. [55] for a review on condensed matter aspects of dense QCD). Well-known example is the chiral density wave [56, 57]. Also in the $1 + 1$ dimensional NJL model, the Gross-Neveu (GN) model, an inhomogeneous (crystalline) phase exists which for the massless GN model (NJL_2) is a "chiral spiral" and a quite complete result for the phase diagram is known, see [58]. It has been shown that these results can be used to construct solutions of the $3 + 1$ dimensional NJL model with one-dimensional modulation of the chiral order parameter [59]. The phase structure of such a model bears similarities with the conjectured quarkyonic phase diagram of Fig. 3.12 in that it has three phases joining in the (tri-)critical point: two homogeneous ones (chirally symmetric and chirally broken) and the inhomogeneous chiral spiral phase which would stand for the quarkyonic one [60]. Such a view on the phase diagram got confirmed recently [61] and suggests that the quarkyonic phase could merely be an island covering the first-order transition which instead of ending in a critical point ends in a Lifshitz point [61].

What significance has the assumption of a one-dimensional modulation of the chiral order parameter for the QCD phase structure? For a chiral quark model with confining (Gribov-Zwanziger) Coulomb-gauge gluon propagator, the $3 + 1$ dimensional theory reduces to a gauge theory in $1 + 1$ dimensions with a local chiral condensate, spatially varying in one direction: the "Quarkyonic Chiral Spiral" [62]. The quarkyonic chiral spiral state which breaks chiral and translational invariance spontaneously forms patches on the quark Fermi sphere which increase in number with increasing quark density [63].

Unfortunately, no credible signals for the quarkyonic chiral spiral phase in heavy-ion collisions have been developed yet by theory. An *ad hoc* conjecture would suggest that baryon number fluctuations should emerge from the hadronization of this baryon-rich, inhomogeneous phase with spatially varying chiral condensate. Recently, Mócsy and Sorensen have examined the consequences of baryon-rich (like quarkyonic) bubble formation in an expanding in an expanding medium and showed how the tw-particle correlations vary in the transverse and longitudinal direction depending on assumptions for radial flow, bubble temperature and baryon emission time [64].

The NICA facility has an excellent opportunity to verify such conjectures experimentally. This would be a scientific discovery of great importance.

3.10 Search for the QCD Critical Point at NICA

X. Luo[a,c], B. Mohanty[b], H.G. Ritter[c], N. Xu[c]

[a] *Department of Modern Physics, University of Science and Technology of China, Hefei, China*
[b] *Variable Energy Cyclotron Center, Kolkata, India*
[c] *Lawrence Berkeley National Laboratory Berkeley, CA,USA*

Lattice QCD calculations predict that a cross-over from the hadronic phase to the Quark Gluon Plasma (QGP) phase occurs above a critical temperature for vanishing baryon chemical potential ($\mu_B = 0$). The corresponding cross-over temperature range has been estimated to be about 170 – 190 MeV [65, 66]. At large μ_B, QCD based model calculations indicate that the transition from the hadronic phase to the QGP phase is of first order. The end point of the first order phase transiton line is the QCD Critical Point [67, 68]. There are large theoretical uncertainties of its location and even its existence is not confirmed [69–72]. Experimentally,

we study the QCD phase diagram by high energy heavy ion collisions [73–75]. By tuning the collision energy, we can vary the baryon chemical potential in the region of interest.

The characteristic feature of a critical point is the increase and divergence of the correlation length (ξ) and of critical fluctuations. Recently, theoretical calculations have shown that higher moments of multiplicity distributions of conserved quantities, such as net-baryon, net-charge, and net-strangeness, are sensitive to the correlation length ξ [3].

In Lattice QCD calculations with $\mu_{\rm B} = 0$, higher order susceptibilities of the baryon number, which can be related to the higher order moments of the net-baryon multiplicity distributions, show a non-monotonic behavior near T_c [76]. A similar behavior is expected for the finite $\mu_{\rm B}$ region. Experimentally, it is hard to measure the net-baryon number while the net-proton number is measurable. Theoretical calculations show that fluctuations of the net-proton number can be used to infer the net-baryon number fluctuations at the critical point [77]. The NICA facility will cover the energy range from $\sqrt{s}$=4 GeV to 11 GeV at the collider and $E_{\rm lab}$ up to 5.5 AGeV for fixed target experiments. Therefore, we propose to study the energy dependence of kurtosis and skewness and other higher order moment products in order to search for the QCD critical point.

We introduce various moments definitions of the event-by-event multiplicity distributions: Mean, $M = < N >$, Variance, $\sigma^2 = < (\Delta N)^2 >$, Skewness, $S = < (\Delta N)^3 > / \sigma^3$, and Kurtosis, $\kappa = < (\Delta N)^4 > / \sigma^4 - 3$, where $\Delta N = N - < N >$. Skewness and Kurtosis are equal to zero for gaussian distributions. Thus, they are ideal probes to demonstrate the non-Gaussian fluctuations feature near the critical point, in particularly a sign change of the skewness or kurtosis may be a hint of that the system is evolving in the vicinity of the critical point [3, 78]. We have calculated the various moments of net-proton ($\Delta p = N_{\rm p} - N_{\bar{\rm p}}$) distributions from transport models. The kinetic coverage of protons and anti-protons used in our analysis is $0.4 < p_{\rm T} < 0.8$ GeV/c and $|y| < 0.5$. Fig. 3.14 (left panel) shows the number of participant ($N_{\rm part}$) dependence of moment

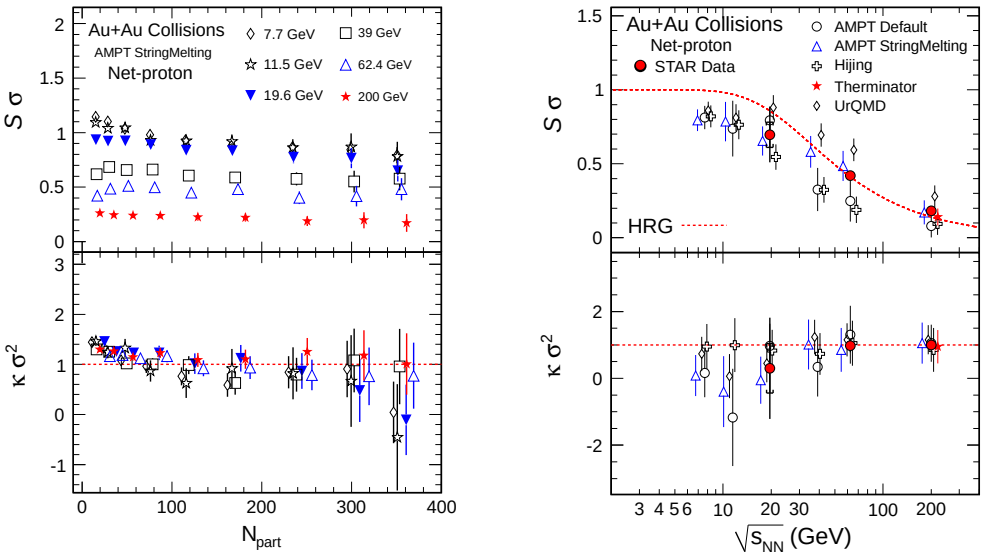

Figure 3.14: **Left panel:** Centrality dependence of moment products $S\sigma$, $\kappa\sigma^2$ of net-proton distributions for Au + Au collisions of various energies from AMPT String Melting model calculation. **Right panel:** Energy dependence of moment products $S\sigma$, $\kappa\sigma^2$ of net-proton distributions for Au + Au collisions of various models and STAR data.

products $S\sigma$, $\kappa\sigma^2$ of net-proton distributions from the AMPT string melting model for various energies. In Fig. 3.14 (right panel), the energy dependence of moment products $S\sigma$, $\kappa\sigma^2$ for most central net-proton distributions from STAR data [79] are compared with the results from various models. We see the data are in good agreement with the HRG model ($\kappa_{\rm B}\sigma^2_{\rm B} = 1$, $S_B\sigma_{\rm B} = tanh(\mu_{\rm B}/T)$) [80] and the thermal model (Therminator) results. A large deviation from constant as a function of $N_{\rm part}$ and collision energy for $\kappa\sigma^2$ may indicate new physics, such as critical fluctuations [3]. Recent lattice QCD calculations from [81] have shown that $\kappa\sigma^2$ non-monotonically depends on colliding energy in the neighbourhood of the critical point.

3.11 Probing the hadron-quark mixed phase at finite temperature, baryon and isospin chemical potentials

G.Y. Shao[a], M. Di Toro[a,b], M. Colonna[a], S. Plumari[a,b], B. Liu[c,d], V. Greco[a,b], Y.X. Liu[e,f]

[a] *INFN-Laboratori Nazionali del Sud, Catania, Italy*
[b] *Physics and Astronomy Dept., University of Catania, Italy*
[c] *IHEP, Chinese Academy of Sciences, Beijing, China*
[d] *Theoretical Physics Center for Scientific Facilities, Chinese Academy of Sciences, Beijing, China*
[e] *Department of Physics and State Key Laboratory of Nuclear Physics and Technology, Peking University, China*
[f] *Center of Theoretical Nuclear Physics, National Laboratory of Heavy Ion Accelerator, China*

The exploration of the phase diagram of strongly interacting matter and search for the signals of the phase transition from hadronic to quark-gluon phase are very important in both theory and experiment. As a fundamental tool, lattice QCD provides us a framework for investigation of non-perturbative phenomena such as confinement and quark-gluon plasma formation at finite temperature and vanishing (small) chemical potential [82–84]. However, lattice QCD suffers the sigh problem of the fermion determinant with three color at finite μ. Although several approximation methods has been taken to try to evade this problem [67,85,86], the validity of lattice simulations at finite chemical potential is still limited in the region $\mu_{\rm q}/T < 1$. The results given with $\mu_{\rm q}/T > 1$ should be taken with care [87].

On the other hand, many phenomenological models [25,31,40,42], as well as the more microscopic Dyson-Schwinger equations (DSEs) approach [88], have been proposed to give a completed description of QCD phase diagram. Among these effective models, the Nambu–Jona-Lasinio model (NJL) is a predominant one, which offers a simple illustration of chiral symmetry breaking and restoration, a key feature of QCD [89–91], and it presents a complicated phase diagram of color superconductivity at high density [92, 93]. One deficiency of the standard NJL model is that quarks are not confined. Recently, an improved version of the NJL model coupled to Polyakov loop (PNJL) has been proposed [94]. The PNJL model takes into both the chiral symmetry and (de)confinement effect, giving a good interpretation of lattice data at zero chemical potential and finite temperature, and make predictions in the region that cannot be reached in lattice calculation [95,96,223].

Most effective models, including the PNJL model, study the hadron-quark-gluon phase transition based on quark degrees of freedom. As a matter of fact, at low temperature and small chemical potential, the QCD dynamics is governed by hadrons. Therefore, it is natural to describe the strongly interacting matter with hadronic degrees of freedom at low T and small μ and quarks at high T and large μ. This picture can be realized in the two equation of state (Two-EoS) approach in which hadronic and quark phases are connected by Gibbs (Maxwell) criteria. This frame is widely used in describing the phase transition in the interior of compact star in weak equilibrium (e.g., [97–100]). Recently, it has also been taken to explore the phase diagram of hadron-quark transition at finite temperature and density concerned with heavy-ion collision [23,101–105]. Moreover, more attention was paid to asymmetric matter, and some observable effects have been already suggested in Ref. [23,102].

We have studied the hadron-quark phase transition in the Two-EoS model by using the Relativistic Mean Field EoS for the hadron sector and various effective approaches for the quark phase, the static MIT-Bag model [102,105], the NJL model [106] with the chiral dynamics and finally the extension to the Polyakov-Loop coupling (PNJL) [107] to include also the (de)confinement dynamics.

We obtain the phase diagrams of hadron–quark-gluon phase transition in $T-\rho_{\rm B}$ and $T-\mu_{\rm B}$ planes. The calculations show that some interesting signatures of the transition are very robust, in the sense that they appear for all the different quark EoS:

- The transition is of the first order at finite temperatures and chemical potentials.
- For isospin asymmetric matter the onset density of the mixed phase is much smaller than the one of symmetric matter. This appears important for the possibility of observations in heavy ion collisions at intermediate energies.
- The Isospin Distillation Effect, i.e. the isospin enrichement of the quark component in the mixed phase in the case of asymmetric matter, is always present, in particular at lower temperatures.

All that leads to some confidence about the possibility of an experimental confirmation.

Besides, the results show that the phase-transition region is greatly modified when both the chiral dynamics and (de)confinement effect are considered. The phase-transition at high T is more close to the result given by lattice calculation at small chemical potential. A Critical-End-Point (CEP) is found at $T \simeq 170\ MeV$ and baryon chemical potential $\mu_{\rm B} \simeq 600\ MeV$, i.e. at a quark chemical potential $\mu_{\rm q}/T_c \simeq 1$, in a region that could be tested by extended lattice calculations.

Hadron matter, quark matter and the mixed phase

In the Two-EoS model , the hadron matter at finite temperature and density/chemical potential is described by the non-linear Walecka model, the Relativistic Mean Field (RMF) effective theory which provides an excellent description of nuclear matter and finite nuclei as well as of of compressed matter properties probed with heavy ion collisions at high energies [23,101,108,109]. The exchanged mesons include the isoscalar-scalar meson σ and isoscalar-vector meson ω (NL force, for isospin symmetric matter), isovector-vector meson ρ and isovector-scalar meson δ, ($NL\rho$ and $NL\rho\delta$ forces, for isospin asymmetric matter).

The quark matter at the same conditions is described by the MIT-Bag [102,105], NJL [106] and PNJL [107] models. For the mixed phase between the pure hadronic and quark phase, the two phases are connected each other with the Gibbs conditions with the thermal, chemical and mechanical equilibriums.

Our aim is to compare mixed phase results obtained with different quark models but keeping the same hadron EoS. However we face a problem since while the microscopic NJL and PNJL approaches have no free parameters, in the MIT-Bag picture the Bag constant can be largely varied, in particular at high densities. Here we have chosen the Bag constant value in order to reproduce the same critical point at high chemical potential as in the NJL and PNJL cases (for isospin symmetric matter). From the systematic study reported in ref. [105] a good choice seems to be $B^{1/4} = 160\ MeV$.

Based on the conservations of baryon number and isospin during the strong interaction, the Gibbs conditions describing the phase transition can be expressed by

$$\begin{aligned}
&\mu_{\rm B}^H(\rho_{\rm B},\rho_3,T) = \mu_{\rm B}^Q(\rho_{\rm B},\rho_3,T)\\
&\mu_3^H(\rho_{\rm B},\rho_3,T) = \mu_3^Q(\rho_{\rm B},\rho_3,T)\\
&P^H(\rho_{\rm B},\rho_3,T) = P^Q(\rho_{\rm B},\rho_3,T),
\end{aligned} \tag{3.6}$$

where $\rho_{\rm B} = (1-\chi)\rho_B^H + \chi\rho_B^Q$ and $\rho_3 = (1-\chi)\rho_3^H + \chi\rho_3^Q$ are the total baryon density, isospin density of the mixed phase, respectively, and χ is the fraction of quark matter, The global asymmetry parameter α for the mixed phase is

$$\alpha \equiv -\frac{\rho_3}{\rho_{\rm B}} = \frac{(1-\chi)\rho_3^H + \chi\rho_3^Q}{(1-\chi)\rho_{\rm B}^H + \chi\rho_{\rm B}^Q} = \alpha^H\ |_{\chi=0} = \alpha^Q\ |_{\chi=1}, \tag{3.7}$$

which is determined by the heavy-ion source used in experiment.

Before showing detailed phase diagrams we can already predict the effects of chiral and (de)confinement dynamics on the quark pressure and then on the phase transition. The chiral symmetry restoration at finite temperature and low chemical potentials will largely increase the quark pressure leading to an End-Point for the pressure matching with the hadron part. When the confinement dynamics is added we will also get a reduction of the quark degrees of freedom and so in general the quark pressure will be reduced. This will imply the shift of the matching with the hadron pressure, and so also of the Critical-End-Point, to higher temperatures [107].

Numerical results and discussions

We present firstly the phase transition from hadronic to deconfined quark phase in $T-\rho_B$ plane for isospin symmetric matter in Figs. 3.15 (solid lines), 3.16 and 3.17 using the same NL hadron interaction and the MIT-Bag, NJL, PNJL respectively for the quark sector. In the Figs. 3.15 (dot-dashed lines), 3.18 and 3.19 the corresponding transition curves for isospin asymmetric matter with the global asymmetry parameter $\alpha = 0.2$. The same $NL\rho\delta$ interaction is used for the hadron matter.

For symmetric matter at a fixed T, the first order phase transition takes place with the same pressure and μ_B in both phases, but a jump in extensive variables, like density, energy density and entropy. In the mixed phase, the pressures of both phases keep unchanged and $\alpha = \alpha^H = \alpha^Q = 0$ for any quark fraction χ.

These features are quite different for the mixed phase in isospin asymmetric matter. For all the different quark EoS, MIT-Bag [23, 102, 105], NJL [106] and PNJL [107] we see a clear Isospin Distillation effect, i.e. a strong enhancement of the isospin asymmetry in the quark component inside the mixed phase, as reported in

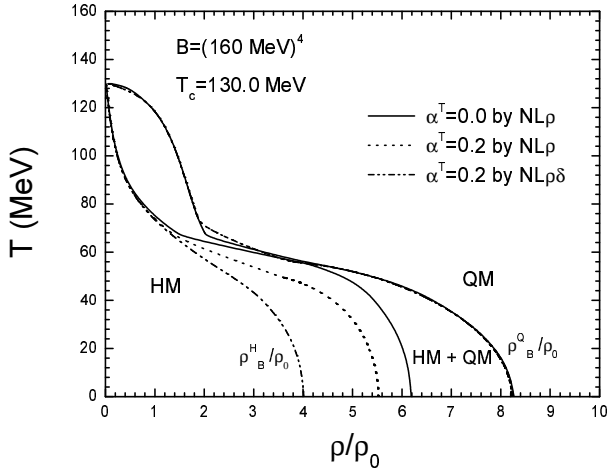

Figure 3.15: Phase diagram in $T-\rho_{\mathrm{B}}$ plane in the Two-EoS Hadron-MIT Bag model for isospin symmetric and asymmetric matter. $NL\rho$, $NL\rho\delta$ hadron interactions.

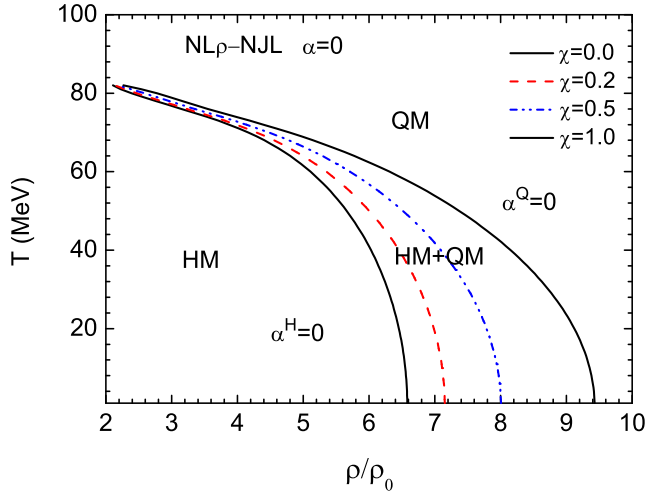

Figure 3.16: Phase diagram in $T-\rho_{\mathrm{B}}$ plane in the Two-EoS Hadron-NJL model for symmetric matter. NL hadron interaction.χ is the quark fraction in the mixed phase.

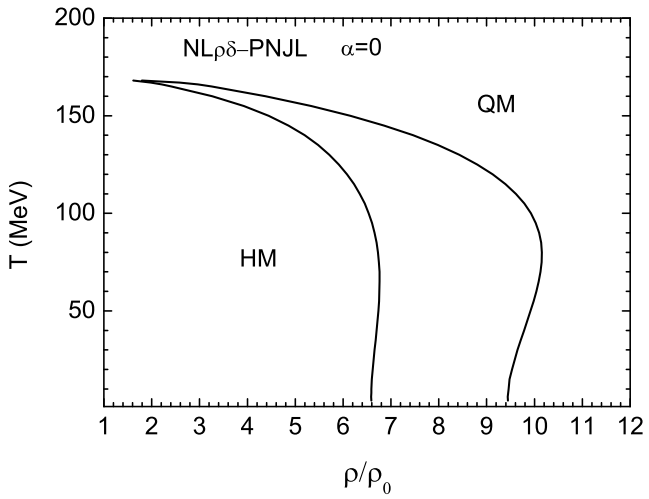

Figure 3.17: Phase diagram in $T-\rho_{\rm B}$ plane in the Two-EoS Hadron-PNJL model for symmetric matter. NL hadron interaction.

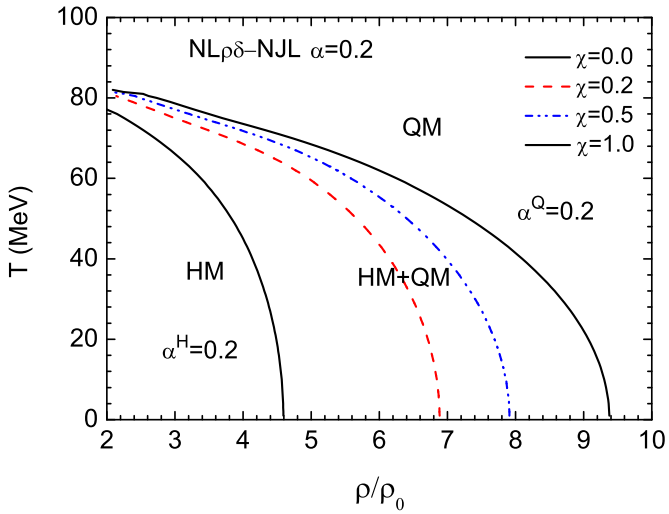

Figure 3.18: Phase diagram in $T-\rho_B$ plane in the Two-EoS Hadron-NJL model for asymmetric matter with the global asymmetry parameter $\alpha=0.2$. χ represents the fraction of quark matter. $NL\rho\delta$ hadron interaction.

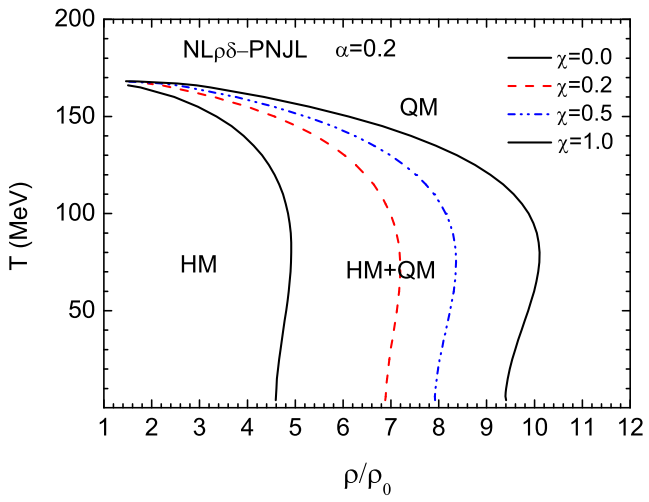

Figure 3.19: Phase diagram in $T-\rho_B$ plane in the Two-EoS Hadron-PNJL model for asymmetric matter with the global asymmetry parameter $\alpha = 0.2$. χ represents the fraction of quark matter. $NL\rho\delta$ hadron interaction.

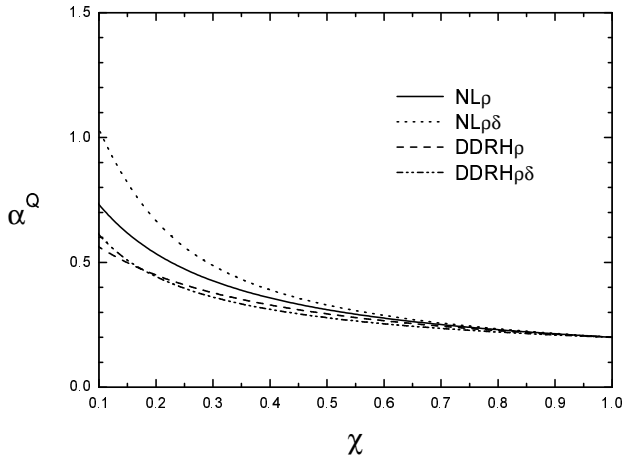

Figure 3.20: The behavior of local asymmetric parameter α^Q in the mixed phase at zero temperature in the Hadron-MIT Bag model. Dotted line: $NL\rho\delta$ hadron interaction. Global asymmetry $\alpha = 0.2$.

Figs. 3.20 (dotted line), 3.21, 3.22, where the asymmetry parameters in the two components are plotted vs. the quark fraction χ. As a consequence the pressure in the mixed phase keeps rising with χ, more rapidly for quark concentrations below 50 %, see details in [102, 106].

From Figs. 3.21, 3.22 we remark that this isospin enrichment of the quark phase is rather robust vs. the increasing temperature. This is important since color pairing correlations at low temperatures will decrease all symmetry energy effects [104].

Such behavior of the local asymmetry parameters will possibly produce some observational signals in the following hadronization during the expansion, see last Section.

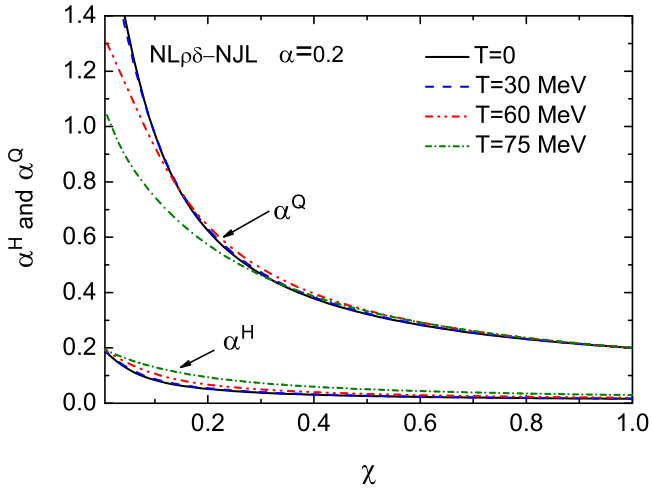

Figure 3.21: The behaviors of local asymmetric parameters α^H and α^Q in the mixed phase with several values of temperature. Hadron-NJL picture with $NL\rho\delta$ hadron interaction.

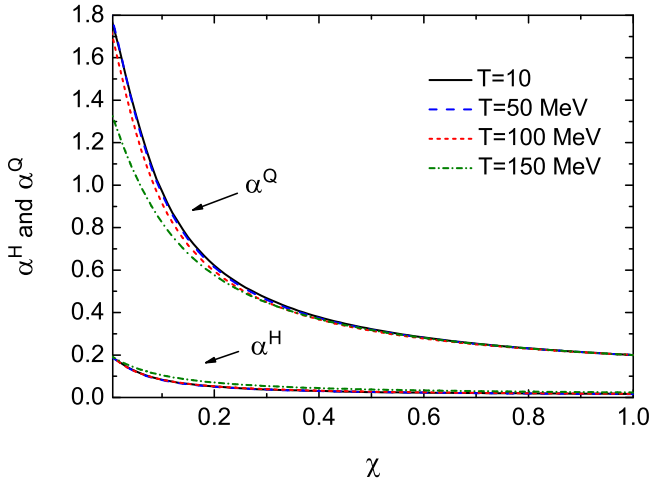

Figure 3.22: The behaviors of local asymmetric parameters α^H and α^Q in the mixed phase with several values of temperature. Hadron-PNJL picture with $NL\rho\delta$ hadron interaction.

We plot the $T-\mu_B$ phase diagrams in Figs. 3.23 (MIT-Bag quark EoS) and 3.24 (upper: Hadron-PNJL; lower: Hadron-NJL) for symmetric matter with the NL hadron interaction. In the Figs. 3.25 (Hadron-MIT Bag) and 3.26 (upper: Hadron-PNJL; lower: Hadron-NJL) the corresponding for asymmetric matter are shown.

Figs. 3.23, 3.24 clearly show that there is only one phase-transition line, not dependent on the quark fraction χ, in the $T-\mu_B$ plane. At variance, for asymmetric matter, the phase transition curve varies for different quark

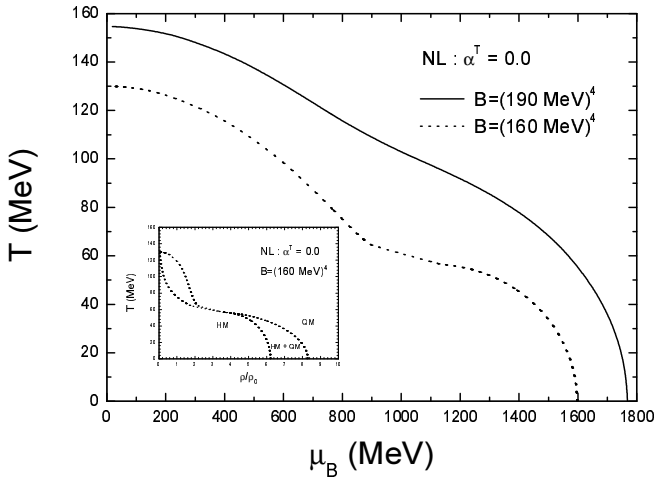

Figure 3.23: Phase diagram in $T - \mu_{\rm B}$ plane for symmetric matter. NL/Hadron-MIT-Bag picture.

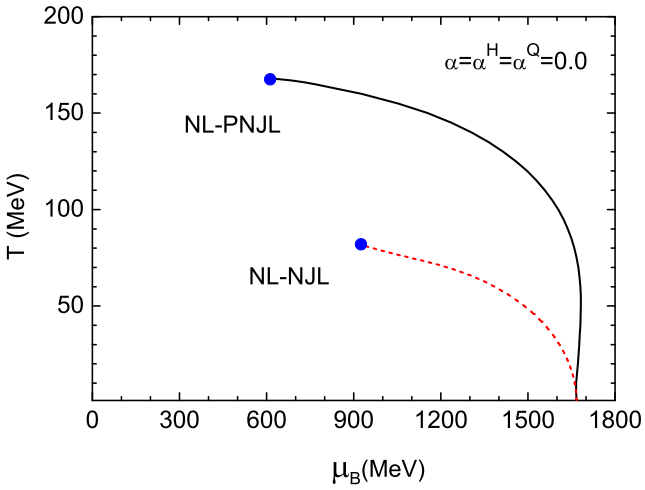

Figure 3.24: Phase diagram in $T - \mu_{\rm B}$ plane for symmetric matter. Upper: Hadron-PNJL. Lower: Hadron-NJL.

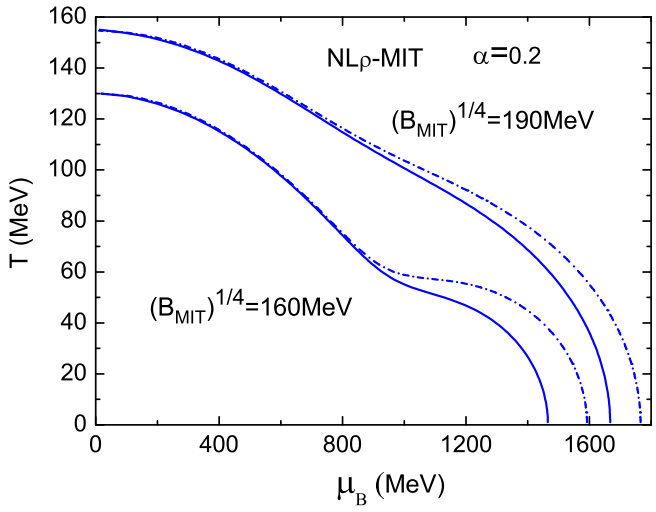

Figure 3.25: Phase diagram in $T-\mu_{\rm B}$ plane for asymmetric matter with the global asymmetry parameter $\alpha=0.2$. .$NL\rho\delta$/Hadron-MIT-Bag picture.

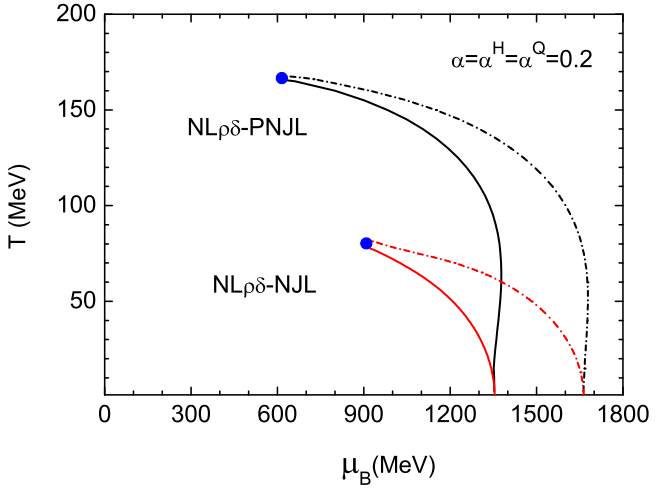

Figure 3.26: Phase diagram in $T-\mu_{\rm B}$ plane for asymmetric matter with the global asymmetry parameter $\alpha=0.2$. Upper: Hadron-PNJL; Lower: Hadron.NJL. $NL\rho\delta$ hadron interaction.

fraction χ. The two lines in Figs. 3.25, 3.26 are obtained with $\chi = 0$ and 1, representing the beginning and the end of hadron-quark phase transition, respectively.

In Figs. 3.24, 3.26 we compare the phase transition curves with the same hadron EoS and the two NJL/PNJL quark pictures. For the NJL model with only chiral dynamics, no physical solution exists when the temperature is higher than ~ 80 MeV. The corresponding temperature is enhanced to about ~ 166 MeV with the Hadron-PNJL model, which is closer to the phase transition temperature given by full lattice calculation at zero or small chemical potential [82–84].

Besides the critical end points given by the Hadron-PNJL model and Hadron-NJL model, the difference of the phase diagrams given by the two models is quite large, even at lower temperatures and chemical potentials. This can be qualitatively understood from the analysis of the quark pressures discussed at the end of Section II.

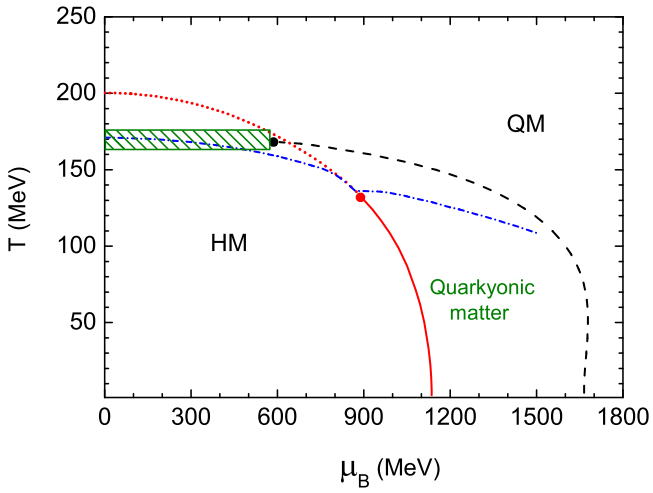

Figure 3.27: Phase diagrams of the PNJL model and the Two-EoS model

Finally in Fig.3.27 we present together the phase diagrams obtained by the PNJL pure quark model and the two EoS Hadron-PNJL approach. We find that the deconfined phase transition curve in the PNJL model is close to the one obtained in the Hadron-PNJL scheme at high temperature and intermediate chemical potential. At larger chemical potential, the deconfinement phase transition curve in the PNJL model is still at rather high temperature. This is naturally leading to the formation of a *quarkyonic* phase (chirally restored but still deconfined) [50], although the interpretation of the Polyakov Loop Φ as order parameter at low temperatures and large chemical potentials is not clear. In any case this is also a strong indication that presently we must rely on the Two-EoS approach for predictions in the region of interest for heavy ion experiments at intermediate energies, i.e. at high $\rho, \mu_{\rm B}$ and finite temperatures.

Summary and suggested observables In this study, the hadron-quark phase transition are investigated in the Two-EoS approach. We describe the hadron matter with nonlinear Walecka model and separately the quark matter with the MIT-Bag and the NJL(PNJL) models. We follow the Gibbs criteria to construct the mixed phase with baryon number and isospin conservations, likely reached during the hot and dense phase formed in heavy-ion collision at intermediate energies. The parameters in both models are fitted to give a good reproduction of the properties of nuclear matter, also at suprasaturation densities, and of lattice data at high temperature with zero/small chemical potential.

The phase diagrams for symmetric and asymmetric matter are explored in the $T - \rho_{\rm B}$ and $T - \mu_{\rm B}$ planes. In both Hadron-(P)NJL calculations we get a first order phase transition with a Critical-End-Point at finite temperature and chemical potential. In the PNJL case the CEP is shifted to larger temperatures and smaller chemical potential, to the $(166, 600)$ MeV point in the $(T, \mu_{\rm B})$ plane. This appears a nice indication of a decrease of the quark pressure when confinement is accounted for. Such result is particularly interesting since the CEP is now in the region of $\mu_{\rm q}/T_c \simeq 1$ (where μ_q is the quark chemical potential) and so it could be reached with some confidence by lattice-QCD complete calculations.

Isospin effects are almost negligible when we approach the CEP. At variance the calculation shows that the onset density of asymmetric matter is lower than that of symmetric matter. Moreover in the mixed phase of asymmetric matter, the decreasing of local asymmetry parameter α^H and α^Q with the increasing quark fraction χ may produce some observable signals. In particular we remark the noticeable isospin distillation mechanism (isospin enrichment of the quark phase) at the beginning of the mixed phase, i.e. for low quark fractions, that should show up in the hadronization stage during the expansion. We also see from Figs.3.20, 3.21 and 3.22 that this effect appears in all quark EoS models and it is still there even at relatively large temperatures, certainly present in the high density stage of heavy ion collisions at relativistic energies [23, 109].

Expected observables

A first expectation of the Isospin Distillation will be a kind of *neutron trapping* in the quark phase, supported by statistical fluctuations [23] as well as by the symmetry energy difference in the two phases [102]. In fact while in the pure hadron matter (neutron-rich) at high density we have a large neutron potential repulsion (in both $NL\rho$, $NL\rho\delta$ cases), in the quark phase the d-quarks see a smaller symmetry repulsion essentially only due to the kinetic contribution from the Fermi gas. As a consequence while in a pure hadronic phase neutrons are quickly emitted or "transformed" in protons by inelastic collisions [110], when the mixed phase starts forming, neutrons are kept in the interacting system, in the quark phase, where they can even thermalize, up to the subsequent hadronization in the expansion stage. Observables related to such neutron "trapping" could be

- (i). An inversion in the trend of emission of fast neutron rich clusters with increasing beam energy, to be seen in the n/p, $^3H/^3He$.. ratios at high kinetic energies;
- (ii). An enhancement of the production of isospin-rich nucleon resonances and subsequent decays, that can be evaluated via equilibrium statistical approaches [111];
- (iii). Related to the previous point, an increase of π^-/π^+, K^0/K^+ yield ratios for mesons coming from high density regions, to be selected via large transverse momenta, corresponding to a large radial flow.

If such kinetic selection of particles from the mixed phase can really be successful also other potential signatures would become available. One is related to the general softening of the matter, due to the contribution of more degrees of freedom, that should show up in the damping of collective flows [112].

The azimuthal distributions (elliptic flows) will be particularly affected since particles mostly retain their high transverse momenta escaping along directions orthogonal to the reaction plane without suffering much rescattering processes. Thus a further signature could be the observation, for the selected particles, of the onset of a quark-number scaling of the elliptic flow: a property of hadronization by quark coalescence that has been predicted and observed at RHIC energies, i.e. for the transition at $\mu_B = 0$ [113].

Finally, an evident feature of Figs. 3.15 (dot-dashed lines), 3.18, 3.19 is that the onset density of hadron-quark phase transition for asymmetric matter is much lower than that of the symmetric one, and therefore it will be easier to probe in heavy-ion collision experiments at intermediate energies.

All that support the possibility of an experimental observation in the new planned facilities, for example, FAIR at GSI-Darmstadt and NICA at JINR-Dubna, with realistic isospin asymmetries for stable/unstable beams.

3.12 Physics at Large Baryon Density at NICA

A. Tawfik

Egyptian Center for Theoretical Physics (ECTP), MTI University, Cairo-Egypt

Apparently, the NICA facility at JINR (Dubna) shall provide a unique possibility to study *relativistic* nuclear matter under extreme conditions (high temperatures and baryon densities). Lattice QCD simulations give strong evidence that the *confined* hadronic matter can be expected to go over through phase transition(s) to a *strongly* correlated quark-gluon plasma (sQGP). Actually, for small baryochemical potentials it is a (rapid) crossover. Various QCD-like effective models designed to describe matter at high baryon densities show that the crossover goes over into a phase transition of first-order. There are several indications that the two regions are separated by a critical endpoint. So far, there is no rigorous proof for its location or even its ultimate existence. The experimental investigations at NICA are expected to help elucidating this issue and to develop experimental tools to explore the QCD phase diagram. In the following, we outline several studies that could

be carried out at NICA energy.

Higher moments, chemical freeze-out and QCD critical endpoint

The possibility of the existence of a QCD endpoint has motivated the RHIC beam energy scan program [114, 115] and was one of the basic motivations for FAIR and NICA. By tuning the collision energy from a center of mass energy of 200 GeV down to ~ 5 GeV, one is able to vary the baryon chemical potential from $\mu_b \sim 20$ to μ_b of about 500 MeV. Concerning the critical endpoint, there are large theoretical uncertainties of its location and even its existence is not fully confirmed [69–72]. Higher moments of various physical quantities are conjectured to reflect through their non-monotonic behaviour to be close to the QCD endpoint. It is of great interest to carry out a systematic study for the higher moments of the multiplicity distribution and show their ability to reflect the fluctuations throughout the QCD phase diagram.

Higher Moments

A general expression for r-th non-normalized moment can be deduced from [116]

$$m_r(T,\mu_b) \;=\; \frac{g}{2\pi^2} T \sum_{l=1}^{r} a_{r,l} \int_0^\infty k^2\, dk \frac{e^{l\,\frac{\mu_b-\epsilon}{T}}}{\left(1 \pm e^{\frac{\mu_b-\epsilon}{T}}\right)^l}\,, \tag{3.8}$$

where the coefficients read

$$a_{r,l} \;=\; (\pm 1)^l (-1)^{l+1} \left[l\; a_{r-1,l} + (l-1)\; a_{r-1,l-1} \right], \tag{3.9}$$

where $l \leq r$ and $a_{r,l}$ vanishes for $\forall\, r < 1$. It obvious that the coefficients of a certain moment are to be determined from the chain of previous coefficients. Thus, all moments are entirely depending on the previous ones. The normalization of the higher moments gives additional insights about their properties. The standard deviation σ of the distribution, which is a susceptibility is utilized for this purpose. The quantity σ is related to the correlation length ξ. It provides us with a tool to relate various orders of moments obtained in a measurement. A systematic study of the higher moments within the hadron resonance gas model at finite chemical potentials is introduced in [116].

Advantages at NICA

Recently, various calculations have shown that the higher moments of the multiplicity distributions of some conserved quantities, such as net-baryon, net-charge, and net-strangeness, are sensitive to the correlation length ξ [3, 116, 117], which in turn is related to all moments. NICA provides a unique possibility to study all these variables at large density. In [116], we have shown that strong dynamical fluctuations and correlations appear starting from the normalized third moment (skewness S). The signatures of non-monotonicity in the normalized fourth moment (kurtosis κ) and its products are very clear.

Freeze out conditions

At high temperature and/or density, QCD predicts that the confined hadronic matter dissolves into quark-gluon plasma (QGP) [118]. Reducing the temperature, QGP is conjectured to hadronize again. At some temperature T_{ch}, the produced hadrons entirely freeze out, concerning their chemical composition. The corresponding freeze-out parameters, T_{ch} and baryo-chemical potential μ_B can be determined fropm thermal models by combining various ratios of integrated particle yields [119, 120]. In such a way, we obtain a window in the $T_{ch} - \mu_B$ phase-diagram compatible to the experimental values. The search for common properties of the freeze-out parameters in heavy-ion collisions has a long tradition [121, 122]. Different models have suggested different criteria, for example the average energy per average particle number $< E > / < n >= 1$ GeV [121], the total baryon number density $n_b + n_{\bar{b}} = 0.12$ fm^{-3} [122] and the percolation threshold between the constituents of the hadronic matter [123]. We propose that this objective is achieved best by assigning a specific constant value to the entropy density s divided by T^3 [124, 125]. The meaning of this criterium can be summarized in the following way: produced hadronic matter in its rest frame can be characterized by exceeding a certain number

density of degrees of freedom, otherwise it breaks into separate hadrons. Putting the quantity s/T^3 equal to $\pi^2/4$ results in effective degrees of freedom corresponding to a free gas [126], see the top panel in Fig. 3.28. For vanishing free energy, i.e. at the chemical freeze-out, the *equilibrium* entropy gives the amount of energy which can not be used to produce additional work. We can in this context define the entropy as the ability of sharing and spreading the energy inside the equilibrium system. Furthermore, we find that the strangeness degrees of freedom are essential at low collision energies, where the strangeness chemical potential μ_S is as large as μ_B. According to the strangeness conservation in the heavy-ion collisions, we find that the higher is the collision energy, the smaller is μ_S [127].

The production rates of particles decrease exponentially with their masses. This phenomenological observations are regarded in the way, that increasing energy/temperature is considered by including heavy resonances. Changing energy with changing particle number is given by chemical potential. The amount of energy which produces no additional work, i.e. vanishing free energy, is the entropy at chemical equilibrium.

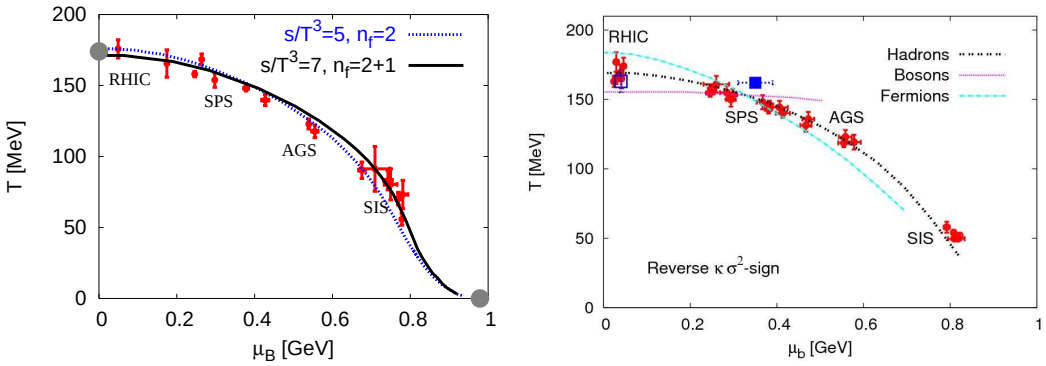

Figure 3.28: Left panel: freeze-out parameters according to constant s/T^3 on top of the experimentally estimated freeze-out parameters (small full circles with errors). For non-strange hadron resonances, we use $s/T^3 = 5$ and for all hadron resonances we assign s/T^3 to 7. Both values have been taken from lattice QCD simulations at zero baryo-chemical potential [124, 125]. We find that strangeness degrees of freedom are essential for reproducing the freeze-out parameters at large densities. Right panel: another condition based on higher moments (double dotted curve). The chemical freezes out is fulfilled when the sign of $\kappa\sigma^2$ is flipped leading to $\kappa = 3\,\chi^2$, where χ is the susceptibility in particle number and κ the kurtosis.

Advantages at NICA

Measuring the multiplicity of particle yields and their ratios besides various thermodynamic properties at NICA energies can be utilized in favour for certain freeze-out parameters. Based on higher moments [116], we introduce a novel condition describing the chemical freeze-out curve. The chemical freeze-out curve is defined by $\kappa = 3\,\chi^2$, where χ is the susceptibility in particle number and κ the kurtosis, see the bottom panel in Fig. 3.28. Besides characterizing the freeze-out parameters, NICA is suitable to study the evolution of κ and χ among other normalized higher moments in thermal and dense medium.

QCD critical Endpoint

In bottom panel of Fig. 3.28, it is interesting to notice that both fermionic and bosonic curves intersect at the hadronic curve at one point. Furthermore, based on the convergence radius of the Taylor expansion in μ_B as obtained in lattice simulations, the critical endpoint as determined in Ref. [70, 71] is given by the solid square. The critical behavior and the existence of the QCD CEP can be identified by means of signatures sensitive to singular parts of the free energy, especially those reflecting dynamical fluctuations of conserved charges, such as baryon number and charge density. The feature that the fermionic and bosonic higher moments are crossing in a point very close to the QCD critical endpoint (CEP) could eventually become confirmed at NICA. To get a clear understanding of why the phase transition at low densities is driven by bosonic degrees of freedom, while the fermionic ones are dominant at large densities, further theoretical and experimental studies have to be pursued. To this destination, NICA shall play an essential role.

Advantages at NICA

The characteristic feature of the CEP is the large correlation length, ξ, and strong dynamical fluctuations. The higher moments are conjectured to be able to reflect the fluctuations associated with the hadron-quark phase transition. This has motivated a remarkable number of experimental and theoretical studies [116,128–132] to be checked in NICA, especially at large densities.

Chiral Condensations

An essential milestone on running NICA is the chiral transition. The quark-antiquark condensates for light (up and down) and strange quark flavors at finite temperatures and chemical potentials have been calculated in HRG, and the results are drawn in Fig. 3.29 [133]. Apparently, the quark-antiquark condensates are given by the derivative of the pressure with respect to the constituent quark masses:

$$< \bar{q}q > \quad = \quad < \bar{q}q >_0 + \sum_h \frac{\partial m_h}{\partial m_q} \frac{\partial \Delta p}{\partial m_h}, \tag{3.10}$$

$$< \bar{s}s > \quad = \quad < \bar{s}s >_0 + \sum_h \frac{\partial m_h}{\partial m_s} \frac{\partial \Delta p}{\partial m_h}, \tag{3.11}$$

where $< \bar{q}q >=< \bar{u}u >=< \bar{d}d >$ represents the light quark-antiquark condensate. Both first terms, $< \bar{q}q >_0$ and $< \bar{s}s >_0$ which are indicating the value of the light and strange quark-antiquark condensates in the vacuum, respectively, have to be modelled [133]. The second quantity which we have to model in order to calculate the quark-antiquark condensates in the hadron gas model is the quark mass dependence of the hadron masses. Results from lattice simulations [135–138] indicate that

$$\frac{\partial m_h}{\partial (m_\pi^2)} \quad = \quad \frac{A}{m_h}, \tag{3.12}$$

where $A \sim 0.9 - 1.2$.

At zero chemical potential (dominating particle production at RHIC and LHC), we find that at the temperature, where the light quark-antiquark condensates entirely vanish, the strange quark-antiquark condensate still keeps a relatively large fraction of its vacuum value. This is in agreement with results obtained in lattice simulations and in chiral perturbation theory at finite temperature and zero chemical potentials. Furthermore, we find that this effect of separation slowly disappears at larger baryon chemical potential (describing to FAIR and NICA). These results might have significant consequences for our understanding of QCD at finite temperatures and chemical potentials. Concretely, our results imply that there might be a domain of temperatures where chiral symmetry is restored for light quarks, but still broken for the strange quark, and that this persists at small chemical potentials. This might have practical consequences for heavy ion collision experiments.

Advantages at NICA

We conclude that the strange quark-antiquark condensate can be relatively large at temperatures where the light quark-antiquark condensate is very small. We obtained these results from the hadron resonance gas model. Our results agree with the recent MILC lattice simulations at zero temperature and chemical potentials. The uncertainty of the value of the strange quark-antiquark condensate at this critical temperature is however rather large. This is due to the uncertainty in the values of the condensates at high temperatures which we have calculated by the hadron resonance gas model. This uncertainty could be considerably reduced, if the factor A in Eq. (3.12) were more precisely known.

The chiral symmetry restoring transition is conjectured to be accompanied with a remarkable increase in mass of the lightest Goldstone bosons, pions. Decreasing T, quarks and gluons are assumed to get confined to hadrons (deconfinement-confinement phase transition) and the chiral symmetry almost simultaneously breaks down, i.e., orientation of right- and left-handed quarks. The latter likely leads to production of Goldstone bosons. Dynamical fluctuations of these particles and/or disoriented chiral condensates (DCC) would manifest this transition.

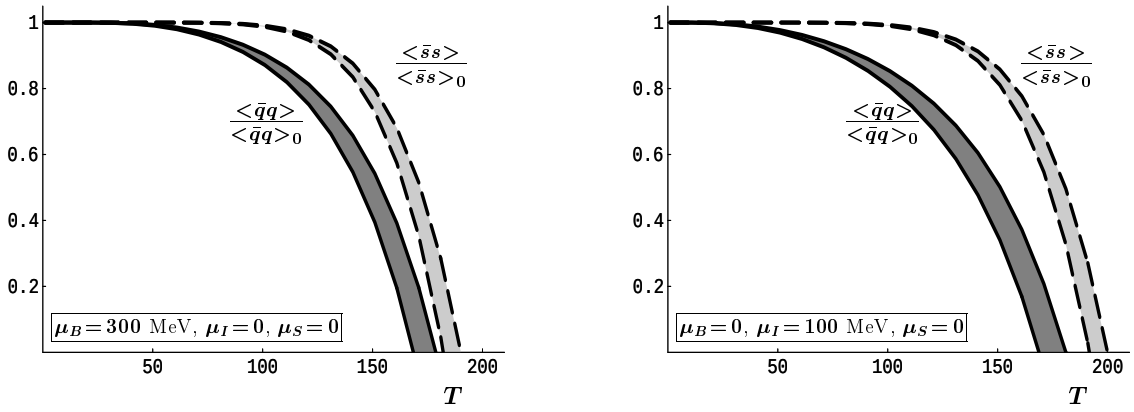

Figure 3.29: The quark-antiquark condensates as a function of temperature at different values of baryon, isospin, and strangeness chemical potentials. The light quark-antiquark condensate $\frac{<\bar{q}q>}{<\bar{q}q>_0}$ is in dark gray and solid curve. The strange quark-antiquark condensate $\frac{<\bar{s}s>}{<\bar{s}s>_0}$ is given in light gray and dashed curve. Left panel: $\mu_B = 300$ MeV, $\mu_I = 0$, and $\mu_S = 0$. Right panel: $\mu_B = 0$, $\mu_I = 100$ MeV, and $\mu_S = 0$. Although chemical potentials have been set to finite values, the critical temperature corresponding to the light quark condensate is still smaller than that of the strange quark.

In-Medium Modifications of essential hadronic properties

The screening masses of different hadronic states are studied in thermal and dense medium on lattice [134]. It has been found that screening masses increase with the temperature. In the deconfined phase, the chemical potential also enhances the screening masses and screening masses are expected to approach $l\pi T$, the lowest Matsubara frequency. Therefore, we suggest to use screening masses normalized to lowest Matsubara frequency to determine the temperatures, at which hadronic bound states dissolve into free quarks. In this limit, the screening mass does not depend on the *parent* bound states. At very high temperatures, one would expect a universal line of screening masses from different hadronic states, $m_D = l\pi T a = l\pi/N_\tau$, where a is lattice spacing and N_τ is the time extention of the lattice (in lattice units). The values of l depend on hadronic states, $l = 2$ for mesons and $l = 3$ for baryons. The temporal masses vanish in the limit of free fields. Interactions with thermal and dense medium drive temporal masses away from free field limit. In other words, differences between temporal and spatial (screening) masses show how close is an interacting system to the case of free quarks.

The screening masses can be used to characterize different physical quantities. Their values depend on the properties of the medium. Therefore, screening masses may provide a useful tool to investigate the properties of quark-gluon plasma phase. Values of screening masses can also quantize the response of the medium to weak perturbations, like hadrons. The response likely appears in form of dynamical Debye screening of long-range Coulomb potential. There are different definitions for screening masses. They are related to the inverse of the Debye screening length. On the other hand, they are the static limits of longitudinal vacuum polarization tensor $\prod_{00}(p \to 0)$. It has been found that different hadronic states have different dissolving temperatures and their chance of survival is considerably improved at finite chemical potential.

$$\frac{m_D(T,\mu_q)}{T} = \frac{m_D(T)}{T}\bigg|_{\mu_q=0} + \left(\frac{\mu_q}{T}\right)\frac{\partial m_D(T)}{\partial \mu_q}\bigg|_{\mu_q=0} + \left(\frac{\mu_q}{T}\right)^2 \frac{T}{2}\frac{\partial^2 m_D(T)}{\partial \mu_q^2}\bigg|_{\mu_q=0} + \cdots$$

Many results given in [134] may considerably improve our understanding of deconfinement, QCD phase structure and critical phenomenon at high temperatures and densities.

The screening masses at finite temperatures are defined by the exponential spatial falloff of the correlation of two static sources. The screening mass depends significantly on the bare mass. Debye screening mass, M_D, is a quantity of special interest. Its inverse gives the screening length of static choromo-electric fields. It plays an important role in regulating some infra-red singularities.

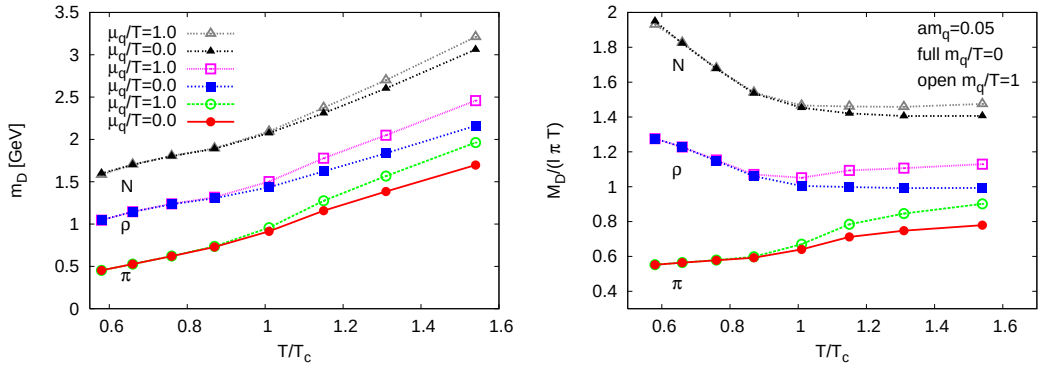

Figure 3.30: Left panel: Screening masses, m_D as function of T/T_c for three hadronic states at $am_q = 0.05$. We set physical units according to $T_c = 0.225$ GeV. Right panel: m_D are normalized to lowest Matsubara frequency $l\pi T$, where $l = 2$ for mesons and $l = 3$ for baryons.

3.13 Lattice QCD constrained CEP prediction in nonlocal PNJL models

G. A. Contrera[a,b,c], A. G. Grunfeld[b,d,e], D. Blaschke[c,f]

[a] *Gravitation, Astrophysics and Cosmology Group, FCAyG, UNLP, La Plata, Argentina*
[b] *CONICET, Rivadavia 1917, 1033 Buenos Aires, Argentina*
[c] *Institute for Theoretical Physics, University of Wrocław, Poland*
[d] *Departamento de Física, Comisión Nacional de Energía Atómica, (1429) Buenos Aires, Argentina*
[e] *Department of Physics, Sultan Qaboos University, Sultanate of Oman*
[f] *Joint Institute for Nuclear Research, Dubna, Russia*

We discuss a scheme for extracting the location of the CEP in the QCD phase diagram based on nonlocal PNJL models where the formfactors of the covariant interaction model are constrained by lattice QCD data for the quark propagator and the strength of the vector coupling is adjusted such as to reproduce the slope of the pseudocritical temperature of the chiral phase transition at low chemical potential extracted recently from lattice QCD simulations. Our study supports the existence of a critical point and favors for its location the region 69.9 MeV $\leq T_{\rm CEP} \leq$ 129.8 MeV and 276.6 MeV $\leq \mu_{\rm CEP} \leq$ 319.1 MeV.

The conjecture for the existence of a critical endpoint (CEP) of first order phase transitions in the QCD phase diagram is the basis for recent as well as future beam energy scan (BES) programs in relativistic heavy-ion collision experiments at RHIC, SPS, NICA and FAIR which try to identify the parameters of its position $(T_{\rm CEP}, \mu_{\rm CEP})$. The theoretical situation is very unsatisfactory since the predictions for this position form merely a skymap in the $T - \mu$ plane [139].

Given the now well-established result from lattice QCD that at zero and small chemical potential μ the chiral and deconfinement transitions are crossover with a pseudocritical temperature of $T_c(0) = 154 \pm 9$ MeV [140] leaves us with a variety of possibilities for the phase structure at nonzero μ of which we want to mention a few:

- no CEP at all [141], since the transition is crossover in the whole phase diagram.
- no CEP, but a Lifshitz point [61],
- one CEP, but with largely differing predictions of its position [139]
- second CEP [142–144]
- CEP and triple point, possibly coincident, due to another phase (i.e. color superconducting [145] or quarkyonic [49] matter) at low temperatures and high densities

This situation is rather unsatisfactory in view of the upcoming experimental programmes. In the present contribution, we discuss the existence and location of a CEP within the class of nonlocal chiral quark models coupled to the Polyakov loop potential on the selfconsistent meanfield level.

The Lagrangian of these models is given by

$$\mathcal{L} = \bar{q}(i\not{D} - m_0)q + \mathcal{L}_{\rm int} + \mathcal{U}(\Phi) \ , \tag{3.13}$$

where q is the $N_f = 2$ fermion doublet $q \equiv (u,d)^T$, and m_0 is the current quark mass (we consider isospin symmetry, that is $m_0 = m_u = m_d$). The covariant derivative is defined as $D_\mu \equiv \partial_\mu - iA_\mu$, where A_μ are color gauge fields.

The nonlocal interaction channels are given by

$$\mathcal{L}_{\rm int} = -\frac{G_S}{2}\Big[j_a(x)j_a(x) - j_P(x)j_P(x)\Big] - \frac{G_V}{2} j_V(x)\, j_V(x), \tag{3.14}$$

where the nonlocal currents are

$$\begin{aligned} j_a(x) &= \int d^4z\ g(z)\ \bar{q}\left(x+\frac{z}{2}\right)\ \Gamma_a\ q\left(x-\frac{z}{2}\right)\ , \\ j_P(x) &= \int d^4z\ f(z)\ \bar{q}\left(x+\frac{z}{2}\right)\ \frac{i\overleftrightarrow{\not\partial}}{2\ \kappa_p}\ q\left(x-\frac{z}{2}\right)\ , \\ j_V(x) &= \int d^4z\ g(z)\ \bar{q}\left(x+\frac{z}{2}\right)\ \gamma^0\ q\left(x-\frac{z}{2}\right). \end{aligned} \tag{3.15}$$

with $\Gamma_a = (\Gamma_S, \Gamma_P) = (\mathbf{1}, i\gamma_5\vec{\tau})$ for scalar and pseudoscalar currents respectively, and $u(x')\overleftrightarrow{\partial} v(x) = u(x')\partial_x v(x) - \partial_{x'}u(x')v(x)$. The functions $g(z)$ and $f(z)$ in Eq.(3.15), are nonlocal covariant form factors characterizing the corresponding interactions. The scalar-isoscalar component of the $j_a(x)$ current will generate the momentum dependent quark mass in the quark propagator, while the "momentum" current, $j_P(x)$, will be responsible for a momentum dependent wave function renormalization of this propagator. Note that the relative strength between both interaction terms is controlled by the mass parameter κ_p introduced in Eq. (3.15). Finally, $j_V(x)$ represents the vector channel interaction current, whose coupling constant G_V is usually taken as a free parameter.

In what follows it is convenient to Fourier transform into momentum space. Since we are interested in studying the characteristics of the chiral phase transition we have to extend the effective action to finite temperature T and chemical potential μ. In the present work this is done by using the Matsubara and imaginary time formalisms. Concerning the gluon fields we use the same prescription as in previous works [146, 147], but in this case, the we have chosen a μ-dependent logarithmic effective potential described in [148].

$$\mathcal{U}(\Phi, T, \mu) = (a_0 T^4 + a_1\mu^4 + a_2 T^2\mu^2)\Phi^2 + a_3 T_0^4 \ln\left(1 - 6\Phi^2 + 8\Phi^3 - 3\Phi^4\right), \tag{3.16}$$

where there parameters are $a_0 = -1.85$, $a_1 = -1.44\text{x}10^{-3}$, $a_2 = -0.08$, $a_3 = -0.40$. In the present work we set the T_0 parameter by using the value corresponding to two flavors $T_0 = 208$ MeV, as it has been suggested in Refs. [150, 199, 224].

Finally, in order to fully specify the nonlocal model under consideration we fix the model parameters as well as the form factors $g(q)$ and $f(q)$ following Refs. [152] and [147], i.e. considering two different types of functional dependencies for these form factors: exponential forms (Set A and Set B) and Lorentzians (Set C). In order to compare with some recent results [141], we have included a local parametrization, using in this case the parameters in [38].

In Fig. 11.5 we show the shapes of normalized dynamical masses and wave function renormalization for the models under discussion here, i.e., the nonlocal models of set A (rank-one), set B and set C (rank-two) as well as the local limit.

The model inputs have been constrained with results from recent lattice QCD studies. In particular, the form factors of the nonlocal interaction can be chosen such as to reproduce the dynamical mass function $M(p)$ and the wave function renormalization (WFR) $Z(p)$ of the quark propagator in the vacuum [153], see Fig. 11.5.

Within this framework the mean field thermodynamical potential $\Omega^{\rm MFA}$ results

$$\Omega^{\rm MFA} = -4T\sum_c\sum_n\int\frac{d^3\vec{p}}{(2\pi)^3}\ln\left[\frac{(\tilde{\rho}^c_{n,\vec{p}})^2 + M^2(\rho^c_{n,\vec{p}})}{Z^2(\rho^c_{n,\vec{p}})}\right] + \frac{\sigma_1^2 + \kappa_p^2\ \sigma_2^2}{2\,G_S} - \frac{\omega^2}{2G_V} + \mathcal{U}(\Phi, T). \tag{3.17}$$

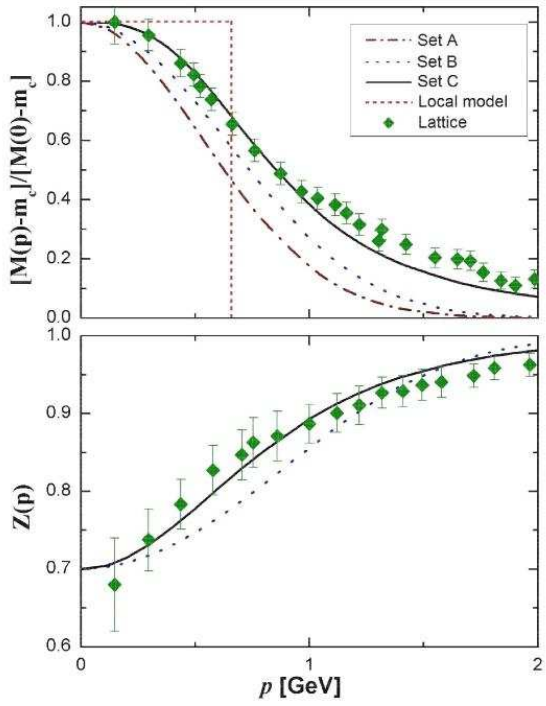

Figure 3.31: (Adapted from Ref. [152]). Normalized dynamical masses for the different form factors under study and wave function renormalization for Set B and Set C, fitted to lattice data [153].

where $M(p)$ and $Z(p)$ are given by

$$\begin{aligned} M(p) &= Z(p)\,[m+\sigma_1\ g(p)]\,, \\ Z(p) &= [1-\sigma_2\ f(p)]^{-1}\,. \end{aligned} \tag{3.18}$$

In addition, we have defined [136]

$$\left(\rho^c_{n,\vec{p}}\right)^2 = \left[(2n+1)\pi T - i\mu + \phi_c\right]^2 + \vec{p}^{\,2}\ , \tag{3.19}$$

where the quantities ϕ_c are given by the relation $\phi = \mathrm{diag}(\phi_r, \phi_g, \phi_b)$. Namely, $\phi_c = c\ \phi_3$ with $c = 1, -1, 0$ for r, g, b, respectively. In the case of $\left(\tilde{\rho}^c_{n,\vec{p}}\right)$ we have used the same definition as in Eq.(3.19) but shifting the chemical potential according to

$$\tilde{\mu} = \mu\ - \omega\ g(p)\ Z(p). \tag{3.20}$$

$\Omega^{\rm MFA}$ turns out to be divergent and, thus, needs to be regularized. For this purpose we use the same prescription as in Refs. [147, 155]. The mean field values $\sigma_{1,2}$, ω and ϕ_3 at a given temperature or chemical potential, are obtained from a set of four coupled "gap" equations which come from the minimization of the regularized thermodynamical potential, that is

$$\frac{\partial\Omega^{\rm MFA}_{reg}}{\partial\sigma_1} = \frac{\partial\Omega^{\rm MFA}_{reg}}{\partial\sigma_2} = \frac{\partial\Omega^{\rm MFA}_{reg}}{\partial\omega} = \frac{\partial\Omega^{\rm MFA}_{reg}}{\partial\phi_3} = 0. \tag{3.21}$$

The vector coupling channel is considered a free parameter which in the mean field approximation (MFA) may be adjusted such as to reproduce the behaviour of $T_c(\mu)$ which has recently been obtained by Taylor expansion technique in lattice QCD [156]

$$T_c(\mu)/T_c(0) = 1 - \kappa(\mu/T_c)^2 + \mathcal{O}[(\mu/T_c)^4]\ , \tag{3.22}$$

with $\kappa = 0.059(2)(4)$.

We also want to include in our analysis the results arising from a local PNJL model. For that purpose, we started from the Lagrangian in [157] with two flavors instead of three. Moreover, we consider that the chemical potential is shifted by

$$\tilde{\mu} = \mu \ - \omega. \tag{3.23}$$

We use the same set of parameters as in [38].

In Fig. 3.32 we compare the lattice result with the values for the coefficient κ obtained within the nonlocal PNJL models for different strengths $\eta_V = G_V/G_S$ of the vector coupling.

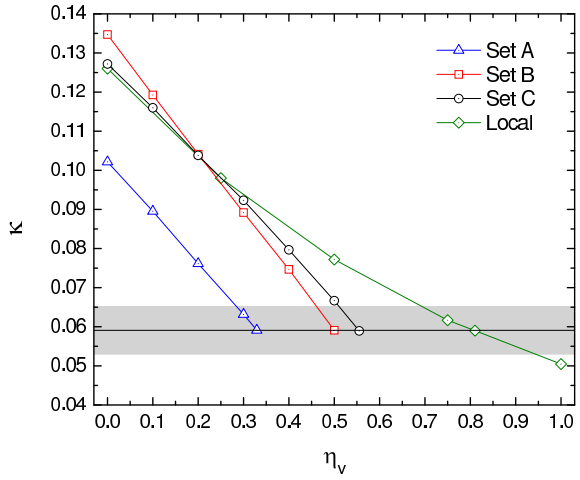

Figure 3.32: Curvature κ of the pseudocritical temperature $T_c(\mu)$ of the chiral crossover transition at low values of μ/T. The black line corresponds to the lattice QCD prediction of $\kappa = 0.059(2)(4)$ [156].

Note that for fitting the lattice QCD value in the local model a larger vector coupling is required than in the nonlocal ones. The consequences for predictions about the existence and location of the CEP are dramatic, see Fig. 3.33. Also the absolute value of the critical temperature $T_c(0)$ in the local model is significantly different (larger) than in the nonlocal one.

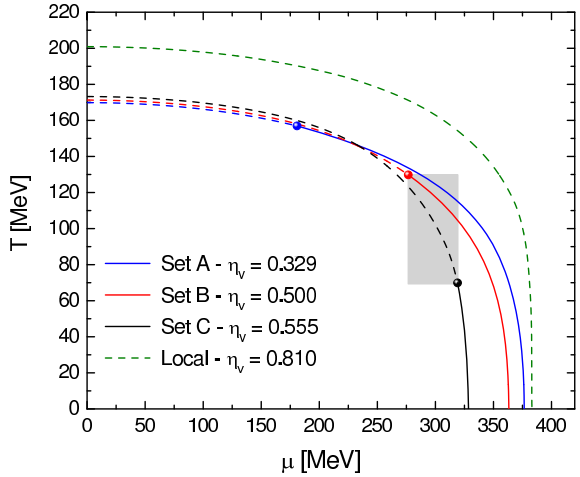

Figure 3.33: Phase diagrams with (pseudo)critical temperatures $T_c(\mu)$ and critical points for nonlocal PNJL models (set A-C) compared to the local one. Dashed (full) lines correspond to crossover (first order) transitions. The vector coupling strength η_V is chosen so that these models reproduce the lattice QCD result $\kappa = 0.059(2)(4)$ [156] for the curvature at low μ-values. The corresponding values for $T_c(\mu = 0)$ (in MeV) are 169.9, 171.3, 173.2 and 200.9, for Sets A, B, C and local, respectively. The highlighted rectangular region denotes the CEP position favored by the present study.

The results indicate that the $T_c(0)$ of nonlocal covariant PNJL models is rather insensitive to the choice of the form factors parametrizing the momentum dependence (running) of dynamical mass function and WFR of the quark propagator as measured on the lattice at zero temperature [153], whereas the position of the CEP and critical chemical potential at $T = 0$ strongly depends on it.

In view of this finding, the absence of a CEP reported recently in the local limit [141] as well as the result for set A which neglects WFR cannot be trusted. The region of CEP's suggested by our study is between the results for set B and set C, i.e. $(T_{\rm CEP}, \mu_{\rm CEP}) = (129.8\ {\rm MeV}, 276.6\ {\rm MeV})$ and $(69.9\ {\rm MeV}, 319.1\ {\rm MeV})$, respectively.

This means that the search for CEP signatures in the BES programs is justified and should be continued. The energy range of the NICA and FAIR facilities shall be particularly promising. As a characteristic feature of the region around the CEP any phase transition signals based on changes in the bulk properties are not pronounced. Therefore, sensible observables are required for the identification of the CEP position like, e.g., higher moments of the identified particle distributions [126, 159] or the flow of nuclear clusters [160].

In conclusion, we have presented progress in the extraction of the CEP location in the QCD phase diagram based on nonlocal PNJL models constrained by lattice QCD. Note that in this exploratory study the lattice QCD data for the quark propagator data and for the curvature of the pseudocritical line are obtained with different lattice actions. A more consistent study should be based on the same discretization of the action, provide a continuum extrapolation and work with physical quark masses.

As a next step it is necessary to investigate the robustness of the results of the nonlocal PNJL models when modifying the choice of the Polyakov-loop potential taking into account recent developments [161–163] and, in particular, when going beyond the mean field approximation. A scheme for going beyond the meanfield in nonlocal PNJL models by including hadronic correlations (bound states and their dissociation in the continuum of scattering states) has recently been developed [164] and shall be generalized for studies of the chiral and deconfinement phase transition in the QCD phase diagram. A key quantity for such studies will be the hadronic spectral function and first results using a generic ansatz [165] for joining the hadron resonance gas and PNJL approaches are promising [166].

Acknowledgement

We would like to thanks to C. Schmidt and K. Redlich for useful comments and discussions. D.B. acknowledges hospitality and support during his visit at University of Bielefeld and funding of his research provided by the Polish NCN under the "Maestro" Grant programme as well as by the Russian Fund for Basic Research under Grant No. 11-02-01538-a. G.C. is grateful for support by CONICET (Argentina) and by the Polish Ministry for Science and Higher Education within the CompStar-POL project.

3.14 From ultra-high densities towards NICA densities: color-flavor locking and other color superconductors

A. Schmitt

Institut für Theoretische Physik, Technische Universität Wien, Austria

Experiments at NICA are expected to produce the highest baryon densities ever seen in a laboratory, exploring a theoretically extremely challenging and so far poorly understood regime of Quantum Chromodynamics (QCD). One guide for what we may expect and what we should be looking for comes from lower-density physics, for instance from heavy-ion collisions at RHIC or CERN as well as from theoretical studies within lattice gauge theory, nuclear physics or perturbative approaches. What can we learn from approaching NICA densities "from above", i.e., by making use of what we know about even higher densities? Clearly, our knowledge about this ultra-dense regime of QCD seems much less solid. However, we do observe matter (in an indirect way) that is at least as dense, probably a few times denser, than collisions at NICA will be able to produce, namely in the interior of compact stars. And, from the theoretical point of view, we do have solid knowledge about asymptotically dense QCD, where asymptotic freedom ensures that quarks are weakly interacting. In the following, I will comment on this asymptotic regime and about what we can learn from taking this regime as a starting point for a theoretical journey towards lower densities that can possibly be reached by NICA.

Color-flavor locking at asymptotically large densities

In sufficiently cold and dense matter a condensate of quark Cooper pairs is formed, analogous to Cooper

pairing of electrons in a superconductor. Since the interactions are weak at ultra-high density, the ground state can essentially be described within BCS theory, i.e., Cooper pairs are formed only in a small vicinity around the Fermi surface. In order to minimize the free energy, it is advantageous to pair as many quark species as possible. In three-flavor quark matter[5] there is one unique possibility (up to rotations in color and flavor space that don't change the physics) to pair *all* quark species, and one can prove rigorously that the resulting state is the ground state at asymptotically large quark chemical potential μ. This state is called the color-flavor locked (CFL) state [167] and is best characterized by its spontaneous symmetry breaking pattern (local groups in square brackets),

$$[SU(3)_c] \times U(1)_B \times \underbrace{SU(3)_L \times SU(3)_R}_{\supset [U(1)_Q]} \to \underbrace{SU(3)_{c+L+R}}_{\supset [U(1)_{\tilde{Q}}]} \times \mathbb{Z}_2 \,. \tag{3.24}$$

The left-hand side is the symmetry group of QCD, while the CFL state is invariant under transformations of the group on the right-hand side. Several properties of CFL are suggested by this symmetry breaking pattern: CFL is a color superconductor, i.e., the gluons acquire a Meissner mass. A combination of one of the gluons and the photon remains massless, hence there is a residual gauge symmetry group $U(1)_{\tilde{Q}}$ with a "rotated" charge $\tilde{Q}$. As a consequence, CFL is not an electromagnetic superconductor. CFL breaks chiral symmetry, and as a result there are eight Goldstone modes, very similar to the meson octet at low densities due to "usual" chiral symmetry breaking. At asymptotic densities we can neglect all quark masses, and thus chiral symmetry is exact, leading to exactly massless Goldstone modes.[6] CFL is a superfluid since baryon number conservation symmetry $U(1)_B$ is broken spontaneously. Since this group is an exact symmetry of QCD, there is another, exactly massless Goldstone mode.

These arguments are rigorous and based on first principle QCD calculations since we have chosen to work at sufficiently large densities. However, these densities are larger by many orders of magnitude than any density possibly reached in collider experiments and compact stars. We thus have to ask what happens if we go down in density. Two difficult challenges arise. First, we leave the region of asymptotic freedom and enter the strong coupling regime. Currently, there is no reliable first-principle method that tells us how to describe dense QCD matter at large, but not asymptotically large, density. The second challenge arises from the strange quark mass m_s which can no longer be neglected and thus disrupts the particularly symmetric CFL state. Many studies using perturbative methods, effective theories, and phenomenological models such as the Nambu-Jona-Lasinio (NJL) model have investigated this scenario and the emerging picture is as follows (see Ref. [**?**] for many more details and more references).

Towards NICA densities

A difference in quark masses induces a difference in Fermi momenta of the quarks that form Cooper pairs, because in the energetically favorable spin-zero channel quarks of different flavor pair. Therefore, there is a cost in free energy associated with pairing at an average, common Fermi momentum. If the mismatch in Fermi momenta is small enough, the condensation energy from pairing can overcome this cost and the usual superconducting state survives. In the case of dense quark matter, this is the case if m_s^2/μ is small compared to the energy gap Δ in the quasiparticle excitation spectrum. Starting from CFL and going down in density thus means to increase m_s^2/μ, and at large densities we may treat m_s^2/μ as a small parameter, going beyond pure CFL in a controlled way.[7] At first, CFL reacts on the stress imposed in the strangeness sector by producing anti-strangeness via a kaon condensate [168,169], the kaon being the lightest CFL meson [170]. This modification of CFL is called CFL-K^0. Importantly, all quarks remain gapped in this phase and thus the low-energy properties of CFL-K^0 are dominated by the meson sector, including the additional Goldstone mode that arises from the condensation of kaons.

All other color superconductors – with the possible exception of the so-called color-spin locked phase – have unpaired fermionic modes (which may form Cooper pairs among themselves, however with much smaller energy gaps). The reason is that, if the mismatch in Fermi momenta becomes too large, Cooper pairs start to break, first in certain directions in momentum space. The resulting phases typically have counter-propagating

[5] We ignore the three heavy quark flavors even though they will be populated for asymptotically large chemical potentials. The reason is that we are ultimately interested in much lower densities where only up, down, and strange quarks play a role.

[6] This is no longer true for densities relevant for compact stars or NICA, where the CFL mesons are pseudo-Goldstone modes (if CFL exists at these densities).

[7] Of course, m_s, Δ, and also the strong coupling constant are actually functions of μ and thus in a complete treatment there is only a single parameter, the chemical potential.

currents [171, 172] and may exhibit crystalline structures where the quasiparticle gap varies periodically in position space and vanishes on certain surfaces. These so-called Larkin-Ovchinnikov-Fulde-Ferrell (LOFF) phases with CFL pairing pattern have the interesting property of being a superfluid and a crystal at the same time. If we further increase m_s^2/μ, we may reach a regime where only up and down quarks form Cooper pairs $\langle ud \rangle$ ("2SC phase" [173]), or where only single-flavor pairs $\langle uu \rangle$ etc are formed, then in the spin-one channel with interesting possible phases not unlike the phases of superfluid helium-3 [174, 175]. Since we do not know the density dependence of the strange quark mass, we do not know which of these phases reside in which region of the QCD phase diagram. It is possible that the CFL phase persists down to the phase transition to hadronic matter, in which case a smooth crossover to the hadronic phase is conceivable [144, 176, 177]. Or there may be a very rich phase structure in between, which would not be surprising given the complicated phase diagrams of ordinary condensed-matter systems. Of course, in this regime close to the hadronic phase we are already deep in the strong coupling region where we cannot exclude that even more exotic phases occur. At the very least, Cooper pairing will not be restricted anymore to a small vicinity of the Fermi surface, and one can speculate whether there is something like a BCS-BEC crossover similar to ultra-cold gases where the interaction strength can be tuned experimentally [178].

For a possible creation of color-superconducting phases at NICA it is also relevant at which temperatures they can be expected to be found. In the asymptotic regime, weak-coupling results yield a relation between the critical temperature and the quasiparticle gap Δ that is similar, but not identical [179], to BCS theory. For CFL,

$$T_c = 2^{1/3} \frac{e^\gamma}{\pi} \Delta \simeq 0.71\, \Delta\,, \tag{3.25}$$

with the Euler-Mascheroni constant γ. The weak-coupling result for the gap is $\Delta \propto \mu \exp(-\text{constant}/g)$, where g is the strong coupling constant.[8] Extrapolating this result to quark chemical potentials of $\mu \sim 400\,\text{MeV}$ gives a critical temperature of about $T_c \sim 20\,\text{MeV}$. This is a bold extrapolation over many orders of magnitude. It is interesting, however, that this estimate is in approximate agreement with estimates from the NJL model which predicts $T_c \simeq (10 - 100)\,\text{MeV}$. The fact that two completely different approaches agree, one from ultra-high density and one from a phenomenological model with parameters matched to low-density quantities, gives us some confidence that this estimate for the critical temperature is meaningful. One concludes that compact stars (which cool down very quickly from about 10 MeV at their birth to temperatures in the keV regime) are clearly cold enough to accommodate color superconductors. For matter created at NICA a prediction is naturally less firm, but temperatures around or even below T_c are certainly conceivable.

Color-superconducting phases have interesting phenomenological properties which have mostly been studied in view of astrophysical applications. In this context, one is interested in the equation of state, neutrino emissivity, and various transport properties. There is a qualitative difference in the neutrino emissivity and the transport properties of CFL and all other non-CFL color superconductors. The reason is that CFL is the only quark matter phase where all fermionic modes are gapped and the low-energy properties are entirely determined by the Goldstone modes, see for instance Refs. [180–182]. Moreover, since CFL is a superfluid, its hydrodynamic properties are nontrivial. Especially in the kaon-condensed phase, CFL appears to be a complicated multi-component fluid, and first attempts towards a complete hydrodynamic description have been made recently [183]. It will be interesting to see whether NICA may provide sufficiently cold and dense matter to find signatures of these nontrivial hydrodynamics or other manifestations of color-superconducting quark matter.

3.15 Restoration of singlet axial symmetry at finite temperature and density

S. Benić[1], D. Horvatić[1], D. Kekez[2], D. Klabučar

[1] *Physics Department, University of Zagreb, Zagreb, Croatia*
[2] *Rugjer Bošković Institute, Zagreb, Croatia*

To accommodate recent RHIC data on η' multiplicity, the present authors proposed [in Phys. Rev. **D84**, 016006 (2011)] a modification of the Witten-Veneziano relation at high temperature (T). This predicted theo-

[8] Taking into account that due to asymptotic freedom $1/g^2$ increases logarithmically with μ, we know that $\exp(-\text{constant}/g)$ decreases more slowly than $1/\mu$. Consequently, Δ (and thus also T_c) *increases* with μ at asymptotically large μ (while Δ/μ decreases).

retically a significant drop of η' mass at high T, signaling a partial restoration of the $U(1)_A$ symmetry of QCDat temperatures around and beyond the temperature of the chiral symmetry restoration.

This happens because our theoretical approach predicts that the anomalous contribution to the η' mass is related to the chiral quark condensate. Therefore, a partial restoration of the $U(1)_A$ symmetry should also happen at a sufficiently high density. We therefore propose herewith, that NICA should investigate the fate of the $U(1)_A$ symmetry in the accessible areas of the (T, μ)-phase diagram.

The ultra-relativistic heavy-ion collider facilities like RHIC at BNL, LHC at CERN, and NICA at JINR aim to produce and study a new form of hot and/or dense QCD matter - quark-gluon plasma (QGP). The most compelling signal for production of QGP would be a restoration - in hot and/or dense QGP - of the symmetries of the QCD Lagrangian which are broken in the vacuum.

One of them is [$\mathrm{SU}_A(N_f)$ flavor] chiral symmetry, whose dynamical breaking leads, for $N_f = 3$ light quark flavors, to the octet of light, (almost-)Goldstone pseudoscalar mesons $\pi^0, \pi^\pm, K^0, \bar{K}^0, K^\pm, \eta$.

The second one is $\mathrm{U}_A(1)$ symmetry. Its breaking by the non-Abelian axial Adler-Bell-Jackiw anomaly ('gluon anomaly' for short) makes the remaining pseudoscalar meson of the light-quark sector, the η', much heavier, preventing its appearance as the ninth (almost-)Goldstone boson of dynamical chiral symmetry breaking (DChSB) in QCD.

The first experimental signature of a partial restoration of $\mathrm{U}_A(1)$ symmetry seems to have been found in the $\sqrt{s_{NN}} = 200$ GeV central Au+Au reactions at RHIC. Namely, Csörgő *et al.* [184] analyzed combined data of PHENIX [185] and STAR [186] collaborations very robustly, through six popular models for hadron multiplicities, and found that at 99.9% confidence level, the η' mass in the vacuum is reduced by more than 200 MeV inside the fireball: $M_{\eta'}(\text{vacuum}) = 957.8$ MeV drops to $M_{\eta'}(\text{fireball}) = 340^{+50+280}_{-60-140} \pm 45$ MeV [184], thus signaling restoration of the Goldstone character of η' [187] and, consequently, the restoration of $\mathrm{U}_A(1)$ symmetry, which would otherwise preclude this.

The Witten-Veneziano relation (WVR) [188, 189]

$$M_\eta^2 + M_{\eta'}^2 - 2M_K^2 = \frac{2\,N_f}{f_\pi^2}\,\chi_{\mathrm{YM}}. \tag{3.26}$$

indicates that the anomalously high mass of η' is contributed by the glue sector, since it is determined, at least at $T = 0$, by the Yang-Mills topological susceptibility χ_{YM}. This is seen especially clearly in the chiral limit of vanishing current quark masses, $m_q \to 0$, for all N_f light flavors $q = u, d, s$, where all non-anomalous pseudoscalar meson masses vanish according to Gell-Mann–Oakes–Renner (GMOR) relation and η' is purely singlet, $\eta' = \eta_0$. Then WVR relation (3.26) becomes

$$\Delta M_{\eta_0}^2 = \Delta M_{\eta'}^2 = \frac{2\,N_f}{f_\pi^2}\,\chi_{\mathrm{YM}}\,, \tag{3.27}$$

since in the chiral limit the only nonvanishing pseudoscalar meson mass is the anomalous contribution ΔM_{η_0}, which M_{η_0} receives because the divergence of the singlet axial quark current $\bar{q}\gamma^\mu\gamma_5\frac{1}{2}\lambda^0 q$ is nonvanishing even for $m_q = 0$ due to the gluon anomaly. The chiral-limit version (3.27) is a very good approximation to the full WVR relation (3.26) even realistically away from the chiral limit, since the non-anomalous contributions to the pseudoscalar meson masses largely cancel in Eq. (3.27), as shown [190], for example, by using GMOR relation. Thus Eq. (3.27) points out especially transparently the ratio $\chi_{\mathrm{YM}}(T)/f_\pi(T)^2$ as crucial for the anomalous η' mass and its evolution with temperature T.

Previous studies [191] using the straightforward extension of WVR to $T > 0$, found that η' mass increases as T approaches the chiral restoration temperature T_{Ch}. The problem is that this is *contrary* to the experimental findings of Csörgő *et al.* [184]. This is happening as T approaches T_{Ch}, due to the fact that there $f_\pi(T)$ starts decreasing significantly, but $\chi_{\mathrm{YM}}(T)$, being a pure-glue quantity, does **not**, until much higher T. (Namely, the pseudocritical temperatures for the chiral and deconfinement transitions in the full QCD are lower than T_{YM} by some 100 MeV or more, due to the presence of the quark degrees of freedom – for example, see Ref. [192].)

One must therefore conclude that either WVR breaks down as soon as T approaches T_{Ch}, or that the T-dependence of its anomalous contribution is different from the pure-gauge $\chi_{\mathrm{YM}}(T)$. Refs. [190, 193] showed that the latter alternative is possible, since WVR can be reconciled with experiment thanks to the existence of another relation which, similarly to WVR, connects the YM theory with full QCD. Leutwyler-Smilga (LS) relation (derived at $T = 0$) [194]

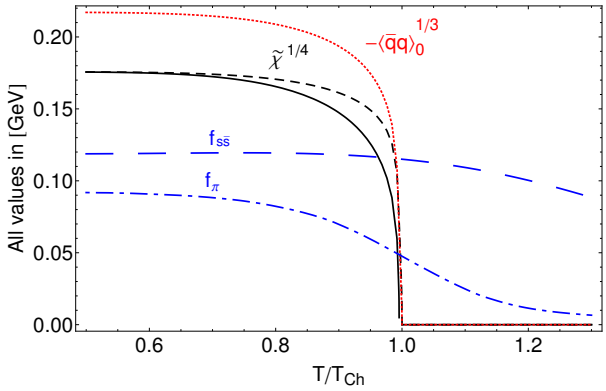

Figure 3.34: The relative-temperature dependences, on $T/T_{\rm Ch}$, of $\widetilde{\chi}^{1/4}$, $\langle\bar{q}q\rangle_0^{1/3} \equiv \Sigma^{1/3}$, f_π and $f_{s\bar{s}}$. The solid curve depicts $\widetilde{\chi}^{1/4}$ for $\delta = 0$, and the short-dashed curve is $\widetilde{\chi}^{1/4}$ for $\delta = 1$. At $T = 0$, both $\widetilde{\chi}$'s are equal to $\chi_{\rm YM} = (0.1757\,{\rm GeV})^4$, the weighted average [191] of various lattice results for $\chi_{\rm YM}$.

$$\chi_{\rm YM} \;=\; \frac{\chi}{1+\frac{\chi}{\Sigma}\left(\frac{1}{m_u}+\frac{1}{m_d}+\frac{1}{m_s}\right)} \;\equiv\; \widetilde{\chi} \tag{3.28}$$

expresses $\chi_{\rm YM}$ by QCD quantities: the QCD topological susceptibility χ and the *chiral-limit* quark condensate $\langle\bar{q}q\rangle_0 \equiv \Sigma$. Their combination, which we call $\widetilde{\chi}$, is equal to $\chi_{\rm YM}$ at $T = 0$. Nevertheless, their behavior must at some $T > 0$ start being different (and this indeed happens around $T \sim T_{\rm Ch}$), since the full QCD is much less resistant to changes of T than the pure-glue YM theory.

The LS relation (3.28) shows that the QCD topological susceptibility χ approaches $\chi_{\rm YM}$ only for large quark masses whereas $\chi_{\rm YM}$ and χ are very different for light quarks. We denoted by $\tilde{\chi}$ the whole right hand side of Eq. (3.28), and proposed that it should replace $\chi_{\rm YM}$ in WVR (3.26) in order that WVR may remain applicable for $T > 0$. Of course, nothing changes at $T = 0$ where $\tilde{\chi} = \chi_{\rm YM}$. Nevertheless, at $T > 0$ the difference turns out to become dramatic when T gets close to $T_{\rm Ch}$. This is because for light quark flavors, χ turns out to be driven by the chiral quark condensate $\langle\bar{q}q\rangle_0 \equiv \Sigma$; in the leading order of expansion in small quark masses,

$$\chi = -\frac{m\,\Sigma}{N_f} + \mathcal{C}_m\,, \quad \text{where} \quad \frac{N_f}{m} \equiv \sum_f \frac{1}{m_f}. \tag{3.29}$$

The first equation above is the Di Vecchia-Veneziano result [**?**, 194]. The existence of the nonvanishing next term in this expansion, $\mathcal{C}_m$, is essential as it keeps the LS relation (3.28) from blowing up. The value of $\mathcal{C}_m$ is fixed at $T = 0$ since $\tilde{\chi}(0) = \chi_{\rm YM}$ at $T = 0$.

For the T-dependence of χ, and of its correction term $\mathcal{C}_m$ in particular, we use the Ansatz justified in Ref. [190]:

$$\chi(T) = -\frac{m\,\Sigma(T)}{N_f} + \mathcal{C}_m(0)\left[\frac{\Sigma(T)}{\Sigma(0)}\right]^\delta.$$

The definition of $\tilde{\chi}$ then gives

$$\tilde{\chi}(T) = \frac{m\,\Sigma(T)}{N_f}\left\{1 - \frac{1}{\mathcal{C}_m(0)}\frac{m\,\Sigma(T)}{N_f}\left[\frac{\Sigma(0)}{\Sigma(T)}\right]^\delta\right\} \tag{3.30}$$

The interesting window for δ is then $0 \le \delta \le 1$ since the lower limit gives no thermal dependence for the correction term, and a quadratic one in the last equation for $\tilde{\chi}$. With $\delta = 1$, an unwelcome enhancement of the η' mass [190] starts building up. Therefore, $\delta \sim 1$ is around the upper limit of interest, even though the respective results for the T-dependence of the meson masses are quantitatively not much different for $\delta = 0$ and $\delta = 1$, as can be seen in, respectively, upper and lower panel of Fig. 3.35.

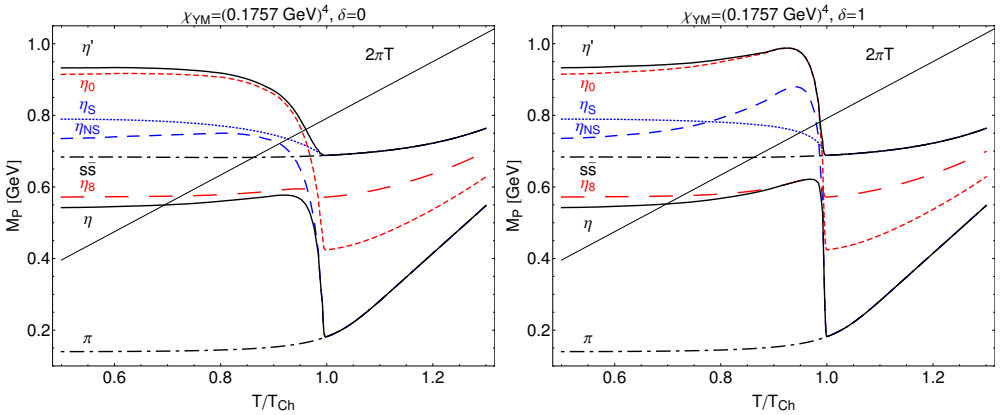

Figure 3.35: The relative-temperature dependence, on $T/T_{\rm Ch}$, of the pseudoscalar meson masses for two $\widetilde{\chi}(T)$, namely Eq. (3.30) with $\delta = 0$ (left panel) and with $\delta = 1$ (right panel). The meaning of all symbols is the same on the both panels: the masses of η' and η are, respectively, the upper and lower solid curve, those of the pion and non-anomalous $s\bar{s}$ pseudoscalar are, respectively, the lower and upper dash-dotted curve, M_{η_0} and M_{η_8} are, respectively, the short-dashed (red) and long-dashed (red) curve, $M_{\eta_{\rm NS}}$ is the medium-dashed (blue), and M_{η_S} is the dotted (blue) curve. The straight line $2\pi T$ is twice the lowest Matsubara frequency.

Mesons are constructed as $q\bar{q}$ bound states via the Bethe-Salpeter equation in the ladder approximation. Dynamical quarks are build up from the Dyson-Schwinger equation in rainbow approximation. We use the successful rank-2 separable model [196] for the gluon propagator, which was also used in Ref. [191]. Rainbow-ladder approximation is the simplest symmetry preserving truncation, necessary for the correct chiral behavior of the theory.

The bound state approach in the ladder approximation can yield only the non-anomalous part of the meson masses. Therefore, the anomalous part is inferred from Eq. (3.26).

The strategy is to use flavor mass matrices to extract η and η' masses from the calculated non-anomalous sector. This is presented in detail in Ref. [191].

The T-dependence of the pseudoscalar meson masses found in Ref. [190] is presented in Fig. 3.35. The main result is that the theoretically predicted reduction in the η' mass is around 200 MeV, which is in quantitative agreement with RHIC data. This is possible only due to the proposed modification of the WVR relation at finite T.

Relevance for NICA

We are presently preparing the extension of the theoretical investigation of Refs. [190, 193] to finite density. We want to point out that this proposed modification of the WVR relation and its effects at finite T described above, have the direct analogy at finite density and finite chemical potential μ. Everything we said about the effects of $T > 0$, has its analogy for $\mu > 0$. Namely, we explained above that the proposed mechanism has the effect of tying (through the LS relation and $\widetilde{\chi}$) the gluon anomaly contribution to the η' mass with the chiral condensate $\langle\bar{q}q\rangle_0$. This condensate would decrease not only for sufficiently high T, but also for sufficiently high μ. This suggests that partial $U_A(1)$-symmetry restoration would also happen if matter density is increased sufficiently, so that the chiral symmetry restoration takes place, and $\Sigma(T,\mu) \equiv \langle\bar{q}q\rangle_0(T,\mu)$ decreases, and even vanishes.

The prediction of the WVR relation with the proposed modified $T, \mu > 0$ behavior [190, 193] turned out to be compatible with the experimental findings [184] on the partial $U_A(1)$-symmetry restoration. However, that was at RHIC, at high T, but $\mu \approx 0$. NICA has the ability to explore the phase diagram for $T > 0, \mu > 0$. This way it can either find the partial $U_A(1)$-symmetry restoration in the (T,μ)-regimes which are complementary to that of RHIC. We hope that the method used at RHIC, namely the study of η' multiplicity, is also feasible at NICA.

Alternatively, NICA may find that the WVR relation breaks down when the critical density is reached and

refute our extension thereof. This would also be an interesting result, and of wider significance, especially since the proposed modification of the WVR relation [190, 193] fits in nicely with the recent *ab initio* theoretical analysis using functional methods [200], which finds that the anomalous breaking of $U_A(1)$ symmetry is related to DChSB (and confinement) in a self-consistent manner, so that one cannot have one of these phenomena without the other.

3.16 Search for the hot color superconducting phase and low-temperature critical point at NICA

Zh. Zhang [1], *T. Kunihiro* [2]

[1] *School of Mathematics and Physics, North China Electric Power University, Beijing, China*
[2] *Department of Physics, Kyoto University, Kyoto, Japan*

It is generally believed that the strongly interacting matter exhibits a rich phase structure in an extreme environment such as at high temperature and/or high baryon chemical potential. Experimentally, RHIC, LHC, FAIR and NICA are providing and should provide more information on this topics. Theoretically, some results have been already obtained on a sound basis: Indeed, the lattice simulations of quantum chromodynamics (QCD) indicate that, for physical quark masses, the transition from the hadronic phase to the quark gluon plasma (QGP) is a smooth crossover at finite temperature and vanishing baryon chemical potential; whereas in the low temperature and very high density region, the asymptotic-free nature of QCD may allow the weak-coupling analysis of the quark matter and thus the color flavor locking (CFL) phase is proved to be the ground state of QCD. However, the above methods based on the first principle fail at the low temperature and moderate density region, due to the sign problem or inherent strong coupling effects. Phenomenologically, such a region in the T-μ plane has relevance to reality such as the physics of compact stars. On that account, chiral models of QCD such as the NJL model that embody the basic low-energy characteristics of QCD such as symmetry properties have been extensively used to explore the T-μ phase diagram of strongly interacting matter. In particular, such model calculations suggest that two-flavor color superconducting (2CSC) phase may occur at low or even moderate temperature and intermediate density region, which belongs to the energy scan range of NICA facility. We propose to explore the possible abnormal chiral phase boundary with large fluctuations of the order parameters of the chiral and diquark condensates to be created by NICA.

Three mechanisms for the possible low-temperature critical point of QCD in the presence of color superconducting phase.

Since the work by Asakawa and Yazaki [53], it is widely believed that there may exist a chiral critical point (CP) in the T-μ phase diagram of QCD. Such a point may be located at the relatively high temperature region, which is promising to be scanned by Heavy ion collisions. On the other hand, there *is* a possibility that the QCD phase diagram may have new chiral CP($'s$) in the low temperature area due to the influence of other phases, especially of the color superconductivity. In the literature, three mechanisms for realizing the low-temperature CP($'s$) are known, which are all due to the interplay between the chiral and diquark condensates.

1. Vector interaction:

In [142], it is found that the vector interaction can effectively enhance the competition between the chiral and diquark condensates and can lead to a low-temperature CP; the competition leads to a small but finite coexistent region (COE) with the chiral and (2CSC-)diquark condensates, and the chiral transition becomes a crossover in the low-temperature region including zero temperature.

2. Axial anomaly in the presence of CFL:

The possible cubic coupling between the chiral and diquark condensates due to the axial anomaly may lead to a low-temperature CP for the three-flavor case, according to the idealized analysis based on a Ginzburg-Landau(G-L) action in the chiral limit [144]. It is to be noted that the color superconducting phase is necessarily the CFL in such an idealized situation, and it is totally obscure whether the new CP thus obtained is robust in the realistic situation with finite and different quark masses for three flavors. One should also note that the G-L analysis would lose its validity if a phase transition is a strong first-order one.

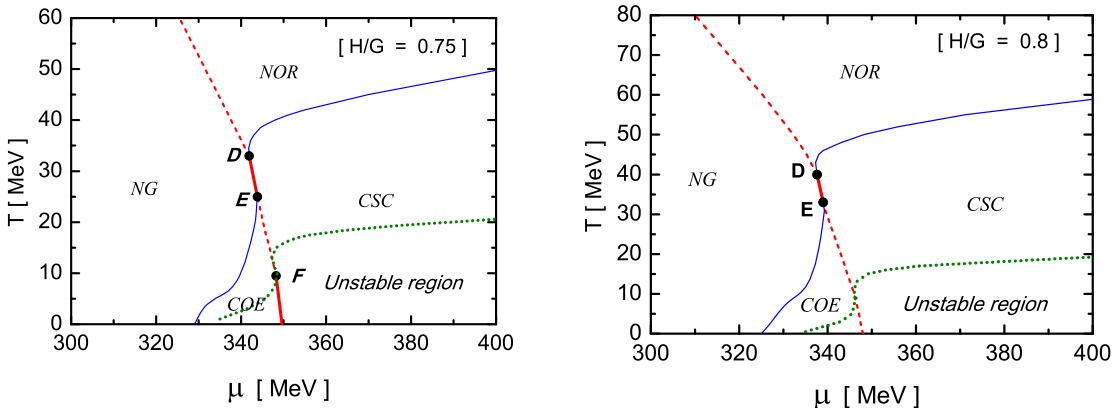

Figure 3.36: The phase diagram with the low-temperature CP($'s$) induced by the electric chemical potential required by charge-neutrality in the presence of 2CSC. The thick solid line, thin solid line and dashed line denote the first order transition, second order transition and chiral crossover, respectively. The unstable region is characterized by the chromomagnetic instibility. The figures are taken from [202], which are obtained in a two-flavor NJL model.

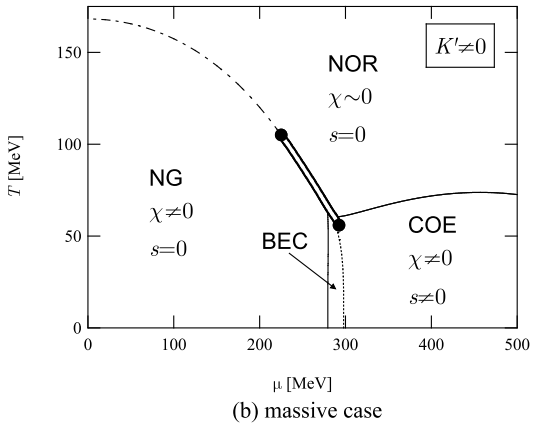

(b) massive case

Figure 3.37: The T-μ phase diagram in a three-flavor NJL model obtained in [144] by considering the cubic chiral-diquark coupling induced by the axial anomaly in the presence of CFL. The SU(3) flavor symmetry is adopted with m_u=m_d=m_s=5.5 MeV and the ratio K'/K is 4.2. Here, K' and K refer to the couplings of the new axial anomaly interaction and traditional Kabayashi-Maskawa-'t Hooft interaction, respectively. K is fixed as it's vacuum value.

3. Electric chemical potential required by the charge-neutrality and β-equilibrium:

It is first reported in [202] that the electric chemical potential μ_e required by the charge-neutrality can effectively strengthen the chiral-diquark interplay and gives rise to one or even two low-temperature CP($'s$): see Fig.3.36. In this mechanism, the μ_e plays double roles on the phase transition: First, it delays the chiral transition towards to a larger chemical potential, just like what the vector interaction does. Second, the finite μ_e implies a Fermi-surface mismatch between u and d quarks leading to an abnormal temperature dependence of the diquark condensate, which causes the multiple CP$'s$.

Note that for the mechanisms 1 and 3, the 2CSC is the the favored color superconducting phase in the COE. So it is naturally expected that the COE should be enlarged when both the vector interaction and the charge-neutrality are taken into account. This has been confirmed in [203] and even four CP$'s$ are observed in the calculation based on the NJL model.

The three-flavor (two-plus-one-flavor) NJL model doesn't support the phase diagram with a low-temperature critical point induced by the Axial Anomaly

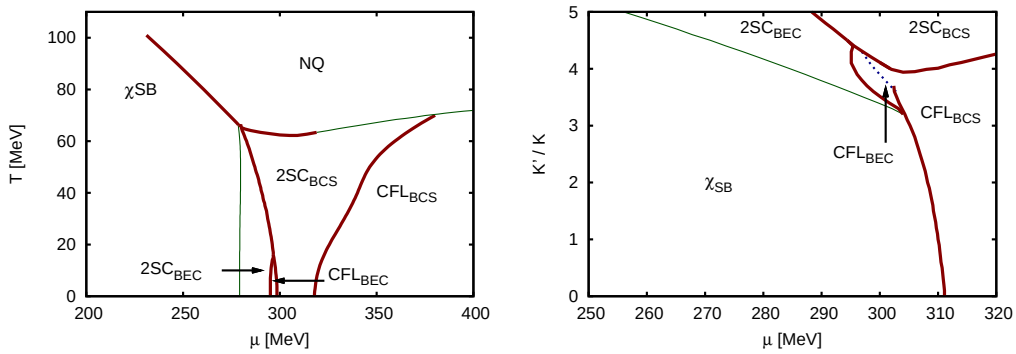

Figure 3.38: The T-μ phase diagram (left) and the K'-μ phase diagram (right) obtained in [209] by taking into account both the 2CSC and CFL phases. The model and model parameters are same as that in Fig. 3.37. One can see that the CFL is disfavored near the low-temperature chiral boundary and there is no new low-temperature CP in the phase diagram.

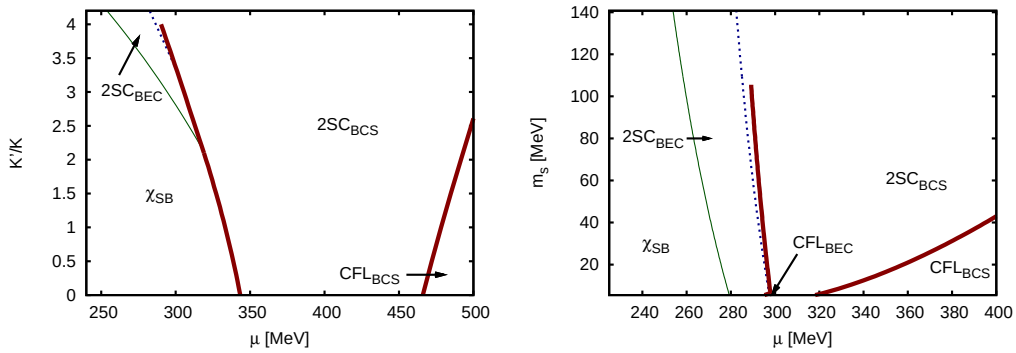

Figure 3.39: The K'-μ phase diagram with physical quark masses for T=0 (left) and the m_s-μ phase diagram with $K'/K = 4.2$ for T=0 (right) obtained in [209] by taking into account both the 2CSC and CFL phases in NJL model. The model parameters for left figure are same as that in Fig. 3.37. One can see that the CFL is disfavored near the low-temperature chiral boundary for both cases.

The advantage of the G-L theory is that it is model-independent. However, the coefficients in the G-L expansion can not be dynamically determined by the theory itself. So a natural question is that whether such a prediction of a new low-temperature CP based on this method could be fulfilled in a dynamical model of QCD. A work toward this problem has been done by Abuki et al. [204] using a three-flavor NJL model with a new axial anomaly term K' [205, 206] as well as the traditional Kobayashi-Maskawa-'t Hooft interaction K [**?**, 207] in the flavor-symmetric case. As shown in Fig. 3.37, the low-temperature CP induced by the axial anomaly is really observed again in such an idealized model.

However, there exists two shortcomings in their study: First, as stated above, the SU(3) flavor symmetry is assumed and it is set that $m_u(m_d) = m_s$. Second, the new CP only appears for very strong K' region (namely, for $K'/K > K'_c/K$=3.8, where K is fixed as it's vacuum value). It is known that the large mass difference between m_s and $m_u(m_d)$ gives rise to a so significant effect on the phase transitions at moderate density region that the CFL is disfavored [40, 42]. Furthermore, K' should become weaker due to the suppression of the instanton.

A more serious problem was pointed out in [209] by using the same model and parameters with the SU(3) flavor symmetry: if K' is too strong, the 2CSC phase is favored over the CFL phase assumed in [204] near the chiral boundary, even in the three-flavor symmetry case. This point is clearly shown in Fig. 3.38. Then, one can further infer that for the physical quark masses, the CFL will be more unlikely in competition with the 2CSC because of the mass mismatch. This point has been confirmed in [209], as shown in Fig. 3.39. Therefore, the investigations in [209] indicate that the NJL model does not support the proposed new CP induced by the axial anomaly in [144] for both the three-flavor and two-plus-one-flavor cases.

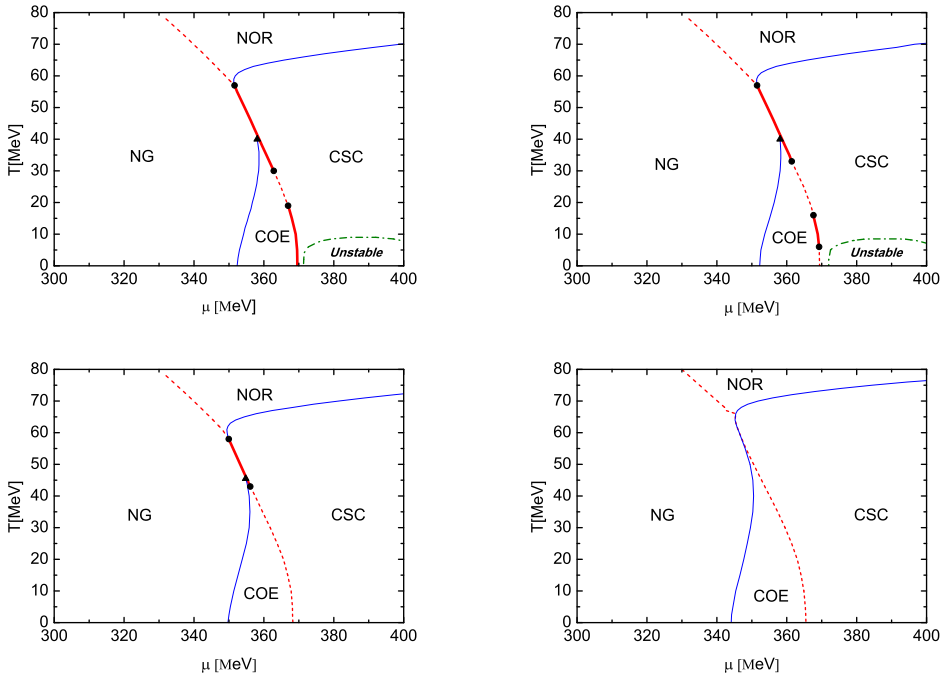

Figure 3.40: The T-μ phase diagrams of the two-plus-one-flavor NJL model for several values of K'/K and fixed $G_V/G_S = 0.25$, where the charge-neutrality constraint and β-equilibrium condition are imposed. The meanings of the different line types are the same as those in Fig. 3.36. With the increase of K'/K, the number of the critical points changes and the unstable region characterized by the chromomagnetic instability (bordered by the dash dotted line) tends to shrink and ultimately vanishes in the phase diagram. The figures are taken from [210].

Dose the two-plus-one-flavor NJL model support the phase diagram with a low-temperature critical point when taking into account the Axial Anomaly, Vector Interaction, and/or Charge-neutrality?

Then, a question naturally arises: does the NJL model support the low-temperature CP when taking into account the axial anomaly, the vector interaction, and the charge-neutrality and β-equilibrium in the presence of 2CSC ? The present authors have investigated this problem in a two-plus-one-flavor NJL model by taking into account all these ingredients [210]. Our study suggests that, besides the vector interaction G_V and the electric chemical potential μ_e, the new axial anomaly interaction K' also favors the COE with 2CSC. The reason is that, near the chiral boundary, the strange quark condensate σ_3 has still a relatively large value and can effectively enhance the Majarona mass for the u-d paring due to the flavor mixing induced by the anomaly term K':

$$\Delta_3 = 2(G_D - \frac{K'}{4}\sigma_3)s_3\,, \tag{3.31}$$

where s_3 stands for the u-d diquark condensate. So unlike its role in the mechanism 1, the heavy strange quark gives a positive contribution for the emergence of the low-temperature CP by enhancing the chiral-diquark interplay for u and d quarks.

Figure. 3.40 shows the T-μ phase diagram of a two-plus-one-flavor NJL with the charge-neutrality and β-equilibrium for different K' and fixed vector interaction G_V. Due to the strengthened chiral-diquark competition, the low-temperature CP($'s$) and crossover for the chiral transition appear in the T-μ plane. One observes that the number of the critical points changes as $1 \to\ 3 \to 4 \to 2 \to 0$ when K' is increased. Owing to the effect of G_V and μ_e, the low-temperature CP($'s$) can be realized with a relatively small K' (Note that without the charge-neutrality constraint, we do not find the low-temperature CP in this model if only the axial anomaly and vector interaction are considered). In Fig. 3.41, the similar chiral CP structures appear for fixed $K'/K = 1$ (The Fierz transition of Kabayashi-Maskawa-'t Hooft interaction gives $K'/K = 1$) but varied G_V.

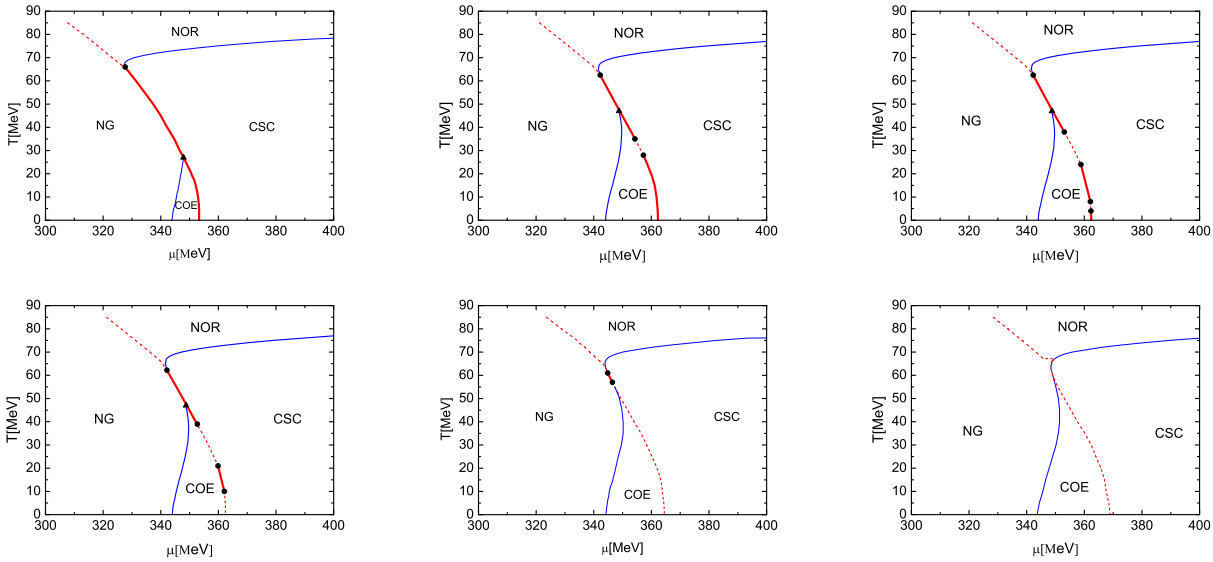

Figure 3.41: The T-μ phase diagrams in the two-plus-one-flavor NJL model for fixed $K'/K = 1.0$ with G_V/G_S being varied, where the charge-neutrality constraint and β-equilibrium condition are taken into account. The meanings of the different line types are the same as those in Fig. 3.36. The number of the critical points changes along with an increase of G_V/G_S. All the phase diagrams are free from the chromomagnetic instability. The figures are taken from [210].

Thus one sees that the chiral-diquark interplay in the COE region becomes complicated once the axial anomaly, the vector interaction and the charge-neutrality are all taken into account. Figures. 3.40 and 3.41 tell us that there exists a parameter region in the K'-G_V plane for the low-temperature CP($'s$) in the NJL model. The above parameter area seems to include the physical region since K' is expected to be suppressed near the chiral boundary while the instanton molecular liquid model predicts that G_V/G_S=0.25.

The suppression of Chromomagnetic Instability by Axial Anomaly and Vector Interaction

Another important role of the axial anomaly and vector interaction is that they can effectively suppress the chromomagnetic instability [211] associated to the gapless 2CSC [212]. This is shown in Fig. 3.42: The unstable region with the instability in the T-μ plane shrinks with increasing K'. Figure. 3.42 also tells us that such a suppression becomes more significant when the vector interaction is included.

The reason for the suppression of the chromomagnetic instability can be attributed to two facts: First,

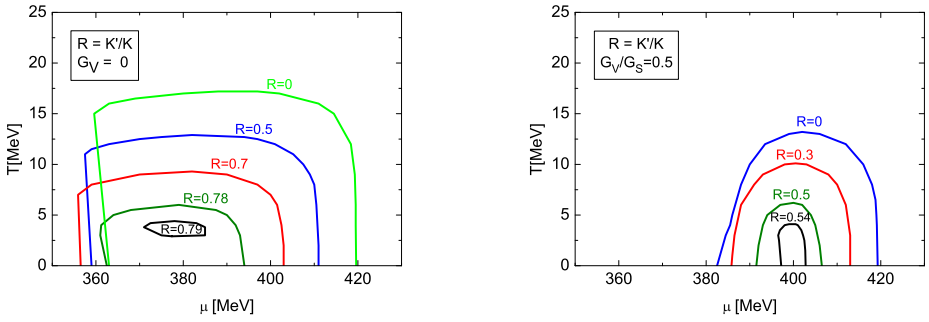

Figure 3.42: The boundary between the stable and unstable homogenous 2CSC regions with (right figure) and without (left figure) the vector interaction in two-plus-one-flavor NJL model. With the increase of the ratio $K'/K \equiv R$, the unstable region with the chromomagnetic instability in the T-μ plane shrinks and eventually vanishes. The figures are taken from [210].

the u-d diquark coupling is enhanced by the s quark due to the nonzero K', which can suppress the instability [213]. Second, the effective chemical potential difference is shifted towards smaller values by G_V. So the hot asymmetric homogeneous 2CSC may be free from the instability and thus could be formed at NICA densities.

Implication for the experiments at NICA densities

Our study suggests that the mixed phase with both chiral symmetry breaking and 2CSC may coexist in the low temperature and moderate density region near the chiral boundary. The interplay of chiral and diquark condensates may be enhanced by the axial anomaly, vector interaction, and electric chemical potential, which may lead to low temperature chiral crossover and CP($'s$). For not very low temperature, such a color superconducting phase may be free from the chromomagnetic instability. Our results are obtained in the mean-field approximation. The appearance of the multiple critical points may suggest that there exist large fluctuations of the chiral and diquark fields around the phase boundary in reality. This possible phase structure can be explored in the future experiments of Heavy Ion Collision at NICA, which aiming at the physics of intermediate baryon density of QCD (In Heavy Ion Collisions, the role of μ_e can be partially replaced by a finite isospin chemical potential. That means the possible low-temperature crossover or CP of our proposal can be tested at NICA by producing the isospin asymmetric quark matter).

Z.Z. was partially supported by the NSFC (No.11275069), by the Fundamental Research Funds for the Central Universities of China, and by the University Plan of NCEPU for the Promotion of Arts and Science. T.K. was partially supported by a Grant-in-Aid for Scientific Research by the Ministry of Education, Culture, Sports, Science and Technology (MEXT) of Japan (No.20540265), by Yukawa International Program for Quark-Hadron Sciences, and by the Grant-in-Aid for the global COE program " The Next Generation of Physics, Spun from Universality and Emergence " from MEXT.

Bibliography

[1] M. Stephanov, K. Rajagopal and E. Shuryak, Phys. Rev. **D 60,** 1140281, (1999); [hep-ph/9903292].

[2] B. Berdnikov and K. Rajagopal, Phys. Rev. **D 61,** 105017, (2000); [hep-ph/9912274].

[3] M. Stephanov, Phys. Rev. Lett. **102,** 032301, (2009); [arXiv:0809.3450].

[4] E.E. Kolomeitsev, D.N. Voskresensky, Nucl. Phys. **A 759,** 373, (2005).

[5] T. Klahn *et al.*, Phys. Rev. **C 74,** 035802, (2006).

[6] A.S. Khvorostukhin, V.D. Toneev and D.N. Voskresensky, Nucl. Phys. **A 791,** 180, (2007).

[7] D.N. Voskresensky, Nucl. Phys. **A 744,** 378, (2004); **812**, 158, (2008).

[8] V.V. Skokov and D.N. Voskresensky, [arXiv:0811.3868]; Nucl. Phys. **A 828,** 401, (2009); [arXiv:0903.4335].

[9] D.N. Voskresensky, Phys. Rev. **C 69,** 065209, (2004).

[10] R.A.L. Jones, *Soft Condensed Matter*, (Oxford University Press, 2002) [ISBN 0198505892].

[11] Ph. Chomaz, M. Colonna and J. Randrup, Phys. Rep. **389,** 263, (2004).

[12] I.C. Arsene *et al.*, Phys. Rev. **C 75,** 034902, (2007).

[13] J. Randrup, arXiv:0903.4736.

[14] V.N. Russkikh and Yu.B. Ivanov, Phys. Rev. **C 74,** 034904, (2006).

[15] Yu.B. Ivanov and V.N. Russkikh, **PoS CPOD07,** 008, (2007).

[16] Yu.B. Ivanov, V.N. Russkikh, and V.D. Toneev, Phys. Rev. **C 73,** 044904, (2006).

[17] K.A. Bugaev, Phys. Part. Nucl. **38,** 447, (2007)..

[18] K.A. Bugaev, Phys. Rev. **C 76,** 014903, (2007); Phys. Atom. Nucl. **71,** 1615, (2008).

[19] K.A. Bugaev, V.K. Petrov and G.M. Zinovjev, *The New Class of Exactly Solvable Models for the QCD Critical Endpoint* (in preparation).

[20] K.A. Bugaev, V. K. Petrov and G. M. Zinovjev, Europhys. Lett. **85**, 22002, (2009); [arXiv:0801.4869]; [arXiv:0807.2391]; K.A. Bugaev, [arXiv:0809.1023].

[21] K.A. Bugaev, *Testing the Influence of Surface Tension and Finite Width of QGP Bags on the QCD Matter Equation of State Properties at NICA Energies*, 2009 (in preparation).

[22] H. Muller, Nucl. Phys. **A 618,** 349, (1997).

[23] M. Di Toro, A. Drago, T. Gaitanos, V, Greco and A. Lavagno, Nucl. Phys. **A 775,** 102, (2006).

[24] M. Di Toro *et al.*, Progr. Part. Nucl. Phys. **62,**389, (2009).

[25] D. Toublan and J.B.Kogut, Phys. Lett. **B 605,** 129, (2005).

[26] B.D. Serot and J.D. Walecka, Adv. Nucl. Phys. **16**, 1 (1985).

[27] V. Baran, M. Colonna, V. Greco and M. Di Toro, Phys. Rep. **410,** 335, (2005).

[28] A. Chodos, *et al.*, Phys. Rev. **D 9,** 3471, (1974).

[29] P. Danielewicz, R.Lacey, W.G.Lynch, Science **298**, 1592 (2002)

[30] N.K. Glendenning, S.A. Moszkowski, Phys. Rev. Lett. **67,** 2414, (1991).

[31] Y. Nambu and G. Jona-Lasinio, Phys. Rev. **122,** 345, (1961); **124**, 246, (1961).

[32] M. Frank, M. Buballa and M. Oertel, Phys. Lett. **B 562,** 221, (2003).

[33] Guo-yun Shao et al., Phys. Rev. **D 73,** 076003, (2006).

[34] S. Plumari, Ph.D.Thesis, Univ.Catania 2008.

[35] B. Liu, V. Greco, V. Baran, M. Colonna, and M. Di Toro, Phys. Rev. **C 65,** 045201, (2002).

[36] A. Bazavov *et al.*, [arXiv:0903.4379 [hep-lat]].

[37] S. Roessner, C. Ratti and W. Weise, Phys. Rev. **D 75,** 034007, (2007); [hep-ph/0609281].

[38] D. Gomez Dumm, D. B. Blaschke, A. G. Grunfeld and N. N. Scoccola, Phys. Rev. **D 78,** 114021, (2008); [arXiv:0807.1660].

[39] D. Blaschke S. Fredriksson, H. Grigorian, A. M. Oztas and F. Sandin, Phys. Rev. **D 72,** 065020, (2005); [hep-ph/0503194].

[40] S.B. Ruester, V. Werth, M. Buballa, I. A. Shovkovy and D. H. Rischke, Phys. Rev. **D 72,** 034004, (2005); [hep-ph/0503184].

[41] H.J. Warringa, D. Boer and J.O. Andersen, Phys. Rev. **D 72,** 014015, (2005); [hep-ph/0504177].

[42] H. Abuki and T. Kunihiro, Nucl. Phys. **A 768,** 118 (2006); [hep-ph/0509172].

[43] S. Typel, Phys. Rev. **C 71,** 064301, (2005); [nucl-th/0501056].

[44] K. Fukushima, Phys. Rev. **D 77,** 114028, (2008); **78**, 039902, (2008); [arXiv:0803.3318].

[45] M.K. Volkov, E. A. Kuraev, D. Blaschke, G. Ropke and S. M. Schmidt, Phys. Lett. **B 424,** 235, (1998); [hep-ph/9706350].

[46] S. Chiku and T. Hatsuda, Phys. Rev. **D 57,** 6, (1998); [hep-ph/9706453].

[47] T. Kunihiro, M. Kitazawa and Y. Nemoto, **PoS CPOD07,** 041 (2007); [arXiv:0711.4429].

[48] S. Wheaton and J. Cleymans, Comput. Phys. Commun. **180**, 84 (2009).

[49] A. Andronic *et al.*, Nucl. Phys. **A 837,** 65 (2010); [arXiv:0911.4806.

[50] L. McLerran and R. D. Pisarski, Nucl. Phys. **A 796,** 83 (2007)

[51] K. Fukushima, Phys. Lett. **B 591,** 277, (2004).

[52] C. Ratti, M. A. Thaler and W. Weise, Phys. Rev. **D 73,** 014019, (2006).

[53] L. McLerran, K. Redlich and C. Sasaki, Nucl. Phys. **A 824,** 86 (2009).

[54] D. B. Blaschke, F. Sandin, V. V. Skokov and S. Typel, Acta Phys. Polon. Supp. **3**, 741 (2010).

[55] K. Rajagopal and F. Wilczek; arXiv:hep-ph/0011333.

[56] M. Kutschera, W. Broniowski and A. Kotlorz, Nucl. Phys. **A 516,** 566 (1990).

[57] E. Nakano and T. Tatsumi, Phys. Rev. **D 71,** 114006 (2005).

[58] G. Basar, G. V. Dunne and M. Thies, Phys. Rev. **D 79,** 105012, (2009).

[59] D. Nickel, Phys. Rev. **D 80,** 074025, (2009).

[60] D. Nickel, Phys. Rev. Lett. **103,** 072301 (2009).

[61] S. Carignano, D. Nickel and M. Buballa, Phys. Rev. **D 82,** 054009 (2010).

[62] T. Kojo, Y. Hidaka, L. McLerran and R. D. Pisarski, Nucl. Phys. **A 843,** 37 (2010).

[63] T. Kojo, R. D. Pisarski and A. M. Tsvelik, Phys. Rev. **D 82,** 074015, (2010).

[64] A. Mocsy and P. Sorensen, Phys. Lett. **B 690,** 135 (2010).

[65] Y. Aoki*et al.*, Nature **443**, 675(2006).

[66] M. Cheng, Phys. Rev. **D 74,** 054507, (2006).

[67] S. Ejiri, Phys. Rev. **D 78,** 074507, (2008).

[68] E. S. Bowman, J. I. Kapusta, Phys. Rev. **D 79,** 015202, (2009).

[69] M. A. Stephanov, Int. J. Mod. Phys. **A 20,** 4387, (2005).

[70] Z. Fodor *et al.*, **JHEP 0404**, 50 (2004).

[71] R. V. Gavai, S. Gupta, Phys. Rev. **D 78,** 114503, (2008);

[72] de Forcrand Philippe and O. Philipsen, Nucl. Phys. **B 642,** 290 (2002).

[73] J. Adams *et al.*, Nucl. Phys. **A 757,** 102 (2005).

[74] X. F. Luo *et al.*, Phys. Lett. **B 673,** 268 (2009).

[75] B. Mohanty, Nucl. Phys. **A 830,** 899, (2009).

[76] M. Cheng *et al.*, Phys. Rev. **D 79,** 074505, (2009).

[77] Y. Hatta and M. A. Stephanov, Phys. Rev. Lett. **91,** 102003, (2003).

[78] M. Asakawa, arXiv:0904.2089.

[79] M. M. Aggarwal *et al.* (STAR Collaboration), Phys. Rev. Lett. **105,** 022302, (2011).

[80] F. Karsch and K. Redlich, Phys. Lett. **B 695,** 136, (2011).

[81] R. V. Gavai and S. Gupta, arXiv:1001.3796.

[82] F. Karsch, E. Laermann, and A. Peikert, Nucl. Phys. **B 605,** 579 (2001).

[83] F. Karsch, Nucl. Phys. **A 698,** 199 (2002).

[84] M. Kaczmarek and F. Zantow, Phys. Rev. **D 71,** 114510, (2005).

[85] Z. Fodor, S.D. Katz, and C. Schmidt, JHEP **03**, 121 (2007).

[86] M. D'Elia and F. Sanfilippo, Phys. Rev. **D 80,** 014502 (2009).

[87] K. Fukushima and T. Hatsuda, Rep. Prog. Phys. **74**, 014001 (2011).

[88] Si-xue Qin, Lei Chang, Huan Chen, Yu-xin Liu, Craig D. Roberts, Phys. Rev. Lett. **106,** 172301 (2001).

[89] S. P. Klevansky, Rev. Mod. Phys. **64**, 649, (1992).

[90] T. Hatsuda and T. Kunihiro, Phys. Rep. **247,** 221 (1994).

[91] M. Buballa, Phys. Rep. **407,** 205 (2005).

[92] M. Huang and I. Shovkovy, Nucl. Phys. **A 729,** 835 (2003).

[93] M. Alford, A. Schmit, K. Rajagopal, and T. Schäfer, Rev. Mod. Phys. **80**, 1455 (2008), and refs. therein..

[94] K. Fukushima, Nucl. Phys. **B 591,** 277 (2004).

[95] W. J. Fu, Z. Zhang, Y. X. Liu, Phys. Rev. **D 77,** 014006 (2008).

[96] T. K. Herbst, J. M. Pawlowski, B-J. Schaefer, Phys. Lett. **B 696,** 58 (2011).

[97] N. K. Glendenning and J. Schaffner-Bielich, Phys. Rev. Lett. **81,** 4564 (1998); Phys. Rev. **C 60,** 025803 (1999).

[98] G. F. Burgio, M. Baldo, P. K. Sahu, and H.-J. Schulze, Phys. Rev. **C 66,** 025802 (2002).

[99] G. Y. Shao and Y. X. Liu, Phys. Rev. **C 82,** 055801 (2010).

[100] J. Xu, L. W. Chen, C. M Ko, and B. A. Li, Phys. Rev. **C 81,** 055803 (2010).

[101] H. Müller, Nucl. Phys. **A 618,** 349 (1997).

[102] M. Di Toro *et al.*, Phys. Rev. **C 83,** 014911 (2011).

[103] R. Cavagnoli, C.'Providência, and D. P. Menezes, [arXiv:1009.3596v1].

[104] G. Pagliara and J. Schaffner-Bielich, Phys. Rev. **D 81,** 094024 (2010).

[105] B. Liu, M. Di Toro, G.Y. Shao, V.Greco, C.W. Shen, Z.H. Li, [arXiv:1105.0555[nucl.th]].

[106] G. Y. Shao, M. Di Toro, B. Liu, M. Colonna, V. Greco, Y.X. Liu, S. Plumari, [arXiv:1102.4964], to be published in Phys. Rev. D (2011).

[107] G.Y. Shao, M. Di Toro, V. Greco, M. Colonna, B.Liu, Y.X. Liu, S. Plumari, *Phase diagrams in the Hadron-PNJL model*, in preparation.

[108] V. Baran, M. Colonna, V. Greco, M. Di Toro, Phys. Rep. **410,** 335 (2005)

[109] M. Di Toro *et al.*, Progr. Part. Nucl. Phys. **62,**389 (2009).

[110] G. Ferini, T. Gaitanos, M. Colonna, M. Di Toro. H.H. Wolter, Phys. Rev. Lett. **97,** 202301 (2006).

[111] G. Ferini, M. Colonna, T. Gaitanos, M. Di Toro, Nucl. Phys. **A 762,** 147 (2005).

[112] L. Csernai, D. Rohrich, Phys. Lett. **B 458,** 454 (1999).

[113] R.J. Fries, V. Greco V, P. Sörensen, Ann.Rev.Nucl.Part.Sci. **58** 177 (2008).

[114] B. I. Abelev *et al.*, [arXiv:0909.4131].

[115] B.I. Abelev et al., Phys. Rev. **C 81**, 024911 (2010).

[116] A. Tawfik, [arXiv:1205.1761 [hep-ph]].

[117] Y. Zhou, *et al.*, Phys. Rev. **C 82**, 014905 (2010).

[118] H. Satz, *talk given at ERC Physics of High Energy Heavy Ions, Vuosaari, Finland, June 17 - 22*, (1994).

[119] J. Sollfrank, U. W. Heinz, H. Sorge, and N. Xu, *J. Phys.* **G 25**, 363 (1999).

[120] H. Cleymans, J. Oeschler and K. Redlich, *J. Phys.* **G 25**, 281–285 (1999).

[121] J. Cleymans and K. Redlich, *Phys. Rev.* **C 60**, 054908 (1999).

[122] P. Braun-Munzinger and J. Stachel, *Nucl. Phys.* **A 606**, 320 (1996); J. Phys. **G 28**, 1971 (2002).

[123] V. Magas and H. Satz, *Eur. Phys. J.* **C 32**, 115, 2003.

[124] A. Tawfik, Europhys. Lett. **75**, 420 (2006).

[125] A. Tawfik, Nucl. Phys. **A 764**, 387-392 (2006).

[126] J. Cleymans, M. Stankiewicz, P. Steinberg, and S. Wheaton, 2005.

[127] A. Tawfik, *Phys. Rev.* **D 71**, 054502 (2005).

[128] C. Athanasiou, K. Rajagopal and M. Stephanov, Phys. Rev. **D 82**, 074008 (2010).

[129] Xiaofeng Luo (STAR Collaboration), [arXiv:1111.5671 [nucl-ex]]; J. Phys. Conf. Ser. **316**, 012003 (2011).

[130] T. J. Tarnowsky (STAR Collaboration), J. Phys. **G 38**, 124054 (2011).

[131] T. K. Nayak (STAR Collaboration), Nucl. Phys. **A 830**, 555 (2009).

[132] M. A. York, G. D. Moore, [arXiv:1106.2535 [hep-lat]].

[133] A. Tawfik and D. Toublan, Phys. Lett. **B 623**, 48-54 (2005).

[134] A. Tawfik, Soryushiron Kenkyu **114**, 48 (2006).

[135] F. Karsch, K. Redlich and A. Tawfik, Eur. Phys. J. **C 29**, 549 (2003).

[136] F. Karsch, K. Redlich and A. Tawfik, Phys. Lett. **B 571**, 67 (2003).

[137] K. Redlich, F. Karsch and A. Tawfik, J. Phys., **G 30**, 1271 (2004).

[138] A. Tawfik, Phys.Rev. **D 71**, 054502 (2005); J. Phys. **G 31**, 1105 (2005).

[139] M. A. Stephanov, PoS LAT **2006**, 024 (2006).

[140] A. Bazavov *et al.*, Phys. Rev. **D 85**, 054503 (2012).

[141] N. M. Bratovic, T. Hatsuda and W. Weise, [arXiv:hep-ph/1204.3788].

[142] M. Kitazawa, T. Koide, T. Kunihiro and Y. Nemoto, Prog. Theor. Phys. **108**, 929 (2002).

[143] D. Blaschke, M. K. Volkov and V. L. Yudichev, Eur. Phys. J. **A 17**, 103 (2003).

[144] T. Hatsuda, M. Tachibana, N. Yamamoto and G. Baym, Phys. Rev. Lett. **97**, 122001 (2006).

[145] D. Blaschke, H. Grigorian, A. Khalatyan and D. N. Voskresensky, Nucl. Phys. Proc. Suppl. **141**, 137 (2005).

[146] G. A. Contrera, D. Gomez Dumm and N. N. Scoccola, Phys. Lett. **B 661** (2008) 113.

[147] G. A. Contrera, M. Orsaria and N. N. Scoccola, Phys. Rev. **D 82**, 054026 (2010).

[148] V. A. Dexheimer and S. Schramm, Phys. Rev. **C 81**, 045201 (2010).

[149] B. -J. Schaefer, J. M. Pawlowski and J. Wambach, Phys. Rev. **D 76**, 074023 (2007).

[150] V. Pagura, D. Gómez Dumm and N. N. Scoccola, Phys. Lett. **B 707**, 76 (2012).

[151] D. Horvatic, D. Blaschke, D. Klabucar, O. Kaczmarek, Phys. Rev. **D 84**, 016005 (2011).

[152] S. Noguera and N. N. Scoccola, Phys. Rev. **D 78**, 114002 (2008).

[153] M. B. Parappilly, P. O. Bowman, U. M. Heller, D. B. Leinweber, A. G. Williams and J. B. Zhang, Phys. Rev. **D 73**, 054504 (2006).

[154] D. B. Blaschke, D. Gomez Dumm, A. G. Grunfeld, T. Klähn and N. N. Scoccola, Phys. Rev. **C 75**, 065804 (2007).

[155] D. Gomez Dumm and N. N. Scoccola, Phys. Rev. **C 72**, 014909 (2005).

[156] O. Kaczmarek, F. Karsch, E. Laermann, C. Miao, S. Mukherjee, P. Petreczky, C. Schmidt, W. Soeldner and W. Unger, Phys. Rev. **D 83**, 014504 (2011).

[157] K. Fukushima, Phys. Rev. **D 77**, 114028 (2008).

[158] B. Friman, F. Karsch, K. Redlich and V. Skokov, Eur. Phys. J. **C 71**, 1694 (2011).

[159] F. Karsch and C. Schmidt, in: NICA White Paper (Dubna, 2011).

[160] P. Danielewicz, T. Klähn, W. Reisdorf and D. Blaschke, in: NICA White Paper (Dubna, 2012).

[161] C. Sasaki and K. Redlich, [arXiv:1204.4330 [hep-ph]].

[162] M. Ruggieri, P. Alba, P. Castorina, S. Plumari, C. Ratti and V. Greco, [arXiv:1204.5995 [hep-ph]].

[163] K. Fukushima and K. Kashiwa, arXiv:1206.0685 [hep-ph].

[164] A. E. Radzhabov, D. Blaschke, M. Buballa and M. K. Volkov, Phys. Rev. **D 83**, 116004 (2011).

[165] D. B. Blaschke, J. Berdermann, J. Cleymans and K. Redlich, Phys. Part. Nucl. Lett. **8**, 811 (2011).

[166] L. Turko, D. Blaschke, D. Prorok and J. Berdermann, Acta Phys. Polon. Supp. **5**, 485 (2012).

[167] M. G. Alford, K. Rajagopal, and F. Wilczek, Nucl. Phys. **B 537**, 443 (1999), [hep-ph/9804403].

[168] P. F. Bedaque and T. Schäfer, Nucl. Phys. **A 697**, 802 (2002), [hep-ph/0105150].

[169] D. B. Kaplan and S. Reddy, Phys. Rev. **D 65**, 054042 (2002), [hep-ph/0107265].

[170] D. T. Son and M. A. Stephanov, Phys. Rev. **D 61**, 074012 (2000), [hep-ph/9910491].

[171] T. Schäfer, Phys. Rev. Lett. **96**, 012305 (2006), [hep-ph/0508190].

[172] A. Kryjevski, Phys. Rev. **D 77**, 014018 (2008), [hep-ph/0508180].

[173] D. Bailin and A. Love, Phys. Rept. **107**, 325 (1984).

[174] T. Schäfer, Phys. Rev. **D 62**, 094007 (2000) [hep-ph/0006034].

[175] A. Schmitt, Phys. Rev. **D 71**, 054016 (2005), [nucl-th/0412033].

[176] T. Schäfer and F. Wilczek, Phys. Rev. Lett. **82**, 3956 (1999), [hep-ph/9811473].

[177] A. Schmitt, S. Stetina and M. Tachibana, Phys.Rev. **D 83**, 045008 (2011).

[178] J. Deng, A. Schmitt, and Q. Wang, Phys.Rev. **D 76**, 034013 (2007), [nucl-th/0611097].

[179] A. Schmitt, Q. Wang and D. H. Rischke, Phys. Rev.**D 66**, 114010 (2002), [nucl-th/0209050].

[180] P. Jaikumar, M. Prakash, and T. Schäfer, Phys. Rev. **D 66**, 063003 (2002), [astro-ph/0203088].

[181] C. Manuel, A. Dobado and F. J. Llanes-Estrada, JHEP **09**, 076 (2005), [hep-ph/040605].

[182] M. G. Alford, M. Braby and A. Schmitt, J. Phys. **G 35**, 115007 (2008)[0806.0285].

[183] M. G. Alford, S. K. Mallavarapu, A. Schmitt and S. Stetina [1212.0670].

[184] T. Csorgo, R. Vertesi and J. Sziklai, Phys. Rev. Lett. **105**, 182301 (2010); [arXiv:0912.5526 [nucl-ex]].

[185] S. S. Adler *et al.* (PHENIX Collaboration), Phys. Rev. Lett. **93**, 152302 (2004); [arXiv:nucl-ex/0401003].

[186] J. Adams *et al.* (STAR Collaboration), Phys. Rev. **C 71**, 044906 (2005); [arXiv:nucl-ex/0411036].

[187] J. I. Kapusta, D. Kharzeev and L. D. McLerran, Phys. Rev. **D 53**, 5028 (1996); [arXiv:hep-ph/9507343].

[188] E. Witten, Nucl. Phys. **B 156**, 269 (1979).

[189] G. Veneziano, Nucl. Phys. **B 159**, 213 (1979).

[190] S. Benić, D. Horvatić, D. Kekez, D. Klabučar, Phys. Rev. **D 84**, 016006 (2011); [arXiv:1105.0356 [hep-ph]].

[191] D. Horvatić, D. Klabučar and A. E. Radzhabov, Phys. Rev. **D 76**, 096009 (2007); [arXiv:0708.1260 [hep-ph]].

[192] Z. Fodor and S. D. Katz, arXiv:0908.3341 [hep-ph].

[193] S. Benić, D. Horvatić, D. Kekez and D. Klabučar, Acta Phys. Polon. Supp. **5**, 941 (2012); [arXiv:1207.3068 [hep-ph]].

[194] H. Leutwyler and A. V. Smilga, Phys. Rev. **D 46**, 5607 (1992).

[195] P. Di Vecchia and G. Veneziano, Nucl. Phys. **B 171**, 253 (1980).

[196] D. Blaschke, G. Burau, Yu. L. Kalinovsky, P. Maris and P. C. Tandy, Int. J. Mod. Phys. A **16**, 2267 (2001); [arXiv:nucl-th/0002024].

[197] B. Alles, M. D'Elia and A. Di Giacomo, Nucl. Phys. **B494**, 281 (1997), [hep-lat/9605013].

[198] G. Boyd *et al.*, Nucl. Phys. **B 469**, 419 (1996); [hep-lat/9602007].

[199] D. Horvatić, D. Blaschke, D. Klabučar and O. Kaczmarek, Phys. Rev. **D 84**, 016005 (2011); [arXiv:1012.2113 [hep-ph]].

[200] R. Alkofer, PoS **FACESQCD**, 030 (2011). [arXiv:1102.3166 [hep-th]].

[201] M. Asakawa and K. Yazaki, Nucl. Phys. A **504**, 668 (1989).

[202] Z. Zhang, K. Fukushima and T. Kunihiro, Phys. Rev. D **79**, 014004 (2009) [arXiv:0808.3371 [hep-ph]].

[203] Z. Zhang and T. Kunihiro, Phys. Rev. D **80**, 014015 (2009) [arXiv:0904.1062 [hep-ph]].

[204] H. Abuki, G. Baym, T. Hatsuda and N. Yamamoto, Phys. Rev. D **81**, 125010 (2010) [arXiv:1003.0408 [hep-ph]].

[205] R. Rapp, T. Schafer, E. V. Shuryak and M. Velkovsky, Annals Phys. **280**, 35 (2000) [arXiv:hep-ph/9904353].

[206] A. W. Steiner, Phys. Rev. D **72**, 054024 (2005) [arXiv:hep-ph/0506238].

[207] M. Kobayashi and T. Maskawa, Prog. Theor. Phys. **44**, 1422 (1970).

[208] G. 't Hooft, Phys. Rev. D **14**, 3432 (1976) [Erratum-ibid. D **18**, 2199 (1978)]. G. 't Hooft, Phys. Rept. **142**, 357 (1986).

[209] H. Basler and M. Buballa, Phys. Rev. D **82**, 094004 (2010) arXiv:1007.5198 [hep-ph].

[210] Z. Zhang and T. Kunihiro, Phys. Rev. D **83**, 114003 (2011) [arXiv:1102.3263 [hep-ph]].

[211] M. Huang and I. A. Shovkovy, Phys. Rev. D **70**, 094030 (2004) *ibid.* D **70**, 094030 (2004) [arXiv:hep-ph/0408268].

[212] I. Shovkovy and M. Huang, Phys. Lett. B **564**, 205 (2003).

[213] M. Kitazawa, D. H. Rischke and I. A. Shovkovy, Phys. Lett. B **637**, 367 (2006) [arXiv:hep-ph/0602065].

4 Hydrodynamics and hadronic observables

The rich structure of the QCD phase diagram at high baryon densities discussed in the previous section, suggests the possibility of a first order phase transition and the existence of a critical end point, eventually a triple point. This section is devoted to the discussion of the effects of a phase transformation in the evolving hot, dense hadronic system on the particle distributions. Critical behaviour and changes in the thermodynamical degrees of freedom shall be revealed in flow observables as well as in the higher moments of (measurable) distribution functions and their ratios. In particular the latter quantities can also be studied in lattice QCD simulations and thus providing a direct link between hadronic observables and *ab-initio* QCD theory.

4.1 Hadronic signals of non-equilibrium phase transition

B. Tomášik

Univerzita Mateja Bela, Banská Bystrica, Slovakia

As pointed out in Jorgen Randrup's contribution, NICA will operate in the regime likely near to and slightly below the critical point of QCD. There a first-order phase transition is expected. In quickly expanding systems this is accompanied with the appearance of spinodal decomposition. In this scenario, bulk fireball matter decays into droplets which evaporate hadrons. Droplets copy the original local expansion velocity of the bulk and recede from each other. Therefore, this would lead to clumps in momentum space: hadrons coming from the same droplet have similar velocities, while those coming from a different droplet have velocities grouped around a different mean. It is also important to realize that in each event the droplets will be in different positions. Therefore, each event will be described by different hadronic distributions.

Various observables have been proposed for the identification of such a scenario. In general, one would not be able to identify it in observables which are integrated over a large number of events, like e.g. hadronic spectrum. Instead, it is necessary to look at correlation and fluctuation signals. Many have been proposed: multiplicity fluctuations, mean p_{T} fluctuations, rapidity and azimuthal angle hadronic correlations, proton rapidity distributions, etc. A promising new way of analyzing data is the use of Kolmogorov-Smirnov (KS) test on a large number of event pairs. Generally, the test has been developed to measure, to what extent two sets of data are similar, i.e. resemble the same underlying probability density. If it is applied to a large number of event pairs then it is rather easy to decide whether the collection of test results corresponds to all events being described by the same distribution or whether there are some non-statistical differences between the events [1]. Recall that the latter can be caused by fragmentation.

The KS test is more sensitive to non-statistical differences between events than any other tool proposed so far. The advantage is that it is not constructed specifically to look at certain moment of the distribution function, but compares the whole empirical distributions. We should also stress that it does not focus exclusively on fragmentation, but indicates non-statistical fluctuations due to any mechanism. Once indicated with the help of the KS test, the exact cause must be identified by other means.

To perform the KS test, measured rapidities (angles, momenta, ...) of all hadrons must be available. It is not sufficient to have only filled histograms. This is the requirement on data reconstruction and analysis. We have checked that even a poor momentum resolution of the detector does not eliminate the signal completely [1]. Efficiency of the detector, which may be a function of the phase space position should also not influence the results qualitatively since it modifies the measurement the same way in all events. Careful Monte Carlo studies to check the last statement should be done, though.

4.2 Scalar mesons properties at finite temperature and density at NICA energy

P. Costa[a] and Yu.L. Kalinovsky[b]

[a] *Departamento de Física, Universidade de Coimbra, Coimbra, Portugal*
[b] *Laboratory for Information Technologies, JINR, Dubna, Russia*

Understanding the behavior of matter under extreme conditions is one of the most important task in physics of strong interactions. In the last years, major theoretical and experimental efforts have been dedicated to the physics of relativistic heavy-ion collisions, looking for signatures of the quark gluon plasma (QGP) formation.

A region of particular interest, that has been so far explored, is the $T - \mu_B$ phase boundary in order to try to explore different regions of the QCD phase diagram. The existence of the Critical End Point (CEP) in QCD was suggested in the end of the eighties, and its properties have been studied since then (for a review see [2]).

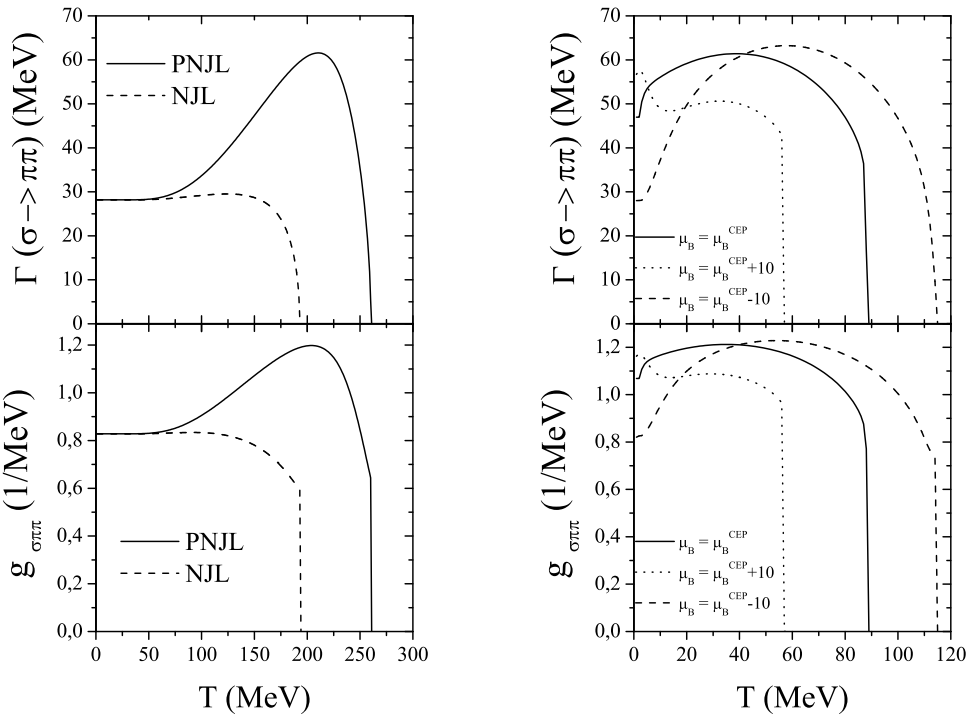

Figure 4.1: The temperature dependencies of decay width $\Gamma(\sigma \to \pi\pi)$ and interaction constant $g_{\sigma\pi\pi}$. These quantities are zoomed in the right panel to show their behavior in the vicinity of $\mu_{\rm CEP}$.

At the CEP the phase transition is of second order, belonging to the three - dimensional Ising universality class, and this kind of phase transitions is characterized by longwavelength fluctuations of the order parameter. As pointed out in [3], the critical region around the CEP is not point-like but has a very rich structure. This critical region is defined as the region where the mean field theory of phase transitions breaks down and nontrivial critical exponents emerge. The size of the critical region is important for future searches for the CEP in heavy ion collisions, particularly in the NICA energy.

It is also expected that experimental signatures peculiar to CEP can be observed through spectral changes in the presence of abnormally light σ mesons. The σ meson in a hot medium can decay through different processes like $\sigma \to \pi\pi$, $\sigma \to \gamma\gamma$, etc. Once the σ mass is so reduced around the chiral transition temperature, the σ meson cannot decay into two pions and thus the spectral function in the σ-channel must be significantly enhanced (the threshold point of the decay is defined by the mass equation $M_\sigma(T,\ \mu) = 2M_\pi(T,\ \mu)$). Using the resulting spectral functions it is possible to evaluated the multiplicity of diphoton emission [4].

In our project we aim to investigate the chiral phase transition and the CEP in quark matter. We perform our calculations in the framework of the two- and three-flavor NJL [5–8] and PNJL models [9]. The generalized PNJL model plays the important role for explaining the equation of state and the critical behavior around the critical end point.

As an example, we present in Fig. 4.1 the $\sigma \to \pi\pi$ at the critical end point. When we are in the region of first order transition (from the chirally symmetric phase to the broken phase), the M_σ and M_π are discontinuous, so M_σ jumps up and M_σ jumps down. The σ decay starts not at the threshold, but at some value beyond the threshold. This means that the decay in the first - order transition region happens suddenly and the decay rate behaves like a step function as a function of the temperature.

When approaching to the critical endpoint from the first-order transition side, the jump of the mass difference disappear. The decay rate becomes continuous, while the coupling strength has still a jump.

4.3 Hadron abundances at high baryon density

H. Satz

Fakultät für Physik, Universität Bielefeld, Germany

Consider the medium formed in an energetic nucleus-nucleus collision. At low baryon density, the constituents of this medium are mostly mesons, and the dominant interaction is resonance formation; with increasing collision energy, different resonance species of increasing mass are formed, leading to a gas of ever increasing degrees of freedom. They are all of a typical hadronic size (with a radius $R_{\rm h} \simeq$1 fm) and can overlap or interpenetrate each other. For baryochemical potential $\mu_{\rm B} \simeq 0$, the contribution of baryons/antibaryons and baryonic resonances is relatively small, but with increasing baryon density, they form an ever larger section of the species present in the medium, and beyond some baryon density, they become the dominant constituents. Finally, at vanishing temperature, the medium consists essentially of nucleons.

For vanishing or low baryon number density, when the interactions are resonance dominated, the system can be described as an ideal gas of all possible resonance species [10–12], contained in an overall spatial volume V. The temperature of this gas is (for $\mu_{\rm B} \simeq 0$ and high collision energy) found to attain a universal value $T_{\rm H} \simeq$ 175 MeV, over a wide range of collision configurations, from e^+e^- annihilation to nucleus-nucleus interactions, and for all CMS collision energies above 10 – 20 GeV. For nuclear collisions at lower $\sqrt{s_{\rm NN}}$, applying the same resonance gas analysis leads to temperatures which become dependent on the baryochemical potential $\mu_{\rm B}$; they decrease for increasing $\mu_{\rm B}$ [13].

At high baryon density, however, the dominant interaction is non-resonant. Nuclear forces are short-range and strongly attractive at distances of about 1 fm; but for distances around 0.5 fm, they become strongly repulsive. The former is what makes nuclei, the latter (together with Coulomb and Fermi repulsion) prevents them from collapsing. The repulsion between a proton and a neutron shows a purely baryonic "hard-core" effect and is connected neither to Coulomb repulsion nor to Pauli blocking of nucleons. As a consequence, the volumes of nuclei grow linearly with the sum of its protons and neutrons. With increasing baryon density, the conceptual basis of a resonance gas thus becomes less and less correct, so that eventually one should encounter a regime of quite different nature.

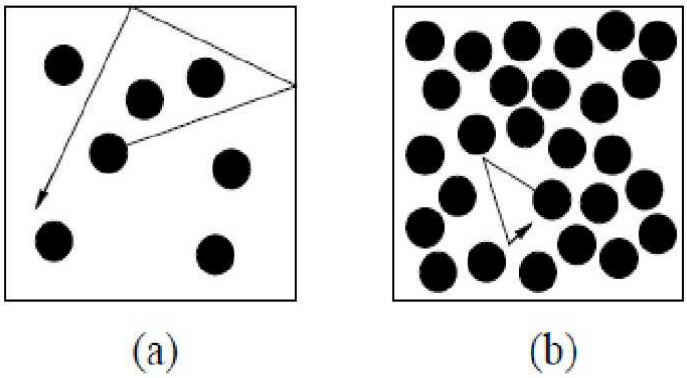

Figure 4.2: States of hard core baryons: full mobility (a), "jammed" (b).

It would seem very interesting to investigate experimentally, through a study of hadron abundances, this change of regimes. If NICA can reach large baryon densities and measure a variety of hadron species, this would appear to be a promising field of research.

In closing, we note that the conceptual differences of the low and the high baryon density regimes of the phase diagram for strongly interacting matter have recently been studied in terms of the underlying critical features [14]. While at low baryon density, hadron percolation leads to the universal chemical freeze-out temperature $T_{\rm H}$ specifying the species abundances, at high baryon density there occurs a "jamming" of nucleons: the mobility of baryons in the medium becomes strongly restricted by the presence of other baryons, leading to a jammed state, as shown in Fig. 4.2. A study of this region could thus help in the understanding of new, high baryon-density phenomena, which have also been discussed in the context of "quarkyonic matter" [15].

4.4 Directed flow as a signal of a liquid state of transient matter

S. M. Troshin

Institute for High Energy Physics, Protvino, Russia

Directed flow v_1, observable introduced for description of nucleus collisions is discussed. We consider a possible origin of the flow in hadronic reactions as a result of rotation of the transient matter and trace analogy with nucleus collisions. It is argued that the presence of directed flow can serve as a signal that transient matter is in a liquid state.

The deconfined state of transient matter found in the four major experiments at RHIC [16–18] reveals the properties of the perfect liquid, being strongly interacting collective state and therefore it was labelled as sQGP [19]. The nature of new form of matter discovered is not known, many different interpretations were proposed for the explanations of the experimental findings. The utmost significance of these experimental discoveries lies in the fact that the matter is strongly correlated and reveals high degree of the coherence when it is well beyond the critical values of density and temperature.

Important tools in the studies of the nature of the new form of matter are the anisotropic flows which are the quantitative characteristics of the collective motion of the produced hadrons in the nuclear interactions. With their measurements one can obtain a valuable information on the early stages of reactions and observe signals of QGP formation.

At the same time, the measurements of anisotropic flows and constituent quark scaling demonstrated an importance of the constituent quarks [20] and their role as effective degrees of freedom of the newly discovered state of matter. Of course the dynamics of strong interactions is the same for the hadron and nucleus collisions, and therefore the following question naturally arises, namely: To which extent, if at all, are the recent discoveries at RHIC relevant for hadronic interactions?

In this note we try to address in a model way one aspect of this broad problem, i.e. we discuss the role of the coherent rotation of the transient matter in hadron collisions as the origin of the directed flow in these reactions and stress that behavior of collective observable v_1 in hadronic and nuclear reactions would be similar and originates from the liquid state of transient matter.

The experimental probes of collective dynamics in AA interactions [20, 21], the momentum anisotropies v_n are defined by means of the Fourier expansion of the transverse momentum spectrum over the momentum azimuthal angle ϕ. The angle ϕ is the angle of the detected particle transverse momentum with respect to the reaction plane spanned by the collision axis z and the impact parameter vector $\mathbf{b}$ directed along the x axis. Thus, the anisotropic flows are the azimuthal correlations with the reaction plane. In particular, the directed flow is defined as

$$v_1(p_\perp) \equiv \langle \cos\phi \rangle_{p_\perp} = \langle p_x/p_\perp \rangle = \langle \hat{\mathbf{b}} \cdot \mathbf{p}_\perp/p_\perp \rangle \tag{4.1}$$

From Eq. (4.1) it is evident that this observable can be used for studies of multiparticle production dynamics in hadronic collisions provided that impact parameter $\mathbf{b}$ is fixed. Therefore we discuss hereabout directed flow v_1 in hadron collisions at fixed impact parameters and refer after that those considerations to the collisions of nuclei keeping in mind the same nature of the transient states in both cases. We amend the model [22, 23] developed for hadron interactions (based on the chiral quark model ideas) and consider the effect of collective rotation of a quark matter in the overlap region. We formulate a hypothesis on connection of the strongly interacting transient matter rotation with the directed flow generation.

Effective degrees of freedom and transient state of matter in hadron collisions

We assume that the origin of the transient state and its dynamics along with hadron structure can be related to the mechanism of spontaneous chiral symmetry breaking (χSB) in QCD [24], which leads to the generation of quark masses and appearance of quark condensates. This mechanism describes transition of the current into constituent quarks. The gluon field is considered to be responsible for providing quarks with masses and its internal structure through the instanton mechanism of the spontaneous chiral symmetry breaking. Massive constituent quarks appear as quasiparticles, i.e. current quarks and the surrounding clouds of quark–antiquark pairs which consist of a mixture of quarks of the different flavors. Quark radii are determined by the radii of the surrounding clouds. The quantum numbers of the constituent quarks are the same as the quantum numbers of current quarks due to the conservation of the corresponding currents in QCD.

Collective excitations of the condensate are the Goldstone bosons and the constituent quarks interact via exchange of the Goldstone bosons; this interaction is mainly due to pion field. Pions themselves are the bound

states of massive quarks. The interaction responsible for quark-pion interaction can be written in the form [25]:

$$\mathcal{L}_I = \bar{Q}[i\partial\!\!\!/ - M\exp(i\gamma_5\pi^A\lambda^A/F_\pi)]Q, \quad \pi^A = \pi, K, \eta. \tag{4.2}$$

The interaction is strong, the corresponding coupling constant is about 4. The general form of the total effective Lagrangian ($\mathcal{L}_{\rm QCD} \to \mathcal{L}_{\rm eff}$) relevant for a description of the non–perturbative phase of QCD includes the three terms [26]

$$\mathcal{L}_{\rm eff} = \mathcal{L}_\chi + \mathcal{L}_I + \mathcal{L}_C.$$

Here $\mathcal{L}_\chi$ is responsible for the spontaneous chiral symmetry breaking and turns on first.

To account for the constituent quark interaction and confinement the terms $\mathcal{L}_{\rm I}$ and $\mathcal{L}_{\rm C}$ are introduced. The $\mathcal{L}_{\rm I}$ and $\mathcal{L}_{\rm C}$ do not affect the internal structure of the constituent quarks.

The picture of a hadron consisting of constituent quarks embedded into quark condensate implies that overlapping and interaction of peripheral clouds occur at the first stage of hadron interaction. The interaction of the condensate clouds assumed to of the shock-wave type, this condensate clouds interaction generates the quark-pion transient state. This mechanism is inspired by the shock-wave production process proposed by Heisenberg [27] long time ago. At this stage, part of the effective lagrangian $\mathcal{L}_{\rm C}$ is turned off (it is turned on again in the final stage of the reaction). Nonlinear field couplings transform then the kinetic energy to internal energy [27, 28]. As a result the massive virtual quarks appear in the overlapping region and a transient state of matter is generated. This state consists of $\bar{Q}Q$ pairs and pions strongly interacting with quarks. This picture of quark-pion interaction can be considered as the origin for a percolation mechanism of deconfinement resulting in the liquid nature of the transient matter [29].

A part of the hadron energy carried by the outer condensate clouds being released in the overlap region goes to the generation of massive quarks interacting by pion exchange and their number was estimated as follows:

$$\tilde{N}(s,b) \propto \frac{(1-\langle k_{\rm Q}\rangle)\sqrt{s}}{m_{\rm Q}}\, D_c^{h_1} \otimes D_c^{h_2} \equiv N_0(s) D_{\rm C}(b), \tag{4.3}$$

where $m_{\rm Q}$ is the constituent quark mass and $\langle k_{\rm Q}\rangle$ the average fraction of hadron energy carried by the constituent valence quarks. The function D_c^h describes the condensate distribution inside the hadron h and b is the impact parameter of the colliding hadrons. Thus, $\tilde{N}(s,b)$ quarks appear in addition to $N = n_{h_1} + n_{h_2}$ valence quarks.

The generation time of the transient state $\Delta t_{\rm tsg}$ in this picture obeys to the inequality

$$\Delta t_{\rm tsg} \ll \Delta t_{\rm int},$$

where $\Delta t_{\rm int}$ is the total interaction time. The newly generated massive virtual quarks play a role of scatterers for the valence quarks in elastic scattering; those quarks are transient ones in this process: they are transformed back into the condensates of the final hadrons.

Under construction of the model for elastic scattering [22] it was assumed that the valence quarks located in the central part of a hadron are scattered in a quasi-independent way off the transient state with interaction radius of valence quark determined by its inverse mass:

$$R_{\rm Q} = \kappa/m_{\rm Q}. \tag{4.4}$$

The elastic scattering S-matrix in the impact parameter representation is written in the model in the form of linear fractional transform:

$$S(s,b) = \frac{1+iU(s,b)}{1-iU(s,b)}, \tag{4.5}$$

where $U(s,b)$ is the generalized reaction matrix, which is considered to be an input dynamical quantity similar to an input Born amplitude and related to the elastic scattering scattering amplitude through an algebraic equation which enables one to restore unitarity [30]. The function $U(s,b)$ is chosen in the model as a product of the averaged quark amplitudes

$$U(s,b) = \prod_{\rm Q=1}^{N} \langle f_{\rm Q}(s,b)\rangle \tag{4.6}$$

in accordance with assumed quasi-independent nature of the valence quark scattering. The essential point here is the rise with energy of the number of the scatterers like $\sqrt{s}$. The b–dependence of the function $\langle f_{\rm Q}\rangle$ has a simple form $\langle f_{\rm Q}(b)\rangle \propto \exp(-m_{\rm Q}b/\xi)$.

These notions can be extended to particle production with account of the geometry of the overlap region and properties of the liquid transient state. Valence constituent quarks would excite a part of the cloud of the virtual massive quarks and those quark droplets will subsequently hadronize and form the multiparticle final state. This mechanism can be relevant for the region of moderate transverse momenta while the region of high transverse momenta should be described by the excitation of the constituent quarks themselves and application of the perturbative QCD to the parton structure of the constituent quark. The model allow to describe elastic scattering and the main features of multiparticle production [22, 23, 31]. In particular, it leads to asymptotical dependencies

$$\sigma_{\rm tot,el} \sim \ln^2 s, \;\; \sigma_{\rm inel} \sim \ln s, \;\; \bar{n} \sim s^{\delta}. \tag{4.7}$$

Inclusive cross-section for unpolarized particles integrated over impact parameter $\mathbf{b}$, does not depend on the azimuthal angle of the detected particle transverse momentum. The s–channel unitarity for the inclusive cross-section could be accounted for by the following representation

$$\frac{d\sigma}{d\xi} = 4\int_0^\infty d\mathbf{b}\frac{I(s,\mathbf{b},\xi)}{|1-iU(s,\mathbf{b})|^2}. \tag{4.8}$$

The set of kinematic variables denoted by ξ describes the state of the detected particle. The function I is constructed from the multiparticle analogues $U_{\rm n}$ of the function U and is in fact an non-unitarized inclusive cross-section in the impact parameter space and unitarity corrections is given by the factor

$$w(s,b) \equiv |1-iU(s,b)|^{-2}$$

in Eq. (4.8). Unitarity modifies anisotropic flows. When the impact parameter vector $\mathbf{b}$ and transverse momentum $\mathbf{p}_\perp$ of the detected particle are fixed, the function $I = \sum_{n\geq 3} I_n$, where n denotes the number of particles in the final state, depends on the azimuthal angle ϕ between vectors $\mathbf{b}$ and $\mathbf{p}_\perp$. It should be noted that the impact parameter $\mathbf{b}$ is the variable conjugate to the transferred momentum $\mathbf{q} \equiv \mathbf{p}'_a - \mathbf{p}_a$ between two incident channels which describe production processes of the same final multiparticle state. The dependence on the azimuthal angle ϕ can be written in explicit form through the Fourier series expansion

$$I(s,\mathbf{b},y,\mathbf{p}_\perp) = I_0(s,b,y,p_\perp)[1+\sum_{n=1}^{\infty} 2\bar{v}_n(s,b,y,p_\perp)\cos n\phi]. \tag{4.9}$$

The function $I_0(s,b,\xi)$ satisfies the following sum rule

$$\int I_0(s,b,y,p_\perp)p_\perp dp_\perp dy = \bar{n}(s,b){\rm Im}U(s,b), \tag{4.10}$$

where $\bar{n}(s,b)$ is the mean multiplicity depending on impact parameter. The "bare" flow $\bar{v}_n$ is related to the measured flow v_n as follows

$$v_n(s,b,y,p_\perp) = w(s,b)\bar{v}_n(s,b,y,p_\perp).$$

In the above formulas the variable y denotes rapidity, i.e. $y = \sinh^{-1}(p/m)$, where p is a longitudinal momentum. Evidently, corrections due to unitarity are mostly important at small impact parameters, i.e. they provide an additional suppression of the anisotropic flows at small centralities, while very peripheral collisions are not affected by these corrections.

The geometrical picture of hadron collision at non-zero impact parameters described above implies that the generated massive virtual quarks in overlap region will obtain large initial orbital angular momentum at high energies. The total orbital angular momentum can be estimated as follows

$$L(s,b) \simeq \alpha b\frac{\sqrt{s}}{2}D_C(b). \tag{4.11}$$

The parameter α is related to the fraction of the initial energy carried by the condensate clouds which goes to rotation of the quark system and the overlap region, which is described by the function $D_{\rm C}(b)$, has an ellipsoidal form (Fig. 4.3). [h] It should be noted that $L \to 0$ at $b \to \infty$ and $L = 0$ at $b = 0$ (Fig. 4.4).

Rotating transient matter and directed flow in hadronic reactions

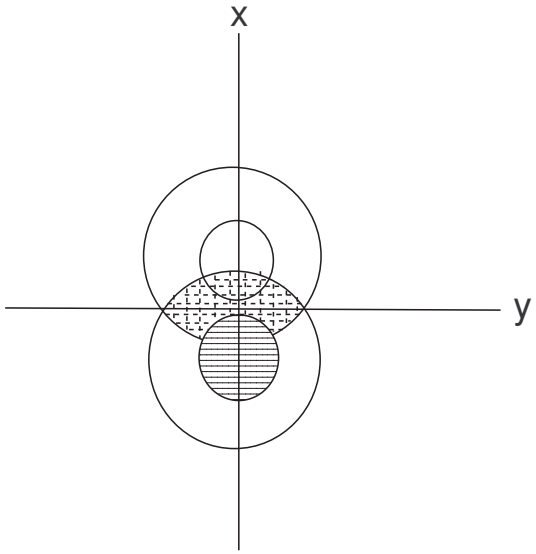

Figure 4.3: Schematic view in frontal plane of the hadron collision as extended objects. Collision occurs along the z-axis.

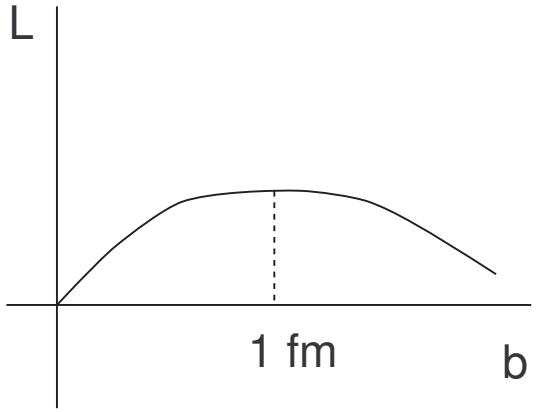

Figure 4.4: Qualitative dependence of the orbital angular momentum L on the impact parameter b.

Now we would like to discuss the experimental consequences of the described picture of hadron collisions. The important problem here is the experimental determination of the impact parameter **b**. To proceed that way the measurements of the characteristics of multiparticle production processes in hadronic collisions at fixed impact parameter should be performed with selection of the specific events sensitive to the value and direction of impact parameter. The determination of the reaction plane in the non-central hadronic collisions could be experimentally realizable with the utilization of the standard procedure [32, 33]. The relationship of the impact parameter with the final state multiplicity is a useful tool in these studies similar to the studies of the nuclear interactions. For example, in the Chou-Yang geometrical approac [34] one can restore the values of impact parameter from the charged particle multiplicity [35]. The centrality is determined by the fraction of the events with the largest number of produced particles which are registered by detectors (cf. [36]). Thus, the impact parameter can be determined through the centrality and then, e.g. directed flow, can be analyzed by selecting events in a specific centrality ranges. Indeed, the relation

$$c(N) \simeq \frac{\pi b^2(N)}{\sigma_{\rm inel}}, \tag{4.12}$$

between centrality and impact parameter was obtained [37] and can be extended straightforwardly to the case of hadron scattering. In this case we should consider $\bar{R}$ as a sum of the two radii of colliding hadrons and $\sigma_{\rm inel}$

as the total inelastic hadron-hadron cross–section. The centrality $c(N)$ is the centrality of the events with the multiplicity larger than N and $b(N)$ is the impact parameter where the mean multiplicity $\bar{n}(b)$ is equal to N.

At this point we would like to emphasize again the liquid nature of transient state. Namely due to strong interaction between quarks in the transient state, it can be described as a quark-pion liquid. Therefore, the orbital angular momentum L should be realized as a coherent rotation of the quark-pion liquid as a whole in the xz-plane (due to the aforementioned strong correlations between particles present in the liquid). It should be noted that for a given value of the orbital angular momentum L the kinetic energy has a minimal value if all parts of liquid rotate with the same angular velocity. We assume therefore that the different parts of the quark-pion liquid in the overlap region indeed have the same angular velocity ω. In this model the spin of the polarized hadrons has its origin in the rotation of the matter the hadrons consist of. In contrast, we assume rotation of the matter during intermediate, transient state of hadronic interaction.

Collective rotation of the strongly interacting system of the massive constituent quarks and pions is the main point of the proposed mechanism of the directed flow generation in hadronic and nuclei collisions. We concentrate on the effects of this rotation and consider directed flow for the constituent quarks supposing that directed flow for hadrons is close to the directed flow for the constituent quarks at least qualitatively.

The assumed particle production mechanism at moderate transverse momenta is the excitation of a part of the rotating transient state of massive constituent quarks (interacting by pion exchanges) by the one of the valence constituent quarks with subsequent hadronization of the quark-pion liquid droplets. Due to the fact that the transient matter is strongly interacting, the excited parts should be located closely to the periphery of the rotating transient state. Otherwise absorption would not allow the quarks and pions to leave the region (quenching). The mechanism is sensitive to the particular rotation direction and the directed flow should have opposite signs for the particles in the fragmentation regions of the projectile and target respectively. It is evident that the effect of rotation (shift in p_x value) is most significant in the peripheral part of the rotating quark-pion liquid and is to be weaker in the less peripheral regions (rotation with the same angular velocity ω), i.e. the directed flow v_1 (averaged over all transverse momenta) should be proportional to the inverse depth Δl where the excitation of the rotating quark-pion liquid takes place (Fig. 4.5) i.e.

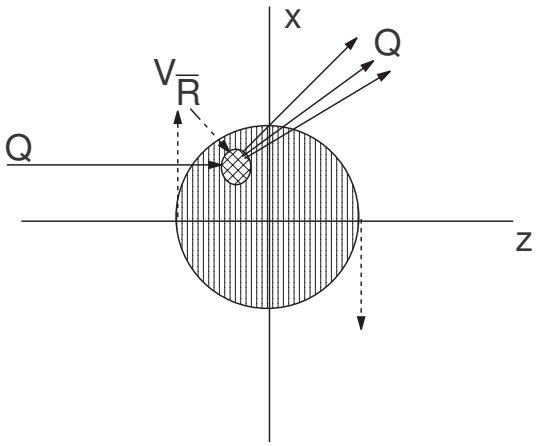

Figure 4.5: Interaction of the constituent quark with rotating quark-pion liquid.

$$|v_1| \sim \frac{1}{\Delta l} \tag{4.13}$$

In its turn, the length Δl is related to the energy loss of constituent valence quark in the medium due to elastic rescattering (quark-pion liquid) prior an excitation occurs, i.e. before constituent quark would deposit its energy into the energy of the excited quarks (those quarks lead to the production of the secondary particles), i.e. it can be assumed that

$$\Delta l \sim \Delta y,$$

where $\Delta y = |y - y_{\rm beam}|$ is the difference between the rapidities of the final particle and the projectile. On the other hand, the depth length Δl is determined by elastic quark scattering cross-section σ and quark-pion liquid

density n. Therefore, the averaged value of v_1 should be proportional to the particle density of the transient state and include the cross-section σ, i.e.

$$\langle |v_1| \rangle \sim \sigma n. \tag{4.14}$$

This estimate shows that the magnitude of the directed flow could provide information on the properties of the transient state. The magnitude of the observable v_1 (determined by the shift of transverse momentum due to rotation) is proportional to $(\Delta l)^{-1}$ in this mechanism and depends on the rapidity difference as

$$|v_1| \sim \frac{1}{|y - y_{\rm beam}|}. \tag{4.15}$$

It does not depend on the incident energy. Evidently, the directed flow $|v_1|$ decreases when the absolute value of the above difference increases, i.e. $|v_1|$ increases at fixed energy and increasing rapidity of final particle and it decreases at fixed rapidity of final particle and increasing beam energy. The dependence of $|v_1|$ will be universal for different energies when plotted against the difference $|y - y_{\rm beam}|$ (Fig. 4.6).

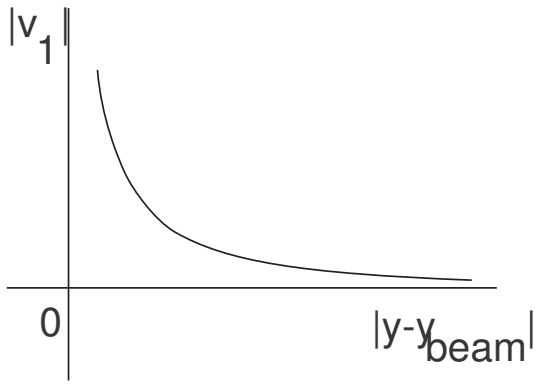

Figure 4.6: Universal dependence of directed flow on the rapidity difference.

The centrality dependence of $|v_1|$ is determined by the orbital momentum dependence L on the impact parameter, i.e. it should be decreasing towards higher and lower centralities. The decrease towards high centralities is evident: no overlap of hadrons or nuclei should be at high enough impact parameters. The decrease of v_1 towards lower centralities is a specific prediction of the proposed mechanism based on rotation since central collisions with smaller impact parameters would lead to slower rotation or its complete absence in the head-on collisions[9]. Thus, the qualitative centrality dependence of $|v_1|$ corresponds to Fig. 4.4.

Now we can consider the transverse momentum dependence of the directed flow $v_1(p_\perp)$ (integrated over rapidity) for constituent quarks. It is natural to suppose that the size of the region where the virtual massive quark Q comes from the quark-pion liquid is determined by its transverse momentum, i.e. $\bar{R} \simeq 1/p_\perp$. However, it is evident that $\bar{R}$ should not be larger than the interaction radius of the valence constituent quark $R_{\rm Q}$ (interacting with the quarks and pions from the transient liquid state). The production processes with high transverse momentum such that $\bar{R}$ is much less than the geometrical size of the valence constituent quark $r_{\rm Q}$ resolves its internal structure as a cluster of the non-interacting partons. Thus, at high transverse momenta the constituent quarks will be excited themselves and hadronization of the uncorrelated partons would lead to secondary particles with high transverse momenta and vanishing directed flow. If the production mechanism rendering to the constituent quark excitation is valid, then similar conclusions on the small anisotropic flows at large transverse momenta should be applicable for $v_n(p_\perp)$ with $n > 1$. Obviously, it should not be valid in the case of the polarized hadron collisions.

The magnitude of the quark interaction radius $R_{\rm Q}$ can be taken from the analysis of elastic scattering [22]; it has a dependence on its mass in the form (4.4) with $\kappa \simeq 2$, i.e. $R_{\rm Q} \simeq 1\ fm$ [10], while the geometrical radius of quark $r_{\rm Q}$ is about $0.2\ fm$. The size of the region[11], which is responsible for the small-$p_\perp$ hadron production, is large, valence constituent quark excites rotating cloud of quarks with various values and directions of their

[9] Of course, there is another reason for vanishing v_1 at $b = 0$, it is rotational invariance around collision axis.
[10] This is the light constituent quark interaction radius which is close to the inverse pion mass.
[11] For simplicity we suppose that this region has a spherically symmetrical form

momenta in that case. The effect of rotation will be averaged over the volume $V_{\bar{R}}$ and therefore $\langle \Delta p_x \rangle_{V_{\bar{R}}}$ and $v_1(p_\perp)$ should be small.

When we proceed to the region of higher values of $p_\perp^Q$, the radius $\bar{R}$ is decreasing and the effect of rotation becomes more prominent, the valence quark excites now the region where most of the quarks move coherently in the same direction with approximately equal velocities. The mean value $\langle \Delta p_x \rangle_{V_{\bar{R}}}$ and the directed flow, respectively, can have a significant magnitude and increase with increasing $p_\perp$. When $\bar{R}$ becomes smaller than the geometrical radius of constituent quark, the interactions at short distances start to resolve its internal structure as an uncorrelated cloud of partons. The production of the hadrons at such high values of transverse momenta is due to the excitation of the constituent quarks themselves and subsequent hadronization of the partons. The collective effects of rotating transient cloud in v_1 at large $p_\perp^Q > 1/r_Q$ will disappear as well as the directed flow of final particles. The value of transverse momentum, where the maximal values in the $p_\perp$-dependence of v_1 are expected, are in the region 1 GeV/c since $r_{\rm Q} \simeq 0.2\ fm$. The qualitative $p_\perp$-dependence of the directed flow is illustrated on Fig. 4.7.

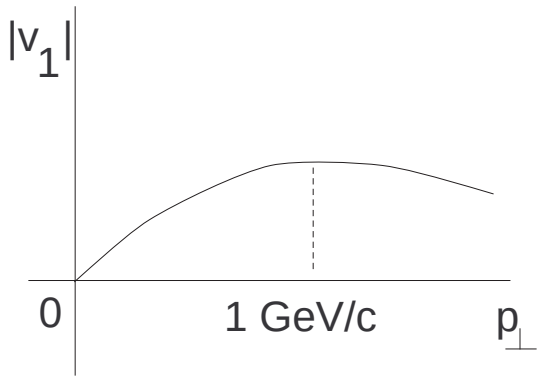

Figure 4.7: Qualitative dependence of directed flow on transverse momentum $p_\perp$.

Directed flow in nuclear collisions

Until now we considered hadron scattering and directed flow in this process, but a significant ingredient in this consideration was borrowed from the AA studies, namely we supposed that the transient matter is a strongly interacting one and it is the same in pp and AA reactions. Using the experimental findings of RHIC, we assumed, in fact, that it is a liquid consisting of massive quarks, interacting by pion exchange, and characterized by the fixed interparticle distances determined by the quark interaction radius. The assumption of the almost instantaneous, shock-wave type of generation of the transient state obtains then support in the very short thermalization time revealed in heavy-ion collisions at RHIC [18, 38]. The existence of massive quark matter in the stage preceding hadronization seems to be supported also by the experimental data obtained at CERN SPS [39].

The geometrical picture of hadron collision has an apparent analogy with collisions of nuclei and it should be noted that the appearance of large orbital angular momentum should be expected in the overlap region in the non-central nuclei collisions. And then due to the strongly interacting nature of the transient matter we assume that this orbital angular momentum realized as a coherent rotation of a liquid. Thus, it seems that underlying dynamics could be similar to the dynamics of the directed flow in hadron collisions.

We can go further and extend the production mechanism from hadron to nucleus case also. This extension cannot be straightforward. First, there will be no unitarity corrections for the anisotropic flows and instead of valence constituent quarks, as a projectile we should consider nucleons, which would excite a rotating quark liquid. Of course, those differences will result in significantly higher values of directed flow. But, the general trends in its dependence on the collision energy, rapidity of the detected particle and transverse momentum, should be the same. In particular, the directed flow in nuclei collisions as well as in hadron reactions will depend on the rapidity difference $y - y_{\rm beam}$ and not on the incident energy. The mechanism therefore can provide a qualitative explanation of the incident-energy scaling of v_1 observed at RHIC [40]. In the projectile frame the directed flow has the same values for the different initial energies. In Fig. 4.8 experimental data are shown along with the dependence

$$v_1 \sim (\eta - y_{\rm beam})^{-1}, \tag{4.16}$$

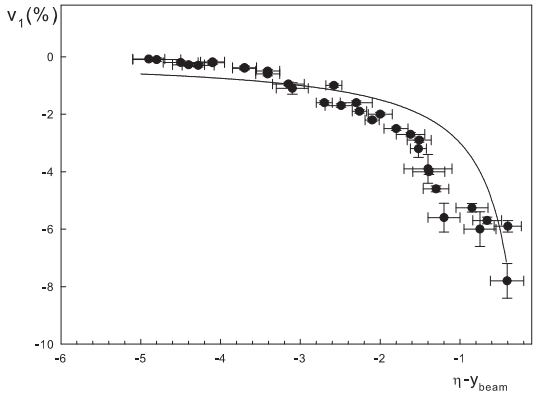

Figure 4.8: Dependence of directed flow on $\eta - y_{\rm beam}$ in Au+Au and Cu+Cu collisions at 62.4 GeV and 200 GeV at RHIC (preliminary data of STAR Collaboration [40])

where η is the pseudorapidity. This dependence reflects the trend in the experimental data and, therefore, the mechanism described in the previous section obtains an experimental justification, qualitatively, of course. In addition, we would like to note that the azimuthal dependence of the suppression factor $R_{\rm AA}$ found in the experiment PHENIX at RHIC [44] can also be explained by a rotation of the transient state. Since the correlations result from the rotation in this mechanism and therefore are maximal in the rotation plane, a similar dependence should be observed in the azimuthal dependence of the two-particle correlation function. The effect of rotation should be maximal for the peripheral collisions and therefore the dependence on ϕ should be steepest at larger impact parameter (or centrality) values. The discussed rotation mechanism should contribute to the elliptic flow too. However, since the regularities already found experimentally for v_1 and v_2 in nuclear interactions imply different dynamical origin for these flows, we should conclude that this mechanism does not provide a significant contribution to the elliptic flow.

Directed flow at the NICA and LHC energies and conclusion

Nowadays, with approaching start of the LHC, and planning of the NICA project at JINR Dubna it is interesting to predict what should be expected at such energies [45], [46] in particular: would deconfined matter produced in *pp* and A + A collisions be weakly interacting or will it remain to be a strongly interacting one as it was observed at RHIC in A + A collisions? In the latter case one can expect that the proposed rotating mechanism will be working at the LHC energies and at NICA and therefore the observed at RHIC incident-energy scaling in v_1 will remain to be valid also, i.e. directed flow plotted against the difference $y - y_{\rm beam}$ will be the same as it is at RHIC. However, if the transient matter at the LHC energies or at NICA will be weakly interacting, then one should expect the absence of the coherent rotation and the vanishing of the directed flow. This conclusion is valid provided that the rotation is the only mechanism of the directed flow generation. If it is so, vanishing directed flow can serve as a signal of a genuine quark-gluon plasma (gas of free quarks and gluons) formation.

I would like to thank Nikolay Tyurin, in collaboration with him the results described here were obtained. I am grateful to Oleg Teryaev for the interesting discussions and proposal to write this contribution for the NICA Project. I would like to aknowledge also many discussions with Laszlo Jenkovszky which were very helpful and interesting.

4.5 Importance of third moments of conserved charges in relativistic heavy ion collisions

M. Asakawa

Department of Physics, Osaka University, Toyonaka, Japan

Quantum chromodynamics (QCD) is believed to have a rich phase structure in the temperature (T) and baryon chemical potential ($\mu_{\rm B}$) plane. Lattice QCD calculations indicate that the chiral and deconfinement phase transitions are a smooth crossover on the temperature axis [47], while various models predict that the

phase transition becomes of first order at high density [48]. The existence of the QCD critical point is thus expected.

One may expect that the singularity at the critical point, at which the transition is of second order, may cause enhancements of fluctuations if fireballs created by heavy ion collisions pass near the critical point during the time evolution. Because of finite size effects and critical slowing down, however, such singularities are blurred and its experimental conformation may not be possible [49, 50].

Here we propose to employ *signs* of third moments of conserved charges around the averages, which we call, for simplicity, the third moments in the following, to infer the states created by heavy ion collisions. In particular, we consider third moments of conserved quantities, the net baryon and electric charge numbers, and the energy,

$$m_3(ccc) \equiv \frac{\langle (\delta N_c)^3 \rangle}{VT^2}, \quad m_3(\mathrm{EEE}) \equiv \frac{\langle (\delta E)^3 \rangle}{VT^5}, \tag{4.17}$$

where N_c with $c = \mathrm{B}, \mathrm{Q}$ represent the net baryon and electric charge numbers in a subvolume V, respectively, E denotes the total energy in V, $\delta N_c = N_c - \langle N_c \rangle$, and $\delta E = E - \langle E \rangle$. We also make use of the mixed moments defined as follows:

$$m_3(cc\mathrm{E}) \equiv \frac{\langle (\delta N_c)^2 \delta E \rangle}{VT^3}, \quad m_3(c\mathrm{EE}) \equiv \frac{\langle \delta N_c (\delta E)^2 \rangle}{VT^4}. \tag{4.18}$$

To understand the behaviors of these moments around the QCD phase boundary, we first notice that the moments Eqs. (4.17) and (4.18) are related to third derivatives of the thermodynamic potential per unit volume, ω, with respect to the corresponding chemical potentials and T. The simplest example is $m_3(\mathrm{BBB})$, which is given by

$$m_3(\mathrm{BBB}) = -\frac{\partial^3 \omega}{\partial \mu_\mathrm{B}^3} = \frac{\partial \chi_\mathrm{B}}{\partial \mu_\mathrm{B}}, \tag{4.19}$$

where the baryon number susceptibility, χ_B, is defined as

$$\chi_\mathrm{B} = -\frac{\partial^2 \omega}{\partial \mu_\mathrm{B}^2} = \frac{\langle (\delta N_\mathrm{B})^2 \rangle}{VT}. \tag{4.20}$$

The baryon number susceptibility χ_B diverges at the critical point and has a peak structure around there.

Since $m_3(\mathrm{BBB})$ is given by the μ_B derivative of χ_B as in Eq. (4.19), the existence of the peak in χ_B means that $m_3(\mathrm{BBB})$ changes its sign there. Although the precise size and shape of the critical region are not known, various models predict that the peak structure of χ_B well survives far along the crossover line. For also $m_3(cc\mathrm{E})$ and $m_3(c\mathrm{EE})$, a similar argument applies.

Once the negativeness of third moments is established experimentally, it is direct evidence of two facts: (1) the existence of a peak structure of corresponding susceptibility in the phase diagram of QCD, and (2) the realization of hot matter beyond the peak, i.e. the quark-gluon plasma, in heavy ion collisions. We emphasize that this statement using the *signs* of third moments is free from any theoretical ambiguities.

The range of μ_B/T where lattice simulations are successfully applied is limited to small μ_B/T with the present algorithms. In particular, thermodynamics around the critical point cannot be analyzed with the Taylor expansion method. In order to evaluate the qualitative behavior of the third moments in such a region, one has to resort to effective models of QCD. To make such an estimate, here we employ the two-flavor Nambu-Jona-Lasinio model [51, 52] with the standard interaction $\mathcal{L}_\mathrm{int} = G\{(\bar{\psi}\psi)^2 + (\bar{\psi} i\gamma_5 \tau_i \psi)^2\}$, where ψ denotes the quark field. For the model parameters, we take the values determined in Ref. [51]; $G = 5.5$ GeV^{-2}, the current quark mass $m = 5.5$ MeV, and the three-momentum cutoff $\Lambda = 631$ MeV. For the isospin symmetric matter, this model gives a first order phase transition at large μ_B.

The region where each moment becomes negative in the T-μ_B plane is shown in Fig. 4.9. One sees that all the moments become negative on the far side of the critical point as it should be, whereas the extent of the region depends on the channel. The figure shows that areas with $m_3(\mathrm{BBB}) < 0$ and $m_3(\mathrm{BBE}) < 0$ extend to much lower μ_B and much higher T than the critical point. This suggests that even if the critical point is located at high μ_B the negative third moments can be observed by heavy ion collision experiments. It should be, however, remembered that the results in Fig. 4.9, are obtained in an effective model. In particular, the model employed here gives the critical point at relatively low T and high μ_B [53]. If the critical point is at much lower μ_B, the areas with negative moments in Fig. 4.9 should also move toward lower μ_B and higher T.

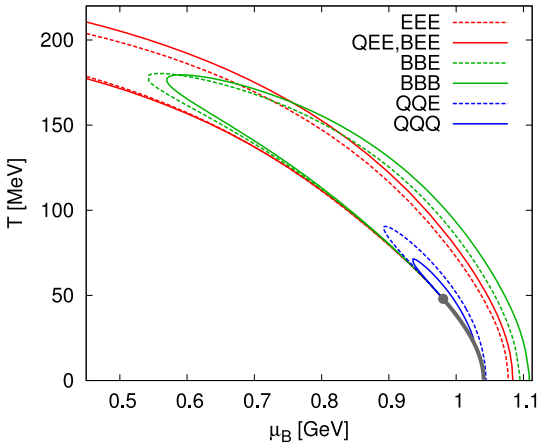

Figure 4.9: Regions where third moments take negative values in the T-$\mu_{\rm B}$ plane. The regions are inside the boundaries given by the lines.

It cannot be emphasized too much that it is essential to cover the entire phase space by changing colliding energy to draw a figure like Fig. 4.9 and get the full information on the QCD phase diagram. From this point of view, NICA project is as important as RHIC and LHC.

4.6 Baryon Stopping in Heavy-Ion Collisions at $E_{\rm lab}$ = 2–160 GeV/nucleon

Yu.B. Ivanov[a,b]

[a] *GSI Helmholtzzentrum für Schwerionenforschung GmbH, Darmstadt, Germany*
[b] *Kurchatov Institute, Moscow, Russia*

The degree of stopping of colliding nuclei is one of the basic characteristics of the collision dynamics, which determines the part of the incident energy of colliding nuclei deposited into produced fireball and hence into the production of secondary particles. The deposited energy in its turn determines the nature (hadronic or quark-gluonic) of the produced fireball and thereby its subsequent evolution. Therefore, a proper reproduction of the baryon stopping is of primary importance for the theoretical understanding of the dynamics of nuclear collisions. A direct measure of the baryon stopping is the net-baryon rapidity distribution. However, since experimental information on neutrons is unavailable, we have to rely on proton data.

Available data on the proton (at AGS energies) and net-proton (at SPS energies) rapidity distributions from central heavy-ion collisions are presented in Fig. 4.10. Only the midrapidity region is displayed in Fig. 4.10, since it is of prime interest in the present consideration. The data at 10 AGeV are repeated in the right panel of Fig. 4.10 in order to keep the reference spectrum shape for the comparison. The data are plotted as functions of a "dimensionless" rapidity $(y - y_{\rm cm})/y_{\rm cm}$, where $y_{\rm cm}$ is the center-of-mass rapidity of colliding nuclei. In particular, this is the reason why the experimental distributions are multiplied $y_{\rm cm}$. This representation is chosen in order to make different distributions of approximately the same width and the same height. This is convenient for comparison of shapes of these distributions. To make this comparison more quantitative, the data are fitted by a simple formula

$$\begin{aligned} \frac{dN}{dy} &= a\,(\exp\{-(1/w_s)\cosh(y - y_{cm} - y_s)\} \\ &+ \exp\{-(1/w_s)\cosh(y - y_{cm} + y_s)\}) \end{aligned} \tag{4.21}$$

where a, y_s and w_s are parameters of the fit. The form (4.21) is a sum of two thermal sources shifted by $\pm y_s$ from the midrapidity. The width w_s of the sources can be interpreted as w_s = (temperature)/(transverse mass), if we assume that collective velocities in the sources have no spread with respect to the source rapidities $\pm y_s$. The parameters of the two sources are identical (up to the sign of y_s) because we consider only collisions of identical nuclei. Results of these fits are demonstrated in Fig. 4.10.

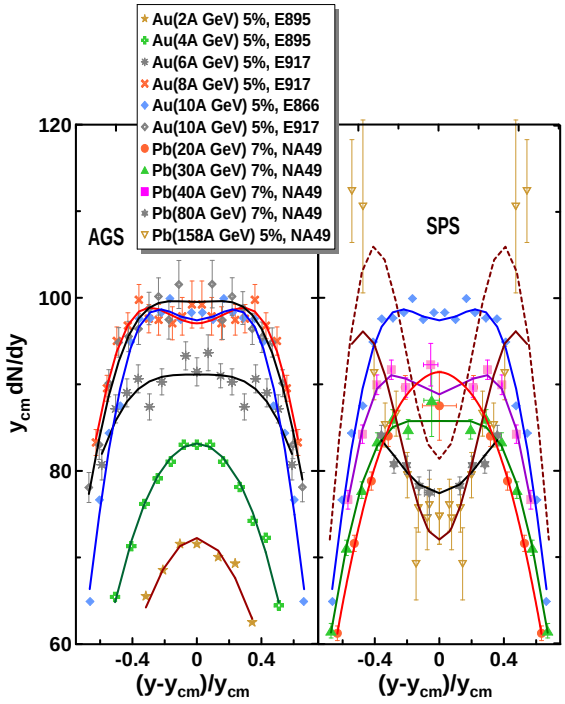

Figure 4.10: Rapidity spectra of protons (for AGS energies) and net-protons ($p - \bar{p}$) (for SPS energies) from central collisions of Au + Au (AGS) and Pb+Pb (SPS). Experimental data are from collaborations E802 [54], E877 [55], E917 [56], E866 [57], and NA49 [58–62]. The percentage shows the fraction of the total reaction cross section, corresponding to experimental selection of central events. Solid lines connecting points represent the two-source fits by Eq. (4.21). The dashed line is the fit to old data on Pb(158 AGeV)+Pb [58], these data themselves are not displayed.

The above fit has been done by the least-squares method. Data were fitted in the rapidity range $|y - y_{cm}|/y_{cm} < 0.7$. The choice of this range is dictated by the data. As a rule, the data are available in this rapidity range, sometimes the data range is even more narrow (40, 80 AGeV and new data at 158 AGeV [62]). We put the above restriction in order to treat different data in approximately the same rapidity range. Notice that the rapidity range should not be too wide in order to exclude contribution of cold spectators.

Inspecting evolution of the spectrum shape with the incident energy rise, we observe an irregularity. Beginning from the lowest AGS energy to the top one the shape of the spectrum evolves from convex to slightly concave at 10 AGeV. However, at 20 AGeV the shape again becomes distinctly convex. With the further energy rise the shape again transforms from the convex form to a highly concave one. In order to quantify this trend, we introduce a reduced curvature of the spectrum in the midrapidity defined as follows

$$\begin{aligned} C_y &\equiv \left(y_{\rm cm}^3 \frac{d^3N}{dy^3}\right)_{y=y_{\rm cm}} \Big/ \left(y_{\rm cm}\frac{dN}{dy}\right)_{y=y_{\rm cm}} \\ &= (y_{cm}/w_s)^2 \left(\sinh^2 y_s - w_s \cosh y_s\right). \end{aligned} \tag{4.22}$$

This curvature is defined with respect to the "dimensionless" rapidity $(y-y_{\rm cm})/y_{\rm cm}$. The factor $1/\left(y_{\rm cm}dN/dy\right)_{y=y_{\rm cm}}$ is introduced in order to get rid of overall normalization of the spectrum, i.e. of the a parameter in terms of fit (4.21). The second part of Eq. (4.22) presents this curvature in terms of parameters of fit (4.21).

Values of the curvature $C_{\rm y}$ deduced from fit (4.21) to experimental data are displayed in Fig. 4.11. The irregularity observed in Fig. 4.10 is distinctly seen here as a "zig-zag" irregularity in the energy dependence of $C_{\rm y}$.

Fig. 4.11 also contains $C_{\rm y}$ deduced from results of 3FD simulations with a hadronic equation of state (hadr. EoS) [65] and a EoS involving a first-order phase transition into the quark-gluon phase (2-ph. EoS) [66]. To obtain y_s and w_s, the 3FD spectra were also fitted by the form (4.21). The 3FD model with the hadronic EoS reasonably reproduces a great body of experimental data in a wide energy range from AGS to SPS, see Ref. [63]. Description of the rapidity distributions with the hadronic EoS is reported in Refs. [63, 64]. The reproduction of the distributions is quite good at the AGS energies and at the top SPS energies. At 40 AGeV the description is still satisfactory. However, at 20 and 30 AGeV the hadr.-EoS predictions completely disagree with the data,

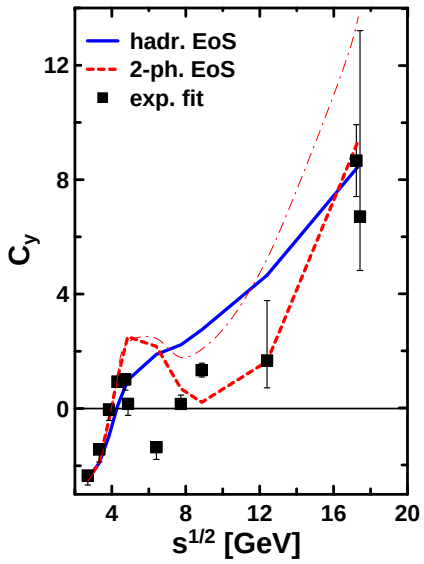

Figure 4.11: Midrapidity reduced curvature of the (net)proton rapidity spectrum as a function of the center-of-mass energy of colliding nuclei as deduced from experimental data and predicted by 3FD calculations with hadronic EoS (hadr. EoS) [65] and a EoS involving a first-order phase transition into the quark-gluon phase (2-ph. EoS) [66]. The thin dashed-dotted line demonstrates the effect of the 2-ph. EoS without changing the friction in the quark-gluon phase.

cf. [64]. At 20 AGeV instead of a bump at the midrapidity the hadronic scenario predicts a quite pronounced dip.

The 3FD simulations have been also done with a EoS involving a first-order phase transition into the quark-gluon phase (2-ph. EoS) [66]. In 2-ph. EoS the Gibbs construction was used for the mixed phase. These calculations well reproduce the AGS data up to the energy of 6 AGeV, where the purely hadronic scenario is realized. The data at the top SPS energy are also reproduced, which is achieved by a proper tune of the inter-fluid friction in the quark-gluon phase. Quality of the reproduction of above data is approximately the same as that with the hadronic EoS, as it is, e.g., seen from Figs. 4.11. However, at top AGS and lower SPS energies (8 – 80 AGeV), where the mixed phase turns out to be really important, the 2-ph. EoS completely fails. This failure cannot be cured by variations of neither the friction nor the freeze-out criterion.

However, the $C_{\rm y}$ curvature energy dependence in the first-order-transition scenario manifests qualitatively the same "zig-zag" irregularity (Fig. 4.11), as that in the data fit, while the hadronic scenario produces purely monotonous behaviour.

The baryon stopping depends on a character of interactions (e.g., cross sections) of the matter constituents. If during the interpenetration stage of colliding nuclei a phase transformation[12] of the hadronic matter into quark-gluonic one happens, one can expect a change of the stopping power of the matter at this time span. This is a natural consequence of a change of the constituent content of the matter because hadron-hadron cross sections differ from quark-quark, quark-gluon, etc. ones. This can naturally result in a non-monotonous behaviour of the shape of the (net)proton rapidity-spectrum at an incident energy, where onset of the phase transition occurs. The friction in the quark-gluon phase was tuned to reproduce the data at the top SPS energy. Naturally, it does not continuously match the friction in the hadronic phase.

However, if even the same friction is used in both phases, the calculated (with 2-ph. EoS) reduced curvature still reveals a "zig-zag" behaviour but with considerably smaller amplitude (see the thin dashed-dotted line in Fig. 4.11). This happens because the EoS in a generalized sense of this term, i.e. viewed as a partition of the total energy between kinetic and potential parts, also affects the stopping power. The friction is proportional to the relative velocity of the counter-streaming nuclei [63]. Therefore, it is more efficient when the kinetic-energy part of the total energy is higher, i.e. when the EoS is softer. The latter naturally results in a non-monotonous

[12]The term "phase transition" is deliberately avoided, since it usually implies thermal equilibrium.

evolution of the proton rapidity spectra with the energy rise.

Fig. 4.12 demonstrates that the onset of the phase transition in the calculations indeed happens at top-AGS–low-SPS energies, where the "zig-zag" irregularity takes place. Similarly to that it has been done in Ref. [69], the figure displays dynamical trajectories of the matter in the central box placed around the origin $\mathbf{r} = (0, 0, 0)$ in the frame of equal velocities of colliding nuclei: $|x| \leq 2$ fm, $|y| \leq 2$ fm and $|z| \leq \gamma_{\rm cm}$ 2 fm, where $\gamma_{\rm cm}$ is Lorentz factor associated with the initial nuclear motion in the c.m. frame. Initially, the colliding nuclei are placed symmetrically with respect to the origin $\mathbf{r} = (0, 0, 0)$, z is the direction of the beam. The ε-$n_{\rm B}$ representation is chosen because these densities are dynamical quantities and, therefore, are suitable to compare calculations with different EoS's. Subtraction of the $m_{\rm N} n_{\rm B}$ term is taken for the sake of suitable representation of the plot. Only expansion stages of the evolution are displayed, where the matter in the box is already thermally equilibrated. Nevertheless, the matter in the box still amounts to a minor part of the total matter of colliding nuclei. Therefore, only the minor part of the total matter undergoes the phase transition at 10 AGeV energy. As seen, the trajectories for two different EoS's are very similar at AGS energies and start to differ at SPS energies because of the effect of the phase transition.

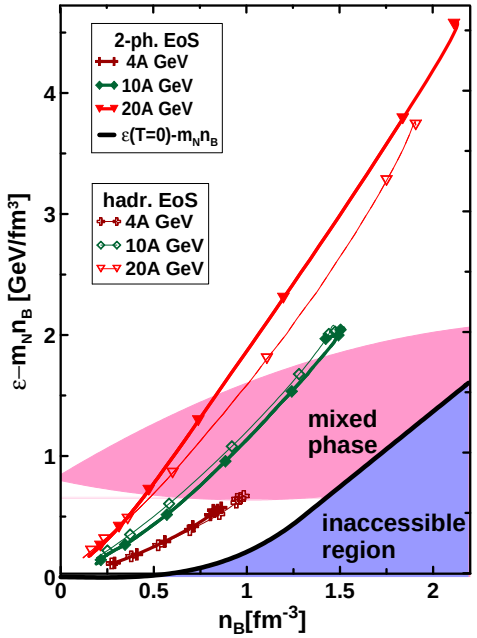

Figure 4.12: Dynamical trajectories of the matter in the central box of the colliding nuclei (4fm×4fm×$\gamma_{\rm cm}$4fm), where $\gamma_{\rm cm}$ is the Lorentz factor associated with the initial nuclear motion in the c.m. frame, for central ($b = 0$) collisions of Au+Au at 4 and 10 AGeV energies and Pb+Pb at 20 AGeV. The trajectories are plotted in terms of baryon density ($n_{\rm B}$) and the energy density minus $n_{\rm B}$ multiplied by the nucleon mass ($\varepsilon - m_{\rm N} n_{\rm B}$). Only expansion stages of the evolution are displayed for two EoS's. Symbols on the trajectories indicate the time rate of the evolution: time span between marks is 1 fm/c.

In conclusion, the experimentally observed baryon stopping may indicate (within the present experimental uncertainties) a non-monotonous behaviour as a function of the incident energy of colliding nuclei. This reveals itself in a "zig-zag" irregularity in the excitation function of a midrapidity reduced curvature of the (net)proton rapidity spectrum. Notice that the energy location of this anomaly coincides with the previously observed anomalies for other hadron-production properties at the low SPS energies [67,70]. The 3FD calculation with the hadronic EoS fails to reproduce this irregularity. At the same time, the same calculation with the EoS involving a first-order phase transition into the quark-gluon phase (within the Gibbs construction) [66] reproduces this "zig-zag" behaviour, however only qualitatively. This non-monotonous behaviour of the baryon stopping is a natural consequence of a phase transition. The question why these calculations do not qualitatively reproduce the "zig-zag" irregularity deserves special discussion elsewhere. It is very probable that either the Gibbs and Maxwell constructions are inappropriate for the fast dynamics of the heavy-ion collisions or the phase transition is not of the first order.

It is somewhat suspicious that the "zig-zag" irregularity happens at the border between the AGS and SPS energies. It could imply that this irregularity results from different ways of selecting central events in AGS and SPS experiments. New data taken at the same acceptance and the same centrality selection in this energy range are highly desirable to clarify this problem. Hopefully such data will come from new accelerators FAIR at GSI and NICA at Dubna, as well as from the low-energy-scan program at RHIC. An advantage of NICA is that it covers precisely the whole energy range of the present interest. Therefore, the measurements can be taken with the same experimental conditions within the whole energy range. This will allow to confirm or reject the discussed experimental trend.

A report on this work in more detail can be found in [71].

4.7 Statistical hadronization phenomenology in a low-energy collider

G. Torrieri[a,b]

[a] *FIAS, J.W. Goethe Universität, Frankfurt A.M., Germany*
[b] *Department of Physics, Columbia University, New York, USA*

Fluctuation observables play an obvious primary role for searches of a lot of new physics planned at NICA. The most universal and model-independent signature of critical point physics is that fluctuations should spike close to the critical point [72] (a "remnant" of their divergence in the thermodynamic limit). Spinodal regions [73], triple points [74], color superconductivity transitions [75] etc. should also produce a qualitatively strong fluctuation enhancement. Before data can be compared to theory, however, two important issues need to be examined and clarified:

The first issue is the formulation of the fluctuation observable least affected by fluctuations not connected to the microscopic physics of the system, like initial state fluctuations and fluctuations due to limited detector acceptance. While an order-of-magnitude shift in fluctuations will probably be visible over a non-thermal background, the background could well overwhelm a smaller spike, especially, as is likely, if the onset of the critical point is also correlated with non-equilibrium dynamical effects.

The second issue is a thorough understanding of the fluctuations due to statistical mechanics *independently* of the critical point. Obviously, they form part of the background to any critical point signal. But more generally, fluctuations can be used to thoroughly constrain the free parameters in statistical models, and determine in what domain, in energy and system size, is statistical mechanics a valid description for particle production.

This task is important in and of itself: As an analogy from another field where fluctuations are crucial, Cosmic Microwave Background fluctuations have not yet yielded evidence of novel physics. Their use to constrain the dominant paradigm of cosmology, inflation, has however been invaluable enough to entitle the leaders of the COBE project to a Nobel Prize. The equivalent job in soft hadronic physics, using fluctuations to Gauge and constrain the statistical model of particle production, is far from being completed, and a low-energy collider is essential to complete it.

The idea of modeling the abundance of hadrons using statistical mechanics has a long history [76–79]. In a sense, any discussion of the thermodynamic properties of hadronic matter (e.g. the existence of a phase transition and a critical point) *requires* that statistical mechanics be applicable to this system. Indeed, there is a consensus that statistical models can fit most particles from very high energies to energies comparable with NICA [80–86].

There are, however, several points of contention to this understanding: Some scientists [76] interpret the statistical model results in terms of nothing more than phase space dominance. If this is the case, the applicability of the statistical model has nothing to do with a genuine equilibration of the system,so using statistical mechanics inspired techniques to look for the critical point is useless. Others [74, 80] believe that the applicability of the statistical model is a sign of a phase transition, as the chemical equilibration of hadrons signals a regime in which multi-particle processes and high-lying resonances dominate.Still others [83] think that in soft QCD processes particles are "born in equilibrium", and the applicability of the statistical model to even smaller systems (itself controversial [87]) is a fundamental characteristic of QCD.

How can these scenarios be differentiated? One observable "at the heart" of statistical mechanics is event-by-event fluctuations. It is a fundamental principle of statistics that variances around averages scale a calculable way w.r.t. averages. In our context "Averages" are particle multiplicities per event and fluctuations are event-by-event fluctuations. For macroscopic systems, this principle ensures that fluctuations become negligible and

the expectation that the state of the system is the maximum entropy one is nearly certain to be realized. The typical event multiplicity, $\sim 100--1000$ particles is not enough for this to be the case, but, if statistical mechanics applies, one should still see that yields, fluctuations and higher cumulants scale in a way calculable from the partition function.

There are, however, some experimental issues specific to heavy ion collisions that need to be explored before this can be transformed into a quantitative test. "standard" fluctuation calculations assume that the volume stays constant. System size fluctuations due to initial geometry and dynamics obviously make this assumption invalid, and contaminate any straight-forward fluctuation observable.

The simplest way to eliminate system size fluctuations unrelated to statistical mechanics is to focus on fluctuations of *ratios* of particles ($\pi^+/\pi^-, p/\pi, K/\pi$, and so on). It can be shown that, at least in the thermodynamic limit, volume becomes a proportionality constant at the level of the partition function so that the scaled variance of a ratio is inversely proportional of the average, $\sigma_{N_1/N_2} \sim 1/\langle N_{1,2}\rangle$ and *strictly independent* of fluctuations in volume. This scaling, for *all yields* and *all fluctuations of ratios* is *specific* to statistical mechanics in the thermodynamic limit, *provided they are measured at the same value* with the same acceptance cuts. In other words, for all particles i, j, $\langle N_i\rangle\sigma_{N_i/N_j}$ is strictly independent of system size, and any dependence of it on $\sqrt{s}$ can be described by the same T and μ_B that *also* describe $\langle N_i\rangle/\langle N_j\rangle$. This is a very tight constraint, equivalent of using CMB fluctuations to tune inflationary cosmology models precisely [88]. Codes capable of doing this are already publically available [85,86], but data to perform this kind of analysis reliably, for reasons explained below, is only available at high (top Relativistic Heavy Ion Collider) energy [88] (see Fig. 4.13 for the main result).

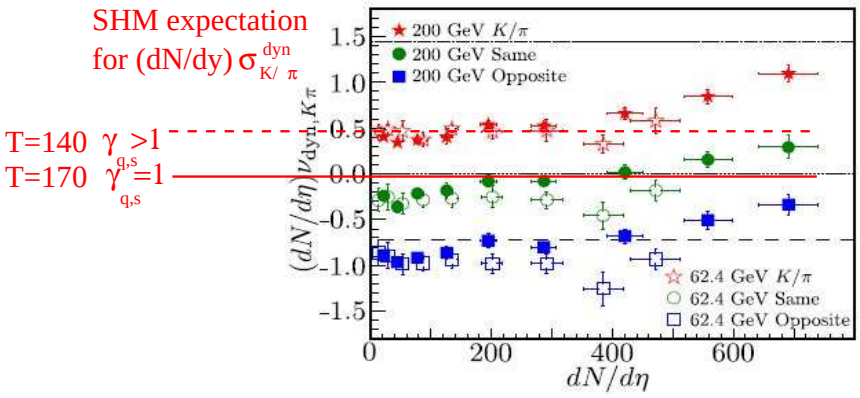

Figure 4.13: A comparison between statistical models and K/π fluctuation data at RHIC energies, see [88] for details.

The applicability and definition of the term "volume" is itself problematic in a dynamical quantum system. Statistical particle production *assumes* a volume, but leaves unexplained how this volume is defined, e.g. if acceptance cuts can be considered as "cuts in volume". If particles are created with a boost-invariant flow (spacetime and flow rapidity coincide) then cuts in rapidity are equivalent to cuts in volume (Fig. 4.14). To make such an approximation, however, the detector must be able to apply a simple rapidity cut for *all* particles at *all* energies under consideration, and to freely vary this cut to see how both the yield and the fluctuation scale. Only at a collider experiment capable of scanning in energy,such as NICA, can these criteria be satisfied. A different but related problem is the effect of particle misidentification, limited momentum resolution etc on fluctuation observables. These are much more difficult to model reliably than averages, and an observable needs to be constructed insensitive to them. Hence, the necessity of mixed event subtraction [86]. Such a mixed event subtraction is however most feasible in a collider, since a fixed target experiment has non-trivial energy dependent phase space cuts that make mixed event subtraction suspect.

Currently, the scaling of fluctuations at low energies is *not* understood [88]. Consequently, the relationship between fluctuation systematics and the structures seen in the *average* chemical properties of events (such as the "Kink" and the "horn" [67], suggesting deconfinement [70]) are ambiguus.

[89] has done a very useful job of showing that the scaling of fluctuations with $\sqrt{s}$ reflects, to a good approximation, that of yields. Of course, in the statistical model the scaling of $\sigma^{K/\pi}$ with $\langle K\rangle, \langle\pi\rangle$ in collisions

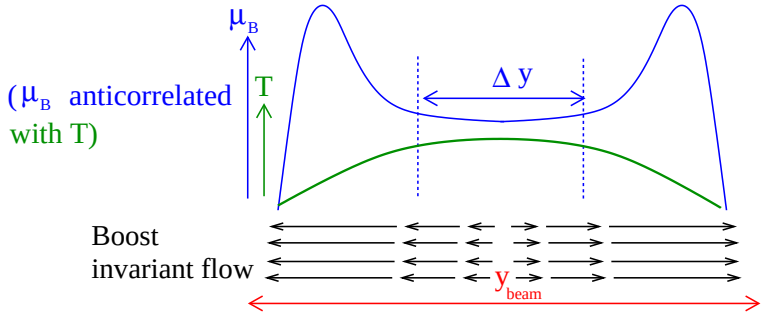

Figure 4.14: A schematic illustration of the Bjorken acceptance on fluctuations.

at different energies is more complicated than any of the models studied in [89], since it reflects changes in T, μ and possibly phase space occupancy γ [86] with $\sqrt{s}$.

It is impossible to go further with the data taken in [89], since the phase space cuts used to measure ratio fluctuations are highly particle and energy-specific. A quantitative separation between "statistical physics" and "detector acceptance" free of systematic errors is, therefore, impossible. To go further, measurements need to be made at mid-rapidity for all energies, with phase space cuts which are the same for all particles. The NICA accelerator is the idea laboratory where such measurements can be made.

If this program is successful, we will know the scaling of ratio fluctuations and abundances of π, K,protons and hyperons. Using the methods outlined in [85,86,88] it will be straightforward to understand in what energy and system size range does statistical particle production apply, how to temperatures, chemical potentials and phase space occupancies vary across energies and system sizes, and what is the relationship between the fluctuation systematics to the systematics of yields [67,70]. Independently from the finding of the critical point or other new physics, this will be a crucial piece of knowledge for the study of hot QCD.

4.8 Flow scaling in a low energy collider: When does the perfect fluid turn on?

G. Torrieri[a,b]

[a] *FIAS, J.W. Goethe Universität, Frankfurt A.M., Germany*
[b] *Department of Physics, Columbia University, New York, USA*

A lot of attention, both in the academic and popular press, has been bestowed on the claim that the Relativistic Heavy Ion Collider (RHIC) has produced a "perfect fluid", of minimally low viscosity [17,18,90–93].

This claim comes from the reasonably good description of the second Fourier component of flow (v_2, "elliptic flow") by ideal hydrodynamics [51, 94, 95, 97–100], and by the under-prediction of v_2 when the viscosity over entropy density (η/s) in the calculation is not small, $\eta/s \geq 0.1$

Indeed, it is still a mystery why the matter created at RHIC has such a small viscosity w.r.t. the naive expectation. Proposed explanations range from strong field plasma instabilities [101] over strongly coupled theories captured by Gauge-gravity correspondence [93] to multi-particle microscopic reactions, partonic [102] or hadronic [103]. A conclusive link between RHIC hydrodynamics and microscopic QCD dynamics is, however, still missing.

Consequently, we do not know the temperature range at which the perfect liquid turns on, or *how* it turns on: Is it a phase transition to a strongly coupled quark-gluon phase, or is it a smooth descent of the mean free path from a dilute weakly interacting hadron gas limit to a gas of overlapping resonances to quarks?

Going further in our understanding is also hampered by the large number of "free" (or, to be more exact, poorly understood from first principles) parameters within the hydrodynamic model, initial conditions as well as transport coefficients: While the equation of state is thought to be understood from lattice simulations, the behavior of shear and bulk viscosity is quantitatively not known around T_c, where it is expected it could be non-trivial. The same goes for the large number of second-order transport coefficients. While we have some understanding of the initial transverse density of the system, we do not as yet have control over the degree of transparency: Is it closer to a Landau "firestreak" or transparent "Bjorken" pancakes that pass through each-other leaving Hubble-expanding gas in between? How does the system move between these limits as the

energy is varied? The thermalization time, and the amount of flow created before thermalization, are similarly unknown. All of these effects need to be understood before the transport coefficients can be determined without large systematic errors.

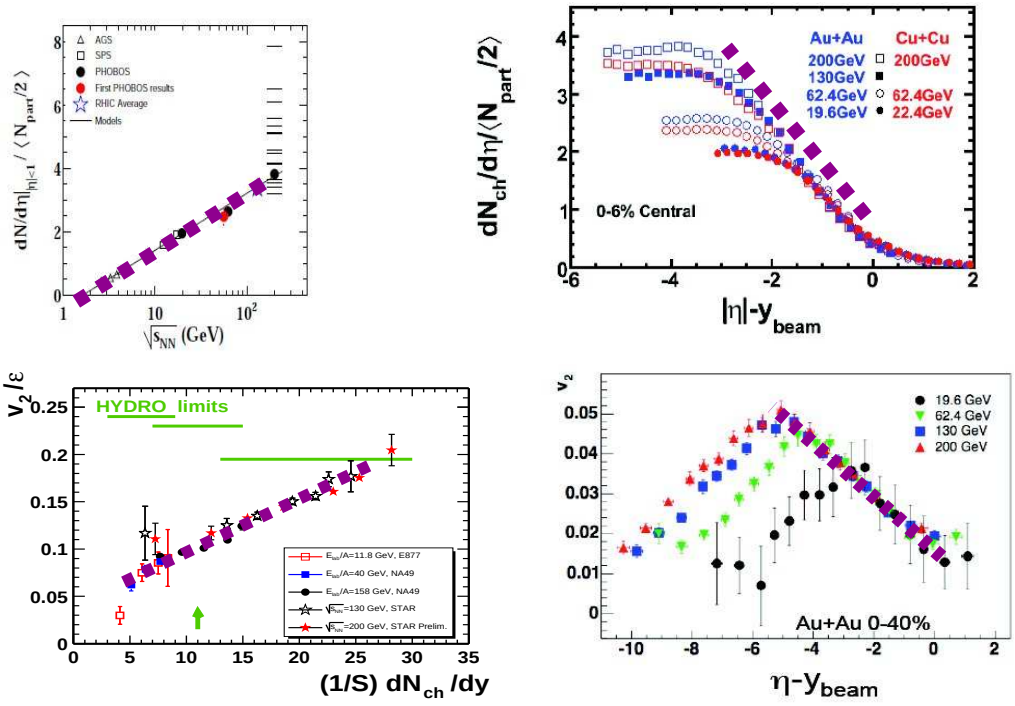

Figure 4.15: Top panels: The experimentally observed scaling of mid-rapidity dN/dy with $\sqrt{s}$ (left), as well as dN/dy away from mid-rapidity (right panel, known as limiting fragmentation). Bottom panel: elliptic flow normalized by eccentricity v_2/ϵ, integrated over rapidity (left panel) and as a function of rapidity (right panel, known as limiting fragmentation of v_2). All experimental plots from [104] and references therein, with the dashed line indicating the scaling trend.

A tool with the potential of overcoming these difficulties is scaling naturalness. Experiments have collected an extraordinary amount of flow data, encompassing a wide range of Energy,centrality, system size, rapidity, particle species and momentum. "Simple" patterns have been found [104], centered around the flow at different energies, system sizes and rapidities scaling with a few global dimensionless parameters (such as eccentricity and multiplicity density). This scaling is by no means natural when the flow is a function of many parameters, some set in the equilibrium phase and some not. Exploring which parameter combinations lead to the most natural scaling, therefore, could be used as a powerful tool to cut through the available parameter space.

What is remarkable is how well flow observables scale with $dN/(Sdy)$ (Fig. 4.15, bottom panel), the particle rapidity density normalized by the Glauber overlap area, over a wide range of energies and system sizes [105,106]. $dN/(Sdy)$, in the Boost-invariant picture, is related to the initial particle density. In the absence of chemical potential, this is in turn related to the initial temperature. It is therefore natural to expect the scaling to hold to some extent. A non-trivial dependence of viscosity and speed of sound on temperature, and/or changes in initial transparency, however, are nearly certain to break the scaling [105–107].

The excellent scaling observed suggests that η/s, the speed of sound and the longitudinal structure of the system stay broadly the same in the energy range accessible to RHIC. The fact that multiplicity dN/dy scales so well both in rapidity and (top panels of Fig. 4.15, known as limiting fragmentation) and across energies (down to NICA energies, as the top panel in Fig. 4.15 shows) corroborates this conclusion, since strong changes in phase structure and viscosity, together with lumpy initial conditions, should lead to entropy generation.

A further, potentially much tighter constraint, is provided by the universal limiting fragmentation-like dependence of elliptic flow [104, 107] (Fig. 4.15 bottom-right panel). This seems to indicate that the transport properties do not vary too much across rapidity in the RHIC domain, and that the initial conditions obey a

"universal ansatz" largely independent of energy [104, 107]. It is to date unknown at what (lower) energy does the system experience a change in its collective properties or initial dynamics capable of breaking this scaling. Such a change could very well signal the transition of the system into the "fluid" phase.

Thus, the scaling of flow observables in a *low* energy accelerator could very well be crucial in understanding the collective properties of QCD matter. NICA is optimally configured for such a study, due to the fact that it is a collider, capable of performing rapidity and energy scans with minimal changes in the detectors acceptance. The NICA energy range is particularly interesting since, if one constructs the initial conditions from Bjorken flow and universal fragmentation, the initial temperature at mid-rapidity should approach the lattice critical temperature T_C close to the top NICA energy range [107] (Fig. 4.16 left panel,see [107] for details).

Given the limiting fragmentation observed in multiplicity and flow, a promising endeavor for low-energy measurements is to look for limiting fragmentation in other soft observables. In particular, it might be worthwhile to look for a similar limiting fragmentation in the average transverse momentum $\langle p_T \rangle$, a break of which could signal the "step" [50,109] in rapidity space. $\langle p_T \rangle \sim T + m_\pi v_T^2$, and the transverse flow v_T should decrease significantly when the initial T is around T_c due to the dip of the speed of sound in the mixed phase regime. Similarly, rapidity dependence of $R_{\rm out}$ and $R_{\rm side}$ HBT radii could be used to check whether the scaling seen in *global* $R_{out,side} \sim \left(\frac{dN}{dy}\right)^{1/3}$ radii [110] is also local in rapidity. Such measurements will clarify whether the compressibility of the system does indeed change with rapidity, as its expected to in local thermal equilibrium where it mirrors the softness of the equation of state.

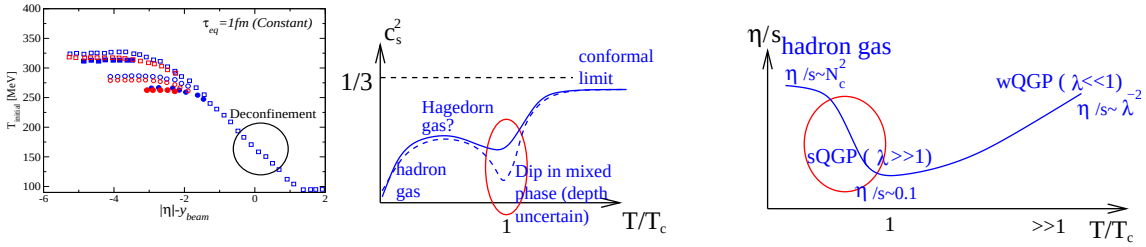

Figure 4.16: The initial temperature from limiting fragmentation (left) and the expected temperature dependence of speed of sound (center) and η/s (right), see [107] for details. The right panel shows qualitative expectations from scaling in number of colors N_c and 't Hooft coupling constant λ.

In conclusion, RHIC has shown the existence of a highly liquid phase in a regime where the initial temperature $\gg T_c$. It is however completely unclear when and how does this phase turn on, as RHIC has also shown the collective properties scale very well across energy, multiplicity and rapidity. A lower limit of this scaling could help us understand how hydrodynamics turns on in heavy ion collisions, and could well signal the transition from a weakly interacting hadron gas to strongly interacting QCD matter. For such a study, a collider capable of scanning in energy and rapidity, with the upper energy compatible with the lower energies studied at RHIC, would be optimal. NICA fulfills these criteria fully.

4.9 Dissipative hydrodynamics effects at NICA

L. Turko

Institute of Theoretical Physics, University of Wrocław, Poland

The NICA collider and the related MPD detector cover a very interesting energy range where crucial phenomena of phase transitions can take place. This is the region of the maximum net baryon density [111] available in heavy ion collision processes. The range of other expected parameters gives the possibility to observe phenomena such as the confinement-deconfinement and the chiral phase transition; it allows to test the equation of state at high baryonic density. The collider geometry provides also a better acceptance coverage than in the case of fixed target experiments.

These conditions should allow for a systematic treatment of fluctuations, correlations and higher order moments of physical quantities in a baryon-rich environment. It is also possible to study hydrodynamical flow properties with conservation laws and dissipative processes taken into account. The entropy of the QGP phase at hadronization determines the observable particle multiplicity so it is important to take into account

contributions due to particle production processes. Standard continuity equations are generalized to incorporate diffusion and particle production or chemical reactions. This results in a hydrodynamic model with dynamical chemical reactions and multi-fluid effects included. The equations have now the form

$$\partial_\mu \tilde{\rho}_i^\mu \equiv \partial_\mu(\rho_i^\mu + \triangle^{\mu\nu}\partial_\nu \mathcal{R}_i) = \mathcal{J}_i \ , \tag{4.23}$$

with $\triangle_{\mu\nu} \equiv g_{\mu\nu} - u_\mu u_\nu$, $g_{\mu\nu} = \mathrm{diag}(1,\text{-}1,\text{-}1,\text{-}1)$ being the flat space-time metric.

$\mathcal{R}$ is the diffusion term which is determined consistently [112,113] with the Second Law of Thermodynamics. $\mathcal{J}_i$ are sources of particle production. They are determined by microscopic reaction cross sections. In the local rest frame one gets the gain and loss equation

$$\mathcal{J}_i = \sum_j [G_{i\leftarrow j}\rho_j - L_{j\leftarrow i}\rho_i] \ , \tag{4.24}$$

The entropy production in a dissipative relativistic fluid is given by:

$$\begin{aligned} T\partial_\mu s^\mu &= -\sum_i \mu_i \mathcal{J}_i - T^{-1}(\partial_\mu T)u_\nu \delta T^{\mu\nu} + (\partial_\mu u_\nu)\delta T^{\mu\nu} \\ &\quad + \sum_i (\mu_i + T\mathcal{L}_i)\partial_\mu \triangle^{\mu\nu}\partial_\nu \mathcal{R}_i + T\sum_i (\partial_\mu \mathcal{L}_i)\triangle^{\mu\nu}\partial_\nu \mathcal{R}_i \ , \end{aligned} \tag{4.25}$$

where T is the temperature, $u^2 = 1$, and we employed natural units $\hbar = c = k_B = 1$. The heat-flow four-vector is defined by

$$\mathcal{Q}_\mu \equiv \partial_\mu T - T u^\nu \partial_\nu u_\mu \, , \tag{4.26}$$

and the shear tensor is given by

$$\mathcal{W}_{\mu\nu} \equiv \partial_\mu u_\nu + \partial_\nu u_\mu - \frac{2}{3} g_{\mu\nu}\partial_\gamma u^\gamma \, . \tag{4.27}$$

The First Law of Thermodynamics implies

$$0 = T\partial_\mu \tilde{s}^\mu + \sum_i \mu_i(\mathcal{J}_i - \partial_\mu \triangle^{\mu\nu}\partial_\nu \mathcal{R}_i) + u_\nu \partial_\mu \delta T^{\mu\nu} \ , \tag{4.28}$$

with an auxiliary entropy four-current, $\tilde{s}^\mu \equiv s u^\mu$, and $\rho_i^\mu \equiv \rho_i u^\mu$.

The chemical potentials μ_i do not imply traditional chemical equilibrium as they are space and time dependent parameters here. They are related to the conservation of abelian charges such as the electric charge, the strangeness or the baryon number. In the case of a conserved abelian charge the corresponding chemical potential is written as

$$\bar{\mu} = \sum_i q_i \mu_i \, ,$$

where q_i denotes the charge of particles of species "i".

The proper entropy four-current is

$$s^\mu \equiv \tilde{s}^\mu + T^{-1}u_\nu \delta T^{\mu\nu} + \sum_i \mathcal{L}_i \triangle^{\mu\nu}\partial_\nu \mathcal{R}_i \ . \tag{4.29}$$

The condition of increasing entropy leads to constraints on the particle source terms $\mathcal{J}_i$ and the diffusion terms $\mathcal{R}$ and $\mathcal{L}$ [112]. The system is driven towards chemical equilibrium if

$$\sum_i \mu_i \mathcal{J}_i \leq 0 \ . \tag{4.30}$$

This condition is closely related to abelian charge conservation of the system.

The structure of the dissipative term $\delta T^{\mu\nu}$ compatible with $\partial_\mu s^\mu \geq 0$ is given as

$$\delta T^{\mu\nu} = \kappa(\triangle^{\mu\gamma}u^\nu + \triangle^{\nu\gamma}u^\mu)\mathcal{Q}_\gamma + \eta \triangle^{\mu\gamma}\triangle^{\nu\delta}\mathcal{W}_{\gamma\delta} + \zeta \triangle^{\mu\nu}\partial_\gamma u^\gamma \ , \tag{4.31}$$

where κ, η and ζ denote the coefficients of heat conductivity, shear viscosity, and bulk viscosity, respectively. The heat-flow is given by

$$\mathcal{Q}_\mu \equiv \partial_\mu T - T u^\nu \partial_\nu u_\mu \,, \tag{4.32}$$

and the shear tensor is

$$\mathcal{W}_{\mu\nu} \equiv \partial_\mu u_\nu + \partial_\nu u_\mu - \frac{2}{3} g_{\mu\nu} \partial_\gamma u^\gamma \,. \tag{4.33}$$

Also, the contribution to the entropy production involving $\mathcal{R}$ becomes nonnegative if one identifies

$$\mathcal{L}_i \equiv -\frac{\mu_i}{T} \quad , \quad \mathcal{R}_i \equiv \sum_j \sigma_{ij} \frac{\mu_j}{T} \quad . \tag{4.34}$$

The symmetric matrix σ consists of the mutual diffusion constants and has only nonnegative eigenvalues. The diffusion current

$$\vec{j}_i \equiv -\nabla \mathcal{R}_i = -\sum_j \frac{\sigma_{ij}}{T} (\nabla \mu_j - \frac{\mu_j}{T} \nabla T) \tag{4.35}$$

involves chemo- and thermo-diffusion contributions.

The entropy production in the relativistic fluid is now given as

$$\begin{aligned} T \partial_\mu s^\mu &= -\sum_i \mu_i \mathcal{J}_i - T \sum_{i,j} \sigma_{ij} (\partial_\mu \frac{\mu_i}{T}) \triangle^{\mu\nu} (\partial_\nu \frac{\mu_j}{T}) \\ &\quad - \frac{\kappa}{T} \mathcal{Q}_\mu \triangle^{\mu\nu} \mathcal{Q}_\nu + \frac{\eta}{2} \mathcal{W}^\beta_\alpha \triangle^\gamma_\beta \mathcal{W}^\delta_\gamma \triangle^\alpha_\delta + \zeta (\partial_\mu u^\mu)^2 \,. \end{aligned} \tag{4.36}$$

This allows us to specify conditions for particular freeze-outs encountered in high energy heavy ion collisions. A complete thermal equilibrium is reached when the entropy is not longer produced, i.e., when the condition $\partial_\mu s^\mu = 0$ is fulfilled.

Dissipative processes are mainly due to bulk and shear viscosities of resulting hadronic fluid and heavy flavor production before chemical equilibrium is reached. In the NICA energy range that would be strangeness production dominated by gluon fusion $g+g \to s+\bar{s}$, with much smaller contributions of light quarks annihilation processes $q + \bar{q} \to s + \bar{s}$. Gluons and light quarks can be treated as a heat bath for strange quarks. Local exact strangeness conservation leads to strong correlations. They can be measured as the event-by-event fluctuations of the number of $s\bar{s}$ pairs. An inclusion of production processes leads to the faster cooling of the fluid. The resulting "effective viscosity" decreases so the fluid becomes more and more "effectively perfect". Flow analysis performed at NICA would allow to look into this effective viscosity problem without influence of heavier flavors processes which lead to separate flavor-specific time scales.

4.10 Hadronic Fluctuations, freeze-out conditions and the QCD (phase) transition line

F. Karsch[a,b] and C. Schmidt[c,d]

[a] *Physics Department, Brookhaven National Laboratory, Upton, NY, USA*
[b] *Fakultät für Physik, Universität Bielefeld, Bielefeld, Germany*
[c] *Frankfurt Institute for Advanced Studies, Frankfurt am Main, Germany*
[d] *GSI Helmholtzzentrum für Schwerionenforschung, Darmstadt, Germany*

Critical behavior is signaled by long range correlations and an increasing size of fluctuations associated with the appearance of massless modes in the vicinity of a second order phase transition. Fluctuations of baryon number, electric charge as well as strangeness have been shown to be sensitive indicators for such critical behavior. In the exploration of the QCD phase diagram at non-zero temperature (T) and baryon chemical potential ($\mu_{\rm B}$) higher moments of baryon number fluctuations play a particularly important role. They will diverge on the chiral phase transition line $T_c(\mu_{\rm B}, m_{\rm q} \equiv 0)$. At physical values of the light and strange quark masses they may still be sensitive to the critical behavior in the chiral limit and may allow to characterize the crossover transition in strongly interacting matter.

It is the intention of this short note to point at some of the recent results on the analysis of charge fluctuations and the exploration of the QCD phase diagram obtained in the framework of lattice QCD calculations. This

short note only discusses results obtained with Taylor expansions. For a more general discussion of the QCD phase diagram and the specific problems with studies of non-zero density QCD on the lattice we refer to recent reviews on this topic [114].

Charge fluctuations

One approach to gain information on QCD at non-zero baryon chemical potential from lattice calculations is based on the usage of Taylor expansions. Within this approach actual numerical calculations are performed at vanishing chemical potential where a set of Taylor expansion coefficients is calculated. An expansion can be set up in terms of baryon ($\mu_{\rm B}$) as well as electric charge ($\mu_{\rm Q}$) and strangeness ($\mu_{\rm S}$) chemical potentials. The expansion coefficients of the resulting Taylor series are given in terms of moments of charges B, Q, S as well as their correlations [115]. The moments of charge fluctuations, $\delta N_{\rm X} \equiv N_{\rm X} - \langle N_{\rm X}\rangle$, with $X = B$, Q or S and their correlations are obtained from derivatives of the logarithm of the QCD partition function, *i.e.* the pressure,

$$\frac{p}{T^4} \equiv \frac{1}{VT^3} \ln Z(V,T,\mu_{\rm B},\mu_{\rm S},\mu_{\rm Q}) \; , \tag{4.37}$$

evaluated at $\mu_{\rm B,Q,S} = 0$,

$$\chi^{BQS}_{ijk} = \left. \frac{\partial^{i+j+k} p/T^4}{\partial \hat{\mu}_B^i \partial \hat{\mu}_Q^j \partial \hat{\mu}_S^k} \right|_{\mu=0} \; , \tag{4.38}$$

with $\hat{\mu}_{\rm X} \equiv \mu_{\rm X}/T$. While the first derivatives, *i.e.* baryon number, electric charge and strangeness densities, vanish for $\hat{\mu}_{\rm B,Q,S} = 0$, their moments and correlation functions with $i+j+k$ even are non-zero. The basic quantities are the quadratic and quartic and also sixth order charge fluctuations,

$$\begin{aligned} \chi_2^X &= \frac{1}{VT^3}\langle N_{\rm X}^2\rangle \\ \chi_4^X &= \frac{1}{VT^3}\left(\langle N_{\rm X}^4\rangle - 3\langle N_{\rm X}^2\rangle^2\right) \; , \\ \chi_6^{\rm X} &= \frac{1}{VT^3}\left(\langle N_{\rm X}^6\rangle - 15\langle N_{\rm X}^4\rangle\langle N_{\rm X}^2\rangle + 30\langle N_{\rm X}^2\rangle^3\right) \end{aligned} \tag{4.39}$$

Some results taken from [115] are shown in Fig. 4.17.

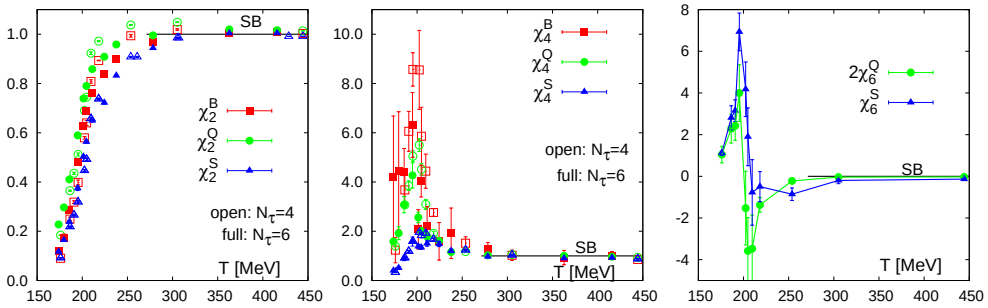

Figure 4.17: Quadratic and quartic fluctuations of baryon number, electric charge and strangeness. All quantities have been normalized to the corresponding free quark gas values. Also shown is the 6th order cumulant of electric charge and strangeness fluctuations without normalization.

Close to the chiral limit of QCD the temperature dependence of moments of charge fluctuations, in particular, higher moments of the baryon number fluctuation, are related to universal critical behavior. For QCD with two massless light quarks (u, d) this is expected to be controlled by critical exponents belonging to the universality class of the 3-dimensional, O(4) symmetric spin models. A consequence of this is that at vanishing baryon chemical potential the fourth moment of baryon number fluctuations will rise close to the transition temperature and will develop a cusp. The sixth order moment is the first moment that diverges in the chiral limit at the phase transition temperature. At non-zero values of the baryon chemical potential such a divergence will show up already in the third order moments. The strength of this divergence, however, will be proportional to $(\mu_{\rm B}/T)^3$

and thus will be difficult to isolate at small values of the baryon chemical potential,

$$\chi_k^B \sim \begin{cases} \left|\frac{T-T_c(0)}{T_c(0)}\right|^{2-\alpha-k/2} & , \text{ for } \mu_B/T = 0, \text{ and } k \text{ even} \\ \left(\frac{\mu_B}{T}\right)^k \left|\frac{T-T_c(\mu_B)}{T_c(0)}\right|^{2-\alpha-k} & , \ \mu_B/T > 0 \end{cases} , \tag{4.40}$$

with $\alpha < 0$ denoting the specific heat critical exponent, which is negative for the 3-d, $O(2)$ symmetric universality class.

Higher moments of charge fluctuations thus are expected to become increasingly sensitive to critical behavior. This also will show up in ratios of moments, χ_B^m/χ_B^n, which have the advantage of being independent of the interaction volume. A comparison with experimental results thus is much easier for ratios of moments rather then the moments themselves.

If matter created in heavy ion collisions is in equilibrium at the time of freeze-out, ratios of moments of charge fluctuations will reflect thermal properties at the freeze-out temperature. A first calculation of ratios of moments along the freeze-out line $T(\mu_B)$, which has been determined by comparing experimental results on particle abundances with results from a hadron resonance gas (HRG) model calculation [116], has been performed in [117]. In Fig. 4.18 we show the variation of a few ratios along the freeze-out line [118]. This calculation has been performed with an improved fermion action on lattice of temporal extent $N_\tau = 4$ and 6.

Calculations of the moments at non-zero baryon chemical potential are obtained from a Taylor expansion, which at present has to be interpreted with caution as these series unfortunately do not go beyond next-to-leading order. We note that results for these ratios agree quite well with HRG model calculations down to collision energies of $\sqrt{s_{\rm NN}} \simeq (20-30)$ GeV. At small values of the beam energy, which of course is the region of interest at NICA, deviations from the HRG model calculations show up. However, in this regime uncertainties in the lattice calculations are large. On the one hand there is need for a much more systematic analysis in order to get the continuum limit under control. On the other hand there clearly is also a need for the calculation of higher order corrections in the Taylor series as next-to-leading order corrections become larger than the leading order result at small $\sqrt{s_{\rm NN}}$, i.e. large values of μ_B. Here one has to worry about the convergence of the series, which of course is closely related to the determination of the location of a critical point in the QCD phase diagram. This too has been studied by using information on the ratio of moments of charge fluctuations.

We also note that HRG model calculations [119] for the ratios of moments shown in Fig. 4.18 are still in good agreement with experimental results [120] also at $\sqrt{s_{\rm NN}} \simeq 20$ GeV.

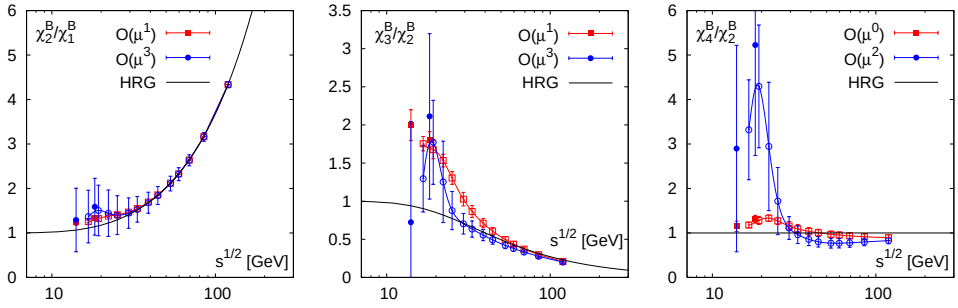

Figure 4.18: Shown are ratios of moments of net-baryon number fluctuations along the freeze-out curve, as a function of the center of mass energy $\sqrt{s_{\rm NN}}$.

Freeze-out curve and crossover line for the QCD transition

Closely related to the calculation of charge fluctuations in lattice QCD is the determination of the phase boundary of the chiral phase transition in the temperature and baryon chemical potential plane. In fact, ratios of moments $\chi_n^{\rm B}/\chi_{n+2}^{\rm B}$ provide estimates for the radius of convergence of the Taylor series of the pressure and may allow to determine a critical point in the QCD phase diagram at physical values of the quark masses [118, 122].

More rigorous results on the transition line at non-zero values of μ_B can be obtained for small $\mu_{\rm B}$ in the chiral limit, where the transition line corresponds to a true second order phase transition. Making use of universal scaling properties of the QCD phase transition in the chiral limit, the phase boundary can be determined to

leading order in the baryon chemical potential,

$$\frac{T_c(\mu_{\rm q})}{T_c} = 1 - \kappa_{\rm q} \left(\frac{\mu_{\rm q}}{T}\right)^2 + \mathcal{O}\left(\left(\frac{\mu_{\rm q}}{T}\right)^4\right) \ , \tag{4.41}$$

from a numerical study of the scaling properties of a mixed susceptibility [121]. Results from such a calculation are shown in Fig. 4.19. They indicate that for small values of the baryon chemical potential the dependence

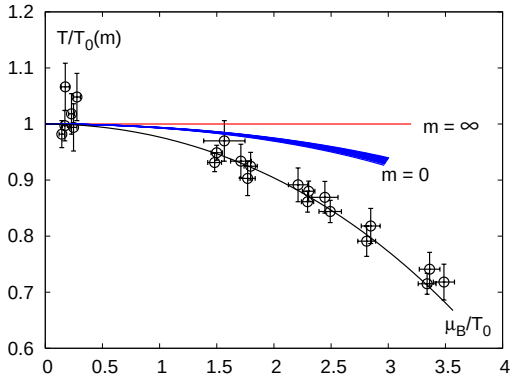

Figure 4.19: Phase boundary for the chiral phase transition in QCD with two massless quarks and a physical strange quark mass. Also shown are data for the freeze-out parameters in heavy ion collisions and the transition line for infinitely heavy quarks (pure gauge theory) which is independent of the chemical potential.

of the chiral phase transition temperature on the baryon chemical potential is rather weak. To what extent this signals that freeze-out occurs at a temperature smaller than the crossover transition in QCD with physical quark masses, still requires further investigations. At larger values of the chemical potential the freeze-out temperatures drop rapidly, which clearly cannot be described by a leading order expansion of $T_c(\mu_{\rm B})$. It has been speculated that this sudden drop may be signal an even richer phase structure of high density QCD [20]. The analysis of higher moments of charge fluctuations will be of great importance in clarifying the structure of the phase diagram in this regime.

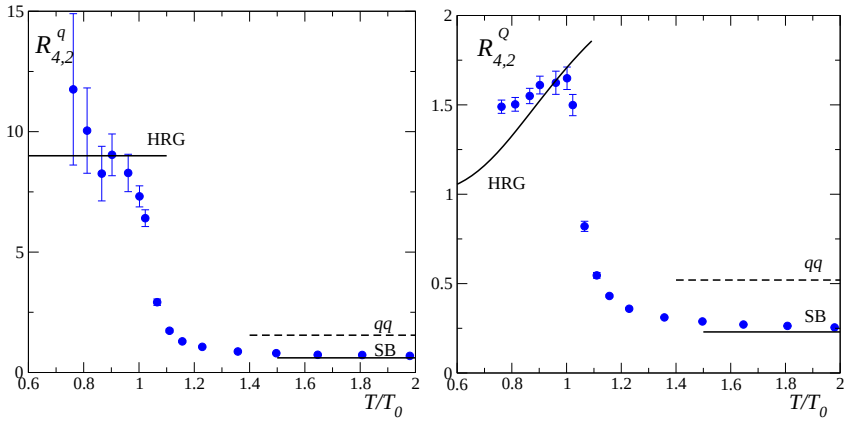

Figure 4.20: The ratio of quartic and quadratic moments of quark number fluctuations (left) [$n_{\rm q} \simeq 3n_{\rm B}$] and electric charge fluctuations (right) as function of temperature evaluated at vanishing baryon chemical potential. Shown in this figure is also an estimate for the high temperature value of these observables, if a significant di-quark component (qq) would contribute to the thermodynamics.

Studies of the phase diagram by NICA

The lattice results presented above and the discussion of the phase diagram in the high temperature, low chemical potential region will eventually form the rigorous background for our understanding of the phase diagram of strongly interacting matter. However, it will not be of direct applicability to the studies of the phase diagram in the energy range accessible at NICA. Experiments at NICA will probe a regime of high baryon number density in which the QCD transition, if at all it is a true phase transition, may well be of first order. In this high density regime direct lattice calculations will be difficult. Nonetheless current lattice results at least tell us that the study of ratios of higher moments of baryon number fluctuations may be of relevance also in this regime. The ratio of e.g. the quartic and quadratic moments of baryon number fluctuations are sensitive to properties of the relevant degrees of freedom that carry the baryonic charge. In Fig. 4.20 we show results from a calculation of ratios of quartic and quadratic moments of quark number and electric charge fluctuations, respectively, performed in a wide temperature range at $\mu_B = 0$ [124]. As one crosses the transition temperature this ratio drops rapidly, indicating the change from baryons ($B = 1$) to quarks ($B = 1/3$) as the dominant degrees of freedom that carry the baryonic charge. If freeze-out at NICA occurs in the mixed phase of a first order transition region one thus may speculate that this will be reflected in a drastic reduction of ratios such as χ_4/χ_2 over conventional values obtained for instance in calculations based on a hadron resonance gas model.

4.11 Exploring hybrid star matter at NICA

T. Klähn[a], D. Blaschke[b,c], F. Weber[d]

[a] *Institute for Theoretical Physics, University of Wrocław, Wrocław, Poland*
[b] *Joint Institute for Nuclear Research, Dubna, Russia*
[c] *Department of Physics, San Diego State University, USA*

Neutron stars (NS) provide valuable insights into the nature of nuclear matter at densities several times beyond nuclear saturation ($n_s \approx 0.16$ fm^{-3}) [125–127]. In particular any extreme (either small or large) value of measured neutron star observables, such as radius, mass, and temperature, is likely to improve our understanding of the properties of cold and dense matter substantially. A prime example underlining this statement is neutron star PSR J1614-2230, whose recently measured mass of (1.97 ± 0.04) M$_\odot$ makes him the heaviest neutron star ever observed with sufficient accuracy and confidence [128]. This measurement has direct consequences for the investiagtion of dense matter in terrestrial heavy-ion collision (HIC) experiments, as planned for NICA. The reason for this is the close relationship that exists between the stiffness of the equation of state (EoS) of symmetric nuclear matter and the highest NS mass supported by the associated EoS for neutron star matter, as illustrated in Figs. 1 and 2 in [127]. In that paper, a testing scheme, consisting of different constraints from astrophysical observations and HIC experiments, had been introduced and consistently applied to a given set of nuclear EoS. At the time of publication of Ref. [127], the most massive NS known was PSR J0751+1807. Its mass was ~ 2.1 M$_\odot$ but was affected by significant uncertainties. Therefore, a second, less strict mass constraint had been formulated, which demanded that the successful nuclear EoS reproduces at least a maximum neutron star mass of 1.6 M$_\odot$. All the EoS investigated back then passed this constraint. Due to the precision of the new mass measurement for PSR J1614-2230, we now update the overall result of this testing scheme (analogously to Table V in [127]). It is evident from Table 4.1 that only four (five) of the formerly eight nuclear EoS are still compatible with the upper (lower) mass value measured for PSR J1614-2230. An additional model for the nuclear EOS–the hybrid EOS "DBHF-NJL"–has been included in Table 4.1, which has several advantages over the purely hadronic EoS. Details about this EOS will be discussed below.

In summary, the important lesson that we learn from high NS masses, as measured for PSR J1614-2230, is that the EoS has to be 'rather stiff' or, conversely, can 'not be too soft' at ultra-high densities in order to be compatible with neutron star masses. In the following we point out how HIC experiments can contribute to constrain the behavior of the nuclear EoS further and, most importantly, provide most valuable information about the existence of quark matter in compact stars.

We focus here on two topics in HIC experiments which are relevant for determining the stiffness of nuclear matter at supersaturation densities and thus have direct implications for the astrophysics of compact stars: (i) strangeness production (see contribution by V. Friese) and (ii) transverse and elliptical particle flow.

According to the present status of the theory, subthreshold K^+ production at $E_{\rm lab} < 1.58$ AGeV appears to require a sufficiently soft equation of state (see [130] for a review) which is an interesting complement to the astrophysical requirement of sufficiently stiff equations of state demanded by the observations of high-mass

Model	$M_{\rm max} \geq 2.01\ M_\odot$	$M_{\rm max} \geq 1.93\ M_\odot$	$M_{DU} \geq 1.5\ M_\odot$	$M_{DU} \geq 1.35\ M_\odot$	4U 1636-536 (u)	4U 1636-536 (l)	RX J1856 (A)	RX J1856 (B)	J0737 (no loss)	J0737 (loss 1% $M_\odot$)	SIS+AGS flow	SIS flow+ K^+ prod.	No. of passed tests	(out of 6)
NLρ	−	−	−	−	−	−	−	−	−	−	+	+	1	1
NL$\rho\delta$	−	−	−	−	−	−	−	−	−	−	+	+	1	1
DBHF	+	+	−	−	+	+	−	+	−	+	−	+	2	5
DD	+	+	+	+	+	+	−	+	−	−	−	−	3	4
D^{3}C	+	+	+	+	+	+	−	+	−	−	−	−	3	4
KVR	−	−	+	+	−	∘	−	−	−	+	+	+	2	4
KVOR	+	+	+	+	−	+	−	−	−	∘	+	+	3	5
DD-F	−	+	+	+	−	+	−	−	−	+	+	+	2	5
DBHF+NJL	+	+	*	*	+	+	−	+	−	+	+	+	4	6

Table 4.1: Summary of results for the testing scheme suggested in [127], updated by the recently measured mass of PSR J1614-2230 ((1.97 ± 0.04) $M_\odot$) and supplemented by the hybrid EoS of Ref. [129] (last line), for which results are shown in Fig. 1. EoS not labeled in bold face fail to reproduce a NS mass of 2.01 $M_\odot$. Non-separated columns show the results for a strict (left) and weakened (right) interpretation of the corresponding constraint. The last column gives the total number of tests passed by a given EOS. (For details, see [127].)

neutron stars (see discussion above).

The analysis of flow data for experiments at different energies ($E_{\rm lab} = 0.4$ to 10 AGeV in Ref. [131]) put a constraint on the cold symmetric nuclear EoS, which represents a region in the nuclear pressure-density plane, $P(n)$, shown in Fig. 4.21.

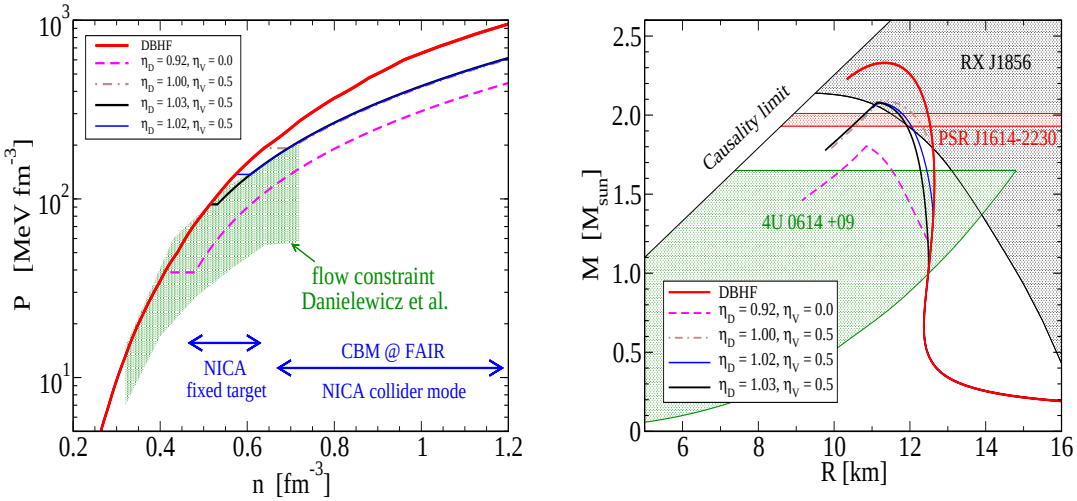

Figure 4.21: Left panel: Flow constraint [131] extracted from HIC experiments in the range $E_{\rm lab} = 0.4$ to 10 AGeV and estimated regions accessible at CBM and NICA experiments [132, 133]. Right panel: Sequences of compact star M-R relations obtained from solution of the Tolman-Oppenheimer-Volkoff [125, 126] equation for different EoS without (DBHF) and with deconfinement transition, as compared to NS constraints.

This constraint is readily applied to the isospin-symmetric part of any neutron star EoS and can therefore be used to derive upper bounds on the maximum mass of compact stars [127], as can be seen by comparing the left and right panels of Fig. 4.21.

From these far-reaching consequences of the latter constraint it is evident that an independent confirmation of this flow constraint is very important, both from the theroretical side as well as by providing sufficiently accurate flow data in the region of $E_{\rm lab} = 2$ to 5 AGeV (Nuclotron fixed-target range), where we suspect the deconfinement phase transition to occur, and just above the limits of the AGS data range, i.e. for $E_{\rm lab} = 10$ to 40 AGeV (CBM range or fixed-target equivalent of the NICA collider range).

According to the flow constraint, the *ab-initio* DBHF EoS for the Bonn-A nucleon-nucleon potential appears to be too stiff at densities above 3.5 times saturation density. Assuming the deconfinement phase transition to provide the softening of the high-density EoS just in this density range at the maximally tolerable stiffness of the Danielewicz et al. constraint would result in an upper limit for the maximum mass of compact stars at 2.1 $M_\odot$. This would be also compatible with the new mass constraint from PSR J1614-2230.

The quark matter EoS used here is the three-flavor color superconducting NJL model one with selfconsistently determined masses and diquark gaps [134] including a vector meson meanfield which entails a sufficient stiffening of the hybrid EoS [129] (a nonlocal, covariant generalization has been provided in Ref. [136]). Neglecting the latter term would result in too soft a hybrid EoS, conflicting with the new neutron star mass constraint (dashed lines in Fig 4.21. Moreover, if the diquark pairing interaction would be sufficiently reduced or even be neglected altogether so that no color superconducting phase can occur, the phase transition would occur at too high densities to be relevant for compact star structure.

Due to isospin asymmetry, in compact stars the deconfinement transition always occurs at lower baryon densities than in symmetric nuclear matter. There is another, indirect argument to expect a deconfinement phase transition in symmetric matter at densities not exceeding about 3 to 4 nuclear saturation densities. This relatively low critical density would correspond to a deconfinement transition in neutron star matter at low enough densities to avoid hyperon formation. In this way the problem could be eliminated that compact stars with hyperons in their interiors would have a too soft EoS to fulfill even much weaker maximum mass constraints than the new one, see Ref. [135].

In conclusion, the question of whether or not quark matter exists in compact stars is very challenging [137] and closely related to the question of deconfinement in heavy-ion collisions at the CBM [138, 139] and NICA facilities [133]. As we don't know a priori the coupling strengths in various interaction channels at high densities, it is important to verify the conjectured EoS in a heavy-ion collision experiment. The energies provided at the NICA facility (both, fixed target and collider) are perfectly suited for providing astrophysically relevant constraints such as to confirm or disprove the possibility that all neutron stars in the observed mass range between 1.23 and 2.01 $M_\odot$ are hybrid stars with color superconducting quark matter cores!

4.12 Testing Hadron Formation and Exotic Bound States in Heavy Ion Collisions at NICA

R. Bellwied[a], *C. Markert*[b]

[a] *Physics Department, University of Houston, USA*
[b] *Physics Department, University of Texas at Austin, USA*

Physics Motivation

The concept of formation time of hadrons in the chirally symmetric deconfined medium produced at RHIC and the LHC has been addressed by the authors in two recent publications [140, 141]. We have conjectured that the hadronization process through parton fragmentation in the deconfined medium is following the same time constraints than in the vacuum, since the hard parton does not thermalize with the system. A calculation based on light cone variables which takes into account not only the Lorentz-boost (inside-outside cascade), but also energy conservation in the medium (outside-inside cascade) shows that there is a finite probability that color-neutral pre-hadrons or bound states can form inside the medium, i.e. above the critical temperature and prior to bulk hadronization. These configurations carry all the necessary quantum numbers, but have not yet developed their full hadron wave function. Two dynamic hadronization scenarios are thus possible. Either these pre-hadron states are very massive (color-neutral resonance clusters or quasi-particles) and subsequently decay into hadronic ground states, or the resonant states of the ground states are formed off mass shell before gaining the necessary on-shell mass. In the second scenario the resonant state might decay with its chiral symmetry still partially restored.

In addition, at NICA, where the energy is lower than at RHIC but the particle density is considerably higher, it is conceivable that these bound states above the critical temperature are surviving states from the hadronic

phase since confined, but chirally symmetric, hadronic states (quarkyonic matter) were proposed recently as a new phase of matter at high baryo-chemical potential [15]. So rather than being formed through recombination of partons in deconfined matter these states survive the phase transition, i.e. they stay confined but their chiral symmetry is restored.

Based on either scenario we propose to actively search for color-neutral bound states around the phase transition in systems with high baryochemical potential but moderate critical temperature.

Model details

In momentum space, expressed through lightcone coordinates, the fragmentation of a parton of mass m_q into a hadron of mass m_h and a light secondary parton is represented through the lightcone $\Delta y^+ = \tau_{\rm form} + l_{\rm form}$ that is conjugate to the non-conserved lightcone momentum component $\Delta p^- = (p^-)_{\rm final} - (p^-)_{\rm initial}$ of the evolving system [141]:

$$\Delta y^+ \simeq \frac{1}{\Delta p^-} = \frac{z p^+}{m_h} \times 2 \left[m_h + \frac{\mathbf{k}^2}{(1-z)m_h} - \frac{z m_q^2}{m_h} \right]^{-1} \tag{4.42}$$

Here $|\mathbf{k}| \sim \Lambda_{\rm QCD} \sim 200\,{\rm MeV}/c$ is the deviation from collinearity and z is the fractional momentum $p^+_{\rm hadron}/p^+$. After further derivation the formation time reads:

$$\tau_{\rm form} = \frac{\Delta y^+}{1+\beta_q}\,, \quad \beta_q = \frac{p_{\rm q}}{E_{\rm q}}\,. \tag{4.43}$$

When compared to the lifetime of the QGP at the LHC we observe that for a wide range of momenta, hadron formation times are well within the anticipated lifetime of the plasma as shown in Fig. 4.22.

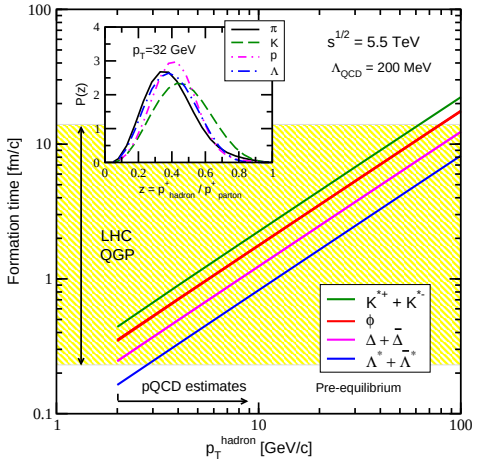

Figure 4.22: Transverse momentum dependence of resonance formation times at LHC energies. The shaded area represents the estimated QGP lifetime at the LHC. Insert shows the meson and baryon distributions P(z) at a fixed momentum (from [141]).

This will not necessarily be the case for NICA energies, where the lifetime of any plasma state is considerably smaller than at the LHC, but since it is anticipated that at least part of the system might contain chirally symmetric (quarkyonic) matter, the off-shell component of the color neutral states should be large, even if the lifetime of the system is small. In that case the argument does not need to be made on the basis of formation time of hadrons from deconfined partons, but rather on the survival probability of confined hadronic states in the chirally symmetric phase. One of the signatures of such a phase should be the measurement of chiral partners with similar or equal mass. Calculations of a common mass for the lowest lying chiral doublet beyond a first order phase transition have been performed in the framework of the PJNL model [142]. Fig. 4.23 shows the

predictions for the pion (π) and sigma (σ) masses above the chiral transition temperature for a baryochemical potential of 340 MeV.

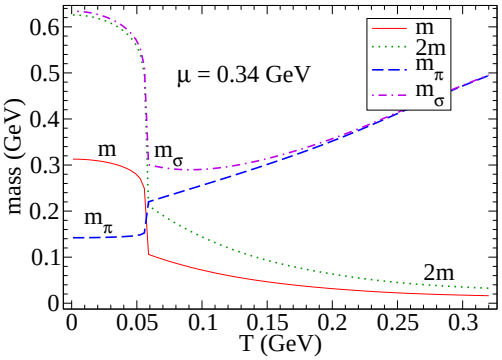

Figure 4.23: Masses of the π and σ as function of the temperature, together with the Hartree quark masses, in the PJNL model at $\mu = 0.34$ GeV. The chiral transition occurs at $T_c = 0.06$ GeV (from [142]).

The resulting chiral partner mass is around 250 MeV, with a remaining slight split between the states due to the finite current mass of the quarks, which explicitly breaks chiral symmetry. A mass peak at 250 MeV should be easily distinguishable from the π or σ on-shell masses.

Proposed measurements

The proposal is too look for the production of color-neutral bound states slightly above T_c in the region of high density. These bound states will be resonant states either above (quasi-particle clusters) or below (chirally symmetric color-neutral states) the known resonance spectrum. They exist either through formation in the deconfined phase or through survival in the confined phase above T_c. The aim is to prevent these states from undergoing medium modifications in the dense hadronic phase after hadronization of the bulk matter, and thus the most proficient way to search for such states is in the di-lepton spectrum. The mass region above the ϕ-meson but below the J/ψ, i.e. the continuum region, as well as the low mass di-lepton region below the ρ and above the π mass, are perfectly suited for such measurements. Beyond the occurrence of any distinct peaks in these regions, any reduction in relative strength or broadening of the pion peak compared to an unmodified cocktail calculation should also provide indications of chiral symmetry restoration for the case of the π,σ chiral doublet.

A dilepton spectrometer (e.g. a gas or silicon based tracking device combined with a time of flight detector) with 2π coverage in NICA collider mode is most appropriate for such measurements. The alternative would be to look for hadronic decay channels of high momentum chiral partners [141] in order to avoid effects due to hadronic re-interactions in the bulk medium, but the luminosity, and thus the sampled statistics of high momentum particles, might not be sufficient at NICA energies.

4.13 Understanding the properties of chemical freeze-out

C. Blume

Institut für Kernphysik der J.W. Goethe Universität, Germany

Is there evidence for an extended hadronic phase ?

The conventional and simplified scenario of the evolution of a high energy heavy ion reaction is the following: Starting from a Quark-Gluon Plasma (QGP) phase particles hadronize at the critical temperature $T_{\rm C}$ and the system then turns into a hadron gas which further evolves as it expands and cools down. It will reach the chemical freeze-out temperature $T_{\rm ch}$ at which all inelastic reactions cease and the relative particle abundances are frozen out. Afterwards elastic scattering processes may still continue and possibly modify the momentum distributions of the hadrons until the kinetic freeze-out temperature $T_{\rm kin}$ is reached. After this final freeze-out only free streaming particles propagate towards the detector. The question to be addressed in the following is whether there is any experimental indication for these different phases after hadronization and, if yes, if there is any way of determining the lifetimes of the different phases by measurements.

It is by no means clear that the above described scenario is realized in nature. In fact, there are several other concepts that do not require any extended period between hadronization and chemical or kinetic freeze-out. Single freeze-out models, for instance, where chemical and kinetic freeze-out coincide, have been quite successful in describing particle spectra and yields as measured at RHIC [143]. The suggestion that chemical equilibration is generally driven by the vicinity of a phase boundary implies that there is no need for an extended hadron gas phase between hadronization and chemical freeze-out [144]. The same applies to sudden freeze-out models as discussed in [145]. A recent review of the experimental situation can be found in [146].

One way to model an extended hadronic phase after hadronization in theory is to couple a hadronic transport model as an afterburner to a hydrodynamic calculation [147]. Alternatively, a hydrodynamical evolution has been combined with an extended freeze-out description [148] to investigate the effect of an extended chemical freeze-out. These approaches allow to study whether particle abundances and spectra are modified by subsequent hadronic interactions as, e.g., the absorption of anti-baryons. As a consequence one might observe deviations from the chemical equilibrium value for certain particle species. It has also been pointed out quite early that particles with low hadronic cross sections (e.g. Ω^-, ϕ) should freeze-out earlier than other hadrons if there was a long lived hadronic phase [149].

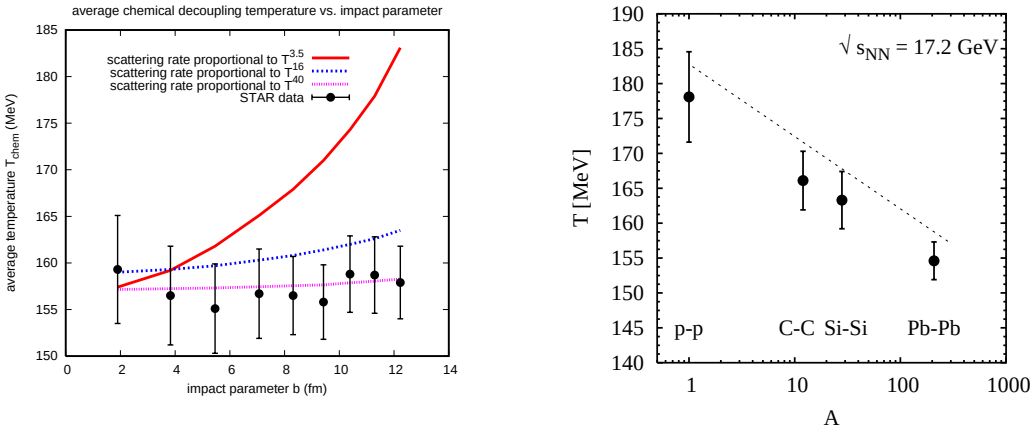

Figure 4.24: Left: The impact parameter dependence of the average chemical decoupling temperature $T_{\rm ch}$ computed from hydrodynamics with different temperature dependences of the scattering rates [150], compared with STAR data for Au+Au collisions at $\sqrt{s_{\rm NN}} = 200$ GeV [152]. Right: The fitted temperature at chemical freeze-out $T_{\rm ch}$ as a function of the mass number A in central heavy ion collisions at $\sqrt{s_{\rm NN}} = 17.3$ GeV (from left to right: p+p, C+C, Si+Si, and Pb+Pb). The dashed line shows a parametrization [153].

The question whether there is any evidence for an extended hadronic phase after hadronization and before chemical freeze-out is much more difficult to answer. One indicator might again be the production of particles with low hadronic cross sections like multi-strange baryons. However, there is no observation yet that any of these particles shows a significant deviation from its statistical equilibrium value as expected in the case of an early hadronic decoupling [151]. However, the error bars on these data, especially at lower energies, are still relatively large so that for a more definite statement also improved data sets would be needed. On the other side, it has also been argued that multi-strange particles might not be too sensitive to a hadronic phase, if they already enter this phase with abundances close to equilibrium [147]. Antibaryons are expected to be much stronger affected due to absorption effects which would cause a reduction of the measured yields relative to the chemical equilibrium value. A caveat here is that antibaryon production can be enhanced in a hadron gas by multi-meson fusion processes [154], which usually are not included in hadronic transport models. A recent study of statistical model fits to data sets including and excluding antibaryons nevertheless indicates that there might be a significant effect [155]. Also, antiprotons exhibit a decrease of their measured yields with increasing system size [156, 157] as expected if they were subject to increasing absorption in hadronic matter. However, this needs to be disentangled from the system size evolution of the effects of baryon number transfer to mid-rapidity that could result in a similar observation. A striking observation that was made recently when results on particle yields for Pb+Pb collisions at $\sqrt{s_{\rm NN}} = 2.76$ TeV were compared to statistical model predictions was

that the measured proton and antiproton yields are significantly lower than the expectations [158]. However, whether this might be an indication for hadronic rescattering in long lived hadron gas phase will still need further investigations.

One remarkable observation made at RHIC is that the system size dependence of $T_{\rm ch}$ and $T_{\rm kin}$ are clearly different. While $T_{\rm kin}$ shows a significant dependence on system size, $T_{\rm ch}$ does not. As pointed out in [150], this is very difficult to be reconciled with a freeze-out from a normal hadron gas. To describe this behavior scattering rates that depend on temperature as T^n with $n > 20$ are required (see left panel of Fig. 4.24). It has been pointed out in [159] that exponents of the order of 60 can be realized if chemical freeze-out happens directly at the phase boundary. At high energies and small $\mu_{\rm B}$ the vicinity deconfinement phase transition would thus provide an explanation for the observed feature. Since at lower energies and consequently higher $\mu_{\rm B}$ the system freeze-out far away from this phase boundary, it is important to do a systematic investigation of the system size dependence of chemical freeze-out parameters also here. One example is shown in the right panel of Fig. 4.24. Here a clear A dependence of $T_{\rm ch}$ is found [153], which is in stark contrast to the observations at RHIC and could be interpreted as an effect of hadronic re-interaction.

Contributions from NICA

For the existence of a hadronic phase before chemical freeze-out no clear evidence can be derived from the current experimental data. Right now, there are several not fully understood features (antiprotons at LHC, system size dependence of $T_{\rm ch}$ at low energies) which might provide some clue for future investigations. However, the limited accuracy and coverage of the existing data does not allow any firm conclusions. Since the distance of the chemical freeze-out curve to the deconfinement phase transition line is much larger at lower energies, any effect of a hadronic rescattering phase should be strongly pronounced there. Therefore, precise measurements of the yields of the antibaryons and of the system size dependences of various hadrons, such as they could be performed with MPD at NICA in the region up to $\sqrt{s_{\rm NN}} = 11$ GeV, will be of high importance for the understanding of the freeze-out conditions. Establishing that also at these low center-of-mass energies no evidence for any rescattering effect as described above is seen, might support the scenario that the chemical freeze-out is driven by a potential phase transition to a quarkyonic phase as conjectured in [74, 144].

4.14 Dynamical development of statistical parameters in phase transition

L.P. Csernai[a], D.J. Wang,[a], C. Anderlik[b], X. Cai[c], Y. Cheng[c], D.M. Zhou[c]

[a] *University of Bergen, Norway*
[b] *Uni-Computing, Bergen, Norway*
[c] *Huazhong Normal University, Wuhan, China*

We suggest to study the development of the mean, variance, skewness and kurtosis of extensive and intensive thermodynamical parameters in fluid dynamical and in hybrid models. In these models these quantities can be correlated with traditional collective flow observables, as the directed and elliptic flow, and higher multiple moments of the azimuthal asymmetry.

These observables are sensitive to a phase transition of the material under study, but also influenced strongly by the details of the collision dynamics.

We study the dynamics of the reaction in a multi module model, with an initial longitudinal Yang-Mills flux tube stage [160], a Computational Fluid Dynamics (CFD) stage where we apply a relativistic 3+1D Particle in Cell (PIC) method [161], and a final stage which is either described by a sudden Freeze Out (FO) using a generalized Cooper-Frye approach with exact conservation laws at the FO hyper-surface or a final parton and hadron transport model, PACIAE, to describe the final rapid hardonization [162].

The development of the thermodynamical and flow parameters in the middle stage of the matter where local thermal equilibrium is established in QGP is described by the CFD model. Here we assume ideal QGi, described with by the MIT Bag model for large ($p > 0$) pressures and decreasing bag constant and quasi-adiabatic expansion at late CFD stages when the pressure drops to zero. The model is tested for different beam energies down to the threshold energy of QGP formation, see Fig. 12.14.

Observations of large strangeness abundance and small HBT radii, indicate rapid hadronization from supercooled plasma [165, 166], thus the fluctuations arising from the phase transition around the critical point must be described by a non-equilibrium, rapid hadronization model. Still the fluid dynamical development leads also to a thermodynamical state, which is not in global equilibrium and shows a spatial distribution of

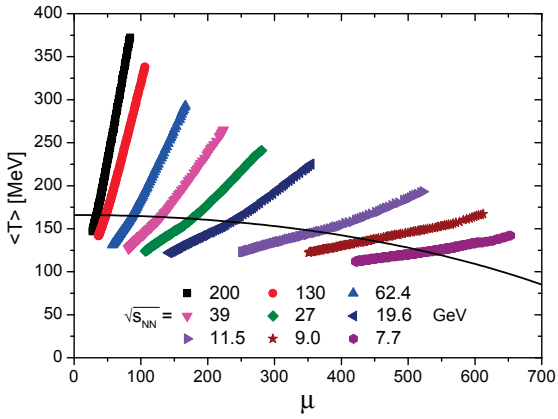

Figure 4.25: The trajectory of fluid dynamical development of QGP fluid at different beam energies as indicated in the figure. Central Au+Au collisions are calculated at a cell size resolution of $dx = dy = dz = 0.575$ fm, and time step $\Delta t = 0.04233$ fm/c. The hadronic freeze out curve [65] is indicated by a full black line. The FD evolution is calculated well beyond this curve. This is possible as the CFD model can describe supercooled QGP fluid also. The viscosity is minimal and only the numerical viscosity is considered in the calculations. These can be performed down to FAIR and NICA energies. From ref. [164].

thermodynamical parameters, with non-zero Skewness and Kurtosis. This is indicated in Fig. 12.15. These parameters are important to locate the critical point, see e.g. [167].

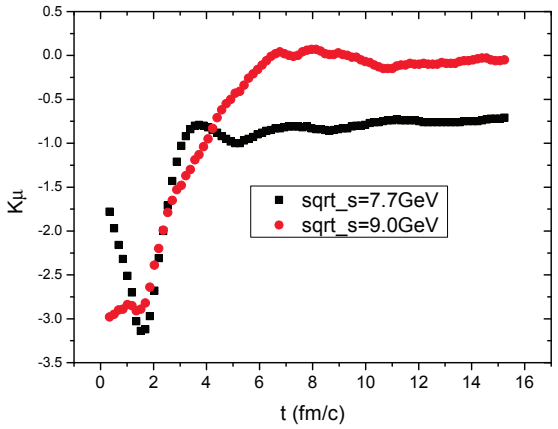

Figure 4.26: The time development of the Kurtosis, K, of the distribution of the chemical potential, μ, due to the fluid dynamical development of QGP fluid at different beam energies relevant for NICA as indicated in the figure. Central Au+Au collisions as described at Fig. 12.14. The transition or FO point is around 4-8 fm/c, but the applied CFD model can describe supercooled GP fluid also.

In addition the final hadronization, if it happens close to the critical point of a 1st order phase transition leads to additional critical fluctuations. We can study this by supplementing the fluid dynamical stage with a transport model, which takes into account the features of the phase transition at the critiacl point.

Csernai and Neda [168] have analysed fluctuations in the coexisting hadronic and quark-gluon plasma phases in small finite volumes. They used a treatment of the fluctuations of the order parameter near phase transitions in a way similar to the Landau theory, by assuming a finite system in a heat-reservoir. This theory describes fluctuations in finite systems. The thermodynamical potential of this system, (e.g. the free energy, $f(e)$) was approximated by a fourth order polynomial. This approach provides a symmetric distribution (zero Skewness), which is wider than a Gaussian near the critical temperature due to critical fluctuations (negative Kurtosis).

In ref. [168] it was pointed out that the transition to QGP is highly asymmetric because the large energy difference between the equilibrated hadronic state, e_h and QGP state, e_q. Thus Landau's theory with a fourth order polynomial approximation to $f(e)$ would lead to similarly wide distribution on both the high and low energy sides, so that fluctuations to unphysical, negative energy density states would be possible. To avoid this unphysical feature, ref. [168] approximated the free energy also as a polynomial, but to obtain the required divergence at $e = 0$ they assume the form

$$f(e) = f_1 + K_1\frac{1}{e} + K_2(e - e_0) + K_3(e - e_0)^2 + K_4(e - e_0)^3 \ .$$

The free-energy density curve of the radiation field can be expanded in Laurent series around e = 0, and for large e the approximation will be the same considered above. This approach does not allow fluctuations with negative energy densities, the distributions will be steeper at the low energy (low particle density) side and wider on the high energy (particle density) side. Thus the approach predicts a positive Skewness for the distribution of thermodynamical quantities arising from fluctuations at the critical point of the Quark-Hadron phase transition. In our multi module approach this feature can be implementad in the final PACIAE stage of the hybrid model [169].

A detailed multi-module model will be able to provide a deeper insight to the development of the final statistical features of the observables at the critical point of the Quark-Hadron phase transition in NICA. It is important to take into account that the fluid dynamical development also provides an energy dependent distribution of the thermodynamical quantities. In addition different initial states or initial state fluctuations may also influence the thermodynamical parameters later. Thus, we need an analysis where the fluctuations from all stages of the reaction dynamics are analysed.

4.15 Challenges to hydrodynamics at NICA

P. Huovinen

Institut für Theoretische Physik, J. W. Goethe-Universität, Frankfurt am Main, Germany

Hydrodynamical models have been important tools for understanding heavy-ion collisions for a long time. However, it is not at all clear whether viscous hydrodynamics is applicable in collisions at NICA energies.

By comparing the numerical solutions of the relativistic Bolzmann equation and Israel-Stewart hydrodynamics, it has been shown that Israel-Steward hydrodynamics is reasonably accurate up to a Knudsen number $Kn \lesssim 1/2$ [170, 171]. It is difficult to estimate the value of the Knudsen number in a heavy-ion collision, but we can cast the requirement $Kn \lesssim 1/2$ in a more intuitive form by using kinetic theory relations as in [170]. In kinetic theory

$$\eta = \frac{4}{5} nT\lambda,$$

and if we assume one-dimensional boost-invariant expansion, the only length scale in the system is time. Thus

$$1/2 \gtrsim Kn = \frac{\lambda}{\tau} = \frac{5\eta}{4nT\lambda} = \frac{5}{T\tau}\frac{\eta}{s},$$

where an approximation $s = 4n$ was used. We get

$$\frac{\eta}{s} \lesssim \frac{T\tau}{10} \approx \frac{1-2}{4\pi}, \tag{4.44}$$

where the last relation is valid at RHIC where $T_0\tau_0 \approx 1$.

Even at RHIC, the viscous hydrodynamics is applicable if, and only if, the shear viscosity to entropy density ratio of the matter is in the vicinity of its postulated lower limit. To estimate similar limit for collisions at NICA, we first have to estimate the initial temperature and thermalization time. Assuming that very little entropy is generated during the expansion, that the expansion is roughly boost invariant, and that entropy density $s \propto T^3$, we can relate the initial temperature at NICA to the initial temperature at RHIC at the same initial time as

$$T_{\rm NICA}(\tau_0) \approx \sqrt[3]{\frac{N_{\rm NICA}}{N_{\rm RHIC}}}\, T_{\rm RHIC}(\tau_0),$$

where N is the final particle multiplicity within one unit of rapidity around midrapidity. At RHIC this is ~ 1000. At the full NICA energy of $\sqrt{s_{NN}} = 11$ GeV, the predicted charged particle multiplicity within ± 1 units of pseudorapidity is 550, and at the lowest NICA energy of $\sqrt{s_{NN}} = 4$ GeV it is 250 [172]. Since the final rapidity distributions at NICA are not flat, we may estimate the total multiplicities within the narrower interval of one unit of rapidity to be 550 and 250 at $\sqrt{s_{NN}} = 11$ and 4 GeV, respectively.

With these numbers we end up with estimates $T_0\tau_0 \approx 0.8$ and 0.6 at $\sqrt{s_{NN}} = 11$ and 4 GeV, respectively. Considering the rough nature of the validity limit in Eq. (4.44), we can estimate that the collisions at the full NICA energy are still within the applicability of viscous hydrodynamics assuming that $\eta/s \lesssim \frac{1}{4\pi}$. But the collisions at the lowest NICA energy seem to require that the shear viscosity coefficient to entropy density ratio should be below the postulated lower limit for viscous hydrodynamics to be applicable.

Alternatively one may assume that the relation $T_0\tau_0 = 1$ still holds at NICA, but the initial time τ_0 is longer than at RHIC. To estimate what the initial time would be in that case, we can use the previous estimate that in the $\sqrt{s_{NN}} = 4$ GeV collisions, $T_0\tau_0 \approx 0.6$, and apply the temperature evolution in ideal boost-invariant expansion with ideal gas equation of state:

$$T = T_0 \left(\frac{\tau_0}{\tau}\right)^{\frac{1}{3}} .$$

When requiring that $T\tau = 1$, we get $\tau \approx 2\tau_0$. When the conventional initial times at RHIC are $\tau_0 = 0.5-1.0$ fm, this would require $\tau_0 = 1-2$ fm at $\sqrt{s_{NN}} = 4$ GeV at NICA. Still a small value, but already large enough that the transverse expansion during thermalization can no longer be neglected, and it is more difficult to estimate the initial state.

Thus a conventional Israel-Stewart hydrodynamics may not be applicable at NICA, at least at all collision energies. Instead we may need to use one of the proposed extensions of the Israel-Stewart theory [67,173], which may be more applicable at lower collision energies.

4.16 Importance of clusters for flow measurements at NICA

P. Danielewicz[a], T. Klähn[b], W. Reisdorf[c], D. Blaschke[b,d]

[a] *National Superconducting Cyclotron Laboratory and Department of Physics and Astronomy, Michigan State University, USA*

[b] *Institute for Theoretical Physics, University of Wrocław, Poland*

[c] *GSI Helmholtzzentrum für Schwerionenforschung, Darmstadt, Germany*

[d] *Joint Institute for Nuclear Research, Dubna, Russia*

We discuss that the measurement of the flow of light nuclear clusters (d, t, h, α) may be advantageous in determining properties of the equation of state for compressed baryon matter as produced in the early stages of nuclear collisions in the energy range provided at the NICA facility.

Constraints for the cold, dense EoS as derived from flow measurements [131] have wide-ranging implications, from possibly signalling the deconfinement phase transition within baryon matter compressed in heavy-ion collisions to consequences in nuclear astrophysics [127,138,175]. Refinement of those constraints, both for zero and finite temperatures, filling in gaps in systematics of flow anisotropies and combining the results from flow with those from other observables, are urgent issues for upcoming experiments. Of particular urgency are the characteristics of the high-density phase transition and the location of the critical endpoint (CEP).

In this contribution, we suggest that the measurement of heavier clusters (such as d, t, h, α) may provide the necessary leverage for such a refinement. Systematics of flow measurements by the FOPI Collaboration at GSI [176], shown in Figure 4.27, illustrates the principal strategy for the refinement, see also [177]. The energy ranges provided by the NICA facility, in fixed target and collider modes, are ideally suited for such an experimental programme, which we explain in the following in a bit more detail.

First and second order flow anisotropies are generated relatively early within the collisions of heavy nuclei and, thus, can serve as useful probes of the early pressure tensor in those collisions [178, 179]. The phase transition to the quark gluon plasma is generally expected to produce a nonmonotonous behavior of derivatives in the equilibrium pressure (e.g. a dip in the speed of sound $c_s = \sqrt{dp/d\varepsilon}$) as a function of early compression and temperature [51]. With different beam energies giving rise to different early compression and temperature, the transition might be identified through a discontinuous behavior of the excitation functions for the flow

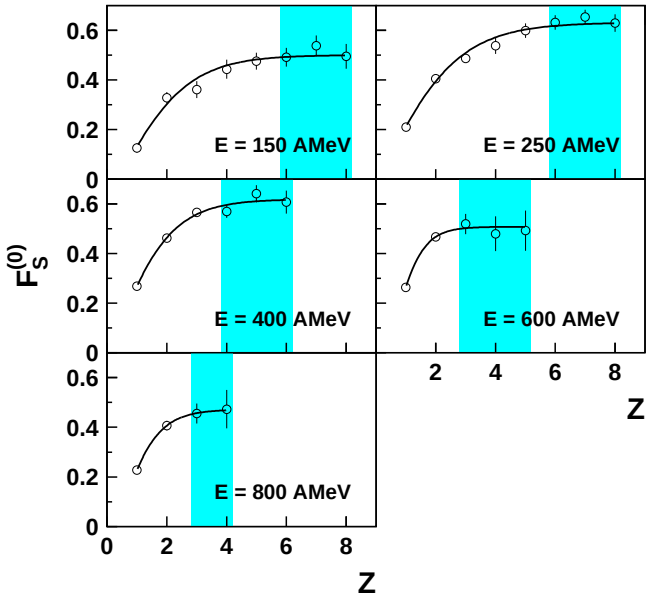

Figure 4.27: Normalized flow parameter as a function of fragment charge in Au + Au collisions at different energies, from the measurements of the FOPI Collaboration [176]. Lines show extrapolations aiming at isolating contribution untainted by thermal motion.

anisotropies [180]. Significance of such a signal could be augmented by finding a parallel discontinuity in the excitation functions for the low-momentum correlation functions or for pion yields, both testing entropy [181].

The above situation is, however, likely complicated by the fact that the observables do not probe instantaneous local pressure but rather its effects integrated over some volume and history of a reaction. To add to this, the transition to quark matter, as crossed in the collisions at NICA, may be weak and might not even be strictly a phase transition in the thermodynamic sense. In particular, energy scan programs of heavy-ion collision experiments such a NICA probe the vicinity of CEP of a first order phase transition. Therefore, the baryon number or energy density as an order parameter change either continuously (at the crossover side of the CEP) or with a very small jump (at the first order side of the CEP). For this reason it is a difficult task to define easily accessible observables which indicate the observation of the phase transition and the relative position to the CEP. Higher order derivatives of particle distributions (susceptibilities) have been suggested as sensible quantities for identifying a phase transition [126]. They require, however, a very high statistics of identified hadrons in order to derive these quantities with sufficient precision from the experiment.

Indeed, if the transition were strong, by now it would have likely been indicated by a significant discontinuity in the pion yield excitation function. Given the opposite, the identification of quite subtle signs of discontinuities in the excitation functions becomes a more important task. In order to succeed in isolating the transition under the previously mentioned circumstances, it is necessary to account as accurately as possible for the effects of the early pressure at any one beam energy.

It has been suggested that the curvature of the proton rapidity distribution at midrapidity might serve as a signal for a phase transition [71]. Otherwise, protons as heavier than pions generally exhibit stronger emission anisotropies than pions. At any one velocity vector of a particle, on account of thermal motion, pions stem from a wider range of freeze-out positions than do protons. The averaging over emission positions suppresses the impact of collective expansion velocities tied to specific locations in space.

Nuclear clusters, though, stem from an even more narrow region in space, than do protons, and their velocity distribution generally better reflects the distribution of collective velocities, with better emphasized anisotropies of the collective flow. In fact, by following the systematics of the velocity distributions as a function of cluster mass, one can attempt, Ref. [176, 177] and Fig. 4.27, to deduce characteristics of collective velocities, free from any effects of thermal motion, through extrapolation. Given the above, to increase prospects of identifying the transition through collective flow anisotropies, it is utterly important to have detectors at NICA capable of measuring clusters, especially d, t, h and α, and this over a wide rapidity range. In addition to helping with

the flow, measurements of clusters would improve precision in assessments of entropy [183] again tied to the transition.

4.17 Baryon stopping probes deconfinement

G. Wolschin

Institut für Theoretische Physik der Universität Heidelberg, Germany

Stopping and baryon transport in central relativistic Pb + Pb and Au + Au collisions are reconsidered with the aim to find indications for deconfinement. At energies reached at the CERN Super Proton Synchrotron ($\sqrt{s_{\rm NN}}$ = 6.3–17.3 GeV) and at RHIC (62.4 GeV) the fragmentation-peak positions as obtained from the data depend linearly on the beam rapidity and are in agreement with earlier results from a QCD-based approach that accounts for gluon saturation. No discontinuities in the net-proton fragmentation peak positions occur in the expected deconfinement region at 6–10 GeV. In contrast, the mean rapidity loss depends linearly on the beam rapidity only at high energies beyond the RHIC scale. The combination of both results offers a clue for the transition from hard partonic to soft hadronic processes in baryon stopping. NICA results could corroborate these findings.

At low relativistic energies in the AGS and SPS region, baryon stopping in central heavy-ion collisions is well described in a relativistic diffusion model that allows to calculate analytically net-baryon rapidity distributions based on non-equilibrium-statistical considerations [184] . However, it does not offer a direct indication whether the physical origin of stopping is of hadronic or partonic nature.

In a partonic QCD-based model such as [185] that is tailored to high-energy processes one should expect deviations from the data in certain net-baryon observables when the energy is reduced and hence, hadronic processes become important. Predictions of this partonic approach are therefore compared to the available data in order to find signatures for the transition from soft hadronic to hard partonic processes in net-baryon (proton) stopping, and the corresponding rapidity distributions.

Stopping in a QCD-based approach

In particular, we investigate both the mean rapidity loss $\langle\delta y\rangle$, and the fragmentation peak position $y_{\rm peak}$ as functions of the beam rapidity $y_{\rm beam}$ (or center-of-mass energy $\sqrt{s_{\rm NN}}$). The peak position in $y-$space occurs somewhat below the beam rapidity. At the maximum LHC energy of 5.52 TeV, for example, it is expected to be about 2 units of rapidity below the beam value, see Fig. 12.14 [185] ($y_{\rm beam}$=8.68).

Most of the physical processes leading to the rapidity loss in the peak region are of partonic nature: Fast valence quarks in the projectile collide with the gluon condensate in the respective other beam, thereby exchanging soft gluons, and reducing the beam energy and rapidity.

This behaviour should persist also at lower incident energies such as those reached at RHIC and SPS, and one therefore expects a linear dependence of the peak position (or the rapidity loss from $y_{\rm beam}$ to $y_{\rm peak}$) on the beam rapidity.

In contrast, the mean rapidity loss that involves physical processes over the whole range from midrapidity to the beam value is not only due to partonic events, but will gradually involve hadronic energy-loss mechanisms. The expected indication for this effect are deviations of the mean rapidity loss $\langle\delta y\rangle$ from a linear dependence on the beam rapidity.

Results for the fragmentation peak position as function of the beam rapidity as extracted [186] from NA49 [187] and BRAHMS [188] data are shown in Fig. 12.15. They fall on a straight line which agrees exactly with the analytical prediction of our partonic model based on gluon saturation [185]

$$y_{peak} = \frac{1}{1+\lambda}\left(y_{beam} - \ln A^{1/6}\right) + const \tag{4.45}$$

for a saturation-scale exponent $\lambda = 0.2$, an empirical const=-0.2, and the mass number A. Here λ determines the Bjorken-x dependent value of the gluon saturation momentum $Q_s^2 = A^{1/3}Q_0^2x^{-\lambda}$, with $Q_0^2 \simeq 0.04$ GeV^2 setting the momentum scale. The saturation-scale exponent $\lambda = 0.2$ corresponds to a gluon saturation momentum of $Q_s \simeq 0.77$ GeV at x=0.01.

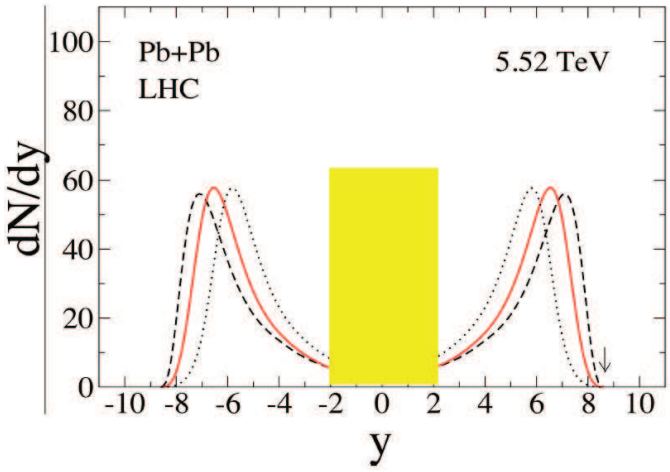

Figure 4.28: Rapidity distribution of net baryons in central Pb + Pb collisions at LHC energies of $\sqrt{s_{\rm NN}} = 5.52$ TeV. The fragmentation peak position depends on the gluon saturation scale Q_s. Theoretical distributions are shown for values of the saturation-scale exponent $\lambda = 0$ (dashed), $\lambda = 0.15$ (solid), and $\lambda = 0.3$ (dotted curve) [185] . ALICE currently provides particle identification only in the shaded midrapidity region, the peaks are experimentally not yet accessible.

This linear dependence of $y_{\rm peak}$ on the beam rapidity $y_{\rm beam}$ is expected to be applicable at RHIC energies and beyond, but as is obvious from Fig. 12.15, the predicted linear growth with $y_{\rm beam}$ is found to be valid also at low SPS energies. This indicates that even in this region of low relativistic energies, the processes that lead to an energy and rapidity loss in the peak region are predominantly partonic.

The mean rapidity loss is obtained by subtracting the average rapidity from the beam rapidity, $\langle \delta y \rangle = y_{\rm beam} - \frac{2}{N_{\rm part}} \int_0^{y_{\rm beam}} y \frac{dN_{B-\bar{B}}}{dy} dy$. It reflects the properties of the system over the whole rapidity range, not just at the peak position, and may therefore show a qualitatively different dependence on the beam rapidity $y_{\rm beam}$ (or the initial c.m. energy $\sqrt{s_{\rm NN}}$) than the fragmentation-peak position $y_{\rm peak}$. Indeed it is found [185, 189, 190] to deviate from a simple straight-line dependence on the beam rapidity, see Fig. 4.45.

For the mean rapidity loss in the high energy limit, the partonic model based on the concept of gluon saturation [185] predicts $\langle \delta y \rangle = \frac{\lambda}{1+\lambda} y_{\rm beam} + const'$. This result is indicated by the straight line in Fig. 4.45 for $\lambda = 0.2$. The limit should be reached in PbPb collsions at the highest LHC energies. At lower energies, the data for the mean rapidity loss (Fig. 4.45) clearly show an increasing deviation that is indicative for the gradual onset of hadronic processes that are not accounted for in the partonic high-energy limit, and thus, for the increasing relevance of confinement.

Conclusion

I conclude that the qualitatively different dependence of the fragmentation peak position, and the mean rapidity loss on the beam rapidity offers a clear indication for the onset of hadronic behaviour at low energies in the midrapidity region. This conclusion is somewhat modified from our arguments in [186] , where we had only considered the dependence of $y_{\rm peak}$ on $y_{\rm beam}$ that is completely linear, and agrees with the partonic prediction.

The transition from partonic to hadronic behaviour in central collisions as the beam energy decreases is gradual, there is no sudden deconfinement with a corresponding jump in the mean rapidity loss at a particular beam energy. Hadronic and partonic processes coexist in a large energy region that extends from AGS to low LHC energies. In the fragmentation peak region, partonic processes are decisive even at low SPS energies.

Acknowledgments I am grateful to Yacine Mehtar-Tani for our collaboration documented in Refs. [185, 186, 191, 192]. This contribution to the white book is scheduled to appear also in the conference proceedings for ISMD2011 at Hiroshima/Miyajima island. The work has been supported by the ExtreMe Matter Institute EMMI.

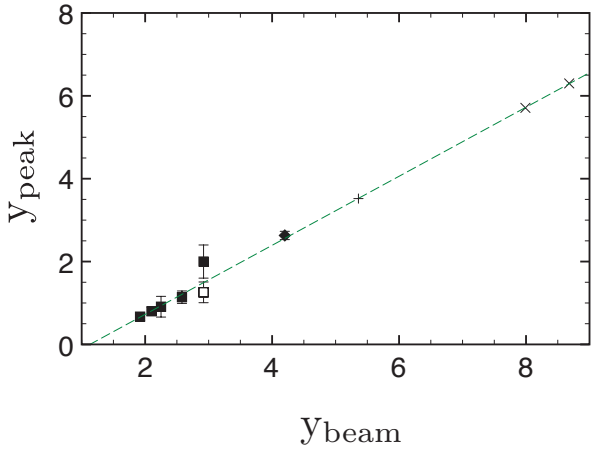

Figure 4.29: Peak positions of the net-proton rapidity distributions in Pb + Pb (black squares) and Au + Au (black diamond) as function of the beam rapidity, determined from double-gaussian fits of the NA49 [61, 187] and RHIC data [190] , see [186] . The open square is based on older NA49 data at 17.3 GeV [58] . The slope agrees well with the analytical expression eq.(4.45) for $\lambda = 0.2$, dashed line. The cross refers to the calculated peak position of Au + Au at 200 GeV, the inclined crosses to Pb + Pb at LHC energies of 2.76 and 5.52 TeV. The data show no deviation from the straight line, indicating the dominance of partonic processes at the peak position. From [186] .

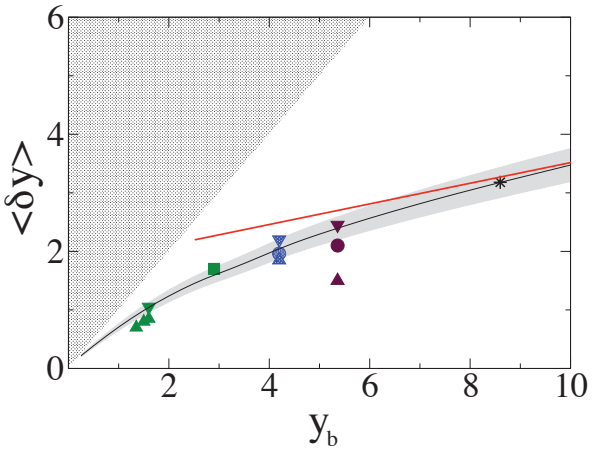

Figure 4.30: The mean rapidity loss $\langle \delta y \rangle$ as obtained in [191] is plotted as a function of beam rapidity $y_{\rm beam}$, solid curve. The star at $y_{\rm beam} = 8.68$ is the prediction for central Pb + Pb at LHC-energies of $\sqrt{s_{\rm NN}} = 5.52$ TeV with $\lambda = 0.2$. Analysis results from AGS Au + Au data (E917, E802/E866, triangles) [189] , SPS Pb + Pb data (NA49, squares [58] ; the preliminary low-rapidity data are from [61]) , RHIC Au + Au data (BRAHMS, dots, with triangles as lower and upper limits [188, 190]) are compared with the calculations [185, 191] . The solid straight line is the analytical prediction of the slope in the high-energy partonic limit for $\lambda = 0.2$. Below the highest RHIC energies there is a clear deviation from the partonic limit due to the gradual onset of hadronic processes in the mean rapidity loss. No such deviation appears in the corresponding fragmentation peak positions, see Fig. 2.

4.18 Can NICA verify BES?

D. Parganlija

Vienna University of Technology Institute for Theoretical Physics, Vienna, Austria

Recent years have seen a lot of activity with regard to scalar-meson spectroscopy by the BES and BES II Collaborations. A new scalar resonance is claimed to have been found by BES – but no subsequent experiments have been performed to approve (or disprove) this claim. This is a question that NICA Project could look into. Additionally, the issue of mass scaling for the (axial-)vector mesons and also of chiral transition is one of the still-unresolved problems in QCD. The NICA Project may give us valuable experimental information also in this regard.

Scalar Mesons

Particle Data Group (PDG) cites the existence of five $IJ^{PC} = 00^{++}$ states (where I, J, P and C respectively denote the isospin, total spin, parity and charge conjugation): $f_0(600)$, $f_0(980)$, $f_0(1370)$, $f_0(1500)$ and $f_0(1710)$. They are known as scalar isoscalar resonances [193]. Claims have been made [194–197] that a sixth such state exists, namely $f_0(1790)$ – a state very close to $f_0(1710)$ but with a different decay behaviour: $f_0(1790)$ decays predominantly into pions whereas $f_0(1710)$ decays predominantly into kaons. However, PDG does not acknowledge the existence of this resonance despite the data on $f_0(1790)$ available until now (see below) – the state is not mentioned even in the 'unconfirmed resonances' section of the PDG compilation. The proposed Project NICA at JINR-Dubna could shed light on this issue of meson phenomenology.

There are four basic production mechanisms for $f_0(1710)$ and $f_0(1790)$ via J/ψ decays:

- (*i*) $J/\psi \to \varphi K^+K^-$,
- (*ii*) $J/\psi \to \varphi\pi^+\pi^-$,
- (*iii*) $J/\psi \to \omega K^+K^-$,
- (*iv*) $J/\psi \to \omega\pi^+\pi^-$.

Reactions (*i*) and (*iii*) allow for reconstruction of $f_0(1710)$ – see Ref. [198–200] – whereas reactions (*ii*) and (*iv*) allow for reconstruction of $f_0(1790)$. Importantly, assuming $f_0(1710)$ and $f_0(1790)$ to be the same resonance leads to a contradiction: such a resonance would have to possess a pion-to-kaon-decay ratio of 1.82 ± 0.33 according to reactions (*i*) and (*ii*) and the pion-to-kaon-decay ratio < 0.11 according to reactions (*iii*) and (*iv*) [196, 197]. The decay ratios must be independent from the production mechanism for a single resonance. Evidently, the BES data demonstrate this not to be the case for $f_0(1710)$ and $f_0(1790)$. Thus the BES data prefer the existence of $f_0(1790)$ – but nonetheless, there has been no additional experimental inspection of this claim after BES results. The NICA Project could reconstruct scalar resonances in the energy region between 1.7 GeV and 1.8 GeV thus either verifying or disproving BES results regarding $f_0(1790)$.

Chiral Transition

There are two established spin-one resonances in the non-strange meson channel: $\rho(770)$ and $a_1(1260)$. Their features are rather well known in vacuum, especially for the case of $\rho(770)$ [**?**, 201] but it is as yet not clear if (and how) their masses change in medium. There are two possible scenarios for the vector mass in particular:

- The mass decreases to zero as the chiral condensate vanishes (i.e., the chiral symmetry of QCD becomes restored) - the "Brown-Rho scenario" [203].
- The mass remains essentially constant or decreases marginally as the chiral condensate vanishes - the "constant-rho scenario" [**?**, 204].

The NICA Project could examine the mass shifts of vector and axial-vector mesons in medium, both at $T \neq 0$ as well as $\mu \neq 0$. This would be extremely helpful for our understanding of QCD, also because the degeneration of ρ and a_1 states can be viewed as an order parameter for the chiral transition [206]. In this sense, there are three possible scenarios for the mass shifts of ρ and a_1 in medium leading to their degeneration: (*i*) both masses decrease and become degenerate; (*ii*) both masses increase and become degenerate; (*iii*) m_ρ increases and m_{a_1} decreases leading to the degeneration of the two masses. NICA could provide us with valuable information regarding which of these scenarios is preferred both at $T \neq 0$ and at $\mu \neq 0$.

4.19 Spinodal amplification of density fluctuations in nuclear collisions at NICA

J. Steinheimer and J. Randrup

Nuclear Science Division, LBNL, Berkeley, California, USA

It is expected that strongly interacting matter, at temperatures below a certain critical value $T_{\rm crit}$, may exist in two different forms, confined and deconfined, at equal temperatures, chemical potentials, and pressures. The search for evidence of this first-order phase transition and the associated critical end point forms a current focus for experimental heavy-ion physics and NICA may be particularly well suited for this endeavour, as discussed below.

When the material under consideration exhibits a phase transition, the associated phase diagram contains a region where uniform matter is both thermodynamcially and mechanically unstable. Therefore, if, in a nuclear collision, the bulk of the system can be brought into that unstable (spinodal) region, small irreguarities may be amplified significantly which, in turn, may lead to observable effects that would signal the existence of the phase transition. This phenomenon was exploited previously to obtain experimental evidence of the nuclear liquid-gas phase transition through event-by-event analysis of the fragment size distribution [207, 208].

It was suggested already several years ago that the spinodal mechanism may also provide useful signals of the deconfinement transition [209]. Indeed quantitative estimates for idealized scenarios have suggested that the time scale for the spinodal amplification may in fact be sufficiently short to prevail over that associated with the overall expansion [210, 211]. It is therefore worthwhile to study the effect by simulating actual collisions with realistic transport treatments.

For this purpose, we have simulated nuclear collisions with finite-density fluid dynamics [212], using a previously developed two-phase equation of state [211]. Fluid dynamics has the advantage that the equation of state, $p_0(\varepsilon,\rho)$, appears explicitly. Because it is essential to incorporate finite-range effects to describe the spinodal phase decomposition [208–211], we follow Ref. [210] and introduce a gradient term into the expression for the local pressure in a nonuniform medium,

$$p(\mathbf{r}) = p_0(\varepsilon(\mathbf{r}),\rho(\mathbf{r})) - a^2\frac{\varepsilon_s}{\rho_s^2}\rho(\mathbf{r})\nabla^2\rho(\mathbf{r}) \ . \tag{4.46}$$

Here $p_0(\varepsilon,\rho)$ is the pressure in *uniform* matter having the energy density ε and the (net) baryon density ρ. In the gradient term, $\rho_s = 0.153/\mathrm{fm}^3$ is the nuclear saturation density and $\varepsilon_s \approx m_N\rho_s$ is the associated energy density, so its strength is then conveniently governed by the length parameter a.

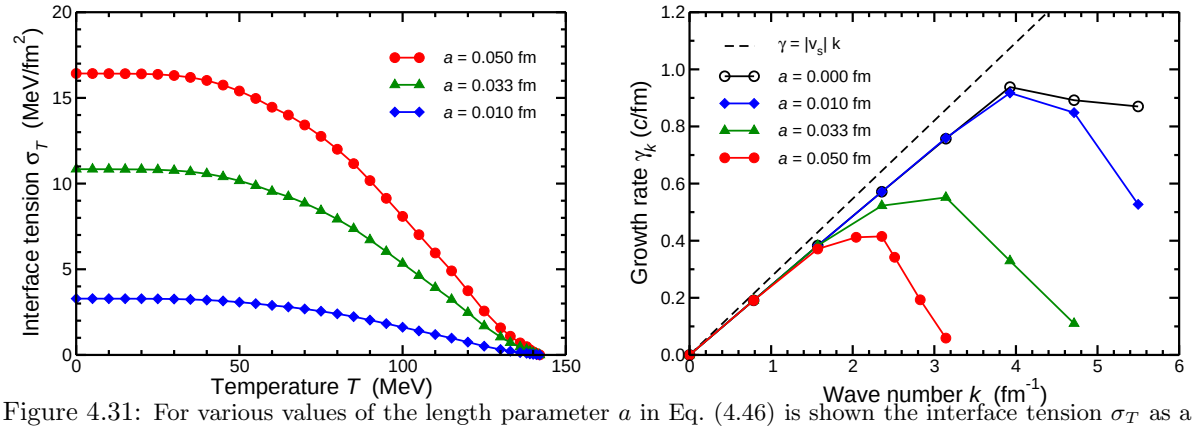

Figure 4.31: For various values of the length parameter a in Eq. (4.46) is shown the interface tension σ_T as a function of the temperature T (*left*) and the spinodal growth rate γ_k as a function of the wave number k, as obtained with ideal finite-range fluid dynamics (*right*) [212].

The gradient term has two interrelated effects that are essential for the proper description of the phase-transition physics, illustrated in Fig. 4.31 above: 1) It will cause a diffuse interface to develop when the two coexisting phases are brought into physical contact and give rise to a temperature-dependent interface tension (which can then readily be determined from the equation of state $p_0(\varepsilon,\rho)$ [210,212]); 2) It will cause the spinodal growth rate γ_k to exhibit a maximum as a function of the wave number of the irregularity being amplified, thus leading to the emergence of a certain length scale in the resulting phase mixture.

The key effect of the first-order phase transition is the spinodal amplification of spatial irregularities [208–211]. For a quantitative measure of the resulting degree of clumping in the system, one may consider the moments of the baryon density distribution $\rho(\mathbf{r})$,

$$\langle \rho^N \rangle \;\equiv\; \frac{1}{A} \int \rho(\mathbf{r})^N \rho(\mathbf{r})\, d^3\mathbf{r}\;, \tag{4.47}$$

where $A = \int \rho(\mathbf{r}) d^3\mathbf{r}$ is the total (net) baryon number. These quantities have observational relevance because they are intimately related to the relative production yield of composite baryons.

In order to ascertain the effect of the phase transition, we employ also a single-phase partner equation of state obtained by performing a Maxwell contruction at each temperature, thereby eliminating the convex anomalies that are responsible for the spinodal instabilities but matching the actual equation of state outside the phase coexistence region.

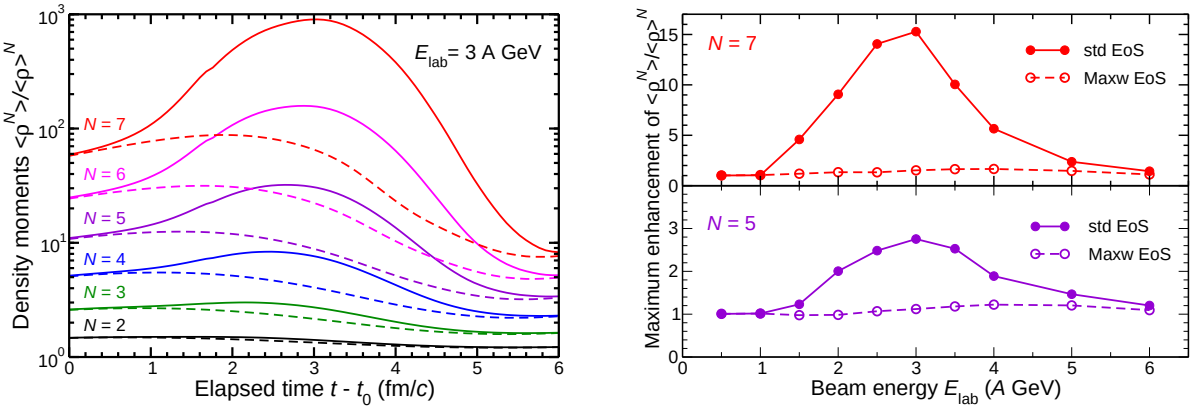

Figure 4.32: *Left:* Mean time evolution of normalized density moments obtained for $E_{\rm lab} = 3A$, GeV with $a = 0.033\,$fm (for which the surface tension is $\sigma_0 \approx 10\,{\rm MeV/fm}^2$), using either the two-phase equation of state (*solid*) or its one-phase partner (*dashed*). *Right:* Mean maximum enhancement of the normalized moments for $N = 7, 5$ (*top, bottom*) as obtained for various energies using either the two-phase equation of state (solid) or its one-phase Maxwell partner (dashed). (From [212].)

The degree of density clumping generated during a collision depends on how long time the bulk of the matter is exposed to the spinodal instabilities. The optimal situation occurs for beam energies that produce maximum bulk compressions lying well inside the unstable phase region because the instabilities may then act for the longest time [208, 210, 211]. At lower energies an ever smaller part of the system reaches instability and the resulting enhancements are smaller. Conversely, at higher energiers the maximum compression occurs beyond the spinodal phase region and the system is exposed to the instabilities only during a relatively brief period during the subsequent expansion. For still higher energies the spinodal region is being missed entirely.

The existence of an optimal collision energy is clearly brought out by the calculated results, see Fig. 4.32 (*right*). The presently employed equation of state (taken from [211]) suggests that this optimal range is $E_{\rm lab} \approx 2 - 4$,A GeV, which is very well matched to the anticipated range of NICA. Furthermore, our studies suggest that the optimal energy is rather insensitive to the range parameter a, which is fortunate because this quantity is not yet well understood. However, it should be recognized that other equations of state may yield different optimum energies, because of difference in compressibilitites and phase-coexistence regions, but the existence of an optimal region is generic. Finally, the degree of clumping also depends on the degree of fluctuation in the initial conditions which in turn are governed by the pre-equilibrium dynamics.

To summarize, by augmenting an existing fluid-dynamical code with a gradient term, we have obtained a transport model that is suitable for simulating nuclear collisions in the presence of a first-order phase transition: it describes both the tension between coexisting phases and the dynamics of the unstable spinodal modes. Applying this novel model to lead-lead collisions, we have found that the associated instabilities may cause significant amplification of initial density irregularities.

How to best observe such clumping is a topic of active research. Because one would expect density enhancements to facilitate the formation of composite particles, such as deuterons and tritons, the effect might be experimentally observable through such yield ratios, but there may well be other possibilities.

4.20 Phenomena at the QCD phase transition in nonequilibrium chiral fluid dynamics (NχFD)

M. Nahrgang[a,b], Ch. Herold[b,c], I. Mishustin[b,d], S. Leupold[e], M. Bleicher[b,c]

[a] *SUBATECH, Université de Nantes, Nantes, France*
[b] *Frankfurt Institute for Advanced Studies (FIAS), Frankfurt am Main, Germany*
[c] *Institut für Theoretische Physik, Goethe-Universität, Frankfurt am Main, Germany*
[d] *Kurchatov Institute, National Research Center, Moscow, Russia*
[e] *Department of Physics and Astronomy, Uppsala University, Uppsala, Sweden*

The search for the critical point of QCD and the study of the first order phase transition is one of the major goals of upcoming heavy-ion experiment facilities like NICA in Dubna and FAIR at GSI.

An enhancement of fluctuations is predicted to be seen for both scenarios, at the critical point and the first order phase transition. At the critical point the correlation length diverges in thermodynamic systems, which leads to a divergency of the fluctuations of the order parameter and is supposed to translate into large event-by-event fluctuations of conserved quantities, such as net-charge or net-baryon number distributions [72, 213]. Systems, which are created in heavy-ion collisions are, however, finite in size and time, spatially inhomogeneous and evolve dynamically. Due to critical slowing down especially finite time effects limit the growth of the correlation length [49].

At the first order phase transition, fluctuations are a result of nonequilibrium effects like supercooling which lead to nucleation and spinodal decomposition [211, 212, 214–216]. These fluctuations should be visible in a careful analysis of single event particle distributions.

In the last couple of years the model of NχFD for the explicit propagation of fluctuations coupled to a dynamic expansion of a heavy-ion collision was developed [217] showing that nonequilibrium effects can have an important influence on the evolution of the fluctuations of the order parameter of chiral symmetry [218, 219]. Recently, we extended this approach to include also the deconfinement-confinement transition with the Polyakov-loop as the order parameter [220]. The expansion of the strongly interacting matter created in a heavy-ion collision is described by ideal fluid dynamics, where the fluid consists of quark and antiquarks with the local thermodynamic properties of the (Polyakov-loop) quark-meson model [221–224].

In order to mimic the phase transition at higher baryonic chemical potentials, which are relevant for the NICA and FAIR experiments, we make use of the fact that for a fixed baryochemical potential μ_B the strength of the phase transition can be tuned via the quark-meson coupling g.

The order parameter of chiral symmetry, the sigma field, and of the deconfinement-confinement transition, the Polyakov-loop interact with the quark fluid and thus are damped. We include damping and fluctuation terms into the equation of motion of the order parameters, which read

$$\partial_\mu \partial^\mu \sigma + \eta_\sigma(T)\partial_t \sigma + \frac{\partial(U + \Omega_{\bar{q}q})}{\partial \sigma} = \xi_\sigma \ , \tag{4.48}$$

$$\eta_\ell \partial_t \ell T^2 + \frac{\partial(\mathcal{U} + \Omega_{\bar{q}q})}{\partial \ell} = \xi_\ell \tag{4.49}$$

It contains a classical Mexican hat potential U, the temperature dependent Polyakov loop potential $\mathcal{U}$, the quark contribution to the thermodynamic potential $\Omega_{\bar{q}q}$ to one-loop level, the damping coefficients η and the stochastic noise fields ξ. The damping term and the stochastic noise are for both order parameters related by the dissipation-fluctuation theorem. The quark degrees of freedom evolve according to energy-momentum conservation, i.e. the equations of relativistic fluid dynamics

$$\partial_\mu T^{\mu\nu} = S^\nu \, , \tag{4.50}$$

where the source term S^ν accounts for the energy-momentum exchange between the fluid and the fields.

First, we present some characteristics of the relaxation process by looking at the intensities of fluctuations of the order parameters, N_σ and N_ℓ. These are shown as a function of the wave number $|k|$ evaluated at late

times of the equilibration in a box scenario in figs. 4.33. At this time the system is equilibrated and the long wavelength modes of both order parameters are enhanced at the critical point.

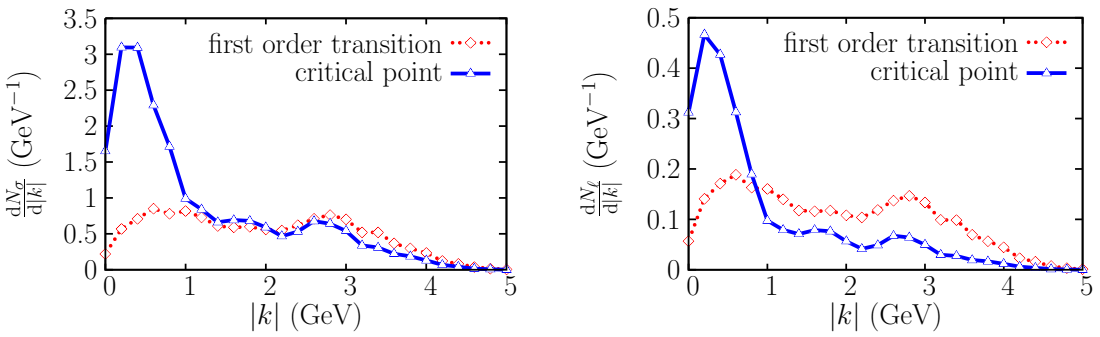

Figure 4.33: The soft modes of the sigma field (left) and the Polyakov-loop (right) after equilibration of the system in a box calculation [220]. See text for details.

Once the dynamic evolution of the quark fluid is included we can track the average values of the order parameters during the expansion of the fireball. The results are shown in figs 4.34. One can observe significant differences in the evolution of the average temperatures: In the scenario with a first order phase transition, the phenomena of reheating occurs after 6 fm as a consequence of the formation of a supercooled phase below the transition temperature. As the average temperature drops below T_c, the average values of the sigma field and Polyakov-loop remain close to their high temperature values at around $\sigma/f_\pi = 0.1$ and $\ell = 0.4$. This supercooled state decays after approximately 2 fm to the global minimum and due to the presence of the source term in eq. (4.49) transfers its energy into the fluid. This process causes an increase in the average temperature.

For the critical point scenario the effect of reheating is not observed. The temperature decreases monotonically with only a small plateau well below the transition temperature. Here, the dynamics slows down slightly due to the flat shape of the effective potential. The evolution of the averaged fields, especially for $\langle\sigma\rangle$, proceeds less rapidly than in the scenario with a first order phase transition.

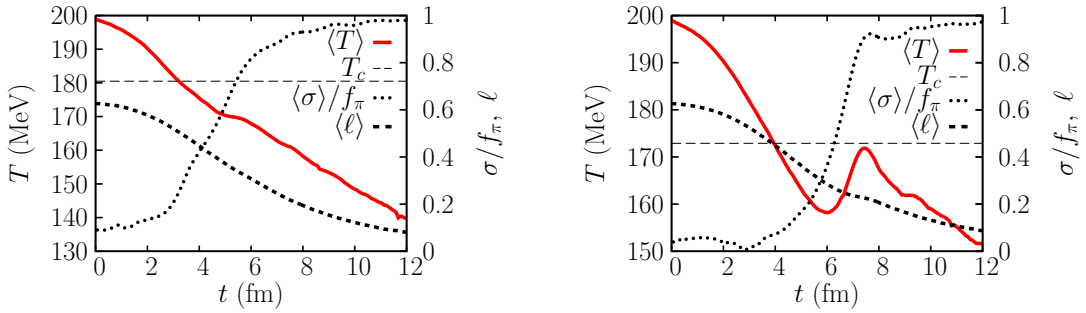

Figure 4.34: Averaged quantities during the expansion in a critical point scenario (left) and a scenario with a first order phase transition (right) [220]. See text for details.

For the critical point scenario we can investigate the growth of the correlation length via the relation

$$\frac{1}{\xi^2} = \left.\frac{\partial^2(U + \Omega_{\bar{q}q}(T))}{\partial\sigma^2}\right|_{\sigma=\sigma_{\rm eq}}, \tag{4.51}$$

which is, however, not a dynamic definition of the correlation of the fluctuations, and should thus be regarded as a very preliminary study. A dynamic investigation of the evolution of the correlation length is work in progress.

In figures 4.35 we study the correlation during different types of the expansion of the medium. In the left plot we demonstrate the influence of the inhomogeneity of the system on the growth of the correlation length. Here, we use the pure quark-meson model (without the Polyakov-loop) as a basis and concentrate on an equilibrium evolution. This means that we do not propagate fluctuations of the sigma fields according to eq. (4.49), but rather use the local equilibrium value of sigma, which corresponds to the local temperature. Since

in a fluid dynamic expansion the temperature is not constant over larger regions, we cannot determine a global correlation length according to eq. (4.51) without averaging. When we first average over the temperature in a central region of the fireball and then calculate the correlation length for this averaged temperature, we find that at an average critical temperature the correlation length obtained from eq. (4.51) diverges. While when we first calculate the correlation length locally (again from eq. (4.51)) and then average over the central region we find that the correlation length remains finite and grows up to 1.5 fm.

On the right plot one sees the comparison between correlation lengths in the two different phase transition models (here with a Polyakov-loop) and for averaging first over temperature. It is obvious that the correlation length in the critical point scenario grows much larger than during the first order phase transition.

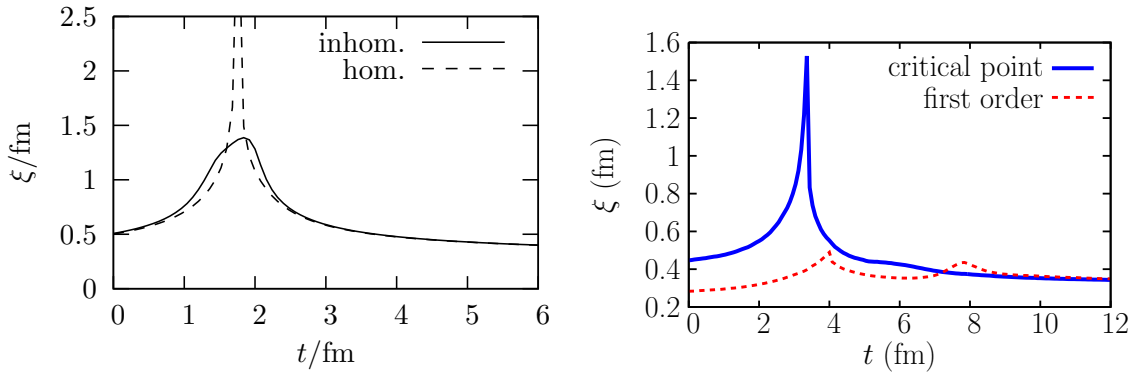

Figure 4.35: The correlation length in a different scenario with a critical point for the quark meson model in equilibrium (left) [225] and the Polyakov-loop extended quark meson model during the expansion (right) [220]. See text for details.

Correlating the stochastic fluctuations in the equations of motion according to the so obtained correlation length enables us to model the domain formation mechanism at the first order transition. Figs. 4.36 show the sigma field for $z = 0$ for a first order and a critical point scenario at the respective transition point. We observe characteristic differences: At the first order phase transition, the structure is bumpy with domains of the chirally broken phase in the chirally symmetric background and vice versa. On the other hand, at the critical point, a regular almond shape is preserved.

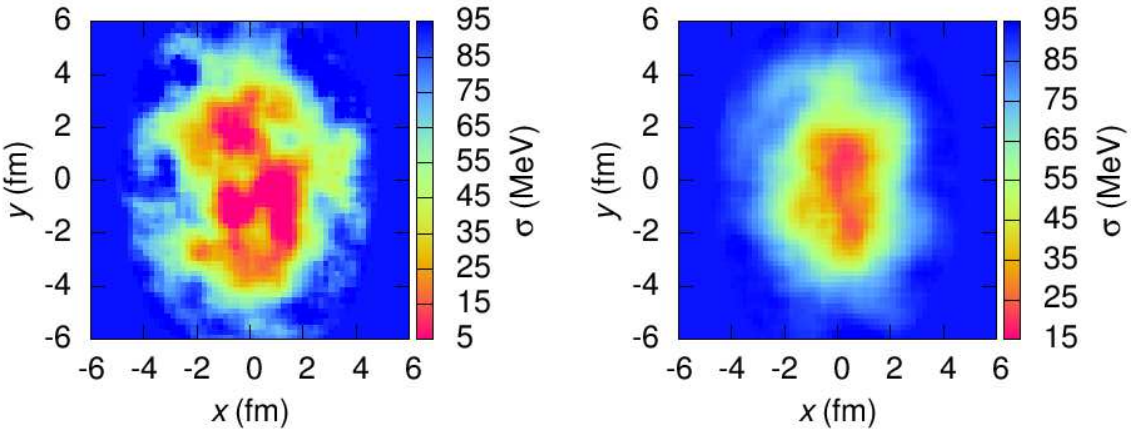

Figure 4.36: The sigma field in the transversal $z = 0$ plane at the first order transition (left) and the critical point (right). See text for details.

This work is ongoing to extend calculations to include fluctuations in net-baryon densities and thus describe the critical point and the first order phase transition realistically. Event-by-event fluctuations and the dynamic

growth of the correlation length in more realistic setups are being investigated.

This ongoing work is supported by the Hessian Excellence Initiative LOEWE through the Helmholtz International Center for FAIR. We are grateful to the Center for Scientific Computing (CSC) at Frankfurt for providing the computing resources.

4.21 Recent Developments of the Hadron Resonance Gas Model and the Chemical Freeze-out of Strange Hadrons

K. A. Bugaev[1], A. I. Ivanytskyi[1], D. R. Oliinychenko[2], E. G. Nikonov[3], V. V. Sagun[1], A. S. Sorin[2] and G. M. Zinovjev[1]

[1] *Bogolyubov Institute for Theoretical Physics, Kiev, Ukraine*
[2] *Bogoliubov Laboratory of Theoretical Physics, JINR, Dubna, Russia*
[3] *Laboratory for Information Technologies, JINR, Dubna, Russia*

Basic elements of the hadron resonance gas model.

The recent findings [226–228] obtained by the hadron resonance gas model (HRGM) resolved a few old puzzles on the chemical freeze-out and gave a novel look at some old problems of QCD phenomenology. The most successful version of the HRGM, the HRGM1, was developed in [229, 230]. The novel version of this model, the HRGM2, which was worked out in [226, 227], has the same basic properties as the HRGM1, namely, it employes the hard-core repulsion between the hadrons, it includes all hadronic resonances with masses up to 2.5 GeV with their finite width, also it accounts both the thermal hadronic multiplicities and the nonthermal ones which are coming from the decay of heavy resonances, and, finally, the HRGM2 explicitly accounts for the strangeness conservation by finding out the chemical potential of the strange charge from a condition of vanishing strangeness. Despite slightly different particle tables employed in the HRGM1 and HRGM2 and a systematic accounting for the resonance width in HRGM2, these models give very similar results for the chemical freeze out (FO) parameters for the same values of the hadronic hard-core radii [226]. This is shown in Fig. 4.37 for the same hadronic hard-core radii $R = 0.3$ fm.

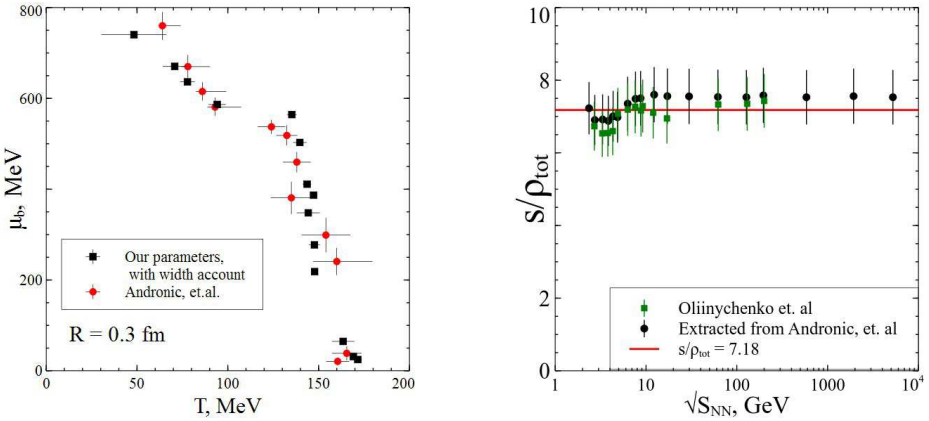

Figure 4.37: Comparison of the chemical FO parameters of HRGM1 [229] and HRGM2 [226]. **Left panel:** baryonic chemical potential vs. the chemical FO temperature for HRGM1 (circles) and HRGM2 (squares). **Right panel:** entropy per particle at chemical freeze-out $s/\rho \simeq 7.18$ vs. the center of mass energy per nucleon $\sqrt{s_{\rm NN}}$. The shown errors are combined the statistical and systematic errors. The results of HRGM2 (squares) are very similar to that ones obtained by HRGM1.

Adiabatic chemical FO criterion and effective hadronic mass spectrum.

A thorough investigation of the traditional chemical FO criteria performed in [226] for the HRGM1 and HRGM2 gave rather valuable results. Although the discussion about the reliable chemical FO criterion has a long history [65, 229], only very recently it was demonstrated that none of the previously suggested chemical FO criteria, including the most popular one of constant energy per particle $E/N \simeq 1.1$ GeV [231, 232] and the

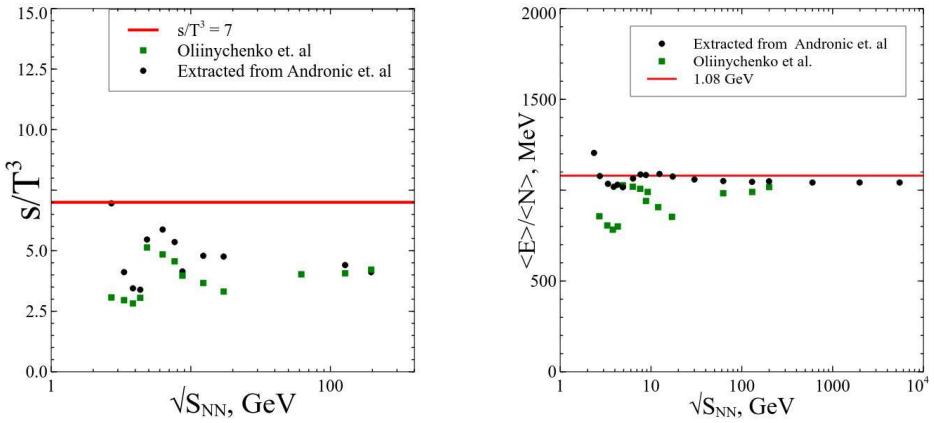

Figure 4.38: Different chemical freeze-out criteria. **Left panel:** ratio of the entropy density to the cube of temperature s/T^3 at chemical freeze-out vs. the center of mass energy $\sqrt{s_{\rm NN}}$. Results of the HRGM1 (HRGM2) are shown by circles (squares). **Right panel**: energy per particle $\langle E\rangle/\langle N\rangle$ at chemical chemical freeze-out vs. $\sqrt{s_{\rm NN}}$. Notations are the same as in the left panel.

criterion of constant entropy density s to the cube of FO temperature ratio, $s/T^3 \simeq 7$ [233, 234], is robust [226], if the realistic particle table with the hadron masses up to 2.5 GeV is used and the hard-core hadronic repulsion is included. This is clearly seen by comparing the right panel of Fig. 4.37 with both panels of Fig. 4.38. At the same time in [226] it was shown that despite an essential difference with the approach used in [229], the both versions of the hadron resonance gas model demonstrate almost the same value 7.18 for the entropy per particle at chemical FO. In other words, the criterion of adiabatic chemical FO is, indeed, the robust one.

A puzzle of the adiabatic chemical FO led us to a formulation of the model equation of state [228]

$$p_M = C_M\ T^{A_M}\ \exp\left[-\frac{m_M}{T}\right]\ , \quad p_B = C_B\ T^{A_B}\ \exp\left[\frac{\mu_B - M_B}{T}\right]\ , \tag{4.52}$$

which successfully parameterizes the baryonic pressure p_B and the mesonic one p_M of the HRGM2. The pressure of antibaryons is also described by the right Eq. (4.52), but for negative value of the baryonic chemical potential extracted from the data at chemical FO, i.e. $\mu_{\bar B} = -\mu_B$. The constants C_a, A_a, m_a with $a \in \{M, B\}$ in (4.52) parameterize the integrated hadronic mass spectrum and should be determined from the fit of the adiabatic chemical FO parameters. The remarkable fact, however, is that one can get rather good description of the constant entropy per particle by fitting only the mesonic and baryonic particle densities for which the mean deviations squared per degree of freedom, respectively, are $\chi^2_M/dof \simeq 0.42/11$ and $\chi^2_B/dof \simeq 7.8/11$. In other words, once the particle densities of the system (4.52) are reproduced, the corresponding entropy densities are automatically reproduced well giving the total mean deviation squared $\chi^2_{tot}/dof \simeq 19.4/36$. The latter includes the sum of mean deviations squared of meson density together with the one of baryons and their full entropy per particle at chemical FO.

The system (4.52) is a further refinement of the original E. Shuryak idea proposed for vanishing baryonic densities [235] and the found powers $A_B \simeq 6.097 \pm 0.38$ and $A_M \simeq 5.31 \pm 0.14$ are very close to the early estimate of Ref. [235]. Additionally, under the well justified assumptions the present model allows us to uniquely determine an effective density of states of hadronic mass spectrum using the inverse Laplace technic [228]. The found density of baryonic states is $\frac{\partial \varrho_B(m)}{\partial m} \sim \frac{(m-M_B)^{A_B-3.5}}{m^{\frac{3}{2}}}$, while the mesonic one is $\frac{\partial \varrho_M(m)}{\partial m} \sim m^{A_M-4}$, i.e. these densities of states are power-like rather than the exponential one. Moreover, numerical estimates show that for hadronic masses below 2.5 GeV these densities of states essentially differ from the empirical power-like hadronic density of states $\frac{\partial \varrho^{emp}(m)}{\partial m} \simeq \frac{4.11}{470\,\rm MeV}\left[\frac{m}{470\,\rm MeV}\right]^{3.11}$ found in [236] from the Particle Data Group [237] data. Our searches for possible reasons of such a difference led to a discovery of two new effects based on the modification of the wide resonance (and quark gluon bag) properties in a thermal medium [228].

Thermal enhancement and sharpening of wide resonances at chemical FO.

In order to demonstrate these new effects, here we consider the Gaussian mass attenuation of wide resonances

instead of the Breit-Wigner one that is used in the actual simulations, since in this case the evaluation is more transparent. Such a treatment gives only about 10 % difference from the Breit-Wigner one, but it also allows us to obtain some important conclusions on the mass spectrum of quark-gluon (QG) bags which according to [238, 239] should unavoidably have the Gaussian mass attenuation. Note that such an estimate provide us with the lower limit, since the Gaussian mass distribution vanishes much faster than the Breit-Wigner one. The typical term of the k-resonance that enters into the mass spectrum of the hadron resonance gas model is given by $F_k(\sigma_k) \exp\left[\frac{\mu_k}{T}\right]$ [226, 229] (here μ_k is the chemical potential of this resonance) with

$$F_k(\sigma_k) \equiv g_k \int\limits_0^\infty dm \, \frac{\Theta\left(m - M_k^{Th}\right)}{N_k(M_k^{Th})} \, \exp\left[-\frac{(m_k - m)^2}{2\,\sigma_k^2}\right] \int \frac{d^3p}{(2\pi\hbar)^3} \exp\left[-\frac{\sqrt{p^2 + m^2}}{T}\right] . \quad (4.53)$$

Here m_k is the mean mass of the k-th resonance, g_k is its degeneracy factor, σ_k is the Gaussian width which is related to the true resonance width as $\Gamma_k = Q\,\sigma_k$ (with $Q \equiv 2\sqrt{2\,\ln 2}$) and the normalization factor is defined via the threshold mass M_k^{Th} of the dominant channel as $N_k(M_k^{Th}) \equiv \int\limits_{M_k^{Th}}^\infty dm \, \exp\left[-\frac{(m_k - m)^2}{2\,\sigma_k^2}\right]$. For the narrow resonances the term $F_k(\sigma_k)$ converts into the usual thermal density of particles, i.e. for $\sigma_k \to 0$ one has $F_k \to g_k\,\phi(m_k, T)$, where the following notation is used $\phi(m, T) \equiv \int \frac{d^3p}{(2\pi\hbar)^3} \exp\left[-\frac{\sqrt{p^2+m^2}}{T}\right]$. The momentum integral in (4.53) can be written using the non-relativistic approximation $\phi(m, T) \simeq \left[\frac{m\,T}{2\,\pi\,\hbar^2}\right]^{\frac{3}{2}} \exp\left[-\frac{m}{T}\right]$. Then to simplify the mass integration of (4.53) one can make the full square in it from the powers of $(m_k - m)$ and get

$$F_k(\sigma_k) \equiv g_k \int\limits_0^\infty dm\, f_k(m) \simeq \tilde{g}_k \int\limits_0^\infty dm \, \frac{\Theta\left(m - M_k^{Th}\right)}{N_k(M_k^{Th})} \, \exp\left[-\frac{(\tilde{m}_k - m)^2}{2\,\sigma_k^2}\right] \left[\frac{m\,T}{2\pi\hbar^2}\right]^{\frac{3}{2}} \exp\left[-\frac{m_k}{T}\right] , \quad (4.54)$$

where an effective resonance degeneracy $\tilde{g}_k$ and an effective resonance mass $\tilde{m}_k$ are defined as

$$\tilde{g}_k \equiv g_k \exp\left[\frac{\sigma_k^2}{2\,T^2}\right] = g_k \exp\left[\frac{\Gamma_k^2}{2\,Q^2\,T^2}\right] , \quad \tilde{m}_k \equiv m_k - \frac{\sigma_k^2}{T} = m_k - \frac{\Gamma_k^2}{Q^2\,T} . \quad (4.55)$$

From Eq. (4.55) one can see that the presence of the width, firstly, may strongly modify the degeneracy factor g_k and, secondly, it may essentially shift the maximum of the mass attenuation towards the threshold or even below it. There are two corresponding effects which we named as *the near threshold thermal resonance enhancement* and *the near threshold resonance sharpening*. These effects formally appear due to the same reason as the famous Gamow window for the thermonuclear reactions in stars [240]: just above the resonance decay threshold the integrand $f_k(m)$ in (4.54) is a product of two functions of a virtual resonance mass m, namely, the Gaussian attenuation is an increasing function of m, while the Boltzmann exponent strongly decreases above the threshold. The resulting attenuation of their product has a maximum, whose shape, in contrast to the usual Gamow window, may be extremely asymmetric due to a threshold presence. Indeed, as one can see from the left panel of Fig. 4.39 the resulting mass attenuation of a resonance may acquire the form of the sharp and narrow peak that closely resembles an icy slide.

To our best knowledge a special attention to the thermal enhancement of the $\Delta_{33}(1232)$ isobar in a thermal medium was for the first time paid in [242], although no detailed explanation of this effect was given in [242]. The mass shift and shape modification of ρ meson in a hot hadronic matter were found in [243]. However, in both cases the found effects were not very strong since the considered resonances are not really wide. An analysis of the wide resonances' modification performed in [228] gave the astonishing results. From the effective resonance degeneracy $\tilde{g}_k$ and the effective resonance mass $\tilde{m}_k$ defined in (4.55) one can see that they essentially differ from their vacuum values for $T \ll \sigma_k$. The left panel of Fig. 4.39 demonstrates a strong modification of the σ-meson mass attenuation at low temperatures which leads to the near threshold resonance sharpening. A simple analysis shows that the effect of resonance sharpening is strongest, if the threshold mass is shifted above the convex part of the Gaussian distribution in (4.54), i.e. for $M_k^{Th} \geq \tilde{m}_k$ or for the temperatures T well below $T_k^+ \equiv \frac{\sigma_k^2}{m_k - M_k^{Th}}$. In this case near the threshold a resonance acquires a narrow effective width [228]

$$\Gamma_k^N(T) \simeq \frac{\ln(2)}{\frac{1}{T} - \frac{1}{T_k^+}} . \quad (4.56)$$

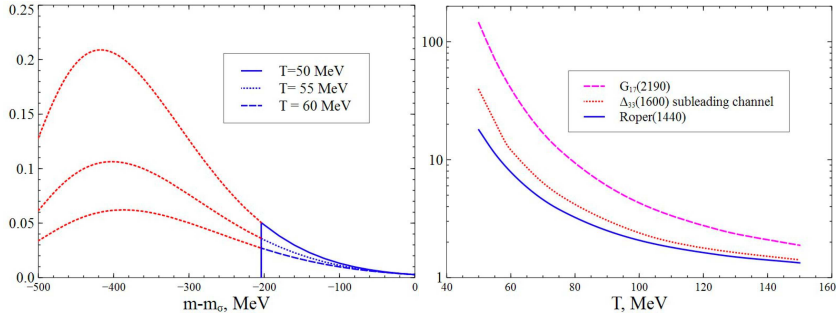

Figure 4.39: **Left panel:** Typical temperature dependence of the mass distribution $f_\sigma(m)/\phi(m_\sigma, T)$ (in units of 1/MeV, see Eq. (4.54)) for σ-meson with the mass $m_\sigma = 484$ MeV, the width $\Gamma_\sigma = 510$ MeV [241] and two pion threshold $M_\sigma^{\rm Th} = 2\,m_\pi \simeq 280$ MeV. In the left panel the short dashed curves demonstrate that at these temperatures the maximum of the full mass distribution is shifted well below the two pion threshold (vertical line at $m - m_\sigma = -204$ MeV) and, hence, the resulting effective mass attenuation of a wide resonance acquires an icy slide shape. **Right panel:** Typical temperature dependence of the resonance enhancement. The ratio $R(T) = \frac{F_k}{g_k\,\phi(m_k,T)}$ is shown for a few hadronic resonance decays. For wide resonances the effect of enhancement can be huge.

The right panel of Fig. 4.39 shows that an effect of near threshold enhancement compared to the thermal particle density of the same resonance taken with a vanishing width can be, indeed, huge for wide ($\Gamma \geq 450$ MeV) and medium wide ($\Gamma \simeq 300 - 400$ MeV) resonances. This effect can naturally explain the strong temperature dependence of hadronic pressure (4.52) at chemical FO, which in its turn generates the discussed power-like mass spectrum of hadrons. The other important conclusion from this analysis is that there is no sense to discuss the mass spectrum of hadronic resonances, empirical or Hagedorn, without a treatment of their width. Furthermore, the same is true for the QG bags which, according to the finite width model [238, 239], are heavy and wide resonances having the mass M_B larger than $M_0 \simeq 2.5$ GeV and the mean width of the form $\Gamma_B \simeq \Gamma_0(T)\left[\frac{M_B}{M_0}\right]^{\frac{1}{2}}$. Here $\Gamma_0(T)$ is a monotonically increasing function of temperature T and $\Gamma_0(0) \in [400; 600]$ MeV [238, 239].

The estimates of [228] based on the finite width model and the approach outlined above show that our best hopes to find the QG bags experimentally may be related to their sharpening and enhancement by a thermal medium. Then at the chemical FO temperatures of about $T \simeq 80 - 140$ MeV the *QG bags may appear directly or in decays as narrow resonances of the width about 50-150 MeV that have the mass about or above 2.5 GeV and that are absent in the tables of elementary particles.* Note that this range of chemical FO temperatures correspond to the center of mass energy of collision $\sqrt{s_{NN}} \in [4; 8]$ GeV [226, 229], which is in the range of the Dubna Nuclotron and NICA energies of collision. This energy range sets the most promising kinematic limit for the QG bag searches.

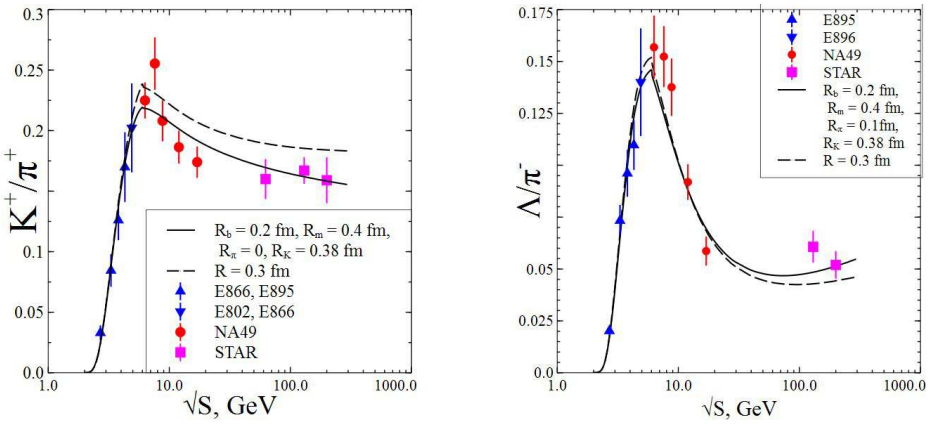

Figure 4.40: $\sqrt{s_{\rm NN}}$ dependences of K^+/π^+ (left panel) and Λ/π^- (right panel) ratios obtained in [227] within the multicomponent model are compared to that ones found within the one-component model [226].

Strangeness Horn description and chemical FO of strange particles.

A novel feature of principal importance implemented into the HRGM2 [226,227] is its multicomponent hard-core repulsion. One of the traditional difficulties of the HRGM was related to the Strangeness Horn description which up to recently was far from being satisfactory, although very different versions of the HRGM were used for this purpose (see [227] for a discussion and references). The HRGM2 with the multicomponent hard-core repulsion allows one to describe the hadron yield ratios from the low AGS to the highest RHIC energies. In [227] it was demonstrated that the variation of the hard-core radii of pions and kaons leads to a drastic improvement of the fit quality of the measured mid-rapidity data and for the first time such a model provides us with a complete description of the Strangeness Horn behavior as the function of the energy of collision without spoiling the fit quality of other ratios. The best global fit with $\chi^2/dof = 80.5/69 \simeq 1.16$ is found for an almost vanishing hard-core radius of pions of 0.1 fm and for the hard-core radius of kaons being equal to 0.38 fm, whereas the hard-core radius of all other mesons is found to be 0.4 fm and that one of baryons is equal to 0.2 fm. Fig. 4.40 demonstrates that within the multicomponent HRGM2 the mean deviation squared per data is $\chi^2/dof \simeq 7.5/14$ for K^+/π^+ and $\chi^2/dof \simeq 14/12$ for Λ/π^- ratios. Note that the value of χ^2/dof obtained for K^+/π^+ ratio is almost three times smaller compared to the best fit of the one-component model.

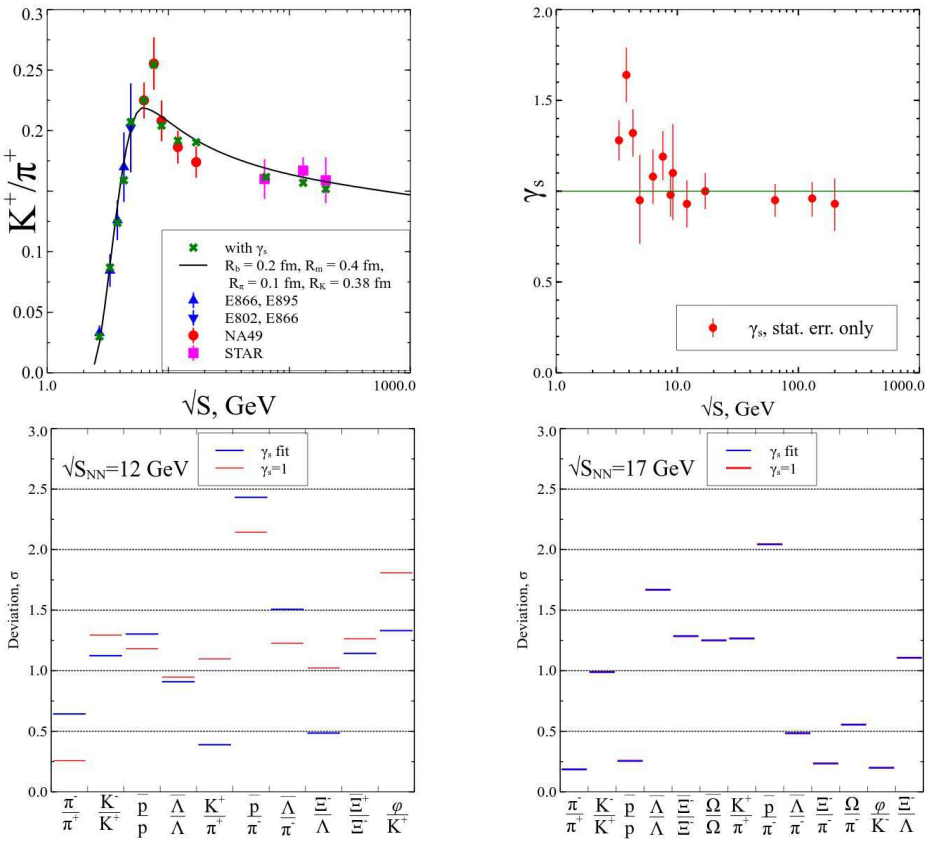

Figure 4.41: **Upper left panel:** $\sqrt{s_{\rm NN}}$ dependence of K^+/π^+ ratio for γ_s included into the fit (crosses) and for $\gamma_s = 1$ (solid curve) [227]. **Upper right panel:** $\sqrt{s_{\rm NN}}$ dependence of γ_s obtained from the new fit shown in the left panel. **Lower panels:** Comparison of the relative deviations of the fit results from experimental ratios is shown for $\sqrt{s_{NN}} \simeq 12$ GeV (left) and $\sqrt{s_{NN}} \simeq 17$ GeV (right).

Note, however, that in the multicomponent HRGM2 [227] in order to demonstrate its new abilities the strangeness suppression factor γ_s [244,245] was kept to be a unity. In the most recent version of the HRGM2 [246] we fixed the hard-core radii values found earlier and included γ_s into the fitting procedure. The obtained results have a better fit quality $\chi^2/dof = 63.4/55 \simeq 1.15$ for all 14 energies of collision in the range from the low AGS to the highest RHIC energies. As one can see from the upper left panel of Fig. 4.41 the γ_s fit greatly improves the K^+/π^+ ratio allowing us to correctly reproduce even the peak of the Strangeness Horn! From the lower

panels of this figure one, however, can deduce that the γ_s fit does not allow us to improve the description of the ratios of antihyperon-hyperon with nonzero strangeness, i.e. $\bar{\Lambda}/\Lambda$, $\bar{\Xi}/\Xi$ and $\bar{\Omega}/\Omega$. Also the antiproton to pion ratio is almost not improved by this fit. Moreover, the γ_s fit does not improve any ratios at $\sqrt{s_{\rm NN}} \simeq 17$ GeV (see the lower right panel in Fig. 4.41)!

In order to get rid of the phenomenological parameter γ_s and to further improve the fit quality of hadron multiplicities, we worked out an alternative concept of the strange particles chemical FO (SPFO). Its main assumption is that the SPFO occurs not at the hypersurface of chemical FO of hadrons (UDFO hereafter), which are built up from u and d quarks. A partial justification for such a hypothesis is given in [247–249], where the early chemical and kinetic FO of Ω hyperons and J/ψ mesons is discussed for the energies above the

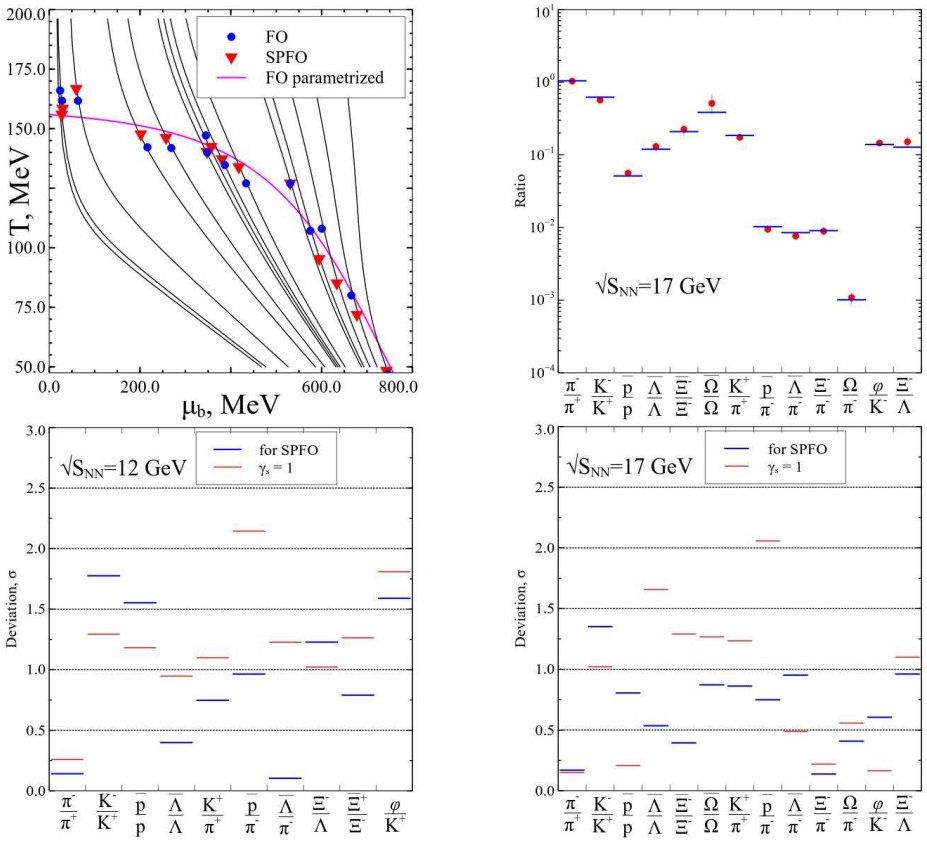

Figure 4.42: **Upper left panel:** μ_b and T values for UDFO (circles) and SPFO (triangles) are shown along with their isentropic trajectories (thin curves). **Upper right panel:** Example of the ratios description within the SPFO approach for $\sqrt{s_{\rm NN}} \simeq 17$ GeV. **Lower panels:** Same as in the lower panels of Fig. 4.41, but for the SPFO approach.

highest SPS energy. In addition to the SPFO temperature, baryonic chemical potential, the chemical potential for a third projection of isospin and strange chemical potential we employ an isentropic evolution of the system between the UDFO and the SPFO, and the conservation laws of baryonic charge, third projection of isospin and strangeness. Then the ratio of hadron $p1$ multiplicity to hadron $p2$ multiplicity is defined as

$$\frac{n_{p1}^{\rm final}}{n_{\rm p2}^{\rm final}} = \frac{\sum_X n_X^{\rm therm}(SPFO) Br(X \to p1) \frac{V_{\rm SPFO}}{V_{\rm UDFO}} + \sum_Y n_Y^{\rm therm}(UDFO) Br(Y \to p1)}{\sum_X n_X^{\rm therm}(SPFO) Br(X \to p2) \frac{V_{\rm SPFO}}{V_{\rm UDFO}} + \sum_Y n_Y^{\rm therm}(UDFO) Br(Y \to p2)}\,, \tag{4.57}$$

where the UDFO and SPFO 'volumes' (in fact, the corresponding hypersurface extents) are related via the baryonic n_B and isospin n_{I3} densities as $\frac{V_{\rm SPFO}}{V_{\rm UDFO}} = \frac{n_B^{\rm UDFO}}{n_B^{\rm SPFO}} = \frac{n_{\rm I3}^{\rm UDFO}}{n_{\rm I3}^{\rm SPFO}}$ due to conservation laws discussed above. The sums in Eq. (4.57) run over over all hadronic species including $p1$ and $p2$. In the latter case the corresponding branching ratios of decay are defined as $Br(p1 \to p1) = 1$ and $Br(p2 \to p2) = 1$, whereas for $X \neq p$ the branching ratios of decay $Br(X \to p)$ are taken from the Particle Data Group [237]. Due to the conservation

laws an effective number of degrees of freedom in the SPFO approach is the same as in case of the γ_s fit, but the fit quality is better $\chi^2/dof = 58.5/55 \simeq 1.06$ than for the γ_s fit. As one can see from Fig. 4.42, the fit of particle ratios which were problematic for the γ_s fit gets better, but not at an expense of an essential worsening of other ratios. Therefore, *the SPFO concept [246] outlined here provides us with more realistic and reliable approach, then a popular concept of strange suppression factor* γ_s.

Conclusions.

In this contribution we discussed the new results obtained within the multicomponent version of the HRGM2. This model allowed us to demonstrate that the most robust criterion of chemical FO is the adiabatic FO criterion of constant entropy per particle equal to 7.18. Searches for a physical explanation of this phenomenon, led us to a thorough analysis of effective hadronic mass spectrum. One of the most important conclusions of our studies is that the width of resonances and QG bags should unavoidably be included into statistical models and, hence, there is no sense to discuss the hadronic mass spectrum, empirical or Hagedorn, without accounting for the width of constituents. Moreover, we showed that the properties of wide resonances are essentially modified at chemical FO. Using the effect of near threshold resonance sharpening, we argued that, if the QG bags are formed in heavy ion collisions, then in experiments they may appear directly or in decays as narrow and heavy resonances with the width about 50-150 MeV which are absent in the tables of elementary particles. Our estimates show that such resonances may appear at the chemical FO temperatures of about $T \simeq 80 - 140$ MeV which corresponds to $\sqrt{s_{NN}} \in [4; 8]$ GeV. This range of the center of mass energy of collision exactly fits into the NICA Project.

Also we demonstrated that the HRGM2 with the multicomponent hard-core repulsion is able to drastically improve the description of K^+/π^+ and Λ/π^- ratios which were problematic for other formulations of HRGM. The most recent development of the HRGM2 includes a novel concept of the SPFO, which seems to be physically more adequate for a description of the strange hadron multiplicity ratios than the popular strangeness suppression factor approach. Therefore, one of the NICA physical tasks will be to find a physical reason of why the chemical FO of strange particles at $\sqrt{s_{\rm NN}} < 5$ GeV occurs at lower temperatures than the FO of hadrons built up from u and d quarks, and why it is vise versa for $\sqrt{s_{\rm NN}} > 9$ GeV.

All versions of the HRGM2 discussed here show that in a narrow range of collision energy $\sqrt{s_{\rm NN}} \in [4.3; 5]$ GeV there exists a certain irregularity in a behavior of the chemical FO temperature, in entropy density and in total particle number density. From the left panel of Fig. 4.37 it is seen that about 15 % increase of $\sqrt{s_{\rm NN}}$ leads to about 10 % change of the baryonic chemical potential μ_B, whereas the chemical FO temperature increases by a factor 1.5. From the left panel of Fig. 4.38 one can also see a simultaneous appearance of irregularity for s/T^3 ratio which jumps over 2 times, leading to 6.75 times resulting increase of entropy density while $\sqrt{s_{\rm NN}}$ increases by about 15 % only! Moreover, due to the adiabatic chemical FO such a small variation of collision energy leads to about 6.75 times increase of the particle density, while the chemical FO 'volume' growth is also about 20 % [226]! To reveal the physical cause for such a huge entropy density increase occurring at the collision energy interval $\sqrt{s_{\rm NN}} \in [4.3; 5]$ GeV and to elucidate its relation to the irregularities observed at slightly higher values of $\sqrt{s_{\rm NN}}$ which are known as the Strangeness Horn, the Step and the Kink, we need an accelerator of new generation working in this energy range with much higher experimental accuracy. It seems that the NICA Project is perfectly suited to resolve these tasks.

4.22 Phase transition signatures in hydrodynamic simulations of heavy-ion collisions at NICA–FAIR energies

A.V. Merdeev[1,2], L.M. Satarov[1,2], I.N. Mishustin[1,2]

[1] *Frankfurt Institute for Advanced Studies, Frankfurt am Main, Germany*
[2] *National Research Center, Kurchatov Institute, Moscow, Russia*

We use (3+1) dimensional ideal hydrodynamics to describe the space-time evolution of strongly interacting matter created in A+A collisions at NICA–FAIR energies. The initial state is represented by two Lorentz–boosted cold nuclei. Two equations of state are used for comparison: the first one corresponding to resonance hadron gas and the second one including the deconfinement phase transition. The parameters of collective flows and hadronic spectra are calculated under assumption of the isochronous freeze–out. It is shown that the deconfinement phase transition leads to broadening of net–baryon rapidity distributions, suppressed directed

flow of protons and formation of pion antiflow in the central rapidity region. These effects are most pronounced at bombarding energies around 10 AGeV, when the system spends the longest time in the mixed phase.

The attractive feature of the hydrodynamic model of heavy–ion collisions is its capability to probe sensitivity of observables to the equation of state (EoS) of matter created in such reactions. We have performed [250] simulations of heavy–ion collisions by using a new version of (3+1)–dimensional ideal hydrodynamics, suitable to the FAIR and NICA energy domain. In these calculations we have used a new EoS [251] (EoS–PT) with the deconfinement phase transition and finite size effects. The hadronic phase of matter in this EoS–PT is described as the hadron resonance gas with the excluded volume corrections. The quark–gluon phase is introduced by using the MIT Bag model. The phase transition boundaries and characteristics of the mixed phase (MP) are found by using the Gibbs conditions with the strangeness neutrality constraint. To probe sensitivity to the phase transition, we also made calculations with the EoS of ideal hadron gas (EoS–HG). To provide stability of initial nuclei we add the Skyrme–like mean field [251].

We start our simulation at the stage when two cold equilibrium nuclei approach each other. It is assumed that they have the Woods-Saxon density distributions in their rest frames.

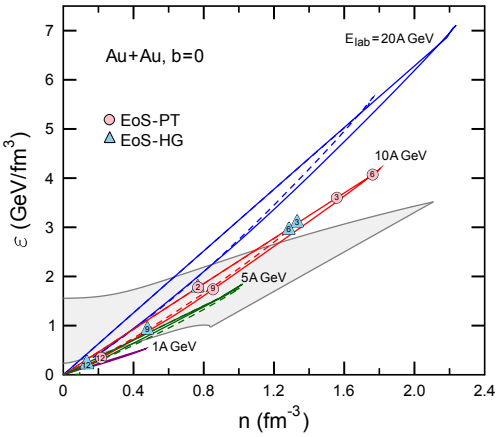

Figure 4.43: Time evolution of matter in central Au+Au collisions at different $E_{\rm lab}$. Shown are values of energy and baryon densities averaged over the central box. The dashed and solid lines correspond to EoS–HG and EoS–PT, respectively. Numbers in triangles and circles give the c.m. time in fm/c. Shading shows the MP region of deconfinement phase transition.

Figure 12.14 represents dynamical trajectories of matter (in the central box $|x|$, $|y|$, $\gamma_0|z| < 1$ fm) produced in central Au+Au collisions at different bombarding energies. As compared with the EoS–HG, the calculations with the phase transition predict longer life-times of states with maximal compression and additional time delays of expansion stages. The largest life times of the MP in central Au+Au collisions are about 4 fm/c. They are reached at $E_{\rm lab} \sim 10$ AGeV. We have checked that properties of states with maximum compression obtained in our simulations agree well with predictions of a simple shock model [252]. At lower energies the MP region is traversed only partly, while at higher $E_{\rm lab}$ the produced matter expands too fast. The MP region can be achieved only for $E_{\rm lab} \gtrsim 4$ AGeV.

The proton rapidity distributions predicted for central Au+Au collisions at $E_{\rm lab} \sim 10$ AGeV are presented in Fig. 12.15. These distributions are calculated by using the Cooper–Frye formula [253]. Up to now we apply the approximation of the isochronous freeze–out, choosing freeze–out times $t_{\rm fr}$ from best fits of observed proton and pion rapidity distributions. In addition to free hadrons, we add contributions from decay of hadronic resonances with masses below 2 GeV. Our calculations with the EoS–PT show that the best choice of $t_{\rm fr}$ corresponds roughly to the end of the hadronization stage for central cells.

As compared to the EoS–HG, the calculation with the phase transition predicts a noticeably broader rapidity distribution. In this case the agreement with experimental data outside the central rapidity region is better than in the purely hadronic scenario. We have checked that this broadening takes place due to larger pressure gradients in the beam direction in the case of EoS–PT.

Figure 4.45 shows our predictions for the proton and pion directed flows v_1 in the 10 AGeV Au+Au and

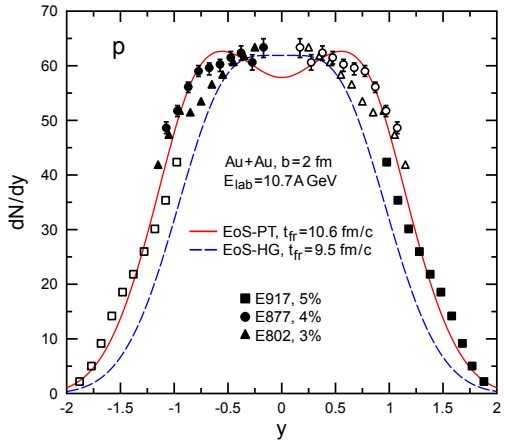

Figure 4.44: Rapidity distributions of protons in 10.7 A GeV Au+Au collision with the impact parameter $b = 2$ fm. Solid and dashed lines are calculated with EoS–PT and EoS-HG, respectively. Full dots are experimental data [254–256], circles are obtained by reflection with respect to midrapidity.

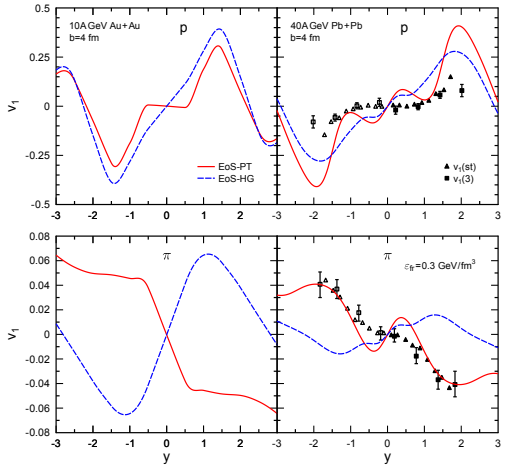

Figure 4.45: Directed flows of protons (upper panels) and charged pions (bottom panels) as functions of c.m. rapidity in 10 A GeV Au+Au (left panels) and in 40 A GeV Pb+Pb (right panels) collisions. Solid (dashed) lines are calculated with EoS–PT (EoS–HG). Full symbols are measured experimental data [257], while the open ones are obtained by reflection.

40 AGeV Pb+Pb collisions. It is assumed that freeze–out occurs when the energy density in the central cell becomes lower than $\varepsilon_{\rm fr} = 0.3$ GeV/fm^3. For both energies the calculations with EoS–PT predict the formation of pion antiflow, i. e. the negative slope of $v_1(y)$ in the central rapidity region ($|y| \lesssim 1$). In this case experimental data at $E_{\rm lab} = 40$ AGeV are in qualitative agreement with our calculation. On the other hand, the simulations with the EoS–HG predict positive slopes of the directed flow. One can see that the sensitivity to the EoS is larger at the AGS energy 10 AGeV. Similar conclusions that the phase transition at AGS energies leads to the proton antiflow in a central rapidity region have been made in [258–260].

In conclusion, we show that the FAIR–NICA energy domain is especially interesting due to possible manifestations of the deconfinement phase transition. According to our analysis, strong pressure gradients are formed at the hadronization stage in this energy domain. These gradients appear due to the excitation of deflagration shocks in the case with phase transition. This leads to an additional acceleration of matter as compared to a purely hadronic scenario. Our calculations with the phase transition lead to an additional broadening of proton rapidity distribution ("extra–push"), to the appearance of antiflow ($v_1'(y) < 0$) in the central rapidity region and to enhanced elliptic flows of secondary hadrons.

This work was supported by the Helmholtz International Center for FAIR (Germany) and the grant NSH–215.2012.2 (Russia).

Bibliography

[1] I. Melo et al., arXiv:0902.1607.

[2] M. A. Stephanov, Prog. Theor. Phys. Suppl. **153**, 139 (2004); Int. J. Mod. Phys. **A 20,** 4385 (2005).

[3] Y. Hatta and T. Ikeda, Phys. Rev. **D 67,** 014028 (2003).

[4] K. Fukushima, Phys. Rev. **C 67,** 025203 (2003).

[5] P. Costa, M.C. Ruivo and Yu.L. Kalinovsky, Phys. Lett. **B 560,** 171 (2003).

[6] P. Costa, M.C. Ruivo, Yu.L. Kalinovsky and C.A. de Sousa, Phys. Rev. **C 70,** 025204 (2004);

[7] P. Costa, M.C. Ruivo, C.A. de Sousa and Yu.L. Kalinovsky, Phys. Rev. **D 70,** 116013 (2004);

[8] P. Costa, M.C. Ruivo, C.A. de Sousa and Yu.L. Kalinovsky, Phys. Rev. **D 71,** 116002 (2005).

[9] P. Costa, M.C. Ruivo, C.A. de Sousa and H. Hansen, Europhysics Letters **86**, 31001 (2009), [arXiv:0801.3616].

[10] E. Beth and G. E. Uhlenbeck, Physica **4**, 915 (1937).

[11] R. Dashen, S.-K. Ma and H. J. Bernstein, Phys. Rev. **187,** 345 (1969).

[12] R. Hagedorn, Nuovo Cim. Suppl. **3**, 147 (1965); Nuovo Cim. **56A**, 1027 (1968).

[13] P. Braun-Munzinger, K. Redlich and J. Stachel; Eds. R. C. Hwa and X.-N Wang *in Quark-Gluon Plasma 3*, (World Scientific, Singapore 2003).

[14] P. Castorina, K. Redlich and H. Satz, Eur. Phys. J. **C 59,** 67 (2009).

[15] L. McLerran and R. D. Pisarski, Nucl. Phys. **A 796,** 83 (2007), [arXiv:0706.2191].

[16] D. Rischke, G. Levin, eds, *Quark Gluon Plasma. New Discoveries at RHIC: A Case of Strongly Interacting Quark Gluon Plasma. Proceedings, RBRC Workshop, Brookhaven*, (Upton, USA, May 14-15, 2004), 2005, p. 169.

[17] J. Adams *et al.* (STAR Collaboration) Nucl. Phys. **A 757,** 102 (2005).

[18] K. Adcox *et al.* (PHENIX Collaboration), Nucl. Phys. **A 757,** 184 (2005).

[19] D. d'Enterria, [arXiv: nucl-ex/0611012].

[20] J.-Y. Ollitrault, Phys. Rev. **D 46,** 229 (1992); S.A. Voloshin, Nucl. Phys. **A 715,** 379 (2003).

[21] D. Molnar, [arXiv: nucl-th/0408044].

[22] S. M. Troshin, N. E. Tyurin, Phys. Rev. **D 49,** 4427 (1994).

[23] S. M. Troshin, N. E. Tyurin, J. Phys. G. **29,** 1061 (2003).

[24] J. D. Bjorken, Nucl. Phys. Proc. Supl. **B 25**, 253 (1992).

[25] D. Diakonov, [arXiv: hep-ph/0406043], JLAB-THY-04-12, Eur. Phys. J. **A 24,** 3 (2005);
D. Diakonov, V. Petrov, Phys. Lett. **B 147,** 351 (1984).

[26] T. Goldman, R. W. Haymaker, Phys. Rev. **D 24,** 724 (1981).

[27] W. Heisenberg, Z. Phys. **133**, 65 (1952).

[28] P. Carruthers, Nucl. Phys. **A 418,** 501 (1984).

[29] L. L. Jenkovszky, S. M. Troshin, N. E. Tyurin, [arXiv:0910.0796].

[30] A. A. Logunov, V. I. Savrin, N. E. Tyurin, O. A. Khrustalev, Teor. Mat. Fiz. 6, 157 (1971).

[31] S.M. Troshin, N.E. Tyurin, Int. J. Mod. Phys. **A 22,** 4437 (2007).

[32] S.A. Voloshin, [arXiv: nucl-th/0410089].

[33] S. A. Voloshin, A. M. Poskanzer, Phys. Lett. **B 474,** 27 (2000).

[34] T. T. Chou, C.-N. Yang, Int. J. Mod. Phys. **A 6,** 1727 (1987); Adv. Ser. Direct. High Energy Phys. 2, 510 (1988).

[35] T. T. Chou, C. N. Yang, Phys. Lett. **B 128,** 457 (1983); Phys. Rev. **D 32,** 1692 (1985).

[36] F. Antinori; Eds. A. Sissakian, G. Kozlov, E. Kolganova *Proc. of the XXXII International Symposium on Multiparticle Dynamics*, (Alushta, Crimea, Ukraine, September 2002), 77.

[37] W. Broniowski, W. Florkowski, Phys. Rev. **C 65,** 024905 (2002).

[38] J. Castillo (STAR Collaboration), Int. J. Mod. Phys. **A 20,** 4380 (2005).

[39] J. Zimányi, P. Lévai, T. S. Biró, *Heavy Ion Phys.* 17, 205 (2003); J. Phys. G. **31,** 711 (2005).

[40] G. Wang (STAR Collaboration), J. Phys. G. **34,** 1093 (2007), [arXiv: nucl-ex/0701045].

[41] B.B. Back et al., (PHOBOS Collaboration), Phys. Rev. Lett. **97,** 012301 (2006).

[42] A.H. Tang (STAR collaboration), J. Phys. G. **31,** S35 (2005).

[43] J. Adams *et al.*, (STAR Collaboration), Phys. Rev. **C 73,** 034903 (2006).

[44] V. S. Pantuev, [arXiv:hep-ph/0604268].

[45] S. Abreu *et al.*, [arXiv:0711.0974].

[46] A.N. Sissakian *et al.*, (NICA Collaboration),J. Phys. G. **36,** 064069 (2009).

[47] T. Hatsuda, J. Phys. G. **34,** S287 (2007)

[48] M. A. Stephanov, PoS **LAT2006**, 024 (2006).

[49] B. Berdnikov and K. Rajagopal, Phys. Rev. **D 61,** 105017 (2000)

[50] C. Nonaka and M. Asakawa, Phys. Rev. **C 71,** 044904 (2005)

[51] T. Hatsuda and T. Kunihiro, Phys. Rep. **247,** 221 (1994)

[52] T. Kunihiro, Phys. Lett. **B 271,** 395 (1991)

[53] M. Asakawa and K. Yazaki, Nucl. Phys. **A 504,** 668 (1989)

[54] L. Ahle *et al.* (E802 Collaboration), Phys. Rev. **C 60,** 064901 (1999).

[55] J. Barrette *et al.* (E877 Collaboration), Phys. Rev. **C 62,** 024901 (2000).

[56] B. B. Back *et al.*, (E917 Collaboration), Phys. Rev. Lett. **86,** 1970 (2001).

[57] J. Stachel, Nucl. Phys. **A 654,** 119 (1999).

[58] H. Appelshäuser *et al.* (NA49 Collaboration), Phys. Rev. Lett. **82,** 2471 (1999).

[59] T. Anticic *et al.* (NA49 Collaboration), Phys. Rev. **C 69,** 024902 (2004).

[60] C. Alt *et al.* (NA49 Collaboration), Phys. Rev. **C 73,** 044910 (2006).

[61] C. Blume (NA49 Collaboration), J. Phys. G. **34,** 951 (2007).

[62] H. Strobele (NA49 Collaboration), [arXiv:0908.2777 [nucl-ex]].

[63] Yu.B. Ivanov, V.N. Russkikh, and V.D. Toneev, Phys. Rev. **C 73**, 044904 (2006).

[64] Yu.B. Ivanov and V.N. Russkikh, PoS(CPOD07)008 (2007), [arXiv:0710.3708 [nucl-th]].

[65] V.M. Galitsky and I.N. Mishustin, Sov. J. Nucl. Phys. **29**, 181 (1979).

[66] A.S.Khvorostukhin, V.V.Skokov, K.Redlich, and V.D.Toneev, Eur. Phys. J. **C 48,** 531 (2006).

[67] C. Alt *et al.* (NA49 Collaboration), Phys. Rev. **C 77,** 024903 (2008).

[68] C. Alt *et al.* (NA49 Collaboration), Phys. Rev. **C 68,** 034903 (2003).

[69] I.C. Arsene, *et al.*, Phys. Rev. **C 75,** 034902 (2007).

[70] M. Gazdzicki and M. I. Gorenstein, Acta. Phys. Polon. **B 30,** 2705 (1999), [arXiv:hep-ph/9803462].

[71] Yu.B. Ivanov, [[arXiv:1001.0670 [nucl-th]], Phys. Lett. **B 690**, 358 (2010).

[72] M. A. Stephanov, K. Rajagopal and E. V. Shuryak, Phys. Rev. Lett. **81,** 4816 (1998), [arXiv:hep-ph/9806219].

[73] I. N. Mishustin, [arXiv:hep-ph/0512366].

[74] A. Andronic *et al.*, Nucl. Phys. **A 837,** 65 (2010), [arXiv:0911.4806 [hep-ph]].

[75] D. B. Blaschke, F. Sandin, V. V. Skokov and S. Typel, Acta Phys. Polon. Supp. **3**, 741 (2010), [arXiv:1004.4375 [hep-ph]].

[76] E. Fermi, Prog. Theor. Phys. **5**, 570 (1950).

[77] I. Pomeranchuk Proc. USSR Academy of Sciences (in Russian) **43**, 889 (1951).

[78] L. D Landau, Izv. Akad. Nauk Ser. Fiz. **17** 51-64 (1953).

[79] R. Hagedorn Suppl. Nuovo Cimento **2**, 147 (1965).

[80] P. Braun-Munzinger, D. Magestro, K. Redlich and J. Stachel, Phys. Lett. **B 518,** 41 (2001)

[81] J. Cleymans, H. Oeschler, K. Redlich and S. Wheaton, [arXiv:hep-ph/0607164].

[82] J. Letessier, J. Rafelski (2002), *Hadrons quark - gluon plasma, Cambridge Monogr.*, Part. Phys. Nucl. Phys. Cosmol. **18**, 1, and references therein

[83] F. Becattini, P. Castorina, A. Milov and H. Satz, Eur. Phys. J. **C 66,** 377 (2010), [arXiv:0911.3026 [hep-ph]].

[84] J. Cleymans, B. Kampfer, M. Kaneta, S. Wheaton and N. Xu, Phys. Rev. **C 71,** 054901 (2005)

[85] G. Torrieri, S. Steinke, W. Broniowski, W. Florkowski, J. Letessier Comput. Phys. Commun. **167**, 229 (2005), [arXiv:nucl-th/0404083].

[86] G. Torrieri, S. Jeon, J. Letessier and J. Rafelski, Comput. Phys. Commun. **175**, 635 (2006), [arXiv:nucl-th/0603026].

[87] K. Redlich, A. Andronic, F. Beutler, P. Braun-Munzinger and J. Stachel, J. Phys. G. **36,** 064021 (2009), [arXiv:0903.1610 [hep-ph]].

[88] G. Torrieri, R. Bellwied, C. Markert and G. Westfall, [arXiv:1001.0087 [nucl-th]].

[89] V. Koch and T. Schuster, [arXiv:0911.1160 [nucl-th]].

[90] I. Arsene *et al.* (BRAHMS Collaboration), Nucl. Phys. **A 757,** 1 (2005)

[91] B. B. Back *et al.*, Nucl. Phys. **A 757,** 28 (2005)

[92] M. Gyulassy and L. McLerran, Nucl. Phys. **A 750,** 30 (2005), [arXiv:nucl-th/0405013].

[93] E. Shuryak, Progr. Part. Nucl. Phys. **53,**273 (2004), [arXiv:hep-ph/0312227].

[94] P. F. Kolb and U. W. Heinz, [arXiv:nucl-th/0305084].

[95] U. W. Heinz and P. F. Kolb, Nucl. Phys. **A 702,** 269 (2002).

[96] D. Teaney, J. Lauret and E. V. Shuryak, [arXiv:nucl-th/0110037].

[97] P. Romatschke and U. Romatschke, Phys. Rev. Lett. **99,** 172301 (2007).

[98] P. F. Kolb, U. W. Heinz, P. Huovinen, K. J. Eskola and K. Tuominen, Nucl. Phys. **A 696,** 197 (2001), [arXiv:hep-ph/0103234].

[99] W. Broniowski, M. Chojnacki, W. Florkowski and A. Kisiel, [arXiv:0801.4361 [nucl-th]].

[100] T. Hirano and K. Tsuda,Nucl. Phys. **A 715,** 821 (2003)

[101] J. Randrup and S. Mrowczynski, Phys. Rev. **C 68,** 034909 (2003), [arXiv:nucl-th/0303021].

[102] O. Fochler, Z. Xu and C. Greiner, Phys. Rev. Lett. **102,** 202301 (2009) [arXiv:0806.1169 [hep-ph]].

[103] J. Noronha-Hostler, J. Noronha and C. Greiner, Phys. Rev. Lett. **103,** 172302 (2009), [arXiv:0811.1571 [nucl-th]].

[104] W. Busza (PHOBOS Collaboration), [arXiv:0907.4719 [nucl-ex]].

[105] G. Torrieri, [arXiv:0911.4775 [nucl-th]].

[106] H. Song and U. W. Heinz, Phys. Rev. **C 78,** 024902 (2008), [arXiv:0805.1756 [nucl-th]].

[107] G. Torrieri, Phys. Rev. **C 76,** 024903 (2007), [arXiv:nucl-th/0702013].

[108] L. Van Hove, Phys. Lett. **B 118,** 138 (1982).

[109] P. Seyboth *et al.* (NA49 Collaboration), Acta. Phys. Polon. **B 36,** 565 (2005).

[110] M. Lisa, AIP Conf. Proc. **828**, 226 (2006), [arXiv:nucl-ex/0512008].

[111] J. Randrup and J.Cleymans, Phys. Rev. **C 74,** 047901 (2006)

[112] H-Th. Elze, J. Rafelski and L. Turko, Phys. Lett. **B 506,** 123 (2001)

[113] L. Turko, J. Phys. G. **35,** 044019 (2008)

[114] S. Gupta, PoS(Lattice 2010) 007, [arXiv:1101.0109 [hep-lat]].

[115] M. Cheng *et al.*, Phys. Rev. **D 79,** 074505 (2009), [arXiv:0811.1006 [hep-lat]].

[116] A. Andronic, P. Braun-Munzinger, K. Redlich and J. Stachel, Phys. Lett. **B 571,** 36 (2003), [arXiv:nucl-th/0303036].

[117] R. V. Gavai and S. Gupta, [arXiv:1001.3796 [hep-lat]].

[118] C. Schmidt, Net-baryon number fluctuations in (2+1)-flavor QCD, arXiv:1007.5164 [hep-lat].

[119] F. Karsch and K. Redlich, Phys. Lett. **B 695,** 136 (2011), [arXiv:1007.2581 [hep-ph]].

[120] M. M. Aggarwal *et al.* (STAR Collaboration), Phys. Rev. Lett. **105,** 022302 (2010), [arXiv:1004.4959 [nucl-ex]].

[121] O. Kaczmarek *et al.*, Phys. Rev. **D 83,** 014504 (2011), [arXiv:1011.3130 [hep-lat]].

[122] R. V. Gavai and S. Gupta, Phys. Rev. **D 78,** 114503 (2008), [arXiv:0806.2233 [hep-lat]].

[123] A. Andronic, D. Blaschke, P. Braun-Munzinger *et al.*, Nucl. Phys. **A 837,** 65-86 (2010), [arXiv:0911.4806 [hep-ph]].

[124] C. R. Allton, M. Doring, S. Ejiri *et al.*, Phys. Rev. **D 71,** 054508 (2005), [hep-lat/0501030].

[125] F. Weber, *Pulsars as astrophysical laboratories for nuclear and particle physics*, (IOP Publishing, Bristol, 1999).

[126] N. K. Glendenning, *Compact Stars*, (Springer, New York, 2000).

[127] T. Klähn *et al.*, Phys. Rev. **C 74,** 035802 (2006), [arXiv:nucl-th/0602038].

[128] P. Demorest, T. Pennucci, S. Ransom, M. Roberts and J. Hessels, Nature **467**, 1081 (2010), [arXiv:1010.5788 [astro-ph.HE]].

[129] T. Klähn *et al.*, Phys. Lett. **B 654,** 170 (2007) [arXiv:nucl-th/0609067].

[130] C. Fuchs, Progr. Part. Nucl. Phys. **56,**1 (2006).

[131] P. Danielewicz, R. Lacey and W. G. Lynch, Science **298**, 1592 (2002), [arXiv:nucl-th/0208016].

[132] I. C. Arsene *et al.*, Phys. Rev. **C 75,** 034902 (2007), [arXiv:nucl-th/0609042].

[133] D. B. Blaschke, F. Sandin, V. V. Skokov and S. Typel, Acta Phys. Polon. Supp. **3**, 741 (2010) [arXiv:1004.4375 [hep-ph]].

[134] D. Blaschke, S. Fredriksson, H. Grigorian, A. M. Öztas and F. Sandin, Phys. Rev. **D 72,** 065020 (2005), [arXiv:hep-ph/0503194].

[135] M. Baldo, G. F. Burgio and H. J. Schulze,]arXiv:astro-ph/0312446].

[136] D. B. Blaschke, D. Gomez Dumm, A. G. Grunfeld, T. Klähn and N. N. Scoccola, Phys. Rev. **C 75,** 065804 (2007) [arXiv:nucl-th/0703088].

[137] M. Alford, D. Blaschke, A. Drago, T. Klähn, G. Pagliara and J. Schaffner-Bielich, Nature **445**, E7 (2007), [arXiv:astro-ph/0606524].

[138] D. Blaschke, T. Klähn and F. Weber, "Constraints on the High-Density Nuclear Equation of State from Neutron Star Observables," in: *Astronomy and Relativistic Astrophysics – New Phenomena and New States of Matter in the Universe*, (Word Scientific, 2010), p. 31, [arXiv:0808.1279 [astro-ph]].

[139] D. Blaschke, T. Klähn and F. Weber, "Compact star constraints on the high-density equation of state," in: *Strongly Interacting Matter - The CBM Physics Book*, Lecture Notes in Physics **814**, (Springer, 2011), p. 158.

[140] R. Bellwied, C. Markert, Phys. Lett. **B 691,** 208 (2010).

[141] C. Markert, R. Bellwied, I. Vitev, Phys. Lett. **B 669,** 92 (2008).

[142] H. Hansen *et al.*, Phys. Rev. **D 75,** 065004 (2007).

[143] W. Broniowski and W. Florkowski, Phys. Rev. Lett. **87**, 272302 (2001).

[144] P. Braun-Munzinger and J. Stachel, *arXiv*:1101.3167.

[145] J. Rafelski, J. Phys. **G 28**, 1833 (2002).

[146] C. Blume, *arXiv*:1111.7140.

[147] S. Bass and A. Dumitru, Phys. Rev. **C 61**, 064909 (2000).

[148] J. Knoll, Nucl. Phys. **A 821**, 235 (2009).

[149] H. van Hecke, H. Sorge, and N. Xu, Phys. Rev. Lett. **81**, 5764 (1998).

[150] U. Heinz and G. Kestin, PoS(CPOD2006), **038** (2006).

[151] C. Blume and C. Markert, Prog. Part. Nucl. Phys. **66**, 834 (2011).

[152] J. Adams *et al.*, (STAR Collaboration), Phys. Rev. Lett. **92**, 112301 (2004).

[153] F. Becattini, J. Manninen, and M. Gaździcki, Phys. Rev. **C 73**, 044905 (2006).

[154] R. Rapp and E. Shuryak, Phys. Rev. Lett. **86**, 2980 (2001).

[155] R. Stock *et al.*, *arXiv*:0911.5705.

[156] M.M. Aggarwal *et al.*, (STAR Collaboration), Phys. Rev. **C 83**, 034910 (2011).

[157] T. Anticic *et al.*, (NA49 Collaboration), Phys. Rev. **C 83**, 014901 (2011).

[158] M. Floris *et al.* (for the ALICE Collaboration), *arXiv*:1108.3257.

[159] P. Braun-Munzinger, J. Stachel, and C. Wetterich, Phys. Lett. **B 596**, 61 (2004).

[160] V.K. Magas, L.P. Csernai and D.D. Strottman, Phys. Rev. **C 64**, 014901 (2001); and V.K. Magas, L.P. Csernai and D.D. Strottman, Nucl. Phys.**A 712**, 167 (2002).

[161] Martha W. Evans, Francis H.Harlow, "The Particle In Cell Method for Hydrodynamic Calcultions", Los Alamos Scienific Laboratory, (1957).

[162] Ben-Hao Sa, Xiao-Mei Li, Shou-Yang Hu, Shou-Ping Li, Jing Feng, and Dai-Mei Zhou. Phys. Rev. **C 75**, 054912 (2007); and Yu-Liang Yan, Dai-Mei Zhou, Bao-Guo Dong, Xiao-Mei Li, Hai-Liang Ma, and Ben-Hao Sa. Phys. Rev. **C 79**, 054902 (2009); arXiv: 0903.0915 v2 [nucl-th].

[163] J. Cleymans, H. Oeschler, K. Redlich and S. Wheaton, Phys. Rev. **C 73**, 034905 (2006).

[164] L.P. Csernai *et al.*, submitted to Cent. Eur. J. Phys. (2012)

[165] J. Rafelski, Phys. Lett. **B 262**, 333 (1991).

[166] T. Csörgő, and L.P. Csernai, Phys. Lett. **B 333**, 494 (1994).

[167] M. A. Stephanov, Phys. Rev. Lett. bf 102, 032301 (2009); and M. Asakawa, S. Ejiri and M. Kitazawa, Phys. Rev. Lett. **103**, 262301 (2009).

[168] L.P. Csernai, and Z. Néda, Phys. Lett. **B 337**, 25 (1994).

[169] Yu-Liang Yan, Yun Cheng, Dai-Mei Zhou, Bao-Guo Dong, Xu Cai, Ben-Hao Sa, and Laszlo P. Csernai, submitted to Journal of Physics G (2012).

[170] P. Huovinen and D. Molnar, Phys. Rev. **C 79**, 014906 (2009).

[171] I. Bouras *et al.*, Phys. Rev. **C 82**, 024910 (2010).

[172] A. N. Sissakian *et al.*, MPD Conceptual Design Report, `http://nica.jinr.ru/files/CDR_MPD/MPD_CDR_en.pdf`

[173] A. El, Z. Xu and C. Greiner, Phys. Rev. **C 81**, 041901 (2010).

[174] G. S. Denicol, T. Koide and D. H. Rischke, Phys. Rev. Lett. **105**, 162501 (2010).

[175] T. Klähn, D. Blaschke and F. Weber, [arXiv:1101.6061 [nucl-th]].

[176] F. Rami *et al.* (FOPI Collaboration), Nucl. Phys. **A 646**, 367 (1999) [nucl-ex/9812005].
[177] W. Reisdorf *et al.* (FOPI Collaboration), Nucl. Phys. **A 876**, 1 (2012).
[178] H. Sorge, Phys. Rev. Lett. **78**, 2309 (1997) [nucl-th/9610026].
[179] L. Shi, P. Danielewicz and R. Lacey, Phys. Rev. **C 64**, 034601 (2001) [nucl-th/0104074].
[180] P. Danielewicz *et al.,* Phys. Rev. Lett. **81**, 2438 (1998) [nucl-th/9803047].
[181] D. H. Rischke and M. Gyulassy, Nucl. Phys. **A 608**, 479 (1996) [nucl-th/9606039].
[182] B. Friman, F. Karsch, K. Redlich and V. Skokov, Eur. Phys. J. **C 71**, 1694 (2011).
[183] S. Pal and S. Pratt, Phys. Lett. B **578**, 310 (2004) [nucl-th/0308077].
[184] G. Wolschin, Prog. Part. Nucl.Phys **59**, 374 (2007).
[185] Y. Mehtar-Tani, G. Wolschin, Phys. REv. Lett **102**, 182301 (2009).
[186] Y. Mehtar-Tani, G. Wolschin, EPL **94**, 62003 (2011).
[187] C. Blume *et al.*, PoS (*Confinement*) **8**, 110, (2008).
[188] I. G. Bearden *et al.*, Phys. Rev. Lett **93** 102301 (2004).
[189] F. Videbaek, O. Hansen, Phys. Rev. **C 52**, 2684 (1995).
[190] I. C. Arsene *et al.*, Phys. Lett. **B 677**, 267 (2009).
[191] Y. Mehtar-Tani, G. Wolschin, Phys. Rev. **C 80**, 054905 (2009).
[192] Y. Mehtar-Tani, G. Wolschin, Phys. Lett.**B 688**, 174 (2010).
[193] K. Nakamura *et al.* (Particle Data Group), J. Phys. **G 37**, 075021 (2010) and 2011 partial update for the 2012 edition.
[194] A. V. Anisovich *et al.*, Phys. Lett. **B 449**, 154 (1999);
[195] B. S. Zou, Nucl. Phys. **A 692**, 362 (2001) [arXiv:hep-ph/0011174].
[196] M. Ablikim *et al.* (BES Collaboration), Phys. Lett. **B 603**, 138 (2004) [arXiv:hep-ex/0409007];
[197] M. Ablikim *et al.* (BES Collaboration), Phys. Lett. **B 607**, 243 (2005) [arXiv:hep-ex/0411001].
[198] D. Barberis *et al.* (WA102 Collaboration), Phys. Lett. **B 453**, 305 (1999);
[199] D. Barberis *et al.* (WA102 Collaboration), Phys. Lett.**B 453**, 316 (1999) [arXiv:hep-ex/9903043];
[200] D. Barberis *et al.* (WA102 Collaboration), Phys. Lett. **B 462**, 462 (1999) [arXiv:hep-ex/9907055].
[201] R. R. Akhmetshin *et al.* (CMD-2 Collaboration), Phys. Lett. **B 648**, 28 (2007) [hep-ex/0610021];
[202] M. Alekseev *et al.* (COMPASS Collaboration), Phys. Rev. Lett. **104**, 241803 (2010) [arXiv:0910.5842 [hep-ex]].
[203] G. E. Brown and M. Rho, Phys. Rev. Lett. **66**, 2720 (1991).
[204] D. Parganlija, F. Giacosa, D. H. Rischke, Phys. Rev. **D 82**, 054024 (2010) [arXiv:1003.4934 [hep-ph]].
[205] S. Janowski, D. Parganlija, F. Giacosa and D. H. Rischke, Phys. Rev. **D 84**, 054007 (2011) [arXiv:1103.3238 [hep-ph]].
[206] S. Strüber and D. H. Rischke, Phys. Rev. **d 77**, 085004 (2008) [arXiv:0708.2389 [hep-th]].
[207] B. Borderie *et al.*, Phys. Rev. Lett. **86**, 3252 (2001).
[208] Ph. Chomaz, M. Colonna, and J. Randrup, Phys. Rep. **389**, 263 (2004).
[209] J. Randrup, Phys. Rev. Lett. **92**, 122301 (2004).
[210] J. Randrup, Phys. Rev. **C 79**, 054911 (2009).
[211] J. Randrup, Phys. Rev. C **82**, 034902 (2010).
[212] J. Steinheimer and J. Randrup, Phys. Rev. Lett. **109**, 212301 (2012).
[213] M. A. Stephanov, K. Rajagopal and E. V. Shuryak, Phys. Rev. **D 60**, 114028 (1999).
[214] L. P. Csernai, J. I. Kapusta, Phys. Rev. **D 46** , 1379 (1992).
[215] I. N. Mishustin, Phys. Rev. Lett. **82**, 4779 (1999).
[216] P. Chomaz, M. Colonna, J. Randrup, Phys. Rept. **389** , 263 (2004).
[217] M. Nahrgang, S. Leupold, C. Herold, M. Bleicher, Phys. Rev. **C 84** , 024912 (2011).
[218] M. Nahrgang, S. Leupold, M. Bleicher, Phys. Lett. **B 711**, 109 (2012).
[219] M. Nahrgang, C. Herold, S. Leupold and I. Mishustin, M. Bleicher, [arXiv:1105.1962 [nucl-th]].
[220] C. Herold, M. Nahrgang, I. Mishustin and M. Bleicher, [arXiv:1301.1214 [nucl-th]].
[221] O. Scavenius, A. Mocsy, I. N. Mishustin and D. H. Rischke, Phys. Rev. **C 64**, 045202 (2001).
[222] B. -J. Schaefer and J. Wambach, Nucl. Phys. **A 757**, 479 (2005).
[223] C. Ratti, M. A. Thaler, W. Weise, Phys. Rev. **D 73** , 014019 (2006).
[224] B. -J. Schaefer, J. M. Pawlowski, J. Wambach, Phys. Rev. **D 76**, 074023 (2007).

[225] M. Nahrgang, C. Herold and M. Bleicher, [arXiv:1301.2577 [nucl-th]].

[226] D.R. Oliinychenko, K.A. Bugaev and A.S. Sorin, Ukr. J. Phys. **58**, 211 (2013).

[227] K. A. Bugaev, D. R. Oliinychenko, A. S. Sorin, G. M. Zinovjev, Eur. Phys. J. A **49**, (2013) 30.

[228] K. A. Bugaev, D. R. Oliinychenko, E. G. Nikonov, A. S. Sorin and G. M. Zinovjev, PoS Baldin ISHEPP XXI (2012) 017, 1-14; arXiv:1212.0132 [hep-ph].

[229] A. Andronic, P. Braun-Munzinger and J. Stachel, Nucl. Phys. **A 772**, 167 (2006).

[230] A. Andronic, P. Braun-Munzinger and J. Stachel, Phys. Lett. **B 673**, 142 (2009) and references therein.

[231] J. Cleymans, K. Redlich, Phys. Rev. Lett. **81**, 5284 (1998).

[232] J. Cleymans, K. Redlich, Phys. Rev. **C 61**, 054908 (1999).

[233] A. Tawfik, Europhys. Lett. **75**, 420 (2006).

[234] A. Tawfik, Nucl. Phys. **A 764**, 387 (2006).

[235] E. V. Shuryak, Sov. J. Nucl. Phys. **16**, 220 (1973).

[236] T. D. Cohen and V. Krejcirik, J. Phys. G **39**, 055001 (2012).

[237] C. Amsler *et al.*, Phys. Lett. **B 667**, 1 (2008) [http://pdg.lbl.gov].

[238] K.A. Bugaev, V.K. Petrov and G.M. Zinovjev, Europhys. Lett. **85**, 22002 (2009).

[239] K. A. Bugaev, V. K. Petrov and G. M. Zinovjev, Phys. Rev. **C 79**, (2009) 054913.

[240] C. S. Rolfs and W. S. Rodney, *Cauldrons in the Cosmos*, University of Chicago Press, 1986.

[241] R. Garcia-Martin, J. R. Pelaez and F. J. Yndurain, Phys. Rev. **D 76**, 074034 (2007).

[242] K. G. Denisenko and St. Mrowczynski, Phys. Rev. C **35**, 1932 (1987).

[243] H.W. Barz *et al.*, Phys. Lett. **B 265**, 219 (1991).

[244] F. Becattini *et al.*, Phys. Rev. **C 69**, 024905 (2004).

[245] J. Letessier, J. Rafelski, nucl-th/0504028.

[246] K. A. Bugaev *et al.*, On Chemical Freeze out of Strange Hadrons, 2013 (in preparation).

[247] K. A. Bugaev, J. Phys. G **28**, 1981 (2002).

[248] M. I. Gorenstein, K. A. Bugaev and M. Gazdzicki, Phys. Rev. Lett. **88**, 132301 (2002).

[249] K. A. Bugaev, M. Gazdzicki, M. I. Gorenstein, Phys. Lett. **B 544**, 127 (2002).

[250] I.N. Mishustin, A.V. Merdeev, and L.M. Satarov, Phys. Atom. Nucl. **75**, 776 (2012).

[251] L.M. Satarov, M.N. Dmitriev, and I.N. Mishustin, Phys. Atom. Nucl. **72**, 1390 (2009).

[252] A.V. Merdeev, L.M. Satarov, and I.N. Mishustin, Phys. Rev. C **84**, 014907 (2011).

[253] F. Cooper and G. Frye, Phys. Rev. D **10**, 186 (1974).

[254] L. Ahle *et al.* (E802 Collaboration), Phys. Rev. C **57**, R466 (1998).

[255] B.B. Back *et al.* (E917 Collaboration), Phys. Rev. Lett. **86**, 1970 (2001).

[256] J. Barrette *et al.* (E877 Collaboration), Phys. Rev. **C 62**, 024901 (2000).

[257] C. Alt *et al.* (NA49 Collaboration), Phys. Rev. **C 68**, 034903 (2003).

[258] D.H. Rischke, Y. Pürsün, J.A. Maruhn, H. Stöcker, and W. Greiner, Heavy Ion Phys. **1**, 309 (1995).

[259] J. Brachmann, A. Dumitru, J.A. Maruhn, H. Stöcker, W. Greiner, and D.H. Rischke, Nucl. Phys. **A 616**, 391 (1997).

[260] L.P. Csernai and D. Röhrich, Phys. Lett. B **458**, 454 (1999).

5 Femtoscopy, correlations and fluctuations

Femtoscopy, HBT correlations and event-by-event fluctuations reveal important information about the space-time history of the hot deconfined matter, and can help to understand the nature of the phase transition at high baryon density. Indeed, if the phase transition is of the first order, it should reveal itself through a number of observables discussed in this section, in particular, through the transverse momentum asymmetry of identified hadrons. Event-by-event fluctuations are also expected to provide a signature of the chiral critical point addressed in the previous section.

5.1 Femtoscopic search for the 1-st order phase transition

R. Lednicky

Joint Institute for Nuclear Research, Dubna

Since the pioneering papers of Kopylov and Podgoretsky, it is well-known that the width of the two-particle correlation function in the out-direction (parallel to the pair transverse velocity) is sensitive to the duration of particle emission (see, e.g., [1–3]). In the case when the hot and dense system created in the collision process passes through the quark-gluon (partonic) phase back to the hadronic phase according to the 1-st order phase transition, the latent heat and the related soft equation of state is expected to substantially increase the emission duration [4–6]. The corresponding increase of the out Gaussian radius of the two-pion correlation function or, the increase of the ratio of the out and side radii, has not been however observed experimentally. Instead, the measured out and side radii appear to be nearly equal and almost constant in a wide energy range from AGS, SPS up to the highest RHIC energies.

Assuming the scenario with the first order phase transition taking place somewhere in the AGS-SPS energy region, one can explain the lack of the signal of increased emission duration in the measured Gaussian radii by the two following reasons (besides the effects of flows and resonance decays - both decreasing the ratio of the out to side radii - underestimated or neglected in the original calculations within ideal hydrodynamics):

- according to the Parton-Hadron-String-Dynamics transport calculations, a dramatic decrease of the partonic phase with the decreasing energy is expected, the most of the energy being carried out by the large hadronic corona; particularly, the maximal partonic energy fraction during the evolution of the system created in the central Pb+Pb collisions at $E_{\rm lab}$ =20 and 158 AGeV is estimated on the level of $\sim 10\%$ and $\sim 40\%$, respectively [7];
- in the presence of two or more essentially different characteristic radii (time scales), the single-(3D)Gaussian fit of the correlation function is dominated by the smaller scales even if the contribution of the larger ones is of comparable size (the large space-time separations of the particle emitters leading mainly to a decrease of the correlation strength parameter lambda) [8].

The femtoscopic search for the first order phase transition thus requires sufficiently high statistics allowing one to perform the multiparametric 2D-(3D-)Gaussian or Hamp function fits of the multidimensional correlation functions (with up to 8 parameters taking into account two sets of the three radii and the corresponding fractions) or, to apply the imaging techniques, for a systematic study of the energy dependence of the contribution of different space-time scales. The multidimensional analysis is important to disentangle e.g. the effect of resonances (contributing to non-Gaussian tails in all directions) from the emission duration effect (absent in the side direction).

The first attempts of such an analysis have been done for two-pion correlation functions measured in central heavy ion collisions at the top SPS and RHIC energies [9, 10]. The non-Gaussian tails observed in the out and side directions can be mainly explained by resonance decays while the one in the longitudinal direction is nearly consistent with the Bjorken longitudinal flow. At the same time, the finite exponential emission duration of 2 fm/c and 4 fm/c (corresponding to the 1.4 times larger r.m.s. width of the exponential distribution of the proper lifetime, i.e. - to the 1.4 times larger r.m.s. width of the original Blast Wave Gausssian distribution characterized by the same duration parameters) is required to fully describe the non-Gaussian tails in the out and longitudinal directions found in the RHIC and SPS data, respectively.

A similar analysis of the lower energy heavy ion data on correlation functions of various particle species already available and planned to be measured in future experiments is obviously called for. The analysis of

correlation functions of various particle species (including nonidentical particles) is important to better control the contribution of the non-lifetime effects (resonance decays, flows, rescatterings etc.) to the non-Gaussian tails. The simultaneous search for other signals of the first order phase transition or the critical point (e.g., the decrease of transverse flow or increased fluctuations) is required having in mind a tiny size of the expected effects. Such a detailed and complex study will require high statistics and precise data with a good particle identification which will hopefully be provided by the future dedicated NICA and FAIR facilities.

5.2 Brief arguments for studying azimuthally sensitive HBT

M. Lisa

Ohio State University, USA

It is well known that collective flow carries important and characteristic information about the bulk sector - i.e. the non-perturbative sector - of a heavy-ion collision. Transport calculations (e.g. Kolb and Heinz) repeatedly predict telltale signatures of flow observables as a function energy density, if a threshold from confined to deconfined matter is crossed. Beyond the existence of threshold, detailed excitation functions should reveal

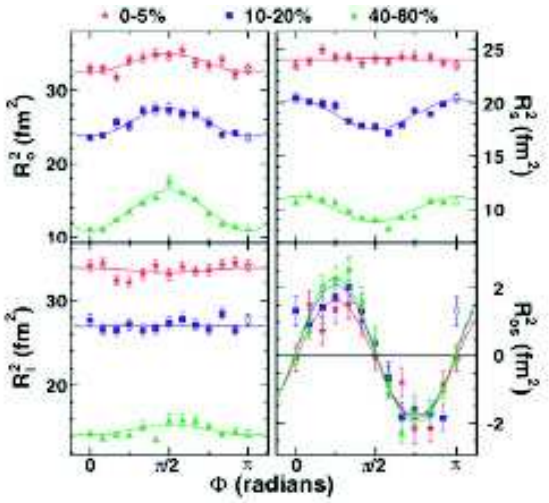

Figure 5.1: HBT radii relative to the 2nd-order event plane in Au + Au collisions at $\sqrt{s_{\rm NN}}$ =200 GeV [14].

important thermodynamic quantities, like any quasi-latent heat or the speed of sound associated with the transition. Common measures of flow include $p_{\rm T}$ spectra (radial flow), and momentum anisotropy (directed and elliptic flow).

But momentum-only observables tell only half of the story of collective flow. The bulk response of the system has a non-trivial structure in both space and time and femtoscopic studies are required to extract this information [21]. Just the $p_{\rm T}$ dependence of azimuthally-integrated HBT radii gives access to the geometric substructure generated by *radial* flow (e.g. [12]), HBT measured relative to the first- and second-order event plane are the spatial analogs of directed and elliptic flow [12,13], respectively, and contain important information not accessible in momentum space alone. As explained below, these measurements can be sensitive to a "softening" in the equation of state, related to a first-order phase transition, or even rapid crossover.

STAR has measured oscillation of pion HBT radii relative to the second-order event plane (Fig. 5.1) [14]. In addition to the overall size of the source, these reveal the transverse *shape*, which is found to be extended out of the reaction plane at freezeout (the stage probed by HBT). It is, however, less anisotropic (equivalently, more round) than the initial source defined by the overlap of the colliding nuclei at finite impact parameter, reflecting the evolution over time in preferential in-plane expansion.

The anisotropy has been measured at a few lower energies, as well. Since the lifetime of the system and elliptic flow increase with energy, one naively expect that, for a fixed initial anisotropy, the freezeout anisotropy becomes less and less out-of-plane extended and may even become in-plane extended (as predicted [15] for example at

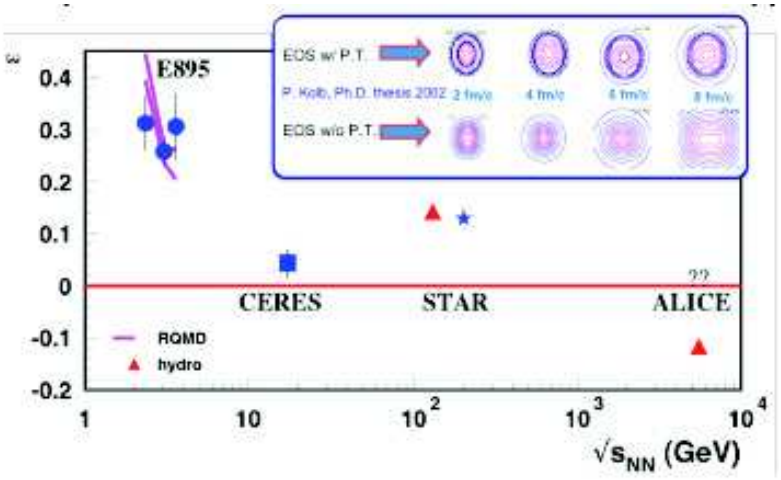

Figure 5.2: Freezeout anisotropy from 2nd-order oscillations of HBT radii. Inset shows hydro evolution of source shape for an equation of state with (upper) and without (lower) softening due to finite latent heat [16].

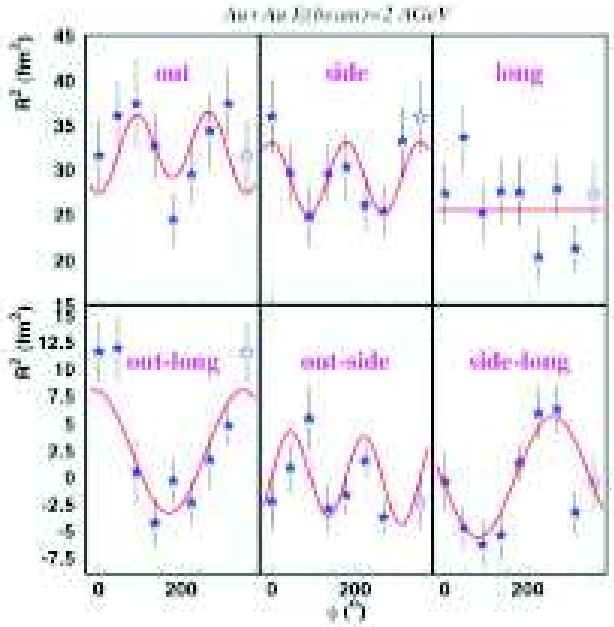

Figure 5.3: HBT radii measured in very low energy ($E_{\rm lab}$ =2 GeV) Au+Au collision at AGS [19], versus the first-order reaction plane. Note that there are now six HBT radii and ϕ is defined over the entire range $0-2\pi$. Lines indicate a fit corresponding to a tilted three-dimensional emission ellipse in coordinate space [13].

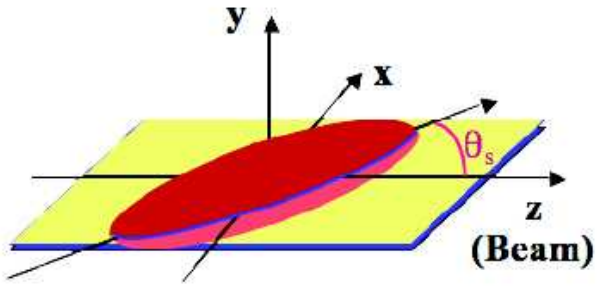

Figure 5.4: The emission source generated at midrapidity may be tilted - in coordinate space - relative to the beam direction [13]. This tilt is revealed in the first order oscillations of the "out-long" and "site-long" cross-terms HBT radii. See Fig. 5.3.

LHC). However, Fig. 5.2 shows instead an intriguing non-monotonic behavior. A possible explanation may be as follows: at low energies (say $E_{\rm lab}$ =3 – 10 AGeV) a stiff equation of state of a hadronic system generates a large pressure pushing the system quickly towards a round shape. But at some energy (say 20 AGeV), a threshold energy required to generate a phase transition is crossed, characterized by a finite latent heat. This generates a "soft point" in the equation of state and the push towards a round state is stalled briefly. As the energy increases beyond this threshold, the time spent in the "soft state" grows, and the "out-of-plane-ness" at freezeout *grows* with energy until some point (say 70 AGeV). Then, at even higher energy, the system spends most of its time in the (stiff) QGP phase, and "out-of-plane-ness" again decreases with energy with no further non-monotonic behaviour. This would be the direct analog of non-monotonic excitation function of v_2 originally predicted by ideal hydro model with softening due to a phase transition [17]. The signal in v_2 has not been observed perhaps because increasing viscous effect at lower energies smears the structure. However, the spatial anisotropy probed by HBT is weighted in the time evolution differently, so may retain sensitivity to the softest point. Fig. 5.2 represents one of very rare bulk-sector probes with a non-monotonic excitation function. Especially given its potential to probe the long sought "soft point", this excitation function cries out to be mapped.

Measuring correlations relative to the *first*-order event plane gives even more unique geometrical information. In particular, if one approximates the spatial configuration of freezeout system as an ellipse, on can extract the angle between its major axis and the beam direction. This "tilt" angle [13] is the spatial analog of the so called "flow angle" [18] formally used to characterized directed flow. It is however, much larger ($\sim 40^o$ at AGS energies [19], compared to flow angles $< 2^o$) and may even have an opposite sign. Simultaneous measurement of both anisotropies provide unique insight on the nature and physics behind the directed flow at lower energies, Fig. 5.3. At RHIC energies, the directed flow becomes even more important, since here we are studying the *bulk* response of the system at the very earliest stages of the collision. Crossing a threshold to a phase transition will generate a "wiggle" in the directed flow at midrapidity, as the system spends most of relevant time (keeping in mind that very small time window to generate directed flow is of order of the crossing time) in the "soft" state. This same physics scenario is predicted to generate non-trivial fingerprint on coordinate-space configuration (of which the tilt angle is the dominant component) [20]. The geometry Fig. 5.4 will probe the physics *behind* the "third component" of flow generating the v_1 wiggle [20, 21].

5.3 Physics at NICA-MPD: particle correlations

V. A. Okorokov

National Research Nuclear University MEPhI, Moscow, Russia

Correlation measurements allow us to get unique information about space-time structure of strong interaction. Moreover study of collective effects is promising tool for investigation of fundamental symmetries and invariances in QCD matter. The requirements for MPD general design suppose reliable identification of various types of charged particles. Thus the detector geometry and characteristics allow us to investigate collective

effects via wide set of correlation measurements.

Azimuthal correlations

The heavy ion investigations at all facilities prove the importance of study of correlations with respect to the reaction plane (flows) for understanding of early stages of final state evolution. Moreover the azimuthal correlation measurements are the promising tool for investigation of fundamental symmetries in hot and dense strongly interacting matter [7,24–26]. Recent investigations at high energies at STAR/RHIC indicate at possible topology-induced local parity violation in strong interactions [27,28]. This effect is an integral part of QCD and it is dominated by non-trivial topology structure of QCD vacuum. Effect of fundamental symmetry violation can serve as a signature of deconfinement state formation and chiral symmetry restoration. It seems QCD vacuum contains high irregular field con-figurations [29]. The features of geometry of these configurations may influence on the fundamental symmetry breaking in particular on the local parity violation in hot strongly interacting matter. Event-by-event charge asymmetry with respect to the reaction plane is observable signature of strong parity violation in heavy ion collisions [30]. There are significant theoretical uncertainties in dependences of effect value on beam energy, atomic number of colliding nuclei etc. so far [24]. The preliminary estimates and general theoretical expectations indicate that the magnetic field at intermediate energies is larger significantly that that for high energy domain [31]. The first correlator calculations show the increasing of experimental observable with energy decreasing for some choice of initial time. But the theoretical estimates never expect decreasing correlator value (as long as deconfinement state of matter is formed) with collision energy decreasing. Some of important characteristics of TPCs for STAR and MPD project are shown in Table 5.1. One can see that the TPC MPD characteristics are suitable for study of fundamental symmetries in hot and dense strongly interacting matter via correlation techniques. Therefore the investigation of topology-induced local parity violation effect can be important task for collectivity / correlation part for physics program of NICA-MPD project.

Characteristic	Main tracker (TPC)	
	NICA/MPD (requirements)	RHIC/STAR
Sizes, cm (TL x IR x OR)	$300 \times 20 \times 110$	$420 \times 50 \times 200$
Rapidity range	$\|\eta\| \leq 1.0$	$\|\eta\| \leq 1.8$
P_t range, GeV/c (ident.)	0.1 -? 3.0	0.1 -? 1.0
dE/dx resolution	$\approx 6\%$	$\approx 7\%$
Momentum resolution	$< 2.5\%$	2 – 3 %
Tracking efficiency	$> 90\%$	80 – 90 %
Two-track resolution	< 5 MeV/c (≈ 1 cm)	0.8 (is) / 1.3 (os) cm
Rate capability	≈ 10 kHz	≈ 0.1 - 1 kHz

Table 5.1: Some characteristics of main trackers for MPD [32] and STAR [33].

Femtoscopy

Femtoscopy is one of the important experimental tasks for first stage of NICA-MPD project. It seems the AGS/SPS have measured the energy range 3 – 17 GeV in detail for identical charged pion pair. The new experimental data with high statistics are important for resolving radii discrepancy in energy range under study. Perhaps, such data can be useful for detail study of freeze-out geometry which can be high irregular in general. Investigation of correlation peak structure and influence of resonances on the pion correlations could be considered as some additional item for NICA-MPD pion femtoscopy. Study of heavier identical meson (kaons) and baryon (lambdas) correlations, correlations of non-identical particle pairs [34, 35] can be one of the focuses and significant part of NICA-MPD femtoscopy program. Study for identical kaon HBT interferometry can be considered as important physical point because of, in particular, very poor sample of experimental data at intermediate energies [36]. Neutral strange particle (Λ, K^0) HBT correlations can be considered as useful tool for study of space-time evolution and size of baryon-rich final state. Moreover, the $\Lambda\Lambda$ correlations can be used for search of exotic states in QCD, for example, H dibaryons [37]. The non-identical particle correlations with kaons (charged and neutral) allow us to obtain information about space-time asymmetry of particle emission, final state interaction, some exotic objects as well as kaonic atoms. Study of femtoscopy correlations for non-identical particle pairs includes correlations with baryons. Possibly, the study of correlations with particles heavier than kaons/lambdas will be some difficult at NICA-MPD because of low corresponding multiplicities.

But even available particle types give us wide additional opportunities for femtoscopy program.

5.4 Event-by-event fluctuations in nucleus-nucleus collisions

M. Gorenstein

Bogolyubov Institute for Theoretical Physics, ? ? Kiev, Ukraine

The energy dependence of most hadron observables demonstrates rapid non-monotonic changes in the SPS energy range. This suggests the onset of the deconfinement in nucleus-nucleus A + A collisions at $E_{\rm lab} = 30$ AGeV [38]. The experimental study of event-by-event fluctuations in A + A collisions gives a unique possibility to reveal a new physical information about the transitions between different phases of the QCD matter. The interest in the study of fluctuations in strong interactions is motivated by expectations of anomalies in the vicinity of the onset of deconfinement [39, 40]. In particular, a critical point of strongly interacting matter may be signaled by a characteristic power-law pattern in fluctuations [41]. The measurements require a large (ideally full) acceptance tracking detector and a precise control of collision centrality. It is also recommended to identify charged hadrons (pions, kaons and protons) on an event-by-event basis, which would allow to study baryon number and strangeness fluctuations as well as the fluctuations of the particle number ratios. Recent theoretical results on event-by-event fluctuations within the statistical and transport models can be found in [42–44]. From the experimental point of view the NICA energy range seems to be ideal for these measurements. This is because a moderate particle multiplicity and their relatively broad angular distribution simplifies efficient detection of all produced charged particles. Up to now only results in a very limited acceptance at high energy A + A collisions are available.

5.5 Flow and freeze-out in relativistic heavy-ion collisions at NICA

L. Bravina and E. Zabrodin

Department of Physics, University of Oslo, Oslo, Norway

One of the observables especially sensitive to the changing of the equation of state (EOS) is the collective flow [18, 45]. The softening of the EOS in the proximity of the QCD phase transition [4, 21, 46] should be seen in the excitation functions of the transverse directed flow of baryons. Its experimental observation would be an important discovery, and an unambiguous signal for the transition to QGP. In microscopic models [**?**, 47–49, 51] the softening of the directed flow [52] of nucleons in semi-peripheral collisions was found at energies from AGS and higher. The origin of the disappearance is traced to nuclear shadowing (or screening). Since the effect is stronger for a light S + S system [47–50], it can be distinguished from the similar phenomenon caused by the quark-gluon plasma formation. In the latter case the disappearance of the flow due to the softening of the equation of state should be most pronounced in collisions of heavy ions.

Some results on the development of anisotropic flow of pions and protons at 40 AGeV have been reported in [53]. The data demonstrate significant softness of the directed flow v_1^p accompanied by the collapse of the elliptic flow v_2^p at the midrapidity range. Several microscopic models cannot reproduce this feature, which can be taken as another evidence of the QGP formation [21]. Here we would like to mention that the trend predicted in the QGSM calculations [47, 48] is similar to that obtained experimentally. Therefore, further microscopic study of this phenomenon at 20 – 40 AGeV is necessary to make any conclusive statements.

The formation and evolution of the anisotropic flow is closely related to the freeze-out of particles. It was found [54, 55] that the freeze-out picture, predicted by the microscopic models for heavy ion collisions at AGS and SPS energies, is quite different from the one, adopted in fluid dynamical models. Even for the most heavy systems particle emission takes place from the whole space-time domain available for the system evolution, but not from the thin freeze-out hypersurface.

Pions are continuously emitted from the whole volume of the reaction and reflect the main trends of the system evolution. Nucleons in heavy ion collisions at both AGS and SPS initially come from the surface region. Therefore, nucleons with large rapidity show a small longitudinal size of the emitting source, while particles from the midrapidity region indicate a large longitudinal size and lifetime of the source. For both reactions there is a separation of the elastic and inelastic freeze-out. Particles which have a small interaction cross section leave the system earlier than those with a large cross section. Thus, the observed interferometric time average

depends on the particle species and on the relative momentum of the pair and so does the correlation function (see also [56]).

It appears that particles with large transverse momenta p_t are predominantly produced at the early stages of the reaction. They are emitted from a spatial domain with small longitudinal and large transverse dimensions. The low p_t-component is populated mainly by the decay products of resonances. This explains naturally the increasing source sizes with decreasing p_t, as observed in HBT interferometry.

The shapes of the emitting sources are far from Gaussians, and the τ -scaling, that is often used in the parameterizations, is not confirmed. Therefore, more realistic source shapes and freeze-out criteria should be used in the analysis of HBT interferometric data. These findings are supported by the results of Ref. [57], in which the HBT correlators of both identical and nonidentical pions are shown to depend strongly on the pion production scenario. The problem with several different emitting sources for hadrons is quite complex and requires further theoretical analysis.

5.6 Perspectives of anisotropic flow measurements at NICA

V. Korotkikh, I. Lokhtin, L. Malinina, S. Petrushanko, L. Sarycheva, A. Snigirev

D.V. Skobeltsyn Institute of Nuclear Physics;
M.V. Lomonosov Moscow State University, Moscow, RUSSIA

Measurements of collective flow phenomena are one of the important tools for studying the properties of the dense matter created in relativistic heavy ion collisions (such as the equation of state EoS, formation conditions, etc.). In non-central collisions of two nuclei the beam direction and the impact parameter vector define a reaction plane for each event. The azimuthal anisotropy of particle production with respect to the reaction plane is an important signature of the physics dynamics at early stages of non-central heavy ion collisions [58,59]. An initial nuclear overlap region has an almond form at non-zero impact parameter. If the produced matter interacts and thermalizes, pressure is built up within the almond shaped region leading to anisotropic pressure gradients. This pressure pushes against the outside vacuum and the matter expands collectively. The expansion is fastest along the largest pressure gradient, i.e. along the shortest axis of the almond. The result is an anisotropic azimuthal angle distribution of the detected particles. One can expand this azimuthal angle distribution in a Fourier series. The second coefficient of the expansion v_2 is often called the elliptic flow and it is expected to be the dominant contribution in the relativistic domain of heavy ion energies. According to the typical hydrodynamic scenario, the values $v_2(p_{\rm T})$ at relatively low transverse momenta ($p_{\rm T} < 2$ GeV/c) are determined mainly by the internal pressure gradients of an expanding fireball during the initial high density phase of the reaction. The ideal hydrodynamics predicts non-monotonic $\sqrt{s_{\rm NN}}$-dependence of v_2 as a result of EoS softening near the critical temperature of quark-hadron phase transition [60].

The elliptic flow was measured in a wide range of heavy ion beam energies (AGS, SPS, RHIC). Besides the integral elliptic flow, differential measurements of v_2 (e.g. as a function of particle transverse momentum $p_{\rm T}$ for various hadron species) are of a great interest. In particular, one of the most striking features of the RHIC experimental data for Au+Au collisions at $\sqrt{s_{\rm NN}} = 200$ and 62.4 GeV per nucleon pair is a so-called constituent quark scaling approximate independence of $v_2/n_{\rm q}$ as a function of $p_{\rm T}/n_{\rm q}$ on hadron species up to $p_{\rm T}/n_{\rm q} \sim 1$ GeV/c (where $n_{\rm q}$ is a number of constituent quarks for the given hadron type), which can be explained in terms of the elliptic flow formation on a partonic level [61]. The breaking such scaling at lower energies may carry the information about changes in properties of a created dense matter. In particular, decrease of the baryon flow and increase of the meson flow are predicted as the signal of a first order quark-hadron phase transition in the presence of critical point [21, 62]. Since at SPS energies the energy dependence of v_2 for baryons is not established, the better measurements (including $p_{\rm T}$ -dependence of v_2 up to high $p_{\rm T} \sim (2-3)$ GeV/c) are required for SPS energy range.

It is expected that the high-accuracy and high-luminosity measurements of differential anisotropic flow for various hadron types over full NICA energy range will provide important constraints on the early dynamics of heavy ion reactions under the conditions where a first order quark-hadron phase transition may occur. We estimated the statistical reach for elliptic flow measurements at NICA with HYDJET++ heavy ion event generator [63]. For NICA energies, input parameters of the model were tuned using SPS and recent low-energy RHIC data. We have found that for MPD acceptance, the statistical $p_{\rm T}$ reach up to $p_{\rm T}/n_{\rm q} = 1$ GeV/c ($p_{\rm T} = 3$ GeV/c for protons and $p_{\rm T} = 2$ GeV/c for pions and kaons) is expected to be achieved within first million

minimum bias Au+Au events at the NICA energy $\sqrt{s_{\rm NN}} = 9$ GeV per nucleon pair. It corresponds to the "first day" physics at designed NICA luminosity. Thus at long time scale measurements, the statistical error in differential v_2 determination (hopefully not only for pions, kaons and protons, but also for other identified hadrons like ρ, ω and ϕ mesons Λ, Σ and Ω baryons) is expected to be much less than the systematic uncertainties. The latter needs to be investigated in the future using different wide-spread flow analysis methods.

5.7 Fluctuations and non-equilibrium processes in collective flow

T. Kodama

Instituto de Física, Universidade Federal do Rio de Janeiro, Caixa, Rio de Janeiro, Brazil

Dissipative hydrodynamics has been applied to relativistic heavy ion collisions to understand the viscous nature of the matter produced by relativistic collision of heavy nuclei. Several works have been done to extract the shear viscosity from the experimental data of the collective flow parameter v_2 [64–66]. Now the hydrodynamic approach is widely accepted as an essential tool to describe the flow dynamics of relativistic heavy ion collisions.

On the other hand, a hydrodynamic description of heavy ion collisions requires many external inputs such as the equation of state, transport coefficients, initial condition and freeze out mechanism. They are exactly what we want to extract from the experimental data applying the hydrodynamic model analysis. Unfortunately (or fortunately), these external "parameters" are all entangled in a complicated way in the final state physical observables. This means that each of any single type of experimental data alone, e.g., particle spectra, collective flow, etc., is not sufficient to specify quantitatively the required information directly from them. Therefore, correlations among the observables, especially those reflect the (estimated) geometrical information of the initial condition like the centrality are invoked to determine, for example, the viscosity coefficients.

One important factor in relativistic hydrodynamics is the relaxation time. To keep the causality and stability of the system, a finite value of the relaxation time related to the viscosity is mandatory. However, this new parameter increases the uncertainty of the hydrodynamic approach. For example, we know that the shear viscosity η/s takes different value in QGP and hadronic phases, and it even depends on the temperature(see Fig. 5.5). This is the same for the relaxation time, τ_Π. Even though, due to the interplay between the effects of viscosity and relaxation time (a large relaxation time reduces the effect of shear viscosity), it is possible to fit the behavior of collective flow in terms of one unique (constant) effective shear viscosity per entropy, $\eta_{\rm eff}/s$ shown by the grey line in Fig. 5.5 [67].

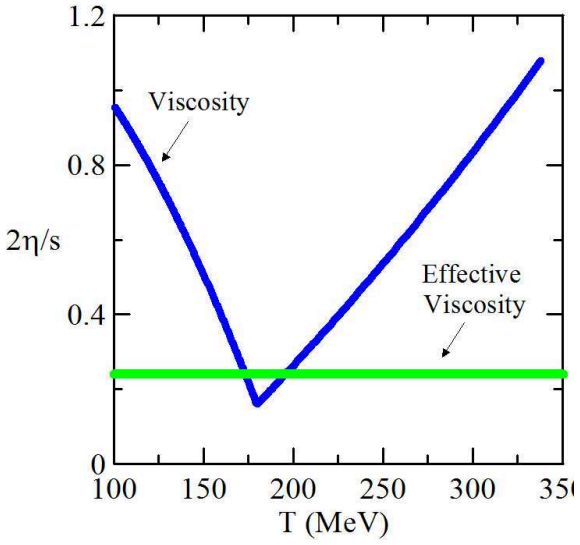

Figure 5.5: Shear viscosity as function of temperature. In spite of the large temperature dependence (black line), the same behaviour of the final values of collective flow parameter can be obtained with a constant (and relatively small) effective shear viscosity (grey line) [67].

The value of effective viscosity depends critically on the evolution of the system. Specifically, this value is

affected by the time span for which the system remains in different phases. For the LHC energies, for example, we would expect a different value for the effective viscosity since the system will stay longer in the quark gluon plasma phase. It is thus quite important to study the behaviour of collective flow as function of energy. We further expect that the finite value of baryon chemical potential, $\mu_{\rm B}$, also changes the behaviour. Therefore, the study of these quantities near the first order phase transition domain will reveal more exclusive information on transport coefficients.

In addition to the above mentioned correlations among inclusive observables, a very important information can be obtained by studying event by event (EbyE) fluctuations [68, 69]. There are many origins of EbyE fluctuations but within a hydrodynamical scenario, we may classify them in three categories: fluctuations in the initial condition (IC), dynamical fluctuations due to the hydrodynamical instabilities, and the fluctuations in hadronization stage. In conventional hydrodynamic models, these fluctuations are usually neglected. For example, the initial conditions for the hydrodynamic expansion are usually parametrized as smooth distributions of thermodynamic quantities and four velocity. However, in the case of relativistic heavy ion collisions, the system is relatively small compared to the inhomogeneity scale so that important event-by-event fluctuations are expected in the IC of the real collisions. Moreover, each set of ICs should presents strongly inhomogeneous structure [70].

Fluctuations of observables also happen due to hydrodynamical instabilities such as turbulences. This may take place when the system passes through the phase boundary and meet the instabilities of order parameters [71, 72]. In particular, at the mixed phase the sound velocity vanishes, so that any inhomogeneity in the velocity field easily generates shocks. At the same time, the relaxation time becomes very large, and when this becomes comparable to the hydrodynamic time scale, the hydrodynamical description may loose its validity. This is because hydrodynamic equations are usually considered as a theory where the local thermodynamical equilibrium is attained. There, we may expect some new features of the collective dynamics, specifically associated with the first order phase transition such as nucleation or spinodal instabilities [73]. These dynamics depend crucially on the coarse-graining scale for the hydrodynamics. Therefore, we need observables sensitive to the small coarse-graining scale of the collective flow.

Another origin of fluctuations comes from the final stage of hydrodynamics, where the observed hadrons are emitted from the fluid. The most common (because it is simple) way to treat this is use the Cooper-Frye formula applied to a sharp freeze-out hyper surface. Recent calculations include the final state interactions of hadrons using the hadronic cascade codes like rQMD [74, 75]. These hadronization process also induces dynamical and statistical fluctuations. Furthermore, if one considers the emission of hadrons from any space time point, EbyE fluctuations also changes according to the kinematical domain (continuous emission mechanism) [76, 77].

One should note that several very different physical scenarios within the hydrodynamical approaches (e.g. smooth initial conditions vs. bumpy initial conditions, single shear viscosity vs. temperature dependent viscosity plus corresponding relaxation time, etc.) can give rise somewhat equally good results in reproducing several sets of observables with suitable choices of parameters. In a way, one may say that the hydro signature is "robust", but on the other hand, this could be a synonym of "insensitive". Recent sophisticated studies, with the combination of adequate initial condition, equation of state and final state interactions, show that most of collective features of the data are well reproduced, even solving the HBT puzzle [78]. Nevertheless, we are still not able to say that these are unique description of the real situation.

With respect to this point, one should remind an important point of the collective flow. We usually say that the hydrodynamic description is valid *only* when the local thermal equilibrium is attained. This is because, by using the assumption of local thermal equilibrium, we introduce the equation of state to describe the pressure as function of density to close the hydrodynamic equations. However, is the inverse of this statement true? That is, does the use of thermodynamical relations really imply the local thermal equilibrium? Unfortunately, the answer is NO, in general. To prove this, we need just find any counter example. As is well-known, for a massless relativistic gas, any *isotropic* momentum distribution leads to the ideal massless equation of state, $\varepsilon = 3p$, irrespective of its energy distribution. More generally, this relation holds for any traceless energy and momentum tensor, if the system is locally isotropic. This means that the use of such an equation of state does not mean at all that the system is in thermal equilibrium.

There exist indeed another situations where the equations of state are valid but their microscopic energy states do not follow the Boltzmann distribution [79, 80]. In such cases, the equations of hydrodynamics can be viewed simply as a coarse-grained (in time and space) effective theory for conserved quantities such as energy and momentum tensor and charge currents. They are essentially a set of continuity equations for these effective

conserved quantities, complemented with the "so-called" equation of state and time evolution equation for the off-diagonal elements of the energy and momentum tensor to close the system. In this vision, it is dangerous to exclude from the beginning any other possibilities than the equation of state and transport coefficients calculated from the real thermal equilibrium, such as those of the lattice QCD calculations. The exclusion should be done using the experimental data. Some people explores the so-called non-extensive statistical approach [82–85]. If this is the case, it would be possible that the effective equation of state that we should use in hydrodynamical analysis does not necessarily be that of the Lattice QCD calculations, and so the transport coefficients.

To clarify these aspects, more observables related directly to genuine hydrodynamical modes, such as shock waves or density waves should be explored [86], without introducing any prejudice for the equation of state and transport coefficients. In this direction, two or more particle correlations in the EbyE analysis are good candidates and some interesting interpretation of double peaks in azimuthal two particle correlations is being studied [87, 88]. In addition, the study of the behavior of universal signatures, such as scaling phenomena is extremely important [89].

There exist still several fundamental questions for the hydrodynamical description of relativistic heavy ion collisions, especially around the domain where the first order phase transition occurs. Thus, more extensive and precise studies, both experimental and theoretical, are required for the determination of properties of the fluid. The NICA program certainly will give a crucial contribution to a large advance of understandig the dynamics of QCD matter near the first order phase transition domain when combined with the energy scan program at the RHIC [90].

5.8 The prospects for experimental study of directed, elliptic, and triangular flows in asymmetric heavy ion collisions at NICA energies

M. Bleicher[a,c], K. A. Bugaev[b], P. Rau[a,c], A. S. Sorin[d], J. Steinheimer[a,c] and H. Stöcker[a,e]

[a] *Frankfurt Institute for Advanced Studies (FIAS), Frankfurt, Germany*
[b] *Bogolyubov Institute for Theoretical Physics, National Academy of Sciences of Ukraine, Ukraine*
[c] *Institut für Theoretische Physik, Goethe-Universität, Frankfurt, Germany*
[d] *Joint Institute for Nuclear Research (JINR), Dubna, Russia*
[e] *GSI Helmholtzzentrum fur Schwerionenforschung, Darmstadt, Germany*

Introduction.

The experimental study of strongly interacting matter has reached a decisive moment: it is hoped that the low energy heavy ion collisions programs performed at the CERN SPS and the BNL RHIC and two new programs that are planned to begin in a few years at NICA (JINR, Dubna) and FAIR (GSI, Darmstadt) will allow the heavy ion community to locate the mixed phase of the deconfinement phase transition and to discover a possible (tri)critical endpoint [91, 92]. The major experimental information is provided by the measurements of particle yields, one particle momentum spectra, two particle correlations, and the Fourier components of the collective hadronic flow [98] known as v_1-coefficient (directed flow), v_2-coefficient (elliptic flow) and v_3-coefficient (triangular flow). Although the great success of experiments at the BNL RHIC and at the CERN LHC proved the high efficiency of modern experimental methods, their results also clearly demonstrated that the heavy ion collisions programs at RHIC, SPS, NICA and FAIR energy range are not simpler and they require further development of both new experimental approaches and far more sophisticated theoretical models in order to reach their goals. Therefore, in view of new opportunities opening with the Nuclotron program Baryonic Matter@Nuclotron (BMN) [91, 92] which will start at JINR (Dubna) in 2014, we would like to address here some new physical issues that can be studied at laboratory energies of 2–5 AGeV for a wide range of colliding nuclei in the fixed target mode. In future, they can further be investigated at the accelerators of new generation like NICA (JINR, Dubna) and FAIR (GSI, Darmstadt) at a center of mass energy up to 11 AGeV.

This range of energies was thoroughly investigated in the past at the GSI SIS and the BNL AGS experiments, but only for symmetric, i.e. A + A, nuclear collisions. In this paper we demonstrate by using the Ultrarelativistic Quantum Molecular Dynamics transport model UrQMD [73, 74] that one of the major tasks of the low energy programs at JINR and GSI could be a systematic study of directed, elliptic, and triangular flows for non-central asymmetric nuclear collisions (ANC), i.e. for non-central $A + B$ reactions with $1 \ll B \ll A$ (see Fig. 5.6). This aspect of heavy ion physics was not yet systematically explored. Until today there were only a few works reported for ANC [95–97]. Moreover, these works were completed before a systematic investigation of the

Fourier components [98] of hadronic flow was proposed. Only recently there appeared the first predictions for this energy range in Ref. [99] which also studied the influence of high density Mach shock waves formed in ANC on the resulting spatial particle and cluster distribution. Using the comprehensive analysis of the v_1, v_2 and v_3 Fourier-coefficients of the azimuthal particle distributions obtained in [100] for non-central ANC, here we argue that a comprehensive experimental study of ANC can help us to essentially improve our understanding of the hadronic matter equation of state at high densities. In addition, under certain conditions, highest baryonic charge densities can be reached in these experiments [99], what could help clarifying the question, whether the mixed quark-hadron phase [91, 92, 101] or the predicted chiral quarkyonic phase [101] can be formed in this energy range.

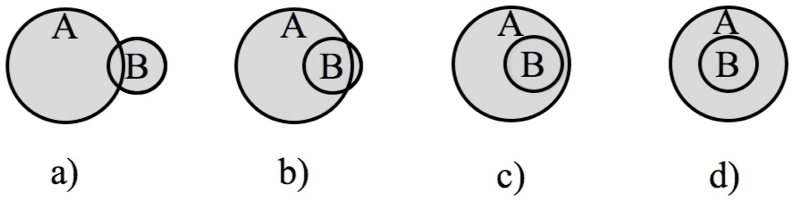

Figure 5.6: Schematic picture of an asymmetric nuclear collision of nuclei A (large circle) with B (small circle) shown in the transverse plane. The common area of two nuclei is shown for very peripheral collisions (panel a)), for semi-peripheral collisions (panels b) and c)) and for the most central collision (panel d)). Clearly, for semi-peripheral collisions the effect of the shadowing of particle motion to the right hand side of the nucleus B is very weak.

The unusual features of ANC.

ANC have some history since they were suggested long ago (see, for instance, [95, 102, 103]), but in those days the analysis of Fourier coefficients of the azimuthal particle distributions was not even suggested. Since that time the analysis of the Fourier coefficients $v_1, v_2, ...$ has become a powerful tool of experimental studies of the evolution process of symmetric heavy ion collisions at high energies [104–106]. Thus, the quark scaling of the v_2 dependence on the transverse momentum p_T [106] clearly demonstrated the partonic source of elliptic flow of hadrons at RHIC energies, while the triangular flow is reflecting the correlations that appear at the early stage of collisions [107].

A principally new element of the ANC compared to symmetric nuclear collisions is the formation of strong and asymmetric gradients of energy density and baryonic density at the initial stage of the collision process along with a stronger flow from the target towards the projectile for a specific choice of the impact parameter values. In contrast to symmetric collisions, in ANC the reflection symmetry between the left nucleus A and the right nucleus B (see panels a)-c) in Fig. 5.6) is broken from the very beginning. This leads to an entirely different shape and location of the overlap region between the colliding nuclei which, in its turn, results in different flow patterns compared to symmetric collisions. Indeed, if the impact parameter value is close to $b_{ANC} \approx 1.1\,\text{fm} \cdot (A^{\frac{1}{3}} - B^{\frac{1}{3}}) \pm 1$ fm (see the panels b) and c) of Fig. 5.6) and if the size of the target nucleus is chosen close to $B^{\frac{1}{3}} \approx \frac{1}{2}A^{\frac{1}{3}}$, then there is sufficient room to vary the impact parameter in the experiment and to select values close to b_{ANC} using an event-by-event analysis. In this case ANC allow us to scan the interior of the target nucleus as well as to study in detail the variety of surface phenomena such as the surface formation of light nuclear fragments like deuterons, tritons, and helium nuclei, the emission of high p_T pions, the isospin dependence of hadron surface emission, and so on.

The discussion of new possibilities opened up by ANC can be found in [100]. In Figs. 5.7-5.9 we show a few results on the directed, elliptic, and triangular flow coefficients obtained by the UrQMD transport model containing in medium potentials [108–110] which was thoroughly tested on the available data in a wide range of collision energies. The left panel of Fig. 5.7 shows the energy and centrality dependence of the v_1^{AS} coefficient for all charged particles at longitudinal midrapidity in the equal velocity frame of the colliding Ne and Au nuclei. Such a system is convenient to compare the results with both the data obtained in the symmetric nuclear collisions. As one can see from Fig. 5.7 the v_1^{AS} coefficient of charged particles is essentially non-zero at $|y| < 0.1$ for ANC, whereas it is zero for $y = 0$ in the symmetric case since it is an odd function of the center of mass rapidity. The right panel of Fig. 5.7 shows the v_1^{AS} coefficient of charged particles found for the

configuration that contains a fluctuating high density spot in the target nucleus [100].

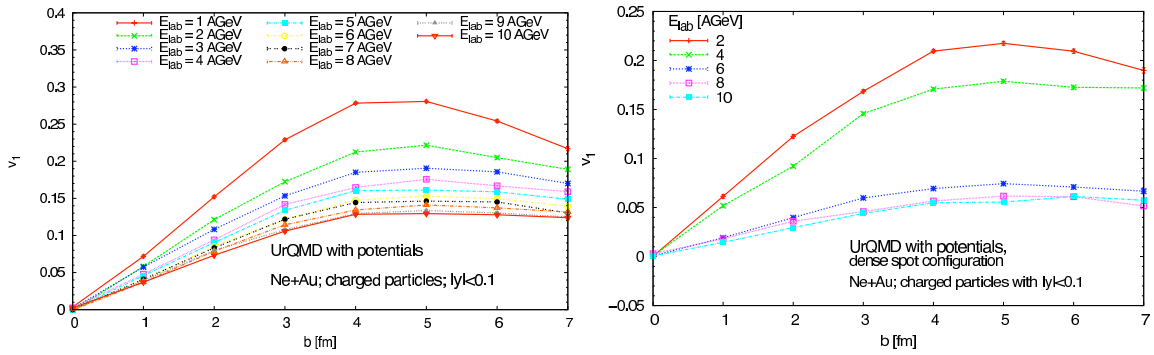

Figure 5.7: Energy and centrality dependence of the v_1^{AS} coefficient of charged particles from Ne+Au collisions as calculated with the UrQMD model with potentials for the standard initialisation (left panel) and with a fluctuating high density spot in the target nucleus (right panel). For more details see the text.

An existence of high density fluctuations in ordinary nuclei is debated for a long time [111, 112] along with their possible applications in the context of the heavy ion reactions [113, 114]. Here we would like to draw attention to this issue and to demonstrate the influence of the high density fluctuations on the v_1^{AS}, v_2^{AS}, and v_3^{AS} coefficients for ANC. To estimate this effect, we randomly put 20 nucleons from the Au-nucleus in a narrow Gaussian distribution inside of the ordinary Monte Carlo sampled nucleus. This gives us a fluctuating dense spot initial configuration. Such an assumption is far from the extremely high densities discussed with respect to flucton [111, 114]. The dense spot is fixed in the center of the Au target with an offset in x-direction of half of the impact parameter in order to make sure the Ne projectile always hits the high density region. Thus, for all impact parameters below 12 fm there is an overlap of the dense spot with Ne-nucleus. The right panel of Fig. 5.7 shows the non-monotonic energy dependence which indicates [100] the change of regimes from the dominance of the target break up process at $E_{lab} = 2 - 4$ AGeV to a strong compression and more intense thermalization of the reaction zone for $E_{lab} \geq 5$ AGeV.

In Figs. 5.8 and 5.9 we also show the v_2^{AS} and v_3^{AS} coefficients calculated for ANC with and without the fluctuating dense spot in the target. These figures show that the 50 % reduction of the directed flow for the dense spot configurations at $E_{\rm lab} \geq 4$ AGeV does not lead to a dramatic change of the corresponding elliptic, and triangular flows at these energies.

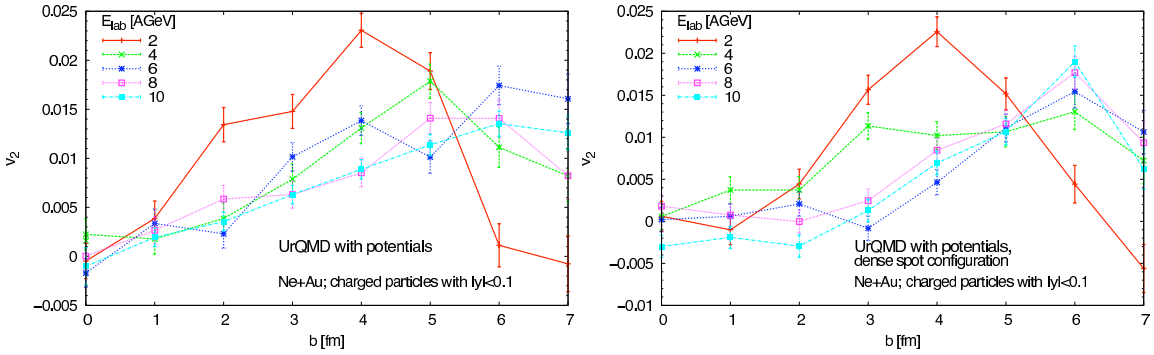

Figure 5.8: Energy and centrality dependence of the v_2^{AS} coefficient of charged particles found by the UrQMD model for the asymmetric Ne + Au collision with the dense spot (right panel) and without it (left panel).

Conclusions and perspectives.

Our analysis of the v_1^{AS}, v_2^{AS} and v_3^{AS} coefficients from ANC revealed [100] that they have a richer and more complicated structure compared to symmetric collisions. Also we find that these flow patterns are very sensitive to the details of the employed interaction which can be used both for fine tuning of the transport codes and for elucidation of the essential features of the hadron interaction in the medium.

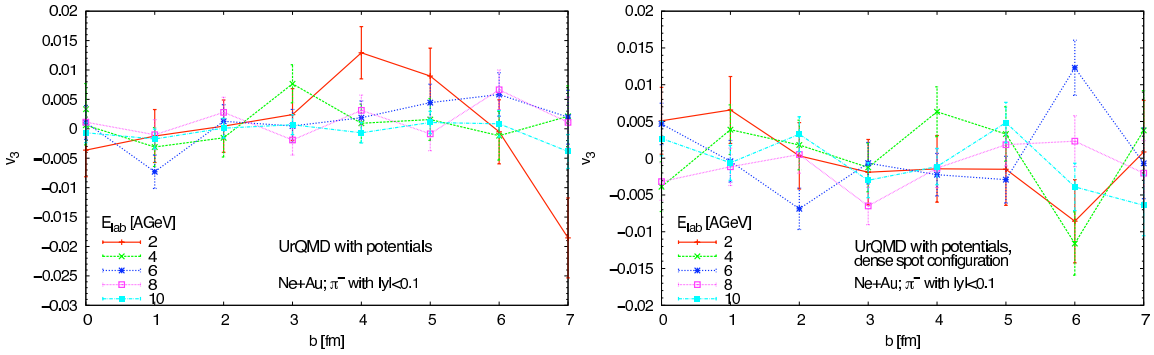

Figure 5.9: Energy and centrality dependence of the v_3^{AS} coefficient of negative pions found by the UrQMD model for the asymmetric Ne+Au collision with the dense spot (right panel) and without it (left panel).

Therefore, one can hope that a systematic study of the directed, elliptic and, perhaps, triangular flows of strange particles would provide us with the information about the modification of the strange particle interaction with the dense hadronic media that exhibits strong density gradients.

Perhaps, it is reasonable to expect, that in the BMN program energy range the impact parameter dependence of the triangular flow coefficient v_3^{AS} will be uncorrelated (or weakly correlated) to that one of the v_2^{AS}-coefficient even for the semi-peripheral collisions. Such a conclusion is based on the triangular flow pattern developed at highest RHIC energies, where the proportionality of v_2^S and v_3^S is established both experimentally [107] and theoretically [115], and it indicates long-range rapidity correlations occurring at the initial stage due to the color flux tube. Then one can expect that the appearance of such correlations in ANC with the dense spot initial state can signal a possible color flux tube formation.

Furthermore, for the semi-peripheral ANC one can expect the appearance of a sizable flow of deuterons, tritons, ^{3}He and ^{4}He nuclei in the out-of-plane direction [99] which are born during the crush of a narrow layer of nucleus A that surrounds the reaction zone from above and below of the reaction plane (see panels b) and c) of Fig. 5.6). We hope that the investigation of such a flow will allow us to study the dynamical and statistical aspects of nuclear cluster formation.

There is also a hope to identify the case of (partial) chiral symmetry restoration without deconfinement by studying the recently suggested chiral vortaic effect [26] which can be stronger in ANC due to large density gradients [116].

5.9 Baryon number cumulants in relativistic heavy ion collisions

M. Kitazawa, M. Asakawa

Department of Physics, Osaka University, Toyonaka, Japan

Fluctuation observables, especially the baryon number cumulants, are invaluable tools to diagnose the primordial stage of heavy ion collisions. In experiments, however, the baryon number is not a direct observable. We show that the isospin distribution of nucleons at kinetic freezeout is binomial and factorized. This leads to formulas that express the baryon number cumulants solely in terms of proton number fluctuations, which are experimentally observable.

Experimental analysis of the QCD phase diagram is one of the most challenging subject of relativistic heavy ion collisions. The analysis of the matter with various temperature T and baryon chemical potential $\mu_{\rm B}$ is acheived in heavy ion collisions by varying the collision energy per nucleon pair, $\sqrt{s_{\rm NN}}$. Such a project is now ongoing at the Relativistic Heavy Ion Collider (RHIC) [117]. Experimental data at LHC, as well as those which will be obtained in the future facilities at the NICA and FAIR designed for lower beam-energy collisions, will also provide complementary information on this subject.

Fluctuations, which are experimentally measured by event-by-event analyses in heavy ion collisions, are promising observables to probe properties of created fireballs [118], as their behaviors are sensitive to the state of the matter. For example, because of the singularity at the critical point, fluctuations of various physical

quantities, including skewness and kurtosis, behave anomalously near the critical point [119–121]. One can also argue that ratios between cumulants of conserved charges are sensitive to the magnitudes of the charge carried by quasi-particles composing the system, and hence behave differently in the hadronic and quark-gluon phases [122–124]. Recently, it was also pointed out that some higher order cumulants of conserved charges change signs around the phase boundary of QCD, which would serve as clear experimental signatures to determine the location of the matter in the phase diagram [125–127].

Among the fluctuation observables, those of conserved charges can reflect fluctuations produced in earlier stages during the time evolution of fireballs than non-conserved ones. This is because the variation of a conserved charge in a volume is achieved only through diffusion, which makes the relaxation to equilibrium slower. In fact, it is argued that if the rapidity range of a detector is taken to be sufficiently large, effects of diffusion are well suppressed and fluctuations produced in the quark-gluon phase can be detected experimentally [122, 123].

QCD has several conserved charges, such as baryon and electric charge numbers and energy. Among these conserved charges, theoretical studies suggest that the cumulants of the baryon number have the most sensitive dependences on the phase transitions and phases of QCD. Experimentally, however, the baryon number fluctuations are not directly observable, because chargeless baryons, such as neutrons, cannot be detected by most detectors. Proton number fluctuations can be measured [117], and recently its cumulants have been compared with theoretical predictions for baryon number cumulants. Indeed, in the free hadron gas in equilibrium the baryon number cumulants are approximately twice the proton number ones, because the baryon number cumulants in free gas are simply given by the sum of those for all baryons, and the baryon number is dominated by proton and neutron numbers in the hadronic medium relevant to relativistic heavy ion collisions. In general, however, these cumulants behave differently. In fact, we will see later that the non-thermal effects which exist in baryon number cumulants are strongly suppressed in the proton number ones.

In Refs. [128, 129], it is argued that, whereas the baryon number cumulants are not the direct experimental observables as discussed above, they can be determined in experiments by only using the experimentally measured proton number fluctuations for $\sqrt{s_{\rm NN}} \gtrsim 10$GeV. The key idea is that isospins of nucleons in the final state are almost completely randomized and uncorrelated, because of reactions of nucleons with thermal pions in the hadronic stage. This leads to the conclusion that, when $N_{\rm N}$ nucleons exist in a phase space of the final state, the probability that N_p nucleons among them are protons follows the binomial distribution. More generally, the probability distribution that N_p protons, N_n neutrons, $N_{\bar{p}}$ anti-protons, and $N_{\bar{n}}$ anti-neutrons are found in the final state in a phase space is factorized as

$$\mathcal{P}_{\rm N}(N_p, N_n, N_{\bar{p}}, N_{\bar{n}}) = \mathcal{F}(N_{\rm N}, N_{\bar{\rm N}}) B_r(N_p; N_{\rm N}) B_{\bar{r}}(N_{\bar{p}}; N_{\bar{\rm N}}), \tag{5.1}$$

where the nucleon and anti-nucleon numbers are $N_{\rm N} = N_p + N_n$ and $N_{\bar{\rm N}} = N_{\bar{p}} + N_{\bar{n}}$, respectively, and

$$B_r(k; n) = \frac{n!}{k!(n-k)!} r^k (1-r)^{n-k}, \tag{5.2}$$

is the binomial distribution function with probabilities $r = \langle N_p \rangle / \langle N_{\rm N} \rangle$ and $\bar{r} = \langle N_{\bar{p}} \rangle / \langle N_{\bar{\rm N}} \rangle$. The function $\mathcal{F}(N_{\rm N}, N_{\bar{\rm N}})$ describes the distribution of nucleons and anti-nucleons and the correlation between them in the final state, which are determined by the dynamical history of fireballs. Using the factorization Eq. (5.1), one can obtain formulas to represent the (anti-)nucleon number cumulants by the (anti-)proton number ones, and vice versa. The (anti-)nucleon number in Eq. (5.1) can further be promoted to the (anti-)baryon number in practical analyses with a simple treatment for strange baryons to a good approximation. These formulas enable to determine the baryon number cumulants solely with the experimentally measured proton number fluctuations, and, as a result, to obtain insights into the present experimental results on the proton number cumulants.

In the following, we first show that the isospin of nucleons in the final state is random and uncorrelated, and then derive formulas to represent baryon number cumulants.

In order to understand the correlation between nucleon isospins in heavy ion collisions, let us first consider how the nucleons evolve in the hadronic stage. The most important interaction of nucleons in the hadronic stage is Nπ reactions mediated by $\Delta(1232)$ resonances. In particular, those mediated by $\Delta^+(1232)$ and $\Delta^0(1232)$,

$$p(n) + \pi \to \Delta^{+,0} \to n(p) + \pi, \tag{5.3}$$

which are called the charge exchange reactions, are responsible for the variation of nucleon isospins. Because of a little energy required and the large cross sections, these reactions proceed even after chemical freeze-out. In

fact, the mean time of this reaction is $3-4$fm for $T=150-170$MeV [128, 129], which is significantly shorter than the lifetime of the hadronic stage. Therefore, nucleons in the fireball undergo this reaction several times on average in the hadronic stage. The ratio of the probabilities that a proton in medium produces a Δ^+ or Δ^0, and then decays into p and n is $5:4$, which is determined by the isospin SU(2) algebra. Whereas this probability is not even, after repeating the above processes several times in the hadronic stage nucleons tend to completely forget their initial isospin. It is also shown that the medium effects on this argument are well suppressed [128, 129]. One thus can conclude that the isospin of nucleons in the final state is random and uncorrelated. This conclusion leads to the factorization Eq. (5.1).

Using Eq. (5.1), one can obtain concrete formulas to relate the baryon and proton number cumulants. In relativistic heavy ion collisions at sufficiently large $\sqrt{s_{\rm NN}}$ and small impact parameters, the isospin density is negligibly small and one can take $r=\bar{r}=1/2$ in Eq. (5.1). One then obtains [128, 129]

$$\langle N_p^{(\rm net)}\rangle = \frac{1}{2}\langle N_{\rm B}^{(\rm net)}\rangle, \tag{5.4}$$

$$\langle(\delta N_p^{(\rm net)})^2\rangle = \frac{1}{4}\langle(\delta N_{\rm B}^{(\rm net)})^2\rangle + \frac{1}{4}\langle N_{\rm B}^{(\rm tot)}\rangle, \tag{5.5}$$

$$\langle(\delta N_p^{(\rm net)})^3\rangle = \frac{1}{8}\langle(\delta N_{\rm B}^{(\rm net)})^3\rangle + \frac{3}{8}\langle\delta N_{\rm B}^{(\rm net)}\delta N_{\rm B}^{(\rm tot)}\rangle, \tag{5.6}$$

$$\langle(\delta N_p^{(\rm net)})^4\rangle_c = \frac{1}{16}\langle(\delta N_{\rm B}^{(\rm net)})^4\rangle_c + \frac{3}{8}\langle(\delta N_{\rm B}^{(\rm net)})^2\delta N_{\rm B}^{(\rm tot)}\rangle + \frac{3}{16}\langle(\delta N_{\rm B}^{(\rm tot)})^2\rangle - \frac{1}{8}\langle N_{\rm B}^{(\rm tot)}\rangle, \tag{5.7}$$

and

$$\langle N_{\rm B}^{(\rm net)}\rangle = 2\langle N_p^{(\rm net)}\rangle, \tag{5.8}$$

$$\langle(\delta N_{\rm B}^{(\rm net)})^2\rangle = 4\langle(\delta N_p^{(\rm net)})^2\rangle - 2\langle N_p^{(\rm tot)}\rangle, \tag{5.9}$$

$$\langle(\delta N_{\rm B}^{(\rm net)})^3\rangle = 8\langle(\delta N_p^{(\rm net)})^3\rangle - 12\langle\delta N_p^{(\rm net)}\delta N_p^{(\rm tot)}\rangle + 6\langle N_p^{(\rm net)}\rangle, \tag{5.10}$$

$$\begin{aligned}\langle(\delta N_{\rm B}^{(\rm net)})^4\rangle_c =& 16\langle(\delta N_p^{(\rm net)})^4\rangle_c - 48\langle(\delta N_p^{(\rm net)})^2\delta N_p^{(\rm tot)}\rangle + 48\langle(\delta N_p^{(\rm net)})^2\rangle \\ &+ 12\langle(\delta N_p^{(\rm tot)})^2\rangle - 26\langle N_p^{(\rm tot)}\rangle.\end{aligned} \tag{5.11}$$

Using Eqs (5.8) - (5.11), the baryon number cumulants are determined in experiments with experimentally measured proton number cumulants. We emphasize that no explicit form of $\mathcal{F}(N_{\rm B}, N_{\bar{\rm B}})$ is assumed in deriving these results. Whereas the effect of nonzero isospin density on Eqs (5.8) - (5.11) becomes non-negligible at low beam energy, explicit calculation shows that the effect is less than 10% in magnitude for $\sqrt{s_{\rm NN}} \simeq 10$GeV [128, 129].

Finally, let us consider the difference between the baryon and proton number cumulants using the above results. In order to estimate the contributions of terms including $N_{\rm B}^{(\rm tot)}$ in these equations, we temporary postulate that $N_{\rm B}$ and $N_{\bar{\rm B}}$ have thermal distributions determined at chemical freeze-out, as the statistical model indicates. For the second and third order relations one then obtains,

$$\langle(\delta N_p^{(\rm net)})^2\rangle = \frac{1}{4}\langle(\delta N_{\rm B}^{(\rm net)})^2\rangle + \frac{1}{2}\langle(\delta N_p^{(\rm net)})^2\rangle_{\rm HG}, \tag{5.12}$$

$$\langle(\delta N_p^{(\rm net)})^3\rangle = \frac{1}{8}\langle(\delta N_{\rm B}^{(\rm net)})^3\rangle + \frac{3}{4}\langle(\delta N_p^{(\rm net)})^3\rangle_{\rm HG}. \tag{5.13}$$

These results show that the second terms on the RHSs, which come from the binomial distributions of the nucleon isospin, have significant contribution to the cumulants of the proton number, and the contribution of the net baryon number cumulants, $\langle(\delta N_{\rm B}^{(\rm net)})^n\rangle$, are relatively suppressed. Since the second terms give the thermal fluctuations, these results show that the deviation of $\langle(\delta N_{\rm B}^{(\rm net)})^n\rangle$ from the thermal value is hard to be seen in the proton number cumulants. Although one cannot transform the fourth-order relation Eq. (5.7) to a simple form as in Eqs. (5.12) and (5.13), from the factor $1/16$ in front of $\langle(\delta N_B^{(\rm net)})^4\rangle_c$ in Eq. (5.7) it is obvious that the direct contribution of this term to experimentally measured $\langle(\delta N_p^{(\rm net)})^4\rangle_c$ is more suppressed compared to the lower-order cumulants, and that its experimental confirmation is more difficult. The analysis of the baryon number cumulants with Eqs. (5.8) - (5.11) enables to remove the thermal contribution in the proton number cumulants and makes the direct experimental observation of signals in $\langle(\delta N_p^{(\rm net)})^n\rangle_c$ possible.

In conclusion, we derived relations between baryon and proton number cumulants, Eqs. (5.4) - (5.7) and Eqs. (5.8) - (5.11), on the basis of the binomial nature of (anti-)nucleon isospin numbers in the final state. These results enable to immediately determine the baryon number cumulants with experimental results in heavy ion collisions, which will provide significant information on the QCD phase diagram.

5.10 Thermal Conductivity and Chiral Critical Point in Third Generation Heavy Ion Collision Experiments

J. I. Kapusta, J. M. Torres-Rincon

School of Physics and Astronomy, University of Minnesota, Minneapolis, USA
Departamento de Fisica Teorica I, Universidad Complutense de Madrid, Madrid, Spain

Quantum Chromodynamics is expected to have a phase transition in the same static universality class as the 3D Ising model and the liquid-gas phase transition. Using mode coupling theory we developed a model of the thermal conductivity, which diverges at the critical point, and used it to study the impact of hydrodynamic fluctuations on observables in high energy heavy ion collisions. The effect of the thermal conductivity on correlation functions is studied in a boost invariant hydrodynamic model via fluctuations, or noise. We find that the closer a thermodynamic trajectory comes to the critical point the greater is the magnitude of the fluctuations in thermodynamic variables and in the 2-particle correlation functions in momentum space. It may be possible to discern the existence of a critical point, its location, and thermodynamic and transport properties near to it in heavy ion collisions using the methods developed here.

It has now been firmly established, via lattice calculations, that QCD with its physical quark masses does not exhibit a phase transition at finite temperature and zero baryon density but only a very rapid crossover from quark-gluon plasma-like behavior to hadronic gas-like behavior [130]- [134]. However, since the up and down quark masses are so small, and chiral symmetry is nearly exact, there are reasons to suspect that there is a curve of first order phase transition in the temperature T versus baryon chemical potential μ plane, terminating at a critical point at $T_c > 0$ and $\mu_c > 0$. The existence of such a critical point has been found in various effective field theory models, such as the Nambu–Jona-Lasinio model [135]- [137], a composite operator model [138], a random matrix model [139], a linear σ model [137], an effective potential model [140], and a hadronic bootstrap model [141]. Lattice QCD has yet to confirm or deny the existence of a critical point. The reason is that inclusion of a chemical potential does not allow for straight-forward Monte Carlo samplings of the field configurations. For reviews see Refs. [142] and [143].

High energy heavy ion collisions may provide experimental evidence for a critical point and provide information on the behavior of the equation of state in its vicinity. Relevant to this are low energy runs at the Relativistic Heavy Ion Collider (RHIC), and in the future at the Facility for Antiproton and Ion Research (FAIR), at the SPS Heavy Ion and Neutrino Experiment (SHINE), and at Nuclotron-based Ion Collider Facility (NICA). Critical points are characterized by large fluctuations. This led to the suggestion to study fluctuations in conserved quantities, such as electric charge, baryon number, and strangeness on an event-by-event basis [**?**,**?**]. The effect is proportional to the spatial size of the domain or correlated region, which is probably rather small due to the finite size and lifetime in heavy ion collisions [144]. Therefore, it was suggested to measure higher moments to search for non-Gaussian behavior [145]. However, at present there is no experimental evidence for anomalous fluctuations of this kind [**?**].

A crucial issue is whether the critical point can ever be reached in a heavy ion collision. Colliding nuclei is necessary to reach high baryon density, but at the same time it creates entropy. If the initial entropy per baryon is much larger than that at the critical point, then the expanding matter will never pass close to it, even under the assumption of an ideal adiabatic expansion, since entropy can only increase with time, not decrease. The problem is similar to that of trying to create superheavy nuclei by colliding nuclei: too much entropy is created.

For this contribution, we summarize the main findings of our recent work [146]. In that paper we have constructed a semi-realistic model for the thermal conductivity due to an assumed critical point in the QCD phase diagram. At a critical point the thermal conductivity diverges, as does the shear viscosity. However, the critical exponent for the shear viscosity is much smaller than that for the thermal conductivity, with the implication that the influence of the divergence of the shear viscosity is confined to a very narrow window

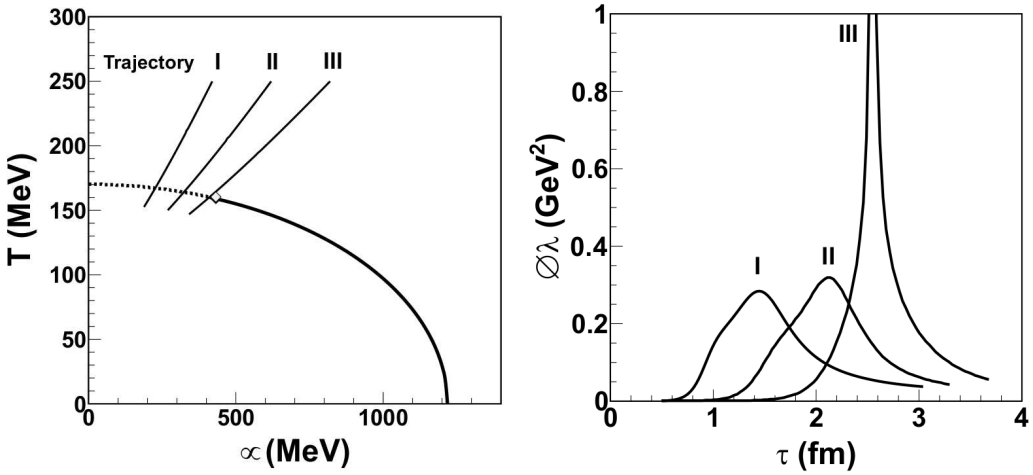

Figure 5.10: Left panel: The phase diagram showing the crossover curve and the three trajectories used in the computation. Right panel: Thermal conductivity as a function of proper time and trajectory.

in temperature, probably too small to have any effect on the matter produced in a heavy ion collision. In contrast, the temperature window for the enhancement of the thermal conductivity is much wider. These transport coefficients, along with the bulk viscosity, control the strength of hydrodynamic fluctuations in heavy ion collisions [147]. In particular, the strength of the hydrodynamic fluctuations due to thermal conductivity λ are quantified by the correlation function

$$\langle f(x_1) f(x_2) \rangle = 2\lambda \left(\frac{nT}{sw} \right)^2 \delta(x_1 - x_2) \ , \tag{5.14}$$

where $f(x)$ is a dimensionless fluctuation, or noise term, that appears in the hydrodynamic equations. Reference [147] applied the relativistic theory of hydrodynamic fluctuations to heavy ion collisions, with a specific example worked out for matter created with zero average baryon density.[13] In this paper we will focus on thermal conductivity and ignore viscosities for simplicity of exposition. This allows us to study the influence of a critical point on the produced matter in a controlled and quantitative manner, although the model we use is not realistic enough for direct comparison with experiment. The Landau-Lifshitz definition of flow velocity is used in this paper since it naturally extends to baryon-free matter, whereas the Eckart definition becomes ambiguous in that limit; see, for example, [147, 150]. Due to this rational choice of reference frame the behavior of the shear and bulk viscosities near the critical point only affect the background solution of the hydrodynamic equations for which, in this exploratory study, we use the perfect fluid solutions. Even greater effects may be anticipated when all of these effects are incorporated self-consistently.

Reference [151] constructed the free energy in the vicinity of the critical point that incorporated both the critical exponents and critical amplitudes. Using this free energy, the Landau theory of fluctuations was applied to estimate the probability of fluctuations away from the equilibrium state and were found to be very large. However, the Landau theory considers baryon number fluctuations in a finite volume in contact with a heat reservoir at fixed temperature, which does not adequately represent the space-time evolution of matter in a heavy ion collision. Dynamical simulations of spinodal decomposition, or phase separation, were done in [152] and [153], but without the incorporation of intrinsic hydrodynamical fluctuations or noise. In this article we assume that the entropy created in the collision is too high to allow any trajectories in the $T - \mu$ plane to pass through the coexistence region. Rather, following the earlier remarks on entropy in heavy ion collisions, we assume that the trajectories always pass to the left of the critical point, never entering the coexistence region or crossing the line of first order phase transition. This is a more conservative scenario for heavy ion experiments.

On the basis of mode coupling theory applied within a boost invariant hydrodynamics scenarium we have studied in [146] the influence of the hydrodynamic fluctuations on the 2-particle correlation functions. Figure 5.10 (right panel) shows the thermal conductivity as a function of time for the three trajectories chosen earlier.

[13] Earlier studies for extracting the shear viscosity in heavy ion collisions were done by [148] and for the bulk viscosity by [149].

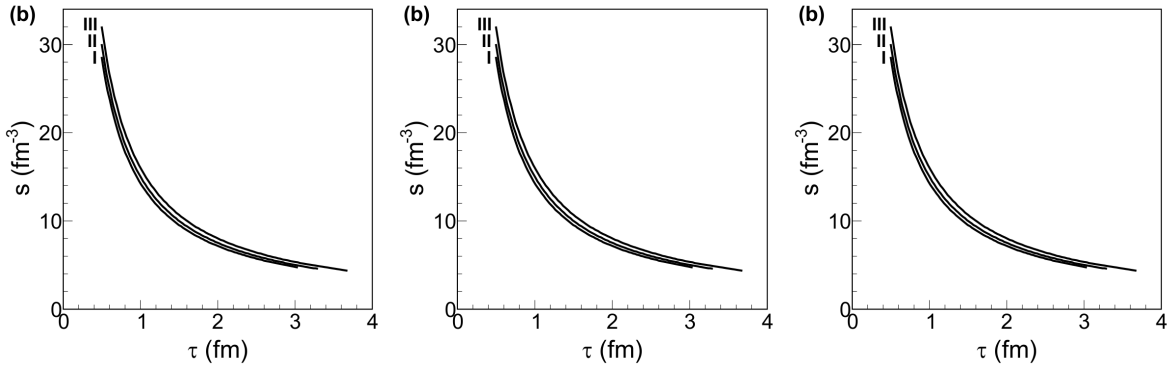

Figure 5.11: Left panel: Particle correlation function for protons. Middle and right panel: Particle correlation function for pions at zero chemical potential. (a) Non-zero fluctuations of chemical potential. (b) No fluctuations of chemical potential.

As the trajectory passes closer to the critical point the enhanced thermal conductivity is probed ever more closely. The effect of this on the 2-particle correlation functions is shown in Fig. 5.11 for protons ($d = 2$, $m_p = 939$ MeV, the left panel) and for charged pions ($d = 2$, $m_\pi = 138$ MeV, zero chemical potential, middle and right panels). We show the 2-particle correlation function for pions with no chemical potential fluctuation ($\delta\mu = 0$) (middle panels) and with pion chemical potential fluctuation equal to that of the protons (right panels). Which one is closer to reality cannot be determined without explicitly introducing a conserved electric current on the same footing as the baryon current. The presence of additional fluctuations enhances the magnitude of the correlation between particles. Both pions and protons exhibit the influence of the thermal conductivity. The shape is approximately the same for all trajectories. The protons have a maximum at $\Delta y = 0$ and a minimum near $\Delta y = 0.95$; the pions have a maximum at $\Delta y = 0$ and a minimum near $\Delta y = 1.7$ (with chemical potential fluctuations) or near 1.3 (without chemical potential fluctuations). The magnitude of the correlation, on the other hand, increases dramatically as one goes from trajectory I to II to III. As mentioned earlier, the boost invariant hydrodynamical model is not sufficiently realistic to consider any comparison to experiment, especially since one needs a large initial baryon number. Nevertheless, the size of the effect in this model bodes well for future theoretical studies and experiments.

We applied mode coupling theory, together with a parameterization of the equation of state that incorporates the correct critical exponents and amplitudes, to develop a model for the thermal conductivity in the vicinity of the critical point. This contribution to the thermal conductivity incorporates the correct critical behavior but can be used in the non-asymptotic region as well. The thermal conductivity quantifies the strength of particular hydrodynamic fluctuations via the fluctuation-dissipation theorem. To obtain insight into what effects might result in heavy ion collisions as a consequence of the critical point, we studied a simple boost-invariant hydrodynamic model. We conservatively assumed that the entropy per baryon created in a heavy ion collision is too large for an adiabat to enter the mixed phase. The thermal conductivity along the adiabatic trajectory is enhanced the closer the trajectory comes to the critical point. The flyby of the critical point results in fluctuations in the temperature, baryon chemical potential, and local flow velocity which evolve with time and are not the same as fluctuations in the initial conditions. We found that the growth of the thermal conductivity near the critical point implies the existence of two-particle correlations over 2 units of rapidity for protons. The strength of this correlation increases the closer the expansion trajectory comes to the critical point. In particular, the magnitude of the correlation is directly proportional to the time-integrated history of the thermal conductivity, making the correlation a sensitive probe of the thermal conductivity and of the presence of a critical point. With the inclusion of other transport coefficients (shear and bulk viscosities) this correlation can be further enhanced. We have found that the fluctuations in the baryon density –in particular the chemical potential fluctuations– are the most important effect for the magnitude of correlations compared to the thermal and velocity fluctuations alone. For this reason, we think that the usually neglected baryon diffusion coefficient –alternatively, the thermal conductivity– could be of interest for accessing the critical behavior by two-particle correlations. However, their practical use relies on the ability of the heavy-ion factories to produce

trajectories that pass close to the critical point.

There are many natural extensions to this study. For example, inclusion of the regular part of the thermal conductivity would increase the magnitude of the fluctuations and hence correlation functions in the final state observables. To quantify fluctuations due to electric charge, pions for example, requires the introduction of the electric charge current in addition to the baryon current. Introduction of the strangeness degree of freedom –the kaon multiplicity is typically larger than proton multiplicity– would also enhance the correlation function as one includes additional fluctuations in the strange chemical potential. Inclusion of the thermal conductivity into the fluid equations of motion, not only in the fluctuations, should certainly be done. This could potentially increase correlations because it couples some of the fluctuations among them in such a way that the drift matrix does not contain any nonvanishing element. The effect of this modification for the shear and bulk viscosities has been studied in [147] leading to a smoothing of the singularities appearing at the sound horizon.

An extension to the region of first order phase transition would be interesting. Decreasing the initial entropy per baryon below its value at the critical point would result in instabilities and phase separation, with probably greater consequences than a flyby of the critical point as studied here. The importance of the thermal conductivity in this regard has already been noted [154]. Ultimately a 3+1 dimensional calculation for the fireball evolution is necessary to study the hydrodynamical correlations not only in rapidity but also as a function of the azimuthal angle, analogous to what was done in Ref. [155]- [157] for initial state fluctuations. Their effects on the flow harmonics and the angular correlation of particles ought to be important. Such a study is of course much more difficult than the one presented here since one must perform extensive numerical calculations.

Bibliography

[1] G. I. Kopylov and M. I. Podgoretsky, Sov. J. Nucl. Phys. **15**, 656 (1973).

[2] G. I. Kopylov, Phys. Lett. **B 50,** 472 (1974).

[3] M. I. Podgoretsky, Sov. J. Part. Nucl. **20**, 266 (1989).

[4] D. H. Rischke and M. Gyulassy, Nucl. Phys. **A 608,** 479 (1996).

[5] J. W. Harris and B. Muller. Ann. Rev. Nucl. Part. Sci. **46**, 71 (1996).

[6] A. Bass, M. Gyulassy, H. Stoecker, and W. Greiner, J. Phys. G. **25,** R1 (1999).

[7] W. Cassing and E. Bratkovskaya, *Talk at the Symposium on The Physics of Dense Baryonic Matter*, (Darmstadt, March 9-10, 2009); https://www.gsi.de/ documents/FOLDER-9871235706286.html .

[8] R. Lednicky and M. I. Podgoretsky, Sov. J. Nucl. Phys. **30**, 432 (1979).

[9] C. Alt *et al.*, (NA49 Collaboration), [arXiv:0809.1445].

[10] S. Afanasiev *et al.*, (PHENIX Collaboration), Phys. Rev. Lett. **100,** 232301 (2008).

[11] M. A. Lisa, S. Pratt, R. Soltz and U. Wiedemann, Ann. Rev. Nucl. Part. Sci. **55**, 357 (2005).

[12] F. Retiere and M. A. Lisa, Phys. Rev. **C 70,** 044907 (2004).

[13] M. A. Lisa, U. Heinz and U. Wiedemann, Phys. Lett. **B 489,** 287 (2000).

[14] J. Adams *et al.*, (STAR Collaboration), Phys. Rev. Lett. **90,** 12307 (2004).

[15] U. Heinz and B. Kolb, Phys. Lett. **B 542,** 216 (2002).

[16] M. A. Lisa and S. Pratt, [arXiv:0811.1352].

[17] U. Heinz and B. Kolb, Phys. Lett. **B 469,** 557 (1999).

[18] W. Reisdorf and H. G. Ritter, Ann. Rev. Nucl. Part. Sci. **47**, 663 (1997).

[19] M. A. Lisa *et al.*, (E895 Collaboration), Phys. Lett. **B 496,** 1 (2000).

[20] J. Brachman *et. al.*, Phys. Rev. **C 62,** 024909 (2000), [nucl-th/9908010].

[21] L. P. Csernai and R. Rohrich, Phys. Lett. **B 458,** 458 (1999), [nucl-th/9908034].

[22] H. Stoecker, Nucl. Phys. **A 750,** 121 (2005).

[23] D. Kharzeev, Phys. Lett. **B 633,** 260 (2006).

[24] D. E. Kharzeev *et al.*, Nucl. Phys. **A 803,** 227 (2008).

[25] V. A. Okorokov, [0809.3130 [nucl-ex]].

[26] O. Rogachevsky, A. Sorin and O. Teryaev, Phys. Rev. **C 82,** 054910 (2010), [arXiv:1006.1331 [hep-ph]].

[27] B. I. Abelev *et al.*, Phys. Rev. Lett. **103,** 251601 (2009).

[28] B. I. Abelev *et al.*, Phys. Rev. **C 81,** 054908 (2010).

[29] D. E. Kharzeev, *private communications.*

[30] S. A. Voloshin, Phys. Rev. **C 70,** 057901 (2004).

[31] V. A. Okorokov, [0908.2522 [nucl-th]].

[32] H. U. Abramyan *et al.*, *The MultiPurpose Detector (MPD) to study Heavy Ion Collisions at NICA*. Letter of Intent. Version 1, Dubna, 2008.

[33] K. H. Ackermann *et al.*, Nucl. Phys. **A 661,** 681 (1999).

[34] R. Lednicky *et al.*, Phys. Lett. **B 373,** 30 (1996).

[35] R. Lednicky, [arXiv : nucl-th/0112011]; [nucl-th/0212089].

[36] V.A. Okorokov, Proceedings of the XVIII International Baldin Seminar on High Energy Physics Problems, Dubna. V.II, 101 (2008). Eds. by A.N. Sissakian, V.V. Burov, A.I. Malakhov.

[37] C. Greiner, B. M?ller, Phys. Lett. **B 219,** 199 (1989).

[38] M. Gazdzicki and M. I. Gorenstein, Acta. Phys. Polon. **B 30,** 2705 (1999); M. I. Gorenstein, Phys. Atom. Nucl. **71**, 1594 (2008).

[39] M. Gazdzicki, M. I. Gorenstein and S. Mrowczynski, Phys. Lett. **B 585,** 115 (2004);

[40] M. I. Gorenstein, M. Gazdzicki and O. S. Zozulya, Phys. Lett. **B 585,** 237 (2004).

[41] M. Stephanov, K. Rajagopal and E. Shuryak, Phys. Rev. **D 60,** 1140281 (1999) [hep-ph/9903292].

[42] M. I. Gorenstein, Phys. Part. Nucl. **39,** 1102 (2008).

[43] V. P. Konchakovski, B. Lungwitz, M. I. Gorenstein and E. L. Bratkovskaya Phys. Rev. **C 78,** 024906 (2008), [arXiv:0712.2044]].

[44] M. I. Gorenstein, M. Hauer, V. P. Konchakovski, E. L. Bratkovskaya, Phys. Rev. **C 79,** 024907 (2009), [arXiv:0811.3089].

[45] H. Stoecker and W. Greiner, Phys. Rep. **137,** 277 (1986).

[46] C. M. Hung and E. V. Shuryak, Phys. Rev. Lett. **75,** 4003 (1995).

[47] L. V. Bravina, A. Faessler, C. Fuchs and E. E. Zabrodin, Phys. Rev. **C 61,** 064902 (2000).

[48] E. E. Zabrodin, C. Fuchs, L. V. Bravina and A. Faessler, Phys. Rev. **C 63,** 034902 (2001).

[49] L.V. Bravina, Phys. Lett. **B 344,** 49 (1995).

[50] L.V. Bravina, E.E. Zabrodin, A. Faessler and C. Fuchs, Phys. Lett. **B 470,** 27 (1999).

[51] M. Bleicher and H. Stoecker, Phys. Lett. **B 546,** 309 (2002).

[52] S. Voloshin and Y. Zhang, Z. Phys. **C70**, 665 (1996).

[53] C. Alt *et al.*, (NA49 Collaboration), Phys. Rev. **C 68,** 034903 (2003).

[54] L. V. Bravina *et al.*, Phys. Lett. **B 354,** 196 (1995); Nucl. Phys. **A 594,** 425 (1995).

[55] L. V. Bravina, I. N. Mishustin, J. P. Bondorf, A. Faessler and E. E. Zabrodin, Phys. Rev. **C 60,** 044905 (1999).

[56] F. Gastineau and J. Aichelin, Phys. Rev. **C 65,** 014901 (2002).

[57] A. Makhlin and E. Surdutovich, Phys. Rev. **C 59,** 2761 (1999).

[58] J.-Y. Ollitrault, Phys. Rev. **D 46,** 229 (1992).

[59] H. Sorge, Phys. Rev. Lett. **82,** 2048 (1999).

[60] P. Kolb, J. Solfrank and U. Heinz, Phys. Rev. **C 62,** 054909 (2000).

[61] S. A. Voloshin, J. Phys. Conf. Ser. **9**, 276 (2005).

[62] E. Shuryak, [hep-ph/0504048].

[63] I. P. Lokhtin, L. V. Malinina, *et al.*, Comput. Phys. Commun. **180**, 779 (2009).

[64] M. Luzum and P. Romatschke, Phys. Rev. **C 78,** 034915 (2008), **79**, 039903 (2009).

[65] H. Song and U. Heinz, Nucl. Phys. **A 830,** 287 (2009)

[66] G. S. Denicol, T. Kodama, T. Koide and Ph. Mota, Phys. Rev. **C 2009** 80 064901, A. Monnai and T. Hirano, Phys. Rev. **C 80,** 054906 (2009).

[67] G. S. Denicol, T. Kodama and T. Koide, [arXiv: nucl-th/1002.2394v1] .

[68] S. Jeon and V. Koch; eds. R.C. Hwa and X.-N. Wang *Quark-Gluon Plasma 3*, (World Scientific, Singapore) [arXiv:hep-ph/0304012v1].

[69] S. A. Voloshin, V. Koch, H. G. Ritter, Phys. Rev. **C 60,** 024901 (1999).

[70] R. P. G. Andrade *et al.*, Phys. Rev. Lett. **101,** 112301 (2008); Acta. Phys. Polon. **B 40,** 931 and 993 (2009) [arXiv:hep-ph/0901.2849v1].

[71] C. E. Aguiar, E. S. Fraga and T. Kodama, J. Phys. G. **32,** 179 (2006), [arXiv:nucl-th/0306041v2].

[72] K. Paech, H. Stoecker and A. Dumitru, Phys. Rev. **C 68,** 044907 (2003); K. Paech and A. Dumitru, Phys. Lett. **B 623,** 200 (2005).

[73] A. Mocsy and P. Sorensen, Phys. Lett. **B 690,** 135 (2010), [arXiv:nucl-th/0908.3983v2].

[74] T. Hirano, J. Phys. G: Nucl. Part. Phys. **30**, S845 (2004).

[75] K. Werner *et al.*, J. Phys. G: Nucl. Part. Phys. **36**, 064030 (2009), [arXiv:nucl-th/0907.5529v2].

[76] F. Grassi, Y. Hama and T. Kodama, Phys. Lett. **B 355,** 9 (1995).

[77] S. V. Akkelin, Y. Hama, Iu. Karpenko and Yu. M. Sinyukov, Phys. Rev. **C 78,** 034906 (2008), [arXiv:nucl-th/0804.4104v4]

[78] K. Werner *et al.*, [arXiv:1004.0805v1[nucl-th]]; S. Pratt, Nucl. Phys. **A 830,** 51 (2009), [arXiv:nucl-th/0907.1094].

[79] J. Berges, S. Borsanyi and C. Wetterich, Phys. Rev. Lett. **93,** 142002 (2004), [arXiv:hep-ph/0403234]

[80] C. Tsallis, J. Stat. Phys. **52**, 479 (1988).

[81] A. S. Parvan, T. S. Biro, [arXiv:1003.5630v1 [cond-mat.stat-mech]]

[82] G. Wilk and Z. Wlodarczyk, Phys. Rev. Lett. **84,** 2770 (2000).

[83] T. Osada, Phys. Rev. **C 81,024907** (2010), [arXiv:nucl-th/0911.2303v2]

[84] T. S. Biro, G. Purcsel and K. Urmossy, Eur. Phys. J. **A 40,** 325 (2009).

[85] A. Adare *et al.* (PHENIX collaboration), [arXiv:1005.3674v1[hep-ex]] .

[86] C. Sasaki, B. Friman and K. Redlich, J.Phys.G: Nucl. Part. Phys. **35**, 104095(2008)

[87] J. Takahashi et al., Phys. Rev. Lett. 103, 242301 (2009) [arXiv:nucl-th 0902.4870v2].

[88] R. Andrade, F. Grassi, Y. Hama and W.-L. Qian, [arXiv:0912.0703v3 [nucl-th]] .

[89] G. Torrieri, *Flow scaling in a low energy collider: When does the perfect fluid turn on?'*, this volume.

[90] G. Odyniec (STAR collaboration), J. Phys. G: Nucl. Part. Phys. **35**, 104164 (2008).

[91] A. N. Sissakian, A. S. Sorin, M. K. Suleymanov, V. D. Toneev and G. M. Zinovjev, Phys. Part. Nucl. Lett. **5**,1 (2008).

[92] NICA White Paper v.3.3, Chapter I, http://theor.jinr.ru/twiki/pub/ NICA/WebHome/

[93] S. A. Bass *et al.*, Prog. Part. Nucl. Phys. **41**, 255 (1998).

[94] M. Bleicher *et al.*, J. Phys. G. **25,** 1859 (1999).

[95] H. G. Baumgardt *et al.*, Z. Phys. **A273** , 359 (1975).

[96] J. Gosset *et al.*, Phys. Rev. Lett. **62,** 1251 (1989).

[97] B. Adyasevich *et al.*, Nucl. Phys. B (Proc. Suppl.) **16**, 419 (1990).

[98] S. Voloshin and Y. Zhang, Z. Phys. C **70**, 665 (1996).

[99] P. Rau, J. Steinheimer, B. Betz, H. Petersen, M. Bleicher and H. Stöcker, [arXiv:1003.1232 [nucl-th]].

[100] M. Bleicher, K.A. Bugaev, P. Rau, A.S. Sorin, J. Steinheimer, H. Stöcker, [arXiv:1106.xxxx [nucl-th]].

[101] for a discussion and estimates see D. Blaschke, F. Sandin, V. Skokov and S. Typel, *NICA White Paper* v.3.3, http://theor.jinr.ru/twiki/pub/ NICA/WebHome/ and refences therein.

[102] H. Stöcker, J. A. Maruhn and W. Greiner, Z. Phys. A **293**, 173 (1979).

[103] H. Stöcker, J. A. Maruhn and W. Greiner, Phys. Rev. Lett. **44,** (1980) 725.

[104] J. Y. Ollitrault, Nucl. Phys. **A 638,** 195 (1998) and references therein.

[105] see R. Stock, J. Phys. **G 30**, (2004) S633 and references therein.

[106] S. S. Adler *et al.*, (PHENIX Collaboration), Phys. Rev. Lett. **91,** (2003) 182301.

[107] B. Alver and G. Roland, Phys. Rev. **C 81,** 054905 (2010).

[108] Q. -f. Li, Z. -x. Li, S. Soff, M. Bleicher, H. Stoecker, J. Phys. **G32** , 151 (2006).

[109] Q. -f. Li, Z. -x. Li, S. Soff, M. Bleicher, H. Stoecker, J. Phys. **G32** , 407 (2006).

[110] H. Petersen, Q. Li, X. Zhu and M. Bleicher, Phys. Rev. **C 74,** 064908 (2006).

[111] D. I. Blokhintsev, ZhETP **6**, 995 (1958).

[112] A. Bohr and B. Mottelson, *"Nuclear Structure", Benjamin Press*, (New York, 1975), Vol.2.

[113] D. Seibert, Phys. Rev. Lett. **63,** 136 (1989).

[114] A. Stavinskiy *et al.*, *NICA White Paper v.3.3*, http://theor.jinr.ru/twiki/pub/NICA/WebHome/

[115] H. Petersen, G.-Y.Qin, S. A. Bass and B. Müller, [arXiv:1008.0625v2 [nucl-th]].

[116] D. E. Kharzeev and D. T. Son, [arXiv:1010.0038v1 [hep-ph]].

[117] M. M. Aggarwal *et al.* (STAR Collaboration), Phys. Rev. Lett. **105**, 022302 (2010).

[118] V. Koch, [arXiv:0810.2520 [nucl-th]].

[119] M. A. Stephanov, K. Rajagopal, and E. V. Shuryak, Phys. Rev. **D 60**, 114028 (1999).

[120] Y. Hatta and M. A. Stephanov, Phys. Rev. Lett. **91**, 102003 (2003) [Erratum-ibid. **91**, 129901 (2003)].

[121] M. A. Stephanov, Phys. Rev. Lett. **102**, 032301 (2009).

[122] M. Asakawa, U. W. Heinz, and B. Müller, Phys. Rev. Lett. **85**, 2072 (2000).

[123] S. Jeon and V. Koch, Phys. Rev. Lett. **85**, 2076 (2000).

[124] S. Ejiri, F. Karsch and K. Redlich, Phys. Lett. **B 633**, 275 (2006).

[125] M. Asakawa, S. Ejiri, and M. Kitazawa, Phys. Rev. Lett. **103**, 262301 (2009).

[126] B. Friman, *et al.*, Eur. Phys. J. **C 71**, 1694 (2011).

[127] M. A. Stephanov, Phys. Rev. Lett. **107**, 052301 (2011).

[128] M. Kitazawa and M. Asakawa, Phys. Rev. **C 85**, 021901R (2012).

[129] M. Kitazawa and M. Asakawa, [arXiv:1205.3292 [nucl-th]].

[130] Y. Aoki, G. Endrodi, Z. Fodor, S. D. Katz, and K. K. Szabo, Nature **443**, 675 (2006).

[131] Y. Aoki, Z. Fodor, S. D. Katz, and K. K. Szabo, Phys. Lett. **B 643**, 46 (2006).

[132] Y. Aoki, Sz. Borsanyi, S. Durr, Z. Fodor, S. D. Katz, S. Krieg, and K. K. Szabo, JHEP **0906**, 088 (2009).

[133] S. Borsanyi, Z. Fodor, C. Hoelbling, S. D. Katz, S. Krieg, C. Ratti, and K. K. Szabo, JHEP **1009**, 073 (2010).

[134] A. Bazavov, *et al.*, Phys. Rev. **D 85**, 054503 (2012).

[135] M. Asakawa and K. Yazaki, Nucl. Phys. **A 504**, 668 (1989).

[136] J. Berges and K. Rajagopal, Nucl. Phys. **B 538**, 215 (1999).

[137] O. Scavenius, A. Mòcsy, I. N. Mishustin, and D. H. Rischke, Phys. Rev. **C 64**, 045202 (2001).

[138] A. Barducci, R. Casalbuoni, S. De Curtis, R. Gatto, and G. Pettini, Phys. Lett. **B231**, 463 (1989); Phys. Rev. D **41**, 1610 (1990); A. Barducci, R. Casalbuoni, G. Pettini, and R. Gatto, *ibid.* **49**, 426 (1994).

[139] M. A. Halasz, A. D. Jackson, R. E. Shrock, M. A. Stephanov, and J. M. Verbaarschot, Phys. Rev. **D 58**, 096007 (1998).

[140] Y. Hatta and T. Ikeda, Phys. Rev. **D 67**, 014028 (2003).

[141] N. G. Antoniou and A. S. Kapoyannis, Phys. Lett. **B 563**, 165 (2003).

[142] M. Stephanov, Prog. Theor. Phys. Suppl. **153**, 139 (2004); Int. J. Mod. Phys. **A 20**, 4387 (2005); PoS(LAT2006)024.

[143] B. Mohanty, Nucl. Phys. **A 830**, 899c (2009) .

[144] B. Berdnikov and K. Rajagopal, Phys. Rev. D **61**, 105017 (2000).

[145] M. A. Stephanov, Phys. Rev. Lett. **102**, 032301 (2009).

[146] J. I. Kapusta and J. M. Torres-Rincon, Phys. Rev. **C 86**, 054911 (2012).

[147] J. I. Kapusta, B. Müller, and M. Stephanov, Phys. Rev. **C 85**, 054906 (2012).

[148] S. Gavin and M. Abdel-Aziz, Phys. Rev. Lett. **97**, 162302 (2006).

[149] A. Dobado, F. J. Llanes-Estrada and J. M. Torres-Rincon, Eur. Phys. J. C **72**, 1873 (2012).

[150] J. I. Kapusta and C. Gale, *Finite Temperature Field Theory*, Cambridge University Press, Cambridge, 2nd edition, 2006.

[151] J. I. Kapusta, Phys. Rev. **C 81**, 055201 (2010).

[152] D. Bower and S. Gavin, Phys. Rev. **C 64**, 051902 (2001).

[153] J. Randrup, Phys. Rev. **C 79**, 054911 (2009).

[154] V. V. Skokov and D. N. Voskresensky, Nucl. Phys. **A 847**, 253 (2010)

[155] E. Shuryak, Phys. Rev. **C 80**, 054908 (2009).

[156] P. Staig and E. Shuryak, Phys. Rev. **C 84**, 034908 (2011).

[157] P. Staig, E. Shuryak, Phys. Rev. **C 84**, 044912 (2011).

6 Mechanisms of multi-particle production

The mechanism by which the energy of the colliding hadrons or nuclei is converted into the final-state particles is a long-standing problem in physics. There has been significant progress in understanding this mechanism at high energies, where the strong color fields inside the colliding hadrons or nuclei play an important role. The systematics of data on hadron production shows that such an approach formulated in terms of gluons and quarks applies starting from the c.m.s. energy of 15 GeV. Below that energy, the dynamics of multi-particle production should probably be described in terms of some effective low-energy degrees of freedom. The deviations from the trends established earlier at higher energies at RHIC and SPS should provide an important clue to this dynamics. An important part of the NICA program is the physics of high multiplicity events, which are expected to give an access to QCD in the high parton density regime even at a moderate energy. It will be very interesting to explore the evolution of the produced system towards freeze-out through a possible mixed phase, as discussed in this section. A detailed study of multi-particle production in the energy range of the NICA collider will thus contribute to the understanding of Quantum Chromo-Dynamics in the non-perturbative domain.

6.1 My several thoughts on NICA

E. Levin

Department of Particle Physics, Tel Aviv University, Tel Aviv, Israel

First, I would like to state clear why I think that we need the nucleus-nucleus collider for the intermediate range of energy. My own experience in describing the ion-ion collision at RHIC taught me that starting from $W = \sqrt{s} \approx 17\ GeV$ we can expect that the best theoretical approach to ion-ion interaction is the QCD cascade in terms of quark and gluons, while at low energies the successful description has been given in terms of hadron cascade. The intermediate energies are needed just to study the transition from hadron cascade to the QCD one.

Having this idea in mind, I think that the NICA project has one shortcoming and one advantage.

The shortcoming is obvious: the upper energy is too low. Indeed, in our paper [1] we showed that starting with $W = 17\ GeV$ we can describe the data on multiplicity using the QCD approach based on saturation of the gluon density and on Colour Glass Condensate (CGC). Therefore, I believe that we need the accelerator which will cover the range: $2 \div 20\ GeV$, From this point of view the upper energy of NICA ($W = 12\ GeV$ is too low.

The advantage is the fact that it is a new machine and we can adjust construction to our specific goals. As I have mentioned the most interesting phenomena occur at large parton densities where the CGC gives the effective theory to describe the QCD cascade. We have explored two ways to penetrate the region of high parton density: the high energy scattering (Tevatron, HERA and coming LHC) and ion-ion collisions (RHIC and LHC).

However, there is another way to enter this region: to measure the events with high hadron multiplicities. The density of hadrons as well as partons are expected to be high in these events and, therefore we can expect to see all high-density QCD predictions.

The second key question that NICA can shed the light is the thermodynamic equilibrium. The data show that the spectrum of the produced particle behaves as $\exp(-E/T)$ where E is the energy of the particle. This spectrum is an indication that we reach the equilibrium. However, the real thermodynamic equilibrium means that all correlations have the same exponential behaviour or very small. I have not found any systematical study of correlation for ion-ion collisions. I believe that NICA can provide the first of this study.

Summarizing, I see two major goals for NICA:

- Study the high multiplicity events to penetrate into the kinematic region suitable for high density QCD: roughly speaking we have to do the multiplicity of the order of multiplicities in high energies, say $W > 15\ GeV$.
- Systematic study of particle correlations to find out whether we have the stage of thermodynamic equilibrium in ion-ion collisions.

Frankly speaking I have only preliminary list of possible experiments which I want to share with you.

- The p_T distribution in high multiplicity events. We expect that the typical transverse momentum $Q_s^2 \propto \rho$ where ρ is the density of partons (particles) in the transverse plane. Therefore, we expect that the mean p_T increases for larger values of ρ.

- The rapidity distribution in high multiplicity events. The KLN approach [2] predicts the rapidity distribution at different and large multiplicities and these formulae can give us the first estimates for what we can expect in ion-ion collisions at this energies. However much work is needed to take into account the effect of rather low energies.

- The azimuthal angle correlations. Qualitatively, CGC leads to the suppression of azimuthal angle correlations for particle with transverse momenta close to the saturation momentum ($p_T \approx Q_s$) since the transverse momentum of the detected particle can be compensate by several particles with the transverse momentum Q_s. In our paper we suggest several way to measure this effect. As far as I know the best way is to measure the correlation between particles with sufficiently large difference in rapidity [3]. The main idea to measure these correlations as a function of the multiplicity is to observe how the number of uncorrelated pair increases with the value of multiplicity.

- One of interesting features of ion-ion collisions is the existence of a hydrodynamical stage in the final state (for some time after collision). I am sure that the measurement of the elliptic flow (v_2 as a function of the multiplicity) will clarify the question how hydro works and at what distances and time.

Certainly this is not full list of the interesting experiments, but at this stage of planning it is enough to think about.

6.2 Some issues in NICA-related research at LPI

I. Dremin and A. Leonidov

P. Lebedev Physics Institute, Moscow, Russia

One of the crucial characteristics of dense strongly interacting matter created in heavy ion collisions is a collective flow of final hadrons. To quantify the amount of flow present in collisions at given energy it is very important to make a careful subtraction of rescattering effects that are present already in proton-nucleus collisions and can mimic some part of collective flow. In fact a model based on parametrizing effects of transverse rescattering in terms of transverse rapidity [4, 5] was shown to provide a very good description of transverse and longitudinal hadron spectra for different hadron types (with an interesting exception of kaons). One can argue that a more natural description of the effects of transverse broadening is to use transverse momentum, not transverse rapidity as a variable quantifying an amount of this rescattering. To analyze this issue one has to work out a corresponding version of the model of [4, 5]. This work is currently underway.

In a more distant perspective our group is planning to study several issues directly related to the main object of experimental studies at NICA, the mixed baryon-rich phase of QCD:

- Kinetic description of fluctuations in the expanding mixed phase. Comparative analysis of baryonless and baryon-rich case.

- Possible role of gluon junctions in the physics of mixed phase.

- Microcanonical description of the physics of mixed phase.

6.3 Hydrokinetic analysis of space-time evolution and properties of strongly interacting matter formed at the NICA and FAIR energies

Yu. Sinyukov

Bogolyubov Institute for Theoretical Physics, Kiev, Ukraine

The phase evolution of strongly interacting matter created at the NICA and FAIR energies is expected to occur near the bondary of the first order phase transition and possibly in vicinity of the critical QCD point. The initially hot and dense matter, produced in A+A collisions, cools down and loses density because of fast

expansion, and passes, therefore, all the thermodynamic phases crossing, possible, phase boundary. The lifetime of such a system is around 10 fm/$c = 10^{-22}$ sec. The information about evolution and properties of the matter can be extracted only from one- and multi-particle momentum spectra for different particle species. The hadrons appears as a result of their gradual liberalization from the interacting matter, this process lasts, typically, a half of the total lifetime of the created finite system [6, 7]. So, the peculiarities and distinctive properies of observables related to characteristics of the new states of matter have to be analysed only within the reliable approach allowing one to describe correctly the evolution, particle emission and spectra formation from the system undergoing the phase transition during its fast expansion.

Hydrodynamic models gives possibility to describe the space-time evolution of the system basing on the hypothesis of local thermalization and energy-momentum conservation low. The microscopic properties of the matter, including complicated kinetics of the possible phase transition, are encoded then only in corresponding equation of state - it is the main advantage of the hydrodynamic models. At the same time, the application of this approach to finite explosively expanding systems faces difficulties since the particles are emitted continuously and so, especially at the later stage, the system is not in local equilibrium. So, the standard Landau/Cooper-Frye prescription, treating the spectra formation as the result of a sudden transition from an ideal fluid to an ideal gas that corresponds to instant switching of very big value of particle cross section in perfect fluid to zero value, is too rough approximation [6, 7]. The hybrid models [8] that match hydrodynamics with cascade models, like UrQMD, collide with problem of causality [9]. Our description of particle emission and spectra formation is based on the hydrokinetic approach (shortly HKM - Hydro-Kinetic Model) [6, 10] that initially has been applied for the systems with the cross-over type of equation of state and zero or small baryonic densities at the RHIC energies [11–13]. The HKM method is based on an analysis of the kinetic equations in terms of probabilities of particles to escape from the hydrodynamically expanding system consisting of these particles. It deals with non-locally equilibrium distribution functions and accounts for a back reaction of the emitted particles on the system evolution.

To simulate the hadron emission and spectra formation at the NICA and FAIR energies we are planning to develop the theoretical basis allowing include into the HKM the modified properties of hadrons in the strongly interacting medium with high baryonic density. The non-equilibrium effects, connected with continuous hadron emission, and viscosity are taken into account in a generalized relaxation time approximation [6, 13]. The local hydrodynamic variables evolve according to hydrodynamic equations of ideal fluid with sources/sinks in the right hand side [6] and account for a possible phase transition and critical QCD point. The corresponding numerical code serves then as an effective tool for calculation of the one- and multi-particle hadronic spectra depending on the properties of the formed matter and initial conditions at the energies of NICA and FAIR.

Collective flows in expanding matter, that are reflected in the spectra of emitting hadrons, depend essentially on properties of super-dense states of the strongly interacting matter, e.g., on its equation of state. A few types of flows are marked out in the experimental analysis: radial flow (isotropic component) and elliptic one - azimuthally asymmetric flows, which appears due to the almonds-like form of the initial interacting region of two nuclei in non-central collisions. We plan to provide a detail study of both types of flows, the transverse momentum spectra and its azimuthal anisotropy as well as the two-particle Bose-Einstein correlation functions. The latter contain main information as for space and time scales of the systems formed in relativistic A + A collisions.

Definitive aim of the hydrokinetic study for NICA and FAIR energies is a search for "anomalies" in spectra and correlation functions which become apparent when the phase trajectory of evolving system passes in vicinity of the critical point or crosses the boundary of the first order phase transition, as well as a search of signatures of in-medium modification of hadron spectral function in hot and dense strongly interacting nuclear surrounding.

The hydro-kinetic approach, which directly accounts for particle interaction inside the matter, allows one to calculate and compare the spectra and correlations for hadrons with different cross-sections, including the particles with "open" and "hidden" charm having a relatively small cross-sections. Because a value of cross-section affect essentially probabilities of the particle emission, it allows one to study varied temporal "slices" of the hadronic matter associated with the different temperatures using corresponding particle species. Such an investigation of the spectra and correlations of particles with different cross-sections is also important because the hadron cross-section in dense medium is different from those which is in the vacuum. This allows one to study off-vacuum modifications of the hadron properties in dense strongly interacting medium. The method can be a useful supplement to the CBM program of an analysis of an influence of the dense medium on hadron properties based on a study of short-lived vector mesons which decay inside the medium on free-emitted lepton pairs.

6.4 Open and hidden strangeness production

E. Kolomeitsev and B. Tomášik

Univerzita Mateja Bela, Banská Bystrica, Slovakia

Since a long time an enhancement of strangeness production in heavy ion collisions has been considered as a signal for quark-gluon plasma formation. The discovery of the sharp peak of K^+/π^+ multiplicity ratio for collisions at beam energy of 30 AGeV is interpreted as a signal for QGP formation, since purely hadronic models without a deconfinement phase transition were not able so far to reproduce the peak. Mainly two quantities are decisive for how much strangeness is produced in a collision: available energy and time. Clearly, more energy increases the rates for production of strange particles. Furthermore, in an environment with under-represented strangeness the abundance of strange particles grows with time.

In Ref. [15] we argued that the peak can be explained as a combination of two effects:

- due to an increase of the collision energy more energy becomes available for strangeness production that enhance the strangeness production;
- the lifespan of the fireball decreases with a collision energy increase, this can lead to the sharp decrease of that ratio.

The physics picture behind the second assumption is that nuclear stopping is stronger at lower energies and expansion is mainly built up from pressure. This takes some time. On the other hand at higher collision energy transparency regime is reached and the longitudinal expansion is, to a large amount, due to original motion of the nuclei. Thus expansion may be quick. The fireball disintegrates when the energy density drops below some critical value, depending also on the expansion speed. Alternatively, one can argue that at higher collision energy the expansion also starts from higher initial (energy) density and might need longer time to drop to its freeze-out value. Hence, the lifetime as a function of collision energy results from two competing effects: the initial energy density which increases with $\sqrt{s_{\rm NN}}$ and tends to prolong the lifetime, and the stopping power which decreases with $\sqrt{s_{\rm NN}}$ and leads to a shortening of the lifetime.

The quantitative question how the fireball lifetime depends on $\sqrt{s_{\rm NN}}$ is non-trivial and cannot be answered conclusively with the present theoretical studies at hand.

The practical results of [15] is that the K^+/π^+, K^-/π^- and Λ/π ratios can be qualitatively described if the the fireball lifetime varies from 15 – 20 fm at the collision energies E = 11.6 AGeV to 25-30 fm at $E_{\rm lab}$ = 30 AGeV and decreases gradually down to 15 fm between 30 and 80 AGeV. We have to note that the obtained lifetimes are sizeably longer than that follow from the hydrodynamical calculations, e.g., [14]. The observed amount of strangeness can hardly be produced during the shorter time unless there is some mechanism to enhance the in-medium production rates, which is operative even at the lower collision energies below an expected phase transition region.

So there is a need in more detailed and thorough study of strangeness production in heavy ion collision which can reveal some details of collision dynamics. For complete reconstruction of the strangeness production dynamics it is mandatory to measure not only strange mesons, but also hyperons. A sensitive test of strangeness production mechanism is also the measurement of multistrange baryons (Ξ, Ω).

Another messenger of the strangeness dynamics in heavy-ion collision is ϕ meson of which the dominant component is a spin-one bound state of s and $\bar{s}$ quarks. The ϕ meson production is an important part of the study program of different nucleus-nucleus collision experiments in the whole range of collision energies: at the AGS, the SPS, RHIC, and even at deeply subthreshold energies at the SIS. As the longest-living vector meson, the ϕ is considered to be a good probe of the collision dynamics: it would decay mainly outside the fireball and the daughter hadrons would be weakly affected by rescattering. The dominant hadronic decay is $\phi \to \bar{K} K$, hence, the production of ϕ's interplays with the production of strange mesons in nucleus-nucleus collisions.

In [**?**] we propose a new mechanism of ϕ meson production in nucleus-nucleus collisions—the catalytic reactions on strange particles, e.g., $\pi Y \to \phi Y$ and $\bar{K} N \to \phi N$. These reactions are OZI-allowed and their cross section can be by an order of magnitude larger than the cross section of conventional OZI-suppressed ϕ production reactions $\pi N \to \phi N$ and $N\Delta \to \phi N$, etc, considered so far. These reactions require only one strange

particle in the entrance channel and therefore are less suppressed than the strangeness coalescence reactions, $K\bar{K} \to \phi$ and $KY \to \phi N$ in collisions where strangeness is statistically suppressed. Comparison of the rates of ϕ production in the catalytic reactions and in the $\pi N \to \phi N$ reaction shows that the former can be competitive in collisions with the maximal temperature above 110 MeV and the collision time $\gtrsim$ 10 fm. The efficiency of catalytic reactions increases if some strangeness is presented in the fireball right in the beginning after the first most violent nucleon-nucleon collisions and if the fireball lifetime is longer. Thus the ϕ meson production can serve as a timer for a nucleus-nucleus collision.

Summarizing, we suggest that the NICA/MPD research program should put some emphasize on the strange particle production, including *hyperons*, and the ϕ mesons. Important complementary information on the production mechanisms can be extracted from the centrality dependence of the particle yields.

6.5 Chemical freeze-out and strangeness production study at NICA

F. Becattini

University of Florence, Italy

Chemical freeze-out in relativistic heavy ion collisions has been studied systematically from few to few hundreds GeV/s in the nucleon-nucleon centre-of-mass energy [16–18]. The picture that has emerged from such studies is that of a regular behaviour of the parameters which determine the state of the source, i.e. temperature and baryon-chemical potential: a steep increase (decrease) of temperature (baryon-chemical potential) in the

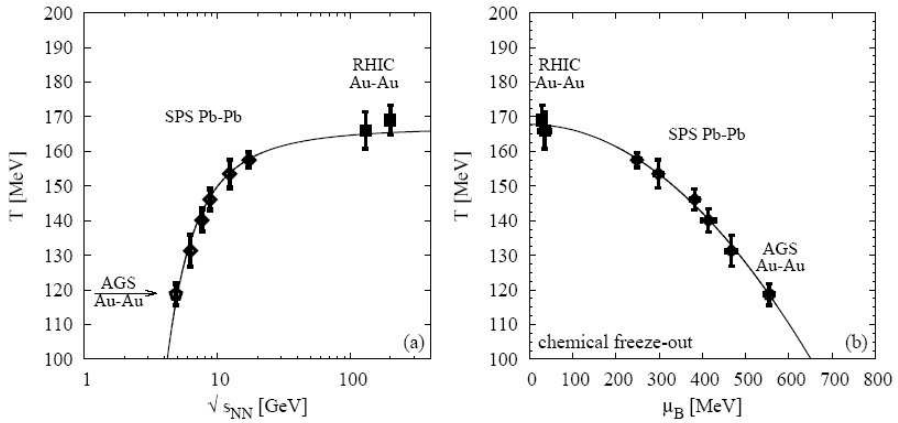

Figure 6.1: Chemical freeze-out temperature as a function of center-of-mass energy in central heavy-ion collisions at AGS, SPS and RHIC (from Ref. [19]).

low energy region followed by a saturation at large energy (see Fig. 6.1). Moreover, it has been observed that also a strangeness undersaturation parameter γ_S is needed to describe the final abundances of hadrons. This parameter also shows a regular behaviour slowly increasing from $\simeq 0.65$ to 1 going from $\sqrt{s_{\rm NN}} = 4.5$ GeV to 200 GeV (see Fig. 6.2). By studying the behaviour of strange particle production as a function of centrality in high-energy heavy-ion collisions, it has been recently argued [20, 21] that the appearance of γ_S is geometrical in origin. Namely, the apparent undersaturation of strangeness might be the effect of single nucleon-nucleon collisions taking place in the outer rim of the colliding nuclei overlapping region, coexisting with a central fully equilibrated hadron gas possibly originated from the quark-gluon plasma (core-corona effect [22–24]). If this was the case, the intriguing question arises whether this superposition is able to account for strangeness undersaturation also in the few GeV/s energy range. Particularly, whether and where a fully equilibrated hadron gas sets in, as its formation could be related to the onset of deconfinement itself. The data which has been collected so far in heavy ion collisions are not sufficient to provide a definite answer to this question and especially in the range $\sqrt{s_{\rm NN}} = 2.6$ GeV. It is therefore crucial to collect and analyze a wealthy data in a new generation of experiments to assess these phenomenological issues which could be decisive in our understanding of the production of the quark-gluon plasma in nuclear collisions. Some analyses seem to indicate that the

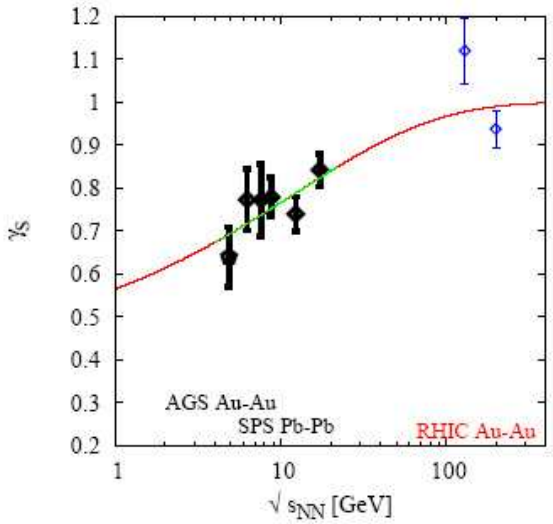

Figure 6.2: γ_S parameter as a function of NN centre-of-mass energy in nuclear collisions.

thermodynamical parameters of the source at very low energy (SIS) follow the general trend [25], however it is not clear whether the hadron-resonance gas model in its zero-order formulation, with non-resonant interaction neglected, can be safely applied at temperatures as low as 100 MeV. The collection of experimental data at low energies will certainly be very important to elucidate this issue.

6.6 MEMO production at high baryon densities

M. Bleicher[a,b], *J. Steinheimer*[a,b]

[a] *Institut für Theoretische Physik, Johann Wolfgang Goethe-Universität, Frankfurt am Main, Germany;* [b] *Frankfurt Institute for Advanced Studies (FIAS), Johann Wolfgang Goethe-Universität, Frankfurt am Main, Germany*

The production of multi-strange meta-stable objects (MEMOs) in Pb+Pb reactions around 30 AGeV is explored in a coupled transport-hydrodynamics model [26]. In addition to making predictions for yields of these particles we are able to calculate particle dependent rapidity and momentum distributions. We argue that this energy regime is the optimal place to search for multi-strange baryonic object (due to the high baryon density, favoring a distillation of strangeness).

Massive heavy-ion reactions provide an abundant source of strangeness. More than 50 hyperons and about 30 Anti-Kaons (i.e. $K^- + \overline{K^0}$ carrying the strange quark) are produced in central collisions of lead nuclei at the CERN-SPS low energy program and before that at the AGS. In the near future, NICA and FAIR will start to investigate this energy regime closer with much higher luminosity and state-of-the-art detector technology. This opens the exciting perspective to explore the formation of composite objects with multiple units of strangeness so far unachievable with conventional methods.

For the microscopic+macroscopic calculation, the Ultra-relativistic Quantum Molecular Dynamics Model (UrQMD) is used to calculate the initial state of a heavy ion collision for a subsequent hydrodynamical evolution [27, 73, 74]. This has been done to account for the non-equilibrium dynamics in the very early stage of the collision. In this configuration the effects of event-by-event fluctuations of the initial state are naturally included. The coupling between the UrQMD initial state and the hydrodynamical evolution proceeds when the two Lorentz-contracted nuclei have passed through each other.

$$t_{\text{start}} = \frac{2R}{\sqrt{\gamma^2 - 1}} \tag{6.1}$$

Cluster	Mass [GeV]	Quark content
He^4	3.750	$12q$
H^0	2.020	$4q+2s$
α_q	6.060	$12q+6s$
$\{\Xi^-,\Xi^0\}$	2.634	$2q+4s$
$\{4\Lambda\}$	4.464	$8q+4s$
$\{2\Xi^-,2\Xi^0\}$	5.268	$4q+8s$
${}^{5}_{\Lambda}He$	4.866	$14q+1s$
${}^{6}_{\Lambda\Lambda}He$	5.982	$16q+2s$
${}^{7}_{\Xi^0\Lambda\Lambda}He$	7.297	$16q+2s$
$\{2n,2\Lambda,2\Xi^-\}$	6.742	$12q+6s$
$\{2\Lambda,2\Xi^0,2\Xi^-\}$	7.500	$8q+10s$
$\{d,\Xi^-,\Xi^0\}$	4.508	$8q+4s$
$\{2\Lambda,2\Xi^-\}$	4.866	$6q+6s$
$\{2\Lambda,2\Sigma^-\}$	4.610	$8q+4s$

Table 6.1: Properties of all considered multibaryonic states (see also [35] for decay systematics).

After the UrQMD initial stage, a full (3+1) dimensional ideal hydrodynamic evolution is performed using the SHASTA algorithm [30, 31]. For the results presented here an equation of state for a hadron-resonance gas without any phase transition is used [32]. The EoS includes all hadronic degrees of freedom with masses up to 2 GeV, which is consistent with the effective degrees of freedom present in the UrQMD model. One should note that we apply a purely hadronic EoS, for energy densities where a transition to the QGP is expected (see also [33] for details on the model and comparison of extracted particle yields to data). Final particle (and MEMO) multiplicities are mainly sensitive on the degrees of freedom at chemical freezeout which is reflected in the hadronic EoS. Dynamical observables such as momentum and rapidity spectra are more sensitive on the underlying dynamics. In addition, a phase transition could catalyse a strangeness destillation process further enhancing MEMO production. However, studying the effects of a phase transition on MEMO production is left subject of future investigations.

The hydrodynamic evolution is stopped, if the energy density of all cells drops below five times the ground state energy density (i.e. ~ 730 MeV/fm^3). This criterion corresponds to a T-$\mu_{\rm B}$-configuration where the phase transition is expected - approximately $T = 170$ MeV at $\mu_{\rm B} = 0$. The hydrodynamic fields are mapped to particle degrees of freedom via the Cooper-Frye equation on an isochronous hyper-surface.

$$E\frac{dN}{d^3p} = \int_\sigma f(x,p)p^\mu d\sigma_\mu \quad \text{with} \quad \mathrm{d}\sigma_\mu = (\mathrm{dx}^3, \tilde{0}) \tag{6.2}$$

Here $f(x,p)$ are the boosted Fermi or Bose distributions corresponding to the respective particle species. Inputs for these distributions are the masses and chemical potentials of the desired particles. For our calculation we assumed the mass of a MEMO to be the sum of the masses of all hadrons it is composed of. Similarly the total chemical potential is the sum of the constituents, and is composed of baryon and strange-quark chemical potentials $\mu_{\rm B}$ and μ_s.

The particle vector information is then transferred back to the UrQMD model, where rescatterings and the final decays are performed using the hadronic cascade. Using this parametrisation of the model one obtains a satisfactory description of data in a energy regime of 1 – 160 AGeV. A more detailed description of the hybrid model including parameter tests and results for multiplicities and spectra can be found in [33].

To calculate the multiplicities of MEMOS in the NICA/FAIR energy region, we employ the introduced hybrid approach to heavy ion collisions. Thus, the fluctuating initial state produced in UrQMD, is coupled to a (3+1) dimensional hydrodynamics evolution. When the energy density drops below $5\epsilon_0(\sim 730\mathrm{MeV/fm}^3)$ the freeze-out is performed and MEMOs and strangelets are produced according to the Cooper-Frye description (6.2). As distinctive inputs for the distribution functions, the chemical potentials $(\mu_{\rm s}, \mu_{\rm B})$ and masses of the MEMOs enter as discussed above. Final state interactions of these MEMOs are neglected for the present study. Table 6.1. gives the properties of all multibaryonic states considered in our analysis. They are the most promising and stable candidates.

Fig. 6.3 provides the total multiplicities per degeneracy factor of various types of MEMOs and strangelets in central Pb + Pb reactions at $E_{\rm lab} = 30A$ GeV. The yields obtained are in good comparison to the statistical model analysis [34], which is describing strange cluster production at AGS energies.

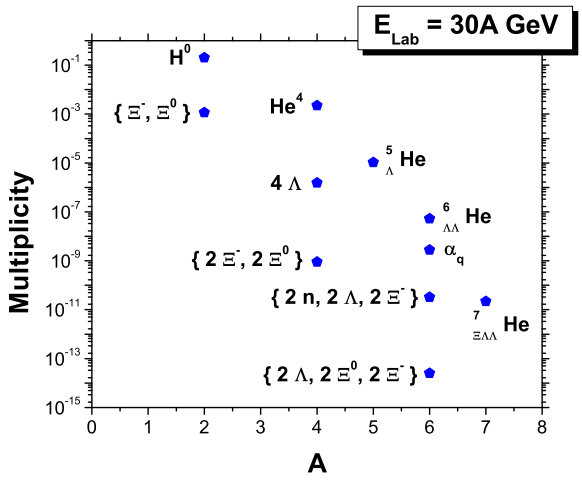

Figure 6.3: Multiplicities of various types of MEMOs and strangelets in central Pb+Pb reactions at $E_{\rm lab} = 30A$ GeV from the hybrid approach.

We have presented results for the thermal production of MEMOs in nucleus-nucleus collisions from a combined micro+macro approach at $E_{\rm lab} = 30$ AGeV. The excitation functions for various MEMO multiplicities show a clear maximum in this energy regime making NICA and FAIR the ideal place to study the production of these exotic forms of multistrange objects.

This work has been supported by GSI and Hessian initiative for excellence (LOEWE) through the Helmholtz International Center for FAIR (HIC for FAIR). We would like to thank Dr. Jürgen Schaffner-Bielich for fruitful discussions. Computational resources were provided by the Center for Scientific Computing (CSC).

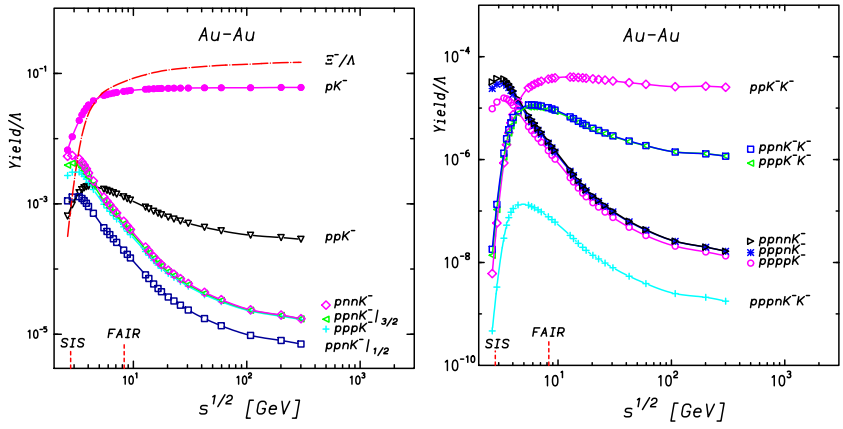

Figure 6.4: Excitation function of the yields of antikaon bound states relative to Λ yields. The calculations are done along the freezeout curve of fixed $E/N = 1$ GeV [39]. For comparison, also show in the left panel is the Ξ^-/Λ yield ratio. The vertical lines indicate the upper energies accessible in experiments at SIS and FAIR. (taken from [37]).

6.7 Statistical production of antikaon nuclear bound states at NICA

A. Andronic[a], P. Braun-Munzinger[a], K. Redlich[a,b]

[a] *GSI Helmholtzzentrum für Schwerionenforschung mbH, Darmstadt, Germany*
[b] *Institute of Theoretical Physics, University of Wrocław, Wrocław, Poland*

It was conjectured that the strongly attractive antikaon–nucleon potential can result in the formation of antikaon nuclear bound states [36]. The experimental and theoretical situation [38] remains rather controversial. The abundance of of single- and double-K^- clusters production in heavy-ion collisions was calculated in terms of the statistical thermal model [37]. The results are shown for central collisions in Fig. 6.4 in terms of production relative to Λ.

If such objects indeed exist, then, in heavy ion collisions, the single-K^- clusters are most abundantly produced at present SIS energies or NICA in fixed target mode, while the double-K^- clusters show a pronounced maximum yield in the energy domain of NICA in collider mode (and at FAIR). This is a direct consequence of: i) the baryonic dominance in low energy heavy ion collisions and the large baryonic content of the antikaonic bound states; ii) the strong energy dependence of strangeness production at low energies.

6.8 Stochastic Hadron Production

H. Satz

Fakultät für Physik, Universität Bielefeld, Germany

Summary The relative species abundances observed in multi-hadron production are in general well described by the statistical hadronisation model, assuming an ideal gas of all possible resonance states, as specified at fixed temperature and baryochemical potential. Such a scenario implies (1) the existence of a thermal hadronic medium and (2) resonance dominated hadron interactions. In e^+e^- annihilation and proton-proton scattering, the former is unlikely, for low energy (high baryon density) nuclear collisions the latter. Nevertheless, in both cases the species abundances appear to remain as predicted by an ideal hadronic resonance gas. We suggest that this is natural if statistical hadron production is quite generally due to a local stochastic process, with the "thermal" distribution arising from tunnelling through a confinement barrier, rather than by a kinetic equilibration process. Hadron production in relatively low energy proton-proton scattering ($\sqrt{s} = 3 - 8$ GeV) would provide an additional test; if it should also follow a resonance gas pattern, local stochastic production would seem as the only explanation.

The statistical hadronisation model, based on a ideal gas of all observed hadronic resonances, provides an excellent general account for hadron production in high energy collisions, from e^+e^- annihilation to the collision of heavy nuclei (see, e.g., [40–43], and references given there). All high energy data lead to a universal hadronisation temperature of about 160 - 170 MeV, in accord with the hadronisation temperature found in finite temperature lattice QCD for low or vanishing baryon density. The only feature distinguishing elementary and nuclear collisions is provided by strangeness production, which in elementary interactions is suppressed by a factor γ_s^n, with $\gamma_s \simeq 0.5 - 0.7$; here n specifies the number of strange quarks and/or antiquarks contained in the measured secondary hadron [45]. Nuclear collisions, in contrast, are in accord with thermal strangeness abundance, i.e., with $\gamma_s = 1$. Such a statistical hadronisation scenario has raised two long-standing questions:

- Why does an elementary process such as e^+e^- annihilation, where per unit rapidity one finds at best two or three secondaries, produce abundances in accord with a hadronic resonance *gas*?
- What is the origin of the strangeness suppression factor γ_s?

A further problem arises in the study of nuclear collisions at low energies. Here again the relative species abundances agree with the predictions of the statistical hadronisation model, in spite of the very small number of secondaries produced [44]. One may argue that the incident nucleons of target and projectile can provide enough constituents to form a gas described in terms of both temperature and baryochemical potential. Then, however, the dominant interaction form in this gas is nucleon repulsion, which has nothing to do with resonance formation. So we encounter the third basic question concerning statistical hadronisation:

- Why does the nucleon-dominated medium given by low energy nuclear collisions, with only very few mesonic secondaries, nevertheless lead to relative abundances of a resonance gas at fixed temperature and baryochemical potential?

We shall here consider some of the answers proposed to these questions, the difficulties they encounter, and a possible further cross-check using low energy proton-proton collisions.

The general solution to the issue of high energy e^+e^- annihilation, as well as for high energy proton-proton collisions, is that while per unit rapidity there are only very few secondaries, one can combine in the study of abundances the clusters or fireballs of different rapidities to a *equivalent global cluster*, whose volume governs the overall multiplicity produced when all rapdities are combined (4π abundances).

The strangeness suppression factor has been interpreted as a phenomenological way to account for the fact that in the production of very few strange particles, strangeness conservation should be accounted for in a rather small strangeness correlation volume, of approximately hadronic size, and not in the overall global cluster volume [46]. In other words, the production of a strange particle has to be compensated *locally* by that of an anti-strange partner, in terms of exact (microcanonical) strangeness conservation.

The aim of this note is two-fold. We shall first argue that such local conservation is generally correct in high energy elementary processes, not only for strangeness. A counterpart of the cosmic horizon problem assures that the fireballs combined to form global equivalent clusters are in general not causally connected and thus cannot form a genuine thermal system. Subsequently, we suggest that the thermal production pattern observed in such a variety of configurations must therefore be of local, non-kinetic origin. Tunnelling through an event horizon with universal surface tension will, through a mechanism of Hawking-Unruh type, produce a universal thermal radiation, whose temperature is determined by the corresponding surface tension. A possible experimental test for this might be the comparison of secondary hadron production in relatively low-energy proton-proton collisions. Here one has rather few secondaries, and the proton-proton interaction itself is not of resonance-type. If they nevertheless should lead to thermal secondary abundance distributions, this would seem to imply a local, stochastic mechanism for such production.

The temperature of the cosmic microwave background radiation (CBR) is, with a precision of better than one part in a thousand, found to be the same, some 2.7 ° Kelvin, throughout the observable universe. This constitutes one of the basic problems of Hot Big Bang cosmology, since at the end of the radiation era, when the CBR first appeared, the presently visible universe consisted of millions of causally disconnected spatial regions. How could such a uniformity in temperature arise without any communication between the radiation sources? The standard explanation, inflation, has the equilibration arising in a pre-inflation world based on a metastable ground state. In the inflation process the transition to the present stable vacuum ground state took place, accompanied by a superluminous spatial expansion. This implies that when the present constituents of matter and radiation first appeared in our world, they were already in the same thermal state throughout all of space. They inherited this thermal behavior from a previous world of very much smaller dimension, in which they were in causal contact and hence able to equilibrate.

The evolution of elementary high energy collisions is generally described in terms of an inside-outside cascade [47]. It specifies a boost-invariant proper time τ_0, at which local volume elements experience the transition from a pre-equilibrium state to a state of thermal equilibrium. This state will eventually lead to the break-up into free-streaming hadrons; we denote the corresponding freeze-out time by τ_h. In a boost-invariant scheme, the space-time coordinates x, t, with x denoting the collision axis, are related to proper time τ and spatial rapidity η through

$$t = \tau \cosh \eta, \quad x = \tau \sinh \eta, \tag{6.3}$$

with $c = 1$. The resulting evolution is illustrated in Fig. 6.5, where the transition curves are determined by $t^2 - x^2 = \tau^2$. Schematically included in this figure is a "fireball" at $\eta = 0$ and one at a larger η. Both the equilibration and freeze-out points for the system at larger η are seen to be well outside the future region of the $\eta = 0$ fireball. More specifically, the hadronization point for the large η fireball just touches the event horizon of the $\eta = 0$ fireball for

$$\tanh \eta_d = \frac{\tau_h^2 - \tau_0^2}{\tau_h^2 + \tau_0^2}, \tag{6.4}$$

defining the fireball range causally connected to the system at $\eta = 0$. Beyond this rapiditiy, i.e., for $\eta > \eta_d$, the two fireballs are causally disconnected and cannot synchronize each other's thermal status.

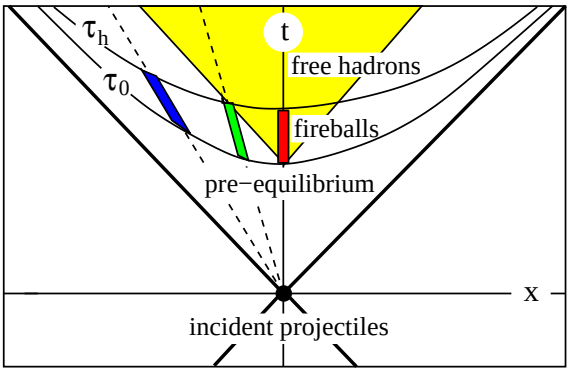

Figure 6.5: The boost-invariant evolution of a high energy collision, from pre-equilibrium ($\tau \leq \tau_0$) to a fireball ($\tau_0 \leq \tau \leq \tau_h$) to free hadrons ($\tau \geq \tau_h$). The region causally connected to a fireball at $\eta = 0$ is colored in yellow, the fireball itself in red. An identical fireball for $\eta = \eta_d$ is marked in green, one for $\eta > \eta_d$ in blue.

To illustrate, we choose $\tau_0 = 1$ fm and $\tau_h = 2$ fm; in this case, a fireball with $\eta > 0.7$ cannot communicate with one at $\eta = 0$. The longer the fireball lifetime is, the larger is the rapidity range of fireballs in causal communication with that at $\eta = 0$. The increase of the range with fireball lifetime is quite slow, however; even for $\tau_h = 7$ fm, the rapidity horizon is only $\eta_d = 2$. In other words, collisions at RHIC or at the LHC will lead to hadron production from causally disconnected fireballs [49].

The observation just made does not, of course, rule out a causal connection (and hence correlations) for hadron production at large rapidity intervals; it only means that any correlations must have originated in the earlier pre-equilibrium stage. It does imply, however, that any state formed at $\eta = 0$ after a finite time interval cannot synchronize its thermal status with a corresponding state at larger rapidity. We thus conclude that any fireball formed in elementary high energy collisions appears in causally disconnected regions, which cannot communicate and thus in particular cannot establish a uniform temperature. If the hadronization temperature is found to be the same for different kinematic origins, this must be due to the local hadronization nature. There does not exist a large *equivalent global system* in thermal equilibrium, since any such equilibrium requires communication (for further details, see [49]).

Recalling the large rapidity ranges for proton-proton collisions at RHIC and at the LHC, as well as those in high energy e^+e^- annihilation, we see that the hadron production in such interactions is due to a number of identical, but causally disconnected fireballs of spatial radius $d \sim 1$ fm. This will retain for all elementary high energy collisions any strangeness suppression emerging from local strangeness conservation. In other words, the production of a kaon requires strangeness conservation within the volume of one fireball, and this effectively suppresses its production and thus accounts the need of a supprression factor γ_s in global equivalent cluster formulations. The basis for this effect is independent of the overall collision energy, and hence γ_s should remain constant for increasing collision energy. The stronger suppression of multi-strange baryons also follows quite naturally from this picture, since all strange quarks needed for their formation have to be compensated locally, thus enhancing the effect.

In the collisions of heavy nuclei, on the other hand, we have in the center of mass on the average around six or seven superimposed nucleon-nucleon collisions, so that there now exists a causally connected region having an equivalent global cluster volume six or seven times larger than that in a nucleon-nucleon collision, with a corresponding increase in the number of produced strange particles. An s quark produced in any specific nucleon-nucleon collision now finds so many $\bar{s}$ from other such collisions in its immediated environment, that no spatial constraints on its partner $\bar{s}$ are necessary. Studies have shown that the resulting equivalent cluster volume should suffice to allow global strangeness conservation and hence drive γ_s to unity, apart from possible small deviations due to corona production.

For e^+e^- annihilation, it was shown hadronisation as Hawking-Unruh radiation arising from quarks tunnelling through their color confinement horizon [48] inherently contain local strangeness conservation [43]. In such a scheme, the maximum separation between s and $\bar{s}$ can never exceed the hadronic scale leading to string breaking, i.e., about 1 fm, thus enforcing § production in a very restricted spatial volume.

More generally, such Hawking-Unruh radiation is a prime example for a local stochastic hadronisation process [48]. The separation of a single quark-antiquark pair leads to stochastic hadron production when the pair reaches the confinement horizon. The "temperature" in this case is the Unruh temperature determined by the confinement string tension and hence universal. A similar picture would arise in the application of the Schwinger mechanism of pair production, which is closely related to Unruh radiation. Moreover, also a potential approach with tunnelling is expected yield such a stochastic production pattern. Given any "thermal" state, one can no longer determine if its origin is kinetic thermalisation or a stochastic pattern; this suggests a statistical equivalence principle, equating the result of the two ways of reaching the observed thermal ratios.

So far, e^+e^- annihilation and high energy proton-proton collisions provide two examples of thermal abundances without "hadron gas" formation. Nuclear collisions lead to such thermal behavior without resonance interaction dominance. Low energy proton-proton collisions, below $\sqrt{s} \simeq 5$ - 6 GeV would constitute a further check, in which one neither has a hadron gas nor resonance interaction dominance. The observation of thermal species abundances in this case would therefore provide a further and very emphatic support for local stochastic hadron production.

6.9 Enhanced strangeness in proton and hard *pp* collisions.

G.I. Lykasov, A.A. Grinyuk, I.V. Bednyakov

Joint Institute for Nuclear Research, Dubna, Russia

The production of the open strangeness at large values of their transverse momenta and rapidities can be a new unique source for estimation of intrinsic strange quark contribution to the proton. We present some predictions for the K-meson production in the pp collision at the $\sqrt{s} \simeq$17 GeV and 7 TeV made within the perturbative QCD including the intrinsic strangeness in the proton that can be verified in the NA61 experiment and at LHC. It is shown that the inclusion of the intrinsic strangeness contribution in the proton, which does not contradict the HERMES data on the DIS, can increase their inclusive spectrum by a factor of 2 or 3 at large transverse momenta and high rapidities of K-mesons.

Intrinsic heavy flavours in the proton

The NA61 (CERN), CBM (Darmstadt) and NICA (Dubna) experiments can be a useful laboratory for investigation of the unique structure of the proton, in particular for the study of the parton distribution functions (PDFs) with high accuracy. It is well known that the precise knowledge of these PDFs is very important for verification of the Standard Model and search for New Physics.

By definition, the PDF $f_a(x,\mu)$ is a function of the proton momentum fraction x carried by parton a (quark q or gluon g) at the QCD momentum transfer scale μ. For small values of μ, corresponding to the long distance scales less than $1/\mu_0$, the PDF cannot be calculated from the first principles of QCD (although some progress in this direction has been recently achieved within the lattice methods [50]). The PDF $f_a(x,\mu)$ at $\mu > \mu_0$ can be calculated by solving the perturbative QCD evolution equations (DGLAP) [51]. The unknown (input for the evolution) functions $f_a(x,\mu_0)$ can usually be found empirically from some "QCD global analysis" [52,53] of a large variety of data, typically at $\mu > \mu_0$.

In general, almost all pp processes that took place at the LHC energies, including the Higgs boson production, are sensitive to the charm $f_c(x,\mu)$ or bottom $f_b(x,\mu)$ PDFs. Nevertheless, within the global analysis the charm content of the proton at $\mu \sim \mu_c$ and the bottom one at $\mu \sim \mu_b$ are both assumed to be negligible. Here μ_c and μ_b are typical energy scales relevant to the c- and b-quark QCD excitation in the proton. These heavy quark components arise in the proton only perturbatively with increasing Q^2-scale through the gluon splitting in the DGLAP Q^2 evolution [51]. Direct measurement of the open charm and open bottom production in the deep inelastic processes (DIS) confirms the perturbative origin of heavy quark flavours [54]. However, the description of these experimental data is not sensitive to the heavy quark distributions at relatively large x ($x > 0.1$).

As was assumed by Brodsky with coauthors in [55,56], there are *extrinsic* and *intrinsic* contributions to the quark-gluon structure of the proton. *Extrinsic* (or ordinary) quarks and gluons are generated on a short time

scale associated with a large-transverse-momentum processes. Their distribution functions satisfy the standard QCD evolution equations. *Intrinsic* quarks and gluons exist over a time scale which is independent of any probe momentum transfer. They can be associated with bound-state (zero-momentum transfer regime) hadron dynamics and are believed to be of nonperturarbative origin. Figure 6.6 gives a schematic view of a nucleon, which consists of three valence quarks q_v, quark-antiquark $q\bar{q}$ and gluon sea, and, for example, pairs of the *intrinsic* charm ($q^c_{in}\bar{q}^c_{in}$) and *intrinsic* bottom quarks ($q^b_{in}\bar{q}^b_{in}$).

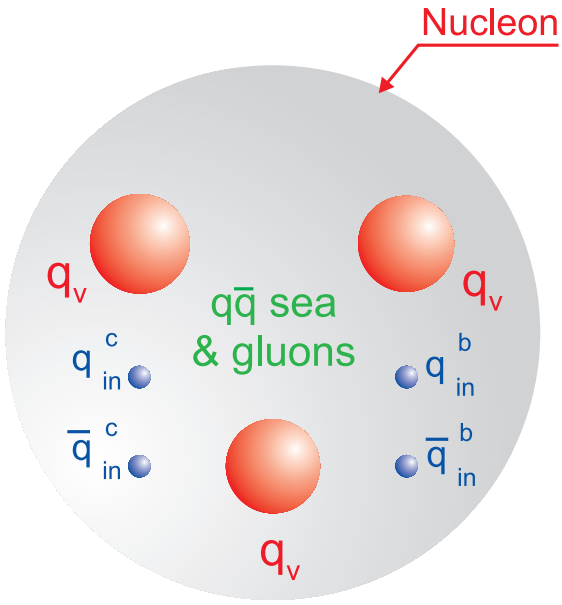

Figure 6.6: Schematic presentation of a nucleon consisting of three valence quarks q_v, quark-antiquark $q\bar{q}$ and gluon sea, and pairs of the intrinsic charm ($q^c_{in}\bar{q}^c_{in}$) and intrinsic bottom quarks ($q^b_{in}\bar{q}^b_{in}$).

It was shown in [56] that the existence of *intrinsic* heavy quark pairs $c\bar{c}$ and $b\bar{b}$ within the proton state could be due to the virtue of gluon-exchange and vacuum-polarization graphs. On this basis, within the MIT bag model [57], the probability to find the five-quark component $|uudc\bar{c}\rangle$ bound within the nucleon bag was estimated to be about 1–2%.

Initially in [55, 56] S.Brodsky with coauthors have proposed existence of the 5-quark state $|uudc\bar{c}\rangle$ in the proton (Fig. 6.6). Later some other models were developed. One of them considered a quasi-two-body state $\bar{D}^0(u\bar{c})\,\Lambda_c^+(udc)$ in the proton [58]. In [58]– [60] the probability to find the intrinsic charm (IC) in the proton (the weight of the relevant Fock state in the proton) was assumed to be 1–3.5%. The probability of the intrinsic bottom (IB) in the proton is suppressed by the factor $m_c^2/m_b^2 \simeq 0.1$ [36], where m_c and m_b are the masses of the charmed and bottom quarks. Nevertheless, it was shown that the IC could result in a sizable contribution to the forward charmed meson production [62]. Furthermore the IC "signal" can constitute almost 100% of the inclusive spectrum of D-mesons produced at high pseudorapidities η and large transverse momenta p_T in pp collisions at LHC energies [63].

If the distributions of the intrinsic charm or bottom in the proton are hard enough and are similar in the shape to the valence quark distributions (have the valence-like form), then the production of the charmed (bottom) mesons or charmed (bottom) baryons in the fragmentation region should be similar to the production of pions or nucleons. However, the yield of this production depends on the probability to find the intrinsic charm or bottom in the proton, but this yield looks too small. The PDF which included the IC contribution in the proton have already been used in the perturbative QCD calculations in [58]- [60].

Due to the nonperturbative *intrinsic* heavy quark components one can expect some excess of the heavy quark PDFs over the ordinary sea quark PDFs at $x > 0.1$. The "signal" of these components can be visible in the observables of the heavy flavour production in semi-inclusive ep DIS and inclusive pp collisions at high energies. For example, it was recently shown that rather good description of the HERMES data on the $xf_s(x,Q^2) + xf_{\bar{s}}(x,Q^2)$ at $x > 0.1$ and $Q^2 = 2.5$ GeV$/c^2$ [64] could be achieved due to existence of *intrinsic* strangeness in the proton, see Fig. 6.7. One can see from Fig. 6.7 that the inclusion of the *intrinsic* strangeness allows us to

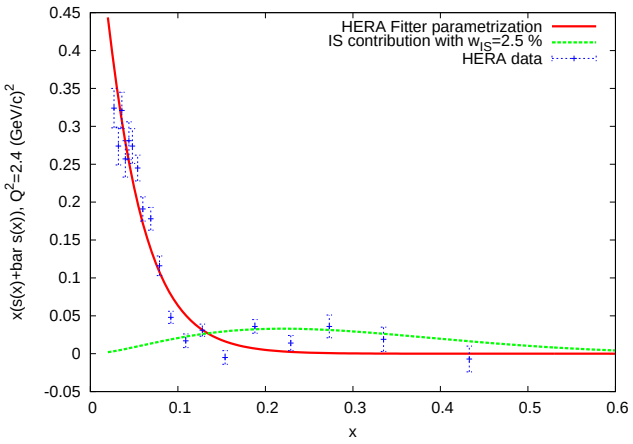

Figure 6.7: The distributions of strange quarks $xS(x) = x(s(x) + \bar{s}(x))$ in the proton; the solid line is the HERA Fitter parametrization of of $xS(x)$ at Q^2 =2.4 GeV/c, the dashed curve is the contribution of the *intrinsic* strangeness (IS) in the proton with the probability 2.5 %

.

describe the HERA data rather satisfactorily in the whole x-region both at $x \leq 0.1$ and $x > 0.1$.

Similarly, possible existence of the intrinsic charm in the proton can lead to some enhancement in the inclusive spectra of the open charm hadrons, in particular D-mesons, produced at the LHC in pp-collisions at high pseudorapidities η and large transverse momenta p_T [63].

Intrinsic heavy quarks in hard pp collisions

Where can one look for the intrinsic heavy quarks?

It is known that in the open charm/beauty pp-production at large momentum transfer the hard QCD interactions of two sea quarks, two gluons and a gluon with a sea quark play the main role. According to the model of hard scattering [71]– [79] the relativistic invariant inclusive spectrum of the hard process $p+p \to h+X$ can be related to the elastic parton-parton subprocess $i + j \to i' + j'$, where i, j are the partons (quarks and gluons). This spectrum can be presented in the following general form [75]– [77] (see also [80, 81]):

$$E\frac{d\sigma}{d^3p} = \sum_{i,j}\int d^2k_{iT}\int d^2k_{jT}\int_{x_i^{\min}}^1 dx_i\int_{x_j^{\min}}^1 dx_j f_i(x_i,k_{iT})f_j(x_j,k_{jT})\frac{d\sigma_{ij}(\hat{s},\hat{t})}{d\hat{t}}\frac{D^h_{i,j}(z_h)}{\pi z_h}. \tag{6.5}$$

Here $k_{i,j}$ and $k'_{i,j}$ are the four-momenta of the partons i or j before and after the elastic parton-parton scattering, respectively; k_{iT}, k_{jT} are the transverse momenta of the partons i and j; z is the fraction of the hadron momentum from the parton momentum; $f_{i,j}$ is the PDF; and $D_{i,j}$ is the fragmentation function (FF) of the parton i or j into a hadron h.

When the transverse momenta of the partons are neglected in comparison with the longitudinal momenta, the variables $\hat{s}$, $\hat{t}$, $\hat{u}$ and z_h can be presented in the following forms [75]:

$$\hat{s} = x_i x_j s, \quad \hat{t} = x_i\frac{t}{z_h}, \quad \hat{u} = x_j\frac{u}{z_h}, \quad z_h = \frac{x_1}{x_i} + \frac{x_2}{x_j}, \tag{6.6}$$

where

$$x_1 = -\frac{u}{s} = \frac{x_T}{2}\cot(\theta/2), \quad x_2 = -\frac{t}{s} = \frac{x_T}{2}\tan(\theta/2), \quad x_T = 2\sqrt{tu}/s = 2p_T/\sqrt{s}. \tag{6.7}$$

Here as usual, $s = (p_1 + p_2)^2$, $t = (p_1 - p'_1)^2$, $u = (p_2 - p'_1)^2$, and p_1, p_2, p'_1 are the 4-momenta of the colliding protons and the produced hadron h, respectively; θ is the scattering angle for the hadron h in the pp c.m.s. The lower limits of the integration in (6.5) are

$$x_i^{\min} = \frac{x_T\cot(\frac{\theta}{2})}{2 - x_T\tan(\frac{\theta}{2})}, \qquad x_j^{\min} = \frac{x_i x_T\tan(\frac{\theta}{2})}{2x_i - x_T\cot(\frac{\theta}{2})}. \tag{6.8}$$

Actually, the parton distribution functions $f_i(x_i, k_{iT})$ also depend on the four-momentum transfer squared Q^2 that is related to the Mandelstam variables $\hat{s}, \hat{t}, \hat{u}$ for the elastic parton-parton scattering [77]

$$Q^2 = \frac{2\hat{s}\hat{t}\hat{u}}{\hat{s}^2 + \hat{t}^2 + \hat{u}^2} \tag{6.9}$$

Calculating spectra by Eq.(6.5) we used the PDF which includes the IS (and does not include it) [60], the FF of the type AKK08 [79] and $d\sigma_{ij}(\hat{s}, \hat{t})/d\hat{t}$ calculated within the LO QCD and presented, for example, in [78].

One can see that the Feynman variable x_F of the produced hadron, for example, the K-meson, can be expressed via the variables p_T and η, or θ the hadron scattering angle in the pp c.m.s,

$$x_F \equiv \frac{2p_z}{\sqrt{s}} = \frac{2p_T}{\sqrt{s}} \frac{1}{\tan\theta} = \frac{2p_T}{\sqrt{s}} \sinh(\eta). \tag{6.10}$$

At small scattering angles of the produced hadron this formula becomes

$$x_F \sim \frac{2p_T}{\sqrt{s}} \frac{1}{\theta}. \tag{6.11}$$

It is clear that for fixed p_T an outgoing hadron must possess a very small θ or very large η in order to have large x_F (to follow forward, or backward direction).

In the fragmentation region (of large x_F) the Feynman variable x_F of the produced hadron is related to the variable x of the intrinsic charm quark in the proton, and according to the longitudinal momentum conservation law, the $x_F \simeq x$ (and $x_F < x$). Therefore, the visible excess of the inclusive spectrum, for example, of K-mesons can be due to the enhancement of the IS distribution (see Fig. 6.7) at $x > 0.1$.

• Intrinsic strangeness

Let us analyze now how the possible existence of the intrinsic strangeness in the proton can be visible in pp collisions. For example, consider the K^--meson production in the process $pp \to K^- + X$. Considering the intrinsic strangeness in the proton [64] we calculated the inclusive spectrum $ED\sigma/d^3p$ of such mesons within the hard scattering model (Eq.(6.5)), which describes satisfactorily the HERA and HERMES data on the DIS. The FF and the parton cross sections were taken from [78, 79], respectively, as mentioned above. In Figs. (6.8,6.9)

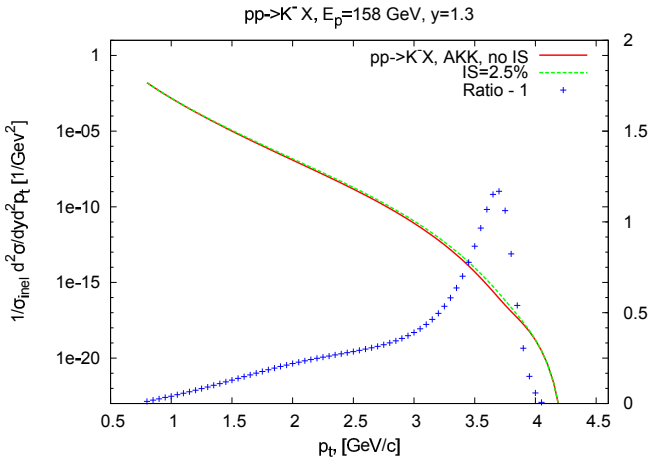

Figure 6.8: The K^--meson distributions (with and without intrinsic strangeness contribution) over the transverse momentum p_t for $pp \to K^- + X$ at the initial energy $E = 158$ GeV, the rapidity y =1.3 and $p_t \geq 0.8$ GeV/c.

the inclusive p_t-spectra of K^--mesons produced in pp collision at the initial energy E_p =158 GeV are presented at the rapidity y =1.3 (Fig 6.8) and y =1.7 (Fig 6.9). The solid lines in Figs. (6.8,6.9) correspond to our calculation ignoring the *intrinsic strangeness* (IS) in the proton and the dashed curves correspond to the calculation including the IS with the probability about 2.5%, according to [64]. The crosses show the ratio of our calculation with the IS and without the IS minus 1. One can see from Figs. (6.8,6.9, right axis) that the IS signal can be above 200 % at $y = 1.3$, p_t = 3.6-3.7 Gev/c and slightly smaller, than 200 % at $y = 1.7$, $p_t \simeq 2.5$

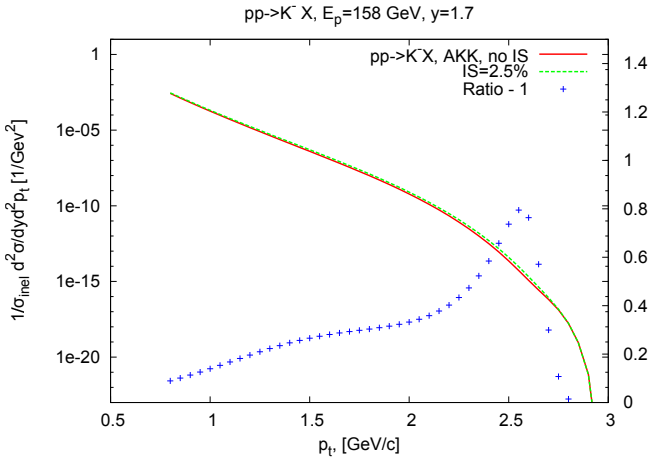

Figure 6.9: The K^--meson distributions (with and without intrinsic strangeness contribution) over the transverse momentum p_t for $pp \to K^- + X$ at the initial energy $E_p = 158$ GeV, the rapidity y =1.7 and $p_t \geq 0.8$ GeV/c.

Gev/c. Actually, this is our prediction for the NA61 experiment that is now under way at CERN.

Conclusion

We analyzed the inclusive K^--meson production in pp collision at the initial energy E_p =158 GeV and gave some predictions for the NA61 experiment going on at CERN. We showed that in the inclusive spectrum of K^--mesons as a function of p_t at some values of their rapidities the signal of the *intrinsic* strangeness can be visible and reach about 200% and more at large momentum transfer we took. The probability of the *intrinsic* strangeness to be about 2.5%, as was found from the best description of the HERA and HERMES data on the DIS, see [64] and references therein. The similar predictions can be made for the open strangeness production at the energies of the CBM (Darmstadt) and NICA (Dubna) experiments. The main goal of such predictions is to show that at the certain kinematical region the contribution of the *intrinsic* strangeness in the proton can result in the enhancement in inclusive spectra by a factor of 2-3. This enhanced strangeness in the nucleon can lead to the enhanced yield of the strange hadrons produced in AA collisions at NICA and CBM in the kinematical region forbidden for the free NN collisions.

Bibliography

[1] D. Kharzeev, E. Levin and M. Nardi, Phys. Rev. **C 71,** 054903 (2005), [hep-ph/0111315].

[2] D. Kharzeev and M. Nardi, Phys. Lett. **B 507,** 121 (2001), [nucl-th/0012025]; **523**, 79 (2001), [nucl-th/0108006]; **561**, 93 (2003), [hep-ph/0210332].

[3] D. Kharzeev, E. Levin and L. McLerran, Nucl. Phys. **A 748,** 627 (2005), [hep-ph/0403271].

[4] A. Leonidov, M. Nardi and H. Satz, Nucl. Phys. **A 610,** 124 (1996).

[5] A. Leonidov, M. Nardi and H. Satz, Z. Phys. **C74**, 535 (1997).

[6] S. V. Akkelin, Y. Hama, Iu. Karpenko and Yu. M. Sinyukov. Phys. Rev. **C 78,** 034906 (2008).

[7] Yu. M. Sinyukov, S. V. Akkelin and Iu. A. Karpenko. Acta. Phys. Polon. **B 40,** 1025 (2009).

[8] S. A. Bass *et al.*, Progr. Part. Nucl. Phys. **41,**225 (1998).

[9] K. A. Bugaev, Phys. Rev. Lett. **90,** 252301 (2003).

[10] Yu. M. Sinyukov and S. V. Akkelin, Y. Hama, Phys. Rev. Lett. **89,** 052301 (2002).

[11] N. Armesto, *et al.*, J. Phys. G: Nucl. Part. Phys. **35**, 054001 (2008).

[12] Yu. M. Sinyukov, S. V. Akkelin and Iu. A. Karpenko, Physics of Atomic Nuclei, **71**, 1619 (2008).

[13] Yu. M. Sinyukov, Iu. A. Karpenko and A. V. Nazarenko, J. Phys. G: Nucl. Part. Phys. **35**, 104071 (2008).

[14] Yu. B. Ivanov, V. N. Russkikh, and V. D. Toneev, Phys. Rev. **C 73,** 044904 (2006).

[15] B. Tomasik and E. E. Kolomeitsev, [arxiv:nucl-th/0512088]; Eur. Phys. J. **C 49,** 115 (2007), [nucl-th/0610041].

[16] J. Cleymans, H. Oeschler, K. Redlich, and S. Wheaton, Phys. Rev. **C 73,** 034905 (2006).

[17] F. Becattini, J. Manninen, and M. Gazdzicki, Phys. Rev. **C 73,** 044905 (2006).

[18] A. Andronic, P. Braun-Munzinger and J. Stachel, Phys. Lett. **B 673,** (2009) 142.

[19] J. Manninen and F. Becattini, Phys. Rev. **C 78,** 054901 (2008).

[20] F. Becattini and J. Manninen, J. Phys. G. **35,** 104013 (2008);

[21] F. Becattini and J. Manninen, Phys. Lett. **B 673,** 19 (2009).

[22] P. Bozek, Acta. Phys. Polon. **B 36,** 3071 (2005).

[23] K. Werner, Phys. Rev. Lett. **98,** 152301 (2007).

[24] V. S. Pantuev, JETP Lett. **85**, 104 (2007).

[25] R. Averbeck, R. Holzmann, V. Metag and R. S. Simon, Phys. Rev. **C 67,** 024903 (2003).

[26] J. Steinheimer, M. Mitrovski, T. Schuster, H. Petersen, M. Bleicher and H. Stoecker, Phys. Lett. **B 676,** 126 (2009), [arXiv:0811.4077 [hep-ph]].

[27] J. Steinheimer, M. Bleicher, H. Petersen, S. Schramm, H. Stocker and D. Zschiesche, Phys. Rev. **C 77,** 034901 (2008), [arXiv:0710.0332 [nucl-th]].

[28] S. A. Bass *et al.*, Progr. Part. Nucl. Phys. **41,**255 (1998); Progr. Part. Nucl. Phys. **41,**225 (1998), [arXiv:nucl-th/9803035].

[29] M. Bleicher *et al.*, J. Phys. G. **25,** 1859 (1999), [arXiv:hep-ph/9909407].

[30] D. H. Rischke, S. Bernard and J. A. Maruhn, Nucl. Phys. **A 595,** 346 (1995), [arXiv:nucl-th/9504018].

[31] D. H. Rischke, Y. Pursun and J. A. Maruhn, Nucl. Phys. **A 595,** 383 (1995); **596**, 717 (1996), [arXiv:nucl-th/9504021].

[32] D. Zschiesche, S. Schramm, J. Schaffner-Bielich, H. Stoecker and W. Greiner, Phys. Lett. **B 547,** 7 (2002), [arXiv:nucl-th/0209022].

[33] H. Petersen, J. Steinheimer, G. Burau, M. Bleicher and H. Stocker, Phys. Rev. **C 78,** 044901 (2008), [arXiv:0806.1695 [nucl-th]].

[34] P. Braun-Munzinger and J. Stachel, J. Phys. G. **21,** L17 (1995), [arXiv:nucl-th/9412035].

[35] J. Schaffner-Bielich, R. Mattiello and H. Sorge, Phys. Rev. Lett. **84,** 4305 (2000), [arXiv:nucl-th/9908043].

[36] Y. Akaishi and T. Yamazaki, Phys. Rev. C 65 (2002) 044005. T. Yamazaki and Y. Akaishi, Phys. Lett. B 535 (2002) 70.

[37] A. Andronic, P. Braun-Munzinger, K. Redlich, Nucl. Phys. A 765 (2006) 211.

[38] C. Curceanu, A. Rusetsky, E. Widmann (eds.), arXiv:hep-ph/0610201

[39] J. Cleymans and K. Redlich, Phys. Rev. Lett. **81**, 5284 (1998) and Phys. Rev. **C 60**, 054908 (1999).

[40] F. Becattini and G. Passaleva, Eur. Phys. J. **C 23,** 551 (2002).

[41] P. Braun-Munzinger, K. Redlich and J. Stachel, in *Quark-Gluon Plasma 3*, R. C. Hwa and X.-N Wang (Eds.), World Scientific, Singapore 2003.

[42] F. Becattini and R. Fries, [arXiv:0907.1031 [nucl-th]], and Landolt-Boernstein 1-23.

[43] F. Becattini *et al.*, Eur. Phys. J. **C 66,** 377 (2010).

[44] J. Cleymans, H. Oeschler and K. Redlich, J. Phys. **G 25**, 281 (1999).

[45] J. Letessier, J. Rafelski and A. Tounsi, Phys. Rev. **C 64,** 406 (1994).

[46] J. S. Hamieh, K. Redlich and A. Tounsi, Phys. Lett. **B 486,** 61 (2000).

[47] J. D. Bjorken, *Lecture Notes in Physics (Springer)* 56 , 93 (1976).

[48] P. Castorina, D. Kharzeev and H. Satz, Eur. Phys. J. **C 52,** 187 (2007).

[49] F. Becattini, P. Castorina and H. Satz, to appear.

[50] J.W.Negele *et al.,* Nucl.Phys. B [Proc.Suppl.] **128**, (2004) 170; W.Schroers, Nucl. Phys. **A 755** (2005) 333.

[51] V.N. Gribov and L.N. Lipatov, Sov.J.Nucl.Phys. **15** (1972) 438; G. Altarelli and G. Parisi, Nucl.Phys. **B 126** (1997) 298; Yu.L. Dokshitzer, Sov.Phys. JETP **46** (1977) 641.

[52] J.Pumplin, D.R.Stump, J.Huston, H.L.Lai, P.Nadolsky and W.K.Tung, J. High Energy Physics **07** (2002) 012; D.R.Stump, J.Huston. J.Pumplin, W.K.Tung, H.L.Lai, S.Kuhlmann and J.F.Owens, J. High Energy Physics **10** (2003) 046.

[53] R.S.T orne, A.d.Martin, W.G.Stirling, and R,G.Roberts, [arXiv:04073 [hep-ph0]].

[54] A.Aktas, *etal.,* (H1 Collaboration), Eur.Phys. J. **C 40**, (2005) 349; [arXiv:0507081 [hep-ex]].

[55] Brodsky S., Hoyer P., Peterson C., Sakai N., Phys.Lett. **B 93** (1980) 451.

[56] Brodsky S., Peterson C., Sakai N., Phys.Rev. **D 23** (1981) 2745.

[57] J.F.Donoghue, E.Golowich, Phys.Rev.D **15** (1977) 3421.

[58] Pumplin J., Phys.Rev. **D 73** (2006) 114015.

[59] Pumplin J., Lai H., Tung W., Phys.Rev. **D 75** (2007) 054029.

[60] Nadolsky P. M., *et. al.,* Phys. Rev. **D 78** (2008) 013004.

[61] Polyakov M. V., Schafer A., Teryaev O. V., Phys.Rev. **D 60** (1999) 051502.

[62] Goncalves V., Navarra F., Nucl.Phys. **A 842** (2010) 59.

[63] G.I.Lykasov, V.A.Bednyakov, A.F.Pikelner and N.I.Zimin, Eur.Phys. Lett. **99** (2012) 21002; arXiv:1205.1131v2 [hep-ph].

[64] Jen-Chieh Peng, Wen-Chen Chang, Published in PoS QNP2012 (2012) 012 Plenary talk at Conference: C12-04-16; [arXiv:1207.2193 [hep-ph]].

[65] A.Airapetian, (HERMES Collaboration), Phys.Lett. **B 666** , 446 (2008); [arXiv:0803.2993 [hep-ex]].

[66] Litvine V. A., Likhoded A. K., Phys. Atom. Nucl. **62** (1999) 679.

[67] V.M.Abazov *et al.,* Phys.Rev.Lett. **102** (2009) 192002; arXiv:0901.0739 [hep-ex].

[68] Vogt R., Prog. Part. Nucl. Phys. **45** (2000) S105.

[69] Navarra F. S., Nielsen M., Nunes C. A. A., Teixeira M., Phys.Rev. **D 54** (1996) 842.

[70] Melnichouk W., Thomas A. W., Phys.Lett. **B 414** (1997) 134.

[71] A.V.Efremov, Sov.J.Nucl.Phys., **19**, 176 (1974).

[72] P.Nasson, S.Dawson & R.K.Ellis, Nucl.Phys. **B 303**, 607 (1988).

[73] P.Nasson, S.Dawson & R.K.Ellis, Nucl.Phys. **B 327**, 49 (1989).

[74] P.Nasson, S.Dawson & R.K.Ellis, Nucl.Phys., **B 3335**, 260(E) (1989)

[75] R.D.Field,R.P.Feyman, Phys.Rev. **D 15** (1977) 2590.

[76] R.P.Feyman, R.D.Field, and G.C.Fox, Nucl.Phys. **B 128** (1977) 1.

[77] R.P.Feyman, R.D.Field, and G.C.Fox, Phys.Rev. **D 18** (1977) 3320.

[78] M.L.Mangano, Physics-Uspekhi, **53** (2010) 109.

[79] S.Albino, B.A.Kniehl, G.Kramer (AKK08), Nucl.Phys. **B 803** (2008) 42.

[80] V.A. Bednyakov, A.A. Grinyuk, G.I. Lykasov, M. Poghosyan, Nucl.Phys. **B 219-220** [Proc.Suppl.] (2011) 225; arXiv:11040532 [hep-ph].

[81] V.A. Bednyakov, A.A. Grinyuk, G.I. Lykasov, M. Poghosyan, Int.J.Mod.Phys. **A 27** (2012) 1250042.

[82] B. Kniehl, G. Kramer, I. Schienbein and H. Spiesberger, Eur.Phys.J. **C 72** (2012) 2082; arXiv:1202.0439v1 (2012) [hep-ph] .

7 Electromagnetic probes and chiral symmetry in dense QCD matter

Dileptons and photons provide a powerful penetrating probe of dense QCD matter. They have been extensively and productively used at RHIC and SPS. Because of the small electromagnetic interaction cross sections, dileptons and photons do not suffer from final state interactions even in a dense medium and deliver unique information about the properties of QCD matter throughout its space-time history. The thermal electromagnetic radiation reveals the temperature of the hot QCD matter. The studies of low-mass dileptons allow access to the properties of dense hadronic matter, and are sensitive to the restoration of chiral symmetry as discussed in this section. The top NICA energy $\sqrt{s_{\rm NN}}$ =11 GeV opens a way to investigate heavy-mass dileptons from J/ψ decays near the threshold. The density of baryons is known to affect the chiral symmetry restoration in a very significant way; therefore the study of electromagnetic probes at NICA energies where a very high baryon density will be achieved would be very valuable.

7.1 Low-mass dileptons at NICA

I. Tserruya

Weizmann Institute of Science, Rehovot, Israel

Dileptons (e^+e^- or $\mu^+\mu^-$ pairs) are an important and powerful tool to diagnose the hot and dense matter produced in relativistic heavy-ion collisions. They play a crucial role in the study of the Quark-Gluon Plasma, the state of matter predicted by lattice QCD numerical calculations and characterized by the deconfinement of quarks and gluons and the restoration of chiral symmetry, the latter being crucial to explore the generation of the hadron masses.

The interest in this probe was first emphasized by Shuryak [1]. Due to their large mean-free-path, dileptons do not suffer from final state interactions and once produced they can escape unaffected to the detector carrying information about the conditions and properties of the medium at the time of production.

The interest is in the detection of radiation emitted in the form of real or virtual photons by the medium in thermal equilibrium. Such radiation is a direct fingerprint of the matter formed. Two well distinct sources are considered:

The thermal radiation emitted by the QGP in the early phase of the collision through quark annihilation ($q\bar{q} \rightarrow l^+l^-$) serves as a proof of deconfinement and provides a direct measurement of the plasma temperature. Theory has singled out dileptons in the mass range $m_{l^+l^-} = (1-3)$ GeV/c^2 as the most appropriate window to observe the thermal radiation from the QGP phase. The challenge is to identify it.

The thermal radiation emitted by the high-density hadron gas in the later phase of the collision through pion annihilation ($\pi^+\pi^- \rightarrow \rho \rightarrow \gamma^* \rightarrow l^+l^-$) contributes primarily to the low-mass region, ($m_{l^+l^-} \leq 1$ GeV/c^2) around and below the ρ mass. This component must always be present since ultimately the system ends in the hadronic phase. It has been identified in the enhancement of low-mass dileptons discovered at the SPS in the mid-nineties primarily by the CERES experiment and later confirmed and studied with much higher precision by the NA60 experiment [2, 3].

The enhancement of low-mass dileptons triggered a huge theoretical activity stimulated mainly by interpretations based on in-medium modifications of the intermediate ρ meson with a possible link to chiral symmetry restoration (CSR). (For a recent theoretical review see [4]). The SPS results motivated also new experiments aiming at precise spectroscopic studies of the vector meson resonances, ρ, ω, and ϕ, to explore in-medium modifications of their spectral properties (mass and width). This topic is of interest in its own right and more so because these modifications could shed light into the behavior of the resonances close to the chiral restoration boundary. The ρ meson with its short lifetime, $\tau \sim 1.3$ fm/c, and its strong coupling to the $\pi\pi$ channel is best suited in this context, making it the most sensitive signal for in-medium modifications and the best probe for CSR. (For a recent review on the experimental results see [5]).

The physics potential of dileptons is confirmed by the wealth of interesting results obtained so far and by the relatively large number of experiments focusing on their study. The energy range covered by the planned NICA facility, $\sqrt{s_{\rm NN}} = (4-11)$ GeV, is unique in several respects. It fills a very important gap where no dilepton measurements exist, providing a crucial complement to the measurements at lower (DLS and HADES) and higher (SPS and RHIC) energies. This is a very promising energy range with considerable discovery potential.

All measurements of dileptons at high energies (SPS and RHIC) have revealed an enhancement with respect to the expected yield from hadronic sources, in particular an enhancement was observed at all SPS energies down to 40 AGeV. The DLS puzzle, referring to the enhancement of low-mass electron pairs originally reported by the DLS experiment at 1 – 2 AGeV, could be close to a solution with the recent HADES results on elementary p+p and p+d collisions indicating no enhancement of low-mass e^+e^- pairs in C+C collisions but rather a mere superposition of nucleon-nucleon collisions. There is no compelling evidence to invoke any new source of dileptons or any in-medium modification of the light vector mesons in this light system and at this low energy. This implies an onset of the low-mass dilepton enhancement somewhere in the energy range of 2 – 40 AGeV. It is interesting to note that this is almost the same energy range where the QCD critical point is being looked for. The NICA facility is thus ideally suited to search not only for the QCD critical point but also for the onset of the low-mass dilepton enhancement.

In the many-body approach of Rapp and Wambach [6,7] the mid-rapidity baryon density plays a crucial role in explaining the low-mass dilepton enhancement. The interpretation invokes pion annihilation $\pi^+\pi^- \to \rho \to \gamma^* \to l^+l^-$ with the intermediate ρ broadened by its scattering off baryons. The importance of baryons prompted the CERES experiment to perform a measurement of low-mass electron pairs at 40 AGeV. An enhancement was indeed observed but the experimental uncertainties were too high for a more elaborate analysis. In the energy range covered by NICA, the mid rapidity baryon density is expected to reach a maximum and thus the NICA facility will allow to measure low-mass dileptons under optimal conditions

Our present knowledge of the QCD phase diagram shows a critical end point at a baryon chemical potential of about $\mu_B = 400$ MeV with a smooth cross over at lower values and a first order phase transition at larger values. Again NICA's planned energy range is ideally suited to explore this region.

7.2 Dileptons at NICA

K. Gudima[a] and V. Toneev[b]

[a] *Institute of Applied Physics, Cishineu, Repubica of Moldova;*
[b] *Joint Institute for Nuclear Research, Dubna, Russia*

Due to weak interaction, dileptons play an exceptional role among different probes providing information on a state of highly compressed and hot nuclear matter formed in relativistic heavy ion collisions. Generally, a dilepton yield depends on both global properties of matter constituents (hadrons and/or quarks, gluons) defined by the equation of state and individual constituent properties related to their in-medium modification. The analysis of the e^+e^- invariant mass spectra from central Pb + Au collisions at the bombarding energy $E_{\rm lab} = 158$ AGeV, measured by the CERES Collaboration, for certain shows an excess radiation in the range of invariant dilepton masses $0.2 \lesssim M \lesssim 0.7$ GeV. Observation of an enhancement of the dilepton rates - at low invariant masses - due to in-medium changes of the vector meson spectral functions as a signal of chiral symmetry restoration in the hot and dense matter. Various scenarios of hadron modification were proposed. However, low statistics, insufficient mass resolution, and large signal/background ratio in the CERES experiments did not allow one to discriminate these scenarios, in particular those based on the Brown-Rho scaling hypothesis [8] assuming a dropping ρ mass and on a strong broadening as found in the many-body approach by Rapp and Wambach [6,7].

However, recent highly precise NA60 [3] results for $\mu^+\mu^-$ pair production in In+In (158 AGeV) collisions have showed a good agreement with Rapp's theoretical predictions within the many-body approach but do not confirm the expected dropping mass scenario of Brown and Rho. We hope that dimuon measurements in the NICA energy range may clarify this situation.

The main Brown-Rho objection to this interpretation is the validity of the vector dominance. In more general theory of the hidden chiral symmetry [9] the vector dominance is valid only at small temperature while in the measured In-In collisions mainly high-temperature states are populated [10].

In Fig. 7.1 the dimuon invariant mass distributions are presented for two limiting energies of colliding Au ions. These spectra are calculated within the Quark-Gluon String Model [11–13] with applying the NICA acceptance. Contributions of channels which are taken into account are shown in figure. Note that no in-medium effects are implemented in these calculations. About 90% of ρ-mesons decay inside the interacting system and therefore should undergo medium influence. Thus, these results may be considered as a reference point for future analysis of muon data.

We expect that at $\sqrt{s_{\rm NN}}$ =11 GeV the broadening of ρ-meson spectral function and an enhancement of the

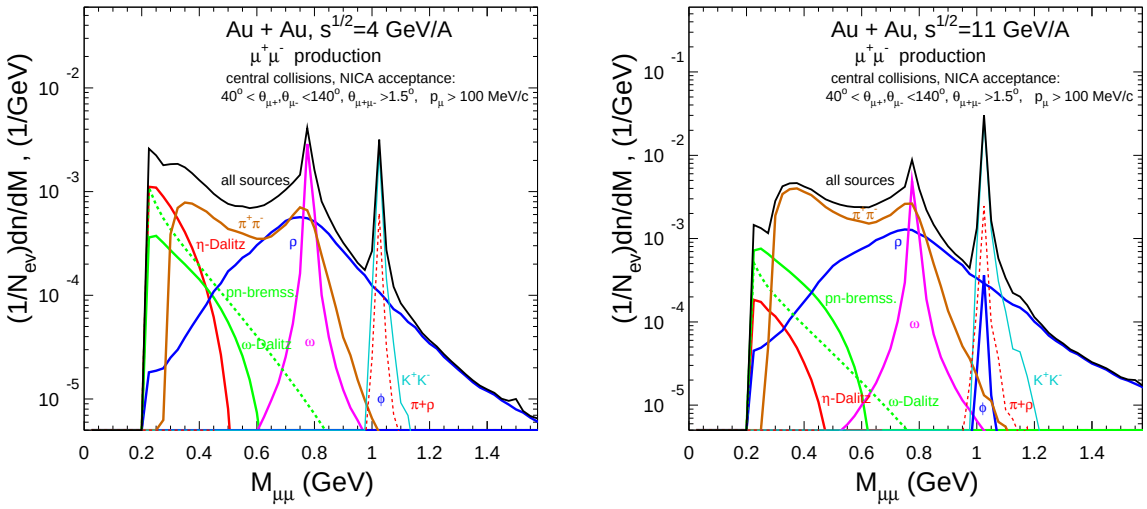

Figure 7.1: Invariant mass spectra of $\mu^+\mu^-$ pairs created in central Au+Au collisions at $\sqrt{s_{\rm NN}}$ = 4 and 11 GeV. Contributions of different dimiuon sources are plotted. The NICA acceptance used is shown in figures.

dilepton rates at low invariant masses, similarly to the case of In - In (158 AGeV) collision, should be observed. But at $\sqrt{s}_{\rm NN}$ =4 GeV the temperature of populated states will be essentially lower and there is a chance for manifestation of the dropping mass scenario as a direct signal of the partial chiral symmetry restoration.

7.3 Electromagnetic probes on NICA

Kh. Abraamyan and A. Friesen

Joint Institute for Nuclear Research, Dubna, Russia

Diphoton production

The two-photon decay of light mesons represents an important source of information. In particular, the $\gamma\gamma$ decay of light scalar mesons was considered as a possible tool to deduce their nature. Also the scalar-isoscalar sector is question at issue presently, since more states are known (including possible glueball candidates) than can be fitted into a single multiplet. Unfortunately, the existing experimental information from $\pi\pi$ scattering has many conflicting data sets at intermediate energies and no data at all close to the interesting threshold region. For many years this fact has made very hard to obtained conclusive results on $\pi\pi$ scattering at low energies or in the sigma region. Interest in the investigation of the photon pair production is bound up with a set of problem:

- To clarify the nature and further investigations of the resonance observed in the invariant mass spectrum of $\gamma\gamma$-pairs in dC-interactions at 2.75 GeV/c per nucleon and dCu-interactions at 3.83 GeV/c per nucleon (see Fig. 7.2) [14].
- To search for some features in the invariant mass spectrum of $\gamma\gamma$-pairs in the interval of 270 – 750 MeV bounding up with the chiral symmetry restoration [15].
- Due to hidden strangeness of η-mesons ($s\overline{s}$ component), comparison η and π^0-productions allows to clarify the mesons production mechanism. The indication on the difference between π^0- and η-mesons production mechanisms was obtained from the comparison of the mesons spectra in the near-threshold region (the PHOTON-2 experiments [16]).

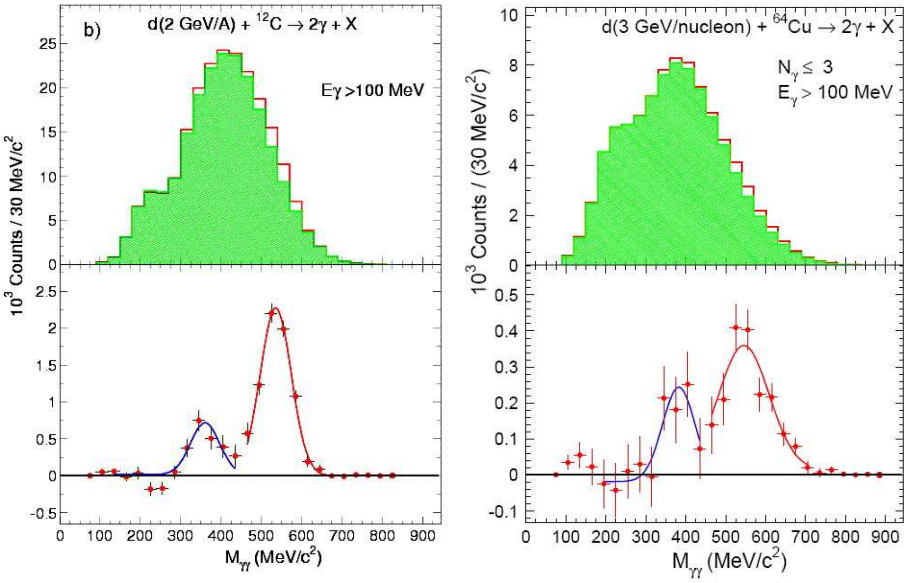

Figure 7.2: Invariant mass distributions of $\gamma\gamma$ pairs without (upper panels) and with (bottom panels) the background subtraction. The left and right figures are obtained for the dC- and dCu-interactions at 2.75 GeV/c and 3.83 GeV/c per nucleon respectively. The curves are the Gaussian approximation of experimental points.

- Investigations of π^0-mesons is of interest in view of the NICA possibilities. The scan of the π^0 spectra in the nuclear-nuclear collision allows one to detect signals of the π-condensate state: the pion vacuum breaking at the strong QCD field in dense nuclear matter.

The NICA advantages

The collider NICA allows one to scan the energy and mass dependence of the resonance production in ion collisions.

To solve above problems a calorimeter with large acceptance and high resolution is needed (in consisting of MPD or as a separate setup), our investigations show that the hexagonal crystal calorimeter meets the requirements. The increasing of the calorimeter acceptance allows to study the invariant mass spectra of $\gamma\gamma$ pairs in a wide range at different energies and transverse momenta of pairs (that means different production mechanisms).

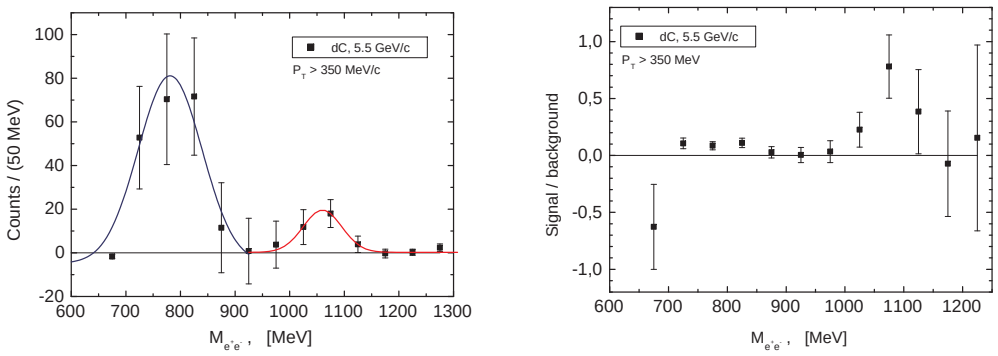

Figure 7.3: Invariant mass distributions of e^+e^- pairs after the background subtraction (left) and signal to background ratio in the reaction $d + C \to e^+e^- + X$ at 2.75 GeV/c per nucleon (right). The curves are the Gaussian approximation of experimental points.

Dilepton production

A possibility of vector mesons detection by e^+e^--decay is shown in Fig. 7.3. The experiment was carried out on the internal Nuclotron beam by the multichannel lead-glass calorimeter with the hexagonal prism modules with length 14 R.L. and the inscribed circle diameter 17.5cm. Emission angles of $e^+(e^-)$ are in the range $20^\circ \div 30^\circ$, opening angles of e^+e^- pairs are $42^\circ \div 66^\circ$. These parameters can be useful for determination of the optimal calorimeter configuration.

7.4 Solving the problem of anomalous J/ψ suppression at NICA MPD

A.B.Kurepin and N.S.Topilskaya

Institute Nuclear Physics, Troizk, Russia

The dissociation of heavy quark resonances by colour Debye screening in a deconfined nuclear matter [17] is one of the possible signature of Quark Gluon Plasma formation in high energy heavy ion collisions.

The absorption of charmonia states at its passing through the ordinary nuclear matter was found by mass dependence in proton-nucleus collisions at the CERN SPS in the NA38 experiment [18]. However in lead-lead collisions an additional anomalous absorption was observed by the NA50 experiment [19, 20] and proposed that it is due to the colour screening in the compressed nuclear matter. Later in some theoretical models the NA50 data were interpreted as the results of charmonia and comover interactions in cold nuclear matter.

However, the experimental results obtained at SPS for indium-indium collisions by the NA60 experiment [21] and at RHIC for gold-gold collisions [22] have shown that the problem is much more complicated.

The amount of anomalous suppression depends on the value of normal absorption. A suppression of J/ψ production (decreasing of J/ψ production cross section per nucleon with increasing the atomic number A) was observed by the NA38 experiment in pA-collisions and in collisions of light ions up to S – U collisions at 200 GeV per nucleon. The results of this experiment were explained by normal nuclear absorption of pre-resonance $c\bar{c}$-state in nuclear matter [18,23]. The cross section for the absorption process, $\sigma_{\rm abs}$, was the same for all nuclei within the range of errors.

The NA50 experiment measured the charmonium production in Pb + Pb collisions at 158 GeV per nucleon [19, 20] and in proton-nucleus collisions at 400 and 450 GeV [24–26]. The normal suppression of J/ψ in proton-nucleus reactions and "anomalous" enhanced suppression was observed in central lead-lead collisions. The suppression grows with increasing centrality. The value of normal nuclear absorption of J/ψ per nucleon was obtained from analysis of proton-nucleus data at 400 and 450 GeV assuming a weak energy dependence and in terms of the Glauber model the value of $\sigma_{\rm abs}$ was 4.2 0.5 mb.

However the recent measurements of pA-collisions at 400 and 158 GeV in the NA60 experiment shows that the energy dependence of $\sigma_{\rm abs}$ is not weak and that it is very important to measure charmonium production in $p+p$, p + A and A + A collisions in the same kinematical domain. The values $\sigma_{\rm abs}(400\ GeV) = 4.3\pm0.8\pm0.6$ mb is in agreement with NA50 results but the appropriatwe value at low energy is different $\sigma_{\rm abs}(158\ GeV) = 7.6\pm0.7\pm0.6$ mb. The In + In collisions measured in the NA60 experiment at 158 GeV per nucleon show small "anomalous" J/ψ suppression $< 10\%$ for central In + In events with this new value of $\sigma_{\rm abs}(158\ GeV)$, while for central Pb + Pb collisions "anomalous" suppression is still near 30%. If anti-shadowing effect (which is very model dependent and previously considered to be important only at high parton density conditions) of EKS model in In + In and Pb + Pb collisions is taken into account. Practically normal, cold nuclear matter J/ψ suppression in In + In collisions and still "anomalous" J/ψ suppression is observed in the most central Pb + Pb collisions [27].

Recent PHENIX experiment at RHIC observed J/ψ suppression in Au + Au and Cu + Cu collisions at $\sqrt{s_{\rm NN}}$ =200 GeV in nucleon-nucleon center-of-mass system [22, 28]. At these energies the results show that the J/ψ suppression at mid-rapidity is of the same order as the suppression at SPS energies for Pb + Pb and is the same for different systems at RHIC. But for forward rapidity range the suppression is stronger.

There are no theoretical models which could explain all the data. Different energy intervals between AGS, SPS, RHIC and LHC are very important to study the mechanism of quarkonium production and suppression, to investigate medium effects and conditions of Quark Gluon Plasma formation.

It is not clear if this problem could be solved at LHC energies, since the multiple charmed production could compensate the effect of color screening. Therefore we can assume that the explanation of anomalous charmonia states suppression could be found at lower energies. It is planned for SIS300 at FAIR, but it is not possible at SIS100 where for heavy ion experiments charmonia production is below threshold.

In conclusion, the measurements of charmonia states production are very important at MPD NICA where the appearance of mixed phase is expected. Although it is not easy to obtain the proton-nuclei data in the collider experiment, the problem could be solved by measurements of the energy dependence for charmonia production in heavy ions collisions at different centralities. The strong effect could be seen near the critical point.

7.5 Low energy J/ψ-hadron interactions

H. Satz

Fakultät für Physik, Universität Bielefeld, Germany

The suppression of J/ψ production has been proposed as a signal for the deconfinement of the medium produced in high energy nuclear collisions [17]. This implies that collisions in a confined thermal medium, i.e., in matter consisting of mesons of thermal momenta, cannot dissociate a J/ψ. To make such considerations quantitative, one first has to calculate the cross-section for the gluon-dissociation of a J/ψ , a QCD analogue of the photo-effect. This can be carried out using the operator product expansion [29, 30], and the result is

$$\sigma_{g-J/\psi} \simeq \frac{1}{m_c^2} \frac{(k/\Delta E_\psi - 1)^{3/2}}{(k/\Delta E_\psi)^5} \ , \tag{7.1}$$

where $\Delta E_{J/\psi} = 2M_D - M_\psi$, k denotes the gluon momentum and m_c the charm quark mass. The corresponding cross-section for the hadron dissociation is then obtained by convoluting the gluon-dissociation cross-section (7.1) with the hadronic gluon distribution function $g(x)$, which for J/ψ -meson interactions leads to

$$\sigma_{g-J/\psi} \simeq \sigma_{\rm geom}(1 - \lambda_0/\lambda)^{5.5} \tag{7.2}$$

with $\lambda \simeq (s - M_\psi^2)/M_\psi$ and $\lambda_0 \simeq (M_{\rm h} + \Delta E_\psi)$. Here $\sigma_{\rm geom} = \pi r_{J/\psi}^2 \simeq 2$ mb is the geometric J/ψ cross-section and $M_{\rm h}$ denotes the mass of the incident meson. In Fig. 7.4, we compare the two dissociation cross-sections (7.1) and (7.2) as function of the incident and pion momentum, respectively.

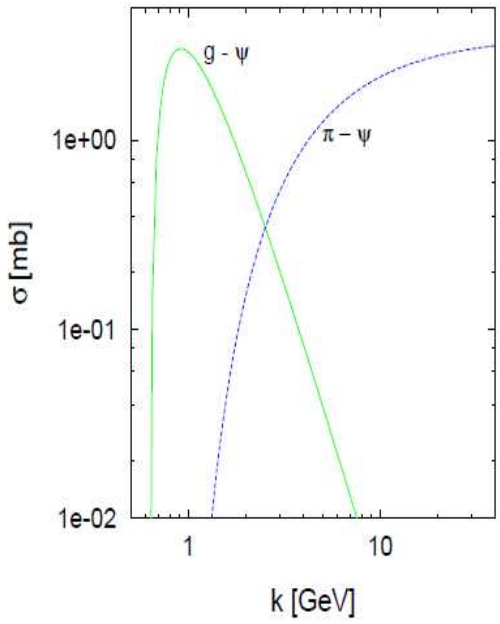

Figure 7.4: Gluon and hadron J/ψ dissociation cross-sections [30].

This result shows that typical thermal gluon momenta near 1 GeV produce a large dissociation cross-section, whereas hadron momenta in a thermal range (up to 1 – 2 GeV) still lead to a vanishingly small cross-section. In other words, the J/ψ should survive in confining media. This assertion is testable experimentally, by studying if slow charmonia in normal nuclear matter suffer significant dissociation.

Such experiments have been proposed for the CERN-SPS [31], but were never carried out, since they would have required major re-arrangements of the NA50 set-up. Studies at Fermilab and at HERA-B do provide some first hints that the inelastic J/ψ -nucleon cross-section indeed decreases for the slowest J/ψ's in nuclear matter accessible there [28].

The argumentation presented so far was based on OPE calculations [29,30], which become exact in the large quark mass limit $m_{\rm q} \to \infty$. It is not clear if the charm quark mass really satisfies this condition, and so the dissociation cross section in J/ψ-hadron collisions has been discussed in other approaches, in particular on the basis of meson exchange reactions, leading to much larger values [32,33]. A possible threshold enhancement has also been discussed. A conclusive experimental study would therefore provide important basic information.

7.6 J/ψ production in high energy nuclear collisions

P. Zhuang

Physics Department, Tsinghua University, Beijing, China

In 1986, Matsui and Satz [17] proposed J/ψ suppression as a signature for the deconfinement phase transition in relativistic heavy-ion collisions. Since the mass of heavy quarks (charm and bottom) is much larger than typical secondary (thermal) excitations of the system created in nuclear collisions, $m_{\rm c,b} \gg T$, they are mainly produced through initial hard processes. Therefore, the background for theoretically calculating heavy flavor production is rather solid and the study of J/ψ production can yield important information on the properties of the quark-gluon plasma (QGP) formed in the early stage of nuclear collisions.

Since $c\bar{c}$ pairs are created via hard processes, the J/ψ yield in p + A collisions should be proportional to the number of binary nucleon-nucleon interactions. However, from the experimental findings in p + A and light nuclear collisions, there exists already J/ψ suppression, the so-called "normal" nuclear suppression induced by multiple scattering between J/ψ (or its pre-resonance state) and spectator nucleons. In addition to the nuclear absorption, the primordially produced charmonia suffer an "anomalous" suppression when they pass though the hot and dense medium created in heavy-ion collisions [34,35].

The number of charm quarks created in the initial stage of heavy-ion collision increases substantially with collision energy. While a small production of charm quarks at SPS energy is expected (about ∼0.2 in central Pb + Pb), there are more than 10 $c\bar{c}$ pairs produced in a central Au + Au collision at RHIC (at $\sqrt{s_{\rm NN}}$ =0.2 TeV), and the number is probably over 200 in heavy-ion collisions at LHC (at $\sqrt{s_{\rm NN}}$ = 5.4 TeV). The large number of uncorrelated $c\bar{c}$ pairs in the QGP can recombine to form charmonia (primarily J/ψ's). Obviously, this regeneration will enhance the J/ψ yield, and the momentum spectra of the total final state J/ψ's may be quite different from the one with only initial production. The J/ψ initial production, continuous regeneration, nuclear absorption and anomalous suppression are schematically illustrated in Fig. 7.5.

Normal and anomalous suppression

Proton-nucleus p + A collisions are believed to be a good measure of normal (nuclear) J/ψ suppression. Suppose the projectile proton collides with a nucleon at $(\mathbf{b}; z)$ (characterizing the transverse and longitudinal positions) in the target nucleus and produces a J/ψ or its pre-resonant state on a very short time scale. On its way out the nucleus, the produced J/ψ collides inelastically with spectators. From the comparison with the SPS data, the average nuclear absorption cross section at SPS energy is extracted at $\sigma_{\rm abs} = 6.5 \pm 1.0$ mb, similar for both J/ψ and J/ψ'. The inelastic J/ψ+nucleon cross section (3.5±0.8 mb) is significantly less than the above value, and the inelastic cross section for ψ' is almost four times the value for J/ψ. The most recent analysis of NA50 data exhibits some of this trend, with $\sigma_{\rm abs} = 4.1 \pm 0.5$ mb and 8.2± 1.0 mb for the J/ψ and ψ', respectively. This indicates that the $c\bar{c}$ states suffering from nuclear absorption have already (at least partially) evolved into their final states, even tough the role of pre-resonant states could still be present.

Note that the effect of nuclear absorption depends strongly on the passing time $d_t = 2R_{\rm A} = sinh\ Y_{\rm B}$ of the two colliding nuclei, where $R_{\rm A}$ is the radius of the nuclei and $Y_{\rm B}$ is their rapidity in the center-of-mass frame. While at SPS energy the collision time is about 1 fm/c and normal suppression is large, the cold nuclear matter effect in extremely high-energy nuclear collisions should be small, due to the small collision time, e.g., $d_t \sim 0.1$

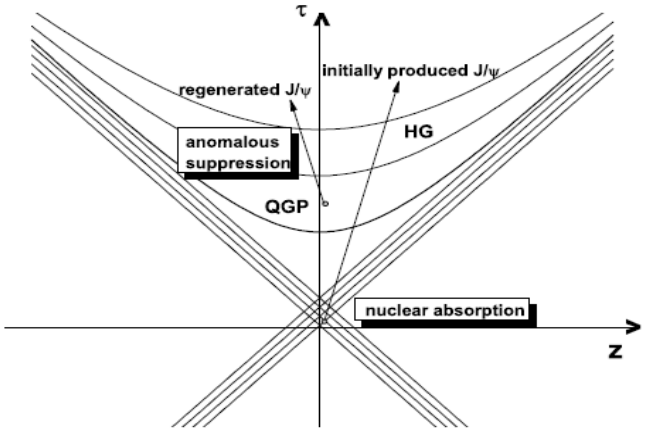

Figure 7.5: A schematic illustration of J/ψ production and suppression in relativistic heavy ion collisions.

fm/c at RHIC and 1/200 fm/c at LHC.

While the nuclear absorption mechanism can well account for the experimental data in p + A and light nuclear collision systems at SPS energy, the experiments with heavy nuclear projectile and target (Pb + Pb and In + In) show that the suppression of J/ψ (and ψ') in semi-/central collisions goes well beyond normal nuclear absorption [36], see Fig. 7.6. This phenomenon, called "anomalous" J/ψ suppression, is considered as one of the most important experimental results in relativistic heavy-ion collisions at SPS. Various theoretical approaches have been put forward to explain the anomalous suppression [30, 37–41].

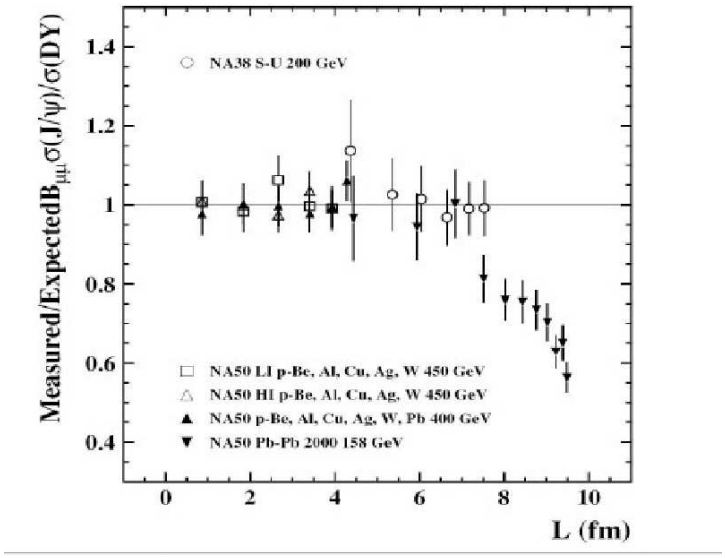

Figure 7.6: The J/ψ anomalous suppression at SPS energy. The figure is taken from Ref. [36].

The first mechanism is based on the original prediction of Matsui and Satz [17]: the Debye screening effect in the QCD medium created in the early stage of nuclear collisions leads to J/ψ melting. The properties of the charmonium states in QGP and in vacuum are very different. In particular, it is currently an open question whether the free energy, $F = U - TS$, or the internal energy is the appropriate quantity to be identified with a heavy-quark potential suitable for use in Schrödinger or Lippmann-Schwinger equation. In any case, due to the weakening of the potential with increasing temperature, the resonant states of $c\bar{c}$ dissociate at some Mott temperature $T_{\rm d}$. If the maximum temperature of the medium produced in heavy nuclear collisions

reaches the Mott temperature, the Debye screening effect results in the anomalous charmonium suppression. Recent lattice calculations of charmonium spectral functions in the deconfined phase suggest that the J/ψ can survive up to temperatures of $T_{\rm d} \simeq 1.6.-2T_c$ (T_c: critical temperature of the deconfined phase transition), while the excited states ψ' and χ_c disappear around T_c. Employing the heavy-quark potential extracted from the lattice calculation, the potential models generally support the above results from the spectral function analysis, even though no quantitative conclusions on the dissociation temperatures have been reached yet. A common conclusion from the lattice-based calculations is that, different charmonium states correspond to different dissociation temperatures. This leads to the sequential dissociation model of describing anomalous charmonium suppression: With continuously increasing temperature of the fireball, ψ' will melt first, then χ_c dissociate and finally J/ψ disappears. Considering the fact that about 40% of the final state J/ψ's originate from the decay of ψ' and χ_c in $p+p$ and p + A collisions, the anomalous J/ψ suppression in Pb + Pb collisions at SPS is associated with the dissociation of ψ' and χ_c in the produced fireball. A precise measurement on ψ' and especially on χ_c yield in the future can help to check the sequential model. Along similar lines, J/ψ suppression in hot and dense medium has been described in a general threshold model without considering microscopic dynamics. In the hot and dense part of the fireball where the density of the system $n_{\rm p}$ is larger than a critical value n_c, all the J/ψ's are absorbed by the matter, and those J/ψ's outside the region suffer only normal suppression. The threshold density n_c in this model is a parameter, e.g., taken as the maximum $n_{\rm p}$ in S+U collisions at SPS (where no anomalous suppression is observed). If the matter with $n_{\rm p} > n_c$ is QGP, the critical density n_c can be considered as the threshold value to create QGP.

The above analysis based on the Debye screening effect is typically based on the simplifying assumption of a constant temperature in connection with a sharp transition of the inelastic charmonium widths from zero (stable below $T_{\rm d}$) to infinity (dissolved above $T_{\rm d}$). However, the volume of the produced fireball in relativistic heavy ion collisions is relatively small and expands rapidly, implying rather fast temperature changes and short fireball lifetimes. In this case, the conclusion from the static Debye screening effect may deviate from the real system, and it becomes essential to include the concrete interactions between partons and charmonia, leading to sizable inelastic reaction rates comparable to the fireball expansion (or cooling) rate. In particular, the charmonia can be destroyed below the dissociation temperature. Debye screening is still operative, by controlling the binding energy which in turn determines the phase space (and thus the width) of the dynamic dissociation reactions. An important such process in the QGP is the (leading-order) gluon dissociation process $g + J/\psi \to c + \bar{c}$, an analogy to the photon dissociation process of electromagnetic bound states. For small binding energies (i.e., when approaching the dissociation temperature), the phase space for gluon dissociation shrinks and next-to-leading order (NLO) processes take over, most notably inelastic parton scattering $g(q,\bar{q}) + J/\psi \to g(q,\bar{q}) + c + \bar{c}$. Not only partons in the deconfined phase can induce anomalous suppression, but also the secondary particles like π, ρ and ω (so-called as comovers) in a hot and dense hadron gas can interact with charmonia inelastically and cause J/ψ suppression. The cross section $\sigma_{\rm co}$ is an adjustable parameter in the calculation. In some calculations the comover densities turn out to be rather high, corresponding to energy densities well above the critical one computed in lattice QCD. Consequently, the pertinent comover-interaction cross section assumes rather small values, e.g., $\sigma_{\rm co}$ =0.65 mb, which are more suitably interpreted as partonic comover interactions.

A more detailed description of the matter evolution together with a dynamical treatment of the interactions between charmonia and comovers has been carried out in the hadronic transport models UrQMD and HSD where the J/ψ motion is traced microscopically throughout the medium. The charmonium-hadron cross sections, however, remain input parameters to these models. Alternatively, one may employ theoretical calculations of charmonium dissociation cross sections with light mesons, as computed in either quark or hadronic models. By adjusting the comover cross sections (and possibly other parameters, such as formation times), interactions at the hadron level can reproduce the SPS data of J/ψ suppression.

Motivated by the lattice QCD findings of surviving J/ψ bound states well above T_c, recent work has treated the formation and evolution of $c-\bar{c}$ correlations more microscopically. In a weakly coupled QGP (wQGP), charm quarks would fly away from each other as soon as enough energy is available, while in a strongly coupled QGP (sQGP), the strong attraction between quarks, as well as their small diffusion constant in the sQGP, opens the possibility of returning to the J/ψ ground state, leading to a substantial increase in survival probability. The charm-quark motion in the medium is described by a Langevin equation. For strongly coupled matter, the drag coeffcient characterizing the thermalization of charm quarks in the medium is large. Taking the internal energy as the heavy-quark potential (extracted from a lattice-QCD computed free energy, the survival probability of charmonia in sQGP is larger than that in wQGP. This explains why there is no large difference

between suppressions at SPS and RHIC. When using effective potentials which are identified with the free energy, F, or a linear combination the internal energy U and F, the charmonium binding is less pronounced leading to dissociation temperatures (i.e., zero binding) below 1.5 T_c even for the J/ψ, as compared to above 2 T_c when employing U. We also recall that a small charm diffusion constant can be obtained from elastic c-quark interactions based on the internal energy as a potential.

Transverse momentum distributions

All models for inclusive J/ψ yields – with and without the assumption of a QGP and with and without regeneration mechanism – describe the observed suppression after at least one parameter is adjusted. Transverse momentum distribution may depend more directly on the production and regeneration mechanisms and therefore contain additional information about the nature of the medium and J/ψ, thus helping to distinguish between different scenarios.

Anomalous suppression is not an instantaneous process, but takes a certain time depending on the mechanism. During this time the produced charmonia with high transverse momentum may "leak" out the parton/hadron plasma and escape suppression. As a consequence, low p_t charmonia are more likely to be absorbed, and consequently the average transverse momentum of the observed charmonia will show an increase which grows monotonically with the average lifetime of the plasma. A self-consistent way to incorporate the effect of leakage into the various models is through charmonium transport equation in phase space [42].

The medium created in high energy nuclear collisions evolves dynamically. In order to extract information about the medium by analyzing the J/ψ distributions, both the hot and dense medium and the J/ψ production processes must be treated dynamically. Due to its large mass, the J/ψ is unlikely fully thermalized with the medium.Thus its phase space distribution should be governed by transport equation including both initial production (incl. anomalous suppression) as well as regeneration. The charmonium distribution function, $f_\Psi(\mathbf{p}_t;\mathbf{x}_t;\tau|\mathbf{b})$ $(\Psi = J/\psi;\psi';\chi_c)$, in the central rapidity region and in the transverse phase space, $(\mathbf{p}_t;\mathbf{x}_t)$, at fixed impact parameter $\mathbf{b}$ is controlled by the classical Boltzmann transport equation

$$\frac{\partial f_\Psi}{\partial \tau} + \mathbf{v}\nabla f_\Psi = -\alpha_\Psi f_\Psi + \beta_\Psi \ .$$

The second term on the left-hand side arises from free streaming of Ψ with transverse velocity $\mathbf{v}_\Psi = \mathbf{p}_t/\sqrt{\mathbf{p}_t^2 + m_\Psi^2}$ which leads to the leakage effect. The anomalous suppression and regeneration mechanisms are reflected in the loss term α_Ψ and gain term β_Ψ, respectively. It is assumed that the medium locally equilibrates at time τ_0 after nuclear absorption of the initially produced J/ψ's has ceased. The latter effect can be included in the initial distribution, $f_\Psi(\mathbf{p}_t;\mathbf{x}_t;\tau_0|\mathbf{b})$, of the transport equation.

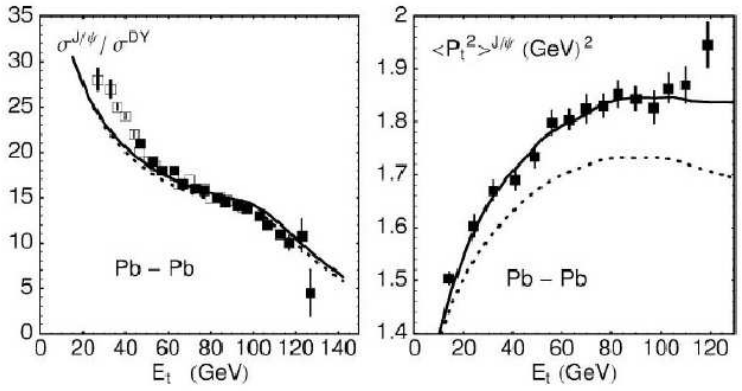

Figure 7.7: The J/ψ suppression and $< \mathbf{p}_t^2 >$ for J/ψ in Pb+Pb collisions at SPS as functions of transverse energy E_t. The dotted and solid lines are calculated in terms of comover model without and with considering the leakage effect, respectively. The figure is taken from Ref. [42].

When the loss and gain terms are known, the transport equation can be solved analytically with the result

$$f_\Psi(\mathbf{p}_t;\mathbf{x}_t;\tau_0|\mathbf{b}) = f_\Psi(\mathbf{p}_t;\mathbf{x}_t-\mathbf{v}(\tau-\tau_0);\tau_0|\mathbf{b})\ e^{\int_{\tau_0}^{\tau} d\tau' \alpha_\Psi(\mathbf{p}_t;\mathbf{x}_t-\mathbf{v}(\tau-\tau');\tau'|\mathbf{b})} + \int_{\tau_0}^{\tau} d\tau' \beta_\Psi(\mathbf{p}_t;\mathbf{x}_t-\mathbf{v}(\tau-\tau');\tau'|\mathbf{b})\ e^{\int_{\tau}^{\prime\tau} d\tau'' \alpha_\Psi(\mathbf{p}_t;\mathbf{x}_t-\mathbf{v}(\tau-\tau'');\tau''|\mathbf{b})}\ .$$

The first and second terms on the right-hand side indicate the contribution from initial production and continuous regeneration, respectively. Both suffer anomalous suppression. The coordinate shift $\mathbf{x}_t \to \mathbf{x}_t - \mathbf{v}_\Psi \Delta\tau$ reflects the leakage effect during the time period $\Delta\tau$.

At SPS energy regeneration can be neglected by setting $\beta_\Psi = 0$. In the comover-interaction model for the suppression mechanism, the J/ψ suppression and averaged transverse momentum $< \mathbf{p}_t^2 >$ are shown in Fig. 7.7. The calculation without leakage, obtained by setting $\mathbf{v}_/Psi = 0$, does not fit the data for $< \mathbf{p}_t^2 >$, even in the domain of low transverse energy, E_t (which in the NA50 experiment is used as a measure of centrality). Only when the leakage effect is taken into account, the calculation agrees well with the data. Since only high-pt charmonia are sensitive to the leakage effect, and since they are only a small fraction of the inclusive yield, both calculations with and without leakage can fit the J/ψ yield very well. The leakage effect on the transverse-momentum distribution is not sensitive to the underlying mechanism; the calculation with the threshold model as the suppression mechanism gives a similar structure of $< \mathbf{p}_t^2 >$ for J/ψ.

Charmonia in heavy-ion collisions at low energies

While in heavy-ion collisions at RHIC and LHC the formed medium is characterized by high temperatures and low (net) baryon densities, at relatively low energies, such as at NICA, highly compressed baryon matter at low temperature is anticipated. Monte Carlo simulations indicate the maximum energy and baryon density in a central Au + Au collision at NICA energy to reach $\varepsilon \sim 5$ GeV/fm^3 and $\rho/\rho_0 \sim 8$. In the following, we will give a qualitative discussion of some of the trends one might expect in the FAIR energy regime, based on the experimental and theoretical lessons at higher energies as discussed above.

Normal vs. Anomalous Suppression.

At low energies, regeneration in both the partonic and hadronic medium is expected to be small and the initial production will dominate the charmonium yield. Normal nuclear absorption of the directly produced charmonia is in the time period $t < t_{\rm d}$. At RHIC and LHC energies, where the collision time $t_{\rm d}$ is small and the lifetime of the partonic medium large, nuclear absorption is not a dominant factor, compared to anomalous suppression. However, at low energies, where the collision time $t_{\rm d}$ is much longer and the lifetime of partonic medium is much shorter, nuclear absorption becomes important, possibly the dominant effect. It has even been argued that heavy quark re-scattering in a cold nuclear medium can fully account for the observed J/ψ suppression in Pb+Pb collisions at SPS energy, without considering further suppression in the hot medium created in the later expansion stages.

Transverse-Momentum Spectra.

In comparison with the regenerated charmonia in the medium, the initially produced charmonia through hard processes have larger transverse momentum. At RHIC, the superposition of initial production and regeneration for J/ψ's leads to a roughly constant (or even slightly decreasing) average transverse momentum squared, $< \mathbf{p}_t^2 >$, with centrality. However, at NICA energy, the $< \mathbf{p}_t^2 >$ of the J/ψ's (dominated by initial production) should increase with centrality, due to the Cronin effect, i.e., the initial multiple scattering of gluons with nucleons (prior to the hard scattering leading to charmonium production).

Formation Time Effects.

The time for the medium created in heavy ion collisions to reach thermal equilibrium is short at high energies, about 0.5 fm/c at RHIC and 0.1 fm/c at LHC, and long at low energies, at least 1 fm/c at NICA (the time for full nuclear overlap is already $\sim$1.5 fm/c). Considering a finite formation time of charmonia, about 0.5 fm/c, J/ψ's are easily dissociated in the hot medium at RHIC and LHC, but might survive in the medium at low energies. Since charmonia are difficult to be thermalized at low energies, their elliptic flow at FAIR will be smaller than that at RHIC and LHC. Charmonia studies at NICA may also present a possible way to distinguish different scenarios of J/ψ suppression. For instance, when after adjusting the suppression at SPS energy, the suppression at NICA by comovers will be stronger than that by threshold melting; in addition, for the ψ/ψ' ratio, the comover scenario predicts a smooth excitation function, contrary to a step-like structure for threshold melting.

Medium Effects.

It is widely believed that chiral symmetry governs the low-energy properties and dynamics of hadrons in the vacuum and at finite temperature and density. The chiral symmetry restoration transition at high temperature (small baryon density) is a crossover, while it presumably becomes a first order phase transition at high density. Both the QCD sum rules analysis and the LO perturbative QCD calculations show that the J/ψ mass is reduced in nuclear matter due to the reduction of the gluon condensate. At SPS energy, chiral symmetry restoration reduces the threshold for charmonium break-up and could lead to a step-like behavior of the reaction rate, as suggested to account for the anomalous J/ψ suppression. The study of the ratio ψ/ψ' at SPS shows the importance of the hadronic phase for ψ' interactions, possibly related to the effect of chiral symmetry restoration. Another high density effect is the Friedel oscillation in the single-particle potential induced by a sharp Fermi surface at low temperature, which is widely discussed in nuclear matter and quark matter. The heavy-quark potential at zero baryon density, decreases monotonously with increasing temperature. In the compressed baryon matter, however, the potential may oscillate and approach the weak coupling limit very slowly. This could imply that J/ψ's survive in a wide region of high densities.

Charmed Baryons.

The importance of charmed baryons at low energies has been recently discussed. While the J/ψ and ψ' yields relative to the total number of $c\bar{c}$ pairs are roughly independent on colliding energy over a wide region from NICA to RHIC, the relative yield for charmed baryon Λ_c decreases strongly with increasing energy, exceeding the yield of D mesons at the low-energy end. This indicates that the investigation of open-charm production at low energies mandates the inclusion of charmed baryons.

7.7 Soft photons at NICA

V. V. Avdeichikov[a], E. S. Kokoulina[a,b], A. Ya. Kutov[c], V. A. Nikitin[a], I. A. Rufanov[a]

[a] *Joint Institute for Nuclear Research, Dubna, Russia*
[b] *Gomel State Technical University, Gomel, Republic of Belarus*
[c] *Komi SC UrD RAS, Syktyvkar, Russia*

Experimental and theoretical studies of direct photon production in hadronic collisions essentially expand our insights about multiparticle production mechanisms [43–45]. These photons are useful probes to investigate nuclear matter at all stages of the interaction. Soft photons (SP) play a particular role in these studies. Until now we have no explanation for the experimentally observed excess SP yield. These photons have low energy transverse momenta $p_T < 0.1$ GeV/c, $|x| < 0.01$ [46–49]. In this domain their yield exceeds the theoretical estimates by 5 – 8 times.

For a qualitative explanation of this effect the assumption of the formation of a cold spot of quark gluon plasma (QGP) or hadronic gas has been made in a number of theoretical papers [50–52]. It is argued that a cold spot is relatively stable and radiates soft photons. SP testify the existence of a new phenomenon connected with the collective behavior of particles [53]. One interesting option currently under discussion is the formation of a pionic condensate when a group of pions with small relative momenta can form a relatively coherent and stable system. It is known from phase shift analysis of low energy pion scattering that pions in the isotopic spin state zero have an attractive potential. In a bosonic system an attractive force is not saturated with the growth of the particle number, because all bosons can occupy one quantum state. As a consequence, the multipionic system acquires additional stability. During the formation of such a system from a hadronic gas, when single pions fall in the lowest quantum state, and an intense soft photon radiation should emerge.

We are preparing for carrying out SP investigations at U-70 (Protvino) and propose to study this unique phenomenon at JINR collider NICA. At high hadron multiplicities available in A + A collisions at collider conditions the probability to form a cold quasistationary (hadron or parton) system is higher than in previous experiments carried out at fixed target. Photons may be detected in a TPC via conversion $\gamma \to e^+e^-$. The estimated count rate of SP is 15 s^{-1} at a beam luminosity of 10^{27} $s^{-1}cm^{-2}$. Another possibility is to implement a small (~ 10 cm^2) special electromagnetic calorimeter with a low energy threshold ($\sim 1 \div 5$ MeV). This module can be incorporated into a barrel calorimeter.

Soft direct photons

Direct photons (DP) by definition are not a decay product of any known particle. In accordance with quantum electrodynamics they may be emitted in the process of charged particle scattering - bremsstrahlung in a parton or hadron cascade. In particular, $q\overline{q} \to g\gamma$ and $gq \to \gamma q$ parton interactions lead to photon emission. The higher the density and the longer the system lifetime, the more DP should be emitted. The produced

photons interact with the surrounding matter only electromagnetically, and therefore they bear the information on properties of the surrounding environment during whole history of evolution.

Special attention is devoted to low energy DP (SP) whose yield surpasses the theoretical predictions by $5 \div 8$ times. This concerns K^+p and $p\bar{p}$ interactions at 70 GeV [46,47] as well as $\pi^\pm p$ and K^+p interactions at 250 and 280 GeV [48,49]. Some results are shown in Fig. 7.8. The recent results on this subject by the DELPHI collaboration [54] are devoted to studying SP inside hadronic jets originated from the $Z^0 \to q\overline{q} \to jet + X$ decay region. The authors claim a clear excess of SP as compared to the theoretical prediction by a factor 3 for charged and a factor 17 for neutral particles.

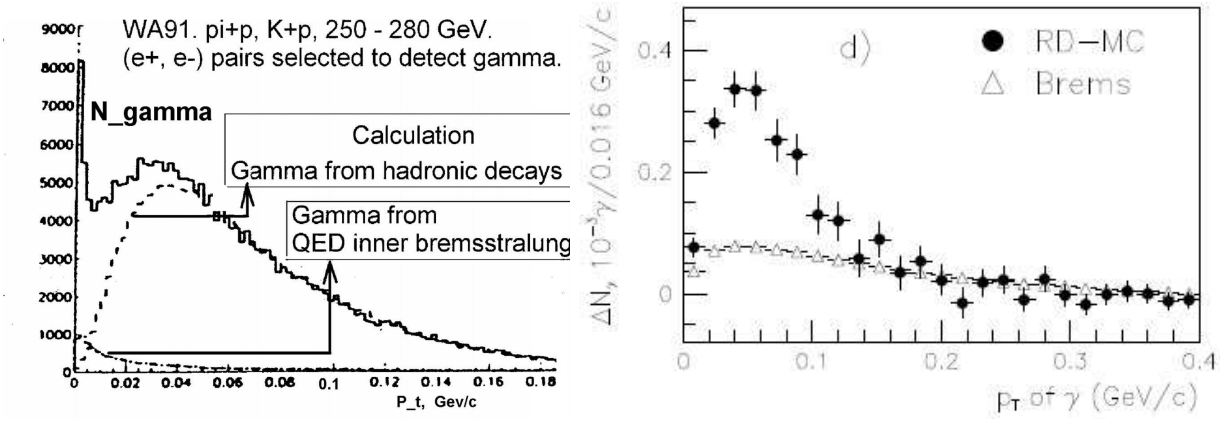

Figure 7.8: Left panel: SP p_t spectrum. The photons from decay of known particles are shown by MC histogram [48]. Right panel: Same as on Left panel, data [54]. RD-MC means real data with MC data subtracted.

The SP surplus can be assigned to unknown physical processes. In the paper [50] the formation of a cold zone of the QGP in a hadronic gas is assumed (model CQGP). The authors believe that cold partons lack energy for fast hadronization. So they recombine in hadrons rather slowly. Therefore a cold QGP droplet has a big lifetime and it reveals itself as a source of low energy DP. The idea of a cold spot of pion gas is considered in the paper [51]. Slow pions get repeatedly reflected from the border of hot and cold areas and have a large lifetime. Again at the cost of a long lifetime the cold spot radiates SP with low energy in the c.m.s.

A new interesting idea has been advanced in [55] where the analogy between expanding hadronic fireball and expanding universe was supposed. In both cases the spectrum and intensity of emerging photons can be described by a black body radiation formula. DP apear as an analogue of the cosmic microwave background radiation. A semiqualitative description of the available experimental data has been achieved.

We have designed a gluon dominance model (GDM) for describing the high multiplicity in lepton (e^+e^-) and hadron (pp, $\overline{p}p$) interactions [56–62]. We assume that the energy of colliding hadrons is transformed to internal energy of initial particles and a quark-gluon system appears. In this case a parton cascade based on QCD is possible whith quark bremsstrahlung and gluon fragmentation. This assumption has been confirmed by our recent multiplicity studies [63]. We have shown that hadron production is realized by active gluons. The comparison of the GDM predictions with experimental data in a wide energy interval shows a good agreement. Half of the active gluons ($\sim 47\%$) produce hadron jets and the remaining gluons form a quark-gluon system (QGS). We suggest that these gluons are the source of the excess rate of SP observable in a number of experiments.

We suppose that at a certain moment the QGS or excited new hadrons may be created in a near-equilibrium state within a short period or finite time. Therefore, to describe massless photons, we used the black body emission spectrum. From experimental data the inelastic cross section is equal to approximately 40 mb. The cross section of SP formation is about $4mb$, and since $\sigma_\gamma \simeq n_\gamma(T) \cdot \sigma_{in}$, the number of SP will be equal to $n_\gamma \approx 0.1$. The estimates of temperature are based on the scale for momentum transfer: $T = p \approx p_T\sqrt{2}$ (1 MeV $= 1.16 \cdot 10^{10}$ K). If $T(p_T)$ is known, using n_γ we can estimate the linear size of the radiating system ($V \simeq L^3$). The obtained linear size of the system from the SP momentum (p_T) is $L \sim 4 - 6$ fm.

It is well-known that the temperature of secondary hadrons is higher than the temperature of SP. We assume that objects with soft gluon content may not transform into hadrons but turn into SP's. The amount of such soft gluons can be estimated by the number of active gluons. The observable dependence of the yield of SP

on the charged, neutral or total multiplicities can be explained the amount of partons converted to the excess SP via QCD-processes. The differences in the excess yield for charged and neutral pions can be explained by the distinction of their constituents. The charged pions consist of different flavors ($u\overline{d}$ or $d\overline{u}$), the neutrals of the same ($u\overline{u}$ or $d\overline{d}$). They are distinguished in masses too. The excess of energy (the cooling of secondary particles) will be transformed to SP. Their yield will be higher for neutral pion (less mass) than for charged meson production.

The study of the DP seems especially interesting for the NICA project and the MPD setup [64] as it aims to deal with a high density system [65, 66]. The goal of the proposed experiment is the investigation of collective behavior of particles in the process of multiple hadron production in pp and AA interactions at the colliding beam energy $E \simeq 5$ AGeV. The domain of high multiplicity (central collisions) will be studied. Near the threshold of a reaction all particles obtain a small relative momentum.

In a thermalized cold and dense hadronic gas as a consequence of multiboson interference a number of collective effects may appear. In particular, an increase in the rate of DP results from bremsstrahlung in the partonic cascade in a dense and cold pionic gas or condensate. The production of a multipion, coherent semibound state is possible. It emits soft pions in the course of its formation. The partonic cascade leads to a high multiplicity of particles in the final state. Many of them are accompanied by bremsstrahlung radiation. At high densities an additional γ source [52] is predicted: pion annihilation $\pi^+\pi^- \to n\gamma$. Close to the region of the chiral phase transition the masses of the constituent quarks decrease which leads to an increase of radiation (bremsstrahlung and annihilation processes). This efect may serve as a more reliable tool to measure density and temperature of the system.

It is necessary to note, that the DP discussed here have energies in the c.m.s. of $E_{c.m.\ \gamma} \leq 30$ MeV or wavelength $\lambda \geq 60$ fm. Obviously, this size is much greater than the size of the formed hadron system. Therefore, such photons should be radiated by system as a whole instead of the separate particles. In this case the pion system can condense [53]. Experimental indications for Bose-Einstein condensation were obtained (Fig. 7.9) by the SVD Collaboration [67].

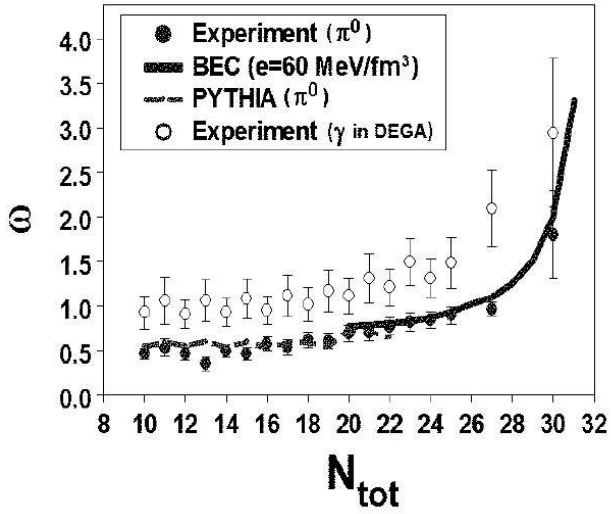

Figure 7.9: Normalized dispersion of neutral pion number as a function of the total number of pions measured in pp interactions at a proton energy of 50 GeV. $\omega = \sigma(\pi^0)^2 / < N(\pi^0) >$ [67].

Photon calorimeter with low energy threshold

A specific feature of the proposed photon detector is its capability to measure low energy deposit $E_{thresh} \leq 5MeV$ [68]. Still none of the known experiments has reached such a small value of the photon energy detection. As it has been mentioned above, it is of importance for check some exotic theoretical models. We suggest to construct an electromagnetic calorimeter (EC) from BGO scintillator. The dimension of one cell should be $\simeq 5 \times 5 \times 120$ cm^3. In this case the spatial localization of a photon is ¡ 5 cm. One should take in to account the transverse dimension of the photon shower ~ 5 cm. From this very qualitative consideration we conclude that the calorimeter transverse dimensions should be $\sim 30 \times 30$ cm^2. Four central cells with a total area of

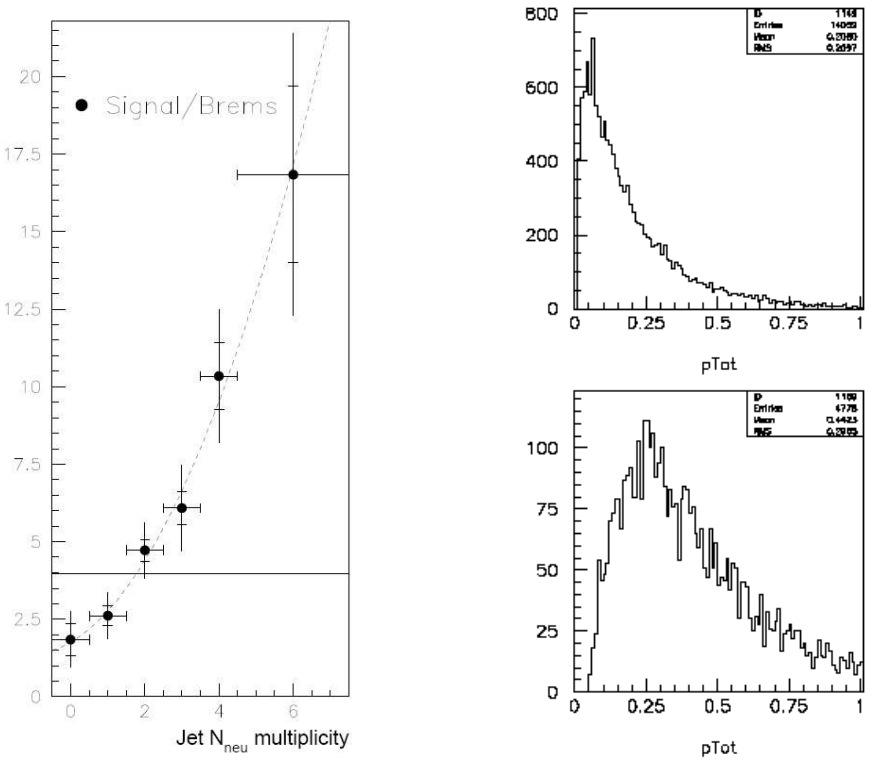

Figure 7.10: Left panel:Intensity of SP as a function of the neutral pion multiplicity in jets [54]. Right panel: MC simulation of γ and π^0 production.

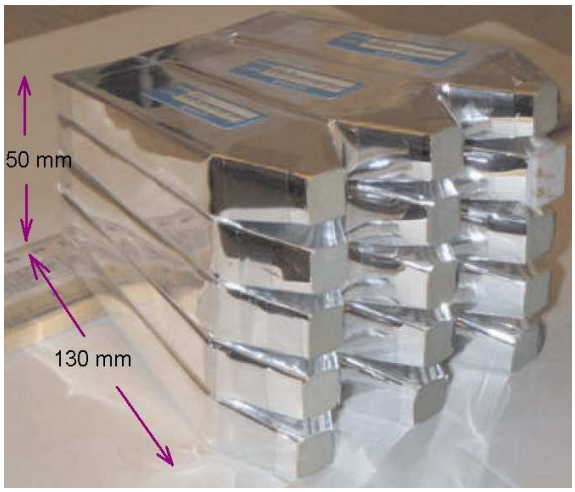

Figure 7.11: Electromagnetic calorimeter prototype [68].

10 cm^2 will provide a high efficiency photon detection. The longitudinal dimension should be as usual ~ 10 radiation lengths. For BGO this is ~ 12 cm. The important problem is to take into account the dissipated particle background in the experimental hall. Reduction of background may be provided by the calorimeter preshower.

According to [46,47] the integrated cross section of the SP production in the domain $p_t \leq 0.1$ GeV/c, $-0.01 \leq x \leq 0.01$ is equal to $2 \div 4$ mb/nucleon. Assuming the SP isotropic angular distribution we get an averaged differential cross section $d\sigma/d\omega = 0.2$ mb/strad/nucleon. For a proton beam luminosity $L \simeq 10^{30}$ cm^{-2} s^{-1} the EC counting rate is equal to $\simeq 1\text{s}^{-1}$. For $Au + Au$ collisions with luminosity $L \simeq 1 \times 10^{27}$ cm^{-2} s^{-1} the count rate is equal to $\simeq 0.4\text{s}^{-1}$. During one day of runtime a statistics of $\simeq 5 \times 10^4$ SP will be accumulated. SP may convert into e^+e^- pairs in the vertex detector material and in the walls of the TPC. Thus another option is the detection of low energy e^+e^- pairs in the TPC. This leads to one order of magnitude higher statistics due to the higher angular acceptance of the TPC. But the pair detection in the TPC is subject to an additional analysis.

Assuming for the photon detector an effective area of 10^2 cm^2, set at a distance of 1.3 m from the target, leads to the following estimate of the DP count rate: 2 events per cycle. One week of runtime will provide a pretty good sample of SP: $\approx 2 \times 10^5$ events.

Let us point to the distinctive features of the present project.

- Photon spectra at several fixed angles will be measured. The lower edge of the spectra is ~ 5 MeV/c.
- Each SP spectrum will be collected at a certain fixed multiplicity of secondaries in pp and AA interactions.
- We plan to study both phenomena, Bose-Einstein condensation [67] and SP yield.

Thus the inelasticity or rate of the primary energy dissipation will be known for each spectrum.

7.8 Electromagnetic probes in heavy-ion collisions

H. van Hees

Frankfurt Institute for Advanced Studies (FIAS), Frankfurt am Main, Germany

In this paper we give a brief review about the important role of precise measurements of electromagnetic probes in relativistic heavy-ion collisions for our theoretical understanding of the properties of strongly interacting hot and dense matter. Since leptons and photons contrary to hadronic observables are probes that penetrate the hot and dense fireball, created in such collisions, nearly undisturbed by final-state interactions, because they do not participate in the strong interaction, the precise measurement of invariant-mass and transverse-momentum spectra of lepton-antilepton pairs ("dileptons") and transverse-momentum spectra of photons offers the unique opportunity to gain insight into the properties of the hot and dense medium in the interior of the fireball at any stage of its evolution. Together with concise theoretical models for both the emission of these electromagnetic probes from a partonic medium (QGP) and the hot and dense hadronic medium one can gain insight on the in-medium properties of the electromagnetic current-correlation function, closely related to the vector current and thus the light vector mesons in the hadronic stages of the fireball evolution. We shall also emphasize the importance of such measurements at high net-baryon-number densities as envisaged with the future NICA project.

Introduction

One of the major goals of relativistic heavy-ion physics is the investigation of strongly interacting matter under extreme conditions of temperature and density. From the fundamental theory of the strong interaction, Quantum Chromodynamics (QCD), which is an asymptotically free non-Abelian gauge symmetry, one expects that in a sufficiently hot and dense medium the hadronic degrees of freedom, governing the thermodynamics of strongly interacting matter at low energies, dissolve into their elementary constituents, quarks and gluons [69]. Ultra-relativistic heavy ion experiments at the CERN SPS and LHC, and the BNL RHIC facilities, have found that many observables concerning the hadron abundances and spectra can be well understood from (nearly ideal) relativistic hydrodynamics assuming the rapid formation of a collectively expanding fireball, which implies rapid local thermalization of the fluid elements. The comparison of the hadron-p_{T} spectra with such a model assumption leads to the conclusion that energy densities have been reached that lie significantly above the

critical density for the deconfinement and chiral phase transition as evaluated in lattice simulations of thermal QCD [70].

A particularly valuable probe are photons and dileptons, i.e., lepton-antilepton pairs, emitted from the hot and dense medium, because in contrast to strongly interacting hadrons they leave the medium nearly unaffected by final-state interactions and thus provide information on the properties of the partonic and hadronic electromagnetic currents in the medium since they directly measure the electromagnetic current-current correlation function in the time-like (dileptons) and light-like (photons) domain. As expected from the various phase transitions, predicted by effective hadronic models of QCD, one expects that the hadrons in a hot and dense medium undergo strong modifications of their spectral properties. Since the electromagnetic probes are directly linked to the vector current of QCD and thus the properties of the vector mesons ρ, ω, and ϕ, which are also directly related to the isovector-vector part of the Noether currents of chiral symmetry, they admit a direct insight to medium modifications governed by chiral-symmetry restoration. Although, of course, the same feature of the only electromagnetic (and weak) coupling of the leptons and photons to the strongly interacting particles, has the experimental drawback of making them to rare probes, their investigation provides unique information about the properties of the hot and dense medium, which is not available from hadron observables, which reflect the (mostly thermal) state of the medium at the end of the fireball evolution when "thermal freeze-out" occurs.

The rest of this contribution is organized as follows: Firstly we briefly review the notion of chiral symmetry in the context of QCD and the relevant quantities in terms of the corresponding vector and axialvector Noether currents and summarize the most important aspects of our current understanding of the vector part in the context of electromagnetic probes and their relation with the chiral-symmetry restoration as well possible experimental observables with the chace to provide some indirect evidence for this phase transition. We conclude with some remarks on the importance of a precise measurement of electromagnetic probes at the future NICA facility, which particularly aims at high net-baryon densities providing insight into a region of the phase diagram at moderate temperatures but high net-baryon densities, which has not been investigated thoroughly yet in the ongoing heavy-ion research programs.

QCD and chiral symmetry

Quantum chromodynamics is the fundamental theory underlying the description of the strongly interacting elementary particles, quarks and gluons. Its Lagrangian is governed first of all by the local color symmetry based on the symmetry group SU(3):

$$\mathscr{L} = \overline{q}(\mathrm{i}\not{\mathrm{D}} - M_q)q - \frac{1}{4}G^a_{\mu\nu}G^{\mu\nu}_a \quad \text{with} \quad \mathrm{D}_\mu = \partial_\mu \mathrm{i}g_2\frac{\lambda_a}{2}A^a_\mu, \tag{7.3}$$

where the quark fields q carry both a color and flavor index. The gluon fields are denoted by A^a_μ, and the λ_a are the Gell-Mann matrices acting in SU(3) color space of the quarks. The non-Abelian field-strength tensor is defined by

$$G^a_{\mu\nu} = \partial_\mu A^a_\nu - \partial_\nu A^a_\mu - f^{abc}A^b_\mu A^c_\nu, \tag{7.4}$$

where the f^{abc} are the SU(3) structure constants. Further $M_q = \mathrm{diag}(m_u, m_d, m_s, \ldots)$ is the current-quark mass matrix in flavor space.

Besides the fundamental local color-gauge symmetry underlying the fundamental structure of the QCD Lagrangian (7.3), QCD shows also other "accidental" symmetries. In our context one of the most important ones is the approximately realized chiral symmetry in the sector of the light u, d, (and s) quarks. Their masses are small compared to typical hadronic scales as the nucleon mass of ~ 940 MeV. In the limit of vanishing quark masses the QCD Lagrangian becomes invariant under the chiral rotations, $q \to \exp(-\mathrm{i}\vec{\alpha_V}\cdot\vec{\tau}/2)$ and $q \to \exp(-\mathrm{i}\gamma_5\vec{\alpha_A}\cdot\vec{\tau}/2)$, where the $\vec{\tau}$ denote the (SU(2)- or SU(3)-) flavor matrices of the light quark sector. This symmetry gives rise to the conserved isovector vector and axial vector currents,

$$\vec{j}^{\,\mu}_V = \overline{q}\gamma^\mu\frac{\vec{\tau}}{2}q, \quad \vec{j}_A = \overline{q}\gamma^\mu\gamma_5\frac{\vec{\tau}}{2}q. \tag{7.5}$$

For non-zero quark masses this symmetry is broken explicitly, but this explicit breaking is quite small and thus can be treated as a perturbation, giving rise to chiral perturbation theory as a tool to derive hadronic models as effective theories for low-energy QCD.

In the vacuum and at low temperatures and densities the chiral symmetry is also spontaneously broken from $\mathrm{SU}(N)_L \times \mathrm{SU}(N)_R$ to $\mathrm{SU}(N)_V$ (with $N = 2$ or 3) due to the formation of a quark condensate, $\langle\overline{q}q\rangle \neq 0$ with the pions (and kaons) as the pseudoscalar pseudo-Goldstone modes.

Effective hadronic models can be built by using chirally symmetric quantum field theories like the linear or non-linear σ model and implementing the heavy particles in a well-defined formalism based on the remaining unbroken isospin symmetry (see, e.g., [71] particularly for the case of vector mesons).

Electromagnetic probes and chiral-symmetry restoration

The emission rates of dileptons or photons from a hot and/or dense equilibrated medium is given by the McLerran-Toimela formula [72, 73]

$$\frac{dN_{\ell\ell}}{d^4x d^4q} = -\frac{\alpha_{\rm em}^2}{\pi^3 M^2} f_{\rm B}(q\cdot u;T)\frac{1}{3} g_{\mu\nu}{\rm Im}\Pi^{\mu\nu}_{\rm em,ret}(q;T,\mu_{\rm B})|_{q^2=M^2}, \tag{7.6}$$

$$q^0\frac{dN_{\gamma}}{d^4x d^3\vec{q}} = -\frac{\alpha_{\rm em}}{\pi^2} f_{\rm B}(q\cdot u;T)\frac{1}{2} g_{\mu\nu}{\rm Im}\Pi^{\mu\nu}_{\rm em,ret}(q;T,\mu_{\rm B})|_{q^2=0}, \tag{7.7}$$

which are exact concerning the strong interactions and in leading order to $\alpha_{\rm em}\simeq 1/137$. Here, q is the four momentum of the ℓ^--ℓ^+ pair ($\ell\in\{{\rm e},\mu\}$), u the four-velocity of the heat bath, and

$$\Pi_{\rm em,ret} = -i\int d^4x \exp(iq\cdot x)\Theta(x^0)\,\langle |j^\mu_{\rm em}(x), j^\mu_{\rm em}(0)|\rangle_{T,\mu_{\rm B}} \tag{7.8}$$

is the (retarded) electromagnetic current-current correlation function, evaluated in the hot and dense medium at given temperature T and net-baryon-number chemical potential $\mu_{\rm B}$.

The electromagnetic current in terms of quark-degrees of freedom is given by

$$j^\mu_{\rm em} = \frac{1}{\sqrt{2}}\left[\frac{\overline{u}\gamma^\mu u - \overline{d}\gamma^\mu d}{\sqrt{2}} + \frac{1}{3}\frac{\overline{u}\gamma^\mu u + \overline{d}\gamma^\mu d}{\sqrt{2}} - \frac{\sqrt{2}}{3}\overline{s}\gamma^\mu s\right]. \tag{7.9}$$

On the other hand in the vacuum it turns out that in the hadronic realm the electromagnetic current of hadrons can be quite well described within effective hadronic models in terms of the vector-meson dominance (VMD) hypothesis, i.e., as to be proportional to the vectorfields, describing the electrically neutral light vector mesons, ρ^0, ω, and ϕ, which have the same quantum numbers as the photon. Thus the current-current correlator in a naive constituent-quark picture of the vector mesons, by comparison with (11.6) obeys the relation

$${\rm im}\Pi_{\rm em,ret} \propto \left[{\rm Im}D_{\rho,\rm ret} + \frac{1}{9}{\rm Im}D_{\omega,\rm ret} + \frac{2}{9}D_{\phi,\rm ret}\right], \tag{7.10}$$

where D_V with $V\in\{\rho,\omega,\phi\}$ denotes corresponding (retarded) vector-meson propagators, whose imaginary part directly gives the spectral functions of these vector mesons, which leads to a direct relation between the emission rates for electromagnetic probes (7.6) to the spectral properties of the vector mesons. Eq. (11.7) identifies the isovector contribution, corresponding to the ρ meson, as the dominant source of dileptons from a hadronic source.

Recently an effective hadronic model [6,74] based on the VMD assumption, including interactions with both mesons and baryons, including all relevant resonances for the evaluation of the vector-meson spectral functions at finite T and μ_B has been used in the rates (7.6). In the partonic phase a hard-thermal-loop improved rate from $q\overline{q}$ annihilation [75] has been applied.

These rates, have been integrated over the whole evolution of a fireball of hot and dense partonic and hadronic medium as created in heavy-ion collisions at the SPS. For the description of a fireball a simple model of an isentropically expanding homogeneous fireball including radial flow with an equation of state with a phase transition from a QGP to a hadronic phase has been used. Also the contribution to the dilepton yield from non-thermal sources (as from the Drell-Yan process, from hard primordially created vector mesons, and from vector-meson decays after thermal freeze-out) have been taken into account [81, 82].

The hadronic many-body model, when evaluated at finite T and μ_B leads to a large broadening of the vector mesons in the medium with negligible mass shifts. This is due to the fact that any interaction channel with mesons and baryons adds to the width of the vector mesons, i.e., the imaginary part of the retarded vector-meson self energies, while there are on the average as many attractive as repulsive resonance channels, leading to a decrease or increase of the vector-meson mass, respectively, nearly compensating each other in

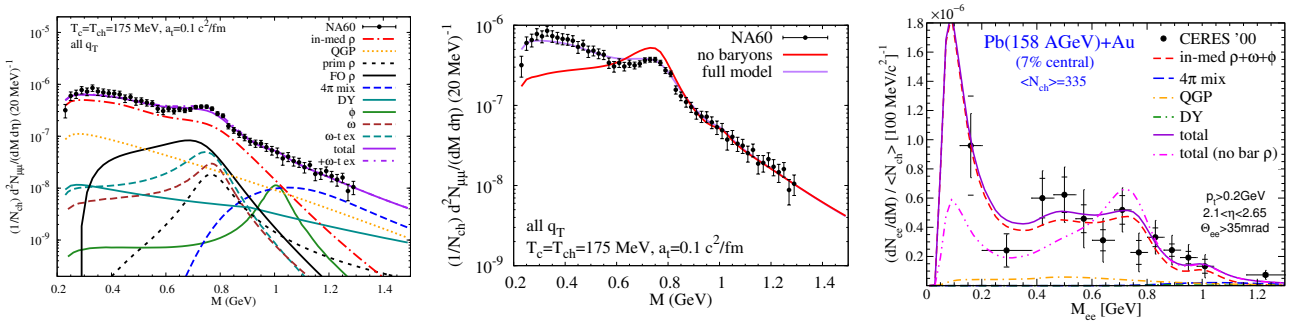

Figure 7.12: Comparison of the evaluation of dilepton invariant-mass spectra in 158 AGeV-In-In collisions (left and middle panel) from partonic and hadronic many-body theory with data from the NA60 collaboration [3, 76–79] and in 158 AGeV-Pb-Pb collisions (right panel) from the CERES/NA45 collaboration [80]. The left panel underlines the importance to take into account all relevant sources during the entire evolution of the fireball. As can be seen, the dominant source in the low-mass region, $M \lesssim 1$ GeV, is the emission from the hadronic phase via the (medium modified) ρ-meson contribution. The middle panel shows that the essential microscopic mechanism underlying the medium modification of the vector mesons are the contributions to their width from direct scatterings of the vector mesons with baryons in the medium, which provides the depletion of the dilepton yield in the peak region at $M \simeq m_\rho = 770$ MeV and, even more pronounced, the substantial enhancement in the low-mass tail down to the dimuon threshold. This latter feature of the medium modifications of the vector-meson spectrum is the more underlined in the comparison to the dielectron data in the right panel, showing compatibility of the model with the dilepton excess data down to $M \simeq 2m_e$.

the real part of the vector-meson self-energy. Another interesting feature of this model is the observation of a kind of "parton-hadron duality" in the following sense: If one evaluates the rates (11.6) on the one hand from the hadronic model and from the hard-thermal-loop improved pQCD-QGP model, extrapolating both models towards the phase-transition region at $T_c \simeq$ 160-180 MeV, one finds very similar results.

By comparison with high-precision data on the invariant-mass and q_T spectra of dimuons from In-In collisions by the NA60 collaboration [3, 76–79] one finds a rather good agreement. The only additional input parameter to be fixed in addition to the hadronic model (which is fixed on input from pp and pA data) and the fireball evolution (which is fixed from collective-flow data in heavy-ion collisions) is the total fireball lifetime, which determines the total yield of dileptons, which in turn leads to a pretty sensitive determination of this lifetime.

It also turned out that an inclusion of the direct interactions of the vector mesons with baryons is crucial for the agreement of the model calculation of the dilepton spectra with the experimental findings. In the first place it is a large contribution to the broadening of the vector mesons (most pronouncedly for the ρ meson), leading to the depletion of the dilepton peak at invariant masses around the vector-meson mass ($m_\rho \simeq 770$ MeV) and the large enhancement at the low-mass tail, down to the dimuon threshold at $M = 2m_\mu$. This is also confirmed for the dielectron measurements by the CERES/NA45 collaboration [80, 83] down to the dielectron threshold at $M = 2m_\mathrm{e}$. The very same model for the in-medium electromagnetic-current correlator is also successful in the description of photon spectra from the WA98 collaboration [84, 85] showing the consistency of the predicted current correlation function between the kinematics for dileptons (timelike momenta) and photons (spacelike momenta).

Conclusions

As has been elaborated in the previous sections, precise measurements of the invariant-mass and q_T spectra of electromagnetic probes, i.e., dileptons and photons, in conjunction with carefully scrutinized models of the in-medium properties of partons in hadrons in the hot and dense strongly interacting medium provide valuable insight in the properties of this medium due to their penetrating nature. Although a direct check for the chiral-symmetry restoration is not yet available, this study provides an important step forward in its general understanding. The model is consistent with chiral-symmetry restoration since the dilepton rates from the hadronic and partonic phase, both extrapolated to the phase-transition region, coincide showing some kind of "parton-hadron duality" via the resonance-melting scheme in contrast to dropping-mass scenarios, which are disfavored by the NA60 data. Since pQCD obeys, of course, unbroken chiral symmetry the phase transition from partonic to hadronic in this model is compatible with chiral-symmetry restoration. Further the accuracy of the absolute yield provided by such high-quality (acceptance-corrected!) data admits a sensitive estimate of

the total fireball lifetime ("ρ clock"), provided the fireball model can be adjusted carefully to corresponding hadronic data to determine the temperature and density on the one hand as well as the collective-flow profile to a sufficient accuracy.

Including the high-precision measurement of electrodynamic probes (dileptons and/or photons) in the future NICA experiment, aiming at the creation of a partonic and hadronic medium at lower temperatures but the highest reachable net-baryon densities, could thus provide further important insights into the properties of strongly interacting matter in a region of the phase diagram not easily accessible by lattice QCD. First of all it could help to further test the models, so far successful at heavy-ion collisions at the SPS and (at least partially) at RHIC, at the lower energies leading to larger net-baryon density at NICA. Particularly this is underlined by the fact that the dominant medium effect on the electromagnetic current correlator is provided particularly by interactions of the vector mesons with baryonic excitations. Further, if the transition behavior indeed changes from the cross-over type at low net-baryon densities as known from lattice QCD calculations at $\mu_{\mathrm{B}} = 0$ (with physical quark masses) to a first-order behavior at larger μ_{B} with a critical second-order transition point, a then possible reliable determination of the fireball lifetime might reveal features like the existence of a mixed parton-hadron phase and perhaps even the critical slowing down of the medium evolution close to a possibly reachable critical endpoint of the first-order transition line. Of course, this also requires further hadronic observables as model input to both the fireball model and the hadronic many-body theory.

7.9 Dilepton and ϕ meson production in elementary and nuclear collisions at the NICA fixed target experiment

M. Zétényi, G. Wolf

Institute for Particle and Nuclear Physics, Wigner Research Centre for Physics, Hungarian Academy of Sciences, Budapest, Hungary

Dileptons are an important probe of relativistic nuclear collisions, because they leave the hot and dense phase of the collision unaffected by strong final state interactions. On the other hand, the dilepton spectrum obtained from a nuclear collision is a complicated superposition of many production channels coming from various stages of the process. Therefore, drawing any reliable conclusions based on the dilepton spectrum is difficult, and depends on understanding many aspects of the underlying physics, like elementary cross sections, in medium modification of particles, reaction dynamics, etc.

In recent years dilepton production was studied at RHIC, SPS, and at much lower energies at GSI SIS by the HADES experiment. The range between the SIS and SPS energies is basically undiscovered, and the NICA fixed target experiment will give a unique opportunity to study dilepton production in this regime.

At low energies elementary hadron collisions were usually described by the resonance dominance model, where in the first step of the collision a baryon resonance is excited, which later decays – possibly in multiple steps – and creates the final state particles. These kinds of models were used to study the dilepton spectrum of nucleon-nucleon collisions in connection with the DLS data (see Ref. [86]). However, a more or less satisfactory agreement between theory and experiment have been reached only with the HADES data and the new calculations in terms of effective field theory (EFT) models [89]. A similar EFT model has been recently applied to dilepton production in pion-nucleon collisions [91].

The spectrum of baryon resonances is known only up to slightly above 2 GeV, with increasing uncertainty at high masses. The resonance model cannot be applied to collisions above the SIS energy range not only because the baryon resonance spectrum is unknown, but also because multiparticle final states become more and more important. These are usually described in terms of string fragmentation models. The calculation of multiparticle production processes in EFT models is complicated by the multi-dimensional phase-space integrals, and many different Feynman diagrams contributing to the same final state. These diagrams have to be added coherently, which results in a large number of interference terms. One further problem is that EFT model calculations contradict the philosophy of transport, where (baryon and meson) resonances propagate as ordinary particles. This prohibits the implementation of certain types of interference terms that appear naturally in EFT models.

All these show that there must be a transition in the applied theoretical models just above the SIS energy range, with probably a pure EFT model for lower energies, supplemented by a string fragmentation model the importance of which is increasing with energy. It is clear that experimental input about elementary cross sections is needed in order to test and calibrate the theoretical models at this regime of transition. The NICA

fixed target experiment is an ideal possibility to provide these important experimental data.

Another reason why the energy range of the NICA fixed target experiment is interesting is ϕ meson production. ϕ, as a neutral vector meson is interesting because it decays directly to the dilepton channel and, therefore, its spectral function can be studied on the dilepton invariant mass spectrum. Furthermore, as a particle containing hidden strangeness, it decays dominantly to the kaon-antikaon channel. The simultaneous study of both decay channels can contribute to a deeper understanding of the underlining physics. In medium modification of antikaon mass can lead to a broadening of the ϕ. At low energy heavy ion reactions, collision of secondary particles plays an important role in the production of ϕ mesons (see [92]), therefore it's sensitive to the reaction dynamics, the EOS etc.

The energy at SIS was not high enough to study the ϕ meson in detail. In particular, it was not seen in the dilepton channel. Only a few measurements have been performed at SIS to study ϕ production via the K^+K^- channel in subthreshold heavy ion collisions [94]. These results by the FOPI collaboration indicate a large ϕ production cross section, which is not explained by the transport calculations of Ref. [92]. The NICA fixed target experiment would be able to study the ϕ meson in both decay channels and, therefore, could contribute to a better understanding of ϕ production around the kinematical threshold.

Bibliography

[1] E. V. Shuryak, Phys. Lett. **B 78,** 150 (1978).

[2] G. Agakachiev *et al.* (CERES Collaboration), Phys. Rev. Lett. **75,** 1272 (1995).

[3] R. Arnaldi *et al.* (NA60 Collaboration), Phys. Rev. Lett. **96,** 162302 (2006); Phys. Rev. **96,** 162302 (2006); Nucl. Phys. **A 774,** 715 (2006).

[4] R. Rapp, J. Wambach and H. van Hees, [arXiv:0901.3289.]

[5] Itzhak Tserruya, [arXiv:0903.0415].

[6] R. Rapp and J. Wambach, Adv. Nucl. Phys. **25**, 1 (2000).

[7] R. Rapp, G. Chanfray and J. Wambach, Phys. Rev. Lett. **76,** 368 (1996).

[8] G.E. Brown and M. Rho, Phys. Rev. Lett. **66,** 2720 (1991).

[9] M. Harada and K. Yamawaki, Phys. Rep. **381,** 1 (2003).

[10] V. V. Skokov and V. D. Toneev, Phys. Rev. **C 73,** 021902 (2006).

[11] N. S. Amelin, K. K. Gudima, S. Y. Sivoklokov and V. D. Toneev, Sov. J. Nucl. Phys. **52**, 172 (1990).

[12] N. S. Amelin, E. F. Staubo, L. P. Csernai, V. D. Toneev and K. K. Gudima, Phys. Rev. **C 44,** 1541 (1991).

[13] V. D. Toneev, N. S. Amelin, K. K. Gudima and S. Yu. Sivoklokov, Nucl. Phys. **A 519,** 463 (1990).

[14] Kh. U. Abraamyan *et al.*, Phys. Rev. **C 80,** 034001 (2009) [arXiv: 0806.2790].

[15] A. N. Sysakian, A. S. Sorin, M. K. Suleymanov, V. D. Toneev and G. M. Zinovjev [arXiv:nucl-ex/0601034]; *Proceedings of the 8th International Workshop "Relativistic Nuclear Physics: From hundreds MeV to TeV"*, (Dubna, 2006), p.306 [arXiv: nucl-ex/0511018].

[16] Kh. U. Abraamyan *et al.*, Phys. Lett. **B 323,** 1 (1994); Phys. Atom. Nucl. **59**, 252 (1996); **60**, 2014 (1997); **60**, 1843 (1997); **68**, 982 (2005).

[17] T. Matsui and H. Satz, plb 178, 416 (1986).

[18] M. C. Abreu *et al.* (NA38 Collaboration), Phys. Lett. **B 466,** 408 (1999).

[19] B. Alessandro *et al.* (NA50 Collaboration), Eur. Phys. J. **C 35,** 335 (2005).

[20] M. C. Abreu *et al.* (NA50 Collaboration), Phys. Lett. **B 477,** 28 (2000).

[21] R. Arnaldi *et al.* (NA60 Collaboration), Phys. Rev. Lett. **99,** 132302 (2007).

[22] A. Adare *et al.* (PHENIX Collaboration), Phys. Rev. Lett. **98,** 232301 (2007).

[23] L. Kluberg, Eur. Phys. J. **C 43,** 145 (2005).

[24] B. Alessandro et *al.* (NA50 Collaboration), Eur. Phys. J. **C 33,** 31 (2004).

[25] P. Cortese *et al.* (NA50 Collaboration), Nucl. Phys. **A 715,** 679 (2003).

[26] M. C. Abreu *et al.* (NA50 Collaboration), Phys. Lett. **B 553,** 167 (2003).

[27] E. Scomparin, R. Arnaldi (NA60 Collaboration), *Quark Matter 2009*, (Knoxvill, TN, USA, March 30-April 4), 2009.

[28] M. J. Leitch, J. Phys. G. **34,** S453 (2007).

[29] M. E. Peskin, Nucl. Phys. **B 156,** 365 (1979); G. Bhanot and M. E. Peskin, Nucl. Phys. **B 156,** 391 (1979).

[30] D. Kharzeev and H. Satz, Phys. Lett. **B 334,** 155 (1994).

[31] D. Kharzeev and H. Satz, Phys. Lett. **B 356,** 365 (1995).

[32] K. Martins, D. Blaschke and E. Quack, Phys. Rev. **C 51,** 2723 (1995).

[33] S. Matinyan and B. Müller, Phys. Rev. **C 58,** 2994 (1998) [nucl-th/9806027].

[34] R. Vogt, Phys. Rep. **310,** 197 (1999).

[35] C. Gerschel and J. Hufner, Annu. Rev. Nucl. Part. Sci. **49**, 225 (1999).

[36] P. Cortese *et al.* (NA50 Collaboration), J. Phys. G. **31,** S809 (2005).

[37] C. Y. Wong and H. W. Crater, Phys. Rev. **D 75,** 034505 (2007).

[38] F. Karsch, D. Kharzeev, and H. Satz, Phys. Lett. **B 637,** 75 (2006).

[39] A. Capella, E. J. Feireiro and A. B. Kaidalov, Phys. Rev. Lett. **85,** 2080 (2000).

[40] E. L. Bratkovskaya, W. Cassing, and H. Stoecker, Phys. Rev. **C 67,** 054905 (2003).

[41] J. P. Blaizot, P. M. Dinh and J. Y. Ollitrault, Phys. Rev. Lett. **85,** 4010 (2000).

[42] J. Hüfner and P. Zhuang, Phys. Lett. **B 559,** 193 (2003).

[43] J. F. Owens Rev. Mod. Phys.**59**, 465 (1987).

[44] W. Vogelsang *et al.*, J. Phys. G: Nucl. Part. Phys. **23**, A1 (1997).

[45] M. M.Aggarwal *et al.*, [nucl-ex /0006007].

[46] P. V. Chlapnikov *et al.*, Phys. Lett. **B 141,** 276 (1984).

[47] M. N. Ukhanov *et al.*, IHEP preprint 86-195, Protvino, (1986).

[48] S. Banerjee *et al.*, Phys. Lett. **B 305,** 182 (1993); A.Belogianni *et al.*, Phys. Lett. **B 408,** 487 (1997).

[49] F. Botterwerk *et al.*, Z. Phys. **C51**, 541 (1991).

[50] P. Lichard and L. Van Hove, Phys. Lett. **B 245,** 605 (1990).

[51] E. V. Shuryak, Phys. Lett. **B 231,** 175 (1989).

[52] M. K. Volkov, E. A. Kuraev, D. Blaschke, G. Röpke, S. M. Schmidt, Phys. Lett. **B 424,** 235 (1998).

[53] S. Barshay, Phys. Lett. **B 227,** 279 (1989).

[54] J. Abdallah (DELPHI Collaboration), Eur. Phys. J. **C 47,** 273 (2006); **57**, 499 (2008).

[55] M. K. Volkov, E. S. Kokoulina, E. A. Kuraev, Ukr. Jour. of Physics. 48, 1252 (2003).

[56] E. S. Kokoulina and V. A. Nikitin, *The International School-Seminar The Actual Problems of Microworld Physics*, (Gomel, Belarus), Dubna, 1 (2004) 221;

[57] E. S. Kokoulina and V. A. Nikitin, *Proceedings of Baldin Seminar on HEP Problems "Relativistic Nuclear Physics and Quantum Chromodynamics"*, (JINR, Dubna, Russia), 319 (2005).

[58] P. F. Ermolov *et al.*, *Proc. of Baldin Seminar on HEP Problems "Relativistic Nuclear Physics and Quantum Chromodynamics"*, (JINR, Dubna, Russia), 327 (2005).

[59] V. V. Avdeichikov *et al.*, *Proposal "Termalization"* (in Russian), JINR-P1-2004-190 (2005).

[60] E. Kokoulina, Acta. Phys. Polon. **B 35,** 295 (2004).

[61] E. Kokoulina and A. Kutov, Phys. Atom. Nucl. 71, 1543 (2008).

[62] E. S. Kokoulina *et al.*, Nucl. Phys. (Rus.) 72, 189 (2009).

[63] *SVD Collaboration, Preprint IHEP*, 2011-4.

[64] V.A. Nikitin, *Nonlinear Phenomena in Complex Systems*, 12, 202 (2010); http://theor.jinr.ru/twiki-cgi/view/NICA/WebHome.

[65] J. Cleymans and K. Redlich, Phys. Rev. **C 60,** 054908 (1999).

[66] F. Becattini, J. Manninen and M. Gazdzicki, Phys. Rev. **C 73,** 044905 (2006).

[67] *SVD Collaboration, Preprint IHEP*, 2011-5.

[68] D. D. Dijulio, V. Avdeichikov *et al.*, NIM, **A612**, 127 (2009).

[69] B. Friman, C. Höhne, J. Knoll, S. Leupold, *et al.* (eds.), The CBM Physics Book, vol. 814 of Lecture Notes in Physics, Springer-Verlag, Berlin, Heidelberg (2011).

[70] F. Karsch, Lect. Notes Phys. **583**, 209 (2002).

[71] U. G. Meissner, Phys. Rept. **161**, 213 (1988).

[72] L. D. McLerran, T. Toimela, Phys. Rev. **D 31**, 545 (1985).

[73] C. Gale, J. I. Kapusta, Nucl. Phys. **B 357**, 65 (1991).

[74] R. Rapp, J. Wambach, Eur. Phys. J. **A 6**, 415 (1999).

[75] E. Braaten, R. D. Pisarski, T.-C. Yuan, Phys. Rev. Lett. **64**, 2242 (1990).

[76] S. Damjanovic, *et al.*, Nucl. Phys.**A 783**, 327 (2007).

[77] R. Arnaldi, *et al.*, Phys. Rev. Lett. **100**, 022302 (2008).

[78] R. Arnaldi, *et al.*, Eur. Phys. J. **C 59**, 607 (2009).

[79] R. Arnaldi, *et al.*, Eur. Phys. J. **C 61**, 711 (2009).

[80] D. Adamova, G. Agakichiev, D. Antonczyk, H. Appelshäuser, *et al.*, Phys. Lett. **B 666**, 425 (2008).

[81] H. van Hees, R. Rapp, Phys. Rev. Lett. **97**, 102301 (2006).

[82] H. van Hees, R. Rapp, Nucl. Phys. **A 806**, 339 (2008).

[83] G. Agakishiev, et al., Phys. Lett. **B 422**, 405 (1998).

[84] S. Turbide, R. Rapp, C. Gale, Phys. Rev. **C 69**, 014903 (2004).

[85] F.-M. Liu, K. Werner, Phys. Rev. Lett. **106**, 242301 (2011).

[86] E.L. Bratkovskaya, W. Cassing, M. Effenberger, and U. Mosel, Nucl. Phys. **A 653**, 301 (1999).

[87] C. Ernst, S.A. Bass, M. Belkacem, H. Stöcker, and W. Greiner, Phys. Rev. **C 58**, 447 (1998);

[88] M. Zétényi and Gy. Wolf, Phys. Rev. **C 67**, 044002 (2003).

[89] R. Shyam and U. Mosel, Phys. Rev. **C 67**, 065202 (2003); **82**, 062201 (2010).

[90] L.P. Kaptari and B. Kämpfer, Phys. Rev. **C 80**, 064003 (2009).

[91] M. Zétényi, Gy. Wolf, Phys. Rev. **C 86**, 065209 (2012).

[92] W.S. Chung, G.Q. Li, and C.M. Ko, Nucl. Phys. **A 625** 347 (1997).

[93] H. W. Barz, M. Zétényi, G. Wolf, and B. Kämpfer, Nucl. Phys. **A 705**, 223 (2002).

[94] N. Herrmann, (FOPI Collaboration), Nucl. Phys. **A 610**, 49 (1996).

[95] R. Kotte, (FOPI Collaboration), in: M. Buballa *et al. (Eds.), Proc. Int. Workshop XXVIII on Gross Properties of Nuclei and Nuclear Excitations, Hadrons in Dense Matter*, (Hirschegg, Austria, January 16-22, 2000), p. 112.

8 Local $\mathcal{P}$ and $\mathcal{CP}$ violation in hot QCD matter

The existence of topological solutions is a very important property of QCD. Topological solutions arise due to the non-Abelian nature of this theory, and lead to a number of important consequences for the properties of the vacuum and hadrons. In hot hadronic matter, the topological fluctuations near the critical temperature can create the space-time domains with locally broken $\mathcal{P}$ and $\mathcal{CP}$ invariances. The local violation of parity can manifest itself in heavy ion collisions through the separation of positive and negative hadrons with respect to the reaction plane; this charge separation would induce an electric dipole moment of the produced hot quark-gluon matter. The charge separation stems from the interplay of strong magnetic field (and/or the angular momentum) in the early stage of the heavy ion collision and the presence of topological configurations in hot matter ("the chiral magnetic effect"). Recent result from RHIC [8] provides an experimental evidence for this phenomenon in heavy ion collisions. This effect should be enhanced in the deconfined quark-gluon plasma phase because it requires the separation of quarks over a large ("macroscopic" on the scale of hot matter size) distance. As discussed in this section, there are reasons to expect that the asymmetry will have a peak at some energy, possibly within the energy range of the NICA collider. It should be emphasized that at high baryon density one can also expect the phenomenon of spontaneous parity violation with a number of unique signatures. The high-energy and low-energy scans at RHIC and the dedicated programs at NICA and FAIR would thus provide a necessary and complementary to each other experimental information.

8.1 Topologically induced local $\mathcal{P}$ and $\mathcal{CP}$ violation in hot QCD matter

D. Kharzeev

Physics Department, Brookhaven National Laboratory, Upton, NY, USA

It has been established experimentally that there is no global violation of $\mathcal{P}$ and $\mathcal{CP}$ invariances in QCD. However, the issue of $\mathcal{P}$ and $\mathcal{CP}$ symmetries in QCD is highly nontrivial because of the existence of topological solutions and the presence of axial anomaly in this theory ("the strong $\mathcal{CP}$ problem"). Even in the absence of global $\mathcal{P}$ and $\mathcal{CP}$ violation, topological fluctuations in QCD vacuum are believed to play an important role in the chiral symmetry breaking, thus being responsible for many properties of hadrons. In hot hadronic matter, the topological fluctuations near the critical temperature can create the bubbles with locally broken $\mathcal{P}$ and $\mathcal{CP}$ invariances [1, 2].

It was suggested in [7] that the local violation of parity can manifest itself in heavy ion collisions at RHIC through the separation of positive and negative hadrons with respect to the reaction plane; this charge separation would induce an electric dipole moment of the produced hot quark-gluon matter. The charge separation stems from the interplay of strong magnetic field (and/or the angular momentum) in the early stage of the heavy ion collision and the presence of topological configurations in hot matter ("the chiral magnetic effect") [5, 6, 8]. The gradients of the topological charge distribution at the boundaries of the domain induce an electric charge [5], and the variation of topological charge with time induces an electric current [6, 8]. Therefore in the presence of very intense magnetic fields, topological fluctuations in hot QCD matter can be observed directly through the spatial separation of positive and negative electric charge signaling a **local** violation of $\mathcal{P}$ and $\mathcal{CP}$ symmetries.

The experimental observable that is sensitive to the local violation $\mathcal{P}$ and $\mathcal{CP}$ invariances has been proposed in [7]. Because the sign of the electric dipole moment is expected to fluctuate from event to event, and one needs to sum over many events to acquire the necessary statistics, the observable is $\mathcal{P}$-even but largely insensitive to the statistical fluctuations [7]. Recent result from RHIC [8] provides an experimental evidence for this phenomenon in heavy ion collisions. This effect should be enhanced in the deconfined quark-gluon plasma phase because it is requires the separation of quarks over a large ("macroscopic" on the scale of hot matter size) distance.

The energy dependence of the local $\mathcal{P}$ and $\mathcal{CP}$ violation is driven by two factors:

- the energy density of the produced hadronic matter and
- the strength and variation with time of the produced magnetic field.

While the initial value of the magnetic field at the time of collision of course increases with energy, the produced field falls off faster at higher energies [8] reflecting a faster separation of the charged spectators and particles produced in the collision. As a result, one expects an increase of the charge asymmetries towards lower energies. On the other hand, at some threshold collision energy the deconfined matter will no longer be produced, and

so the asymmetry should significantly decrease in magnitude. It would be extremely important to explore this behavior in low-energy heavy ion collisions. The low-energy scan at RHIC and the dedicated programs at NICA and FAIR would thus provide a necessary and complementary to each other experimental information.

8.2 Magnetic effects in QCD vacuum: lattice view

P.V. Buividovich[a,b], M.N. Chernodub[b], E.V. Luschevskaya[b] and M.I. Polikarpov[c]

[a] *JIPNR, Minsk, Belarus;*
[b] *ITEP, Moscow, Russia;*
[c] *CNRS, Tours, France*

Chiral magnetic effect

Generation of electric current along the direction of magnetic field takes place on local fluctuations of chirality (= difference between densities of left-handed and right-handed quarks). Can be observed in $\mathcal{CP}$-even quantities only! Observables which can be calculated on the lattice: $\langle j_\mu j_\nu \rangle$, $\sigma^2_{\mu\nu}$, ... Lattice results for quenched vacuum and overlap Dirac fermions:

- Confinement phase: the current along the magnetic field $\langle j^2_\parallel \rangle$ is enhanced with respect to the perpendicular component $\langle j^2_\perp \rangle$ when the magnetic field grows (see Fig. 8.1)
- Deconfinement phase: the current along the magnetic field $\langle j^2_\parallel \rangle$ stays constant, while the perpendicular component $\langle j^2_\perp \rangle$ is suppressed (see Fig. 8.1)

This current can be observed as enhanced emission of charged particles perpendicular to the reaction plane!

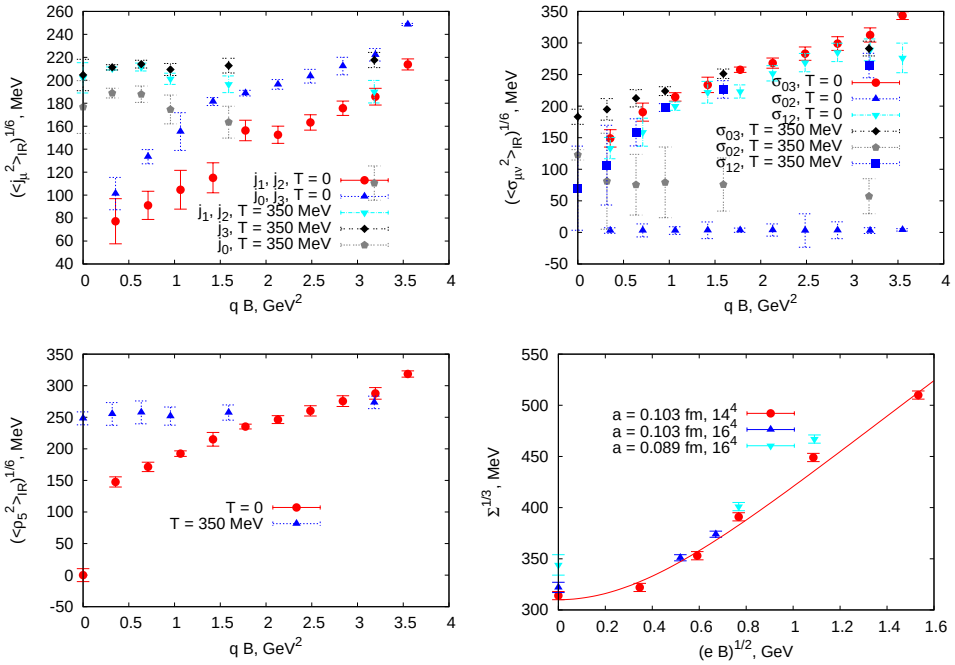

Figure 8.1: Upper panels: Induced fluctuations of electric current and electric dipole moment along and perpendicular to the magnetic field. Magnetic field is directed along the 3rd axis. Lower panels: The dependence of the induced fluctuations of chirality and of the chiral condensate on the magnetic field.

Generation of electric dipole moment (EDM) along the direction of magnetic field

An observable quantity is the square of different components of the EDM associated with spin: $\sigma_{\mu\nu} = i/2\,\bar{q}\,[\gamma_\mu, \gamma_\nu]\,q$. We see a strong enhancement of the fluctuations of moth magnetic moment and the EDM with magnetic field, which are almost equal. In contrast to current, EDM behaves similarly in both confinement and deconfinement phases (see upper panels of Fig. 8.1)

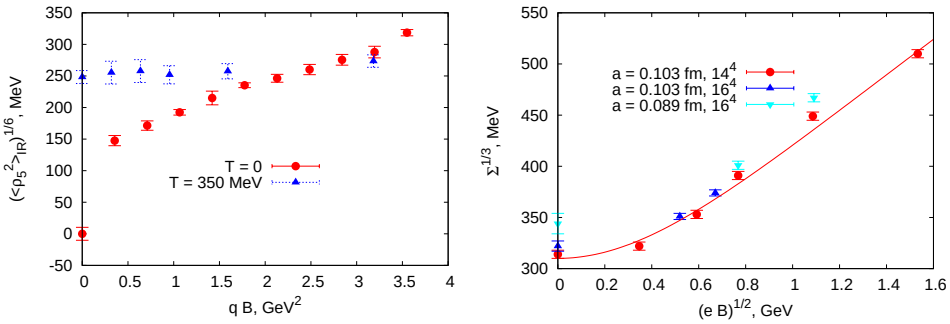

Figure 8.2: The dependence of the induced fluctuations of chirality and of the chiral condensate on the magnetic field. Magnetic field is directed along the 3rd axis.

Enhanced fluctuations of chirality

Magnetic field, as well as temperature, enhances the fluctuations of the difference of the densities ρ_5 of left and right quarks. This, in turn, enhances the chiral magnetic effect (see lower left panel of Fig. 8.2).

Enhancement of the chiral symmetry breaking.

The magnetic field stabilizes the chirally broken (low-temperature) phase of QCD enlarging the value of the chiral condensate and enhancing the chiral symmetry breaking (see lower panels of Fig. 8.2). According to the Gell-Mann-Oakes-Renner relation, the pion mass is proportional to the chiral condensate, which gives a possibility to measure this enhancement.

8.3 Rich physics of non-central heavy-ion collisions

S. Voloshin

Wayne State University, Detroit, Michigan, USA

The idea of the local strong parity violation (due to quark interaction with topologically non-trivial gluonic configuration: topology induced parity violation) has received a lot of developments in the recent years starting from paper [1, 2]. Originally it was noticed that such an effect can lead to difference in the reaction plane reconstructed from positive and negative particles [11], but no effect has been observed at that time. More recently it was noticed [5–8] that in the presence of the strong magnetic of non-central nuclear collision, it could result in the charge separation along the direction magnetic field (or the system angular momentum). The corresponding experimental techniques has been developed in [7] and first results from STAR Collaboration [12] indeed are consistent with theoretical expectations. The effects is expected to depend strongly on the existence of the deconfinement stage. Also, the charge separation depends linearly on the strength of magnetic field, more exactly on the time integral of the magnetic field. It is predicted that the latter is increasing at lower energies. Combined with effect of deconfinement it could lead to a threshold behavior. In this sense the study of the local strong parity violation at NICA become extremely important. At this point I would also mention, that if observed, for the further study of the effect one might need good particle identification and also possibility to collide different nuclei, in particular isobaric nuclei.

The most interesting measurements of the anisotropic flow from my point of view would be

- elliptic flow of charge particles and possible observation of the wiggle in v_2 behavior, in particular in the region of possible deconfinement transition [13–16],
- checking constituent quark number scaling in elliptic flow of identified particles [15, 17], again as an indicator of deconfinement, and
- directed flow of identified particles which is sensitive to the dynamics of baryon stopping and system expansion [18].

Femtoscopy of the system asymmetries, first proposed in [19] and for non-identical particles in [20] (for a review, see [21]), obviously would be necessary to understand the entire picture of the system evolution.

Finally, I mention on interesting possibility of the system global polarization (transfer of the orbital angular momentum into particle spin) [5,23]. Although at RHIC energies it was found to be consistent with zero within experimental uncertainties [24] it will be exciting to repeat these measurements at lower energies

8.4 Spontaneous $\mathcal{P}$-violation in dense matter accessible with NICA

A. Andrianov[a], V. Andrianov[a] and D. Espriu[b]

[a] *St.Petersburg State University, Russia;*
[b] *University of Barcelona, Spain*

Parity violation in QCD can take place spontaneously under extreme conditions due to condensation of neutral pseudoscalar matter. Its detection would constitute an important breakthrough for the understanding of strong interactions at high density and a considerable achievement for heavy-ion experiments. It is conjectured [25] that such a parity breaking phase may be present for densities ranging from 3 to 10 times the normal nuclear density ρ_0 and moderate temperatures. This is sketched in Fig. 8.3

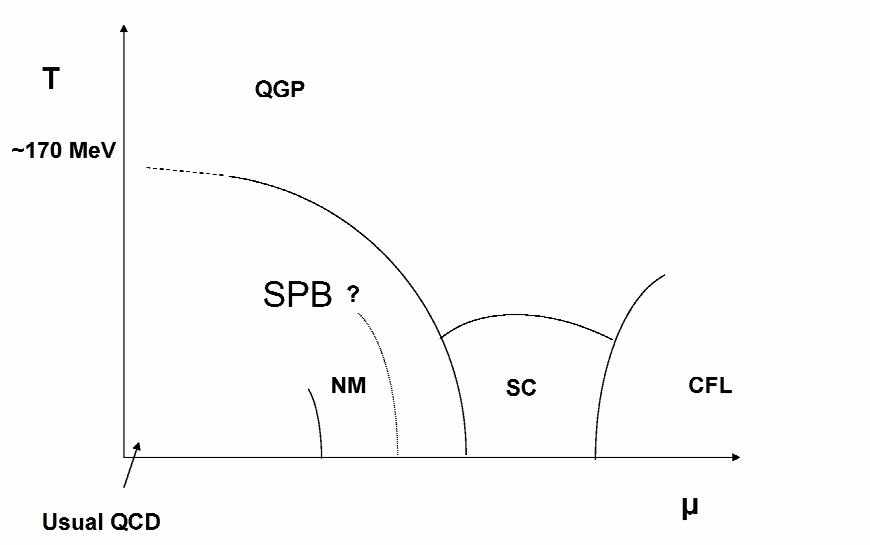

Figure 8.3: Tentative location of the hypothetical parity breaking phase in QCD.

The possibility of spontaneous parity breaking (SPB) may be accessible in the range of nuclear densities where the hadron phase persists and quark percolation does not occur yet (see Fig. 8.4). Since, as it is known, pion condensation is believed to be impossible in models with only one scalar/pseudoscalar isomultiplet, it will be necessary to include the two lowest lying, scalar/pseudoscalar resonances in each channel. While this is not the most general model, it contains the sufficient ingredients for spontaneous parity breaking.

The "pion" condensate may arise as a relative complex phase factor between the two scalar condensates. We arrive at the conclusion that such an effect takes place by using an effective Lagrangian for low-energy QCD that retains the two lowest lying states in the scalar and pseudoscalar sectors. We include [26] a chemical potential for the quarks that corresponds to a finite density of baryons, implement the bound state of normal nuclear matter and investigate the pattern of symmetry violation in its presence. In general this phase is bound by a divide line and it extends across a range of chemical potentials that correspond to nuclear densities where more exotic phenomena such as CFL or CS may occur.

Within this model the expectation values of the two scalar condensates $\langle\sigma_1\rangle$ and $\langle\sigma_2\rangle$ and of the pseudoscalar one $\rho = \langle\Pi\rangle$ has the following qualitative behaviour as the chemical potential is increased.

The mass spectrum differs considerably from the familiar one as seen in Fig. 8.5. At the phase transition point where spontaneous parity breaking occurs three massless states (Goldstone bosons) appear. Throughout the parity breaking phase two charged states remain massless while the third Goldstone boson is light, but not massless.

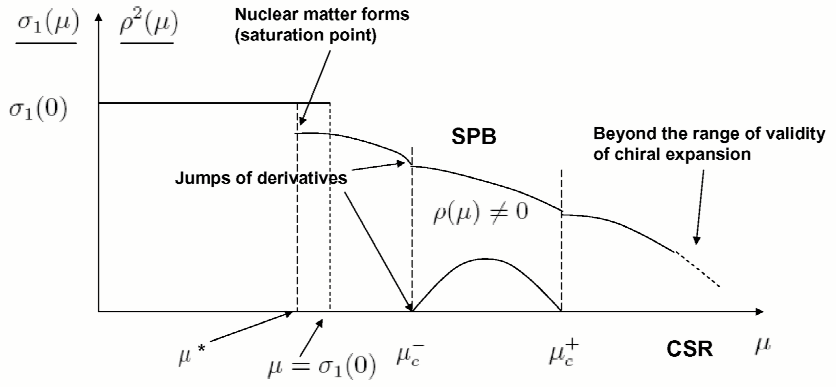

Figure 8.4: The figure shows the dependence of the various expectation values on μ. Notice the *only partial* restoration of chiral symmetry at the saturation point, a considerable achievement of this model

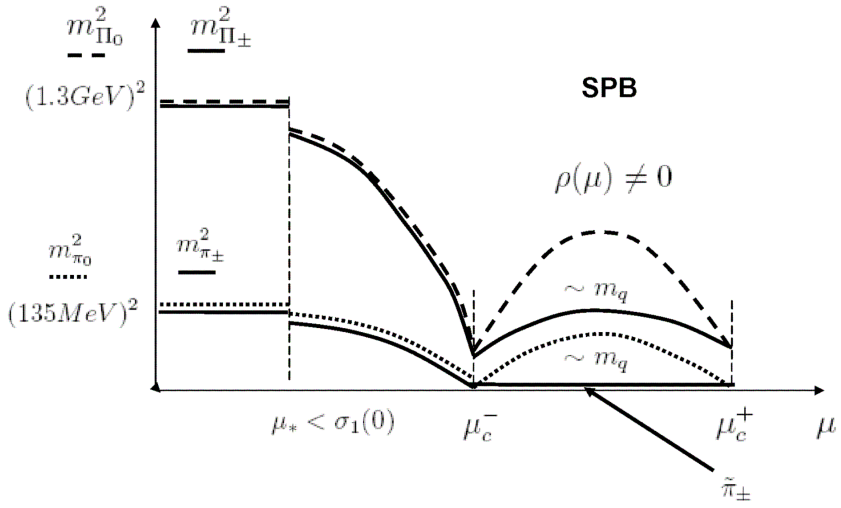

Figure 8.5: The lines indicate the evolution of the usual pion and the heavy pion (1300) multiplets as the chemical potential evolves

A salient characteristics of this phase would be the spontaneous violation of the vector isospin symmetry $SU(2)_V$ down to $U(1)$ as is made evident by the generation two additional massless charged pseudoscalar mesons. The latter cause substantial changes in the nuclear equation of state. The signature of the spontaneous parity breaking is a strong mixing between scalar and pseudoscalar states that translate spontaneous parity violation into meson decays. The mass eigenstates will decay both in odd and even number of pions simultaneously. Isospin violation can also be visible in decay constants.

While parity violation in QCD would lead to striking consequences [25, 26], detecting the changes of characteristics such as the same in-medium resonance being able to decay into even and odd number of pions, isospin violation and the like may be very difficult because the observation of in-medium particle properties is a difficult task. More signatures are wanted which could be detected outside the reaction region and would be suitable to discriminate the SPB phenomenon from other processes going on in ordinary nuclear matter.

Let us focus on central collisions. Then one can expect a pion condensate (if any) $\langle \Pi \rangle$ arising in a rather space-homogeneous configuration but essentially depending on the collision time $\langle \dot{\Pi} \rangle \equiv \eta \neq 0$ (first increasing then decreasing). Then a remarkable phenomenon shows up [27], namely, due to the presence of parity odd interaction, the term $\Pi \, F_{\mu\nu} \, \widetilde{F}^{\mu\nu}$ appears in the Lagrangian relevant for this situation. This term describes the

neutral pion decay into two photons. And in the presence of pion condensation it distorts the photon spectrum via a modification of Maxwell Electrodynamics with a Chern-Simons interaction $\eta\vec{A}\cdot\vec{B}$. As a consequence, the two transversal, circularly polarized, photons obtain different effective masses. When $\eta > 0$ one of them becomes massive $m^2_{\gamma,+} = \eta|\vec{k}|$ with a mass growing with photon momentum $\vec{k}$ and another one appears as a tachyon with negative mass squared $m^2_{\gamma,-} = -\eta|\vec{k}|$. For the opposite sign of the condensate time derivative $\langle\dot{\Pi}\rangle$ the polarizations are interchanged.

As a result, photons with momenta $|\mathbf{k}| > \frac{4m_l^2}{\eta}$ start to decay into lepton pairs $\gamma \to l^+l^-$. A hierarchy of thresholds appear for different leptons (mostly electrons and muons). An additional feature of his type of decay is the creation of dileptons in a rather narrow cone when $\eta \ll m_l$. The decay width $\sim \alpha\ \eta$ is suppressed by the fine structure constant α but may be considerably enhanced if the pion condensate derivative η rapidly increases. If parity breaking occurs spontaneously as a second order phase transition then at the very critical line indeed η increases unboundly, see the Fig. 8.6.

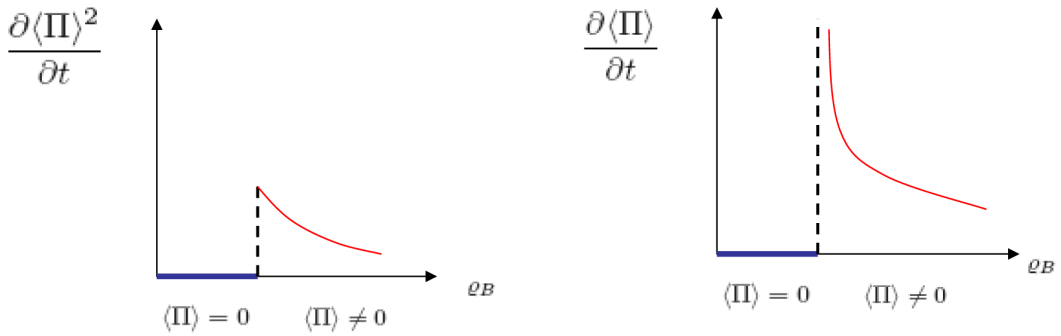

Figure 8.6: The figure shows the evolution of the time derivative of the pseudoscalar condensate $\langle\Pi\rangle$ in the vicinity of the critical density.

However for finite nuclei one should not expect a divergence, but a large enhancement. The decay width will also become large enough to produce abnormal excess of dileptons in spite of being an electromagnetic process.

A still open question is to what extent the $\mathcal{P}$-breaking phase can last with increasing temperatures. It is conceivable that the $\mathcal{P}$-breaking divide line points out directly to the QCD tricritical point. Thus the experimental studies with the NICA facilities of the QCD tricritical point may well detect a more complicated phase structure due to the interplay with the parity violation phase.

8.5 On $\mathcal{CP}$ violation in heavy-ion collisions at the NICA energy

V. Skokov and V. Toneev

Gesellschaft für Schwerionenforschung mbH, Darmstadt, Germany;
Joint Institute for Nuclear Research, Dubna, Russia

In QCD, chiral symmetry breaking is due non-trivial topological effect. Topological transitions have never been observed directly (*e.g.* at the level of quarks in DIS). The best evidence of this physics would be event-by-event strong parity violation.

One of the most exciting signals of the deconfinement and the chiral phase transitions in heavy-ion collisions, chiral magnetic effect, suggested in [8], predicts an observable effect of preferential emission of charged particles along the direction of angular momentum in the case of non-central heavy-ion collisions due to presence of a non-zero chirality. As it was stressed in [6, 8] both deconfinement and chiral phase transitions are essential requirements for chiral magnetic effect to take place. The first one is needed, since only in this case soft quarks can separate over distances greater than the radius of nucleon. The second is also required [6,8], since non-zero values of chiral condensate drives asymmetry between the number of right- and left-handed quarks to zero. Here we compare these conditions at the RHIC and NICA energies.

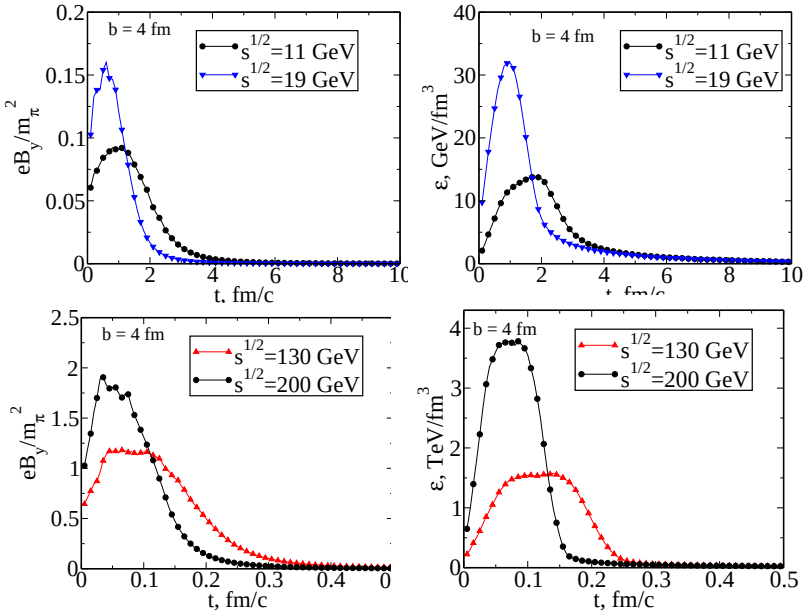

Figure 8.7: Upper panels: The time evolution of the magnetic field strength eB_y (left) and energy density (right) at the central point. The UrQMD calculations are carried out for Au + Au collisions with impact parameter, $b = 4$ fm for $\sqrt{s_{\rm NN}} = 11$, 19 GeV. The symbols are plotted with the step $\delta t = 0.2$ fm/c. Lower panels: the same upper panels for $\sqrt{s_{\rm NN}} = 130$ and 200 GeV, with the time step $\delta t = 0.01$ fm/c.

We focus our calculations [9] on the magnetic field in the central point O of the created fireball (symmetric with respect to the reaction plane $x - z$ in the transverse $x - y$ plane) and energy density of nuclear matter in the Lorentz-contracted box with 2 fm site-length centered around O. Nuclei are colliding along z-axis.

The magnetic field strength at a position $\vec{x}$ and time t is defined by the Lienard-Wiechert potentials

$$e\vec{B}(t,\vec{x}) = \alpha_{\rm EM} \sum_n Z_n \frac{1 - v_n^2}{\left(R_n - \vec{R}_n \vec{v}_n\right)^3} \left[\vec{v}_n \times \vec{R}_n\right], \tag{8.1}$$

where the fine-structure constant $\alpha_{\rm EM} \approx 1/137$, Z_n is the electric charge of the nth particle (in units of the electron charge), $\vec{R_n} = \vec{x} - \vec{x}_n$ is a radius vector of particle, $\vec{v}_n$ is particle velocity. The quantities $\vec{v}_n$ and $\vec{x}_n$ are taken at the time moment t' defined implicitly by the following equation

$$|\vec{x} - \vec{x}_n(t')| + t' = t. \tag{8.2}$$

Summation is to be done over all charged particles.

On the basis of the expression (8.1) one can draw several conclusion for the main properties of the magnetic field at the origin O. First of all, from symmetry reasons it is evident that the magnetic field will be negligible for collision with small impact parameter. From the same symmetry considerations one obtains that the field will have only non-zero B_y-component. Second, the field will be negligible for low collision energies, because the field strength is proportional to the particle velocity. On the other hand for very high, ultrarelativistic energies of the collision the contribution to the magnetic field is feasible only for for particles close to transverse plane $\left(R_n - \vec{R}_n \vec{v}_n\right) \sim 0$. The contribution from particles away from transverse plane is suppressed by factor of $(1 - v^2)$.

In the left panels of Fig. 8.7 , the time evolution of the magnetic field strength is shown for RHIC and NICA energies. The magnetic field is created in non-central Au + Au collision with impact parameter $b = 4$ fm. The resulting field strength is averaged over 100 events to reduce statistical fluctuations. It is clear, however, that magnetic field fluctuation in a single event can be significant for an observable effect.

The key quantity of these effects is a value of a background magnetic field strength created in heavy-ion collisions. The results obtained within the UrQMD very close to the early estimate [8] where it was shown that

the field may reach very high values $eB \sim 3 \cdot m_\pi^2 \sim 3 \times 10^{18}$ Gauss (Note we measure the magnetic field strength in units of squared pion mass, using for definiteness $m_\pi = 140$ MeV. However the magnetic field strength can be translated into cgs system by the following identity $m_\pi^2 = 140^2 \times 0.512 \cdot 10^{14}$ Gauss $\approx 10^{18}$ Gauss).

The large value of the magnetic field strength itself does not guarantee possible observable effects, but additional requirements are needed, *e.g.* for chiral magnetic effect the system should be in deconfinement and chiral restored phase. To demonstrate that matter in central region is, presumably, in QGP phase we calculated the energy density. It is done in the center region of created fireball. The calculated time evolution of energy density in the center region is shown in the right panels of Fig. 8.7. Even for bombarding energy $\sqrt{s_{\rm NN}} = 11$ GeV and impact parameter $b = 4$ fm the energy density in the central region is sufficient to reach QGP phase. However, the question whether the system is in local equilibrium and can it be described by temperature and chemical potential(s) is still open.

Values of magnetic field strength and energy density play an important role in estimations of possible observable effects of deconfinement and chiral phase transition in heavy-ion collisions. Going down from the RHIC to NICA top energy in Au + Au collision at $b = 4$ fm, the magnetic field strength B_y decreases approximately by 17 times which is not too small as would naively expect. However, as compared to RHIC, the peak energy density ϵ, being above the deconfinement transition one, decreases by a factor of ~ 250. This reduces substantially the possibility of appearance of non-zero winding number configurations at the NICA energies. In both limiting energy regions the deconfined state defined as $\varepsilon \gtrsim 1$ GeV/fm^3 is inside the range of the maximal magnetic field strength but at the NICA energy the system stays there longer by a factor of $\sim$20 as compared to the RHIC one. Thus, taking into account theoretical uncertainties, it is still not excluded that a small effect of the charge separation can be observed at the top NICA energy [10].

8.6 Vorticity and neutron asymmetries at NICA

M. Baznat[a,b], K. Gudima[a,b], O. Rogachevsky[b,c], A. Sorin[b,d] and O. Teryaev[b,d]

[a] *Institute of Applied Physics, Academy of Sciences of Moldova, MD-2028 Kishinev, Moldova;*
[b] *JINR Dubna, Dubna, Russia;*
[c] *PNPI RAS, Leningrad district, Russia;*
[d] *Dubna International University, Dubna (Moscow region), Russia*

We study the possibility of testing experimentally signatures of P-odd effects related with the vorticity and hydrodynamoc helicity of the medium. The studies of helicity and vorticity in the framework of kinetic Quark-Gluon String Model for the kinematics of NICA is performed. The Chiral Vortical Effect is generalized to the case of conserved charges different from the electric one. In the case of baryonic charge and chemical potential such effect should manifest itself in neutron asymmetries at the NICA accelerator complex measured by the MPD detector. The required accuracy may be achieved in a few months of accelerator running. We also discuss polarization of the hyperons and P-odd correlations of particle momenta (handedness) as probes of vorticity.

The local violation [6] of discrete symmetries in strongly interacting QCD matter is now under intensive theoretical and experimental investigations. The renowned Chiral Magnetic Effect (CME) uses the (C)P-violating (electro)magnetic field emerging in heavy ion collisions in order to probe the (C)P-odd effects in QCD matter.

There is an interesting counterpart of this effect, Chiral Vortical Effect (CVE) [28, 29] due to coupling to P-odd medium vorticity. In its original form [28] this effect leads to the appearance of the same electromagnetic current as CME. Here we suggest a straightforward generalization of CVE resulting in generation of all conserved-charge currents. In particular, we address the case of the *baryonic* charge and the corresponding asymmetries of baryons, especially neutrons (not affected by CME), which can be measured by the MultiPurpose Detector (MPD) [30] at the Nuclotron-based Ion Collider fAcility (NICA) [31] at the Joint Institute for Nuclear Research (JINR).

Chiral Magnetic and Vortical effects

The basic point in the emergence of CME is the coupling of the topological QCD field θ to the electromagnetic field A_α controlled by the triangle axial-anomaly diagram. Similar interaction of θ with the velocity field V_α exists in relativistic hydrodynamics due to the new coupling

$$e_j A_\alpha J^\alpha \Rightarrow \mu_j V_\alpha J^\alpha \tag{8.3}$$

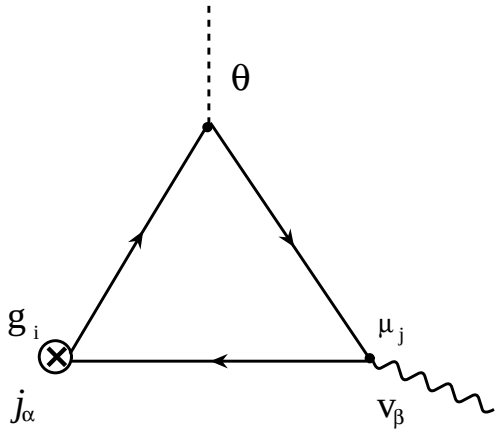

Figure 8.8: The generation of the current of the conserved charge g_i by the chemical potential μ_j.

involving the chemical potentials μ_j (for various flavours j) and the current J^α. It provides also the complementary description [32] of the recently found contribution of fluid vorticity to the anomalous non-conserved current [33]. Note that the similarity between the effects of the magnetic field and the rotation mentioned in [28] is very natural as the rotation is related by the Equivalence Principle to the so called *gravitomagnetic* field (see e.g. [34] and references therein).

CVE leads to similar (to CME) contribution to the electromagnetic current:

$$J_e^\gamma = \frac{N_c}{4\pi^2 N_f}\varepsilon^{\gamma\beta\alpha\rho}\partial_\alpha V_\rho \partial_\beta(\theta \sum_j e_j\mu_j) \ , \tag{8.4}$$

where N_c and N_f are the numbers of colours and flavours, respectively. If variation of the chemical potential is neglected, the charge induced by CVE for a given flavour can be obtained from that due to CME by substitution of the magnetic field with the curl of the velocity: $e_j\vec{H} \to \mu_j\vec{\nabla}\times\vec{V}$.

On one hand, CVE provides another source for the observed consequences of CME, relating with both light and strange [35] quarks (regarded as the heavy ones [36]). On the other hand (this is the basis of our following discussion), CVE leads also to the separation of charges different from the electric one. This becomes obvious if the current is calculated from the triangle diagram, where quark flavours j carry various charges $g_{i(j)}$ (see Fig. 8.8). The calculation may also be performed, following [28], by variation of the effective Lagrangian with respect to the external vector field. In that case this vector field can be not only the electromagnetic potential [28] (entering the Lagrangian describing the interaction with the real electromagnetic field) but also an arbitrary (auxiliary) field coupled to any conserved charge.

If variation of the chemical potential in Eq. (8.4) is neglected, the current of that charge g_i selecting the specific linear combination of quark triangle diagrams is related to electromagnetic one as follows (see Fig.1):

$$J_i^\nu = \frac{\sum_j g_{i(j)}\mu_j}{\sum_j e_j\mu_j}\ J_e^\nu \ . \tag{8.5}$$

In another extreme case of dominance of chemical potential gradients (assumed to be collinear) one get the relation

$$J_i^0 = \frac{|\vec{\nabla}\sum_j g_{i(j)}\mu_j|}{|\vec{\nabla}\sum_j e_j\mu_j|}\ J_e^0 \tag{8.6}$$

which might be useful e.g. for the mixed phase [42] description.

In particular, the large baryonic chemical potential (actually the largest one which is achievable in accelerator experiments [37]), appearing in the collisions at comparatively low energies at the FAIR and NICA (and possibly SPS and RHIC at low energy scan mode) facilities, may result in the separation of the baryonic charge. Of special interest are manifestations of this separation in *neutron* asymmetries with respect to the production

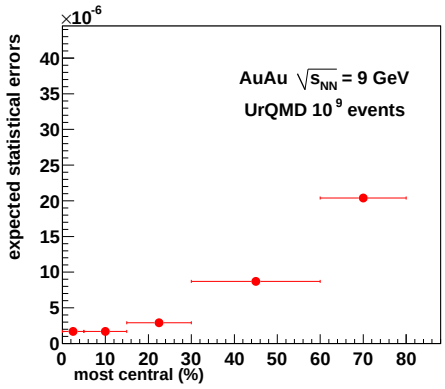

Figure 8.9: Estimation of statistical errors.

plane, as soon as the neutrons, from the theoretical side, are not affected by CME and, from the experimental side, there is a unique opportunity to study neutron production and asymmetries by MPD at NICA. Besides that, the noticeable strange chemical potential at the NICA energy range (see e.g. [38] and references therein) might result in the strangeness separation.

Experiments at NICA and neutron asymmetries

The numerical smallness of such expected vortaic effect makes it highly improbable to search it on an event-by-event basis. To collect statistics from different events one needs to construct a quadratic variable which does not depend on the varying sign of topological field fluctuations.

This problem was solved in the experimental studies of CME [39–41] by consideration of the angular asymmetries of *pairs* of particles with the same and opposite charges with respect to the reaction plane. Moreover, one can use three-particle correlations as well in order to avoid the necessity of fixing the reaction plane.

We suggest to use the similar correlations for baryonic charge. However, this method is not directly applicable in the case of baryon charge separation because of the very small number of produced antibaryons, in particular, antineutrons[14]. Nevertheless, the two-particle correlation for neutrons still might be used as one of the probes of CVE. In the case of three-particle correlations the third particle should not necessarily be the neutron and could also be a charged particle.

Note that the comparison of above-mentioned correlations for various particles could be very useful. Namely, CVE is negligible for pions, due to the rather small chemical potential, so that only CME contributes. On the other hand, for neutrons the correlations are entirely due to CVE, while for protons one should have both such effects. In case the correlations emerged due to other reasons than CVE and CME to quadratic order, then their simultaneous observation would be an important test of their actual existence.

For the studies of CVE we suggest the collider NICA[15] which is expected to operate with average luminosity $L \sim 10^{27} cm^{-2} s^{-1}$ for Au + Au collisions in the energy range $\sqrt{s_{\rm NN}} = 4 \div 11$ GeV/n (for Au^{79+}). In one of the collision points of NICA rings the Multi Purpose Detector (MPD) [30] will be located. MPD is proposed for a study of dense baryonic matter in collisions of heavy ions over the wide atomic mass range $A = 1 \div 197$. Inclusion of neutron detectors is also considered in the conceptual design of the MPD. The multiplicity of the neutrons in these collisions, predicted by the UrQMD model [44], will be about 200 in a full solid angle. The number of registered neutrons in each event depends on the event centrality and varies on the range $10 \div 150$ with a reasonable efficiency $\sim 80\%$ for neutron detection. With the proposed interaction rate for the detector MPD of about 10 kHz [30], it will be possible in a few months of accelerator running time to accumulate $\sim 10^9$ events with different centralities and measure CVE with comparable accuracy to CME or set an upper limit on the value of CVE. For the estimation of CVE we could explore the same three-particle correlator

$$\langle cos(\phi_\alpha + \phi_\beta - 2\phi_c) \rangle \tag{8.7}$$

which was used for the calculation of CME [39–41].

[14] Note that the opposite sign charge correlations for CME are also very small [41].
[15] The value of CME at NICA is under intensive discussion [42].

The possible magnitude of the statistical errors for the three-particle correlator with this number of collected events from the UrQMD model collisions of Au + Au at $\sqrt{s_{\rm NN}} = 9$ GeV is shown in Fig.8.9. The error points were obtained by taking two of the neutrons (α and β in Eq. (8.7)) from the mid-rapidity range ($|\eta| < 1$) and a third one (c in Eq. (8.7)) was taken from the ZDC rapidity range ($|\eta| > 3$). We should mention that the number of neutrons in each event within the mid-rapidity range is much smaller than the number of charged particles. Hence, in order to determine CVE with the same value of precision as in the CME case at RHIC [41], we need a much larger number of events. Precisely while $\sim$ 15M of events were sufficient at RHIC for targeted precision in the CME case, at NICA we need $\sim 1000M$ of events for the same precision in CVE measurements, which could be accumulated in a few months of NICA/MPD running time. More detailed estimates taking into account also neutron detector acceptances and efficiencies will be discussed elsewhere.

Modelling the vorticity and helicity

For estimation of the actual size of neutron asymmetry one should start with the modelling [45] of velocity and vorticity fields At energies higher than about 10 GeV, the Quark-Gluon String Model (QGSM) is used to describe elementary hadron collisions [47, 70]. This model is based on the $1/\mathrm{N}_c$ expansion of the amplitude for binary processes where N_c is the number of quark colours. Different terms of the $1/\mathrm{N}_c$ expansion correspond to different diagrams which are classified according to their topological properties. Every diagram defines how many strings are created in a hadronic collision and which quark-antiquark or quark-diquark pairs form these strings. The relative contributions of different diagrams can be estimated within Regge theory, and all QGSM parameters for hadron-hadron collisions were fixed from the analysis of experimental data. The break-up of strings via creation of quark-antiquark and diquark-antidiquark pairs is described by the Field-Feynman method [48], using phenomenological functions for the fragmentation of quarks, antiquarks and diquarks into hadrons. The modified non-Markovian relativistic kinetic equation, having a structure close to the Boltzmann-Uehling-Uhlenbeck kinetic equation, but accounting for the finite formation time of newly created hadrons, is used for simulations of relativistic nuclear collisions. One should note that QGSM considers the two lowest SU(3) multiplets in mesonic, baryonic and antibaryonic sectors, so interactions between almost 70 hadron species are treated on the same footing. This is a great advantage of this approach which is important for the proper evaluation of the hadron abundances and characteristics of the excited residual nuclei. The energy extremes were bridged by the QGSM extension downward in the beam energy [49].

For investigation of dynamical formation of velocity $\vec{v}$ and vorticity $\vec{\omega}$ ($\equiv rot\,\vec{v}$) fields in relativistic heavy ion collision the coordinate space was divided into $50 \times 50 \times 100$ cells of volume $dxdydz$ with $dx = dy = 0.6fm$, $dz = 0.6/\gamma$ fm, where γ is the gamma factor of equal velocity system of collision. In this reference system the total momentum and total energy of the produced particles were calculated in all cells for each of fixed 25 moments of time t covering the interval of 10 fm/c.

The results were averaged for about 10000 heavy ion collisions with identical initial conditions. The spectator nucleons of projectile or target ions, which at given time momentum do not undergone any individual collision, were included in evaluation of velocity. The velocity field in the given cell was defined by the following double sum over the particles in the cell and over the all simulated collisions:

$$\vec{v}\,(x,y,z,t) \;=\; \frac{\sum_i \sum_j \vec{P}_{ij}}{\sum_i \sum_j E_{ij}} \tag{8.8}$$

where $\vec{P}_{ij}$ and E_{ij} are the momentum and energy of particle i in the collision j, respectively. The vorticity was calculated using the discrete partial derivatives.

We paid a special attention to the pseudoscalar characteristics of the vorticity, that is the hydrodynamical helicity $H \equiv \int dV(\vec{v}\cdot\vec{w})$ which is related to a number of interesting phenomena in hydrodynamics and plasma physics, such as the turbulent dynamo (providing possibly additional mechanism of magnetic filed generation on the later stages of heavy-ion collisions) and Lagrangian chaos. It might be compared the analog of topological charge $Q \;=\; \int d^3x J^0(x)$ where the current $J^\mu \;=\; \epsilon^{\mu\nu\rho\gamma} u_\nu \partial_\rho u_\gamma$ (as usual, the four-velocity $u_\nu \;\equiv\; \gamma\,(1,\vec{v}\,)$) contributes to the hydrodynamical anomaly [33] and the polarization of hyperons [52, 66]. The calculation of the topological charge which is the correct relativistic generalization of the hydrodynamical helicity leads to the extra factor γ^2 in the integrand. Still as the helicity itself is a more traditional quantity, we use it for the numerical calculations. Fig. 8.10 represents the helicities in gold-gold collisions at different impact parameters evaluated in different domains. One can see that the helicity calculated with inclusion of the all cells is zero (black line). For the cells with the definite sign of the velocity components, which are orthogonal to the reaction plane (which may be selected also experimentally), the helicity is nonzero and changes the sign for the different

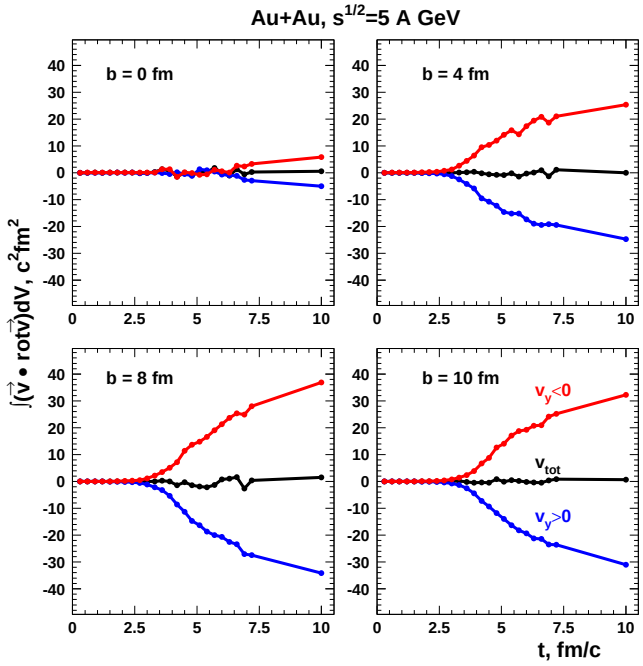

Figure 8.10: Time dependence of helicity at different impact parameters

signs of these components (red and blue lines, respectively). The effect is growing with impact parameter and represents a sort of saturation in time. Let us stress that the calculation in the hybrid UrQMD model manifests

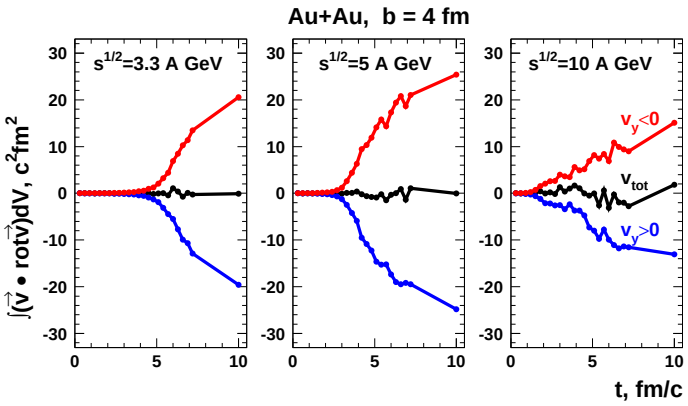

Figure 8.11: Time dependence of helicity at different energies

very similar behavior [53]. This is not surprising as the helicity is in fact generated at the hydrodynamical stage of the model, while the transition from kinetic to hydrodynamical stage should be performed similarly to our Eq. (8.8).

This effect of helicity separation might be qualitatively explained, if the perpendicular components of velocities (which are selected to have different signs) and the corresponding vorticities (assumed to have the same signs) provide the dominant contribution to the scalar product in the helicity definition. However, the numerical analysis showed that the longitudinal components along the beam directions (z-axis) provide even larger contribution to the helicity than contributions from the transverse direction (y-axis). Note that comparable values

of z and y components to helicity is due to larger $z-$components of velocity and $y-$ components of vorticity

So, such qualitative picture is oversimplified, but still provides a correct sign convention for the helicity-separation effect.

Fig. 8.11 represents the energy dependence of helicity which shows that its maximal value is achieved around the NICA energy range.

Conclusions and outlook

We discussed the new tests of P-odd effects in heavy ions collisions due to vorticity in the specific conditions of the MPD detector at NICA. Special attention was paid to the generalization of the Chiral Vorical Effect to the case of separation of the baryonic charge and its manifestation in neutron asymmetries.

We proposed to study the two- and three-particle correlations similar to those used in studies of CME. We compared the required accuracies and found that CVE could be studied with the data collected in a few months of NICA running.

As an outlook, let us first mention that the non-perturbative (in particular, lattice QCD [50]) studies of vorticity effects are very important. Let us also note that the large chemical potential might result in meson decays forbidden in the vacuum, like C-violating $\rho \to 2\gamma$ [54,55] or recently considered CP-violating $\eta \to 3\pi$ [56].

Vorticity is related to the global rotation of hadronic matter, an interesting observable by itself. Its manifestation in the polarization of Λ particles was suggested some time ago although the experimental tests at RHIC [39] did not show any significant effect. One may think that such a polarization can emerge due to the anomalous coupling of vorticity to the (strange) quark axial current via the respective chemical potential, being very small at RHIC but substantial at FAIR and NICA energies. Note that the temperature-dependent contribution In that case the Λ polarization at NICA [42] due to triangle anomaly can be considered together with other probes of vorticity [57] and recently suggested signals [58] of hydrodynamical anomaly. This option may be explored in the framework of the program of polarization studies at NICA [42] performed in the both collision points.

To collect the polarization data from different events one need to supplement the production plane with a sort of orientation. For this purpose one might use the left-right asymmetry of *forward* neutrons as it was done at RHIC [39,40] or another observable, interesting by itself. The last comment regards handedness [59], namely, the P-odd multiparticle momenta correlation. Its exploration in heavy ion collisions provides a way of orienting the event plane and collecting data for Λ polarization and other P-odd observables.

Finally, let us mention the possibility [42] to study P-even angular distributions of dileptons [60] which might be used as probes of quadratic effects of CME [61] and, quite probably, CVE.

8.7 Particle correlations and local P-violation in heavy-ion collisions

V. Koch[a], A. Bzdak[b], J. Liao[b,c]

[a] *Lawrence Berkeley National Laboratory, Berkeley, USA*

[b] *RIKEN BNL Research Center, Bldg. 510A, Brookhaven National Laboratory, Upton, USA.*

[c] *Physics Department and Center for Exploration of Energy and Matter, Indiana University, Bloomington, USA.*

Introduction

Experiments at the Relativistic Heavy Ion Collider (RHIC) have triggered quite a number of interesting fundamental questions to our understanding of strongly interacting matter under extreme conditions. Among them is that of a possible detection of local parity violation due to the non-trivial topological properties of QCD. The suggestions by Kharzeev and collaborators that the topological sphaleron transitions together with a chirally restored phase created in heavy ion collisions could result in the so-called Chiral Magnetic Effect (CME) [8]. The Chiral Magnetic Effect predicts that in the presence of the strong external (electrodynamic) magnetic field at the early stage after a (non-central) collision sphaleron transitions induce a separation of charges along the direction of the magnetic field. Of course, sphaleron and anti-sphaleron transitions are equally likely, and, therefore, the event-averaged charge separation will vanish. However, if present, the event-by-event charge separation should be observable in a suitable correlation measurement. Such a measurement has been proposed by Voloshin in [7] and recently carried out by the STAR collaboration [40, 62]. Here we will discuss to which extent the STAR measurement is indeed sensitive to the CME. Details can be found in [63–65]. A similar line

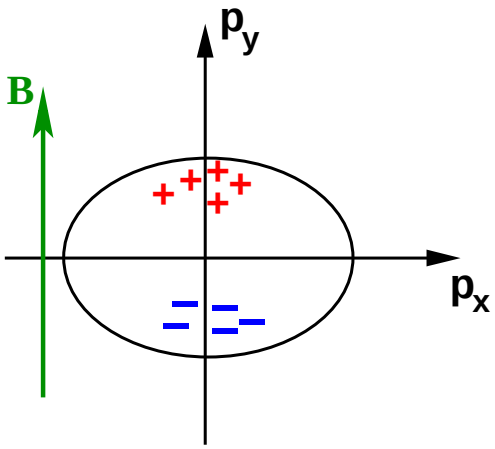

Figure 8.12: A schematic illustration of charge separation due to the Chiral Magnetic Effect in an heavy ion event. The reaction plane is aligned along the p_x-direction on this case.

of argument applies also for the case of the chiral vortical effect (CVE), recently suggested in Ref. [66] with possible relevance for the upcoming NICA facility. The chiral magnetic wave (CMW) may also occur in the baryonic-dense matter to be created at NICA with measurable effects [67].

Local parity violation in heavy ion collisions?

As briefly discussed in the introduction, the Chiral Magnetic Effect (CME) leads to the separation of charges along the direction of the magnetic field generated by the moving ions. This charge separation can be viewed as a dipole in momentum space as depicted in Fig. 8.12. In case of the CME, in a given event the dipole vector will be either parallel or anti-parallel to the magnetic field, depending on the presence of sphaleron- or anti-sphaleron transitions in the reaction. Therefore, the expectation value of the momentum-space dipole-moment vanishes, $\langle \vec{d} \rangle = 0$, as does the expectation value of the parity-odd scalar product with the magnetic field, $\langle \vec{B}\vec{d} \rangle = 0$. However, since in case of charge separation $\langle \vec{d}^2 \rangle \neq 0$ the presence of an event-by-event electric dipole may be observable in the *variance* of a parity-odd operator, or equivalently, in charge-dependent two-particle correlations. Of course, simple statistical fluctuations also give rise to a finite $\langle \vec{d}^2 \rangle$ and suitable observables have to be devised which are not sensitive to these statistical fluctuations (for a discussion see [64]).

One way to obtain information about the presences of the CME is to study charge dependent two-particle correlations with respect to the reaction plane, as proposed by Voloshin [7]. He suggested to measure the following three-particle correlation,

$$\langle \cos(\phi_i + \phi_j - 2\phi_k) \rangle \tag{8.9}$$

for same-charge pairs ($i, j = ++/--$) and opposite-charge pairs ($i, j = +-$) with the third particle, denoted by index k, having any charge. If the correlation with the third particle k is dominated by elliptic flow, then

$$\langle \cos(\phi_i + \phi_j - 2\phi_k) \rangle = v_2 \langle \cos(\phi_i + \phi_j - 2\Psi_{R.P.}) \rangle \tag{8.10}$$

where $\Psi_{R.P.}$ is the angle of the reaction plane, and v_2 denotes the strength of the elliptic flow. Working in a frame where the reaction plane is along the x-axis, $\Psi_{R.P.} = 0$, we get

$$\gamma \equiv \frac{1}{v_2} \langle \cos(\phi_i + \phi_j - 2\phi_k) \rangle = \langle \cos(\phi_i + \phi_j) \rangle \tag{8.11}$$

The STAR collaboration has recently measured this correlator and indeed has verified the above dependence of the elliptic flow. Before we discuss the STAR measurement in detail, however, let us see what to expect for this observable in case of the CME. As can be seen from Fig. 8.12, the CME predicts same-side out-of-plane correlations for same charges and back-to-back out-of-plane correlations for opposite charges. This is best seen by rewriting the correlator γ as

$$\begin{aligned} \gamma = \langle \cos(\phi_i + \phi_j) \rangle \quad &= \quad \langle \cos(\phi_i) \cos(\phi_j) \rangle \\ &\quad - \langle \sin(\phi_i) \sin(\phi_j) \rangle \end{aligned} \tag{8.12}$$

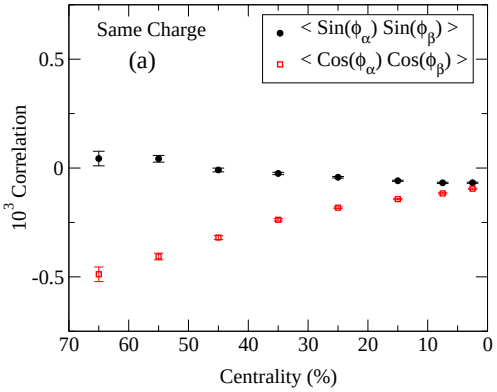

Figure 8.13: In-plane (red) and out-of-plane (black) correlations for same-charge pairs as measured by the STAR collaboration [40, 62]. For details see [63].

In this representation the first term, $\langle \cos(\phi_i)\cos(\phi_j)\rangle$, measures the in-plane correlations while the second term, $\langle \sin(\phi_i)\sin(\phi_j)\rangle$, measures the out-of-plane correlations. The CME predicts that same-charge pairs have either both an angle of $\phi_i, \phi_j \simeq \pi/2$ or $\phi_i, \phi_j \simeq 3\pi/2$. In either case, $\sin(\phi_i)\sin(\phi_j) \simeq 1$. For opposite charges, $\phi_i \simeq \pi/2$; $\phi_j \simeq 3\pi/2$ or vice versa and $\sin(\phi_i)\sin(\phi_j) \simeq -1$. Hence the CME predicts

$$\begin{aligned} \gamma_{CME,\,same-charge} &< 0 \\ \gamma_{CME,\,opposite-charge} &> 0, \end{aligned} \tag{8.13}$$

and indeed this is what the STAR measurement shows. So have we seen the CME and thus local parity violation in an actual experiment? Not quite yet, because there is an alternative scenario for which the correlator γ may be negative for same charge pairs and positive for opposite charge pairs: Suppose we have same-charge *in-plane* back-back correlations, i.e. $\phi_i \simeq 0$ and $\phi_j \simeq \pi$ or vice verse, and opposite-charge *in-plane* same-side correlations, i.e. $\phi_i, \phi_j \simeq 0$ or $\phi_i, \phi_j \simeq \pi$ we obtain the same signs for γ as above, but this time it is the $\langle \cos(\phi_i)\cos(\phi_j)\rangle$ term which controls things. In other words, the correlator γ is not unique and we need another observable to determine whether we are dealing with in-plane or out-of-plane correlations. The obvious candidate is

$$\begin{aligned} \delta \equiv \langle \cos(\phi_i - \phi_j)\rangle &= \langle \cos(\phi_i)\cos(\phi_j)\rangle \\ &\quad + \langle \sin(\phi_i)\sin(\phi_j)\rangle \end{aligned} \tag{8.14}$$

which represents the *sum* of the in-plane ($\langle \cos(\phi_i)\cos(\phi_j)\rangle$) and out-of plane ($\langle \sin(\phi_i)\sin(\phi_j)\rangle$) correlations. With both γ and δ we can extract both in-plane and out-of-plane correlations separately

$$\begin{aligned} \langle \cos(\phi_i)\cos(\phi_j)\rangle &= \frac{1}{2}(\delta + \gamma) \;\; (\mathrm{in-plane}) \\ \langle \sin(\phi_i)\sin(\phi_j)\rangle &= \frac{1}{2}(\delta - \gamma) \;\; (\mathrm{out-of-plane}) \end{aligned} \tag{8.15}$$

Fortunately, STAR has measured the correlator δ allowing for a decomposition of the in-plane and out-of-plane correlations. Those are shown in Fig. 8.13 for same-charge pairs and in Fig. 8.14 for opposite charge pairs. The surprising result is that a) for same charge pairs the measured out of-plane correlations are essentially zero, in contrast to the predictions from the CME. Instead STAR observes an *in-plane* back-to-back correlation! This situation is illustrated in Fig. 8.15. Opposite-charge pairs, on the other hand seem to be equally correlated in both the in-plane and out-of-plane direction. Obviously this is not quite in agreement with the expectation from the CME. Especially the fact that the same-charge pairs do not show any out-of-plane correlations for all centralities is difficult to understand in the context of the CME predictions. Naturally, there will be other effects contributing to the correlators γ and δ, such as the coulomb interaction, transverse-momentum conservation [65], local charge conservation [68,69], cluster-decays [70] etc. However, it is difficult to imagine how for all centralities these "background" contributions conspire to perfectly cancel the correlations expected from the CME. One should note, however, that so far the measured correlation are not understood in terms of conventional physics

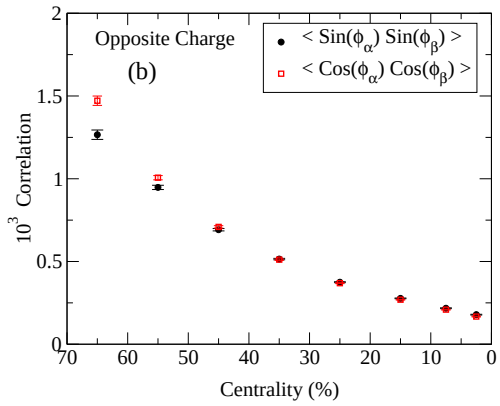

Figure 8.14: In-plane (red) and out-of-plane (black) correlations for opposite-charge pairs as measured by the STAR collaboration [40, 62]. For details see [63].

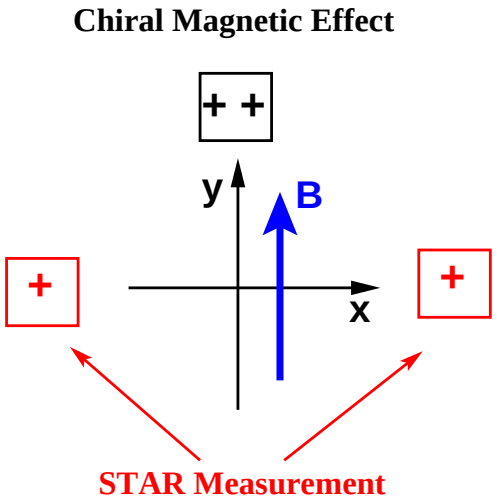

Figure 8.15: Schematic illustration of the actual STAR measurement (red) together with the predictions from the Chiral Magnetic Effect (black) for same-charge pairs.

either, possibly because many effects contribute, as indicated above. Furthermore, it would be very useful to have a more differential information on the above correlations. While STAR has extracted the rapidity and transverse-momentum dependence of γ this information is not yet available for δ. In addition, the value for the above correlations in simple proton-proton collisions would serve as an important reference point. It may also be useful to develop alternative observables [64, 71]. For example in [64] the direct extraction of the magnitude and direction with respect to the reaction plane of the momentum-space dipole-moment has been proposed by introducing a charge-dependent Q-vector analysis [72]. In [64] it was also demonstrated that simple two-particle correlations may mimic the effect of an actual dipole, and only the careful analysis of the distributions of both the magnitude and the angle of the extracted dipole was able to distinguish between an explicit dipole and other correlations.

Conclusions

In this contribution we have critically examined the STAR measurement of charge dependent two and three particle correlations and their relevance for local parity violation. We found that for same charge pairs STAR measures in-plane back-to-back correlations in contradistinction to the prediction from the Chiral Magnetic effect, which predicts out-of plane same side correlations. However, recently the ALICE collaboration reported preliminary results on the same observable measured at LHC energies, which in qualitative agreement with the prediction from the chiral magnetic effect [73]. Therefore, the jury on the existence of local parity violation in heavy ion collision is still out. As a lesson for the discussion of the CVE for NICA and other heavy-ion collision experiments in the high baryon density region one may conclude that it is important to carefully check and therefore to measure the correlations!

8.8 Exploring Dense and Cold QCD Phases in a Magnetic Field

V. de la Incera, E. J. Ferrer

University of Texas at El Paso, USA

The investigation of the nature of the chiral and deconfinement phase transitions, the location of the so-called chiral critical point, and the properties in its vicinity, have attracted a lot of interest during the past three decades [74–87]. Despite the fact that the theory of strong interactions (QCD theory) has been known for quite a long time, there is still a lack of understanding of the fundamental physics involved in the regions of intermediate values of the coupling. The chiral phase transition is known to take place close to the $m = 0$ region, whereas the deconfinement transition, signaled by the Polyakov loop, occurs at $m \to \infty$, where QCD becomes a pure gauge SU(3) theory. A priori, it is not evident that confinement and chiral phase transitions have to occur at the same temperature [88] . Nevertheless, early lattice calculations with large quark masses and/or coarse lattices found that deconfinement and chiral transition happen at the same temperature [89]. However, by using the so-called stout staggered quark action and finer lattices, it was found recently [90] that the two transitions are not interconnected as previously suggested in [88]. New developments in nonperturbative methods, such as lattice gauge theory or functional methods are needed to definitely settle this issue.

Since 2000, collision energies of order of 200 GeV have been reached in the Relativistic Heavy Ion Collider (RHIC) at Brookhaven National Lab (BNL), high enough to form the quark-gluon plasma. New ongoing experiments, as the one running since 2010 in the Large Hadron Collider (LHC) at CERN, will continue exploring the high temperature/low density region, through $\mathrm{Pb}-\mathrm{Pb}$ collisions at energies of order of 2.76 TeV. No doubt, the results of this experiment will serve to increase the precision of the physical findings in that region. On the other hand, the Nuclotron-based Ion Collider Facility (NICA) at JINR will open the possibility to explore the high-baryon-density and small-temperature region, thereby helping us to complete the entire picture of the QCD $(T-\mu_{\mathrm{B}})$-plane.

Of particular interest for the understanding of the phases that can be produced in the above-mentioned experiments is the effects related to the presence of strong magnetic fields. The generation of strong magnetic fields is due to occur in heavy-ion experiments during the peripheral collisions of positively charged ions moving at almost the speed of light. As argued in [14], these strong magnetic fields, produced during the first instants after a collision, can create the conditions for observable QCD effects. These effects can be prominent because the reached magnetic fields are of the order of, or higher than the QCD scale. There are both theoretical and experimental indications that the colliding charged ions can indeed generate magnetic fields estimated to be of order $e\mathrm{B} \sim 2\mathrm{m}_{\pi}^2$ ($\sim 10^{18}$ G) for the top collision, $\sqrt{s_{\mathrm{NN}}} \sim 200$ GeV, in non-central $\mathrm{Au}-\mathrm{Au}$ collisions at RHIC,

or even larger, $eB \sim 15 m_\pi^2$ ($\sim 10^{19}$ G), at future LHC experiments [9, 40, 62, 92]. Even though these magnetic fields decay quickly, they only decay to a tenth of the original value for a time scale of order of the inverse of the saturation scale at RHIC [93, 94], hence they may influence the properties of the QCD phases probed by the experiment. Strong magnetic fields will likely be also generated in the planned experiments at NICA, which will make possible to explore the region of higher densities under a magnetic field.

The production of such strong magnetic fields in heavy-ion collisions and their potential for triggering experimentally observable new QCD effects highlight the urgent need for studying the effects of these powerful fields in QCD and QCD-inspired theories. Some topics that would highly benefit from the availability of NICA experiments in the region of high density and low temperatures are:

1. Confinement/deconfinement and chiral transitions in a magnetic field
2. Magnetic field influence on the location of the critical point
3. Inhomogeneous condensates in the presence of a magnetic field

The relevance of them is reflected in the increasing attraction the effects of an external magnetic field is getting in the literature, as for instance in chiral magnetization [95–98], modification of the nature of the chiral phase transition (e.g. from a crossover to a first-order phase transition) [99, 101–105, 111], the chiral magnetic effect [5–7, 90, 106], spontaneous creation of axial currents [107, 108], formation of π_0-domain walls [109], the influence of the magnetic field on the location and nature of deconfinement [110–115], the influence of a magnetic field in the formation of quarkyonic chiral spirals [116], just to name a few.

Bibliography

[1] D. E. Kharzeev, R. D. Pisarski and M. H. G. Tytgat, Phys. Rev. Lett. **81,** 512 (1998) [arXiv:hep-ph/9804221].

[2] D. Kharzeev and R D. Pisarski, Phys. Rev. **D 61,** 111901 (2000).

[3] D. Kharzeev, Phys. Lett. **B 633,** 260 (2006)

[4] D. Kharzeev, L. McLerran and H. Warringa, Nucl. Phys. **A 803,** 227 (2008), [arXiv:0711.0950].

[5] D. Kharzeev and A. Zhitnitsky, Nucl. Phys. **A 797,** 67 (2007).

[6] K. Fukushima, D. Kharzeev and H. Warringa, Phys. Rev. **D 78,** 074033 (2008), [arXiv:0808.3382].

[7] S.A. Voloshin, Phys. Rev. **C 70,** 057901 (2004), [arXiv:hep-ph/0406311].

[8] S. A. Voloshin, [arXiv:0806.0029].

[9] V. Skokov, A. Illarionov, and V. Toneev, Int. J. Mod. Phys.**A 24**, 5925 (2009); [arXiv:0907.1396].

[10] D. Kharzeev, *talk at the NICA Round Table III*, (Dubna, 2008), http://theor.jinr.ru/ meetings/2008/roundtable/ .

[11] S. A. Voloshin, Phys. Rev. **C 62,** 044901 (2000) [arXiv:nucl-th/0004042].

[12] S. A. Voloshin (STAR Collaboration)*, talk at QM2009.*

[13] S. A. Voloshin, A. M. Poskanzer and R. Snellings, [arXiv:0809.2949].

[14] S. A. Voloshin and A. M. Poskanzer, Nucl. Phys. **B 474,** 27 (2000), [nucl-th/9906075].

[15] S. A. Voloshin, Nucl. Phys. **A 715,** 379 (2003), [nucl-ex/0210014].

[16] H. Satz, Nucl. Phys. **A 715,** 3 (2003) [hep-ph/0209181].

[17] D. Molnar and S. A. Voloshin, Phys. Rev. Lett. **91,** 092301 (2003) [nucl-th/0302014].

[18] R. J. M. Snellings, H. Sorge, S. A. Voloshin, F. Q. Wang and N. Xu, Phys. Rev. Lett. **84,** 2803 (2000), [nucl-ex/9908001].

[19] S. A. Voloshin and W. E. Cleland, Phys. Rev. **C 53,** 896 (1996) [nucl-th/9509025]; **54**, 3212 (1996), [nucl-th/9606033].

[20] S. Voloshin, R. Lednicky, S. Panitkin and N. Xu, Phys. Rev. Lett. **79,** 4766 (1997) [nucl-th/9708044].

[21] M. A. Lisa, S. Pratt, R. Soltz and U. Wiedemann, Ann. Rev. Nucl. Part. Sci. **55**, 357 (2005).

[22] Z. T. Liang and X. N. Wang, Phys. Rev. Lett. **94,** 102301 (2005) [nucl-th/0410079]; **96**, 039901 (2006).

[23] S. A. Voloshin, [arXiv:nucl-th/0410089].

[24] B. I. Abelev *et al.* (STAR Collaboration), Phys. Rev. **C 76,** 024915 (2007), [arXiv:0705.1691].

[25] A. A. Andrianov and D. Espriu, Phys. Lett. **B 663,** 450 (2008).

[26] A. A. Andrianov, V. A. Andrianov and D. Espriu, Phys. Lett. **B 678,** 416 (2009) [arXiv:0904.0413].

[27] A. A. Andrianov, D. Espriu, P. Giacconi and R. Soldati, JHEP **09**, 057 (2009) [arXiv: 0907.3709].

[28] D. Kharzeev and A. Zhitnitsky, Nucl. Phys. **A 797,** 67 (2007), [arXiv:0706.1026 [hep-ph]].

[29] D. Kharzeev, *Talk at the Round Table Discussion IV "Searching for the mixed phase of strongly interacting matter at the Nuclotron-based Ion Collider fAcility (NICA): Physics at NICA (White Paper)"*, (JINR Dubna, September 9 - 12 (2009)), http://theor.jinr.ru/meetings/2009/roundtable/

[30] *MPD Conceptual Design Report*, http://nica.jinr.ru

[31] *NICA Conceptual Design Report*, http://nica.jinr.ru

[32] F. V. Gubarev, V. I. Zakharov, *Talk at JINR/ITEP seminar on heavy ion collisions*, (February 15, 2010).

[33] D.T. Son and P. Surowka, Phys. Rev. Lett. **103,** 191601 (2009), [arXiv:0906.5044 [hep-th]].

[34] Y. N. Obukhov, A. J. Silenko and O. V. Teryaev, Phys. Rev. **D 80,** 064044 (2009), [arXiv:0907.4367 [gr-qc]].

[35] O. V. Teryaev, *Proceeding of SPIN-09 Workshop* (Dubna, September 1-5 2009), p. 147-150.

[36] M. V. Polyakov, A. Schafer and O. V. Teryaev, Phys. Rev. **D 60,** 051502 (1999), [arXiv:hep-ph/9812393].

[37] J. Randrup and J. Cleymans, Phys. Rev. **C 74,** 047901 (2006).

[38] V. D. Toneev, E. G. Nikonov, B. Friman, W. Norenberg and K. Redlich, Eur. Phys. J. **C 32,** 399 (2003), [arXiv:hep-ph/0308088].

[39] I. Selyuzhenkov [STAR Collaboration], J. Phys. G. **32,** S557 (2006), [arXiv:nucl-ex/0605035].

[40] B.I. Abelev *et al.* (STAR Collaboration), Phys.Rev. **C 81**, 054908 (2010), [arXiv:0909.1717 [nucl-ex]].

[41] S. A. Voloshin, [arXiv:1003.1127 [nucl-ex]].

[42] *NICA White Paper*, http://nica.jinr.ru , http://theor.jinr.ru/twiki-cgi/view/NICA/WebHome

[43] M. Bleicher, E. Zabrodin, C. Spieles *et al.*. J. Phys. G: Nucl. Part. Phys. **25** (1999) 1859

[44] M. Bleicher, E. Zabrodin, C. Spieles *et al.*. J. Phys. G: Nucl. Part. Phys. **25** (1999) 1859

[45] M. Baznat, K. Gudima, A. Sorin and O. Teryaev, arXiv:1301.7003 [nucl-th].

[46] V.D. Toneev, N.S. Amelin, K.K. Gudima, S.Yu. Sivoklokov, Nucl. Phys. A **519**, 463c (1990).

[47] N.S. Amelin, E.F. Staubo, L.S. Csernai et al., Phys.Rev. C **44**, 1541 (1991).

[48] R.D. Field, R.P. Feynman, Nucl. Phys. B **136**, 1 (1978).

[49] N.S. Amelin, K.K. Gudima, S.Yu. Sivoklokov, V.D. Toneev, Sov. J. Nucl. Phys. **52**, 272 (1990).

[50] P. V. Buividovich, M. N. Chernodub, E. V. Luschevskaya and M. I. Polikarpov, [arXiv:0909.1808 [hep-ph]].

[51] O. Rogachevsky, A. Sorin and O. Teryaev, Phys. Rev. C **82**, 054910 (2010) [arXiv:1006.1331 [hep-ph]].

[52] J. -H. Gao, Z. -T. Liang, S. Pu, Q. Wang and X. -N. Wang, Phys. Rev. Lett. **109**, 232301 (2012) [arXiv:1203.0725 [hep-ph]].

[53] J. Steinheimer, private communication.

[54] O. Teryaev, Chin. J. Phys. **34**, 1074 (1996).

[55] A. E. Radzhabov, M. K. Volkov and V. L. Yudichev, J. Phys. G. **32,** 111 (2006), [arXiv:hep-ph/0510329].

[56] R. Millo and E. V. Shuryak, [arXiv:0912.4894 [hep-ph]].

[57] B. Betz, M. Gyulassy and G. Torrieri, Phys. Rev. **C 76,** 044901 (2007), [arXiv:0708.0035 [nucl-th]].

[58] B. Keren-Zur and Y. Oz, [arXiv:1002.0804 [hep-ph]].

[59] A.V. Efremov, L. Mankiewicz and N.A. Tornqvist, Phys. Lett. **B 284,** 394 (1992).

[60] E. L. Bratkovskaya, O. V. Teryaev and V. D. Toneev, Phys. Lett. **B 348,** (1995) 283.

[61] P. V. Buividovich, M. N. Chernodub, D. E. Kharzeev, T. Kalaydzhyan, E. V. Luschevskaya and M. I. Polikarpov, [arXiv:1003.2180 [hep-lat]].

[62] B. Abelev *et al.*, (STAR Collaboration), Phys.Rev.Lett. **103**, 251601 (2009), `arXiv:0909.1739`.

[63] A. Bzdak, V. Koch, J. Liao, Phys. Rev. **C 81**, 031901 (2010), `arXiv:0912.5050`.

[64] J. Liao, V. Koch, A. Bzdak, Phys. Rev. **C 82**, 054902 (2010), `arXiv:1005.5380`.

[65] A. Bzdak, V. Koch, J. Liao Phys. Rev. **C 83**, 014905 (2010), `arXiv:1008.4919`.

[66] O. Rogachevsky, A. Sorin and O. Teryaev, Phys. Rev. **C 82**, 054910 (2010) [arXiv:1006.1331 [hep-ph]].

[67] Y. Burnier, D. E. Kharzeev, J. Liao and H. -U. Yee, Phys. Rev. Lett. **107**, 052303 (2011).

[68] S. Pratt (2010), `arXiv:1002.1758`.

[69] S. Pratt, S. Schlichting, S. Gavin (2010), `arXiv:1011.6053`.

[70] F. Wang, Phys.Rev. **C 81**, 064902 (2010), `arXiv:0911.1482`.

[71] N. Ajitanand, R.A. Lacey, A. Taranenko, J. Alexander (2010), `arXiv:1009.5624`.

[72] S.A. Voloshin, A.M. Poskanzer, R. Snellings, *Collective Phenomena in Non-Central Nuclear Collisions* Landolt-Boernstein New Series I/23, Editor: R. Stock, Springer (2010), `arXiv:0809.2949`.

[73] P. Christakoglou (for the ALICE Collaboration), J. Phys. G: Nucl. Part. Phys. 38, 124165 (2011).

[74] K.Fukushima and T. Hatsuda, Rept. Prog. Phys. **74**, 014001 (2011) .

[75] K. Rajagopal and F. Wilczek, [arXiv:hep-ph/0011333].

[76] T. Schafer, [arXiv:hep-ph/0509068].

[77] H.D. Politzer, Phys. Rev. Lett. **30**, 1346 (1973).

[78] D.J. Gross, and F. Wilczek, Phys. Rev. Lett. **30**, 1343 (1973).

[79] A.M. Polyakov, Phys. Lett. **B 72**, 477 (1978) .

[80] G. ?t Hooft, Nucl. Phys. **B 138**, 1 (1978).

[81] T. Banks and A. Casher, Nucl. Phys.**B 169**, 103 (1980).

[82] A. Mocsy, F. Sannino, and K. Tuominen, Phys. Rev. Lett.**92**, 182302 (2004).

[83] Y. Hatta and K. Fukushima, Phys. Rev. **D 69**, 097502 (2004).

[84] B. Gattringer, Phys. Rev. Lett.**97**, 032003 (2006).

[85] C.S. Fischer, Phys. Rev. Lett. **103**, 052003 (2009).

[86] J. Braun, H. Gies and J.M. Pawlowski, Phys. Lett. **B 684**, 262 (2010).

[87] J. Braun, L.M. Haas, F. Marhauser and J.M. Pawlowski, Phys. Rev. Lett. **106**, 022002 (2011).
[88] E. Shuryak, Phys. Lett. **B 107**, 103 (1981).
[89] P. Petreczky, Nucl. Phys. Proc. Suppl. **140**, 78 (2005) .
[90] Y. Aoki et al., Phys. Lett. B 643 (2006) 46; JHEP 0906 (2009) 088.
[91] () D.E. Kharzeev, L.D. McLerran and H.J. Warringa, Nucl. Phys. A 803 (2008) 227.
[92] V. Voronyuk, *et al.*, Phys. Rev. **C 83**, 054911 (2011).
[93] K. Fukushima, (*"QCD matter in extreme environments"*), [arXiv: 1108.2939 [hep-ph]].
[94] L.D. McLerran and R. Venugopalan, Phys. Rev. **D 49**, 2233 (1994) ; ibid.: 3352; **D 50**, 2225 (1994).
[95] T. D. Cohen and E. S. Werbos, Phys. Rev. **C 80**, 015203 (2009).
[96] A. Gorsky and A. Krikun, Phys. Rev. **D 79**, 086015 (2009).
[97] P. V. Buividovich, M. N. Chernodub, E. V. Luschevskaya and M. I. Polikarpov, Nucl. Phys. **B 826**, 313 (2010).
[98] M. D?Elia and F. Negro Phys. Rev. **D 83**, 114028 (2011).
[99] T. D. Cohen, D. A. McGady and E. S. Werbos, Phys. Rev. **C 76**, 055201 (2007).
[100] E. S. Fraga and A. J. Mizher, Phys. Rev. **D 78**, 247 (2008).
[101] N. O. Agasian and S. M. Fedorov, Phys. Lett. **B 663**, 445 (2008).
[102] A. V. Zayakin, J. High Energy Phys. 07 (2008) 116.
[103] A. J. Mizher and E. S. Fraga, Nucl Phys. **A 820**, 247 (2009).
[104] S-I Nam and C-W Kao, Phys. Rev. **D 83**, 096009 (2011) .
[105] C. Chatterjee, H. Mishra and A. Mishra, Phys. Rev. **D 84**, 014016 (2011).
[106] E. Kharzeev, Annals Phys. **325**, 205 (2010).
[107] D. T. Son and A. R. Zhitnitsky, Phys. Rev. **D 70**, 074018 (2004).
[108] M. A. Metlitski and A. R. Zhitnitsky, Phys. Rev. **D 72**, 045011 (2005).
[109] D. T. Son and M. A. Stephanov, Phys. Rev. **D 77**, 014021 (2008).
[110] K. G. Klimenko, Z. Phys. **C 54**, 323 (1992).
[111] F. S. Fraga and A. J. Mizher, Phys. Rev.**D 78**, 025016 (2008).
[112] J. K. Boomsma and D. Boer, Phys. Rev. **D 81**, 074005 (2010).
[113] K. Fukushima, M. Ruggieri, and R. Gatto, Phys. Rev. **D 81**, 114031 (2010).
[114] A. J. Mizher, M. N. Chernodub, and E. S. Fraga, Phys. Rev. **D 82**, 105016 (2010).
[115] R. Gatto and M. Ruggiery Phys. Rev. **D 82**, 05027 (2010); **83**, 034016 (2011).
[116] E. J. Ferrer, V. de la Incera, A. Sanchez, [arXiv:1205.4492 [nucl-th]].

9 Cumulative processes

Cumulative processes are the processes that are kinematically forbidden for (quasi-)free nucleons. Therefore, they necessarily involve collective properties of the nuclear constituents and allow to extract unique information about the short-distance correlations of quarks and gluons in cold and hot hadronic matter. The study of cumulative processes was pioneered at Dubna; these studies can be extended at NICA at a new level. This section details the measurements that can be performed, and discusses the physics issues that can be addressed on the basis of the new data.

9.1 New forms of QCD matter and cumulative processes

A. Kaidalov

Institute for Theoretical and Experimental Physics, Moscow, Russia

It is emphasized that investigation of cumulative processes in nucleus-nucleus collisions can provide an important information on new forms of QCD matter at high baryon density. Properties of cumulative processes are shortly discussed and possible experiments for NICA facility are proposed. It was realized in recent years that the phase diagram of QCD has a rich structure. Besides the confinement-deconfinement phase transition there is a possibility of the color super-conductivity phase at very large baryon densities (see review [1]). On the other hand a structure of the phase diagram for baryon densities, which are several times larger than the usual nuclear density, is poorly known.

A very important question is: how to investigate the phase diagram of QCD and new forms of quark-gluon matter in laboratory? Here I would like to suggest to investigate these problems for the region of large baryon densities in experiments with nucleus-nucleus collisions in the kinematical region forbidden for interactions of quasi-free nucleons (the so called cumulative processes).

Cumulative processes have been discovered in early seventies [2] and were studied in interactions of hadrons and leptons with nuclei [3–5]. Existing experimental information is usually described in terms of dense multi-quark configurations in nuclei ("fluctons" [6]) or short-range correlation of nucleons [7–12]. Such configurations can be considered as small drops of a new QCD phase in nuclei. These configurations exist in fast moving nuclei and may represent a new form of QCD matter.

Let me remind some characteristic properties of cumulative processes, which indicate that they are related to intrinsic properties of nuclei and reflect a new form of QCD matter.

- Universality of spectra in cumulative region. Spectra of hadrons in cumulative region $x > 1$ have a form $E\ d^3\sigma^a_{hA}/d^3p = exp(-\beta^a_A x)$ and the slope of the distribution β^a_A practically does not depend on initial energy, atomic number A and type of the produced hadron a.

- Average transverse momenta of produced hadrons increase as x increases. For pions $< p^2_T >$ reach values $\sim 2\ GeV^2$ at $x \sim 4$ [4]. These values are much larger than average transverse momenta of particles produced in interactions of hadrons and nuclei at high energies. Strange particle suppression is practically absent in cumulative region. There are many other characteristic features of cumulative processes, which can be interpreted as manifestation of dense multi-quark systems in nuclei. An information on cumulative particle production in nucleus-nucleus collisions is very limited and new facilities like NICA can considerably enlarge information on these interesting processes. It is worth to emphasize that colliders of very high energy like RHIC and LHC are not suitable for a study of these processes and the best region for investigation of non-nucleonic configurations in nucleus-nucleus collisions is the intermediate energy region $\sqrt{s_{\rm NN}} \sim 5$ GeV relevant for NICA.

Several observables, which can be studied in nucleus-nucleus collisions, sensitive to the effects considered above, are discussed below:

- It is important to study inclusive spectra of hadrons $E\ d^3\sigma^a_{A_1A_2}(b)/d^3p$ in the cumulative regions of both colliding nuclei. Broadening of spectra can be caused by multiple production of "drops" of a new phase and it is possible to search for a phase transition to the new phase. Deviations from the universality indicated above can be also due to "stopping" of produced fast hadrons by other nucleus. This effect leads to a faster decrease of spectra with x. It would be interesting to study spectra as functions of centrality.

- Is there an extra strangeness enhancement in cumulative region for nucleus-nucleus collisions? How it depends on atomic numbers and collision geometry? Very rich information can be obtained from a study of correlations for particles produced in cumulative regions:

  a) Production of two particles in the fragmentation region of the same nucleus. Here one can study BE-correlations and determine the sizes of production region. It is very interesting to study production of resonances in cumulative region (say ρ, ω, ϕ mesons). A study of multi-baryon resonances from decays of multi-quark configurations looks promising.

  b) Correlations between particles in the opposite fragmentation regions. One can look for interaction of two or more dense fluctuations. Production of particles with large transverse momenta, which can be due to such interactions is studied now at ITEP. To conclude, there is a very interesting and practically unexplored region of dense QCD medium, which can be studied in nuclear collisions at intermediate energies. Investigation of kinematical regions forbidden for quasi-free nucleon-nucleon interactions is the most suitable for these purposes. A rich experimental program of investigation of dense fluctuation for nuclei is formulated and can be realized at NICA.

9.2 The study of dense cold nuclear matter with cumulative trigger

A. Stavinskiy, O. Denisovskaya, Yu. Zaitsev, K. Mikhailov, P. Polozov, M. Prokudin, V. Stolin, R. Tolochek, S. Tolstoukhov and G. Sharkov

Institute for Theoretical and Experimental Physics, Moscow, Russia

It is important to study the phase diagram of nuclear matter and find out signals of phase transitions. The region of large density and small temperature is hardly accessible experimentally but strongly motivated by new theoretical results (see for example [13–17]. Cumulative effect [18] can be considered in terms of dense local multinucleon fluctuations (fluctons [19]), but some problems prevent the interpretation of such fluctons as dense nuclear matter droplet. First of all, flucton is a dynamical fluctuation with zero lifetime. Second it is a virtual configuration. And the last one, it is a small few-nucleon system.

We propose to study light ions collisions (from HeHe to CC) with high p_{T} midrapidity photon trigger(see figure). The maximum possible photon momentum corresponds to maximum c.m.s. collision energy and select a flucton-flucton interaction. High p_{T} process guarantee the locality (system size r of the order of 1 fm). It means that we can expect a dense real multinucleon (6 – 7 nucleons) system in the final state. Kinematical restriction will result in relatively small internal energy of the final multibaryon system with its relatively long lifetime. High density of the system just after collision ($20 \div 40\ \rho_0$) results in small mean-free path length $l << r \sim 1$ fm. It means that multinucleon system in the final state can be considered as a dense nuclear matter droplet [20].

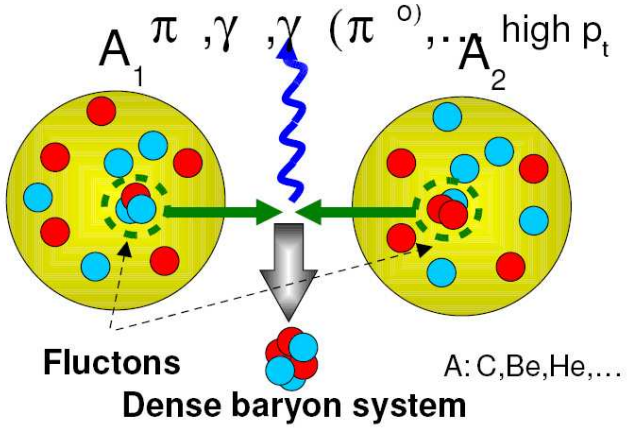

Figure 9.1: Artist's view of the flucton-flucton interaction process.

For the selected events we propose the wide analysis program to study dense nuclear system properties. Some analysis tasks are

- Relative momenta distribution study to check momentum space locality of the system due to kinematical properties of the proposed trigger
- Femtoscopy measurements (two particles correlations at small relative velocity) to check coordinate space locality of the system [21–25]
- Particle ratio ($n/p, \pi^+/\pi^-$) measurements to study the expected izosymmetrization effect [26]
- Strangeness production measurements (strangeness enhancement predicted for a hot QGP [27], expected also for cold dense matter)
- Vector meson production measurements (vector meson enhancement predicted in [28]; it is also interesting to check vector meson properties in dense matter)
- Search for exotic (like dibaryons or pentaquarks [29–31]). Fraction of exotic hadrons expected to be much higher than that for unselected events due to expected saturation of the nucleonic degrees of freedom.
- Search for direct photons (c.m.s. energy for flucton-flucton interactions will be much higher than that for NN collisions at the same beam momenta)
- Search for expected multifermion effects. It was shown that multiboson effects will modify standard meson femtoscopy at high density [32]. We also expect additional analysis items in the proposed program due to theoretical progress during the detector construction period. Program is proposed for MPD. Some program tasks need additional detector components (can be discussed separately; ITEP group responsibility also can be discussed). Trigger rate have being estimated base on real experimental data accumulated by FLINT collaboration in ITEP [33] and proved to be reasonable (see Table 9.2).

	Q1+Q2∼5	Q1+Q2∼6	Q1+Q2∼7
NICA	10^5(CC) 10^4(HeHe)	3.10^3(CC) 3.10^2(HeHe)	10^2(CC) 10^2(HeHe)
RHIC	10^3(CC) 10^2(HeHe)	3.10^1(CC)	

Table 9.1: Estimated data sample for 4π detector (expected number of accumulated events as a function of $Q_1 + Q_2$ for 10^6 sec run; preliminary)

In the table Q_1 and Q_2 are minimal numbers of nucleons in interacting fluctons. Estimate was done for CC (upper row) and HeHe (lower row) collisions at luminosity $L = 10^{30}\ cm^{-2}sec^{-1}$ (NICA) and $L = 10^{28}cm^{-2}sec^{-1}$ (RHIC).

9.3 Quark cluster structures in hypernuclei and compressed nuclear matter at NICA and FAIR

H. J. Pirner[a], J. P. Vary[b]

[a] *Institut für Theoretische Physik der Universität Heidelberg, Germany*
[b] *Department of Physics and Astronomy, Iowa State University, Ames, USA*

Heavy ion experiments and lattice-gauge simulations of Quantum Chromodynamics (QCD) intensively investigate the quark-gluon phase transition relevant to the early universe. Another challenge is to understand, under varying external conditions, the roles of fundamental quarks and gluons in hadronic and nuclear matter. Where are they essential to replace low-energy descriptions of nuclei based on hadrons (neutrons, protons and mesons)? From lattice QCD simulations, we understand quantitatively the masses of the hadrons. Similarly, we know that quark and gluon color charges make the strong coupling constant grow at distances larger than the hadron size and generate their own confinement within color-neutral hadrons. However, a theoretical understanding of longer range QCD dynamics, beyond the size of a hadron, is still a challenge for lattice simulations.

We present evidence for an intermediate-range phenomena, the formation of multi-quark clusters in cold as well as hot equilibrated baryonic matter that blurs the boundary between the hadron and quark-gluon phases. Based on a recent article [34] we summarize here the main implications of our studies for the anticipated experimental program at the upcoming fixed target (BM@N) and collider (NICA-MPD) experiments at the JINR Dubna, paralleling similar developments at FAIR Darmstadt.

We adopt classical percolation theory [35–38] to bridge the gap between quark and hadron physics. In our hybrid approach we take nuclear matter to be composed of color neutral clusters, which consist at zero temperature of 3, 6, 9, 12, ... quarks and at finite temperature we include quark-antiquark ($q\bar{q}$) states for the mesons. These larger units have small probabilities in cold nuclei, but are color conducting, like subdomains of ionized plasma in a electrically neutral gas. We assume there is a common size parameter for the lowest mass nucleon and pion which determines the overlap of hadronic states at finite density and consequently the probabilities to form these multi-hadron clusters. We expect the presently neglected gluon content of these systems to become important at very short distances.

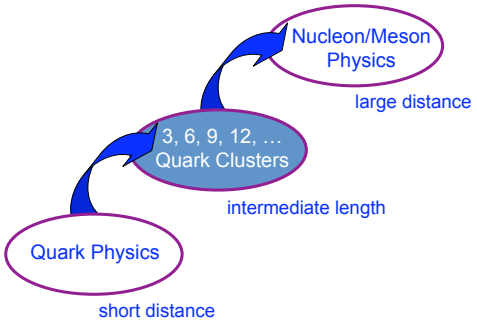

Figure 9.2: The separation of quark physics, the physics of color neutral multi-quark clusters and and nucleon/meson physics.

In Fig. 9.2 we summarize the percolation approach to nuclear physics where, between the well-established hierarchy of quark/gluon physics and nucleon/meson physics, we insert a new layer consisting of color neutral multi-quark clusters. Percolation theory allows us to connect these regions and appears sufficient to unify the microscopic and macroscopic physics with an accuracy of $\approx 10\%$. Solutions for cluster probabilities in nuclei have previously been reported [38, 39].

Relativistic Heavy Ion Collisions

We now show that the quark cluster description is appropriate at high excitation energies produced in relativistic heavy ion collisions. Cluster probabilities are mainly a function of the local hadron density and, to proceed to finite temperature, we introduce a pion component. We assume that the critical separation distance for the pions to transition into larger quark clusters is the same as for nucleon percolation, $d_c = 1$ fm, and that d_c is temperature independent. Therefore we adjust the baryon chemical potential so that the sum of the baryon and pion densities is the same as the density of baryons at $T = 0$ to maintain approximately constant color percolation probability. Then

$$\rho_{\rm hadrons}(\mu, T) = \rho_{\rm baryons}(\mu_b, T) + \rho_{\rm pions}(\mu_\pi, T). \tag{9.1}$$

We set the pion chemical potential $\mu_\pi = 0$ at $T = 0$ to fix the reference baryon chemical potential μ_b at normal nuclear matter density 0.17 baryons/fm^3 (Fermi momentum $k_f = 1.36$ fm^{-1}). The nucleon dispersion relation is influenced by the nuclear mean field potential for which we take [40]

$$\epsilon(k) = \sqrt{(k^2 + (m_N + V_s(k))^2)} + V_0(k) \tag{9.2}$$

where the scalar and vector self-energies are momentum dependent

$$V_s(k) = -0.35GeV(1-0.05(k/k_f)^2) \quad (9.3)$$
$$V_0(k) = +0.29GeV(1-0.05(k/k_f)^2) \quad (9.4)$$

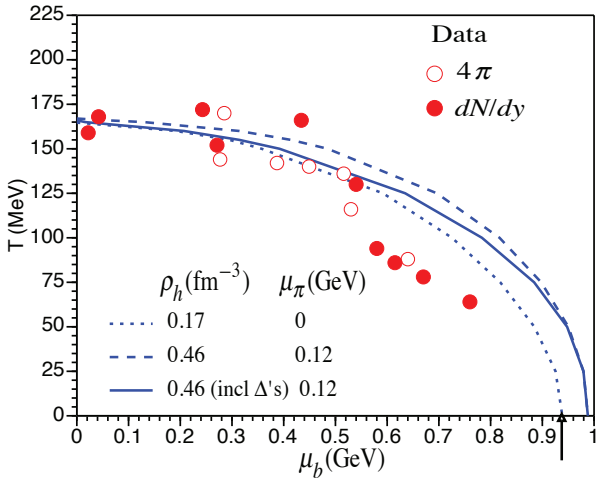

Figure 9.3: The boundary between hadron- and quark/gluon-matter from our quark percolation model for 50% percolation rate (upper curves) and 22% percolation rate (lower curve) in a temperature T versus baryon chemical potential μ_b phase diagram. The parameters of the three theory curves are specified in the legend. The arrow indicates μ_b for nuclear matter at $T = 0$. The freeze-out data are compiled from different experiments [41].

The freeze-out data [41] extracted from heavy ion collisions at high temperatures are shown in Fig. 9.3 as a function of T and μ_b along with the theoretical (dotted) curve which corresponds to a mostly hadronic system of pions and nucleons. On this curve, each quark is percolating 22% of the time in $i > 3$-quark clusters. We also plot in Fig. 3 a curve with a higher percolation rate which we call "percolating nuclear matter" and find μ_b where more than 50% of all nucleons have transitioned to 6, 9, 12, ... -quark clusters at $T = 0$. This $T = 0$ state requires $\rho_{baryon} = 0.46fm^{-3}$ i.e. 2.7 times nuclear density and therefore has a larger chemical potential than nuclear matter. For this case, we also adopted $\mu_\pi = 120MeV$, used to fit the transverse momentum dependence of the pion spectra from a kinetically equilibrated pion distribution [42]. Taking into account also the Δ- resonance at 1.236 GeV shifts the higher temperature percolation curve (solid line) towards the curve corresponding to nuclear matter density (dotted line).

The percolation model is a geometrical model and is not sensitive to the decay properties of resonances, but more to the number of hadronic states in a certain volume. The classical percolation transition is a cross over transition in finite systems and the transition itself is not well defined. Thus quark percolation blurs the boundary between the hadron phase and the quark/gluon phase.

Extended Quark Orbitals in Hypernuclei

Another avenue to explore quark cluster structures is to replace one of the nucleons with a strange spectator, a $\Lambda-$hyperon, producing a hypernucleus. The successful explanation of the hypernucleus spin-orbit potential based on quark dynamics [43] motivates a closer look at possible quark cluster effects. In particular, we focus on a longstanding puzzle [44] of the sudden decrease of the binding energy in $^5He_\Lambda$ compared with the binding energy of a baryon-based calculation with two-body forces. The ^{4}He nucleus is doubly magic in the language of the shell model with protons and neutrons but the full occupation of the 0s -state by protons and neutrons does not preclude the addition of a $\Lambda-$hyperon to the 0s -state. With two-body forces alone one then obtains overbinding of the A=5 hypernucleus by $1-3MeV$. One way out is through effective many-baryon potentials. Indeed, calculations with purely baryonic degrees of freedom and a three-body Λ-NN force resulting from an explicit Σ- component in the wave function [45] seem to show the repulsive character for the total three-body

contributions. However, if the three quark substructure of the Λ matters, i.e. up(u)+down(d)+strange(s), then for the 12-quark cluster configuration of ^{4}He, the Λ's up and down quarks cannot occupy the 0s-shell which can accommodate only 12 u- and d- quarks according to the Pauli principle. The observation of such extended quark orbitals would be the best proof for color percolation in nuclei as G. Baym has already indicated in 1979 [35].

Let us make a simple estimate of this effect. The mean spacing in the constituent quark shell model would be larger by a factor three based on the ratio of nucleon to constituent quark masses

$$\hbar\omega_Q = 3\hbar\omega_N = 75MeV \tag{9.5}$$

Including a size factor for the smaller 12 quark cluster compared to the nuclear size could easily boost this mean spacing by a factor of two.

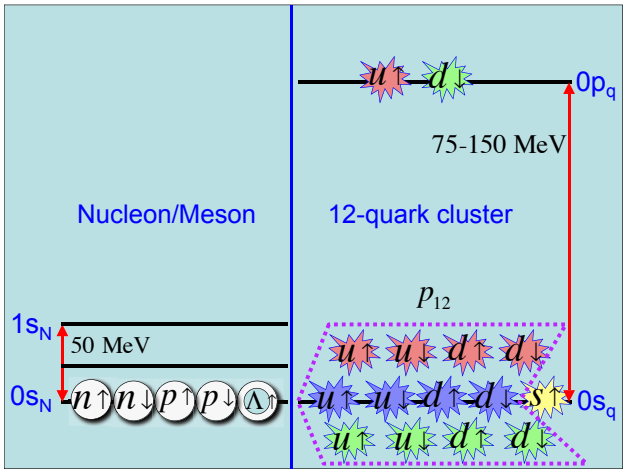

Figure 9.4: Sketch of the two possible views of the Lambda attached to the the lowest configuration of two neutrons(n) and two protons(p). On the left, the Lambda and the nucleons are structureless baryons with spin projections indicated. On the right, their quark substructure is taken into account with spin and color attributes sketched. In the latter case, the 12-quark cluster configuration that appears with probability $p_{12} = 0.007$ in the quark cluster model, forces the up(u) and down(d) quarks of the Lambda to be in the next higher, Pauli-allowed, orbit $0p_q$. The Lambda's strange(s) quark may occupy the lowest $0s_q$ level.

Therefore a 12-quark cluster with two extra u- and d- quarks would need an extra excitation energy of approximately 150-300 MeV. Our quark cluster model provides [38] $p_{12}(^4He) = 0.007$, a small probability for such an extended 12-quark cluster in ^4He (Fig. 9.4). Multiplying this probability with the Pauli-required u- and d- quark excitations of 150-300 MeV would give a decrease in $^5He_\Lambda$ binding of $1-2MeV$, in rough agreement with experiment. This one case is not sufficient to establish the existence of extended quark shell model states. One should look at heavier hypernuclei where the additional Λ has to split up in a low lying s-quark and an excited ud-pair. Future precision experiments could explore the binding energy systematices of heavier closed shell systems such as: $^{16}O_\Lambda$,$^{17}O_\Lambda$ and $^{16}N_\Lambda$,$^{17}N_\Lambda$.

Additional experimental tests of quark clustering can be performed such as measuring high mass di-lepton pair production from nuclear targets [46] (Drell-Yan process).

If one asks whether our understanding of QCD is complete, the question may be recast to whether additional theoretical or experimental work can improve the situation decisively. Compressed baryonic matter [47] is an area where our theoretical and experimental understanding is not as well developed as baryon-free matter. For nuclei a theory which contains nucleons and multi-quark cluster states is an efficient way to describe the transition from purely nucleonic matter to quark matter at high baryon density. A hybrid model with quark clusters would define a major advance if one would be able to rewrite the smooth infrared limit of lattice QCD in a field theoretic continuum picture. Such a picture should also continue the phase diagram into the totally percolated phase where perhaps the formation of a qq -dimer condensate [48] and BCS-pairing [49] of quarks

can be found in analogy to the physics of cold atoms. Quark percolation and these other features of the QCD phase diagram would also impact astrophysics.

Bibliography

[1] K. Rajagopal and P. Wilczek, [hep-ph/0011333]; T. Schafer and E. Shuryak, [nucl-th/0010049]; D. Rischke and R. Pisarsky, [hep-ph/0004016].

[2] A. M. Baldin, EPAN **8**, 429 (1971).

[3] V. S. Stavinsky, EPAN **10**, 949 (1979).

[4] S. B. Boyarinov *et al.*, Yad. Fiz. **34**, 119 (1991); S. B. Boyarinov *et al.*, Yad. Fiz. **57**, 1452 (1994).

[5] K. S. Egiyan *et al.*, Phys. Rev. Lett. **96,** 082501 (2006); E. Piasetsky *et al.*, Phys. Rev. Lett. **97,** 162504 (2006).

[6] D. I. Blokhintsev, JETP **33**, 1295 (1957).

[7] A. V. Efremov, Yad. Fiz. **24**, 1208 (1976).

[8] V. K. Lukyanov and A. I. Titov, EPAN **10**, 815 (1979).

[9] V.V. Burov, V.K. Lukyanov and A.I. Titov, EPAN **15**, 1249 (1984).

[10] A. V. Efremov, A. B. Kaidalov, V. T. Kim *et al.*, Sov. J. Nucl. Phys. **47**, 868 (1988);

[11] A.V. Efremov, A.B. Kaidalov, G.I. Lykasov and N.V. Slavin, Yad. Fiz. **7**, 932 (1994).

[12] M. I. Strikman and L. L. Frankfurt, EPAN **11**, 571 (1980).

[13] B.Barrois, Nucl. Phys. **B 129,** 390 (1977).

[14] D. Bailin and A. Love, Phys. Rep. **107,** 325 (1984).

[15] M. Alford, K. Rajagopal and F. Wilczek, Phys. Lett. **B B422,** 247 (1988).

[16] R. Rapp, T. Schafer, E. V. Shuryak and M. Velkovsky, Phys. Rev. Lett. **81,** 53 (1988).

[17] M. Alford, K. Rajagopal, T. Schafer and A. Schmitt, Rev. Mod. Phys. **80**, 1455 (2008).

[18] A. M. Baldin *et al.*, *JINR Preprint* P1-5819 (1971); Yad. Fiz. **18**, 79 (1973).

[19] D. I. Blokhintsev, JETP **6**, 995 (1958).

[20] D. Seibert, Phys. Rev. Lett. **63,** 136 (1989); R.S. Bhalerao and R.K. Bhaduri, [hep-ph/0009333].

[21] G. I. Kopylov and M. I. Podgortski, Yad. Fiz. **15**, 392 (1972).

[22] S. E. Koonin, Phys. Lett. **B 70,** 43 (1977).

[23] P. Lednitski and V. L. Ljuboshitz, Yad. Fiz. **35**, 1316 (1982).

[24] B. K. Jennings, D. W. Boal and C. J. Shillcock, Phys. Rev. **C 33,** 1303 (1986).

[25] Yu. D. Bajukov *et al.*, Yad. Fiz. **50**, 1023 (1989).

[26] Yu. D. Bajukov *et al.*, Yad. Fiz. **42**, 185 (1985); L.S.Vorobijov *et al.*, Yad. Phys. **59**, 694 (1996).

[27] J. Rafelski and B. Muller, Phys. Rev. Lett. **48,** 1066 (1982).

[28] A. M. Baldin and S. B. Gerasimov, *JINR communication* E2-11804 (1978).

[29] L. A. Kondratjuk *et al.*, Yad. Fiz. **45**, 1252 (1987).

[30] A. A. Grigirjan and A. B. Kaidalov, JETP Letters **28**, 318 (1978); Nucl. Phys. **B 135,** 93 (1978).

[31] D. Diakonov, Prog. Nucl. Phys. **51**, 173 (2003); R.L. Jaffe, [hep-ph/0409362].

[32] R. Lednicky *et.al.*, Phys. Rev. **C 61,** 034901 (2000).

[33] I. Alekseev *et al.*, Yad. Fiz. **71**, 1879 (2008).

[34] H. J. Pirner and J. P. Vary, Phys. Rev. **C 84**, 015201 (2011).

[35] G. Baym, Physica **96 A**, 131(1979); Prog. Nucl. Part. Phys. **8**, 73(1982).

[36] H. Satz, Nucl. Phys. **A 642**, 130 (1998).

[37] H. J. Pirner and J. P. Vary, Phys. Rev. Lett. **46**, 1376 (1981).

[38] M. Sato, S. A. Coon, H. J. Pirner and J. P. Vary, Phys. Rev. **C 33**, 1062 (1986).

[39] F. Guttner and H. J. Pirner, Nucl. Phys. **A 457**, 555(1986); R. Boisgard, J. Desbois, J. F. Mathiot, C. Ngo, Nucl. Phys. **A 489**, 731(1988).

[40] B. Chen and Z. Ma, Phys. Lett. **B 339**, 297(1994).

[41] A. Andronic, P. Braun-Munzinger and J. Stachel, Nucl. Phys. **A 772**, 167(2006).

[42] P. Gerber, H. Leutwyler and J. L. Goity, Phys. Lett. **B 246**, 513(1990).

[43] H. J. Pirner and B. Povh, Phys. Lett. **B 114**, 308(1982).

[44] E. V. Hungerford and L. C. Biedenharn, Phys. Lett. **B 142**, 232(1984).

[45] H. Nemura, Y. Akaishi and Y. Suzuki, Phys. Rev. Lett. **89**, 142504(2002).

[46] A. Harindranath and J. P. Vary, Phys. Rev. **D 34**, 3378 (1986).

[47] B. Friman, C. Höhne, J. Knoll, S. Leupold, J. Randrup, R. Rapp, P. Senger (Editors), *The CBM Physics Book: Compressed Baryonic Matter in Laboratory Experiments, Lecture Notes in Physics*, (Springer-Verlag, NY) (2011).

[48] A. H. Rezaeian and H. J. Pirner, Nucl. Phys. **A 779**, 197 (2006).

[49] T. Schäfer and F. Wilczek, Phys. Rev. **D 60**, 114033 (1999).

10 Polarization effects and spin physics

This section contains the discussion of two important issues: i) polarization effects in heavy ion collisions and ii) the spin program with polarized beams. The studies of polarization effects in heavy ion collisions have just began. The conversion of the huge initial angular momentum available in a heavy ion collision into the angular momentum carried by dense matter, and possibly by the spins of produced particles is an extremely interesting problem. Understanding it will undoubtedly allow to penetrate deeper into the collision dynamics. A number of observables are proposed in this section – most of them have never been studied before in heavy ion experiments. The physics issues include the dynamics of the collision, the chiral properties of the produced medium, and of the possible local violation of $\mathcal{P}$ and $\mathcal{CP}$ invariances discussed above.

The spin program is an important and integral part of the NICA project. Indeed, ever since the "spin crisis" of 1987, the composition of the nucleon's spin in terms of the fundamental constituents – quarks and gluons – remains in the focus of attention of many physicists. This section contains the discussion of the physics goals and perspectives of the spin program at NICA. The highlights of the NICA spin program include the measurements of Drell-Yan processes with longitudinally polarized proton and deuteron beams, spin effects in the inclusive and exclusive production of baryons, light and heavy mesons and direct photons, and the studies of helicity amplitudes and double spin asymmetries in elastic scattering. This section also addresses the issue of the competitiveness of the NICA spin program – it appears that the SPD detector at NICA would allow to contribute significantly to the current and planned international program in spin physics.

10.1 Polarization effects in heavy ions collisions at NICA

A. Efremov, O. Teryaev and V. Toneev

Joint Institute for Nuclear Research, Dubna, Russia

Spin effects are known to be the most sensitive tests of the the adequacy of theoretical description of high energy processes. Their investigation in heavy ion collisions is currently not very well developed, probably because of the experimental difficulties of the polarization measurements having the large number of produced particles. The exploration of spin effects in the new generation of experiments with heavy ions, including NICA, offers a new opportunities for the detailed studies of the patterns of hadronic phases.

The polarization observable which can be studied in the easiest way is the hyperon (in particular, Λ) polarization revealing itself via the angular asymmetry in the parity violating decay. Due to the parity conservation in the case of binary or inclusive reaction it can be only transverse (like all Single Spin Asymmetries in QCD [1]), i.e. directed normally to the scattering plane providing the only available pseudovector. If any kind of (isotropic) hadronic medium is formed and the direction of the colliding beams is "forgotten", the transverse polarization should be diluted. At the same time, the longitudinal polarization emerging in the parity-violating weak Σ decays should be preserved. Such changes in the Λ polarization were suggested [2–4] as a signal for hadronic medium formation. The observation of the effect of dilution of transverse polarization at NICA may be an important complementary probe of the mixed phase.

In order to observe the transverse polarization together with the longitudinal one it is possible to choose its direction normal to the reaction rather than production plane. The latter may be identified in event-by-event analysis. It is also important to have this plane oriented, which was achieved by the identification of left-right asymmetry of forward neutrons. Nevertheless the RHIC data showed that the polarization is compatible with zero. This contradicts to the model [5] of the coupling of the collective orbital momentum of the produced medium to the hyperon spin. This may not be surprising as this orbital momentum is distributed among a large number of hadrons and its amount coupled to the polarization of a single hadron is quite small. One may therefore use various types of the transverse handedness [6] to probe the orbital momentum of the matter.

As soon as Single Spin Asymmetries are $\mathcal{T}$-odd observables, they may emerge due to the effects of spontaneous $\mathcal{CP}$-violation in dense matter. Therefore, the correlations of Λ polarization with with the charge separation (see [7, 8] and references therein) may be used for the search of this effect.

The $\mathcal{T}$-even polarization observables are represented, first of all, by the anisotropy of dileptons [9,10] probing the tensor polarization of virtual photon. The formation of isotropic matter provides the important restrictions to its form, depending only on polar angle in Collins-Soper frame and being sensitive to mechanisms of dilepton productions [11]. The existence of the preferred direction, like the normal to the production plane may give

rise also to azimuthal asymmetries, providing another probe for collective orbital momentum. There are also much more strong effects [12] if the directions of colliding ions momenta are somehow remembered which may be studied in the correlation analysis together with the other observables.

To conclude, the following polarization observables at NICA may be studied:

- Polarization of Λ as a probe of formation of isotropic matter.
- Correlations of Λ polarization with charge sepration as a complementary signal for $\mathcal{CP}$-violation in dense matter.
- Transverse handedness as a probe for collective orbital momentum of the matter.
- Tensor polarization of dileptons as a complementary probe of matter formation, dilepton production mechanisms and collective orbital momentum.

10.2 Spin physics

A. Efremov, A. Nagaytsev, I. Savin, O. Shevchenko and O. Teryaev

Joint Institute for Nuclear Research, Dubna, Russia

The composite nature of the nucleon spin structure has been studied for a long time by means of Deep Inelastic Scattering (DIS) of leptons and production of Drell-Yan (DY) [13] lepton pairs in the Bjorken regime. As a consequence of the high scale Q, scattering occurs in a collinear configuration between the incident lepton and a single parton in the nucleon. The factorization theorem allows the inclusive DIS and DY cross section to be expressed as a convolution of two contributions: one corresponds to the hard process occurring at short distance between probe and parton; the other accounts for the coherent long-distance interactions between parton and target, and is described in terms of parton distributions. In the leading order (leading twist) the variable x can be interpreted as a fraction of the longitudinal momentum of the parent (fast-moving) nucleon carried by the active parton, and one may distinguish three kinds of Parton Distributions Functions (PDF). Two of them are well-known structure functions measured in DIS and other processes: f_1^α (α is a parton flavor, often suppressed) is the density of unpolarized partons with longitudinal momentum fraction x in an unpolarized nucleon, and $g_1(x)$ giving the net helicity of partons in a longitudinally polarized nucleon. The third one, the transversity $h_1(x)$, describing the density of partons with polarization parallel to that of a transversely polarized nucleon minus the density of partons with antiparallel polarization, is chiral-odd and requires a quark helicity flip that cannot be achieved in hard subprocess. Other parts of the cross section have to be explored for that. They are either chiral-odd Fragmentation Function (FF) (e.g. Collins fragmentation function $H_1^\perp$ in semi inclusive DIS (SIDIS) or another transversity of the second polarized incident hadron in the DY).

However, in addition to the information on the longitudinal behaviour in momentum space along the direction in which the nucleon is moving, a complete three-dimensional picture of the nucleon also requires knowledge of the transverse motion of partons [14, 15]. A full account of the orbital motion, which is also an important issue to understand the spin structure of the nucleon, can be given in terms of Transverse-Momentum Dependent parton distribution functions (TMDs). There are eight leading-twist TMDs: $f_1(x, p_\mathrm{T})$, $f_{1T}^\perp(x, p_\mathrm{T})$, $g_{1L}(x, p_\mathrm{T})$, $g_{1T}(x, p_\mathrm{T})$, $h_1(x, p_\mathrm{T})$, $h_{1L}^\perp(x, p_\mathrm{T})$, $h_{1T}^\perp(x, p_\mathrm{T})$, $h_{1L}^\perp(x, p_\mathrm{T})$. Two of them, the Boer-Mulders and Sivers function, $h_1(x, p_\mathrm{T})$ and $f_{1T}^\perp(x, p_\mathrm{T})$ [16,17], are $\mathcal{T}$-odd, *i.e.* they change sign under naive time reversal, which is defined as usual time reversal, but without interchange of initial and final states. The other six leading-twist TMDs are $\mathcal{T}$-even. In order to be sensitive to intrinsic transverse parton momenta, it is necessary to measure adequate transverse momenta of the produced hadrons in the final state, e.g., in processes like semi-inclusive lepton-nucleon DIS (SIDIS), hadron production in e^+e^- annihilation [14–17] or the transverse momentum lepton pair in the Drell-Yan processes in hadron-hadron collisions. Here, factorization has been proved at leading twist [18–20] allowing to access information on TMDs as well as on fragmentation functions (FFs) describing the hadronization process of the hit quark decaying into the detected hadrons. At leading twist, the fragmentation of unpolarized hadrons is described in terms of two fragmentation functions, $D_1(z, K_\mathrm{T})$ and $H_1^\perp(z, K_\mathrm{T})$, where z is the energy fraction taken out by the detected hadron and $K_T = |\vec{K}_\mathrm{T}|$ its transverse momentum. The function $D_1(z, K_\mathrm{T})$ describes the decay of an unpolarized quark, whereas the Collins function $D_1(z, K_\mathrm{T})$ describes a left-right asymmetry in the decay of a transversely polarized quark [6]. By measuring the angular distribution of produced hadrons in SIDIS or lepton pairs in DY, it is possible to access information on all eight leading-twist

TMDs in combinations with the two leading-twist FFs. Restricting ourselves to the one-photon approximation and considering spin degrees of freedom such as the beam helicity and the target spin, the contraction between the lepton and hadron tensors in the cross section can be decomposed in a model-independent way in terms of eighteen structure functions, thus exhibiting a non trivial azimuthal dependence of the detected hadron in SIDIS [21] or lepton pairs in the DY [22]. According to factorization, each of the leading-twist structure functions can be conceived as a convolution between one TMD and one FF in SIDIS or two TMDs (for quark and antiquark) in the DY. Since structure functions enter the cross section with a defined angular coefficient, they can be accessed by looking at specific azimuthal asymmetries. This has become now a powerful tool for studying the three-dimensional structure of the nucleon [23, 24] and many more data are expected to come in the future. The remarkable experimental progress was accompanied by and motivated numerous theoretical and phenomenological studies in literature.

Concerning the Drell-Yan process. During the past decades dilepton production in high-energy hadron-hadron collisions [13, 25] has played an important role in order to pin down parton distributions (PDFs) of hadrons. While the main focus was on PDFs of the nucleon, also information on the partonic structure of the pion was already obtained through Drell-Yan measurements. The crucial tool, required for the extraction of PDFs, is the QCD-factorization theorem if the invariant mass of the dilepton pair is sufficiently large. Experimentally, the Drell-Yan process is quite challenging because of the relatively low counting rates. On the other hand, from the theoretical point of view it is the cleanest hard hadron-hadron scattering process. The fact that no hadron is detected in the final state simplifies the proof of factorization in comparison to hadron-hadron collisions with hadronic final states. This important point is one of the main reasons for the continued interest in the Drell-Yan reaction. Currently, not less than six programs for future Drell-Yan measurements are pursued. These plans comprise dilepton production in nucleon-nucleon collisions (at RHIC [26], J-PARC(KEK) [27, 28], IHEP(Protvino) [29], and at the JINR (Dubna) [30], in antiproton nucleon collisions (at FAIR (GSI) [31], as well as in pion-nucleon collisions at COMPASS (CERN). Past measurements exclusively considered the unpolarized cross section, but all future programs are also aiming at polarization measurements. Including polarization of the incoming hadrons opens up a variety of new opportunities for studying the strong interaction in both the perturbative and the nonperturbative regime. Enough to mention, the opportunities to access the transversity distribution of the nucleon [32, 33] and to other TMDs describing the strength of various intriguing spin-spin or spin-orbit correlations of the parton-hadron system [34, 35] for more information on TMDs.

In order to analyze upcoming and planning new data from polarized Drell-Yan measurements it is necessary to have a general and concise formalism at hand. This step is most conveniently done in a dilepton rest frame like the Collins-Soper frame [36] with z-axis in direction in the sum of incident hadrons momenta. However, to the best of our knowledge, a complete formalism for the polarized Drell-Yan process has not been worked out yet. This is a challenge to theory and availability of the experimental data is very important for this purpose.

In addition to model-independent results, the process in the parton model approximation is usually considered. In the latter case TMDs enter in the parton model description and in a full QCD treatment [19, 20].

The parameters of the NICA collider allows to perform the important spin and polarization effect studies of:

- Drell-Yan (DY) processes with longitudinally and transversely polarized p and d beams. Extraction of unknown (poor known) Parton Distribution Functions (PDFs);
- PDFs from J/ψ production processes;
- Spin effects in baryon, meson and photon production;
- Effects in various exclusive reactions;
- Diffractive processes;
- Cross sections, helicity amplitudes and double spin asymmetries (Krisch effect) in elastic reactions;
- Spectroscopy of quarkonium.

The preliminary design of the SPD detector for spin effects studies is based on the requirements set by the DY and J/ψ productions studies. These requirements are the following:

- almost 4π geometry for secondary particles;

- precision vertex detector;
- precision tracking system ;
- precision momentum measurement of secondary particles;
- good particle identification capabilities for (μ, π, p, e etc.);
- high trigger rate capabilities.

The most of these requirements are also good for other studies mentioned in previous sections. Basing on these requirements several possible scheme of SPD are considered, one of them is similar to the detector of PAX experiment (close to NICA in kinematics) at FAIR GSI, the second one is the SPD of limited possibilities, providing the muon pair detection only and the third is the scheme of SPD based on so-called Muon Range System, which is considered as detector for PANDA muon system. The final version of the SPD will be defined after detailed Monte-Carlo simulations and consideration of requirements for other spin effects studies. The purpose is to have the simple universal detector.

Since the famous "spin crisis" in 1987, the problem of the nucleon spin structure remains one of the most intriguing puzzle of high energy physics. The central component of this problem attracting for many years enormous both theoretical and experimental efforts, is a search for answering the questions, how the spin of the proton is build up from spins and orbital momenta of its constituents. The searches brought up a concept of the parton distribution functions in nucleon, at the beginning two of them, one, f_1, for unpolarized and second, g_1, for polarized nucleons. Now we know that about 50 different parton distributions functions are needed for a complete description of the nucleon structure. While today a part of the polarized distributions can be considered as sufficiently well known, there is a number of PDFs which are either absolutely unknown or poorly known, especially the spin dependent ones, These are longitudinally polarized distributions of valence light sea, strange quarks and gluons, both sea and valence transversely polarized distributions of all flavours. This new class of PDFs is characterized by its non-trivial dependence on a transverse quark momentum. The most significant among them are Sivers and Boer-Mulders PDFs. The studies of these open questions of the nucleon structure is the first priority task for the scientific program of the second IP the NICA facility.

10.3 Polarization of Λ^0 hyperons in nucleus-nucleus collisions at MPD

V. Ladygin, A. Jerusalimov and N. Ladygina

Joint Institute for Nuclear Research, Dubna, Russia

One of the new signature of the phase transition from ordinary nuclear matter to a quark gluon plasma (QGP) can be the change of in the polarization properties of the secondary particles in the nucleus-nucleus collisions compared to the nucleon-nucleon collisions. A number of polarization observables have been proposed as a possible signature of phase transition, namely, decreasing of the Λ^0 transverse polarization in central collisions [37, 38], non-zero $\bar{\Lambda}^0$ longitudinal polarization [2–4, 39], non-zero J/ψ polarization at low $p_{\rm T}$ [12], anisotropy in di-electron production from vector mesons decay [40] (and references therein), global hyperon polarization [5] and spin-alignment of vector mesons [41] in non-central events etc.

However, at the moment there are only few results on the Λ^0 polarization in nucleus-nucleus interaction [42–45]. The precise measurements of Λ^0 polarization in nucleus-nucleus collisions at $\sqrt{s_{\rm NN}}$ of several GeV can be performed using the high luminosity MPD/NICA setup [46].

A significant amount of the data on Λ^0 polarization in pp- and pA-collisions has been accumulated at different nucleon initial energies between 6 and ∼2000 GeV. The data show large effect as a function of transverse momenta $p_{\rm T}$ and $x_{\rm F}$. Most of the models explain the Λ^0 polarization by the recombination of a polarized s-quark with an unpolarized (ud) spectator diquark. For instance, in the framework of the semiclassical recombination model of DeGrand-Miettinen [47] the Λ^0 polarization is defined by the slow s-quark spin precession.

In the case of relativistic nucleus-nucleus collisions, the expectation is that, Λ^0's coming from the region where the critical density for QGP formation has been achieved, are produced through the coalescence of independent slow sea u, d and s quarks. Therefore, the plasma creates Λ^0 with zero polarization [38]. Finally, in the case of QGP formation the depolarization effect compare to proton-induced reaction should be observed.

One expect up to 30–40% of the depolarization effect for the central events [38]. It is shown that the measurable depolarization effect can be observed at the Λ^0 transverse momenta $p_T \geq (0.6 - 0.8)$ GeV/c.

Another novel phenomena is so called global polarization [5, 41]. System in the noncentral collisions have large orbital angular momentum, which manifests in the polarization of secondary particles along the direction of the system angular momentum. Parton interaction in noncentral relativistic nucleus-nucleus collisions leads to the global polarization of the produced quarks.

The main method to measure Λ^0 polarization in nucleus-nucleus collisions is the measurement of the emission angle distribution of the decay proton with respect to the system orbital momentum L (reaction plane). Feasibility of Λ^0 polarization measurement at high energies can be estimated from UrQMD transport model. One can expect production of approximately 20 Λ^0's decaying into $p\pi^-$ pair in the central Au + Au collisions at the energies $\sqrt{s_{NN}}$ of several GeV·A. The collider mode provides more symmetrical acceptance for Λ^0 hyperons than fixed target experiments, that is significant for the proper reconstruction of the polarization. Also, the important feature of MPD setup is quite large acceptance for the detection of the both protons and pions. Therefore, it is possible to detect the Λ^0- hyperons with large transverse momenta p_T, where maximal effect in polarization properties is expected. The $y - p_T$ ideal acceptance for Λ^0's from Au + Au central collisions at $\sqrt{s_{NN}}$= 7.1 GeV for the collider mode (assuming the axial symmetry of MPD) is show in Fig. 10.1.

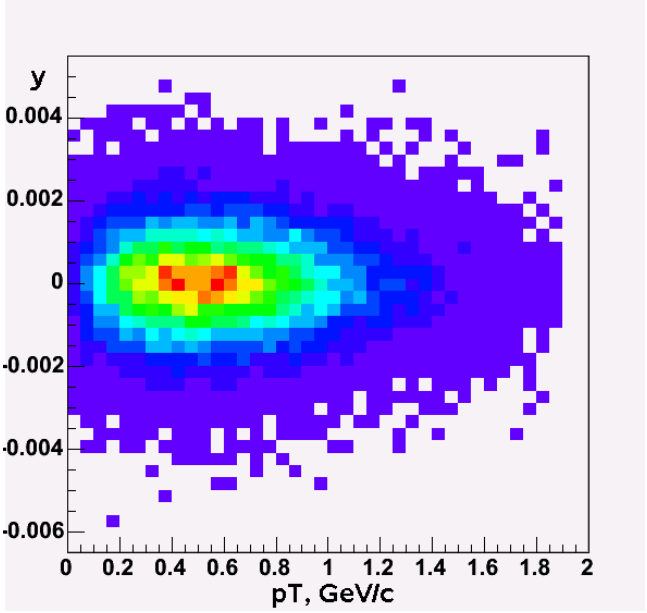

Figure 10.1: The $y - p_T$ acceptance for Λ^0's from Au + Au central collisions at $\sqrt{s_{NN}}$= 7.1 GeV for the collider mode.

Since no particle identification is required the transverse momenta p_T achieved can be large enough to measure sizable polarization effects for Λ^0's production. In this case the main source of the background is K^0_S meson decaying into $\pi^+\pi^-$ pair. The measurement of the Λ^0 polarization requires good knowledge of the kinematical parameters of the Λ^0, as well as the reaction plane and centrality value, which can be measured with zero degree calorimeter PSD or via charged particles energy flow reconstructed in the time-projection chamber.

The measurement of the Λ^0 polarization in nucleus-nucleus collisions at the energies of NICA can be a new important tool in addition to the traditional ones to study the features of mixed phase and phase transition. The study of the polarization effects in hyperon production for the collider mode can be performed at MPD setup and has certain advantages compared to the fixed target experiments.

10.4 Possible effect of mixed phase and deconfinement upon spin correlations in the $\Lambda\bar{\Lambda}$ pairs generated in relativistic heavy-ion collisions

V.L. Lyuboshitz and V.V. Lyuboshitz

Joint Institute for Nuclear Research, Dubna, Russia

Spin correlations for the $\Lambda\Lambda$ and $\Lambda\bar{\Lambda}$ pairs, generated in relativistic heavy ion collisions, and related angular correlations at the joint registration of hadronic decays of two hyperons with nonconservation of space parity are analyzed. Within the conventional model of one-particle sources, correlations vanish at enough large relative momenta. However, under these conditions, in the case of two non-identical particles ($\Lambda\bar{\Lambda}$) a noticeable role is played by two-particle annihilation (two-quark, two-gluon) sources, which lead to the difference of the correlation tensor from zero. In particular, such a situation may arise when the system passes through the "mixed phase" .

Generalities

The spin density matrix of the $\Lambda\Lambda$ and $\Lambda\bar{\Lambda}$ pairs, just as the spin density matrix of two spin-1/2 particles in general, can be presented in the following form [48–50]:

$$\hat{\rho}^{(1,2)} = \frac{1}{4}\left[\hat{I}^{(1)}\otimes\hat{I}^{(2)} + (\hat{\boldsymbol{\sigma}}^{(1)}\mathbf{P}_1)\otimes\hat{I}^{(2)} + \hat{I}^{(1)}\otimes(\hat{\boldsymbol{\sigma}}^{(2)}\mathbf{P}_2) + \sum_{i=1}^{3}\sum_{k=1}^{3} T_{ik}\hat{\sigma}_i^{(1)}\otimes\hat{\sigma}_k^{(2)}\right]; \tag{10.1}$$

in doing so, $tr_{(1,2)}\hat{\rho}^{(1,2)} = 1$.

Here $\hat{I}$ is the two-row unit matrix, $\hat{\boldsymbol{\sigma}} = (\ \hat{\sigma}_x,\ \hat{\sigma}_y,\ \hat{\sigma}_z\ )$ is the vector Pauli operator ($x, y, z \to 1, 2, 3$), $\mathbf{P}_1$ and $\mathbf{P}_2$ are the polarization vectors of first and second particle ($\mathbf{P}_1 = \langle\hat{\boldsymbol{\sigma}}^{(1)}\rangle$, $\mathbf{P}_2 = \langle\hat{\boldsymbol{\sigma}}^{(2)}\rangle$), $T_{ik} = \langle\hat{\sigma}_i^{(1)}\otimes\hat{\sigma}_k^{(2)}\rangle$ are the correlation tensor components . In the general case $T_{ik} \neq P_{1i}P_{2k}$. The tensor with components $C_{ik} = T_{ik} - P_{1i}P_{2k}$ describes the spin correlations of two particles .

It is essential that any decay of an unstable particle may serve as an analyzer of its spin state .

Let us consider the double angular distribution of flight directions for protons formed in the decays of two Λ particles into the channel $\Lambda \to p + \pi^-$, normalized by unity (the analyzing powers are $\boldsymbol{\xi}_1 = \alpha_\Lambda\mathbf{n}_1$, $\boldsymbol{\xi}_2 = \alpha_\Lambda\mathbf{n}_2$). It is described by the following formula [**?**, **?**]:

$$\frac{d^2\,w(\mathbf{n}_1,\mathbf{n}_2)}{d\,\Omega_{\mathbf{n}_1}\,d\,\Omega_{\mathbf{n}_2}} = \frac{1}{16\,\pi^2}\left[1 + \alpha_\Lambda\mathbf{P}_1\,\mathbf{n}_1 + \alpha_\Lambda\mathbf{P}_2\,\mathbf{n}_2 + \alpha_\Lambda^2\sum_{i=1}^{3}\sum_{k=1}^{3} T_{ik}n_{1i}n_{2k}\right], \tag{10.2}$$

where $\mathbf{P}_1$ and $\mathbf{P}_2$ are polarization vectors of the first and second Λ particle, T_{ik} are the correlation tensor components, $\mathbf{n}_1$ and $\mathbf{n}_2$ are unit vectors in the respective rest frames of the first and second Λ particle, defined in the common (unified) coordinate axes of the c.m. frame of the pair ($i, k = \{1, 2, 3\} = \{x, y, z\}$) .

The polarization parameters can be determined from the angular distribution of decay products by the method of moments [49, 50] – as a result of averaging combinations of trigonometric functions of angles of proton flight over the double angular distribution .

The angular correlation, integrated over all angles except the angle between the vectors $\mathbf{n}_1$ and $\mathbf{n}_2$ and described by the formula [49–52]

$$d\,w(\cos\theta) = \frac{1}{2}\,(\,1 + \frac{1}{3}\,\alpha_\Lambda^2 T\,\cos\theta)\sin\theta d\,\theta = \frac{1}{2}\,[\,1 - \alpha_\Lambda^2\,(W_s - \frac{W_t}{3})\cos\theta]\sin\theta d\,\theta, \tag{10.3}$$

is determined only by the "trace" of the correlation tensor $T = W_t - 3W_s$ (W_s and W_t are relative fractions of the singlet state and triplet states, respectively), and it does not depend on the polarization vectors (single-particle states may be unpolarized).

Due to CP invariance, the coefficients of P-odd angular asymmetry for the decays $\Lambda \to p+\pi^-$ and $\bar{\Lambda} \to \bar{p}+\pi^+$ have equal absolute values and opposite signs: $\alpha_{\bar{\Lambda}} = -\alpha_\Lambda =$
$-\,0.642$. The double angular distribution for this case is as follows [49, 50]:

$$\frac{d^2\,w(\mathbf{n}_1,\mathbf{n}_2)}{d\,\Omega_{\mathbf{n}_1}\,d\,\Omega_{\mathbf{n}_2}} = \frac{1}{16\,\pi^2}\left[1 + \alpha_\Lambda\mathbf{P}_\Lambda\,\mathbf{n}_1 - \alpha_\Lambda\mathbf{P}_{\bar{\Lambda}}\,\mathbf{n}_2 - \alpha_\Lambda^2\sum_{i=1}^{3}\sum_{k=1}^{3} T_{ik}n_{1i}n_{2k}\right], \tag{10.4}$$

(here $-\alpha_\Lambda = +\alpha_{\bar\Lambda}$ and $-\alpha_\Lambda^2 = +\alpha_\Lambda\alpha_{\bar\Lambda}$) .

Thus, the angular correlation between the proton and antiproton momenta in the rest frames of the Λ and $\bar\Lambda$ particles is described by the expression:

$$d\,w(\cos\theta) = \frac{1}{2}\,(\,1 - \frac{1}{3}\,\alpha_\Lambda^2 T\,\cos\theta)\sin\theta d\,\theta = \frac{1}{2}\,[\,1 + \alpha_\Lambda^2\,(W_s - \frac{W_t}{3})\cos\theta]\sin\theta d\,\theta, \tag{10.5}$$

where θ is the angle between the proton and antiproton momenta.

Spin correlations at the generation of $\Lambda\,\Lambda$ pairs in multiple processes

We will use the model of one-particle sources [53], which is the most adequate one in the case of collisions of relativistic ions .

Two Λ particles are identical particles. Spin and angular correlations in this case arise due to the Fermi statistics and final-state interaction.

Indeed, it is easy to see that the Fermi-statistics effect leads not only to the momentum–energy $\Lambda\,\Lambda$-correlations at small relative momenta (correlation femtoscopy), but to the spin correlations as well.

The following relation holds, in consequence of the symmetrization or antisymmetrization of the total wave function of any identical particles with nonzero spin (bosons as well as fermions) [54]:

$$(-1)^{S+L} = 1. \tag{10.6}$$

Here, S is the total spin and L is the orbital momentum in the c.m. frame of the pair. At the momentum difference $q = p_1 - p_2 \to 0$ the states with nonzero orbital momenta "die out", and only states with $L = 0$ and even total spin S survive.

Since the Λ-particle spin is equal to $1/2$, at $q \to 0$ the $\Lambda\,\Lambda$ pair is generated only in the singlet state with $S = 0$.

Meantime, at the 4-momentum difference $q \neq 0$ there are also triplet states generated together with the singlet state.

Within the conventional model of one-particle sources emitting unpolarized particles, the triplet states with spin projections $+1$, 0, and -1 are produced with equal probabilities. If correlations are neglected, the singlet state is generated with the same probability – the relative "weights" are $\widetilde{W}_t = 3/4$, $\widetilde{W}_s = 1/4$.

When taking into account the Fermi statistics and s-wave final-state interaction, which is essential at close momenta (at orbital momenta $L \neq 0$ the contribution of final-state interaction is suppressed), the fractions of triplet states and the singlet state are renormalized .

We will perform here the analysis of spin $\Lambda\Lambda$ correlations in the c.m. frame of the $\Lambda\Lambda$ pair . In the c.m. frame, we have: $q = \{0, 2\mathbf{k}\}$, where q is the difference of 4-momenta of the Λ particles, $\mathbf{k}$ is the momentum of one of the particles. In doing so, the momentum $\mathbf{k}$ is connected with the relative momentum $\mathbf{q}$ in the laboratory frame by the Lorentz transformation [55],(we use the unit system with $\hbar = c = 1$):

$$\mathbf{k} = \frac{1}{2}\,\left[\mathbf{q} + (\gamma - 1)\frac{(\mathbf{qv})\mathbf{v}}{|\mathbf{v}|^2} - \gamma\mathbf{v}\,q_0\right]; \tag{10.7}$$

here, $\mathbf{v} = (\mathbf{p}_1 + \mathbf{p}_2)/(\varepsilon_1 + \varepsilon_2)$ is the velocity of the $\Lambda\Lambda$ pair in the laboratory frame, $\gamma = (1 - v^2)^{-1/2}$ is the Lorentz factor, $\mathbf{q} = \mathbf{p}_1 - \mathbf{p}_2$ and $q_0 = \varepsilon_1 - \varepsilon_2$ are the laboratory relative momentum and energy, respectively .

The Lorentz transformations of 4-coordinates are given by the expressions:

$$\mathbf{r}^* = \mathbf{r} + (\gamma - 1)\,\frac{(\mathbf{rv})\mathbf{v}}{|\mathbf{v}|^2} - \gamma\mathbf{v}\,t, \qquad t^* = \gamma(t - \mathbf{vr}), \tag{10.8}$$

where $\mathbf{r} = \mathbf{r}_1 - \mathbf{r}_2$ and $t = t_1 - t_2$ are the differences of coordinates and times for one-particle sources in the laboratory frame .

The interference term connected with identity (quantum statistics) is determined by the expression:

$$\langle\cos 2\mathbf{kr}^*\rangle = \int W_{\mathbf{v}}(\mathbf{r}^*)\cos(2\mathbf{kr}^*)d^3\mathbf{r}^*, \tag{10.9}$$

where

$$W_{\mathbf{v}}(\mathbf{r}^*) = \int W(x)\,d\,t^* = \int W(\mathbf{r}^*, t^*)\,d\,t^*$$

is the distribution of coordinate difference between two sources in the c.m. frame of the $\Lambda\Lambda$ pair.

Meantime, the contribution of s-wave final-state interaction is expressed as follows (at the sizes of the generation region in the c.m. frame, exceeding the effective radius of interaction of two Λ particles):

$$B_{\rm int}(q) = B^{(\Lambda\Lambda)}(\mathbf{k},\mathbf{v}) = \int W_{\mathbf{v}}(\mathbf{r}^*)\, b(\mathbf{k},\mathbf{r}^*) d^3\mathbf{r}^*, \tag{10.10}$$

where the function $b(\mathbf{k},\mathbf{r}^*)$ has the structure [49, 55, 56]:

$$b(\mathbf{k},\mathbf{r}^*) = |f^{(\Lambda\Lambda)}(k)|^2 \frac{1}{(r^*)^2} + 2\,{\rm Re}\left(f^{(\Lambda\Lambda)}(k)\,\frac{e^{ikr^*}\cos\mathbf{kr}^*}{r^*}\right) - 2\,\pi\,|f^{(\Lambda\Lambda)}(k)|^2\, d_0^{(\Lambda\Lambda)}\delta^3(\mathbf{r}^*). \tag{10.11}$$

Here, $k = |\mathbf{k}|$, $r^* = |\mathbf{r}^*|$, $f^{(\Lambda\Lambda)}(k)$ is the amplitude of low-energy $\Lambda\Lambda$ scattering. In the framework of the effective radius theory [54, 57]:

$$f^{(\Lambda\Lambda)}(k) = a_0^{(\Lambda\Lambda)}\left(1 + \frac{1}{2}\,d_0^{(\Lambda\Lambda)}\,a_0^{(\Lambda\Lambda)}\,k^2 - i\,k\,a_0^{(\Lambda\Lambda)}\right)^{-1}, \tag{10.12}$$

where, by definition, $(-a_0^{(\Lambda\Lambda)})$ is the length of s-wave scattering and

$$d_0^{(\Lambda\Lambda)} = \frac{1}{k}\,\frac{d}{d\,k}\left({\rm Re}\,\frac{1}{f^{(\Lambda\Lambda)}(k)}\right)$$

is the effective radius.

The integral (10.10), with expressions (10.11, 10.12) inside, approximately takes into account the difference of the true wave function of two interacting Λ particles with the momenta $\mathbf{k}$ and $(-\mathbf{k})$ at small distances from the asymptotic wave function of continuous spectrum [56, 58].

Information about the parameters of $\Lambda\Lambda$ scattering is contained in the works studying double hypernuclei and pair correlations in the reactions with formation of two Λ particles (see, for example, [59–61]). Analysis of the experimental data leads to the conclusion that the length of $\Lambda\Lambda$ scattering is comparable by magnitude ($\approx (-20)$ fm) with the length of neutron–neutron scattering [61].

Spin correlations at the generation of $\Lambda\bar{\Lambda}$ pairs in multiple processes

In the framework of the model of independent one-particle sources, spin correlations in the $\Lambda\bar{\Lambda}$ system arise only on account of the difference between the interaction in the final triplet state ($S = 1$) and the interaction in the final singlet state . At small relative momenta, the s-wave interaction plays the dominant role as before, but, contrary to the case of identical particles ($\Lambda\Lambda$), in the case of non-identical particles ($\Lambda\bar{\Lambda}$) the total spin may take both the values $S = 1$ and $S = 0$ at the orbital momentum $L = 0$. In doing so, the interference effect, connected with quantum statistics, is absent .

If the sources emit unpolarized particles, then, in the case under consideration, the correlation function describing momentum-energy correlations has the following structure (in the c.m. frame of the $\Lambda\bar{\Lambda}$ pair):

$$R(\mathbf{k},\mathbf{v}) = 1 + \frac{3}{4}\,B_t^{(\Lambda\bar{\Lambda})}(\mathbf{k},\mathbf{v}) + \frac{1}{4}\,B_s^{(\Lambda\bar{\Lambda})}(\mathbf{k},\mathbf{v}). \tag{10.13}$$

The components of the correlation tensor for the $\Lambda\bar{\Lambda}$ pair are as follows:

$$T_{ik} = \frac{B_t^{(\Lambda\bar{\Lambda})}(\mathbf{k},\mathbf{v}) - B_s^{(\Lambda\bar{\Lambda})}(\mathbf{k},\mathbf{v})}{4 + 3\,B_t^{(\Lambda\bar{\Lambda})}(\mathbf{k},\mathbf{v}) + B_s^{(\Lambda\bar{\Lambda})}(\mathbf{k},\mathbf{v})}\,\delta_{ik}; \tag{10.14}$$

here the contributions of final-state triplet and singlet $\Lambda\bar{\Lambda}$ interaction are determined by the expression (analogously to Eqs.(10.10-10.12) for the $\Lambda\Lambda$ interaction [49, 56], with the replacement $\cos\mathbf{kr}^* \to e^{i\,\mathbf{k}\,\mathbf{r}^*}$ in Eq.(10.12) owing to the non-identity of the particles Λ and $\bar{\Lambda}$ [55]) :

$$B_{s(t)}^{(\Lambda\bar{\Lambda})}(\mathbf{k},\mathbf{v}) = |f_{s(t)}^{(\Lambda\bar{\Lambda})}(k)|^2\,\langle\frac{1}{(r^*)^2}\rangle + 2\,{\rm Re}\left(f_{s(t)}^{(\Lambda\bar{\Lambda})}(k)\,\langle\frac{e^{ikr^*}e^{i\,\mathbf{kr}^*}}{r^*}\rangle\right) -$$

$$-\frac{2\pi}{k}\,|f^{(\Lambda\bar{\Lambda})}_{s(t)}(k)|^2\,\frac{d}{d\,k}\left(\mathrm{Re}\,\frac{1}{f^{(\Lambda\bar{\Lambda})}_{s(t)}(k)}\right)\,W_{\mathbf{v}}(0), \tag{10.15}$$

where $f^{(\Lambda\bar{\Lambda})}_{s(t)}(k)$ is the amplitude of the s-wave low-energy singlet (triplet) $\Lambda\bar{\Lambda}$ scattering.

At sufficiently large values of k, one should expect that [56]:

$$B^{(\Lambda\bar{\Lambda})}_{s}(\mathbf{k},\mathbf{v}) = 0, \qquad B^{(\Lambda\bar{\Lambda})}_{t}(\mathbf{k},\mathbf{v}) = 0.$$

In this case the angular correlations in the decays $\Lambda \to p + \pi^-$, $\bar{\Lambda} \to \bar{p} + \pi^+$, connected with the final-state interaction, are absent :

$$T_{ik} = 0, \qquad T = 0.$$

Angular correlations in the decays $\Lambda \to p + \pi^-$ and $\bar{\Lambda} \to \bar{p} + \pi^+$ and the "mixed phase"

Thus, at sufficiently large relative momenta (for $k \gg m_\pi$) one should expect that the angular correlations in the decays $\Lambda \to p + \pi^-$ and $\bar{\Lambda} \to \bar{p} + \pi^+$, connected with the interaction of the Λ and $\bar{\Lambda}$ hyperons in the final state (i.e. with one-particle sources) are absent . But, if at the considered energy the dynamical trajectory of the system passes through the so-called "mixed phase", then the two-particle sources, consisting of the free quark and antiquark , start playing a noticeable role . For example, the process $s\,\bar{s} \to \Lambda\bar{\Lambda}$ may be discussed .

In this process, the charge parity of the pairs $s\bar{s}$ and $\Lambda\bar{\Lambda}$ is equal to $C = (-1)^{L+S}$, where L is the orbital momentum and S is the total spin of the fermion and antifermion . Meantime, the CP parity of the fermion–antifermion pair is $CP = (-1)^{S+1}$.

In the case of one-gluon exchange, $CP = 1$, and then $S = 1$, i.e. the $\Lambda\bar{\Lambda}$ pair is generated in the triplet state; in doing so, the "trace" of the correlation tensor $T = 1$.

Even if the frames of one-gluon exchange are overstepped, the quarks s and $\bar{s}$, being ultrarelativistic, interact in the triplet state ($S = 1$) . In so doing, the primary CP parity $CP = 1$, and, due to the CP parity conservation, the $\Lambda\bar{\Lambda}$ pair is also produced in the triplet state. Let us denote the contribution of two-quark sources by x. Then at large relative momenta $T = x > 0$.

Apart from the two-quark sources, there are also two-gluon sources being able to play a comparable role. Analogously with the annihilation process $\gamma\gamma \to e^+e^-$, in this case the "trace" of the correlation tensor is described by the formula (the process $g\,g \to \Lambda\bar{\Lambda}$ is implied):

$$T = 1 - \frac{4\,(1-\beta^2)}{1 + 2\,\beta^2\,\sin^2\theta - \beta^4 - \beta^4\,\sin^4\theta}, \tag{10.16}$$

where β is the velocity of Λ (and $\bar{\Lambda}$) in the c.m. frame of the $\Lambda\bar{\Lambda}$ pair, θ is the angle between the momenta of one of the gluons and Λ in the c.m. frame (see [62]). At small β ($\beta \ll 1$) the $\Lambda\bar{\Lambda}$ pair is produced in the singlet state (total spin $S = 0$, $T = -3$), whereas at $\beta \approx 1$ – in the triplet state ($S = 1$, $T = 1$). Let us remark that at ultrarelativistic velocities β (i.e. at extremely large relative momenta of Λ and $\bar{\Lambda}$) both the two-quark and two-gluon mechanisms lead to the triplet state of the $\Lambda\bar{\Lambda}$ pair ($T = 1$).

In the general case, the appearance of angular correlations in the decays $\Lambda \to p + \pi^-$ and $\bar{\Lambda} \to \bar{p} + \pi^+$ with the *nonzero* values of the "trace" of the correlation tensor T at large relative momenta of the Λ and $\bar{\Lambda}$ particles may testify to the passage of the system through the "mixed phase" (see also [63]).

Summary

So, it is advisable to investigate the spin correlations of $\Lambda\Lambda$ and $\Lambda\bar{\Lambda}$ pairs produced in relativistic heavy ion collisions .

The spin correlations are studied by the method of angular correlations – method of moments .

The spin correlations, as well as the momentum-energy ones, make it possible to determine the space-time characteristics of the generation region and, besides, the parameters of low-energy scattering of Λ on Λ and Λ on $\bar{\Lambda}$. They should be investigated jointly with the momentum-energy correlations.

One should expect the sufficient statistics for (anti)baryon pairs production at very high energies only. Thus the suggested observables may be considered as a reference point for the studies of phases of lower (NICA) energies.

Bibliography

[1] A. V. Efremov and O. V. Teryaev, Phys. Lett. **B 150,** 383 (1985).

[2] M. Jacob, Z. Phys. **C38**, 273 (1988).

[3] M. Jacob and J. Rafelski, Phys. Lett. **B 190,** 173 (1987).

[4] B. Betz, M. Gyulassy and G. Torrieri, Phys. Rev. **C 76,** 044901 (2007), [arXiv:0708.0035].

[5] Z.T. Liang and X.N. Wang, Phys. Rev. Lett. **94,** 102301 (2005) [nucl-th/0410079].

[6] A.V. Efremov, L. Mankiewicz and N.A. Tornqvist, Phys. Lett. **B 284,** 394 (1992).

[7] D. Kharzeev, Phys. Lett. **B 633,** 260 (2006).

[8] D. Kharzeev, L. McLerran and H. Warringa, Nucl. Phys. **A 803,** 227 (2008), [arXiv:0711.0950].

[9] P. Hoyer, Phys. Lett. **B 187,** 162 (1987).

[10] E.L. Bratkovskaya, O.V. Teryaev and V.D. Toneev, Phys. Lett. **B 348,** 283 (1995).

[11] R. Arnaldi *et al.* (NA60 Collaboration), [arXiv:0812.3100].

[12] B. L. Ioffe and D. E. Kharzeev, Phys. Rev. **C 68,** 061902(R) (2003), [hep-ph/0306176].

[13] S. D. Drell and T. M. Yan, Phys. Rev. Lett. **2,** 316 (1970); **25**, 902 (1970).

[14] J. C. Collins, Acta. Phys. Polon. **B 34,** 3103 (2003).

[15] J. C. Collins, T. C. Rogers and A. M. Stasto, Phys. Rev. **D 77,** 085009 (2008).

[16] D. Boer and P. J. Mulders, Phys. Rev. **D 57,** 5780 (1998).

[17] D. W. Sivers, Phys. Rev. **D 41,** 83 (1990); **43**, 261 (1991).

[18] J. C. Collins and D. E. Soper, Nucl. Phys. **B 193,** 381 (1981); **213**, 545 (1983)].

[19] X. D. Ji, J. P. Ma and F. Yuan, Phys. Rev. **D 71,** 034005 (2005); Phys. Lett. **B 597,** 299 (2004).

[20] J. C. Collins and A. Metz, Phys. Rev. Lett. **93,** 252001 (2004).

[21] A. Kotzinian, Nucl. Phys. **B 441,** 234 (1995).

[22] S. Arnold, A. Metz and M. Schlegel, [arXiv:0809.2262].

[23] A. Airapetian *et al.* (HERMES Collaboration), Phys. Lett. **B 648,** 164 (2007).

[24] R. Seidl, M. Grosse-Perdekamp and A. Ogawa (Belle Collaboration), Phys. Rev. **D 78,** 032011 (2008).

[25] S. D. Drell and T. M. Yan, Annals Phys. **66**, 578 (1971); **281**, 450 (2000).

[26] G. Bunce *et al.*, http://spin.riken.bnl.gov/rsc/report/spinplan_2008/ spinplan08.pdf, *Plans for the RHIC Spin Physics Program.*

[27] J. C. Peng *et al.*, http://j-parc.jp/NuclPart/pac_0606/pdf/p04-Peng.pdf, J-PARC Proposal P04 (2006).

[28] Y. Goto *et al.*, http://j-parc.jp/NuclPart/pac_0801/pdf/Goto.pdf, J-PARC Proposal P24 (2007).

[29] V. V. Abramov *et al.*, [hep-ex/0511046].

[30] A. Sissakian, O. Shevchenko, A. Nagaytsev, and O. Ivanov, [arXiv:0807.2480].

[31] V. Barone *et al.*, (PAX Collaboration), [arXiv:hep-ex/0505054].

[32] M. Anselmino, V. Barone, A. Drago and N. N. Nikolaev, Phys. Lett. **B 594,** 97 (2004).

[33] A. V. Efremov, K. Goeke and P. Schweitzer, Eur. Phys. J. **C 35,** 207 (2004).

[34] U. D'Alesio and F. Murgia, Progr. Part. Nucl. Phys. **61,**394 (2008).

[35] V. Barone, A. Drago and P. G. Ratcliffe, Phys. Rep. **359,** 1 (2002).

[36] J. C. Collins and D.E. Soper, Phys. Rev. **D 16,** 2219 (1977).

[37] A. D. Panagiotou, Phys. Rev. **C 33,** 1999 (1986).

[38] A. Ayala, E. Cuautle, G. Herrera and L. M. Montano, Phys. Rev. **C 65,** 024902 (2002).

[39] G. Herrera, G. Magnin and L. M. Montano, Eur. Phys. J. **C 39,** (2005) 95.

[40] E. L. Bratkovskaya, W. Cassing and U. Mosel, Z. Phys. **C75**, 119 (1997).

[41] Z.-T. Liang and X.-N. Wang, Phys. Lett. **B 629,** 20 (2005).

[42] J. Harris *et al.*, Phys. Rev. Lett. **47,** 229 (1981).

[43] M. Anikina *et al.*, Z. Phys. **C25**, 1 (1984).

[44] R. Bellwied *et al.*, Nucl. Phys. **A 698,** 499 (2002).

[45] B. I. Abelev *et al.*, Phys. Rev. **C 76,** 024915 (2007).

[46] V. P. Ladygin, A. P. Jerusalimov and N. B. Ladygina, [arXiv:0806.3867].

[47] T. A. DeGrand and H. I. Miettinen, Phys. Rev. **D 23,** 1227 (1981); **24**, 2419 (1981); **31**, 661(E) (1985).

[48] V. L. Lyuboshitz and M. I. Podgoretsky, Yad. Fiz. **60**, 45 (1997).

[49] V. L. Lyuboshitz, *Proceedings of XXXIV PNPI Winter School . Physics of Atomic Nuclei and Elementary Particles*, St-Petersburg (2000), p.402.

[50] R. Lednicky and V. L. Lyuboshitz, Phys. Lett. **B 508,** 146 (2001).

[51] G. Alexander and H.J. Lipkin, Phys. Lett. **B 352,** 162 (1995) .

[52] R. Lednicky, V. V. Lyuboshitz and V. L. Lyuboshitz, Yad. Fiz. **66**, 1007 (2003)

[53] M. I. Podgoretsky, Fiz. Elem. Chast. At. Yadra **20**, 628 (1989)

[54] L. D. Landau and E. M. Lifshitz, *Quantum Mechanics. Nonrelativistic Theory* (in Russian), (Nauka, Moscow, 1989).

[55] V. L. Lyuboshitz and V. V. Lyuboshitz,*Proceedings of XXXVII and XXXVIII Winter Schools of the Petersburg Institute of Nuclear Physics. Physics of Atomic Nuclei and Elementary Particles*, St.-Petersburg (2004), p.390 .

[56] R. Lednicky and V.L. Lyuboshitz, Yad. Fiz. **35**, 1316 (1982)

[57] H. A. Bethe and P. Morrison, *Elementary Nuclear Theory* (New York, 1956) p.10.

[58] V. L. Lyuboshitz, Yad. Fiz. **41**, 820 (1985) [Sov. J. Nucl. Phys. **41**, 529 (1985)].

[59] S. Iwao and M. Shako, Progr. Theor. Phys. **48**, 1412 (1972).

[60] A. O. Ohnishi *et al.*, Nucl. Phys. **A 670,** 297 (2000).

[61] I. R. Afnan, Nucl. Phys. **A 639**, 55c (1998).

[62] W. H. McMaster, Rev. Mod. Phys. **33**, 8 (1961).

[63] V. L. Lyuboshitz and V. V. Lyuboshitz, Yad. Fiz. **73**, 836 (2010); Phys. At. Nucl. **73**, 805 (2010).

11 Related topics

11.1 Determination of the equation of state of dense matter

S. Fantoni[a], *S. Gandolfi*[b], *A. Illarionov*[c], *F. Pederiva*[c,d] *and K. Schmidt*[e]

[a] *International School for Advanced Studies, SISSA, Italy and INFN, Trieste, Italy;*
[b] *Theoretical Division, Los Alamos National Laboratory, Los Alamos, USA;*
[c] *Dipartimento di Fisica dell'Universitá di Trento, Trento, Italy;*
[d] *INFN, Gruppo Collegato di Trento, Trento, Italy;*
[e] *Department of Physics, Arizona State University, USA*

In order to understand the properties of matter at intermediate densities and temperatures, it is important to gather knowledge on the regime defined by densities of the order $n_0 < n < (3-4)n_0$, and temperatures between 0 and 10 – 20 MeV. This regime is particularly challenging. At such densities it is completely not obvious that the knowledge on the nucleon-nucleon and many-nucleon interactions, that has been developed essentially fitting properties of small nuclei, is s till applicable. On the other hand, this regime is at present completely unaccesible to QCD.

The constraints coming from astrophysical observations (in particular on the properties of neutron stars) have been partly supplied with information coming from heavy-ion collisions. However, the present situation does not allow for a definitive discrimination among the variety of proposed models that have been developed in the last two decades.

The development of a facility allowing for reaching dense matter conditions might help to improve the situation of uncertainty that permeates the field.

Recent methodological developments allowed for a more systematic approach to the study of the properties of high density nucleonic matter. In particular, by means of the Auxiliary Field Diffusion Monte Carlo (AFDMC) method [1], it is possible to solve with extremely high accuracy the Schrodinger equation with realistic potentials for numbers of nucleons A which might be of order 100, allowing therefore to make predictions on the properties of nuclear [2] and neutron [3] matter.

This is a big step forward, because the limits on number of nucleons that can be treated efficiently has been moved forward by at least one order of magnitude. Even more important, however, is the fact that for a given interaction (more or less phenomenological), it is possible to obtain solutions which are not plagued by uncontrolled approximations. It is therefore possible to start discussing with no ambiguity the portability of current interactions (like Argonne-Urbana AV18+UIX or Illinois ILX potentials) to the high density regime, and to possibly develop alternatives that might at least give phenomenological input for attacking important problems.

In this context, for instance, we have recently developed a density-dependent interaction (DDI) following the initial intuition of Lagaris and Pandharipande [4] which, after fitting three parameters on basic properties of symmetrical nuclear matter (saturation density, energy and compressibility at saturation density), yields an equation of state (EOS) which is by far softer than the celebrated Akmal, Pandharipande and Ravenhall [5] EOS, both for symmetrical nuclear matter and pure neutron matter, and consequently gives estimates of Neutron Star properties (such as Mass/Radius ratio, momentum of inertia, and others) that are much better reconciled with observations, and closer to extrapolated constraints.

Once more, the importance of such an approach is that a sound starting point for phenomenological discussion and further developments is now available. In particular we want to mention two future developments which might be relevant for the regime of densities and temperatures of matter that should be reached in NICA. The study of the occurrence of a transition to a mixed nucleon-hyperon phase. Despite there is a large amount of literature present on the subject, the determination of the onset of the presence of hyperons depends on two unknowns: the hyperon-nucleon interaction (about which the amount of experimental information is very limited) and the equation of state of nuclear/neutron matter.

The presence of these two unknowns at the same time generated a wide variety of predictions. The use of AFDMC and DDI can help to narrow down the range of such predictions, allowing for a more stringent comparison with possible new constraints that should emerge from experiments as exemplified in Fig. 11.1.

The second issue concerns the temperature effects on the equation of state. Once more, the information available is very limited. From the point of view of microscopic calculations the neater approach would be the development of a code capable to compute the expectation of operators in the Quantum Canonical Ensemble

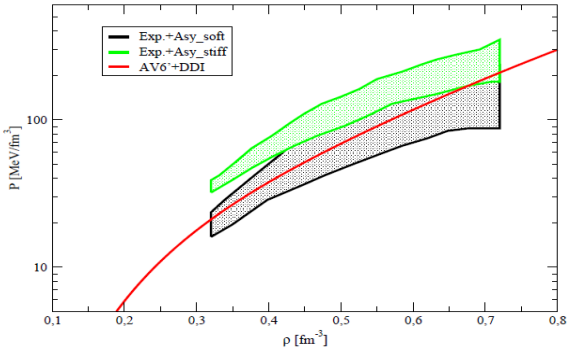

Figure 11.1: Zero-temperature EOS for neutron matter. The upper and lower shaded regions for neutron matter consistent with the experimental of data of heavy-ion collision after inclusion of the pressures from asymmetry terms with strong and weak density dependence, respectively [6]. The line shows our prediction for neutron matter EOS.

(always neglecting relativistic effects) by means of Path Integral Monte Carlo techniques. In principle this would allow for a rigorous study of nuclear/neutron matter up to temperatures and densities very close to the phase transitions of interest in NICA. However, approximated approaches based on the extrapolation of the temperature behavior from Fermi Hypernetted Chain calculations [7] could be used in order to include temperature dependence up to 20 – 25 MeV. This fact is important because it provides a guide the corrections necessary to have a sensible comparison between $T = 0$ results yielded by AFDMC calculations. Work along this line has been already in progress.

We believe that the availability of a facility like NICA will be important to clarify important issues not only from the QCD point of view, but also for as concerns some obscure points that are still present in the understanding of the nucleon-nucleon interactions and of the phase transitions that matter undergoes at medium densities and relatively low temperatures, a physics that is extremely relevant for a theoretical analysis of dense stars, in particular for the properties of the inner crust and of the exterior core.

11.2 Relativistic nuclear fusion reactions and QED of strong fields: novel possibilities at the NICA facility

A. Kovalenko, A. Sissakian and A. Sorin

Joint Institute for Nuclear Research, Dubna, Russia

The main goal of the proposed two storage rings of the NICA facility is to provide head-on collisions of heavy ions [8]. This short remark is aimed at discussing of the proposal for extending the research program at NICA to investigate the interactions of relativistic multi-particle systems having a small difference in the momentum. In other words we would like to consider interactions (collisions) of **relativistic co-moving particles**. Different ion-ion spices, light polarized nuclei with different orientation of spin or even electron-ions can be used as interacting objects. The construction of a facility to study electron-ion collisions was proposed at JINR in 1989 [9]. The electron-ion mode of operation was proposed for the RIKEN facility at Japan [10], nevertheless the maximum ion energy was limited to about 0.8 GeV/A. The peak energy of electron beam was chosen at 2.5 GeV to produce highly brilliant X-rays, if necessary. As it has been shown [11], the optimization of the collider lattice can make it possible to reach practically the same luminosity of ion-ion collisions for the case of co-moving beams as those for head-on collisions.

The use of co-moving particle interactions make it possible to study the interactions of heavy ions near and below the Coulomb barrier, the momentum transfer can be controlled by adjustment of the machine parameters. The observation of ultra-peripheral interactions of different highly charged ions is also possible. The production of e^+e^--pairs can be observed.

The technical realization of the co-moving ion-ion interaction mode appears to be feasible. Several conditions should be taken into account:

- beam crossing angle is not zero in this case to provide necessary separation between the beams after

crossing point;

- beam crossing angle is chosen in some range, let say, between 10 mrad $< \theta <$ 150 mrad.
- the collider magnets power supply system should be flexible enough and provide necessary changing of supply current direction and independent power supplies of the magnetic elements of the insertions near the beam intersection points;
- longitudinal momentum of the reaction products will dominate over the transverse one, thus forward detector and particle separation channel are needed. It is important that in the case of non-zero crossing angle we don't need to work with bunched beams.

Thus, the stochastic cooling will operate well. The conditions for electron cooling system are also very comfortable. The total number of stored particles in the coasting beams can be increased.

The case of co-moving particle interactions is most reasonable to consider in the range of beam kinetic energy of 2 GeV/A. The Coulomb forces in the circulating beams is suppressed by a factor of 10, the transverse component of ion momentum due to non-zero crossing angle will be in the range from 20 MeV/A to 300 MeV/A. The difference between longitudinal momentum of the interacting particles can be varied in fine steps over the range of ± 0.5 GeV/A and wider. Note that it is possible to use co-moving collision mode at large difference of the particles longitudinal momentum to increase the luminosity of heavy ion collisions at the lowest requested energies at NICA. The luminosity of co-moving particle interaction is estimated to $10^{27} cm^{-2} s^{-1}$ for heavy ions and to $10^{31} cm^{-2} s^{-1}$ for the light ions including polarized ones.

11.3 Development of highly charged ion sources for NICA injector and its possible applications for nanofabrication and in medicine

D.E. Donets, E.D. Donets, E.E. Donets, V.V. Salnikov V.B. Shutov

Veksler&Baldin Laboratory of High Energy Physics, JINR, Dubna, Russia

Novel type of highly charged ions sources – Electron String Ion Sources (ESIS) is under development in JINR in framework of NICA project. This ion sources produce intense beams of highly charged ions of heavy elements, up to gold. Two major applications of this ion sources: for nanofabrication and for cancer therapy are briefly discussed.

Novel type of ion sources - Electron String Ion Source of highly charged ions is for injector complex of NICA project. According to the Project parameters this new ion source Krion-6T (which is under construction now) should produce up to $3 \cdot 10^9$ ppp of Au^{32+}. However, this ion source also could produce higher charge states: up to Au^{69+} for Krion-6T. The operational ion source of ESIS type – Krion-2 ESIS has produced ion beams up to Au^{54+} in stand laboratory conditions in 2009 (see [12] and refs therein). In February-March 2010 Krion-2 ESIS was successfully used as injector of highly charged Xe^{42+} ions during 41-st Nuclotron run. Krion-2 ESIS has produced up to 3x10^8 Xe^{42+} ions per pulse; this ion beams were accelerated in LU-20 LINAC and further in Nuclotron up to relativistic energies and used for physics experiments.

As a result, the high ionization efficiency as well as the reliability and stability of Electron String Ion Source Krion-2 in an automatic regime of it's work have been demonstrated. The present status of studies and the tests on a synchrotron show that Electron String Ion Source has become a new and useful tool for accelerator facilities.

However, highly charged ions of heavy elements, produced and slowly extracted from the ion source could be used in many interesting applications. Nonaccelerator physics of highly charged ion is relatively new developing branch. We would like to describe only two possible applications which could be considered in parallel to the main stream of the NICA project development.

Production of nanostructures by slow highly charged ions for information storage and processing at nanometer range

A highly charged ion (HCI) reacts intensely with matter through deposition of its large potential energy. The potential energy is equal to the summation of ionization energy to produce the HCI concerned and increased rapidly with the ion charge. For example, potential energy of Xe^{44+} reaches 48 keV while singly charged Xe^{+1} ion has only 12 eV of potential energy. Another feature is that HCI has a large number of unoccupied orbitals. When HCI approaches to a solid surface, the HCI captures a lot of electrons to the orbitals and releases the

large potential energy with in a short time (< 100 fs) onto a small region of the surface. Such interaction of the HCI with the surface (previously called as "Coulomb explosion") give two important charactersitics; one is a high yield of secondary electron emission and the other is terrawatts power flux deposition onto nanoregion. This effect is essentially different from that induced by irradiation of energetic low charged ions, where the kinetic energy of the primary particles plays a major role.

A nanoscopically modified materials (such as HOPG – highly oriented pyrolithic graphite, Si(111) and others) by slow highly charged ions, such as Xe^{44+}, I^{51+} have craters and hillocks of a typical size of 5 – 10 nm in diameter and about 1.5 nm in depth/height. Such surface modifications result from deposition of huge potential energy of HCIs to a nanometer sized region of the surface within a short time, which corresponds to a power flux density of > 1 TW/cm^2. Although Terawatt power density is also achieved with a short pulsed laser, the laser beam waist is about 500 nm in a diameter at least, while HCI can deposit terawatts power flux onto a nanoregion. Usually images of the surface nanomodifications by HCI are obtained with use of scanning tunneling microscope (STM) [13].

Surface modification by HCI opens possibility to create large-scale devices with dimensions in the 10 nm range. First application could be information storage. The extremely small size of ion damage sites (1-10 nm) suggests that the ultimate limit for information density using this technique is about 10^{12} bits/cm^2, or 1000 Gb/cm^2 that is few order of magnitude higher than the best modern devices.

In order to perform the HCI based nano-processes efficiently, HCI beams should have high flux density and intensity. Therefore HCIs have to be efficiently extracted from the ion source and transported precisely in a beam line with well designed ion optical elements. Nano-sized capillares seem to be one of the efficient tools for precise ion steering transportation [14].

Several areas need to be explored before ion nanofabrication can be exploited: the ion/surface interaction and the nature of the damage; materials and (possibly?) chemical processing; the limits of size and density of independent devices; development of ion sources to higher flux of HCI ions of heavy elements; steering the ions to nanometer precision; information processing in nanometer range et cetera...

The planned development of the ESIS-type ion sources in framework of the NICA project could give an excellent opportunity to develope this area since this ion sources provide intense beams of heavy HCI's up to gold, which are mostly applicable for the described nano-applications.

Resonant combination cancer therapy – newly proposed method with use of highly charged ion source of highest intensity

The new scheme of cancer therapy includes source of highly charged heavy ions of highest intensity only and no any accelerators. Conceptual basis of this scheme is following [15]. Well-tested technology already exists to deliver 1.9 nm gold particles to achieve considerable concentration of gold in tumor, while maintaining an order of magnitude less concentration in the normal tissue due to the trapping of the gold nanoparticles within the tumor vasculature.

The scheme proposed involves impacting slow bare or hydrogen-like heavy ions onto a surface, resulting in one high energy photon (> 30 keV) per K-shell vacancy with the energy of these photons being dictated by the atomic number (Z) of the highly charged ions used. A particular ion is selected so that these photons lie just above the K-edge of a heavy ion species (gold) preferentially incorporated into the tumor leading to a large local dose as required. **Radiation in the 'Desired Radiation Window' efficiently produces K-shell holes in the gold nanoparticle. After a radiative transisition, this system stabilises predominantly by Auger decay that should destroy tumor cells in surroundings of gold nano-particle due to electron flux during fs.**

An example of the set up for the proposed from of radiotherapy is following: ions are transported from a high intensity ion source (ESIS or EBIS) which has been configured to produce predomimantly bare ot hydrogen-like heavy ions, chosen so that the K-alpha radiation from these ions lies just above the K-edge of a heavy atom dopant (gold) previously incorporated into the tumor. These ions are transported through rotatable guntry and focused onto a thin aluminium window (0.25 – 0.5 mm width). This window acts both as an electron rich target, generating the high energy photons and also as a high-pass filter, attenuating low energy (< 20 keV) x-rays. The resultant x-rays are then collimated using s multileaf collimator so as to target tumor.

The ion source requirements for this scheme are following: 10^{11} – 10^{12} ions/second for highly charged (like Au^{78+}) heavy ions. These requirements are still beyond present ion source capabilities. However, ions source development toward more highly charge states and intensity should give a real chance for successful realization of this new, safe and relatively cheap form of nonaccelerator cancer therapy.

Basic and applied researches with highly charged intense ion beams of heavy elements, produced with ESIS-type ion sources have a very wide area for applications in nano-sceiences and medicine. Ion source development program in framework of the NICA project has a great potential for various nonaccelerator applications as well.

11.4 Using Specific Nuclei for NICA Experiments

P. Filip

Institute of Physics, Slovak Academy of Sciences, Bratislava

Ground-state deformation of nuclei in relativistic heavy ion collisions is often neglected, or considered to be a complication. However, strong prolate deformation of some nuclei allows one to increase significantly the energy density of the created hot and compressed QCD matter. The reason for such increase is two-fold: a) transverse area of the interaction zone gets smaller for tip-tip collisions of prolate nuclei if compared to spherical nuclei with similar number of participating nucleons; b) number of binary nucleon-nucleon interactions N_{coll} is higher for tip-tip configuration, which further increases the multiplicity of secondary charged particles N_{ch} in central collisions.

Simulations based on Optical Glauber Model predict [16] maximal transverse energy density ε_T achievable in collisions of prolate ^{165}Ho nuclei ($\beta_2 \approx 0.3$) to be higher than in Pb+Pb collisions (see Fig.11.2). Colliding heavy prolate nuclei with proton number $Z > 90$ allows one to increase further [17] the energy density by 30-40%.

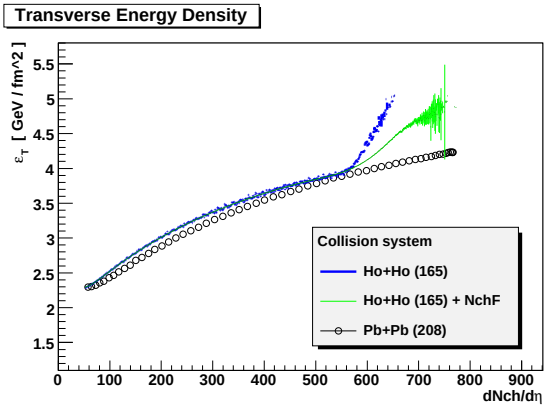

Figure 11.2: Transverse energy density from OGM simulation [16] for $\sqrt{s_{\rm NN}}$=200GeV/n.

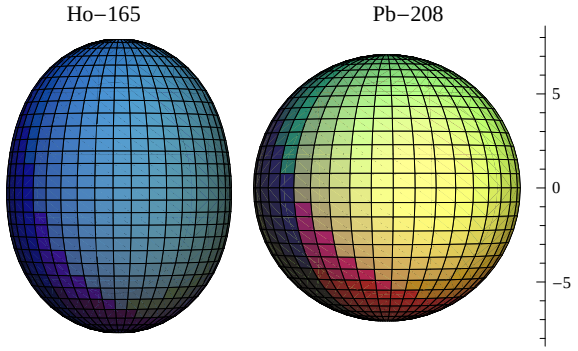

Figure 11.3: The size and shape of ^{165}Ho (deformed) and ^{208}Pb (spherical) nuclei.

Additional reasons exist for colliding specific (deformed) nuclei in a relativistic collider. In the very-high-multiplicity (VHM) collisions of prolate nuclei a cusp-like drop of elliptic flow magnitude v_2 is expected to occur [18]. The observation of such behaviour would confirm our understanding of the secondary particle

generation mechanism and of the relation between the initial eccentricity and observed elliptic flow. Although, at NICA collision energies the elliptic flow magnitude v_2 is expected to be small, one can measure elliptic flow fluctuations σ_{v_2} via difference of v_2 cumulants: $v_2\{2\}^2 - v_2\{4\}^2 \approx 2\sigma^2_{v_2} + \delta_2$ (where δ_2 is non-flow [19]). Since natural Nd and Sm elements contain spherical (^{142}Nd and ^{144}Sm) and strongly deformed [20] stable nuclei (^{150}Nd and ^{154}Sm), one can test the sensitivity of elliptic flow fluctuations to the initial eccentricity fluctuation using a single element in the ion source of a collider.

Understanding the influence of ground-state deformation of nuclei on various observables in heavy ion collisions can be important also for the measurement of specific phenomena. For example, collisions of ^{96}Zr+^{96}Zr and ^{96}Ru+^{96}Ru nuclei are suitable for testing the isospin-dependent quantities, the influence of large magnetic fields (due to spectator protons) on e.g. the elliptic flow of charged particles, or for the attempts to observe chiral magnetic effect [21]. However, ^{96}Ru nucleus is almost spherical, while ^{96}Zr is prolate [20]. Therefore, one needs to understand and subtract deformation effects from the true signal differences expected in $^{96}_{40}$Zr and $^{96}_{44}$Ru collisions. Such subtraction can be done by comparing ^{144}Sm+^{144}Sm with ^{154}Sm+^{154}Sm collisions.

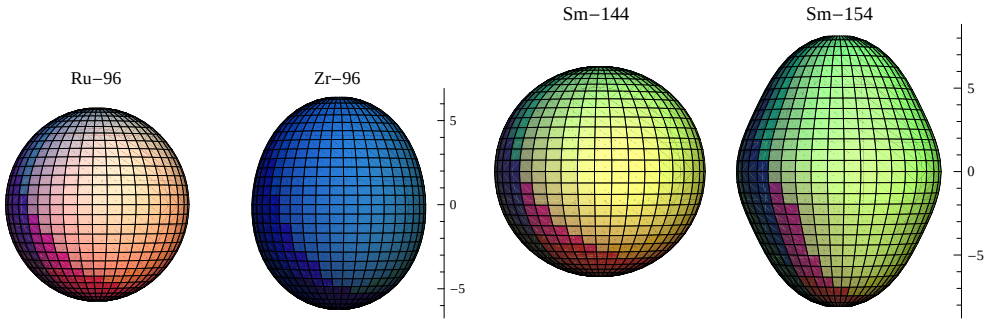

Figure 11.4: *Left:* Nuclei $^{96}_{40}$Ru and $^{96}_{44}$Zr. *Right:* ^{144}Sm and ^{154}Sm nuclei.

Once the equation of state of QCD matter at NICA energies is known well enough, one may also attempt to study internal properties of nuclei using sensitive observables in nucleus-nucleus collisions. Besides the static deformation $\langle\beta_2\rangle$, existence of dynamic quadrupole moment (due to shape vibrations) of some nuclei has been addressed [22] recently. Quantum shape vibration in the ground state (a distribution of β_2 parameter described by wave function $|\psi_{vib}(\beta_2)|^2$) can be large in some nuclei due to the specific shape of their $E(\beta_2)$ potential energy surface. A substantial momentum-space correlation, corresponding to collective quadrupole vibrations of nucleons in the wave function of nuclei, might influence the elliptic flow and initial eccentricity fluctuations. It would be fascinating, if such aspects of the internal structure of nuclei could be observable at NICA experiments. For example, the observed magnitude of elliptic flow [23] in ^{63}Cu+^{63}Cu collisions at $\sqrt{s_{\rm NN}}$=22.4GeV/n exceeds our expectations (the simulations) by factor 2x and the explanation is still missing.

11.5 Inputs for viscous Cosmology from NICA experiments

A. Tawfik

Egyptian Center for Theoretical Physics (ECTP), MTI University, Cairo-Egypt

The dissipative effects, including both bulk and shear viscosity, are supposed to play a very important role in the early evolution of the Universe. The first attempts at creating a theory of relativistic fluids were those of Eckart [24] and Landau and Lifshitz [25]. These theories are now known to be pathological in several respects. Regardless of the choice of the equation of state, all equilibrium states in these theories are unstable and in addition signals may be propagated through the fluid at velocities exceeding the speed of light. These problems arise due to the first order nature of the theory, that is, it considers only first-order deviations from the equilibrium leading to parabolic differential equations, hence to infinite speeds of propagation for heat flow and viscosity, in contradiction with the principle of causality. Conventional theory is thus applicable only to phenomena which are quasi-stationary, i.e. slowly varying on space and time scales characterized by mean free path and mean collision time.

A relativistic second-order theory was found in Ref. [26] and developed by Israel and Stewart (IS) [27], Hiscock and Lindblom [28] and Hiscock and Salmonson [29] into what is called “transient” or “extended” irreversible

thermodynamics. In this model deviations from equilibrium (bulk stress, heat flow and shear stress) are treated as independent dynamical variables, leading to a total of 14 dynamical fluid variables to be determined. For general reviews on causal thermodynamics and its role in relativity see Ref. [30].

Causal bulk viscous thermodynamics has been extensively used for describing the dynamics and evolution of the early universe or in an astrophysical context. But due to the complicated character of the evolution equations, very few exact cosmological solutions of the gravitational field equations are known in the framework of the full causal theory. For a homogeneous universe filled with a full causal viscous fluid source obeying the relation $\xi \sim \rho^{1/2}$, with ξ bulk viscosity coefficient and ρ energy density of the cosmological fluid, exact general solutions of the field equations have been obtained in previous works [32–36]. It has also been proposed that causal bulk viscous thermodynamics can model on a phenomenological level matter creation in the early universe [32]. Exact causal viscous cosmologies with $\xi \sim \rho^s, s \neq 1/2$ have been considered in Ref. [33].

Because of technical reasons, most investigations of dissipative causal cosmologies have assumed Friedmann-Lemaitre-Robertson-Walker (FLRW) symmetry (i.e. homogeneity and isotropy) or small perturbations around it [36]. The Einstein field equations for homogeneous models with dissipative fluids can be decoupled and therefore are reduced to an autonomous system of first order ordinary differential equations, which can be analyzed qualitatively.

The evolution of a flat, isotropic and homogeneous universe, which is filled with a causal bulk viscous cosmological fluid has been studied [37–41, 44, 45]. The viscous properties are described by an ultra-relativistic equation of state, and bulk viscosity coefficient obtained from recent lattice QCD calculations. The basic expression for the Hubble parameter is to be derived by using expressions for the energy density under the assumption of covariant conservation of energy-momentum tensor of the matter filling the background geometry of the Universe. Assuming a power law dependence of bulk viscosity coefficient, temperature and relaxation time on the energy density, we can derive the time evolution of the Hubble parameter. Therefore, the equations of state deduced from recent lattice QCD simulations and heavy-ion collisions play an essential role in deriving approximate solutions of the field equations. Apparently, the time evolution of Hubble parameter and scale factor essentially depends on the type the background matter/radiation and on its viscous property. Such a dependence in not absence in other thermodynamic quantities, like temperature, energy density and bulk pressure.

Physical Properties in Early (viscous) Universe

***A*diabatic Processes in Early (viscous) Universe**

From FLRW equations [43, 45], it is straightforward to appreciate that cosmic expansion is an adiabatic process

$$\dot{\rho} + 3(\rho + p)\, H = 0, \tag{11.1}$$

as the last expression can be rewritten in terms of the internal energy $U = \rho\, a^3$

$$dU = -p\, dV, \tag{11.2}$$

which is equivalent to $d\rho = T\, ds$. When translating such an adiabatic expansion into thermal evolution of a gas consisting of matter (baryons) and radiation (photons), we simply find that the gas cools down as the universe expands

$$p \propto \rho^{\alpha}, \qquad \text{then} \qquad T\, a^{3(\alpha-1)} = \text{constant}, \tag{11.3}$$

where α stands for the ratio of specific heat at constant pressure and volume, respectively. $\alpha = 5/3$ for matter and $\alpha = 4/3$ for radiation leading to $T \propto a^{-2}$ and $T \propto a^{-1}$, respectively. Thus, there is a backward time and the universe simply shrinks accordingly, but T raises.

Following the illustrative model that the cosmic background is characterized by one particle with mass m [43], we add another photon with frequency ν, it is conjectured that the photon completes one oscillation over the whole radius of the universe [45]. Therefore, the photon's frequency $\nu = 1$. Such an assumption fits well with the model [43], where it has been conjectured that the expansion itself is determined by the distance covered by the particle with the mass m. In other words, the size of the universe is given by the distance covered by the particle and simultaneously along which the photon is able to complete one cycle. These two components are located at a distance a from some point in the Universe. In the radial direction, the particle will have a kinetic energy $m\dot{a}^2/2$. The kinetic energy of the photon reads $h\nu$. In the opposite direction, both are affected by a gravitational force due to their masses m_p, m_γ and the mass inside the sphere, which is given as

$M = (4\pi/3)a^3\rho$. The latter characterizes the mass of the *absolute* background. Then, the particle's *gravitational* potential energy is $-GMm_p/a$ and the photon's one is $-GMm_\gamma/a$, where G is the Newtonian gravitational constant. In natural units, $c = k_B = \hbar = G = 1$, where c and k_B being speed of light and Boltzmann constant, respectively. Then $h = 2\pi$, where h is the Planck constant

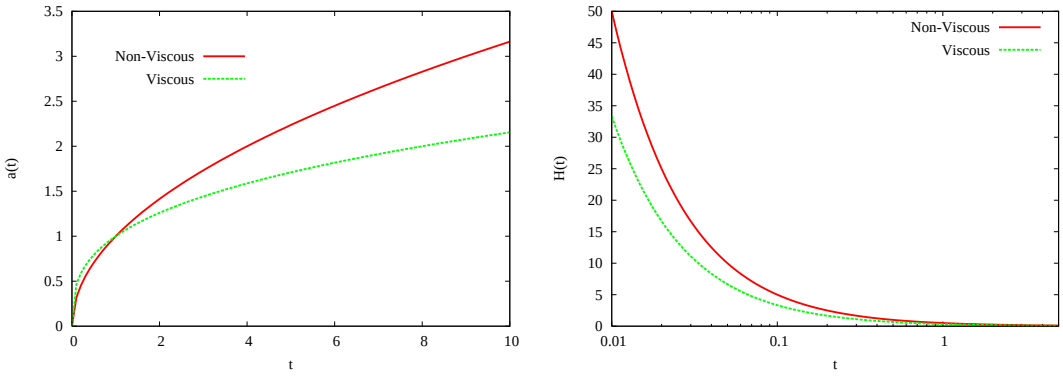

Figure 11.5: The dependence of the scale factor a on the co–moving time t is illustrated in the left panel. The right panel shows the Hubble parameter H in dependence on t. Solid curve represents the case where the background geometry is filled with an ideal content. The dashed curve illustrates the effects of the viscosity. Due to the natural units, physical units are not given.

NICA advantages:
The adiabatic expansion preserves number of particles while volume obviously expands and temperature changes such that $\Delta(a^3\,T^3)$ = constant. The particle production in an adiabatic process are considered as source for the entropy. The dissipative pressure is considered due to decaying of particle production and a cosmological term [52].

***B*aryon Asymmetry in Early (viscous) Universe**
It is essential to mention potential similarities between high energy collisions and Big Bang cosmology [46]. There is a generic similarity between early stages of the early Universe and those of the heavy–ion collisions [47], which apparently reflects the explosive start and successive phases, as well [48]. The formation of QGP in relativistic collisions would constrain even the inhomogeneous cosmologies [49]. The *prompt* first-order phase transition seems to have essential astrophysical consequences. Despite of the order of phase transitions, the QGP era - in early Universe - seems not to be followed by an extreme expansion (inflation). This is apparently the case in heavy-ion collisions, because of the baryon number conservation and the limitation of baryon-to-photon ratio $(n_b - n_{\bar{b}})/n_\gamma \sim 10^{-11}$ [51]. Therefore, $n_{\bar{p}} - n_p$ recently measured by ALICE experiment at 7 GeV can be used to estimate photon number density, $n_\gamma \approx 5.5 \times 10^4$, while in CMB era, $n_\gamma \approx 411.4\ (T/2.73\mathrm{K})$ cm^{-3}. The partonic is followed by hadronization through thermal and chemical equilibrium. Therefore, the QGP era seems to be the last symmetry breaking of strongly interacting matter. With this statement, we mean deconfinement and chiral symmetry breaking and/or restoring. Going back to the analogy with CMB, it is not restricted to the baryon-photon ratio. The quantum fluctuations from the early Universe are conjectured to be explained by WMAP [51]. The temperature-correlations in the heavy-ion collisions have been simulated in hydrodynamic models for Au nuclei (12 fm across) [50]. A power–spectrum from the heavy-ion data has been extracted and compared with CMB.

NICA advantages:
Measuring particle ratios of various species, especially baryons, at NICA energy.

Cosmological Parameters in viscous Background
Generally, the bulk viscous effects can be described by means of an effective pressure Π, which formally is to be included in the effective thermodynamic pressure $p_{eff} = p + \Pi$ [30]. Then, the energy momentum tensor in co-moving frame of reference has the components $T^0_0 = \rho, T^1_1 = T^2_2 = T^3_3 = -p_{eff}$. The Einstein field equations

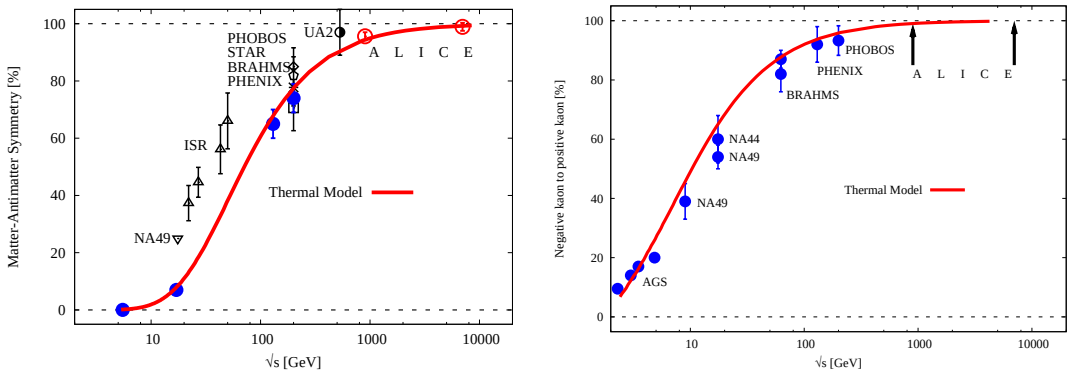

Figure 11.6: *Left panel:* $n_{\bar{p}}/n_p$ ratios depicted in the whole available range of $\sqrt{s}$. Open symbols stand for the results from various pp experiments (labeled). The heavy-ion results from AGS, SPS and RHIC, respectively, are drawn in solid symbols. The solid curve represents results from thermal HRG model at $\mathcal{Q} = 0.5$ and $\gamma = 1.0$, which apparently perfectly describes all heavy–ion collisions, besides the ALICE pp results. At LHC energy, the ratios are very much close to unity indicating almost 100% baryon-antibaryon symmetry. *Right panel:* n_{K^-}/n_{K^+} ratios given in the whole available range of $\sqrt{s}$ in heavy–ion collisions of AGS, SPS and RHIC, respectively. The solid curve represents HRG results. At RHIC energy, the ratios reach 93%, whereas at LHC energy very much close to unity indicating an almost 100% antiboson-boson symmetry. The values predicted at ALICE energies are marked by upwards arrows.

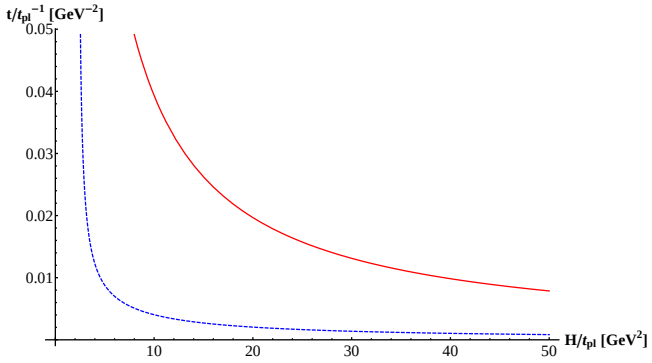

Figure 11.7: The $t - H$ relation in Eckart relativistic QGP fluid. Solid and dotted curves represent viscous and non-viscous QGP fluid filling the background geometry, respectively. It is obvious that the viscosity slows down the evolution of the Hubble parameter.

at vanishing cosmological constant (a type of dark non-baryonic matter, for instance, in the sense that it is not gravitationally clustered at all scales as the usual matter) read

$$\left(\frac{\dot{a}}{a}\right)^2 = \frac{8\pi}{3} G\, \rho, \tag{11.4}$$

$$\frac{\ddot{a}}{a} = -\frac{4\pi}{3} G\, \left(3p_{eff} + \rho\right), \tag{11.5}$$

where one dot denotes derivative with respect to the time t, G is the gravitational constant and a is the scale factor. The Hubble parameter H relates velocity to separation.

Assuming that the total matter content of the universe is conserved, $T^j_{i;j} = 0$, the energy density of the *adiabatic* cosmic matter fulfils the conservation law:

$$\dot{\rho} + 3H\left(p_{eff} + \rho\right) = 0, \tag{11.6}$$

In presence of bulk viscous stress Π,

$$\dot{\rho} + 3H\left(p + \rho\right) = -3\Pi H. \tag{11.7}$$

For the evolution of the bulk viscous pressure we adopt the causal evolution equation [30], obtained in the simplest way (linear in Π) to satisfy the H-theorem (i.e., for the entropy production to be non-negative, $S^i_{;i} = \Pi^2/\xi T \geq 0$ [26, 27]). According to the causal relativistic Israel-Stewart theory, the evolution equation of the bulk viscous pressure reads [30]

$$\tau\dot{\Pi} + \Pi = -3\xi H - \frac{1}{2}\tau\Pi\left(3H + \frac{\dot{\tau}}{\tau} - \frac{\dot{\xi}}{\xi} - \frac{\dot{T}}{T}\right). \tag{11.8}$$

In order to have a closed system from equations (11.4), (11.7) and (11.8) we have to add a set of equations of state for p, T, ξ and relaxation time τ, describing the matter/radiation filling the background geometry.

NICA advantages:
Providing equations of state at large baryon density is likely accessible at NICA energy. It would represent a crucial step in extending previous series of work on viscous early universe [37–41, 44, 45] to cover other eras. In the astrophysical and cosmological context, it is obvious that the evolution of the cosmological parameters in the hadron epoch would have essential consequences. This epoch seems to be accessible by NICA.

Bibliography

[1] K. E. Schmidt and S. Fantoni, Phys. Lett. **B 446,** 99 (1999).

[2] S. Gandolfi, F. Pederiva, S. Fantoni and K. E. Schmidt, Phys. Rev. Lett. **99,** 022507 (2007).

[3] S. Gandolfi, A. Yu. Illarionov, K. E. Schmidt, F. Pederiva and S. Fantoni, Phys. Rev. **C 79,** 054005 (2009).

[4] I. E. Lagaris and V. R. Pandharipande, Nucl. Phys. **A 359,** 331 (1981).

[5] A. Akmal, V. R. Pandharipande and D. G. Ravenhall, Phys. Rev. **C 58,** 1804 (1998).

[6] P. Danielewicz, R. Lacey, W. G. Lynch, Science **298**, 1592 (2002).

[7] K. E. Schmidt and V. R. Pandharipande, Phys. Lett. **B 87,** 11 (1979).

[8] A. N. Sissakian *et al.*, *The Project NICA/MPD at JINR: Search for the Mixed Phase of Strongly Interacting Matter at Nuclotron-based Ion Collider fAcility. XXIII International Symposium on Lepton and Photon Interactions at High Energy, LP07.* (August 13-18, 2007, Daegu, Korea).

[9] A. D. Kovalenko. *On a possible conception of a relativistic nucleus and electron beam facility. JINR Communication* , P9-89-26, JINR, 1989.

[10] T. Katayama, Yu. Batygin *et al.*, Nucl. Phys. **A 626,** 545 1997.

[11] Yu. Batygin and T. Katayama. *Merging Beam-Beam Interactions. Proc. PAC99*, p.1737.

[12] D. E. Donets *et al.*, Rev. Sci. Instrum. **80**, 063304 (2009)

[13] M. Tona *et al.*, Eds. R. W. McCullough *et al.*, *Proceedings of the 13th International Conference on the Physics of Highly Charged Ions* (2007), Journal of Physics conference series **58** 379.

[14] N. Stolterfoht *et al.*, Phys. Rev. Lett. **88,** 133201 (2002)

[15] A. P. Kavanagh *et al.*, Eds. R. W. McCullough, *et al.*, *Proceedings of the 13th International Conference on the Physics of Highly Charged Ions* (2007), Journal of Physics conference series **58**, 439

[16] P.Filip, in *Proceedings of RNP2012 Conference*, Stará Lesná, Slovakia, June 2012.

[17] E.V.Shuryak, Phys. Rev. **C 61**, 34905,(2000).

[18] P.Filip, R.Lednicky, H.Masui, N.Xu, Phys. Rev. **C 80**, 054903 (2009).

[19] G.Agakishiev and STAR Collaboration, Phys. Rev. **C 86**, 014904 (2012).

[20] J.Möller et al., Atomic Data Nucl. Data Tables, **59**, 185 (1995).

[21] K.Fukushima, D.E.Kharzeev, H.J.Warringa, Phys. Rev. **D 78**, 074033 (2008).

[22] I.Boboshin et al., *Proceedings of Int. Conf. on Nuclear Data for Science and Technology*, April 22-27, 2007, France, (ed. Bersillon et al.) EDP Sciences, 65, 2008.

[23] G.Agakishiev and STAR Collaboration, Phys. Rev. **C 85**, 014901 (2012).

[24] C. Eckart, Phys. Rev. **58**, 919 (1940).

[25] L. D. Landau and E. M. Lifshitz, *Fluid Mechanics*, Butterworth Heinemann (1987).

[26] W. Israel, Ann. Phys. **100**, 310 (1976).

[27] W. Israel and J. M. Stewart, Phys. Lett. **A 58**, 213 (1976).

[28] W. A. Hiscock and L. Lindblom, Ann. Phys. **151**, 466 (1989).

[29] W. A. Hiscock and J. Salmonson, Phys. Rev. **D 43**, 3249 (1991).

[30] R. Maartens, Class. Quantum Grav. **12**, 1455 (1995); R. Maartens, `astro-ph/9609119` (1996).

[31] R. Baier, P. Romatschke, D. T. Son, A. O. Starinets and M. A. Stephanov, JHEP **0804**, 100 (2008).

[32] L. P. Chimento and A. S. Jakubi, Class. Quantum Grav. **14**, 1811 (1997); L. P. Chimento and A. S. Jakubi, Int. J. Mod. Phys. **D 7**, 177 (1998); M. K. Mak and T. Harko, Gen. Rel. Grav. **30**, 1171 (1998); Gen. Rel. Grav. **31**, 273 (1999); J. Math. Phys. **39**, 5458 (1998).

[33] T. Harko and M. K. Mak, Int. J. Theor. Phys. **38**, 1561 (1999).

[34] M. K. Mak and T. Harko, Aust. J. Phys. **52**, 659 (1999).

[35] M. K. Mak and T. Harko, Int. J. Mod. Phys. **D9**, 97 (2000); Aust. J. Phys. **53**, 241 (2000); Int. J. Mod. Phys. **D 9**, 475 (2000).

[36] R. Maartens and J. Triginer, Phys. Rev. **D56**, 4640 (1997).

[37] A. Tawfik, M. Wahba, H. Mansour and T. Harko, Uzbek J. Phys. **12**, 316-321 (2010).

[38] A. Tawfik, H. Mansour and M. Wahba, *12th Marcel Grossmann Meeting on "General Relativity"*, (12-18 July 2009 Paris-France).

[39] A. Tawfik, Ann. Phys. **523**, 423 (2011).

[40] A. Tawfik, M. Wahba, H. Mansour and T. Harko, Ann. Phys. **523**, 194 (2011).

[41] A. Tawfik, M. Wahba, H. Mansour and T. Harko, Ann. Phys. **522**, 912 (2010).

[42] A. Tawfik and M. Wahba, Ann. Phys. **522**, 849(2010).

[43] A. Tawfik, Can. J. Phys. **88**, 822 (2010).

[44] A. Tawfik, Ann. Phys. **523**, 423(2011).

[45] A. Tawfik and H. Magdy, Can. J. Phys. **90**, 433 (2012).

[46] D. Schramm and K. Olive, Nucl. Phys. **A 418**, 289c (1984).

[47] L. McLerran, AIP Conf. Proc. **917**, 219 (2007).

[48] F. Gelis, Acta Phys. Polon. Supp. **1**, 395 (2008).

[49] T. Kajino, Phys. Rev. Lett., **66**, 125 (1991).

[50] A. Mocsya and P. Sorensen, Nucl. Phys. **A 855**, 241-244 (2011).

[51] C. Bennett *et al.*, (WAMP Collaboration), App. J. Suppl. **148**, 1 (2003).

[52] S. Bhanja, S. Chakraborty, and U. Debnath, Int. J. Mod. Phys. **D 14**, 1919 (2005).

12 Fixed Target Experiments

With the completion of the booster system in 2014, there will be the possibility to have ion beams with a good quality starting from the year 2015. These beams which are extracted to the experimental hall can be used for experiments full time before the NICA/MPD experiment is ready for operation. Therfore, it is actual to discuss in this section the physics potential of possible experiments using the extracted ion beams with laboratory energies up to 5.5 AGeV.

12.1 Measurement of Elementary Cross Sections

J. Aichelin[1], M. Bleicher[2], E. Bratkovskaya[2], C. Hartnack[1]

[1] *SUBATECH, Laboratoire de Physique Subatomique et des Technologies Associées, Université de Nantes, Nantes, France;*

[2] Frankfurt Institute for Advanced Studies (FIAS), Frankfurt am Main, Germany

Today heavy ion reactions are not made any more to discover single particle spectra of hadrons. These spectra have since long been analysed and for the most frequent particles reproduced by simulation programs like QMD [1, 2], HSD [3] or URQMD [74]. The present goal of heavy ion experiments is much more ambitious. One aims to study in medium properties of particles, the nuclear equation of state, the transition toward a quark gluon plasma or reaction mechanisms which are only present in heavy ion collisions like those reactions which involve a Δ in the initial state. To extract this desired information the experimental results have to be compared with these computer programs which predict observables for different assumptions of the in medium properties, the cross sections etc. The assumption which fits best is than used to predict other observables in order to cross check whether it reflects really the properties of the system. Using this method remarkable progress has been made in the last decade on strangeness production close to the threshold, on the nuclear equation of state and other properties of hadrons in matter.

The problem with these simulation programs for heavy ion reactions is the fact that they use measured elementary cross sections as input quantities. Up to beam energies of around 1.5 GeV these elementary cross sections have been measured in the sixties and seventies by bubble chamber experiments.Therefore many of them suffer from low statistics. In addition, already at 2 GeV yet unknown elementary cross sections limit the predictive power of the heavy ion simulation programs. A good example is the dilepton production in CC at 2 AGeV which has been measured by the HADES collaboration. The experimental data show an enhancement of the dileption yield at an invariant mass corresponding to the mass of the ρ and ω but since the experimental cross sections

$$\begin{aligned} np &\to \rho + x \\ pp &\to \rho + x \\ np &\to \omega + x \\ pp &\to \omega + x \end{aligned} \tag{12.1}$$

are either unknown or known only with large error bars (and theoretical prediction differ by up to a factor of 5) it is difficult to interpret these data yet. One simply cannot say whether the measured yield can be reproduced using free production cross sections or whether the data give a hint that properties of these mesons, like their mass, have changed in the medium, not to talk about more ambitious ideas like to verify experimentally the off-shell propagation of the baryon resonances and mesons in a nuclear environment. This has been discussed extensively at the last collaboration meeting of HADES.

In addition, it would be very important to know the role of nuclear resonances for the meson production (which could in principle be analysed by kinematics) but there almost no information is available presently. This excludes an interpretation of the enhanced dilepton cross section in large systems for intermediate invariant masses observed by the HADES collaboration. Even worse, for mesons like the η, which is one of the candidates for this enhancement,the production in np reactions in unknown in the energy regime of interest . Therefore this enhancement is not accessible for theoretical studies presently.

All the people who are implied in the development of these simulation programs, agree that the present limitation of their predictive power is the lack of knowledge on the cross section.

Today TPCs or similar devices are very effective to measure the complete kinematics of charged particles with a high frequency and, tagging the p in dp reactions, would allow for studying the np collisions. The multiplicity in these elementary reactions is small and therefore the detection does not require sophisticated devices.

Therefore we think that a program "measurement of elementary cross sections from 1.5 GeV upwards" would be extremely helpful for the later coming heavy ion reactions, or, to be more precise, without such a program it will be impossible to extract the physics of the heavy ion reaction in a convincing way.

In addition, this energy regime is also very interesting. At 2 GeV we see that the particles in the exit channel in reactions like $NN \to NNK^+$are distributed according to the three dimensional phase space. At 80 GeV and probably also well below, in order to describe the data one has to assume that strings are formed and the distribution of the particles is governed by the 1-dim longitudinal phase space. In transverse direction the particles have about a pt of 300 MeV. Therefore the transition between a description of the reaction in nuclear degrees of freedom and in quark degrees of freedom takes place in this energy regime and it would by very interesting to identify precisely the energy where the transition takes place.

We would therefore recommend that the experimental program at DUBNA starts out from this proposal of elementary collisions.

12.2 Search for scaling onset in exclusive reactions with lightest nuclei at NUCLOTRON using fixed target.

Yu.N. Uzikov

Joint Institue for Nuclear Researches,LNP, Dubna, Moscow reg. Russia

Search for transition region from hadron to quark-gluon degrees of freedom in nuclear structure at short distances between nucleons ($r_{\rm NN} < 0.5$ fm) is a challenging problem of particle and nuclear physics. This transition is expected to occur in processes at enough high transferred momenta allowing to probe dense fluctuations of nuclear matter in nuclear structure [5].

A possible signature for this transition is related with the constituent counting rules (CCR) [6,7]. According to CCR the differential cross section of a binary reaction $AB \to CD$ at (asympthoticaly) high incident energy $\sqrt{s}$ and transferred momentum t can be parameterized for a given c.m.s. scattering angle $\theta_{\rm cm}$ as

$$\frac{d\sigma}{dt}(AB \to CD) = \frac{f(t/s)}{s^{n-2}}, \tag{12.2}$$

where $n = N_{\rm A} + N_{\rm B} + N_{\rm C} + N_{\rm D}$ and N_i is the minimum number of point-like constituents in the *i-th* hadron (for a lepton and photon one has $N_l = 1$), $f(s/t)$ is a function of $\theta_{\rm cm}$. The CCR follows from the hypothesis of self-similarity [6] and perturbative QCD (pQCD) [7].

Existing high energy data for many measured hard processes with free hadrons appear to be consistent with the CCR [8]. The CCR derived for asympthoticaly high values of kinematical variables $s \to \infty$ and $t \to \infty$, surprisingly, turned out to be valid at moderate energies $\sim$ few GeV in many reactions with **free hadrons** when the condition $\theta_{\rm cm} = const$ is used [8].

For exclusive reactions with **lightest nuclei** at high Q^2, CCR can give a definite signal for transition to the valence quark region. Indeed, the s^{-11} behaviour of the cross section $d\sigma/dt$ of the reaction $\gamma d \to pn$, observed at SLAC/Jlab at $E_\gamma = 1 - 4$ GeV and large scattering angles $\theta_{\rm cm} = 90^\circ$, perfectly follows the CCR (see [9] and references therein, Fig.12.1). A similar behaviour was observed in the reaction ^{3}He$(\gamma, pp)n$ [10] with much lower cross section. On the other hand, the reaction $pp \to d\pi^+$ at very similar kinematics does not demonstrate the CCR behaviour s^{-12} [12].

Further study of this phenomenon, however, is very limited *by small cross sections* of the electromagnetic interactions. Recently, the precise CCR dependence s^{-22} was found in the **pure hadronic reactions** $dd \to {}^3$Hp and $dd \to {}^3$Hen measured at SATURNE at $T_{\rm d} = 0.5 - 1.2$ GeV and large scattering angles $\theta_{\rm cm} = 50 - 60^\circ$ [12] (see Fig.12.2). The $pd \to pd$ cross section demonstrates the s^{-16} dependence but with worse χ^2 [12]. At lower scattering angles, i.e. lower transferred momenta, this behaviour is absent both in the $dd \to {}^3$Hp, $pd \to pd$ and $\gamma d \to pn$ reactions.

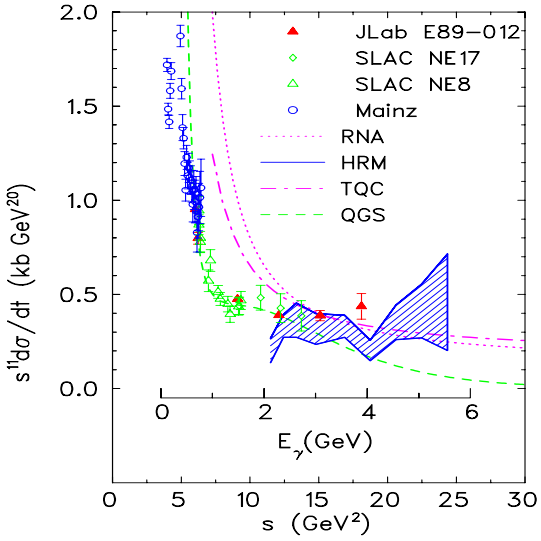

Figure 12.1: The invariant cross section of the reaction $\gamma d \to pn$ at $\theta_{\rm cm} = 90^\circ$ multiplied by s^{11} in comparison with different theoretical models. The figure is taken from Ref. [11]

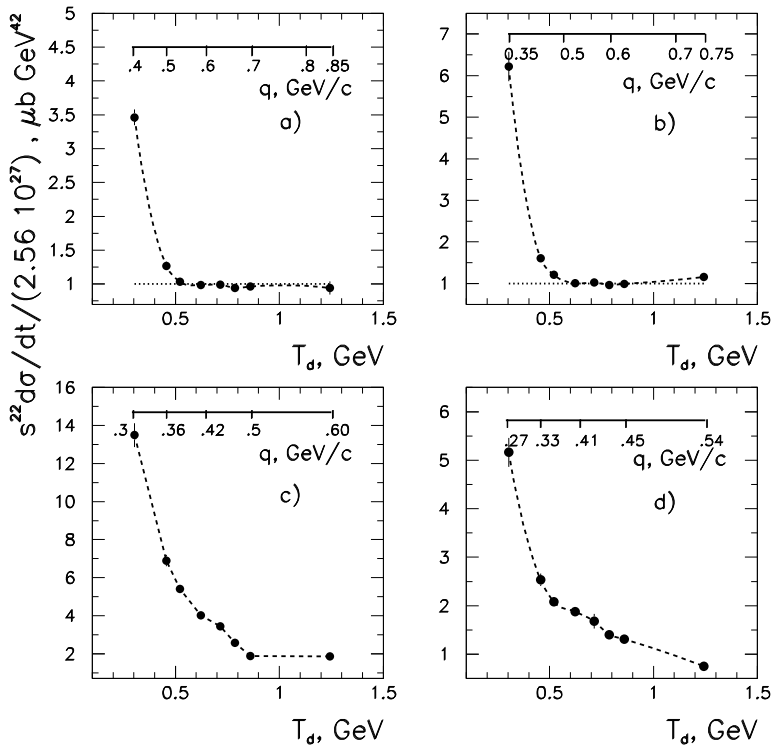

Figure 12.2: The invariant cross section of the $dd \to {}^3Hen$ and $dd \to {}^3Hp$ reactions multiplied by s^{22} versus the deuteron beam energy at different scattering angles $\theta_{\rm c.m.}$: $a - \theta_{\rm c.m.} = 60^o$; $b - 50^\circ - 52^\circ$; $c - 33^\circ - 35^\circ$; $d - 28^\circ$. On the upper scale is shown the minimal relative momentum (GeV/c) between nucleons in the deuteron for the ONE mechanism. The data are taken from Ref. [14]. At lower scattering angles the plateau is not visible in this data, maybe, except for $\theta_{\rm cm} = 33^\circ - 35^\circ$. The figure is taken from Ref. [12]

All these reactions involve nuclear wave functions at very high internal momenta between nucleons $q \sim 1$ GeV/c. The perturbative QCD, however, can be hardly applied at these rather low energies. **New data on these and other exclusive reactions are required to clarify the underlying dynamics. One of the most important task is determination of the scaling onset for different reactions.** Measurement of energy dependence of the differential cross section of the reaction $dd \to {}^3\mathrm{He}\, n$ in the interval $T_\mathrm{d} = 1 - 3$ GeV at fixed cms scattering angles within $\theta_\mathrm{cm} = 30^\circ - 90^\circ$ would be very important to confirm the SATURNE data.

The JINR *Nuclotron with fixed target* facility provides unique possibility to perform this study in dd and pd collisions above 1 GeV. A broad experimental program will include other exclusive reactions with lightest nuclei: $dd \to dd$,$pd \to pd$, $pd \to {}^3\mathrm{H}\pi^+$, $pd \to {}^3\mathrm{He}\eta$, $dd \to {}^4\mathrm{He}\eta$, $pp \to d\rho^+$, $d^3\mathrm{He} \to {}^4\mathrm{He}\, p$.

12.3 Measurement of strange particle production in the NICA fixed-target program

V. Friese

GSI Helmholtzzentrum für Schwerionenforschung mbH, Darmstadt, Germany

The production of strange particles is considered a sensitive probe of the dynamics of nuclear collisions and of the state of the produced matter since the early days of heavy-ion physics, the original perception being that strangeness is more easily produced in parton-parton interactions than in hadronic interactions, and is thus more abundant in the final state should a deconfined phase be transiently reached [15]. This strangeness enhancement was indeed observed [16], but it was soon realised that the measured particle abundances, including those of strange particles, can be described in terms of an equilibrium hadron gas model [17].

The apparent chemical equilibrium was interpreted to be a consequence of the phase transition from deconfined to confined matter, either by phase-space dominance [18] or by multi-particle collisions [19] which become effective near the phase boundary, which, for high collision energies like at SPS or RHIC, is expected to coincide with chemical freeze-out. However, the statistical model was also successfully applied to the final state hadrons emerging from nuclear collisions at lower energy like at AGS or even at SIS, where the creation of deconfined matter is not likely, and where, as suggested by results from lattice QCD calculations, the chemical freeze-out is separated from the deconfinement phase transition by a stage of dense hadronic medium. This observation led recently to the proposal of an additional QCD phase, the quarkyonic phase, where confinement still holds, but chiral symmetry is restored [20]. The phase transition from this quarkyonic medium to hadrons could then act as a thermaliser in the same way as the transition from deconfined to confined matter does for higher collision energies.

The energy regime of the Nuclotron and the future FAIR facility, creating a baryon-dense but moderately hot initial state, is uniquely suited for the study of this part of the QCD phase diagram and the hypothetical quarkyonic phase. A prime tool are again strange particles, the production features of which still bear open questions. Of particular interest, besides the bulk strangeness carriers K and Λ, are multi-strange hyperons, the production of which, close to the threshold in elementary reactions, can be enhanced though strangeness-exchange processes like $\Lambda K \to \Xi\pi$ or $\Lambda\Xi \to \Omega n$ with previously produced strange particles in the entrance channel. Their yield is thus sensitive to both the strangeness production mechanism and the baryon density.

Available experimental data on the production of multi-strange hadrons near the threshold do currently not give rise to a conclusive picture. Recently, the HADES experiment reported a large deviation of the measured Ξ^- yield from the statistical model in Ar + KCl at 1.76 AGeV beam energy [21,22]. The same is true for the η meson yield measured by the TAPS collaboration (Fig. 12.3). In contrast, the experiment E895 at AGS finds the measured Ξ^-/Λ ratio in Au + Au collisions slightly above threshold ($E_\mathrm{beam} = 6$ AGeV) in agreement with both thermal and transport models [23]. At the higher energies of the SPS, the statistical model gives a fair description of the Ξ^- yield (see Fig. 12.4), while the transport model UrQMD fails badly [24]. The particle abundances measured by FOPI in Ni+Ni collisions at SIS energies can be fitted thermally, but the extracted temperature is below that deduced from the transverse momentum spectra, i.e. at kinetic freeze-out.

A fixed-target experiment at the Nuclotron should shed light on these puzzles by a systematic study of strangeness production at energies above SIS and for heavy collisions systems, where the currently available experimental data are either missing, scarce, or cover only a small fraction of the phase space. A detailed measurement of the Ξ^- excitation function in heavy-ion reactions near the elementary threshold would provide substantial input to the understanding of the collision dynamics and the strangeness production processes.

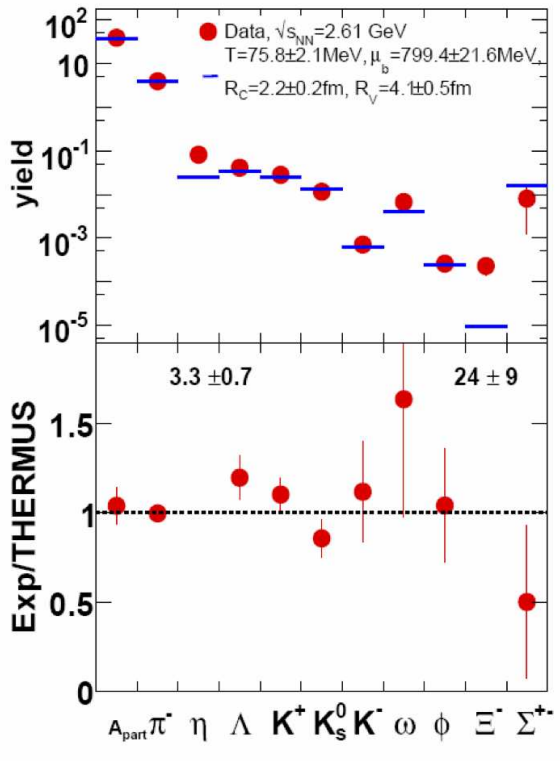

Figure 12.3: Comparison of hadron abundances measured by the HADES experiment and the hadron gas model fit (from [22]). The Ξ^- yield differs by more than an order of magnitude from the model. A large deviation is also observed for the η meson measured by TAPS.

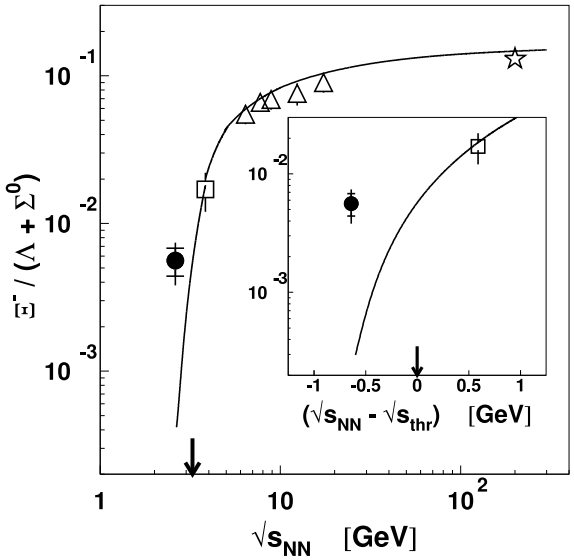

Figure 12.4: Excitation function of the $\Xi^-/(\Lambda+\Sigma^0)$ ratio (from [21]). The full curve shows the results of thermal model fits.

Even more spectacular would be the observation of deep sub-threshold Ω production, where no experimental heavy-ion data below SPS energies exist, or that of the hypothetical multi-strange di-baryons [25].

K^0_S, Λ, Ξ and Ω and di-baryons are all detected by their weak decay topology; these channels can thus be studied by a spectrometer consisting of a magnet and a high-precision tracking device. Such a compact

experiment would allow to characterise the major part of the total strangeness content of the final state. The fixed-target geometry gives access to a large rapidity range and facilitates the detection of the displaced decay vertices because of the Lorentz boost from CM to laboratory frame. As the measurement of the rare probes Ξ and Ω requires high event rates, large-volume gas drift chambers are not applicable. The choice could be a Silicon tracker, covering a large part of the forward hemisphere. The development and construction of such a device is consumptive in terms of budget, manpower and time, but possible synergy effects exist with similar detector developments for the MPD project and for the CBM experiment at FAIR.

A complete characterisation of the final state requires in addition the measurement of protons, charged pions and charged kaons. This task can be covered by a time-of-flight detector which, given the moderate momenta of the produced particles at Nuclotron energies, can be located at about 5 m downstream of the interaction point. State-of-the-art Resistive Plate Chambers can equip this device, but for high interaction rates, their rate capabilities become an issue. Again, a possible experiment could profit from developments at FAIR, where the CBM project faces similar problems.

In the context of strangeness in heavy-ion reactions, the ϕ meson plays an important role, as it carries a strange quark pair but is strangeness-neutral as a hadron. At SPS energies, ϕ meson production is not well described by the statistical model [26], while HADES at SIS reports no deviation from the thermal fit (see Fig. 12.3). In contrast, the microscopic transport model UrQMD describes the ϕ yield at lower energies reasonably well, while it starts to fail a higher energies. The experimental situation at RHIC energies in unclear. At SPS, different yield were claimed to be observed in the hadronic and in the muonic decay channels [27]. Data from the Nuclotron, just above threshold, would be highly desirable for an understanding of these features. In the setup outlined above, the ϕ meson can be observed in its decay into charged kaons. This also requires the selection of decay candidates by time-of-flight to reduce the combinatorial background, but the required precision of kaon identification is lower than for the measurements of direct kaons since the final identification of ϕ is done by invariant mass.

The above outlined observables should be studied systematically not only as function of beam energy, but also of system size. The latter can be varied either by using different projectile and target nuclei, or by the centrality of the collision. In any case, a device controlling the collision centrality is indispensable. A forward calorimeter similar to that developed for the NA61 experiment [28] would be suitable also for a fixed-target experiment at the Nuclotron. The question whether an intermediate tracking device connecting the main tracker and the time-of-flight system is required must be assessed by detailed simulations.

In summary, the production of strangeness at Nuclotron energies (up to 5.5 AGeV incident beam energy) can be studied by a relatively compact detector setup with magnet and tracking system. A time-of-flight detector with moderate size can extend the range of observables towards charged pions and kaons and the ϕ meson. Emphasis should be put on good coordinate resolution of the tracking system, large acceptance coverage and capabilities for high interaction rates to cover also the rare multi-strange hyperons and possible exotic states.

It should be noted that the experimental programme discussed above is in large parts concurrent to the planned activities of the CBM experiment, which will start taking data at the SIS-100 accelerator at beam energies from 2 to 10 AGeV from 2018 on. However, the physics focus of CBM is the energy domain from 10 to 45 AGeV to be covered by the SIS-300 synchroton in a later stage of the realisation of FAIR, whereas an experiment at the Nuclotron will be optimised to its specific energy range. The two activities hence provide complementary approaches to the study of high-density QCD matter.

12.4 Fixed target mode: correlations in relative 4-velocity space

V.A. Okorokov

National Research Nuclear University MEPhI, Moscow, Russia

Investigation of a mixed phase associated with the transition from meson-nucleon to quark-gluon degrees of freedom is one of the hottest topics in the world program of research into the field of strong interactions. Experiments studying hadron interactions at intermediate energies may furnish important information about the emergence of new (color) degrees of freedom.

A relativistically invariant method was proposed in [29, 30] for studying collective effects in multiparticle production processes. Large experimental material for various interaction types was analyzed at intermediate energies (see, for example [31, 32]). In particular, in was observed that the values of mean square of soft jet

size in 4-velocity space are significantly smaller for hadron-hadron reactions at $\sqrt{s} \sim 3$ GeV than those in other interactions at slightly higher energies. Moreover the energy dependence of mean kinetic energy of particles in the jet rest frame shows a sharp growth in a narrow interval of initial energies $\sqrt{s} \sim 3 - 5$ GeV with further smoother behavior [33]. The observations allow to assume that these effects may be due to the involvement of new degrees of freedom in the production of soft pion jets and to the respective transition from the description of these processes in terms of meson?nucleon degrees of freedom to the use of color (quark?gluon) degrees of freedom. But additional experimental investigations with high statistics and better particle identification are important for more detail study these effects at intermediate ener-gies.

In various realms of physics, the onset of manifestations of new degrees of freedom and transition processes is accompanied by the presence of self-affine and fractal effects in collective phenomena. In [34], it was proposed to study geometric properties of pion jets in the space of 4-velocities with the aid of the cluster dimension, which is determined by the relation between the number of particles in the jet and its radius in the relative 4-velocity space. For a number of the reactions investigated in the range $\sqrt{s} \sim 3-20$ GeV the cluster dimensions have fractional values, and this gives sufficient grounds to assume that pion jets have fractal properties [33]. Special features found in the energy dependence of cluster (fractal) dimension for hadron?hadron reactions are compatible with the qualitative assumption made above that new degrees of freedom arise in the region around $\sqrt{s} \sim 3 - 5$ GeV.

Thus, investigations of collective and geometric (fractal) properties in soft hadron reactions at intermediate energies $\sqrt{s} \sim 3 - 5$ GeV with high statistics at modernized Nuclotron can provide new important information about the hadronization mechanism, non-perturbative physics, and the way in which color degrees of freedom become operative in collective phenomena.

12.5 Nuclear and strange matter physics with a fixed-target experiment at the JINR-Nuclotron

P. Senger

GSI Helmholtzzentrum für Schwerionenforschung, Darmstadt, Germany
Goethe Universität Frankfurt, Germany

A dedicated heavy-ion experiment in the fixed-target hall of the JINR-Nuclotron would provide the unique opportunity to perform an internationally competitive research program focused on the physics of dense nuclear and strange matter. The basic setup should comprise a large-acceptance dipole magnet equipped with several large-area highly-granulated detector stations for track reconstruction. An additional time-of-flight detector would be needed for particle identification. In order to measure rare diagnostic probes a high-speed data read-out and acquisition system is mandatory for online event selection. Such a setup will be sufficient to perform a comprehensive study of strangeness production in heavy-ion collisions including multi-strange hyperons. Moreover, heavy-ion collisions in the Nuclotron energy range are very well suited for the production of (multi-strange) hypernuclei via the coalescence of lambda hyperons with light fragments. These pioneering measurements will provide new information on the properties of nuclear matter at neutron star core densities, and will open an avenue to explore the third (strangeness) axis of the nuclear chart.

The physics case

The Nuclotron at JINR will provide beams of heavy ions with energies up to 6 AGeV for isospin symmetric nuclei, and 4.5 A GeV for Au nuclei. In central heavy-ion collisions at these energies, nuclear densities of about 4 times nuclear matter density can be reached. This is illustrated in Fig. 12.5 which depicts the nucleon densities reached in central Au+Au collisions at different beam energies as a function of time as calculated with a transport code [35]. At 3 - 4 times nuclear matter densities the nucleons start to overlap, and it was speculated that under such extreme conditions free quarks and nucleons may coexist [20].

In any case, these conditions are very well suited to investigate the equation-of-state (EOS) of dense nuclear matter which plays a central role for the dynamics of core collapse supernovae and for the stability of neutron stars. At the same time, energetic heavy-ion collisions are a rich source of strange hadrons, and strangeness-exchange reactions in kaon-lambda collisions or the coalescence of lambdas with nucleons will produce a variety of multi-strange hyperons or of light hypernuclei, respectively. Even the production of double-lambda hypernuclei or of double-strange dibaryons is expected to be measurable in heavy-ion collisions at Nuclotron energies with a dedicated experimental setup and with high beam intensities. In the following, we will discuss the physics potential of a fixed target programme at the Nuclotron.

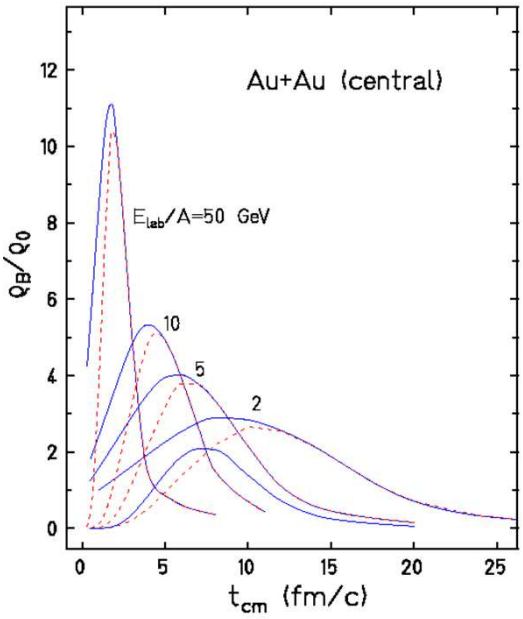

Figure 12.5: Nuclear density reached in the reaction volume of two colliding Au nuclei at various beam energies as function of the elapsed time. Taken from [35].

Exploring the equation-of-state of nuclear matter at high densities

In this chapter we briefly review our knowledge on the equation-of-state of nuclear matter (EOS) at high baryon densities as extracted from experimental data. The general approach to obtain information about the high-density EOS is to measure observables which are related to the density of the fireball produced in heavy-ion collisions, and to compare the experimental data to results of mean-field microscopic transport calculations. These models compute the binding energy per nucleon E/A (for example using a Skyrme parameterisation), and by variation of the nuclear compressibility $k = 9\rho^2 d^2(E/A)/d\rho^2$ (with ρ the nuclear density) one tries to reproduce the experimental data. In Fig. 12.6 presents the binding energy per nucleon as a function of the nuclear density obtained from relativistic Dirac-Brueckner Hartree-Fock calculations, and from a phenomenological model based on Skyrme forces [36].

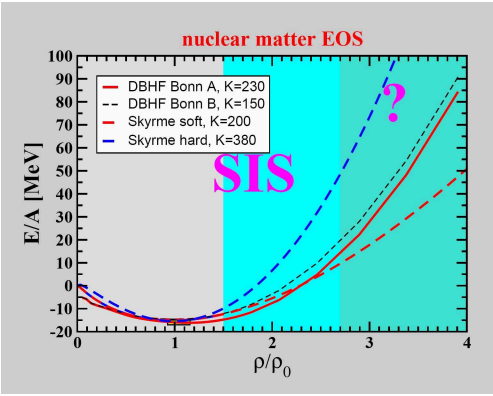

Figure 12.6: Binding energy per nucleon as a function of the nuclear density obtained from relativistic Dirac-Brueckner Hartree-Fock calculations and from a phenomenological model based on Skyrme forces. Taken from [36].

Probing the EOS with collective flow of nucleons

An experimental observable sensitive to the EOS is the collective flow of nucleons which is driven by the pressure built up in the reaction volume. A recent analysis of data on the collective flow of particles in nucleus-

nucleus collisions at beam energies of 0.4 - 1.5 AGeV (corresponding to nuclear densities of about $1-3\rho_0$) are compatible with values of $k \approx 200$ MeV indicating a soft EOS [37]. In order to study the EOS at baryon densities up to about 7 times ρ_0 the excitation function of the collective flow of protons has been measured in Au+Au collisions at beam energies between 2 and 8 AGeV at the AGS. The data have been analyzed with respect to the nuclear compressibility ? using microscopic transport calculations [43]. The experimental data are shown together with the results of the transport model calculations in Fig. 12.7.

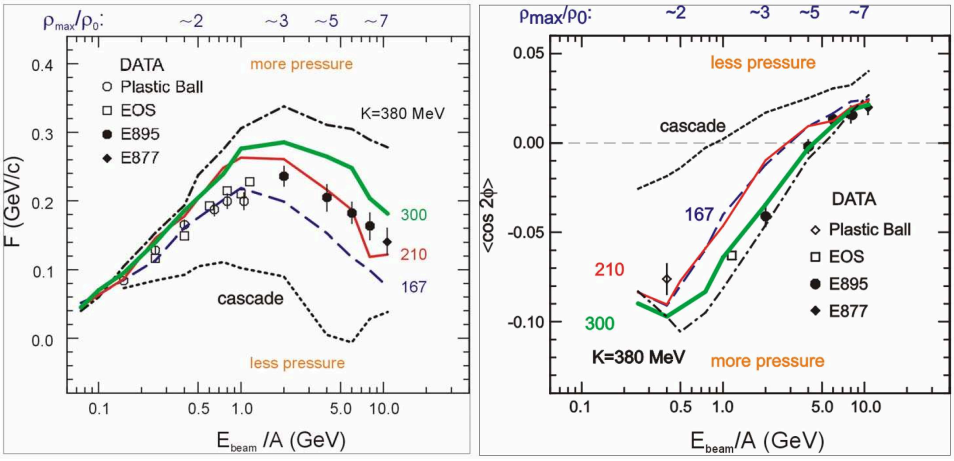

Figure 12.7: Collective flow excitation function for central Au+Au collisions. Data and transport calculations are represented by symbols and lines, respectively. Left panel: Sideward flow. Right panel: Elliptic flow. Taken from [38].

Whereas the AGS data on directed flow (left panel of Fig. 12.7) are compatible with the assumption of a soft EOS ($k \approx 200$ MeV), the elliptic flow (right panel) seems not to be sensitive to the EOS for beam energies above 4 AGeV. Therefore, the authors conclude that the data on proton collective flow presented in Fig. 12.8 constrain the compressibility of symmetric nuclear matter to values of $k = 170 - 380$ MeV.

The wide range of k values as extracted from the available heavy-ion data does not provide sufficient information on the EOS of symmetric nuclear matter at high densities as required for the calculations of neutron star properties. Moreover, the interpretation of flow data from heavy-ion collisions using transport models is not unambiguous because the strength of the collective proton flow does not only depend on the EOS, but also on the assumptions on the in-medium nucleon-nucleon cross sections. Nevertheless, it is worthwhile to provide more accurate data of the collective flow of particles in the Nuclotron energy range, and to compare it to most recent model calculations.

Probing the EOS with kaon production

An approach complementary to the study of collective flow is to investigate the yields of newly produced particles as diagnostic probes of the nuclear compressibility. In particular, it was found that the yield of kaons created in collisions between heavy nuclei at subthreshold beam energies ($E_{\rm beam} = 1.58$ GeV for $NN \to K+\Lambda N$) is sensitive to the EOS of nuclear matter at high baryon densities. This sensitivity is due to the fact that "subthreshold" production of kaons requires multiple nucleon-nucleon collisions or secondary collisions such as $\pi N \to K+\Lambda$. The probability of these processes increases quadratically with the baryon density which depends on the nuclear EOS [2].

The left panel of Fig. 12.8 depicts the measured excitation functions of $K+$ meson production in Au+Au and C+C collisions together with results of QMD transport model calculations [39, 40]. Whereas the kaon yield from the small C+C collision system does not depend on the nuclear EOS, the kaon yield from the heavy Au+Au system supports the assumption of a nuclear matter compression modulus of $k = 200$ MeV. In the right panel of Fig. 12.8 the excitation function of the ratio $(K^+/A)_{\rm (Au+Au)}/(K^+/A)_{\rm (C+C)}$ is shown. In this representation the systematic uncertainties both in experiment (normalization, efficiencies, acceptances etc.) and theory (elementary cross sections etc.) are reduced, and also the effects of the in-medium KN potentials cancel to a large extent. The data are compared to results of different transport model calculations [40,41] which are performed with a compression modulus of $k = 380$ MeV (corresponding to a "hard" equation-of-state) and with $k = 200$ MeV (corresponding to a "soft" equation-of-state). The data clearly favor a soft equation of state.

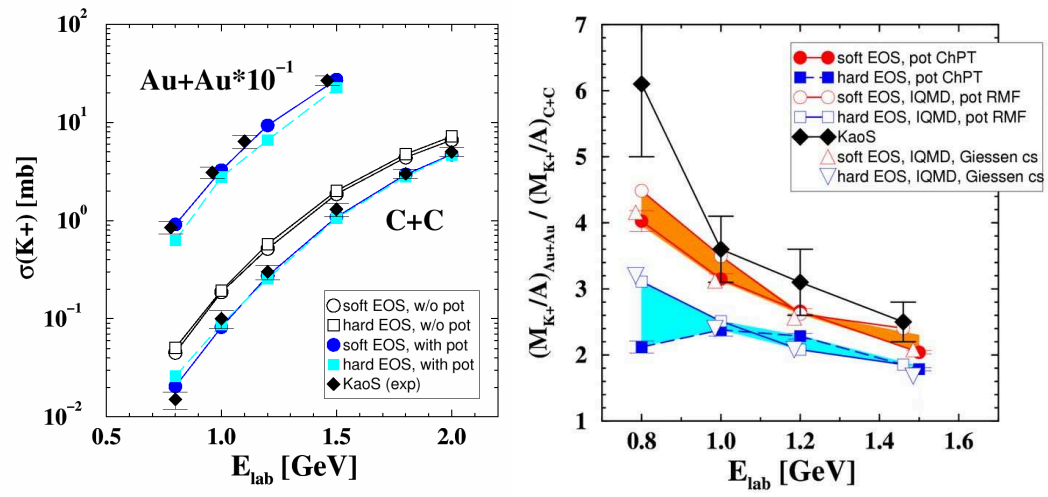

Figure 12.8: Production cross sections of K^+ mesons for Au+Au and C+C collisions as a function of the projectile energy per nucleon [39]. The data (full diamonds) are compared to results of transport calculations assuming a soft (circles) and a hard (squares) nuclear equation-of-state with and without KN in-medium potentials [40]. Right panel: K^+ ratio measured in inclusive Au+Au and C+C collisions as function of beam energy. The data are compared to vari-ous QMD calculations assuming nuclear compressibilities of $k = 200$ MeV and 380 MeV [40, 41]. Taken from [36].

The calculations presented in Fig. 12.8 use momentum-dependent Skyrme forces to determine the binding energy per nucleon. The kaon data would also agree with an EOS obtained from relativistic Dirac-Brueckner Hartree-Fock calculations as shown in Fig. 12.6. At densities larger than about $2.5\rho_0$ the different approaches diverge. Fig. 12.6 illustrates that it is not sufficient to determine the nuclear compressibility (which corresponds to the curvature of $E/A(\rho)$ at saturation density), but rather one has to study the response of nuclear matter at different densities. Therefore, measurements at baryon densities above $3\rho_0$ are necessary to pin down the nuclear EOS at high baryon densities which are relevant for neutron stars. One possibility is to perform precision measurements of K^+ mesons in light and heavy collision systems towards higher beam energies. A novel approach which is discussed in the following would be the investigation of subthreshold hyperon production in heavy-ion collisions.

Probing the EOS with hyperon production

The yield and the phase-space distributions of multi-strange hyperons at beam energies close to their production threshold in nucleon-nucleon collisions are promising observables of the nuclear density of the fireball, and, hence, of the EOS. The threshold beam energies for reactions like $pp \to \Xi^- K^+ K^+ p$ or $pp \to \Omega^- K^+ K^+ K^0 p$ are 3.7 or 7.0 GeV, respectively. However, Ξ^- and Ω^- hyperons can also be created via strangeness exchange reactions like $\Lambda\Lambda \to \Xi^- p$ and $\Lambda\Xi^- \to \Omega^- n$ or $\Lambda K^- \to \Xi^- \pi^0$ and $\Xi^- K^- \to \Omega^- \pi^-$. In these cases, the Λ and the K- have been produced in independent reactions such as $pp \to K^+ \Lambda p$ and $pp?K^+ K^- pp$ which require only 1.6 and 2.5 GeV, respectively. Due to these multi-step (or three body) collisions involving lambdas and kaons the production of multi-strange hyperons is expected to be enhanced at high densities, and their yield is sensitive to the baryon density reached in the fireball. This scenario is supported by results of microscopic transport calculations on the production of Ξ^- hyperons in Au+Au collisions at a beam energy 4 A GeV [42]. According to these calculations, the dominating process is a hyperon-hyperon (YY) collision, followed by baryon-hyperon (BY) and meson-hyperon (MY) reactions. The preliminary results are shown in Fig. 12.9.

Systematic measurements of Ξ^- and Ω^- hyperon production as function of beam energy and size of the colliding nuclei offer the possibility to study the nuclear matter equation-of-state, or baryon density fluctuations as they are expected to occur when the system undergoes a first-order phase transition. These fluctuations may also indicate the existence and the location of a QCD critical endpoint. Moreover, the energy distributions of multi-strange hyperons provide information on the fireball temperature and the radial flow at the time when they are emitted.

A fixed-target experiment at the Nuclotron would deliver the first data on the production of multi-strange hyperons in heavy-ion collisions in this beam energy range. The data situation is illustrated in Fig. 12.10 where

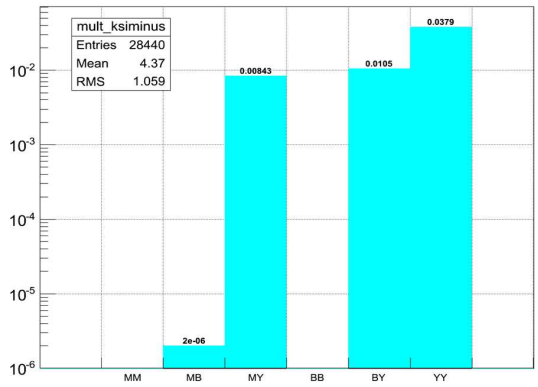

Figure 12.9: Production mechanisms of Ξ^- hyperons in Au+Au collisions at a beam energy 4 AGeV as calculated with the QGSM code [10] : hyperon-hyperon (YY), baryon-hyperon (BY), meson-hyperon (MY), meson-baryon (MB) collisions (preliminary results).

the measured excitation function of strange particles is shown for central collision of heavy nuclei (Au+Au, Pb+Pb) at beam energies above 2 A GeV [43]. In conclusion, the systematic measurement of multi-strange hyperons as diagnostic probes of dense nuclear matter at Nuclotron energies has a substantial discovery potential.

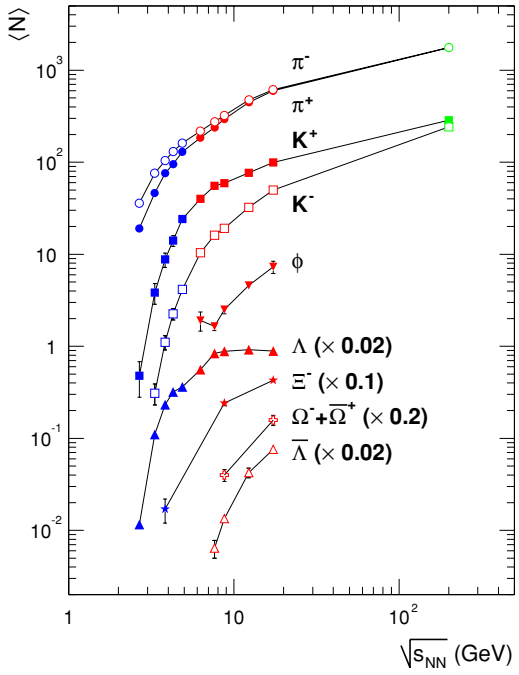

Figure 12.10: Yield of mesons and (anti-) hyperons as function of beam energy measured in central collisions of Au+Au (Pb+Pb). Taken from [43].

Search for strange matter

Hypernuclei

The search for hypernuclei offers the fascination perspective to explore the third (i.e. strange) axis of the chart of nuclei. Moreover, the investigation of (double-lambda) hypernuclei provides information on the hyperon-nucleon and even on the hyperon-hyperon interaction which play an important role in neutron star models. Most of the known hypernuclei have been produced in experiments with K- beams bombarding light

nuclei. In a strangeness exchange reaction the s quark was transferred from the K^- meson to a nucleon forming a lambda hyperon which was trapped in the nucleus. In violent collisions between the K^- meson and the nucleon, a double-strange Ξ^- hyperon may be produced (together with a K^+). If the Ξ^- hyperon is trapped in another nucleus, the two strange quarks may be transferred to two nucleons forming two lambdas, and eventually a double-lambda nucleus is created. In most of the experiments up to date the decay of the double-lambda hypernucleus was observed in emulsions. Only very few double-lambda hypernuclei have been found so far.

In contrast to the method described above we propose to produce (double-lambda) hypernuclei in heavy-ion collision via coalescence of lambdas with nucleons or light fragments. In high-energy nucleus-nucleus collisions lambdas are produced abundantly. Due to the decrease of the baryon-chemical potential with increasing beam energy, the maximum lambda yield is observed at beam energies between 30 and 40 A GeV. In central Pb+Pb collisions at these energies about 50 lambdas are produced (see Fig. 12.10). In central Au+Au collisions at 4 A GeV still 4 lambdas are produced. The probability for coalescence of lambdas with protons or light nuclei like He, however, increases with decreasing beam energy, i.e. with decreasing temperature of the fireball, and, hence, increasing He yield. This is illustrated in Fig. 12.11 where the yield of (multi-strange) hypernuclei as calculated with a thermal model is plotted as function of beam energy [44]. The yield of ^{3}He and ^{4}He strongly increases with decreasing beam energy, and the maximum yield of $\Lambda\Lambda^5H$ and $\Lambda\Lambda^6He$ is predicted for collision energies of $\sqrt{NN} = 4 - 5$ GeV ($\approx 8 - 10$ A GeV beam energy for stationary target experiments). According to this calculation, we expect at Nuclotron energies (4 A GeV) yields of $4 \cdot 10^{-8}$ $\Lambda\Lambda^6He$, $2 \cdot 10^{-6}$ $\Lambda\Lambda^5H$, and $2 \cdot 10^{-2}$ Λ^3H per central collision. Experimentally one has to reconstruct the decay chain of the hypernuclei, for example: $\Lambda\Lambda^5H \rightarrow \Lambda^5He + \pi^-$, $\Lambda^5He \rightarrow^4 He + \Lambda$; $\Lambda \rightarrow p + \pi^-$.

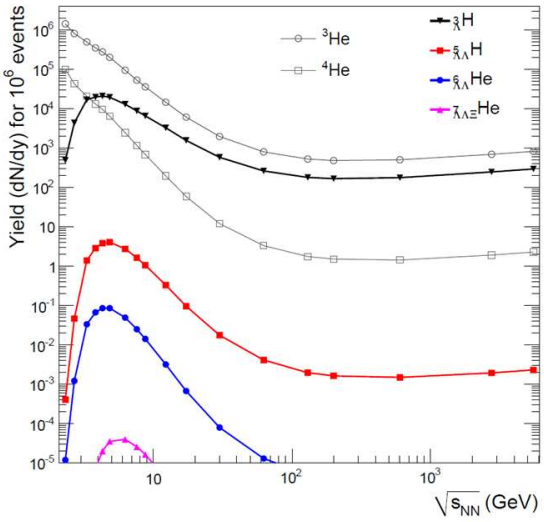

Figure 12.11: Energy dependence of hypernuclei yields at midrapidity for 10^6 central collisions calculated with a thermal model [44]. The predicted yields of ^{3}He and ^{4}He nuclei are included for comparison.

Multi-strange meta-stable objects

Forms of meta-stable or even stable objects with strangeness have been proposed long ago as collapsed states of matter, either consisting of baryons or quarks. Up to date, none of these objects, e.g. strangelets and (strange) di-baryons, have been observed. Moreover, no reliable predictions for the multiplicities of these objects in heavy-ion collisions at Nuclotron energies are available. At higher energies, calculations with a hybrid model have been performed [13]. With a detector system which is able to identify hyperons it is definitely worthwhile to search for a strange dibaryon like a $(\Xi\Lambda)_b$ which decays into two lambdas.

Experimental requirements

Experimentally the Λ, Ξ, and Ω hyperons can be identified via the topology of their weak decays ($\Lambda \rightarrow p\pi$, $\Xi \rightarrow \Lambda\pi$, $\Omega \rightarrow \Lambda K$) (see Fig. 12.12). We have performed simulations using the UrQMD event generator, the CBM detector model in the GEANT transport code, and the event reconstruction algorithms in the CBMRoot software package [46]. The CBM detector model comprises 8 stations of double-sided silicon micro-strip detectors (pitch 60 μm, stereo angle 15°) located in the field of a large aperture dipole magnet. The geometrical

acceptance of the setup is $2.5° - 25°$ for polar angles and $0° - 360°$ for azimuth angles. Some results of the simulations are shown in Fig. 12.13 which depicts the invariant mass spectra for K^0s mesons, Λ hyperons, and Ξ^- hyperons for central Au+Au collisions at 4 A GeV. The analysis is based on topological cuts only, without particle identification via time-of-flight determination. The combinatorial background can be further reduced by identifying the decay protons by a time-of-flight measurement.

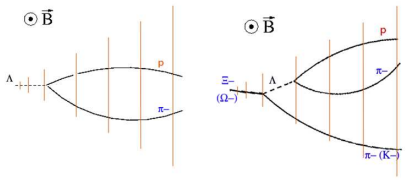

Figure 12.12: Decay topologies of lambda hyperons (left) and of Ξ^- and Ω^- hyperons (right). Detector planes are indicated as lines, the magnetic field is perpendicular to the plane.

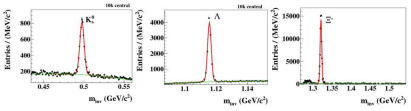

Figure 12.13: Reconstructed K^0s mesons, Λ hyperons, and Ξ^- hyperons (from left to right) for central Au+Au collisions at 4 A GeV using the UrQMD event generator, the CBM model in the GEANT transport code, and the event reconstruction algorithms in the CBMRoot software package [46]. The yields correspond to 10^4 collisions for K^0s and Λ, and to 10^8 collisions for Ξ^-.

The results of the simulations discussed in the last chapter demonstrate that a tracking system consisting of 8 stations of Silicon strip detectors located inside a large aperture dipole magnet field is well suited to perform the hyperon measurements. The last Silicon tracking stations near the exit of the magnet may be replaced by several layers of segmented straw-tube detectors. Here, the hit density is reduced to about 0.05 hits/cm^2 for min. bias collisions of Au+Au at 4 A GeV, and straw-tube of 4 mm diameter with segments of 2 cm length will be sufficient to obtain an occupancy of 4%. The experimental setup will be complemented by a TOFwall based on MRPCs, and by drift chambers for intermediate tracking.

In Table 12.1 the expected hyperon yields from central and minimum bias Au+Au collisions at 4 A GeV are listed. The multiplicities for central collisions are calculated with a statistical model [15], and were divided by a factor of 4 for minimum bias collisions. The yields are calculated assuming a typical reaction rate of 105/s corresponding to a beam intensity of 107 with and a 1% interaction target. The yields of hypernuclei calculated under the same assumptions are given in Table 12.2. According to the calculations the measurement of $\Lambda\Lambda^5H$ seems promising.

It is important to mention that these measurements require a high-speed data read-out and acquisition system to perform an online data analysis in order to select events containing secondary vertices from Λ hyperon decays.

Hyperions	E_{thr}NN GeV	M central	M min.bias	ε %	Yield/s min. bias	Yield/week min. bias
Ξ^-	3.7	$1 \cdot 10^{-1}$	$2.5 \cdot 10^{-2}$	3	75	$4.5 \cdot 10^7$
Ω^-	6.9	$2 \cdot 10^{-3}$	$5 \cdot 10^{-4}$	3	1.5	$9 \cdot 10^5$
Anti-Λ	7.1	$2 \cdot 10^{-4}$	$5 \cdot 10^{-5}$	15	0.15	$9 \cdot 10^4$
Ξ^+	9.0	$6 \cdot 10^{-5}$	$1.5 \cdot 10^{-5}$	3	$4.5 \cdot 10^{-2}$	$2.7 \cdot 10^4$
Ω^+	12.7	$1 \cdot 10^{-5}$	$2.5 \cdot 10^{-6}$	3	$7.5 \cdot 10^{-3}$	$4.5 \cdot 10^3$

Table 12.1: Expected hyperon yields from central and minimum bias Au+Au collisions at 4 A GeV for reaction rates of 10^5/s. The multiplicities per event are calculated with a statistical model [47]. The efficiency is based on the CBM detector model.

Hyper-nucleus	M central	M min.bias	ε %	Yield/s min. bias	Yield/week min. bias
$\Lambda^3 H$	$2 \cdot 10^{-2}$	$5 \cdot 10^{-3}$	1	5	$3 \cdot 10^6$
$\Lambda\Lambda^5 H$	$2 \cdot 10^{-6}$	$5 \cdot 10^{-7}$	1	$5 \cdot 10^{-4}$	300
$\Lambda\Lambda^6 He$	$4 \cdot 10^{-8}$	$1 \cdot 10^{-8}$	1	$1 \cdot 10^{-5}$	6

Table 12.2: Expected yields of hypernuclei from central and minimum bias Au+Au collisions at 4 A GeV for reaction rates of 10^5/s. The multiplicities per event are calculated with a statistical model [44]. The efficiency is based on the CBM detector model.

A new generation fixed-target experiment using the intense nuclear beams from the Nuclotron will offer novel possibilities to investigate the equation-of-state (EOS) of dense nuclear matter which plays a central role for the dynamics of core collapse supernovae and for the stability of neutron stars. Promising observables in this respect are multi-strange hyperons which have not been measured yet in the Nuclotron beam energy range. Moreover, in nucleus-nucleus collisions at Nuclotron energies a variety of hypernuclei will be produced by coalescence of lambdas with nucleons or light fragments. Even double-lambda hypernuclei could be identified with a dedicated experiment and high beam intensities. In addition, such an experiment would be ideally suited for the search for exotic objects like double-strange dibaryons. The detailed study of (multi-strange) hyperons and hypernuclei, and the discovery of strange heavy objects in the Nuclotron energy range will trigger a breakthrough in our understanding of dense and strange matter, and would pave the road for the experimental exploration of the 3rd dimen-sion of the nuclear chart.

12.6 Deeply Subthreshold Particle Production in Nucleus-Nucleus Collisions

S. Mrówczyński

Institute of Physics, Jan Kochanowski University, Kielce, Poland
National Centre for Nuclear Research, Warsaw, Poland

Particle production in nucleus-nucleus collisions is known to occur at initial energies per nucleon smaller than the threshold energy for the process in interactions of two free nucleons. These are the so-called *subthreshold* reactions which are usually described in terms of transport models [48] where the Fermi motion of nucleons of colliding nuclei plays a crucial role in the energy-momentum balance. The models certainly make sense - and indeed they successfully describe the data - if the collision energy is not too small that nucleons responsible for particle production are not far away from the mass shell. In case of deeply subthreshold processes, an applicability of the transport models becomes questionable, as the production process has to be highly collective or equivalently nucleons involved in the process must be driven far away from the mass shell.

Development of experimental techniques allowed one to observe the production of pions in C-C collisions at an energy as small as merely 6 MeV above the absolute threshold [49]. The 'absolute' means that the total kinetic energy of colliding nuclei has to be converted (in the center-of-mass frame) into pion mass to satisfy the energy-momentum conservation. Close to the absolute threshold, a mechanism of particle production has to be maximally collective - a colliding nucleus must act like a single particle. Atomic nuclei behave in such a way when the collision energy is smaller than the binding energy of a single nucleon but in case of pion production in C-C interactions the collision energy in the center-of-mass frame is almost 20 times bigger than the binding energy. This show how nontrivial the production mechanism near the absolute threshold must be.

Experimental data on pion subthreshold pion production are relatively abundant. There are also some data on subthreshold kaon production [50] at a collision energy which is, however, rather far from the absolute threshold. It is not surprising, as the production cross sections dramatically decrease when the collision energy approaches the absolute threshold. The above mentioned cross section of the pion production in C-C collisions observed 6 MeV above the absolute threshold was measured to be only 200 picobarns [49]. And it is certainly an experimental challenge to observe such rare processes. Due to the smallness of the cross section, it is fairly unclear whether the kaon production in, say, C-C collisions close to the absolute threshold is experimentally accessible. The estimate given in [51] is rather pessimistic but the estimate simply extrapolates the nuclear form factor to a high momentum where the form factor is actually no longer known. A surprise is thus possible.

The NICA facility, which is planned to operate both in the fixed target and collider mode, offers a unique possibility to systematically study subthreshold production of pions, kaons, and possibly antiprotons. A broad

range of energies and masses of accelerated ions is particularly useful here. One could start with the particle production in p-p collisions to have a reference point. The threshold energies in the center-of-mass frame for the pion, kaon and antiproton production read, respectively, $m_\pi = 140$ MeV, $m_\Lambda - m_p + m_K = 672$ MeV and $2m_p = 1877$ MeV with $m_\pi, m_p, m_\Lambda, m_K$ being the masses of charged pions, protons, lambdas and kaons. The thresholds correspond to the following laboratory projectile energies in the fixed target p-p collisions: 1 229 MeV, 2 253 MeV and 6 568 MeV. Having the p-p reference point, one would move to light ions like ^{4}He, and finally experiments with heavier ions could start. An observation of pion production a few MeV above the threshold in p-p collisions should not be very difficult. Analogous observation in collisions of heavy-ions is a real challenge. In case of kaons and antiprotons, it is fairly unclear how close the absolute threshold can be approached.

Particle production near absolute threshold is theoretically rather poorly understood because of high momentum transfers occurring in the processes. A nucleus cannot be treated in such a case as a collection of almost independent from each other nonrelativistic nucleons on mass-shell. Inter-nucleon correlations, relativistic effects and propagation of nucleons off mass-shell should be all taken into account. The experimental program at NICA would greatly stimulate theoretical studies of these problems of relativistic nuclear physics has been practiced in Dubna for years.

12.7 Production of exotic hypernuclei and hyper-matter

A. S. Botvina

Institute for Nuclear Research, Russian Academy of Sciences, Moscow, Russia

Pioneering experiments on production of hypernuclei can be performed at the NICA facility with fixed targets. The peripheral collisions of relativistic ions are very promising for searching mutli-strange and exotic hypernuclei which are not easy accessible with other experimental methods. In these experiments one can also get information on the Equation of State of hyper-matter around nuclear saturation density at low and moderate temperatures.

In nuclear reactions at high energies strange particles (baryons and mesons) are produced abundantly, and they are strongly involved in the reaction process. The specifics of hypernuclear physics is that there is no direct experimental way to study hyperon–nucleon (YN) and hyperon–hyperon (YY) interactions ($Y = \Lambda, \Sigma, \Xi, \Omega$). When hyperons are captured by nuclei, hypernuclei are produced, which can live long enough in comparison with nuclear reaction times. Therefore, a nucleus may serve as a laboratory offering a unique opportunity to study basic properties of hyperons and their interactions. Double- and multi-strange nuclei are especially interesting, because they are more suitable for extracting information about the hyperon–hyperon interaction and strange matter properties.

The investigation of hypernuclei allows to answer many fundamental questions: Studying the structure of hypernuclei helps to understand the structure of conventional nuclei too [52] and it leads to an extension of the nuclear chart into the strangeness sector [53]. Hypernuclei provide a bridge between traditional nuclear physics (dealing with protons and neutrons) and hadron physics. Strangeness is an important degree of freedom for the construction of QCD motivated models of strong interactions [54]. Hyperons are also very important in many astrophysical sites, e.g., they are abundantly produced in nuclear matter at high densities, which are realized in the core of neutron stars [55]. The only way to describe realistically these physical conditions is to study the hyperon interactions in laboratory, and select theoretical models which pass the careful comparison with experimental data.

It has been realized that the absorption of hyperons in spectator regions of peripheral relativistic ion collisions is a promising way for producing hypernuclei [56–59]. The basic mechanisms of such reactions were well established in analysis of collisions of conventional nuclei: Nucleons in the overlapping zone between the projectile and the target (participants) interact intensively with each other and produce many new particles including strange ones. These particles can re-scatter and propagate further towards the non-overlapping parts of nuclei (spectator residues) and can be captured there, if their relative kinetic energy is smaller than their potential in nuclear matter. This mechanism will lead to formation of excited normal spectators and hyper-spectators, which later on disintegrate into ordinary and hyper-fragments [60]. Very peripheral collisions lead to spallation of the normal nuclei and to fission of heavy ones. In mid-peripheral collisions, when temperatures of

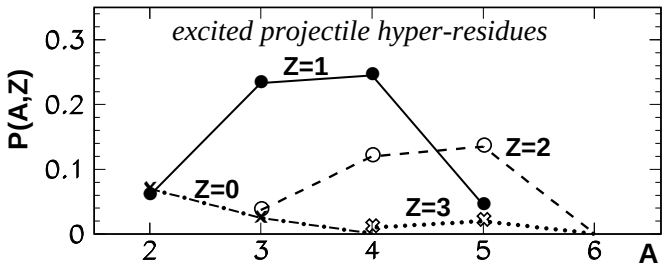

Figure 12.14: Ensemble of the projectile spectators with one absorbed Λ hyperon as predicted by DCM calculations for ^{6}Li (2 A GeV) + ^{12}C reaction: P(A,Z) is relative probability to produce specific excited hyper-residues with mass A and charge Z. The dot-dashed, solid, dashed, and dotted lines correspond to residues with Z=0, 1, 2, and 3, respectively.

excited spectators reach several MeV, multifragmentation reaction takes place, and this allows for investigation of the Equation of State (EOS) in the region of the nuclear liquid-gas phase transition [61, 62]. Since the Λ potential in nuclear matter is of the same order as the nucleon one we expect that similar processes will occur with hyper-spectators too. Such reactions may give access to heavy and exotic hypernuclei, as well as to very strange nuclei beyond S=–2 [59]. It was also predicted that the relative yields of hypernuclei produced in these reactions can reveal important information about their properties and provide a unique way for experimental studying hyper-matter at relatively low temperatures ($T \lesssim 10$ MeV) [60]. These are important advantages of the proposed measurements over experimental methods used presently in hyper-physics, which are mostly limited by investigations of hypernuclei with S=–1 in ground and weakly-excited states.

Actually, early experiments with light-ion beams at the LBL [63] and JINR [64] have demonstrated that hypernuclei can be formed in such reactions. Recently the HypHI collaboration at GSI Darmstadt has reported first results on the production of light hypernuclei in the disintegration of 2 GeV per nucleon ^{6}Li projectiles impinging on a ^{12}C target [65]. This experiment has confirmed the feasibility to produce hypernuclei abundantly in peripheral ion collisions. The observed production of $^{3}_{\Lambda}$H is by about a factor of three larger than the production of $^{4}_{\Lambda}$H. In a still preliminary analysis also indications for a significant bump in the π^--deuteron invariant mass distribution were found [66]. If confirmed in the ongoing analysis this observation could be interpreted as the formation of slightly bound Λ-neutron systems (Λn and Λnn), which seem to dominate over other hypernuclei.

It was theoretically demonstrated that this reaction can be explained within a hybrid approach including dynamical stage of production and capture of hyperons by spectators and statistical stage describing decay of such excited spectators into hypernuclei [67, 68]. The first stage of this collision process was described within the transport Dubna cascade model (DCM) [69, 70] taking into account absorption of Λ-hyperons [59]. The generalized for hyper-nuclei Fermi-break-up model [71] was used for the second stage.

The DCM calculations of ^{6}Li (2 A GeV) + ^{12}C collisions predict formation of a broad ensemble of projectile residues with captured Λ hyperons. After integration over all impact parameters this ensemble is shown in Fig. 12.14. The following evolution depends on excitation energy of these residues: Their baryon content will not change practically if the excitations are low. In the case of high excitations the residues will loose nucleons and small final hypernuclei will be produced predominantly, including exotic Λn hyper-systems [68].

We emphasize specially that the exotic Λ–neutron systems were never observed previously with traditional methods of hyper-physics, which use mainly a capture of hyperons produced by hadrons and leptons of high energy in nuclei without their excitation. The reason may be that a very low binding energy expected for the Λn systems (around few tens keV) can not be seen in such direct interactions releasing particles with large energy. On the other hand, the decay of moderately excited hyper-systems into small hypernuclei [71] is rather sensitive to the tiny binding energy. Therefore, the new reaction mechanism realized in peripheral collisions of relativistic ions makes possible to produce and investigate exotic hypernuclear species.

Another new important possibility is to study fragmentation and multifragmentation of hyper-matter produced in peripheral collisions of heavy ions. In this case one can address the EOS of hyper-matter at moderate

temperatures as previously it was done for conventional matter [72]: The method is to analyze the yields of fragments and hyper-fragments and their velocity correlations, which contain information about hyperon interaction in medium. For illustration, Fig. 12.15 shows probabilities for producing spectator residues with different numbers of captured Λs, in collisions of proton on gold and gold on gold at energies 2 and 20 GeV per nucleons [59].

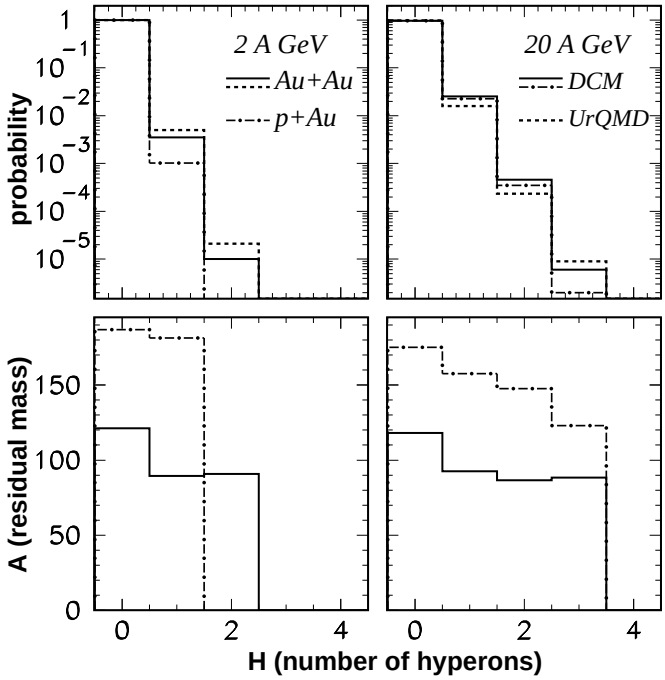

Figure 12.15: Probability for formation of conventional and strange spectator residuals (top panels), and their mean mass numbers (bottom panels) vs the number of captured Λ hyperons (H), calculated with DCM and UrQMD model for p + Au and Au + Au collisions with energy of 2 GeV per nucleon (left panels), and 20 GeV per nucleon (right panels) [59]. The reactions and energies are noted in the figure by different histograms.

The dynamical stage of these reactions was described by DCM [69, 70] and UrQMD (Ultra-relativistic Quantum Molecular Dynamics) [73, 74] models. One can see that both in proton-nucleus and nucleus-nucleus collisions the hyper-spectators can be formed abundantly. For example, the fraction of excited spectator residues with one Λ is in the range of from 0.1% (for the case of 2 GeV proton) to few percent of the total yield at 20 GeV. At the nuclotron's beam energy of 4.5 A GeV the estimated probability of one Λ capture will be around 0.3% for p + Au and more than 1% for Au + Au collisions. The probabilities for capturing two Λs will be by nearly two order lower, and the probability for three Λ to be captured is around 10^{-6}. However, these reaction probabilities are quite sufficient for hyper-physical experiments which are usually adjusted for cross-sections about few nanobarns. The absorption of a higher number of hyperons is also feasible. This new mechanism opens a unique opportunity to produce and study multi-strange systems, which are not conceivable in other nuclear reactions. As discussed, later on the hot spectators disintegrate, and final fragments with products of weak decay of hypernuclei can be measured by detectors. Statistical models, see refs. [60, 61, 71], can be used to describe this stage of the process. Relativistic spectators have also obvious experimental advantages: Because of the Lorentz factor their lifetime is longer, the projectile hyper-fragments can travel a longer distance. This makes possible to use sophisticated vertex detectors and fragment separation technique for their identification.

One should remember, that the considered reaction process is qualitatively different from the production mechanisms of light hypernuclei coming from decay of very excited (T∼ 160 MeV) fireballs with strangeness admixture, which are formed in central relativistic heavy-ion collisions, . In this case coalescence-like processes are most probable for cluster production. There is hard to expect production of big and weakly bound nuclei,

because of a large energy deposited in the fireball [44, 75]. Nevertheless, after full construction of the NICA facility, this kind of measurements may also be done by colliding relativistic beams and detecting species coming from the midrapidity region.

In conclusion, an advantage of the proposed novel experiments is that they can be already performed at the first stage of the NICA project with nuclotron beams by using the fixed targets. It is instructive that the very first experimental identification of a hypernucleus was performed in similar collisions: This event was observed in a multifragmentation reaction induced by a cosmic energetic proton or ion in photo-emulsion [76]. Recently, encouraging results in studying spectator hypernuclei were obtained in GSI experiments [65, 66]. As we have shown theoretically [59, 60, 67, 68, 71], the process of formation of moderately-excited hyper-nuclear systems ($T \approx 1 - 10$ MeV) in peripheral collisions of relativistic ions with their subsequent disintegration is a natural way to produce new and exotic hypernuclei. We know also from studies of conventional nuclei [61, 72] that investigation of such systems can provide effective methods to extract the EOS of hyper-matter at densities around the nuclear saturation density. Hypernuclear physics will benefit strongly from exploring the new production mechanism realized in peripheral ion collisions and the novel detection technique associated with fragmentation reactions of excited nuclei.

12.8 Light Hyper-Fragments Production in Au+Au central collisions at $4AGeV$. Model predictions.

K. K. Gudima

Institute of Applied Physics, Academy of Science of Moldova, Kishinev, Moldova

We study the formation of light hyper-fragments in high energy central collisions of Au+Au ions at Nuclotron energy of $4AGeV$ within intra-nuclear cascade model developed in Dubna [69, 70, 77]. (We refer to it as the Dubna Cascade Model - DCM.) The DCM is based on the Monte Carlo solution of a set of the Boltzmann-Uehling-Uhlenbeck relativistic kinetic equations with the collision terms, including cascade-cascade interactions. For particle energies below $1GeV$ it is sufficient to consider only nucleons, pions and deltas. The model includes a proper description of pion and baryon dynamics for particle production and absorption processes. At energies higher than about $5GeV$, the Quark-Gluon String Model (QGSM) is used to describe elementary hadron collisions. The QGSM considers the two lowest SU(3) multiplets in mesonic, baryonic and antibaryonic sectors, so interactions between almost 70 hadron species are treated on the same footing. The above noted two energy extremes were bridged by the QGSM extension downward in the beam energy using the mix-and-match method.

During collision of heavy ions strangeness is produced abundantly and is likely to form clusters of different sizes. We can discriminate two distinct mechanisms for hyper-cluster formation in heavy ion collisions. First, the absorption of hyperons in the spectator fragments of non central collisions. In this scenario one is interested in hyperons which propagate with velocities close to the initial velocities of the nuclei, i.e. in the vicinity of nuclear spectators [59]. In this case one can obtain rather large and moderately excited hyper-system decaying into hyper-fragments later on [60] approaches. In other scenario we use DCM-QGSM transport model to provide us with the phase space information of all hadrons produced in a heavy ion collisions. This information then serves as an input for coalescence prescription. For the present study the coalescence model has been modified in comparison with its initial formulation in [69].

As usual, the coalescence model forms a deuteron from a proton and a neutron produced after the cascade stage of reaction if their relative momenta are within a sphere of radius p_C, comparable to the deuteron's momentum. The same momentum criterion can be used to describe formation of $tritons$, ^3He, and α-particles. In particular, the parameters $p_C(d) = 90$, $p_C(t) = 108$, $p_C(^3He) = 108$, and $p_C(^4He) = 115(MeV/\mathrm{c})$ were adopted [69] to reproduce the experimental data. An approach disregarding the spacial coordinates of nucleons can be justified only for collisions with moderate energy deposition in nuclei since the region for final state interaction is small enough. However, this is not the case for central heavy ion collisions.

Here we assume that the coalescence criterion used to form the composite particles includes the proximity of nucleons both in the momentum and coordinate space. The coordinate coalescence parameters are determined by the relation $r_C = \hbar/p_C$, with the same values of p_C as were used in [69]. As a first approximation we use the same coalescence parameters for both conventional fragments and hyper-fragments. An example of the calculated invariant yields of the fragments produced in the central $Au + Au$ collisions at projectile momentum $11.5AGeV$ is shown in Fig. 12.16, where model prediction are compared with experimental data [78]. One

can understand that at this energy the coalescence model reproduces qualitatively the experimental data for conventional fragments.

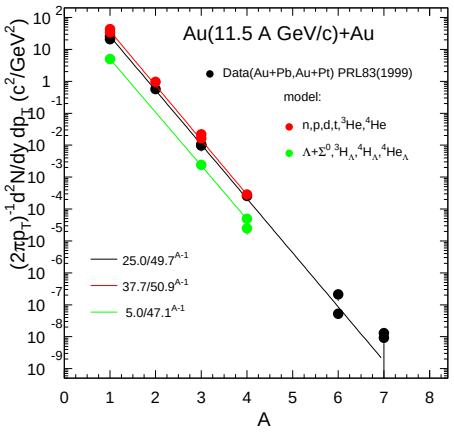

Figure 12.16: Invariant multiplicities of fragments produced in central collisions Au+Au at 11.5 A GeV/c compared with experimental data. Lines are fits of data and model predictions.

The fragments yields fit very close to exponential dependence with a penalty factor of approximately 50 for each nucleon added in agreement with the data. Due to the fact that the same coalescence parameters were used a similar penalty factor is obtained for hyper-fragments, which is supplemented by additional suppression if the neutron is replaced by a Λ. For the following results we fixed the coalescence parameters as described, with a fit to the data at $11.5 AGeV$, and assume that they do not change with beam energy. This allows us to predict cluster production over a wide range of beam energies [75].

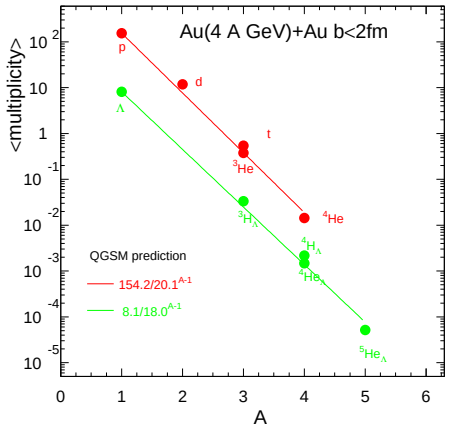

Figure 12.17: Mass number dependence of multiplicity of fragments produced in central collisions Au+Au at 4 A GeV. Lines are fits to the model predictions.

The production of strange particles at Nuclotron energy of 4 A GeV is sufficient to produce observable amount of hyper-fragments. On Fig.12.17 are shown the baryon number dependence of multiplicity of conventional fragments and hyper-fragments produced in central collisions of gold nuclei at this energy.

One can observe that the model predicts the same exponential dependence with a penalty factor close to

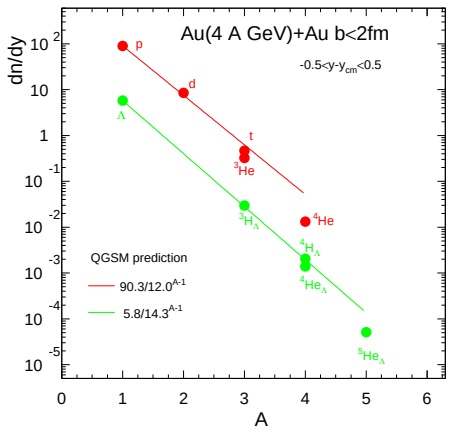

Figure 12.18: Midrapidity yield of fragments produced in central collisions Au+Au at 4 A GeV/c. Lines are fits of model predictions.

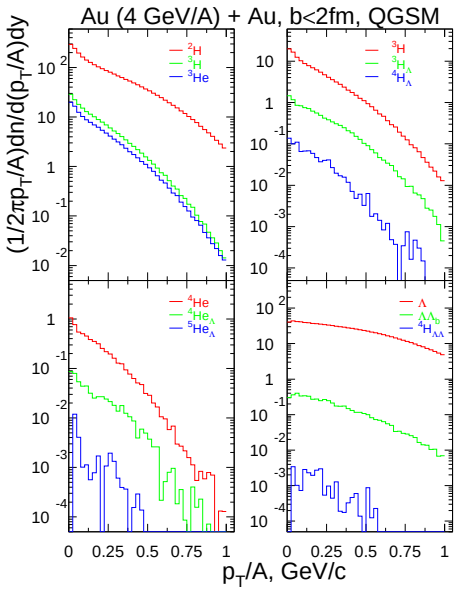

Figure 12.19: Invariant multiplicities of fragments produced in central collisions Au+Au at 4 A GeV at midrapidity.

20 for both conventional and hyper-fragments. Our estimations are based on statistics of 10^6 central collisions of gold nuclei, that is sufficient to present on Fig.12.18 the same dependence of dn/dy at midrapidity. Here the penalty factor is slightly less than for multiplicity. The invariant multiplicities for $-0.5 < y - y_{\rm cm} < 0.5$ of conventional fragments, hyper-fragments, and H di-baryon ($\Lambda\Lambda$) in dependence of transverse momentum p_t/A are presented on Fig.12.19

For another promising experimental observable the double ratio $R_{\rm H} = {}^3_\Lambda H/{}^3He/(\Lambda/p)$ our model predicts 1.67 and a ratio of 1.28 if Λ includes Σ^0 (experiments usually cannot distinguish between Λ's and Σ^0). These ratios are calculated using integrated multiplicities. If for calculation of double ratio $R_{\rm H}$ are used the fragment yields in rapidity window $-0.1 < y - y_{\rm cm} < 0.1$ model gives 1.38 and 1.05 respectively.

These predictions can be useful to planning of experiments within the BM&N project.

12.9 Hypernuclei Production in Heavy Ion Collisions

A. LeFevre[a], Ch. Hartnack[b], Y. Leifels[a], J. Aichelin[b]

[1] *GSI Helmholtzzentrum für Schwerionenforschung GmbH, Darmstadt, Germany*

[2] *SUBATECH, Laboratoire de Physique Subatomique et des Technologies Associées, University of Nantes, Nantes, France*

Hyper nuclei are not only a laboratory to study the interaction among strange and non strange baryons [79] but can be as well a very useful tool to study the space time evolution of heavy ion reactions . Therefore recently the first attempts have been made to produce hypernuclei in heavy ion reactions [**?**,65]. If this method could be established not only hypernuclei can be produced in numbers but their multiplicity and momentum space distribution provides also valuable information on the time evolution of heavy ion reactions. The reason is that the Λ which is formed in these collisions has to find fellow nucleons to form a hyper nucleus and therefore the production yield depends on the phase space distribution (and not only the momentum distribution) of the nucleons around the Λ. As for normal multifragmentation [80] there will be two formation processes. Hypernuclei can be formed by coalescence type processes from participant matter [58, 67] . This will be the dominant process at midrapidity and will create light hypernuclei. Around projectile and target rapidity for hypernucleus formation the Λ has to be absorbed in the preformed target/projecile fragments [80]. There also heavier hypernuclei may be created. Theoretical approaches based on the Simulated Annealing procedure [81] are presently under way.

Because the Λ is produced by participant nucleons the hypernucleus production in the target/projectile region will provide information about the interaction between spectators and participants and therefore about the space time evolution of the system. Such a space time information is necessary to clarify the mechanism of multi fragmentation at these energies, which is still not understood.

Bibliography

[1] C. Hartnack, R. K. Puri, J. Aichelin, J. Konopka, S. A. Bass, H. Stoecker and W. Greiner Eur. Phys. J. **A 1,** 151 (1998), [arXiv:nucl-th/9811015]

[2] J. Aichelin, Phys. Rep. **202,** 233 (1991).

[3] W. Cassing and E. L. Bratkovskaya, Phys. Rep. **308,** 65 (1999).

[4] S. A. Bass *et al.*, Progr. Part. Nucl. Phys. **41,**255 (1998); **41**, 225 (1998), [arXiv:nucl-th/9803035].

[5] G. A. Leksin, Yad Fiz. **65** 2042 (2002).

[6] V. A. Matveev, R. M. Muradyan and A. N. Tavkhelidze, Lett. Nuovo Cim. **7**, 719 (1973).

[7] S. J. Brodsky and G. R. Farrar, Phys. Rev. Lett. **31,** 1153 (1973).

[8] C. White *et al.*, Phys. Rev. **D 49,** 59 (1994).

[9] J. Napolitano, *et al.*, Phys. Rev. Lett. **61,** 2530 (1988); P. Rossi *et al.*, Phys. Rev. Lett. **94,** 012301 (2005).

[10] I. Pomerantz, Phys. Lett. **B 684,** 106 (2010).

[11] S.J. Brodsky *et al.*, Phys. Lett. **B 578,** 69 (2004).

[12] Yu.N. Uzikov, JETP Lett. **87** 387 (2005).

[13] Eds. A. N. Sissakian, V. V. Burov, A. I. Malakhov *Proc. of 18 Int. Baldin Seminar on High Energy Physics Problem* (Dubna, 25-30 Sept., 2006), V.I p.51.

[14] G. Bizard, J.L. Laville, C.Le Brun *et al.*, Phys. Rev. **C 22,** 1632 (1980).

[15] P. Koch, B. Müller and J. Rafelski, Phys. Rep. **142,** 167 (1986).

[16] E. Andersen *et al.*, Phys. Lett. **B 417,** 202 (1999).

[17] see e.g. F. Beccattini, J. Manninnen and M. Gadzdicki, Phys. Rev. C **73**, 044905 (2006).

[18] R. Stock, Phys. Lett. **B 456,** 277 (1999).

[19] P. Braun-Munzinger, C. Wetterich and J. Stachel, Phys. Lett. **B 596,** 61 (2004).

[20] A. Andronic *et al.*, Nucl. Phys. **A 837,** 65 (2010).

[21] G. Agakishiev *et al.*, Phys. Rev. Lett. **103,** 132301 (2009).

[22] S. Wheaton and J. Cleymans, Comp. Phys. Comm. **180**, 84 (2009).

[23] P. Chung *et al.*, Phys. Rev. Lett. **91,** 202301 (2003).

[24] C. Alt *et al.*, Phys. Rev. **C 78,** 034918 (2008).

[25] J. Schaffner-Bielich, R. Matiello and H. Sorge, Phys. Rev. Lett. **84,** 4305 (2000).

[26] C. Alt *et al.*, Phys. Rev. **C 78,** 044907 (2008).

[27] B. Alessandro *et al.*, Phys. Lett. **B 555,** 147 (2003).

[28] A. Kurepin, *6th International Workshop on Critical Point and Onset of Deconfinement, CPOD 2010* (Dubna, Russia, 2010), to appear in Yad. Fiz.

[29] A. M. Baldin, Sov. Phys. Dokl. **20**, 418 (1975).

[30] A. M. Baldin, Sov. Phys. Dokl. **29**, 1031 (1984).

[31] A. M. Baldin and L. A. Didenko, Fortschr. Phys. **38**, 261 (1990).

[32] V. I. Mikhailichenko *et al.*, Phys. At. Nucl. **62**, 1665 (1999).

[33] V. A. Okorokov *et al.*, Phys. At. Nucl. **73**, 1963 (2010).

[34] V. A. Okorokov *et al.*, *Proceedings of the Scientific Session MEPhI-2000*, MEPhI. V.7, 218 (2000); ibid 220.

[35] B. Friman, W. Nurenberg, V.D. Toneev, Eur. Phys. J. **A 3**, 165 (1998).

[36] C. Fuchs, Prog. Part. Nucl. Phys. **56**, 1 (2006).

[37] W. Reisdorf *et al.*, (FOPI collaboration), [arXiv:1112.3180 [nucl-ex]], Nucl. Phys. A in press.

[38] P. Danielewicz, R. Lacey and W.G. Lynch, Science 298, 1592 (2002).

[39] C. Sturm *et al.*, (KaoS collaboration), Phys. Rev. Lett. **86**, 39 (2001).

[40] C. Fuchs *et al.*, Phys. Rev. Lett. **86**, 1974 (2001).

[41] C. Hartnack and J. Aichelin, J. Phys. G **28**, 1649 (2002).

[42] K. Gudima *et al.*, private communication.

[43] C. Blume, J. Phys. G **31** (2005).

[44] A. Andronic *et al.*, Phys. Lett. **B 695**, 203 (2011).

[45] H. St?cker et al., Nucl. Phys. **A 827**, 624 (2009).

[46] I. Vassiliev, CBM Progress Report 2011

[47] A. Andronic, private communication

[48] U. Mosel, Ann. Rev. Nucl. Part. Sci. **41**, 29 (1991).

[49] D. Horn *et al.*, Phys. Rev. Lett. **77**, 2408 (1996).

[50] R. Legrain *et al.*, Phys. Rev. C **59**, 1464 (1999).

[51] St. Mrówczyński, Phys. Lett. B **220**, 337 (1989).

[52] O. Hashimoto, H. Tamura, Prog. Part. Nucl. Phys. **57**, 564 (2006).

[53] J. Schaffner, C.B. Dover, A. Gal, C. Greiner, and H. Stoecker, Phys. Rev. Lett. **71**, 1328 (1993).

[54] P. Papazoglou, S. Schramm, J. Schaffner-Bielich, H. Stoecker, and W. Greiner, Phys. Rev. **C 57**, 2576 (1998)

[55] J. Schaffner and I.N. Mishustin, Phys. Rev. **C 53**, 1416 (1996).

[56] M. Wakai, H. Bando and M. Sano, Phys. Rev. **C 38**, 748 (1988).

[57] Z.Rudy, W.Cassing *et al.*, Z. Phys. **A 351**, 217 (1995).

[58] Th. Gaitanos, H. Lenske, and U. Mosel, Phys. Lett. **B 675**, 297 (2009).

[59] A.S. Botvina, K.K. Gudima, J. Steinheimer, M. Bleicher, I.N. Mishustin, Phys. Rev. **C 84**, 064904 (2011).

[60] A.S. Botvina and J. Pochodzalla, Phys. Rev. **C 76**, 024909 (2007).

[61] J.P. Bondorf, A.S. Botvina, A.S. Iljinov, I.N. Mishustin, and K. Sneppen, Phys. Rep. **257**, 133 (1995).

[62] R. Ogul *et al.*, Phys. Rev. **C 83**, 024608 (2011).

[63] K.J. Nield *et al.*, Phys. Rev. **C 13**, 1263 (1976).

[64] S. Avramenko *et al.*, JETP Lett. **48**, 516 (1988);
S. Avramenko *et al.*, Nucl. Phys. **A 547**, 95 (1992).

[65] T.R. Saito *et al.* (HypHI collaboration), Nucl. Phys. **A 881**, 218 (2012).

[66] T.R. Saito (HypHI collaboration), *ECT workshop 'Strange Hadronic Matter'*, (Trento, Italy, 2011), http://www.ectstar.eu/ ; NUFRA2011 conference, Kemer, Turkey, 2011, http://fias.uni-frankfurt.de/nufra2011/.

[67] A.S. Botvina *et al.*, Nucl. Phys. **A 881**, 228 (2012).

[68] A.S. Botvina, I.N. Mishustin and J. Pochodzalla, Phys. Rev. **C 86**, 011601 (2012).

[69] V.D. Toneev, K.K. Gudima, Nucl. Phys. **A 400**, 173 (1983).

[70] V.D. Toneev, N.S. Amelin, K.K. Gudima, S.Yu. Sivoklokov, Nucl. Phys. **A 519**, 463c (1990).

[71] A.S. Lorente, A.S. Botvina, and J. Pochodzalla, Phys. Lett. **B 697**, 222 (2011).

[72] *Dynamics and thermodynamics with nuclear degrees of freedom*, edited by Ph. Chomaz, F. Gulminelli, W. Trautmann, and S.J. Yennello (Springer, Berlin/Heidelberg/New York, 2006); Eur. Phys. J. **A 30**, 1 (2006).

[73] M. Bleicher *et al.*, J. Phys. **G 25**, 1859 (1999).

[74] S. A. Bass *et al.*, Prog. Part. Nucl. Phys. **41**, 255 (1998).

[75] J. Steinheimer *et al.*, Phys. Lett. **B 714**, 85 (2012).

[76] M. Danysz and J. Pniewski, Philos. Mag. **44**, 348 (1953).

[77] N.S. Amelin, K.K. Gudima, s.Yu. Sivoklokov, V.D. Toneev, Sov. J. Nucl. Phys. 52 (1990) 272

[78] T.A. Armstrong et al. , E864 Collaboration, Phys. Rev. C61 (2000) 064908; Phys.Rev.Lett 83 (1999) 5431.

[79] J. Pochodzalla, Acta Phys. Polon. B **42** (2011) 833 [arXiv:1101.2790 [nucl-ex]].

[80] K. Zbiri, A. L. Fevre, J. Aichelin, J. Lukasik, W. Reisdorf, F. Gulminelli, U. Lynen and W. F. J. Muller *et al.*, Phys. Rev. C **75** (2007) 034612 [nucl-th/0607012].

[81] R. K. Puri and J. Aichelin, J. Comput. Phys. **162** (2000) 245 [nucl-th/9811018].

List of Contributors

1. Abraamyan Kh. (Section 7.3)
   Joint Institute for Nuclear Research, Dubna, Russia.

2. Aichelin J. (Section 12.1,12.9)
   SUBATECH, Laboratoire de Physique Subatomique et des Technologies Associées, Université de Nantes, Nantes, France.

3. Anderlik C. (Section 4.14)
   Uni-Computing, Bergen, Norway

4. Andrianov A. (Section 8.4)
   St.Petersburg State University, St.Petersburg, Russia.

5. Andrianov V. (Section 8.4)
   St.Petersburg State University, St.Petersburg, Russia.

6. Andronic A. (Section 6.7)
   GSI Helmholtzzentrum für Schwerionenforschung mbH, Darmstadt, Germany

7. Asakawa M. (Section 4.5, 5.9)
   Department of Physics, Osaka University, Toyonaka, Japan.

8. Avdeichikov V. V. (Section 7.7)
   Joint Institute for Nuclear Research, Dubna, Russia.

9. Becattini F. (Section 6.5)
   University of Florence, Florence, Italy.

10. Bednyakov I. V. (Section 6.9)
    Joint Institute for Nuclear Research, Dubna, Russia

11. Begun V. V. (Section 2.8)
    Bogolyubov Institute for Theoretical Physics, Kiev, Ukraine
    Institut für Kernphysik, Geothe-University, Frankfurt am Main, Germany.

12. Bellwied R. (Section 4.12)
    Physics Department, University of Houston, Houston, USA.

13. Benić S. (Section 3.15)
    Physics Department, University of Zagreb, Zagreb, Croatia

14. Blaschke D. (Sections 3.7, 3.9, 4.11, 3.13, 4.16)
    Joint Institute for Nuclear Research, Dubna, Russia.
    Institute for Theoretical Physics, University of Wrocław, Poland.

15. Bleicher M. (Sections 5.8, 6.6, 12.1, 4.20)
Frankfurt Institute for Advanced Studies (FIAS), Frankfurt, Germany.
Institut für Theoretische Physik, Goethe-Universität, Frankfurt, Germany.

16. Blume C. (Section 4.13)
Institut für Kernphysik, J. W. Goethe-Universität, Frankfurt, Germany.

17. Botvina S. (Section 12.7)
Institute for Nuclear Research, Russian Academy of Sciences, Moscow, Russia.

18. Bratkovskaya E. (Sections 2.4, 12.1)
Frankfurt Institute for Advanced Studies (FIAS), Frankfurt, Germany.

19. Bravina L.(Section 5.5)
Department of Physics, University of Oslo, Oslo, Norway.

20. Braun-Munzinger P. (Section 6.7)
Helmholtzzentrum für Schwerionenforschung MbH (GSI), Darmstadt, Germany.

21. Brodsky S. J. (Section 2.7)
SLAC National Accelerator Laboratory Stanford University, Stanford, California, USA.

22. Bugaev K. (Sections 3.5, 4.21, 5.8)
Bogolyubov Institute for Theoretical Physics, Kiev, Ukraine.

23. Buividovich P. V. (Section 8.2)
Joint Institute for Power and Nuclear Research, Minsk, Belarus.
Institute for Theoretical and Experimental Physics (ITEP), Moscow, Russia.

24. Bzdak A. (Section 8.7)
RIKEN BNL Research Center, Brookhaven National Laboratory, Upton, USA.

25. Cai X. (Section 4.14)
Huazhong Normal University, Wuhan, China

26. Cassing W. (Section 2.4)
Institut für Theoretische Physik, Universität Giessen, Giessen, Germany.

27. Csernai L. P. (Section 4.14)
University of Bergen, Norway

28. Cheng Y. (Section 4.14)
Huazhong Normal University, Wuhan, China

29. Chernodub M. N. (Section 8.2)
Institute for Theoretical and Experimental Physics (ITEP), Moscow, Russia.

30. Cleymans J.(Section 2.5)
Department of Physics, University of Cape Town, Cape Town, South Africa.

31. Colonna M.(Section 3.11)
INFN-Laboratori Nazionali del Sud (LNS), Catania, Italy.

32. Contrera G. A. (section 3.13)
Gravitation, Astrophysics and Cosmology Group, FCAyG, UNLP, La Plata, Argentina
CONICET, Buenos Aires, Argentina
Institute for Theoretical Physics, University of Wrocław, Poland

33. Costa P.(Section 4.2)
Departamento de Física, Universidade de Coimbra, Coimbra, Portugal.

34. Danielewicz P. (Section 4.16)
National Superconducting Cyclotron Laboratory and Department of Physics and Astronomy, Michigan State University, USA

35. Denisovskaya O. (Section 9.2)
Institute for Theoretical and Experimental Physics (ITEP), Moscow, Russia.

36. Di Toro M. (Sections 3.6, 3.11)
INFN-Laboratori Nazionali del Sud (LNS), Catania, Italy.
University of Catania, Catania, Italy.

37. Donets D. E. (Section 11.3)
Joint Institute for Nuclear Research, Dubna, Russia.

38. Donets E. D. (Section 11.3)
Joint Institute for Nuclear Research, Dubna, Russia.

39. Donets E. E. (Section 11.3)
Joint Institute for Nuclear Research, Dubna, Russia.

40. Dremin I. (Section 6.2)
P. Lebedev Physical Institute, RAS, Moscow, Russia.

41. Efremov A.(Sections 10.1, 10.2)
Joint Institute for Nuclear Research, Dubna, Russia.

42. Espriu D. (Section 8.4)
University of Barcelona, Barcelona, Spain.

43. Fantoni S. (Section 11.1)
International School for Advanced Studies, SISSA, Italy and INFN, Trieste, Italy.

44. Ferrer E. J. (Section 8.8)
University of Texas at El Paso, USA

45. Filip P. (Section 11.4)
Institute of Physics, Slovak Academy of Sciences, Bratislava, Hungary

46. Friese V.(Section 12.3)
Helmholtzzentrum für Schwerionenforschung MbH (GSI), Darmstadt, Germany.

47. Friesen A. (Section 7.3)
Joint Institute for Nuclear Research, Dubna, Russia.

48. Fukushima K.(Section 3.8)
Yukawa Institute for Theoretical Physics, Kyoto University, Kyoto, Japan.

49. Gandolfi S. (Section 11.1)
Theoretical Division, Los Alamos National Laboratory, Los Alamos, USA.

50. Gazdzicki M. (Section 2.1, 2.8)
Institut für Kernphysik, Goethe-Universität, Frankfurt, Germany.
J. Kochanowski University, Kielce, Poland.

51. Gorenstein M. (Section 5.4, 2.8)
Bogolyubov Institute for Theoretical Physics, Kiev, Ukraine.

52. Greco V. (Sections 3.6, 3.11)
INFN-Laboratori Nazionali del Sud (LNS), Catania, Italy.
University of Catania, Catania, Italy.

53. Grinyuk A. A. (Section 6.9)
Joint Institute for Nuclear Research, Dubna, Russia

54. Grunfeld A. G. (Section 3.13)
CONICET, Rivadavia 1917, 1033 Buenos Aires, Argentina
Departamento de Física, Comisión Nacional de Energía Atómica, (1429) Buenos Aires, Argentina
Department of Physics, Sultan Qaboos University, Sultanate of Oman

55. Gudima K. (Section 7.2, 12.8)
Institute of Applied Physics, Cishineu, Repubica of Moldova.

56. Hartnack C. (Section 12.1, 12.9)
SUBATECH, Laboratoire de Physique Subatomique et des Technologies Associées, Université de Nantes, Nantes, France.

57. van Hees H. (Section 7.8)
Frankfurt Institute for Advanced Studies (FIAS), Frankfurt am Main, Germany

58. Herold Ch. (Section 4.20)
Frankfurt Institute for Advanced Studies (FIAS), Frankfurt am Main, Germany
Institut für Theoretische Physik, Goethe-Universität, Frankfurt am Main, Germany

59. Horvatić D. (Section 3.15)
Physics Department, University of Zagreb, Zagreb, Croatia

60. Huovinen P. (Section 4.15)
Institut für Theoretische Physik, Goethe-Universität, Frankfurt, Germany.

61. de la Incera V. (Section 8.8)
University of Texas at El Paso, USA

62. Illarionov A. (Section 11.1)
Dipartimento di Fisica dell'Universitá di Trento, Trento, Italy.

63. Ivanytskyi A. I. (Section 4.21)
Bogolyubov Institute for Theoretical Physics, Kiev, Ukraine

64. Ivanov Yu. (Section 3.4, 4.6)
Helmholtzzentrum für Schwerionenforschung MbH (GSI), Darmstadt, Germany.
NRC "Kurchatov Institute", Moscow, Russia.

65. Jerusalimov A. (Section 10.3)
Joint Institute for Nuclear Research, Dubna, Russia.

66. Kaidalov A. (Section 9.1)
Joint Institute for Nuclear Research, Dubna, Russia.

67. Kalinovsky Yu. L.(Section 4.2)
Joint Institute for Nuclear Research, Dubna, Russia.

68. Kapusta J. I. (Section 5.10)
School of Physics and Astronomy, University of Minnesota, Minneapolis, USA
Departamento de Fisica Teorica I, Universidad Complutense de Madrid, Madrid, Spain

69. Karsch F. (Section 4.10)
Physics Department, Brookhaven National Laboratory, Upton, NY, USA.
Fakultät für Physik, Universität Bielefeld, Bielefeld, Germany.

70. Kekez D. (Section 3.15)
Rugjer Bošković Institute, Zagreb, Croatia

71. Kharzeev D. (Section 8.1)
Physics Department, Brookhaven National Laboratory, Upton, NY, USA.

72. Kitazawa M.(Section 5.9)
Department of Physics, Osaka University, Toyonaka, Japan

73. Klabučar D. (Section 3.15)
Rugjer Bošković Institute, Zagreb, Croatia

74. Klähn T. (Section 4.11, 4.16)
Institute for Theoretical Physics, University of Wrocław, Poland.

75. Kłusek-Gawenda M. (Section 2.9)
H. Niewodniczański Institute of Nuclear Physics, Polish Academy of Sciences, Kraków, Poland

76. Koch V. (Section 8.7)
Lawrence Berkeley National Laboratory, Berkeley, USA

77. Kodama T. (Section 5.7)
Instituto de Física, Universidade Federal do Rio de Janeiro, Rio de Janeiro, Brazil.

78. Kokoulina E. S. (Section 7.7)
Joint Institute for Nuclear Research, Dubna, Russia.
Gomel State Technical University, Gomel, Belarus.

79. Kolomeitsev E.(Section 6.4)
Univerzita Mateja Bela, Banská Bystrica, Slovakia.

80. Korotkikh V. (Section 5.6)
Skobeltsyn Institute of Nuclear Physics of Moscow State University, Moscow, Russia.
M.V. Lomonosov Moscow State University, Moscow, Russia.

81. Kunihiro T. (Section 3.16)
Department of Physics, Kyoto University, Kyoto, Japan

82. Kovalenko A. (Section 11.2)
Joint Institute for Nuclear Research, Dubna, Russia.

83. Kurepin A. B. (Section 7.4)
Institute for Nuclear Research, Troizk, Russia.

84. Kutov A. Ya. (Section 7.7)
Komi SC UrD RAS, Syktyvkar, Russia.

85. Ladygin V. (Section 10.3)
Joint Institute for Nuclear Research, Dubna, Russia.

86. Ladygina N. (Section 10.3)
Joint Institute for Nuclear Research, Dubna, Russia.

87. Lednicky R. (Section 5.1)
Joint Institute for Nuclear Research, Dubna, Russia.

88. LeFevre A. (Section 12.9)
GSI Helmholtzzentrum für Schwerionenforschung GmbH, Darmstadt, Germany

89. Leifels Y. (Section 12.9)
GSI Helmholtzzentrum für Schwerionenforschung GmbH, Darmstadt, Germany

90. Leonidov A. (Section 6.2)
P. Lebedev Physical Institute, RAS, Moscow, Russia.

91. Leupold S. (Section 4.20)
Department of Physics and Astronomy, Uppsala University, Uppsala, Sweden

92. Levin E. (Section 6.1)
Department of Particle Physics, Tel Aviv University, Tel Aviv, Israel.

93. Liao J. (Section 8.7)
RIKEN BNL Research Center, Bldg. 510A, Brookhaven National Laboratory, Upton, USA.
Physics Department and Center for Exploration of Energy and Matter, Indiana University, Bloomington, USA.

94. Lisa M. (Section 5.2)
Ohio State University, Columbus, Ohio USA.

95. Liu B. (Sections 3.6, 3.11)
Center of Theoretical Nuclear Physics, National Laboratory of Heavy Ion Accelerator, Lanzhou, China.
Institute of High Energy Physics, Chinese Academy of Sciences, Beijing, China.

96. Liu Y. X. (Section 3.11)
Center of Theoretical Nuclear Physics, National Laboratory of Heavy Ion Accelerator, Lanzhou, China.
Department of Physics and State Key Laboratory of Nuclear Physics and Technology, Peking University, China.

97. Lokhtin I. (Section 5.6)
Skobeltsyn Institute of Nuclear Physics of Moscow State University, Moscow, Russia.
M.V. Lomonosov Moscow State University, Moscow, Russia.

98. Luo X. (Section 3.10)
Department of Modern Physics, University of Science and Technology of China, Hefei, China.
Lawrence Berkeley National Laboratory Berkeley, California, USA.

99. Luschevskaya E. V. (Section 8.2)
Institute for Theoretical and Experimental Physics (ITEP), Moscow, Russia.

100. Lykasov G. I. (Section 6.9)
Join Institute for Nuclear Research, Dubna, Russia

101. Lyuboshitz V. L. (Section 10.4)
Joint Institute for Nuclear Research, Dubna, Russia.

102. Lyuboshitz V. V.(Section 10.4)
Joint Institute for Nuclear Research, Dubna, Russia.

103. Malinina L. (Section 5.6)
Skobeltsyn Institute of Nuclear Physics of Moscow State University, Moscow, Russia.
M.V. Lomonosov Moscow State University, Moscow, Russia.

104. Markert C. (Section 4.12)
Physics Department, University of Texas at Austin, USA.

105. McLerran L. (Section 3.9)
Physics Department, Brookhaven National Laboratory, Upton, NY, USA.

106. Merdeev A. V. (Section 4.22) *Frankfurt Institute for Advanced Studies, Frankfurt am Main, Germany*
National Research Center, Kurchatov Institute, Moscow, Russia

107. Mikhailov K. (Section 9.2)
Institute for Theoretical and Experimental Physics (ITEP), Moscow, Russia.

108. Mishustin I. (Section 4.20, 4.22)
Frankfurt Institute for Advanced Studies (FIAS), Frankfurt am Main, Germany
Kurchatov Institute, National Research Center, Moscow, Russia

109. Mohanty B. (Sections 2.3, 3.10)
Variable Energy Cyclotron Center, Kolkata, India.

110. Mrówczyński S. (Section 12.6)
Institute of Physics, Jan Kochanowski University, Kielce, Poland

111. Nagaytsev A. (Section 10.2)
Joint Institute for Nuclear Research, Dubna, Russia.

112. Nahrgang M. (Section 4.20)
SUBATECH, Université de Nantes, Nantes, France
Frankfurt Institute for Advanced Studies (FIAS), Frankfurt am Main, Germany

113. Nikitin V. A. (Section 7.7)
Joint Institute for Nuclear Research, Dubna, Russia.

114. Nikonov E. G. (Section 4.21)
Laboratory for Information Technologies, JINR, Dubna, Russia

115. Okorokov V. A. (Section 5.3, 12.4)
Moscow Engineering Physics Institute (National Research Nuclear University MEPhI), Moscow, Russia.

116. Oliinychenko D. R. (Sections 4.21)
Bogoliubov Laboratory of Theoretical Physics, JINR, Dubna, Russia

117. Parganlija D. (Section 4.18)
Vienna University of Technology Institute for Theoretical Physics, Vienna, Austria

118. Pederivax F. (Section 11.1)
Dipartimento di Fisica dell'Universitá di Trento, Trento, Italy.
INFN, Gruppo Collegato di Trento, Trento, Italy.

119. Petrushanko S. (Section 5.6)
Skobeltsyn Institute of Nuclear Physics of Moscow State University, Moscow, Russia.
M.V. Lomonosov Moscow State University, Moscow, Russia.

120. Pirner H. J. (Section 9.3)
Institut für Theoretische Physik der Universität Heidelberg, Germany

121. Plumari S. (Sections 3.6, 3.11)
University of Catania, Catania, Italy.

122. Polikarpov M. I. (Section 8.2)
French National Center for Scientific Research (CNRS), Tours, France.

123. Polozov P. (Section 9.2)
Institute for Theoretical and Experimental Physics (ITEP), Moscow, Russia.

124. Prokudin M. (Section 9.2)
Institute for Theoretical and Experimental Physics (ITEP), Moscow, Russia.

125. Randrup J. (Sections 2.5, 3.3, 4.19)
Lawrence Berkeley National Laboratory Berkeley, California, USA.

126. Rau P. (Section 5.8)
Frankfurt Institute for Advanced Studies (FIAS), Frankfurt, Germany.
Institut für Theoretische Physik, Goethe-Universität, Frankfurt, Germany.

127. Redlich K. (Section 3.9, 6.7)
Institute for Theoretical Physics, University of Wrocław, Poland.
Theory Division, CERN, Geneva, Switzerland.

128. Reisdorf W. (Section 4.16)
GSI Helmholtzzentrum für Schwerionenforschung, Darmstadt, Germany

129. Ritter H. G. (Section 3.10)
Lawrence Berkeley National Laboratory Berkeley, California, USA.

130. Rogachevsky O. (Section 8.6)
Joint Institute for Nuclear Research, Dubna, Russia.
Petersburg Nuclear Physics Institute, RAS, Leningrad district, Russia.

131. Rufanov L. A.(Section 7.7)
Joint Institute for Nuclear Research, Dubna, Russia.

132. Rybicki A. (Section 2.9)
H. Niewodniczański Institute of Nuclear Physics, Polish Academy of Sciences, Kraków, Poland

133. Sagun V. V. (Section 4.21)
Bogolyubov Institute for Theoretical Physics, Kiev, Ukraine

134. Salnikov V. V. (Section 11.3)
Joint Institute for Nuclear Research, Dubna, Russia.

135. Sandin F. (Section 3.7)
Fundamental Interactions in Physics and Astrophysics, University of Liège, Belgium.
EISLAB, Luleå University of Technology, Luleå, Sweden.

136. Sarycheva L. (Section 5.6)
Skobeltsyn Institute of Nuclear Physics of Moscow State University, Moscow, Russia.
M.V. Lomonosov Moscow State University, Moscow, Russia.

137. Satarov L. M. (Section 4.22)
Frankfurt Institute for Advanced Studies, Frankfurt am Main, Germany
National Research Center, Kurchatov Institute, Moscow, Russia

138. Satz H. (Sections 4.3, 6.8, 7.5)
Fakultät für Physik, Universität Bielefeld, Bielefeld, Germany.

139. Savin I. (Section 10.2)
Joint Institute for Nuclear Research, Dubna, Russia.

140. Schmidt C. (Section4.10)
Institut für Theoretische Physik, Goethe-Universität, Frankfurt, Germany.
Helmholtzzentrum für Schwerionenforschung MbH (GSI), Darmstadt, Germany.

141. Schmidt K. (Section 11.1)
Department of Physics, Arizona State University, USA.

142. Schmitt A. (Section 3.14)
Institut für Theoretische Physik, Technische Universität Wien, Austria

143. Senger P. (Section 2.6, 12.5)
Helmholtzzentrum für Schwerionenforschung MbH (GSI), Darmstadt, Germany.

144. Shao G. Y. (Section 3.11)
INFN Laboratori Nazionali del Sud, Catania, Italy

145. Sharkov G. (Section 9.2)
Institute for Theoretical and Experimental Physics (ITEP), Moscow, Russia.

146. Shevchenko O. (Section 10.2)
Joint Institute for Nuclear Research, Dubna, Russia.

147. Shutov V. B. (Section 11.3)
Joint Institute for Nuclear Research, Dubna, Russia

148. Sinyukov Yu. (Section 6.3)
Bogolyubov Institute for Theoretical Physics, Kiev, Ukraine.

149. Sissakian A. (Section 11.2)
Joint Institute for Nuclear Research, Dubna, Russia.

150. Skokov V. (Section 3.7, 8.5)
Brookhaven National Laboratory, Upton NY, USA.

151. Snigirev A.(Sections 5.6)
Skobeltsyn Institute of Nuclear Physics of Moscow State University, Moscow, Russia.
M.V. Lomonosov Moscow State University, Moscow, Russia.

152. Sorin A. (Sections 4.21,5.8, 8.6, 11.2)
Joint Institute for Nuclear Research, Dubna, Russia.
International University "Dubna", Dubna, Russia.

153. Sputowska I. (Section 2.9)
H. Niewodniczański Institute of Nuclear Physics, Polish Academy of Sciences, Kraków, Poland

154. Stöcker H. (Section 5.8)
Frankfurt Institute for Advanced Studies (FIAS), Frankfurt, Germany.
Helmholtzzentrum für Schwerionenforschung MbH (GSI), Darmstadt, Germany.

155. Stavinskiy A. (Section 9.2)
Institute for Theoretical and Experimental Physics (ITEP), Moscow, Russia.

156. Steinheimer J. (Sections 5.8, 6.6, 4.19)
Frankfurt Institute for Advanced Studies (FIAS), Frankfurt, Germany
Institut für Theoretische Physik, Goethe-Universität, Frankfurt, Germany

157. Stephanov M. (Section 3.1)
University of Illinois, Chicago, USA.

158. Stolin V. (Section 9.2)
Institute for Theoretical and Experimental Physics (ITEP), Moscow, Russia.

159. Szczurek A. (Section 2.9)
H. Niewodniczański Institute of Nuclear Physics, Polish Academy of Sciences, Kraków, Poland
University of Rzeszów, Rzeszów, Poland

160. Tawfik A. (Section 3.12, 11.5)
Egyptian Center for Theoretical Physics (ECTP), MTI University, Cairo-Egypt

161. Teryaev O. (Sections 8.6, 10.1, 10.2)
Joint Institute for Nuclear Research, Dubna, Russia.
International University "Dubna", Dubna, Russia.

162. Tolochek R. (Section 9.2)
Institute for Theoretical and Experimental Physics (ITEP), Moscow, Russia.

163. Tolstoukhov S.(Section 9.2)
Institute for Theoretical and Experimental Physics (ITEP), Moscow, Russia.

164. Tomášik B. (Sections 4.1, 6.4)
Univerzita Mateja Bela, Banská Bystrica, Slovakia.

165. Toneev V. (Sections 7.2, 8.5, 10.1)
Joint Institute for Nuclear Research, Dubna, Russia.

166. Topilskaya N. S. (Section 7.4)
Institute for Nuclear Research, Troizk, Russia.

167. Torrieri G. (Sections 4.7, 4.8)
Frankfurt Institute for Advanced Studies (FIAS), Frankfurt, Germany.
Department of Physics, Columbia University, New York, USA.

168. Torres-Rincon J. M. (Section 5.10)
School of Physics and Astronomy, University of Minnesota, Minneapolis, USA
Departamento de Fisica Teorica I, Universidad Complutense de Madrid, Madrid, Spain

169. Troshin S. M.(Section 4.4)
Institute for High Energy Physics, Protvino, Russia.

170. Tserruya I. (Section 7.1)
Weizmann Institute of Science, Rehovot, Israel.

171. Turko L. (Section 4.9)
Institute for Theoretical Physics, University of Wrocław, Poland.

172. Typel S. (Section 3.7)
Helmholtzzentrum für Schwerionenforschung MbH (GSI), Darmstadt, Germany.
Excellence Cluster Universe, Technical University Munich, Garching, Germany.

173. Uzikov Yu. (Section 12.2)
Joint Institute for Nuclear Research, Dubna, Russia.

174. Vary J. P. (Section 9.3)
Department of Physics and Astronomy, Iowa State University, Ames, USA

175. Voloshin S. (Section 8.3)
Wayne State University, Detroit, Michigan, USA.

176. Voskresensky D. (Section 3.2)
Moscow Engineering Physics Institute (National Research Nuclear University MEPhI), Moscow, Russia.

177. Wang D. J. (Section 4.14)
University of Bergen, Norway.

178. Weber F. (Section 4.11)
Department of Physics, San Diego State University, USA.

179. Wolf G. (Section 7.9)
Institute for Particle and Nuclear Physics, Wigner Research Centre for Physics, Hungarian Academy of Sciences, Budapest, Hungary

180. Wolschin G. (Section 4.17)
Institut für Theoretische Physik der Universität Heidelberg, Germany

181. Xu N. (Sections 2.2, 3.10)
Lawrence Berkeley National Laboratory Berkeley, California, USA.

182. Zabrodin E. (Section 5.5)
Department of Physics, University of Oslo, Oslo, Norway.

183. Zaitsev Yu. (Section 9.2)
Institute for Theoretical and Experimental Physics (ITEP), Moscow, Russia.

184. Zétényi M. (Section 7.9)
Institute for Particle and Nuclear Physics, Wigner Research Centre for Physics, Hungarian Academy of Sciences, Budapest, Hungary

185. Zhang Zh. (Section 3.16)
School of Mathematics and Physics, North China Electric Power University, Beijing, China

186. Zhou D. M. (Section 4.14)
Huazhong Normal University, Wuhan, China.

187. Zhuang P. (Section 7.6)
Physics Department, Tsinghua University, Beijing, China.

188. Zinovjev G. M. (Section 4.21)
Bogolyubov Institute for Theoretical Physics, Kiev, Ukraine